Towards the synthesis of weakly coordinating functionalised carborane anions via rhodium-catalysed hydroboration

Perulan, Eduardo Molinos

Award date:
2007

Awarding institution:
University of Bath

TOWARDS THE SYNTHESIS OF WEAKLY COORDINATING FUNCTIONALISED CARBORANE ANIONS VIA RHODIUM-CATALYSED HYDROBORATION

Eduardo Molinos Perulán

A thesis submitted for the degree of Doctor of Philosophy

University of Bath

Department of Chemistry

July 2007

ProQuest LLC
789 East Eisenhower Parkway
P.O. Box 1346
Ann Arbor, MI 48106-1346

Contents

Contents i
Acknowledgements iv
Abbreviations vi
Abstract vii

Chapter 1. Introduction 1
1.1 The [*closo*-$CB_{11}H_{12}$]$^-$ anion 1
1.1.1 Weakly coordinating anions 1
1.1.2 Measurement of the nucleophilic character of anions 5
1.1.3 A versatile cluster: [*closo*-$CB_{11}H_{12}$]$^-$ anion 9
1.1.3.1 Synthesis of [*closo*-$CB_{11}H_{12}$]$^-$ 10
1.1.3.2 Reactivity 11
1.1.4 Functionalisation of [*closo*-$CB_{11}H_{12}$]$^-$ anion 16
1.1.4.1 C-H functionalisation 16
1.1.4.2 {BH} functionalisation 18
1.2 Transition Metal Chemistry of [*closo*-$CB_{11}H_{12}$]$^-$ and its derivatives 22
1.2.1 Available starting materials 22
1.2.2 [*closo*-$CB_{11}H_{12}$]$^-$ and derivative anions complexes 24
1.2.3 Analogous *nido*-carborane complexes 33
1.3 Additional functionalisation methods of {BH} cluster vertexes 35
1.3.1 Metal catalysed alkene hydroboration/borylation 35
1.3.2 Metal induced alkyne hydroboration 37
1.3.3 Friedel-Craft conditions 38
1.3.4 Hydroxylation 38
1.3.5 Ionic liquids 39
1.4 Bibliography 40

Chapter 2. Functionalisation of [*closo* $CB_{11}H_{12}$]$^-$ with the $\{Rh(PPh_3)_2\}^+$ metal fragment .. 45
2.1 Introduction 45
2.1.1 Metal complexes for catalytic carborane functionalisation 45
2.1.2 Scope of the chapter 50
2.2 Results and discussion 50
2.2.1 Functionalisation of [*closo*-$CB_{11}H_{12}$]$^-$ with the $\{Rh(PPh_3)_2\}^+$ fragment 50
2.2.1.1 [$Rh(PPh_3)_2$(7/12-(H_2C=CH)-1-*closo*-$CB_{11}H_{11}$)] 50
2.2.1.2 [$Rh(PPh_3)_2$(nbd)][7/12-(H_2C=CH)-1-*closo*-$CB_{11}H_{11}$] 54
2.2.1.3 [$Rh(PPh_3)_2$(7/12-(H_3C-H_2C)-1-*closo*-$CB_{11}H_{11}$)] 58
2.2.1.4 [$Rh(PPh_3)_2$(nbd)][7/12-(H_3C-H_2C)-1-*closo*-$CB_{11}H_{11}$] 59
2.2.1.5 [$Rh(PPh_3)_2${7-(CH_2=CH)-12-Br-1-*closo*-$CB_{11}H_{10}$}] 60
2.2.1.6 [$Rh(PPh_3)_2$(nbd)][12-Br-7-(CH=CH_2)-1-*closo*-$CB_{11}H_{10}$] 63
2.2.1.7 [$Rh(PPh_3)_2$(nbd)][2,4,8,10,12-$(Et)_5$-1-*closo*-$CB_{11}H_7$] 64
2.2.2 Functionalisation of [1-X-*closo*-$CB_{11}H_{11}$]$^-$ (X = Me, ^{i}Pr_3Si) with the $\{Rh(PPh_3)_2\}^+$ fragment 69
2.2.2.1 [$Rh(PPh_3)_2$(1-X-*closo*-$CB_{11}H_{11}$)], (X = Me, ^{i}Pr_3Si) 69
2.2.2.2 [$Rh(PPh_3)_2$(1-Me-9,11,12-$(Et)_3$-1-*closo*-$CB_{11}H_8$)] 80
2.2.2.3 [$Rh(PPh_3)_2$(nbd)][1-Me-9,11,12-$(Et)_3$-1-*closo*-$CB_{11}H_8$] 83
2.2.2.4 [$Rh(PPh_3)_2$(nbd)][1-(^{i}Pr_3Si)-9,11,12-$(Et)_3$-1-*closo*-$CB_{11}H_8$] 83

2.2.3 Studies on the mechanism of borylation 85
2.2.3.1 $[Rh(PPh_3)_2(\eta^2\text{-}C_2H_4)_3][closo\text{-}CB_{11}H_{12}]$ and $[Rh(PPh_3)_2(\eta^2\text{-}C_2H_4)_3][closo\text{-}CB_{11}H_6Br_6]$ 87
2.3 Conclusions 92
2.4 Bibliography 93

Chapter 3. Monophosphine rhodium complexes partnered with $[closo\ CB_{11}H_{12}]^-$ 95
3.1 Introduction 95
3.1.1 Monophosphine rhodium complexes 96
3.1.2 Scope of the chapter 98
3.2 Results and discussion 98
3.2.1 Synthesis of phosphonium salt precursors of $[closo\text{-}CB_{11}H_{12}]^-$ 99
3.2.1.1 $[HPCy_3][closo\text{-}CB_{11}H_{12}]$ 99
3.2.1.2 $[HPCyp_3][closo\text{-}CB_{11}H_{12}]$ 100
3.2.1.3 $[HP^iPr_3][closo\text{-}CB_{11}H_{12}]$ 100
3.2.2 Synthesis of $[Rh(PR_3)(H)_2(closo\text{-}CB_{11}H_{12})]$ 101
3.2.2.1 $[Rh(PCy_3)(H)_2(closo\text{-}CB_{11}H_{12})]$ 103
3.2.2.2 $[Rh(PCyp_3)(H)_2(closo\text{-}CB_{11}H_{12})]$ 105
3.2.2.3 $[Rh(P^iPr_3)(H)_2(closo\text{-}CB_{11}H_{12})]$ 107
3.2.3 Monophosphine carborane rhodium dimers 111
3.2.3.1 $[(PCy_3)(closo\text{-}CB_{11}H_{11})(H)Rh\text{-}Rh(PCy_3)(closo\text{-}CB_{11}H_{12})]$ 111
3.2.3.2 $[(PCyp_3)(closo\text{-}CB_{11}H_{11})(H)Rh\text{-}Rh(PCyp_3)(closo\text{-}CB_{11}H_{12})]$ 117
3.2.3.3 $[(P^iPr_3)(closo\text{-}CB_{11}H_{11})(H)Rh\text{-}Rh(P^iPr_3)(closo\text{-}CB_{11}H_{12})]$ 118
3.2.3.4 Low temperature studies 119
3.2.3.5 Comments on the formation of **25**, **26** and **27** 121
3.2.4 Reactivity of $[(PR_3)(CB_{11}H_{11})(H)Rh\text{-}Rh(PR_3)(CB_{11}H_{12})]$ with olefins 123
3.3 Conclusions 126
3.4 Bibliography 127

Chapter 4. Monophosphine rhodium complexes partnered with $[closo\ CB_{11}H_6Br_6]^-$ 129
4.1 Introduction 129
4.1.1 Scope of Chapter 131
4.2 Results and discussion 131
4.2.1 Synthesis of $[HPR_3][closo\text{-}CB_{11}H_6X_6]$, R = Cy, Cyp, ^{i}Pr; X = Br, Cl 131
4.2.1.1 $[HPCy_3][closo\text{-}CB_{11}H_6Br_6]$ 132
4.2.1.2 $[HPR_3][closo\text{-}CB_{11}H_6X_6]$, R = Cyp, ^{i}Pr; X = Br, Cl 133
4.2.2 $[Rh(PR_3)(H)_2(closo\text{-}CB_{11}H_6Br_6)]$ 133
4.2.2.1 $[Rh(PCy_3)(H)_2(closo\text{-}CB_{11}H_6Br_6)]$ 134
4.2.2.2 $[Rh(PCyp_3)(H)_2(closo\text{-}CB_{11}H_6Br_6)]$ 138
4.2.2.3 $[Rh(P^iPr_3)(H)_2(closo\text{-}CB_{11}H_6Br_6)]$ 140
4.2.2.4 Reactivity of $[Rh(PR_3)(H)_2(closo\text{-}CB_{11}H_6Br_6)]$ with D_2 145
4.2.3 Reactivity of $[Rh(PR_3)(H)_2(closo\text{-}CB_{11}H_6Br_6)]$ towards olefins 145
4.2.3.1 $[Rh\{(\eta^2\text{-}C_6H_9)P(Cy_2)\}(closo\text{-}CB_{11}H_6Br_6)]$ 146
4.2.3.2 $[Rh\{P(Cyp_2)(\eta^2\text{-}C_5H_7)\}(closo\text{-}CB_{11}H_6Br_6)]$ 152
4.2.3.3 $[Rh(P^iPr_3)(\eta^2\text{-}CH_2{=}CH^tBu)(closo\text{-}CB_{11}H_6Br_6)]$ 163
4.3 Conclusions 168
4.4 Bibliography 170

Chapter 5. [1-Me-1-*closo*-$SnB_{11}H_{11}$]$^-$ as a potential weakly coordinating anion 172
5.1 Introduction 172
5.1.1 Scope of Chapter 173
5.2 Results and Discussion 174
5.2.1 [$Rh(PPh_3)_2$(nbd)][1-Me-*closo*-$SnB_{11}H_{11}$] 174
5.2.2 [$Rh(PPh_3)_2$(1-Me-*closo*-$SnB_{11}H_{11}$)] 175
5.2.3 Reactivity of [$Rh(PPh_3)_2$(1-Me-*closo*-$SnB_{11}H_{11}$)] with ethene 178
5.2.4 DFT calculations 179
5.3 Conclusions 182
5.4 Bibliography 183

Chapter 6. Experimental 184
6.1 General 184
6.1.1 NMR spectroscopy 184
6.1.2 X-ray crystallography 184
6.2 Synthesis and characterization 185
6.2.1 Starting materials 185
6.2.2 Synthesis 185
6.3 Bibliography 224

Appendix I
Appendix A I
Appendix B VI
Appendix C IX

Acknowledgements

I would like to thank Dr Andy Weller for being such an excellent supervisor. I will never forget his encouragement, support and guidance over these years, as well as his help and patience throughout the writing of this thesis. Thanks also to Dr Mary Mahon, Dr Gabriele Kociok-Köhn and Dr Simon K. Brayshaw for their work in collecting and refining the crystal structures and Dr John Lowe and Dr. Anneke Lubben for their help with NMR spectroscopy and mass spectrometry.

I would also like to thank all the people I have shared the lab with, including, Nico, Mike, Mark, Jamie, Gemma and Tom. Special thanks to Tom Player who worked in the stannaborane project, and Simon for his help and always useful comments.

A warm thank you to all who have been here for me in the good and not so good times: Jorge, Luisa, Diego, Lorena, Sonia, Laura, Paqui, Cristina, Yolanda, Julio, Irantzu, Rocco, Domenico, Ismael... for all the moments I have shared with you during the last three years in Bath. Thanks also to Paco, Narad and Edmundo, for the great times in Bath and Bristol, and to my friends in Spain, Santi, Susana, Laura and Cris. Last but certainly not least, immense thanks Walter! for your love and understanding.

Finally I wish to thank those that most deserve it, my mum Tere and sister Ana, for always having faith in me and being there. You are always in my heart with dad and Teresa.

To my Dad and sister Teresa,

Abbreviations

3c2e	3-centre-2-electron
Å	Angstrom (1×10^{-10} metres)
BAr^F_4	$[\{(3,5\text{-}CF_3)_2C_6H_3\}_4B]$
COD	Cyclooctadiene
coe	Cyclooctene
Cp	Cyclopentadienyl
Cp^*	pentamethyl-cyclopentadienyl
Cy	cyclohexyl
Cyp	cyclopentyl
δ	Chemical Shift
dppm	Diphenylphophinomethane
ESI	Electrospray ionization
ESI-MS	Electrospray ionisation mass spectrometry
Et	CH_2CH_3, ethyl
EtOTf	Ethyltriflate
Hz	Hertz
IMes	1,3-dimesitylimidazol-2-ylidene
^iPr	isopropyl
IR	Infrared spectroscopy
Me	CH_3, methyl
MeOTf	Methyltriflate
nbd	norbornadiene
NMR	Nuclear Margnetic Resonance
ppm	parts per million
THF	Tetrahydrofuran
TPP	Tetraphenylporphyrinate
[*closo*-$CB_{11}H_6X_6$]	[7,8,9,10,11,12-X_6-1-*closo*-$CB_{11}H_5$]; X = Cl, Br, I, Me
[*closo*-$CB_{11}HX_{11}$]	[2,3,4,5,6,7,8,9,10,11,12-X_{11}-1-*closo*-$CB_{11}H$]; X = F, Cl, Br, I, Me, Et
[*closo*-$CB_{11}H(Me)_5X_6$]	[2,3,4,5,6-Me_5-7,8,9,10,11,12-X_6-1-*closo*-$CB_{11}H$]; X = Cl, Br

Abstract

Sequential treatment of $[Rh(PPh_3)_2(1\text{-}X\text{-}CB_{11}H_{11})]$ [X = H(**I**), Me (**12**), $^iPr_3Si$(**13**)] with ethene and H_2 at room temperature results in the poly-functionalisation of the [*closo*-$CB_{11}H_{12}]^-$ cage. The process starts with the dehydrogenative borylation of ethene to produce the vinyl-substituted carborane $[Rh(PPh_3)_2\{(H_2C{=}CH)\text{-}closo\text{-}CB_{11}H_{11}\}]$ (**1**) that coordinates to the $\{Rh(PPh_3)_2\}^+$ fragment, blocking further substitutions on the cage. Addition of H_2 to **1** affords $[Rh(PPh_3)_2(Et\text{-}closo\text{-}CB_{11}H_{11})]$ (**3**). Up to five ethyl substitutions have been achieved on the [*closo*-$CB_{11}H_{12}]^-$ carborane anion to give [*closo*-$CB_{11}H_7Et_5]^-$ (**7**, **8**), and three when a methyl or the bulky triisopropylsilyl group are incorporated to the cage carbon atom, [1-X-*closo*-$CB_{11}H_8Et_3]^-$ [Me (**14, 15**), $^iPr_3Si$(**16**). These results are in accordance with the data obtained from the treatment of $[Rh(PPh_3)_2(1\text{-}X\text{-}closo\text{-}CB_{11}H_{11})]$ with deuterium, which gives H/D exchange in the carborane to afford $[Rh(PPh_3)_2(1\text{-}X\text{-}closo\text{-}CB_{11}D_{11})]$, presumably via a (non-observed) Rh-boryl intermediate. Functionalisation of the stannaborane cage in $[Rh(PPh_3)_2(1\text{-}CH_3\text{-}closo\text{-}SnB_{11}H_{11})]$ (**43**) with ethene results in a much slower dehydrogenative borylation rate than that observed for **I**, **12** and **13**. DFT studies suggests that the stronger Rh-H-B interactions of the stannaborane cage, when compared to [*closo*-$CB_{11}H_{12}]^-$, are the responsible of this behaviour.

Monophosphine rhodium complexes $[Rh(PR_3)(H)_2(closo\text{-}CB_{11}H_{12})]$ [R = Cy (**22**), Cyp (**23**), ^{i}Pr (**24**)] have been prepared from reaction of $[Rh(\mu\text{-}OMe)(nbd)]_2$ with $[HPR_3][closo\text{-}CB_{11}H_{12}]$ (**19-21**) in fluorobenzene. Solutions of these complexes under vacuum lose dihydrogen to yield the dimeric species $[(PR_3)(closo\text{-}CB_{11}H_{11})(H)Rh\text{-}Rh(PR_3)(closo\text{-}CB_{11}H_{12})]$ (**25-27**). These complexes show higher reactivity towards dehydrogenative borylation of alkenes, but less selectivity, giving up to nine

substitutions, but never compositionally pure material. The analogous complexes with the weakly coordinating anion [*closo*-$CB_{11}H_6Br_6$]$^-$, [Rh(PR_3)$(H)_2$(*closo*-$CB_{11}H_6Br_6$)] (**32-34**) have been synthesised in the same manner as **22-24**. Treatment of these complexes with an excess of *tert*-butylethene yields bidentate phosphine-alkene complexes [Rh{(η^2-C_6H_9)P(Cy_2)}(*closo*-$CB_{11}H_6Br_6$)] (**36**) and [Rh{P(Cyp_2)(η^2-C_5H_7)}(*closo*-$CB_{11}H_6Br_6$)] (**38**) by alkane transfer dehydrogenation, or [Rh(P^iPr_3)(η^2-CH_2=CH^tBu)(*closo*-$CB_{11}H_6Br_6$)] (**41**) in which no dehydrogenation has occurred.

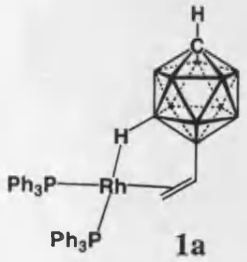

1a

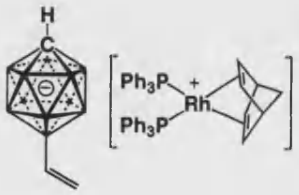

2a

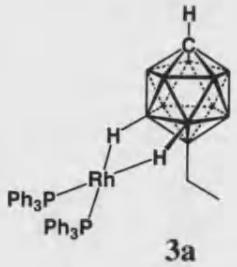

3a

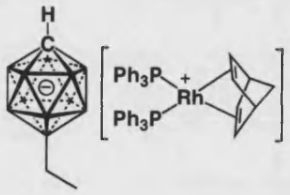

4a

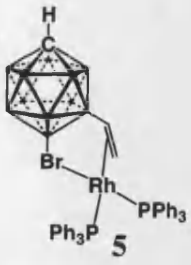

5

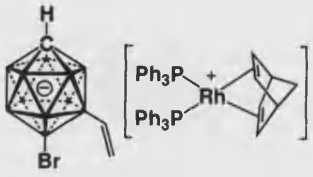

6

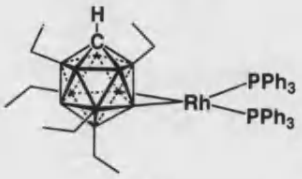

7

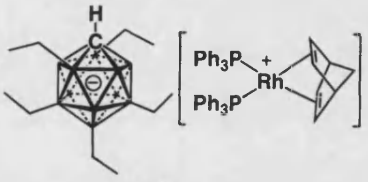

8

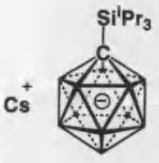

9

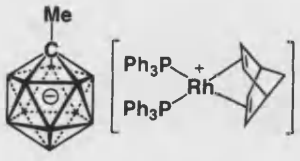

10

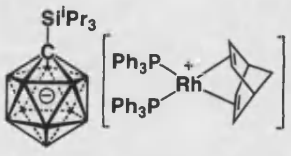

11

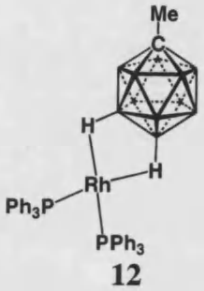

12

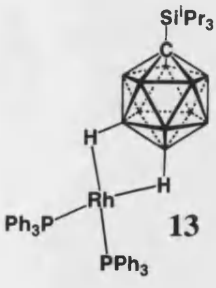

13

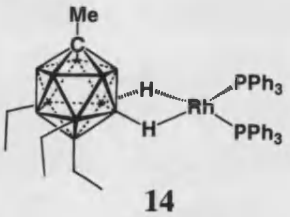

14

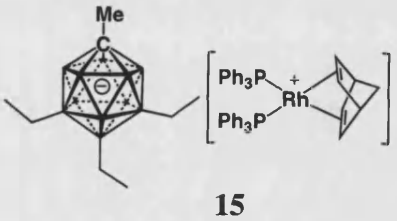

15

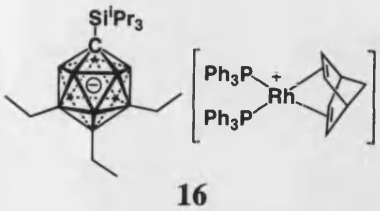

16

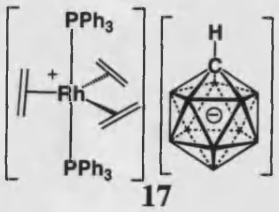

17

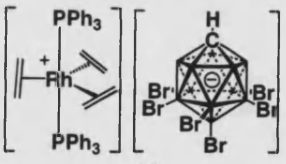

18

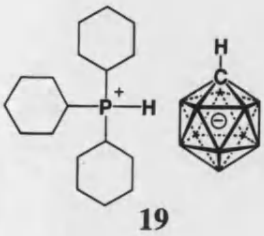

19

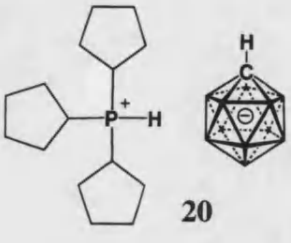

20

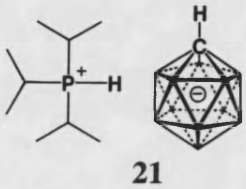

21

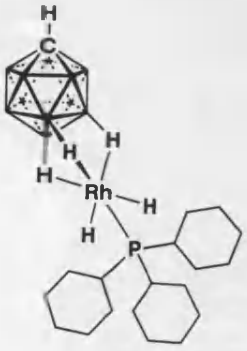

22

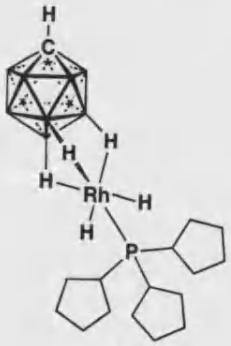

23

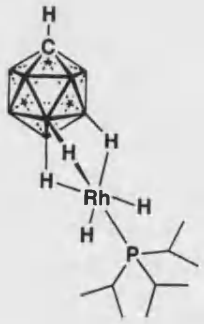

24

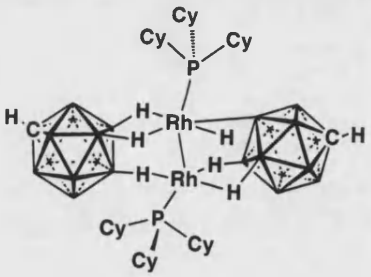

25

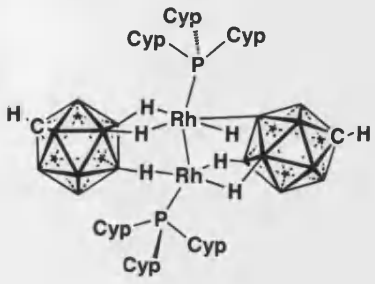

26

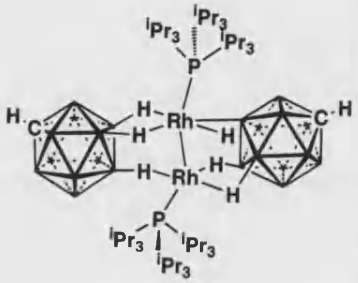

27

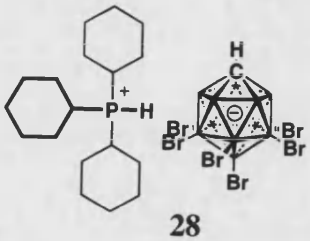

28

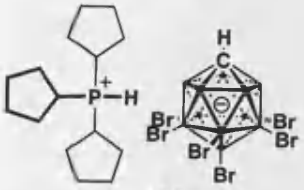

29

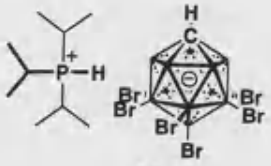

30

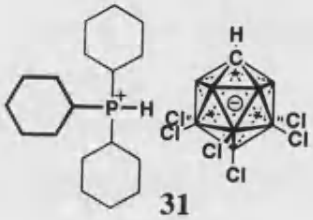

31

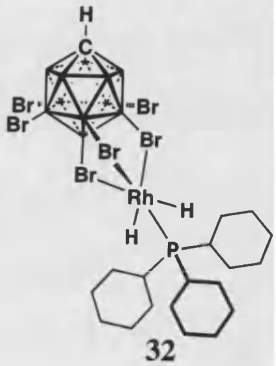

32

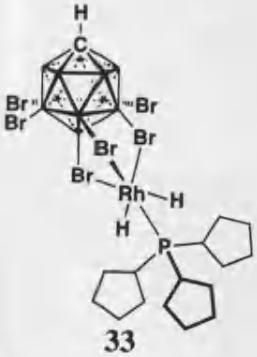

33

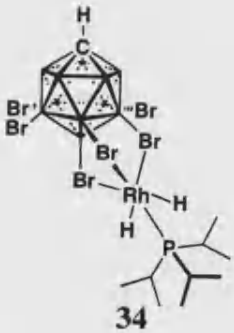

34

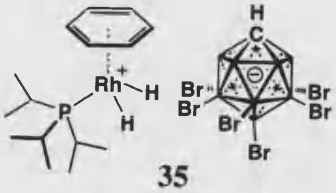

35

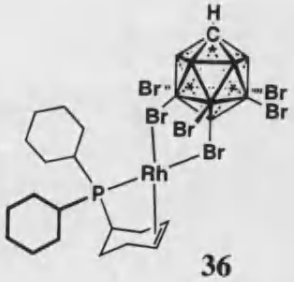

36

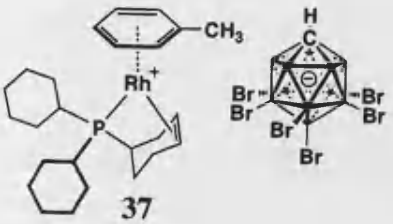

37

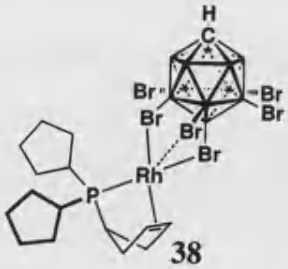

38

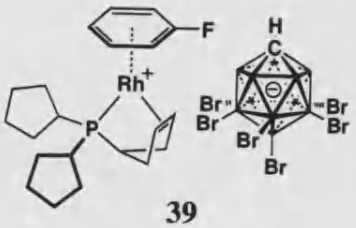

39

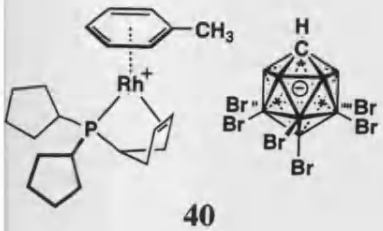

40

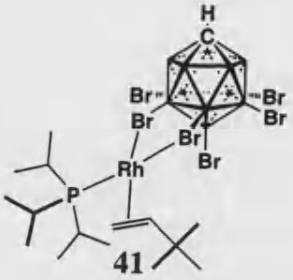

41

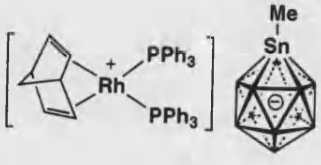

42

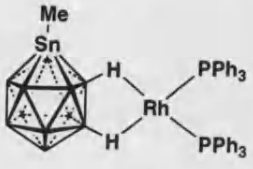

43

Chapter 1. Introduction

1.1 The [*closo*-$CB_{11}H_{12}$]$^-$ anion

1.1.1 Weakly coordinating anions

The use of weakly coordinating anions is an area of growing importance and in constant development[1] since they find application in electrochemistry,[2] ionic liquids[3] and lithium ion batteries.[4, 5] In addition they are used in extraction of radioactive cations or in stabilizing and isolating reactive protonated species as well as producing highly reactive Lewis-acidic cations with "vacant" or latent coordination sites. Such species are also very important in different types of metal-mediated catalysis[6, 7] such as: polymerisation,[8] hydrogenation of olefins[9] and Diels-Alder[10] reactions. As Figure 1.1 shows, there are four main possibilities through which a vacant coordination site can be occupied:[11]

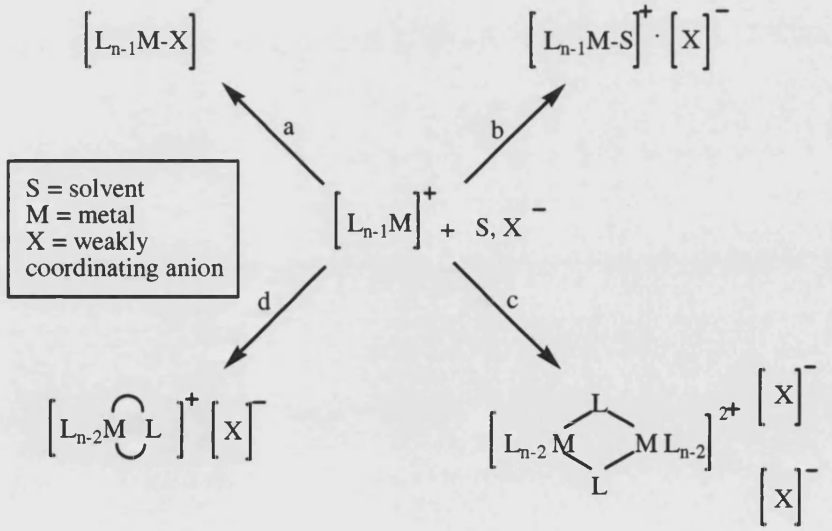

Figure 1.1

(*a*), The vacant coordination site is filled by the anion; (*b*), the solvent coordinates to the metal;[12] (*c*) one of the ancillary ligands become bidentate; and (*d*), two ancillary ligands act as bridges.[9] The solvent also plays an important role, and it may compete with the anion in the stabilisation of the catalytic species.

When using weakly coordinating solvents such as dichloromethane or fluorobenzene, the traditionally known and miscalled "non-coordinating" anions,[13] $[ClO_4]^-$, $[SO_3SF_3]^-$, $[BF_4]^-$, $[PF_6]^-$, $[AsF_6]^-$ and $[SbF_6]^-$, have been found to coordinate to metal cations (Figure 1.2) as demonstrated by Beck in his pioneering work in the 1980s.[14, 15]

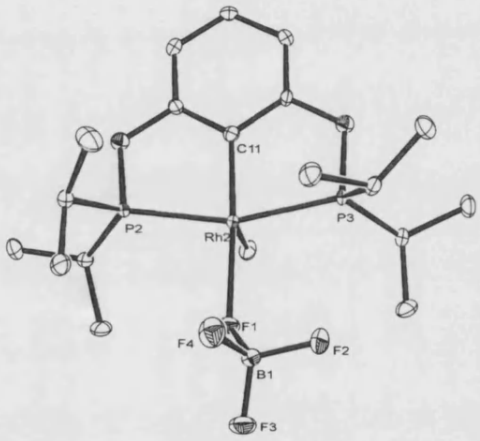

Figure 1.2 Example of coordination of the $[BF_4]^-$ anion to a Rh(III) complex.[16]

The presence of basic sites on the periphery of weakly coordinating anions leads to higher coordination ability, hence anions with oxygen or chlorine atoms should bind to Lewis acidic metal centres more easily that those with hydrogen or fluorine atoms. Thus, one quality of weakly coordinating anions should be the absence of basic or nucleophilic sites (e.g., lone pairs, hydridic hydrogens and multiple bonds, or easily polarised bonds). In addition to this characteristic, weakly coordinating anions should have large size to reduce to a minimum electrostatic interactions and a delocalised charge distribution to avoid an atom or group of atoms having a high local

concentration of charge. Other important properties are kinetic and thermodynamic stability, and in particular resistance to oxidation.

As well as $[BF_4]^-$ and $[PF_6]^-$, other important weakly coordinating anions in chemistry are derivatives of the tetraphenylborate anion $[BPh_4]^-$ and the borane cluster 1-carba-*closo*-dodecaborate anion [*closo*-$CB_{11}H_{12}]^-$. Their importance mainly resides in their usefulness as starting materials for more weakly nucleophilic and less reactive anions.[17] One of the main limitations of the parent $[BPh_4]^-$ anion is that it deactivates metal centres *via* the coordination of one phenyl group through π-interactions (Figure 1.3).[18]

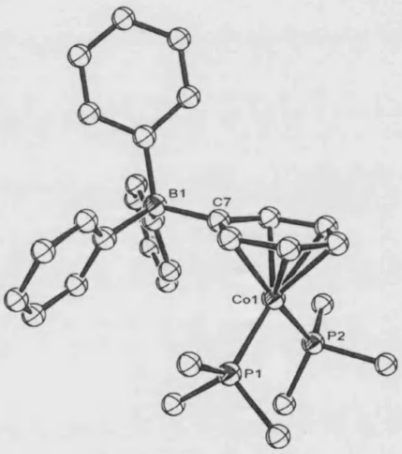

Figure 1.3 Molecular structure of a stabilised cobalt centre through coordination of one phenyl ring of the $[BPh_4]^-$ anion.[18]

The η^6-coordination of one of its phenyl groups has been demonstrated to have the same strength as the interaction of neutral arenes with metal fragments;[19] and in the complex $[Zr(CH_2Ph)_3\{(\eta^6\text{-}C_6H_5)BPh_3\}]$ the $[BPh_4]^-$ anion cannot be displaced by neutral arenes such as toluene.[20] Other limitations are the susceptibility to photochemical decomposition and reactions between $[BPh_4]^-$ and metal ions (e.g. metalation[21] or B-C cleavage[22]). Fluorinated derivatives of $[BPh_4]^-$, for example $[B(C_6F_5)_4]^-$[23] and $[BAr^F{}_4]^-$, $BAr^F{}_4$ = $[\{(3,5\text{-}CF_3)_2C_6H_3\}_4B]$,[24] were developed in order

to reduce the coordinating ability and increase the stability of the tetraphenylborate anion (Figure 1.4).

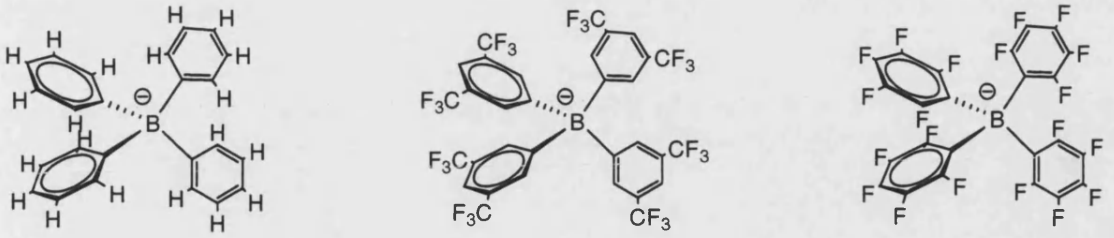

$[BPh_4]^-$ $[BAr^F{}_4]^-$ $[B(C_6F_5)_4]^-$

Figure 1.4 $[BPh_4]^-$ anion and its most utilised fluorinated derivatives.

Active catalytic systems for hydrogenation, olefin polymerisation,[8, 25] carbon monoxide and olefin copolymerisation[26] have been prepared with $[BAr^F{}_4]^-$ and $[B(C_6F_5)_4]^-$ anions. They have also been useful to isolate and stabilise cationic metal complexes with weakly coordinating solvents or molecules (CH_2Cl_2, Et_2O, H_2, N_2)[27-29] and reactive cations,[30] including protonated arenes and the silylium cation.[31]

Although these fluorinated anions have demonstrated a considerable improvement in stability and weak coordination ability compared with $[BPh_4]^-$, there are some examples where these anions have shown reactivity themselves with Lewis-acidic metal fragments. The $[BAr^F{}_4]^-$ anion in the complex *trans*-$[Pt(PPh_3)_2(Me)(OEt_2)][BAr^F{}_4]$ in refluxing C_6H_6 gives C-B cleavage with the formation of *trans*-$[Pt(PPh_3)_2(m\text{-}(CF_3)C_6H_3)_2]$;[32, 33] interactions between aromatic C-F bonds and metal centres are suggested in the complex $[Zr(Cp^*)_2(Me)(B(p\text{-}C_6H_4F)_4)]$ as determined by NMR spectroscopy;[34] and in the solid state, the complex $[Th(Cp^*)_2(Me)(B(p\text{-}C_6F_5)_4)]$[23] showed Th-F distances shorter than the sum of van der Waals radii. However, these distances are longer than the sum of ionic radii of Th^{4+} and F^-, which imply only weak Th-F interactions.[35]

Although the robust [*closo*-$CB_{11}H_{12}$]$^-$ anion[36] is a weakly coordinating anion, its hydridic hydrogens can coordinate and react with Lewis acidic cationic metal fragments. One way of evading these difficulties is by replacement the hydrogens for halogens[37-42] or even better for alkyls,[43, 44] which do not have basic lone pairs of electrons and provides an anion with less coordinating properties (Figure 1.5 shows the [*closo*-$CB_{11}H_{12}$]$^-$ anion, the hexabrominated, perchlorinated and permethylated cages). This thesis is concerned with the development of the synthesis and coordination chemistry of such anions.

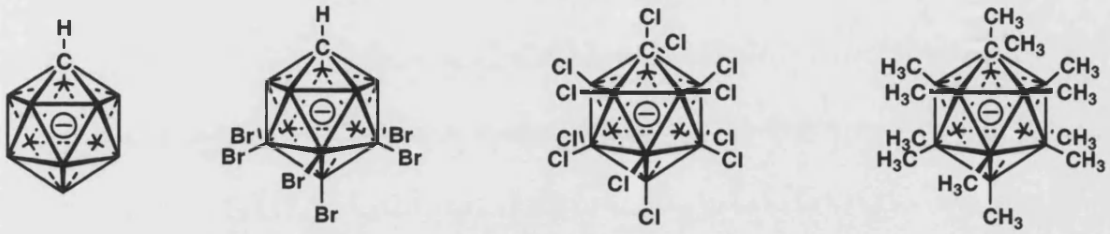

Figure 1.5 Terminal {BH} hydrides are omitted for clarity.

1.1.2 Measurement of the nucleophilic character of anions

Several systems have been developed to measure the coordination strength or weakness of the different weakly coordinating anions. The first of these systems was outlined by C.A. Reed and it consists of measuring, in the solid state, the degree of Fe deviation from the plane in [Fe(TPP)$^+$] (TPP = tetraphenylporphyrinate). The closer to planarity, and hence the shorter the distance between N-Fe, the more weakly coordinating the anion is suggested to be. The shortest distance was obtained for the [*closo*-$CB_{11}H_{12}$]$^-$ anion.[45] This system had to be abandoned when weaker anions, such as halogenated derivatives of [*closo*-$CB_{11}H_{12}$]$^-$, were used, since solvent molecules crystallised closer to the iron complex than the anion (e.g.Figure 1.6), i.e. the limit of the scale was reached.[46]

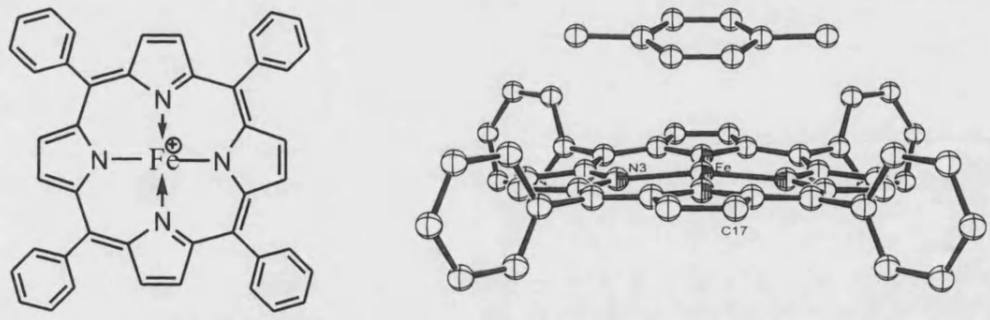

Figure 1.6 $[Fe(TPP)]^+$ cation (left) and crystal structrure of $[Fe(TPP)(p\text{-xylene})]^+$ (right).

Another system, based on the CO stretching frequencies observed for $[Fe(Cp)(CO)_2X]$ (X = anion), was also developed by Reed to rank the coordinating weakness of anions.[17] The less nucleophilic the anion, the less electronic density the metal is going to receive. This increment in the cationic character in the $\{FeCp(CO)_2\}^{\delta+}$ moiety correlates with higher CO frequencies due to a diminution in π-back-bonding from the metal. Therefore the highest stretching frequencies (Table 1.1) will belong to the weakest coordinating anion. As some of the species were prepared *in situ*, and could not be isolated or eventually characterised, these results should be interpreted with caution.

X^-	Average νCO in toluene (cm^{-1})
$[ClO_4]^-$	2049
$[closo\text{-}CB_{11}H_{12}]^-$	2049
$[SbF_6]^-$	2050
$[closo\text{-}CB_{11}Me_{12}]^-$	2098
$[closo\text{-}CB_{11}H_6Br_6]^-$	2108

Table 1.1 Average carbonyl stretching frequencies for $[Fe(Cp)(CO)_2X]$.[17]

The third, and more accurate method, is based in the downfield variation of the ^{29}Si chemical shift in $^{i}Pr_3Si^{\delta+}X^{\delta-}$.[47] By this criterion the more positive values in the ^{29}Si chemical shift will indicate a more deshielded nucleus with more cationic character, "R_3Si^+", and thus the weakest coordinating anions will be established. Due to fluoride

ion abstraction and C-B cleavage, the $[B(C_6F_5)_4]^-$ anion could not be measured in solution, while some measurements have had to be done in the solid state because of solvent – anion competition as the equilibrium in Equation 1.1 shows.

$$^{i}Pr_3Si(anion) + toluene \rightleftharpoons [^{i}Pr_3Si(toluene)]^+ + anion$$

Equation 1.1

Compound	$\delta(^{29}Si)$/ppm
$^{i}Pr_3Si[closo\text{-}CB_{11}H_6I_6]$	97
$^{i}Pr_3Si[B(C_6F_5)_4]$	107.6
$^{i}Pr_3Si[closo\text{-}CB_{11}H_6Br_6]$	110
$^{i}Pr_3Si[closo\text{-}CHB_{11}Cl_{11}]$	114.4
$^{i}Pr_3Si[closo\text{-}CB_{11}H_6Cl_6]$	115
$^{i}Pr_3Si[closo\text{-}CB_{11}HF_{11}]$	120

Table 1.2 Selected ^{29}Si shifts for $[^{i}Pr_3SiX]$.

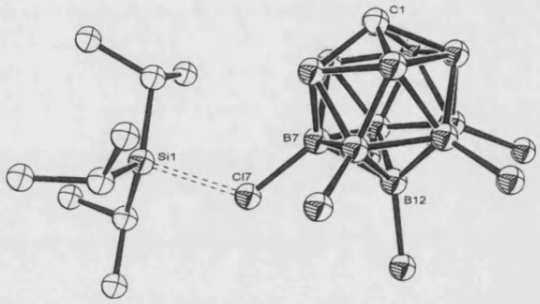

Figure 1.7 $[^{i}Pr_3Si][closo\text{-}CB_{11}H_6Cl_6]$.

Table 1.2 provides the ^{29}Si chemical shifts of a variety of anions in $^{i}Pr_3SiX$. As can be seen, the coordination capacity of halogenated carboranes increases with the accessibility of their lone pairs in the order F < Cl < Br < I. The degree of halogen substitution is usually related to the coordinating weakness of the anion; the higher the number of substitutions the more weakly coordinating the anion, however, there are exceptions as Table 1.2 shows for the hexachloro (Figure 1.7) and undecachlorocarboranes.[39, 42, 48] The permethylated $[closo\text{-}CB_{11}Me_{12}]^-$anion cannot be ranked by this method due to methide abstraction to form $SiMeR_3$.[49]

Other methods have been used recently in order to measure the relative acidity of acids made with weakly coordinating anions as conjugate bases, indicating that halogenated carborane derivatives produce the strongest and most stable acids known. The mesityl oxide scale, which relies on the variation of ^{13}C chemical shifts of C_α and

C_β atoms, has demonstrated that carborane acids possess more acidic character than any oxyacid,[50] but discrimination between carboranes acids is difficult since they move the equilibrium completely to the right of the equation (Equation 1.2).

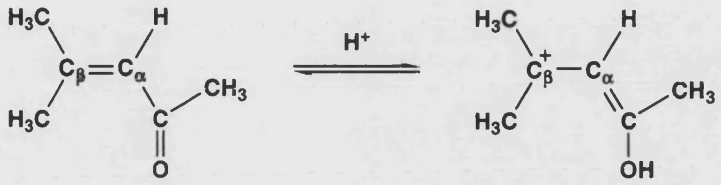

Equation 1.2 Equilibrium formed after addition of an acid to mesityl oxide.

Thus, another system based on IR spectroscopy has been developed in order to accurately measure the relative basicities of carboranes. The ν(NH) stretching frequency of the trioctylammonium salts of carboranes correlates to the degree of interaction between the conjugate base and the proton (Figure 1.8), the weaker the interaction, the higher the ν(NH) frequency (stronger N-H bond) and the less basic the anion (Table 1.3).[50-53]

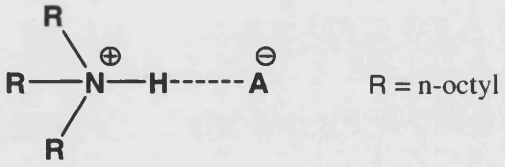

Figure 1.8 N-H ion pair contact with the anion.

Conjugate base	νN-H (± 1 cm^{-1})	Δν (cm^{-1})	Conjugate base	νN-H (± 1 cm^{-1})	Δν (cm^{-1})
$[B(C_6F_5)_4]^-$	3233	0	$[CB_{11}H(Me)_5Cl_6]^-$	3143	90
$[CMeB_{11}F_{11}]^-$	3219	14	$[BF_4]^-$	3133	100
$[PF_6]^-$	3191	42	$[CB_{11}H_{12}]^-$	3129	104
$[CB_{11}HCl_{11}]^-$	3163	70	$[CB_{11}H_6Br_6]^-$	3125	108
$[CB_{11}H(Me)_{11}]^-$	3156	77	$[CB_{11}H(Me)_5Br_6]^-$	3120	113
$[CB_{11}H_6Cl_6]^-$	3148	85	$[CB_{11}H_6I_6]^-$	3097	136

Table 1.3 Selected ν(N-H) frequencies for a range of different anions.

Although relative acidities of anions can be ranked using this method by formation of the corresponding trioctylammonium salts, isolation of free acids is only achievable for those conjugate bases with high kinetic and thermodynamic stability. Consequently, carborane acids are the strongest *isolable* acids, since e.g. $H[B(C_6F_5)_4]$ or $H[PF_6]$ decompose and cannot be isolated.

1.1.3 A versatile cluster: [*closo*-$CB_{11}H_{12}$]$^-$ anion

Since the synthesis of the first boranes in the early 19hundreds, the development of boron containing clusters has been a major research topic. One main characteristic of these polyhedral boron aggregates is the presence of 3-centre-2-electron (3c2e) bonds due to the deficiency of electrons around the {BH} fragment. In the case of carboranes, they can be considered as borane derivatives because a $\{BH\}^-$ fragment is isolobal and isoelectronic with a {CH} fragment.[54] This relationship indicates that the fragments have identical frontier orbitals and number of bonding electrons, and the molecular orbitals have similar symmetry and approximately the same energy; overall implying that, in theory, they can be exchangeable.

The borane polyhedron might be complete or might have up to 3 vertices missing, albeit more than 2 are infrequent. By application of Wade's rules to a borane or carborane it is possible to predict the polyhedral shape of the cluster, which is related with the number of vertices and skeletal electron pairs.[55] A *closo*-cluster has $n + 1$ electron pairs, where n is the number of cluster vertices. Its shape is a closed polyhedron (or deltahedron) with n vertices. A *nido*-cluster has $n + 2$ pairs of electrons and 1 missing vertex, which is the one with the highest connectivity in the polyhedron. Likewise, an *arachno*-cluster has $n + 3$ pairs of electrons (donated to cluster bonding) and 2 vertices missing. A *hypho* cluster means three vertices are short of a complete

polyhedron. Examples of *closo, nido* and *arachno* carboranes based in the icosahedral polyhedron are shown in Figure 1.9.

[*closo*-1-$CB_{11}H_{12}$]$^-$ [*nido*-7,8,9-$C_3B_8H_{11}$]$^-$ *arachno*-$C_2B_8H_{14}$

Figure 1.9 *Closo, nido* and *arachno* clusters based on an icosahedral polyhedron.

Most *arachno*-carboranes are quite reactive because of their open structure and bridging hydrogens. *Nido*-carboranes are less thermally and chemically unstable than *arachno* but still react easily, for example by deprotonation of a bridging B-H-B hydrogen. Finally, the *closo*-counterparts are the most stable within the carborane family, and [*closo*-$CB_{11}H_{12}$]$^-$ anion and its derivatives are among the most stable of these.[56-58]

1.1.3.1 Synthesis of [*closo*-$CB_{11}H_{12}$]$^-$

The attractiveness of the [*closo*-$CB_{11}H_{12}$]$^-$ anion is that it fulfils all characteristics of a weakly coordinating anion: its negative charge is delocalised in the $\{CB_{11}\}^-$ cluster, it has a spherical and large size, is chemically robust, available in multigram scale and its {BH} vertices can be functionalised.

Three synthetic routes have been reported for the synthesis of the [*closo*-$CB_{11}H_{12}$]$^-$ anion. The first one, and the most appropriate for multigram synthesis, was reported by Knoth in 1967 and it starts from decaborane [*nido*-$B_{10}H_{14}$] (Figure 1.10).[36, 59] Different modifications on this synthesis were introduced by Heřmánek[60] and Hughes.[61] The second route, published by Michl *et al*, uses $NaBH_4$ oxidation with I_2 to synthesise [*nido*-$B_{11}H_{14}$]$^-$ and to finally obtain the [*closo*-$CB_{11}H_{12}$]$^-$ anion *via* C-H insertion.[62] This

route has the limitation that can only be run on a 1g scale in order to obtain a reliable yield. However, it is a good synthetic way of obtaining the carbon-substituted [1-Ph-*closo*-$CB_{11}H_{11}$]$^-$ anion (see Figure 1.18 later). The third route, based on the Brelloch's reaction,[63] was firstly used for the [1-Ph-*closo*-$CB_{11}H_{11}$]$^-$ anion synthesis (Figure 1.19).[64] It uses $B_{10}H_{14}$ and an aldehyde RCHO (R = Ph, H) to render the [*nido*-6-R-6-CB_9H_{11}]$^-$ anion, which when treated with $BH_3{\cdot}SMe_2$ or $BH_3{\cdot}NEt_3$ in dichloroethane gives the [1-R-*closo*-$CB_{11}H_{11}$]$^-$ anion (R = Ph, H).[65]

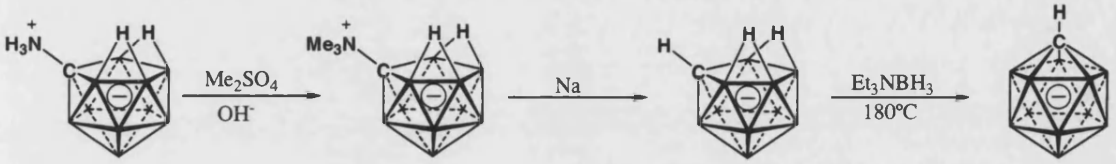

Figure 1.10 Knoth's synthesis of [*closo*-$CB_{11}H_{12}$]$^-$.

1.1.3.2 Reactivity

The great stability of the {*closo*-CB_{11}}$^-$ core is based in the high HOMO-LUMO energy gap, the high oxidation potential and its delocalised σ-bonding framework (σ-bonds are much stronger than π-bonds),[57] which makes this *closo* cluster the three-dimensional analogue of benzene. This σ aromaticity character has been supported by computational studies.[57, 58] However, the periphery of the [*closo*-$CB_{11}H_{12}$]$^-$ anion is easily functionalised *via* electrophilic substitution at the {BH} bonds and *via* lithiation with butyl lithium at the C atom. The difference in electronegativity among carbon, boron and hydrogen results in a slight polarisation of the cage, therefore most of the negative charge is located on the carbon atom (Table 1.4, Figure 1.11). However, the reactivity of the anion relies on the distribution of charges on the anion periphery and consequently the atomic charges on the borons and hydrogens dictate the reactivity of the anion either in coordination to metal centres or in vertex substitution reactions.

$B_{2\text{-}6}$: upper pentagonal belt

$B_{7\text{-}11}$: lower pentagonal belt

B_{12}: antipodal vertex

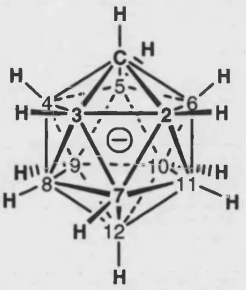

Figure 1.11[*closo*-$CB_{11}H_{12}$]$^-$ labelling scheme.

	n.a.c.	n.a.c. on {H}	*n.a.c. on {EH}*
C	-0.712	+0.322	-0.38
$B_{2\text{-}6}$	-0.022	+0.049	+0.027
$B_{7\text{-}11}$	-0.185	+0.058	-0.127
B_{12}	-0.161	+0.055	-0.106

Table 1.4 n.a.c. (natural atomic charges).

The most susceptible boron to suffer electrophilic attack is the antipodal boron vertex B_{12}, followed by the lower pentagonal belt ($B_{7\text{-}11}$) whose boron atoms are only slightly less reactive. The boron atoms at the upper pentagonal belt are even less reactive and the harshest conditions are needed to functionalise these positions. Although the carbon atom at position 1 is negatively charged, it shows no reactivity to electrophilic attack. This is inhibited by the large positive charge of its hydrogen.

The same reactivity towards electrophilic attack was obtained from *ab-initio* calculations and the use of Frontier Molecular Orbital Theory, which indicates that the selectivity of electrophilic attack is very much dependant on the amplitude of the HOMO at any particular position. Since the HOMO and HOMO-1 are relatively close in energy in [*closo*-$CB_{11}H_{12}$]$^-$, both molecular orbitals have to be considered in order to establish the cage's reactivity pattern. The HOMO vanishes at the carbon and boron at position 12 and only has horizontal tangential amplitudes at both pentagons. The HOMO-1, has a large amplitude at boron 12 (antipodal position) and smaller vertical tangential amplitudes on borons at the lower pentagonal belt (see Figure 1.12). Due to these differences in reactivity at the different boron atoms, the cage can be selectively functionalised by controlling the hardness of electrophiles as well as the conditions of reaction. The brominated derivatives of the [*closo*-$CB_{11}H_{12}$]$^-$ anion constitute a good example of its reactivity.

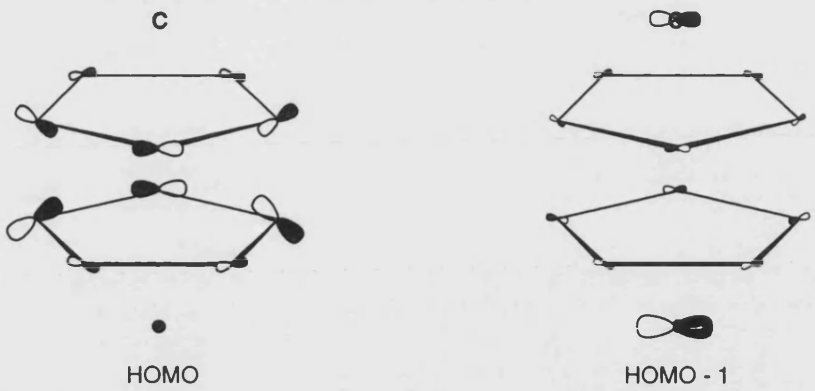

Figure 1.12 HOMO and HOMO-1 of [*closo*-$CB_{11}H_{12}]^-$, showing only one of each degenerate pair.

As Figure 1.13 illustrates, the mono-brominated [12-Br-1-*closo*-$CB_{11}H_{11}]^-$ anion can be prepared at room temperature by two methods: (1) using stoichiometric amounts of a bromine solution in CCl_4 and K_2CO_3 in water, or (2) with one equivalent of N-bromosuccinimide in dimethylformamide. The use of two or more equivalents of N-bromosuccinimide leads to the formation of the [7,12-Br_2-1-*closo*-$CB_{11}H_{10}]^-$ anion. The hexabromo [*closo*-$CB_{11}H_6Br_6]^-$ anion synthesis requires harsher conditions: a solution of [*closo*-$CB_{11}H_{12}]^-$ in glacial acetic acid with Br_2 at 80 °C. The [*closo*-$CB_{11}HBr_{11}]^-$ anion has to be synthesized in triflic acid with bromine at 200 °C for 4 days. To perbrominate the cage (i.e. C-Br), the temperature has to be increased to 250 °C and maintained for 6 days (in triflic acid with bromine).

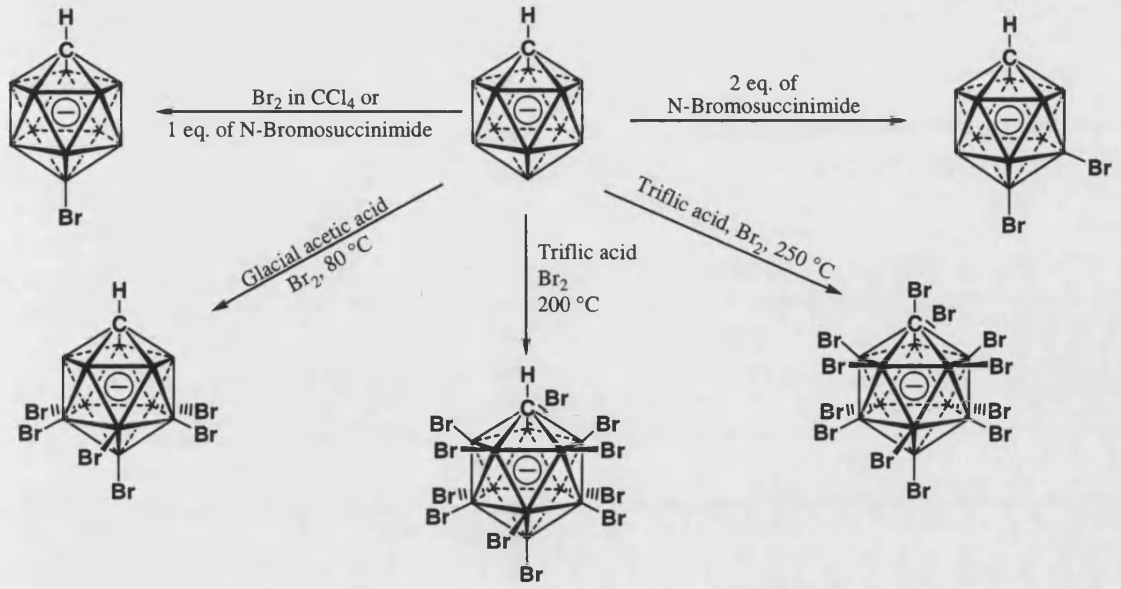

Figure 1.13 Reactivity of [*closo*-$CB_{11}H_{12}$]$^-$ against bromination.

Several results have confirmed the weakly nucleophilic nature of [*closo*-$CB_{11}H_{12}$]$^-$. One consequence is the reduction of the reaction rate in silver metathesis reactions, which was proposed by Reed.[66] Weller and coworkers have confirmed this fact in the reactions of [(L)Mo(CO)$_3$X] (L = Cp, Cp*, X = Cl, I) with the silver complexes of the [*closo*-$CB_{11}H_{12}$]$^-$ and [*closo*-$CB_{11}Br_6H_6$]$^-$ anions.[67] The isolation of the silver intermediate [CpMo(CO)$_3$I·Ag{*closo*-$CB_{11}H_{12}$}]$_2$ was achieved due to the weakly nucleophilic behaviour of the [*closo*-$CB_{11}H_{12}$]$^-$ anion[68] (Figure 1.14)

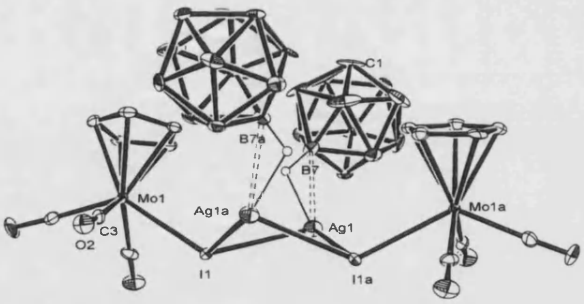

Figure 1.14 X-Ray structure of [CpMo(CO)$_3$I·Ag{*closo*-$CB_{11}H_{12}$}]$_2$.[68]

The differences in reactivity of the {BH} bonds of the [*closo*-$CB_{11}H_{12}$]$^-$ anion, observed in electrophilic substitution reactions, also follow for the coordination of the anion with metal fragments. The 12 vertex and the lower pentagonal belt are usually

involved in the coordination with metals centres, however, there is no example of a coordinated upper pentagonal belt vertex documented. The existence of interaction only *via* the 12 vertex is well documented, for example, the complexes $[Zr(Cp)_2(CH_3)(closo\text{-}CB_{11}H_{12})]$,[69] $[Fe(Cp)(CO)_2(closo\text{-}CB_{11}H_{12})]$[66] exhibit this interaction through a 3c2e bond in the solid state. However, two isomers of $[Fe(Cp)(CO)_2(x\text{-}\mu\text{-}H\text{-}closo\text{-}CB_{11}H_{11})]$ and $[Mo(Cp)(CO)_3(x\text{-}\mu\text{-}H\text{-}closo\text{-}CB_{11}H_{11})]$ (x = 7, 12) can be observed in solution by NMR spectroscopy.[67, 70] Complexes with two {BH} positions interacting to the metal, usually 7 and 12, are known as well; the most representative examples belong to rhodium[71, 72] and platinum[73] complexes with distorted square planar coordination. There are also complexes that coordinate in a tridentate manner, with interactions between the metal fragment and vertices 7, 8 and 12 (e.g. $[Zr(Cp^*)(CH_3)_2(closo\text{-}CB_{11}H_{12})]$[69]).

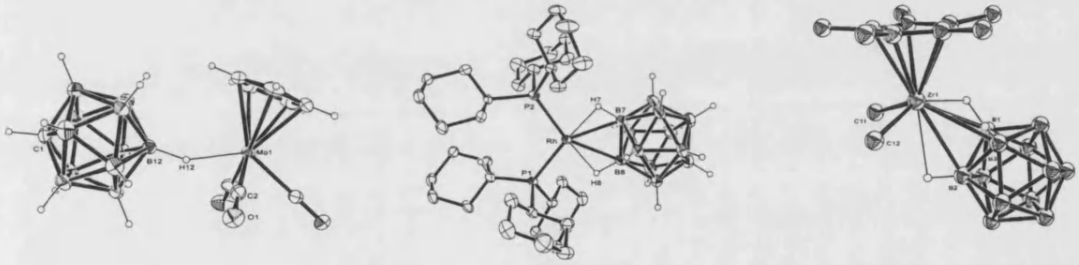

Figure 1.15 Examples of the three known coordination modes of the $[closo\text{-}CB_{11}H_{12}]^-$ anion.[67, 69, 72]

The mode of coordination of these complexes is *via* 3-centre-2-electron bonding. The nature of these interactions plays a very important role in catalytic systems and they may be strong enough to reduce the catalytic activity of cationic Lewis acid metals. An illustrative example is the decrease of the catalytic activity in ethylene polymerisation and copolymerisation of propene of $[Zr(Cp^*)(CH_3)_2(\eta^3\text{-}closo\text{-}CB_{11}H_{12})]$, which shows much less reactivity with olefins than $[Zr(Cp)_2(\eta^2\text{-}CH_2Ph)(\eta^1\text{-}closo\text{-}CB_{11}H_{12})]$ and $[Zr(Cp')_2(CH_3)(\eta^1\text{-}closo\text{-}CB_{11}H_{12})]$ (Cp' = C_5H_4Me).[69] This fact may be due to the

tridentate coordination mode of the carborane, which is not as easily displaced as when it is coordinated through one Rh-H-B interaction.

A similar cluster but with a completely different reactivity pattern, due to the replacement of {CH} for {Sn^-} as a vertex, has been widely studied by Wesemann. [*closo*-$SnB_{11}H_{11}]^{2-}$ has been mainly used as a two electron donor ligand, however there are a few examples of B-H coordination to metals through 3c2e bonding as is exemplified in Figure 1.16.[74] This X-ray crystal structure shows coordination of the tin cage to the metal centre through B-H bonds from the upper and lower pentagonal belts.

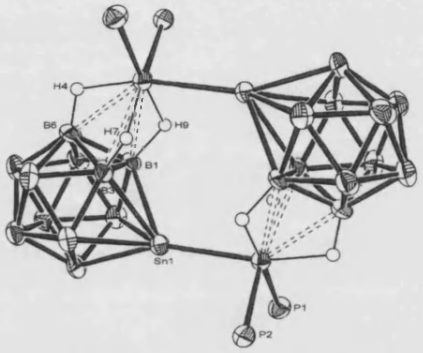

Figure 1.16 [$Ru(PPh_3)_2$(1-*closo*-$SnB_{11}H_{11}$)]$_2$.[74]

Less nucleophilic polysubstituted carboranes have been developed in order to reduce these interactions and enhance the catalytic activity of metal cations. Halogenation and alkylation of the {*closo*-CB_{11}}$^-$ core have been the most important routes of obtaining more weakly coordinating carboranes, as is discussed next.

1.1.4 Functionalisation of [*closo*-$CB_{11}H_{12}]^-$ anion

1.1.4.1 C-H functionalisation

The most frequent route of C-H functionalisation is by treatment of the parent [*closo*-$CB_{11}H_{12}]^-$ with a suitable base, such as butyllithium, to make the carbon vertex the most nucleophilic,[75] and therefore amenable to be attacked by electrophilic reagents

such as alkyl halides.[38] It is worth noting that if the carborane is already substituted in all, or some of its boron vertices, the acidity on the C-H proton varies. For example, there is yet to be a base strong enough to deprotonate [*closo*-$CB_{11}HMe_{11}]^-$, however [1-X-1-*closo*-$CB_{11}Me_{11}]^-$ (X = Br, I) can be converted into the permethylated anion by treatment with butyllithium and MeI.[76] In contrast the cluster [*closo*-$CB_{11}HF_{11}]^-$ can be easily attacked on the C-H proton with a basic aqueous hydroxide solution.[40]

Figure 1.17 General procedure for C-substituted carboranes.

Other groups different from alkyls have also been inserted by this route, such as silyls, phosphino, sulphide or copper.[38, 60, 77-79]

The 1-alkylated [1-R-1-*closo*-$CB_{11}H_{11}]^-$ anions are accessible by carbon or boron insertion in precursors such as [*nido*-$B_{11}H_{14}]^-$, [*nido*-7-$CB_{10}H_{10}]^{3-}$ or *nido*-$B_{10}H_{14}$. Michl's final step of the carborane cage synthesis can be modified, and as can be seen in Figure 1.18, by the use of the appropriate reagent to give access to new C substituted derivatives by carbene insertion into the anion [*nido*-$B_{11}H_{14}]^-$.[62] The inclusion of aryl groups by this method or *via* palladium catalysed routes, as is explained later, leads to functionalised carboranes that are not ideally designed for use as weakly coordinating anions, as they easily coordinate to metals through π arene interactions.

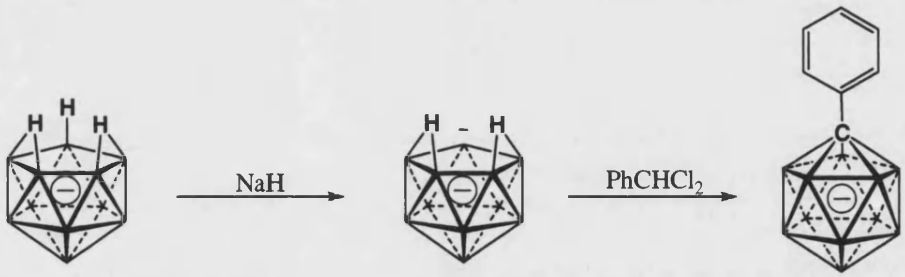

Figure 1.18 Carbene insertion method.

Brelloch's reaction is another alternative route of preparing 1-substituted carboranes by changing the aldehyde substitute (*R*-CHO) as pictured in Figure 1.19.[64, 80]

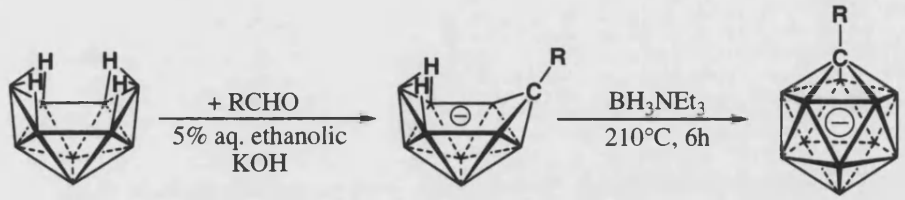

Figure 1.19 Brelloch's reaction.

Replacement reactions are another alternative in the synthesis of more C-substituted derivatives. An example of this kind of reaction is given in Figure 1.20 where treatment of [1-(NH_3)-1-*closo*-$CB_{11}H_{11}$] with nitrous acid inserts a hydroxide group on the carbon.

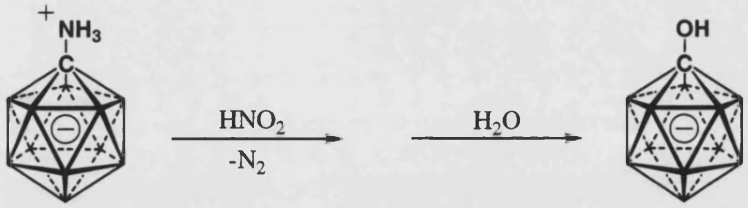

Figure 1.20 Hydroxylation at the {CH} vertex.[77]

1.1.4.2 {BH} functionalisation

Alkylation and halogenation of the parent [*closo*-$CB_{11}H_{12}$]$^-$ {BH} vertices have been widely studied techniques in {BH} functionalisation. They have provided a broad number of new weakly coordinating anions with enhanced properties, such as: more

stable and less reactive carboranes (from halogenation) and more soluble anions in non-polar solvents (from alkylation).

Halogenation. Selective halogenation of the different positions at the [*closo*-$CB_{11}H_{12}]^-$ anion has been accomplished by modifying the conditions of reaction and harshness of the reactants. An illustrative example has already been described in Figure 1.13 for the selective bromination of the vertices of the [*closo*-$CB_{11}H_{12}]^-$ anion. Similar processes but with different reagents are necessary for the synthesis of [12-X-1-*closo*-$CB_{11}H_{11}]^-$, [7,12-X_2-1-*closo*-$CB_{11}H_{10}]^-$, [*closo*-$CB_{11}H_6X_6]^-$, [*closo*-$CB_{11}HX_{11}]^-$ (X = F, Cl, Br, I) and [*closo*-$CB_{11}Br_{12}]^-$.[38, 39, 41, 77] The mono, di, and hexa-chloro derivatives are prepared under the same conditions as the brominated analogues. The mono and dichlorinated [12-Cl-1-*closo*-$CB_{11}H_{11}]^-$, [7,12-Cl_2-1-*closo*-$CB_{11}H_{10}]^-$ are synthesized using 1 or 2 equivalents of N-chlorosuccinimide respectively,[38] and the hexachlorinated [*closo*-$CB_{11}H_6Cl_6]^-$ requires Cl_2 in glacial acetic acid.[77] The different iodinated derivatives are prepared with iodine (mono and disubstituted) or with ICl (for the hexa and periodinated cages).[41] The perfluorinated [*closo*-$CB_{11}HF_{11}]^-$ anion can be synthesized using F_2 in hydrofluoric acid at room temperature.[40] Mixed halocarborane anions [2,3,4,5,6-Y_5-7,8,9,10,11,12-X_6-1-*closo*-$CB_{11}H$] (X, Y = Cl,Br, I) were also reported by Xie and coworkers in 2000.[42]

Alkylation. Alkylated anions are available after treatment of the parent carborane with a strong methylating reagent, such as methyl triflate, coupled with the strong base CaH_2 in sulfolane. This reaction, reported by Michl,[43] proceeds readily since the incorporation of one methyl group activates the cluster for subsequent {BH} substitutions. The combination of methylation and halogenation renders an important number of mixed halo-methylated carborane derivatives.

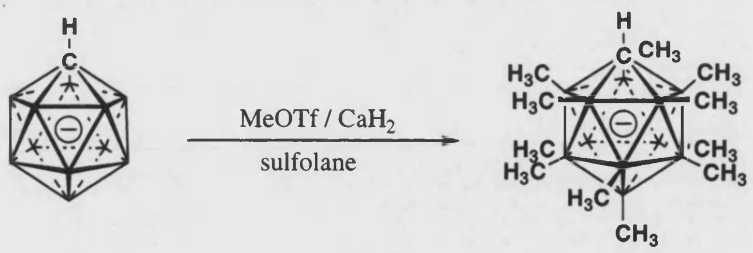

Figure 1.21 Synthesis of the undecamethylated anion [*closo*-$CB_{11}HMe_{11}]^-$.[43]

According to unpublished results but commented on in a recent review,[81] Michl and co-workers have inserted ethyl groups using similar reaction conditions as described above. In this sense, ethyl triflate has been used along with [1-^{i}Pr$_3$Si-1-*closo*-$CB_{11}H_{11}]^-$ or [*closo*-$CB_{11}H_6Me_6]^-$ to form [1-^{i}Pr$_3$Si-7,8,9,10,11,12-Et_6-1-*closo*-$CB_{11}H_5]^-$ and [2,3,4,5,6-Et_5-7,8,9,10,11,12-Me_6-1-*closo*-$CB_{11}H]^-$, the isopropyl group is believed to block the positions at the upper pentagonal belt from methyl or ethyl substitution by steric effects. However, methylation is electronically retarded by the halogen on the C position; when the halogen is fluorine, complete methylation is not feasible.

Xie and coworkers have also reported the synthesis of the permethylated [*closo*-$CB_{11}HMe_{11}]^-$ and [*closo*-$CB_9Me_9]^-$ anions along with the perethylated [*closo*-$CB_{11}HEt_{11}]^-$ anion. The synthesis uses an excess of RBr (R = Me, Et) with [*closo*-$CB_{11}H_{12}]^-$ or [*closo*-$CB_9H_{10}]^-$ anions in a sealed pyrex tube at 200 °C (Figure 1.22).[44] The low yields and difficult purification are the limitations to the repeatability of this synthetic route; therefore it is not a convenient method for starting material preparation for further reactions.[82]

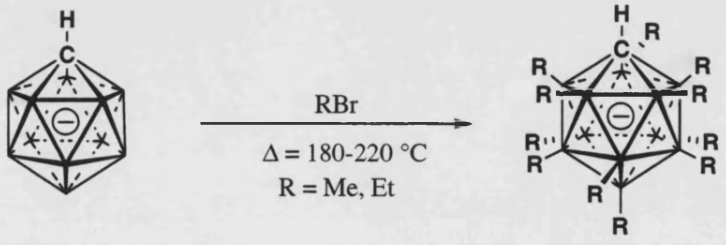

Figure 1.22 Xie's synthesis of the undecaalkylated anions [*closo*-$CB_{11}HR_{11}]^-$.[44]

Incorporation of alkyl and aryl substituents is also possible by conversion of B-I vertices of iodocarbaboranes to B-C vertices *via* palladium-catalysed cross-coupling reaction with Grignard reagents and CuI as co-catalyst (Figure 1.23). This technique results in the 12-substituted carboranes [12-R-1-*closo*-$CB_{11}H_{11}]^-$ (R = Me, Et, butyl, hexyl, Ph, $C_7H_6^+$).[83]

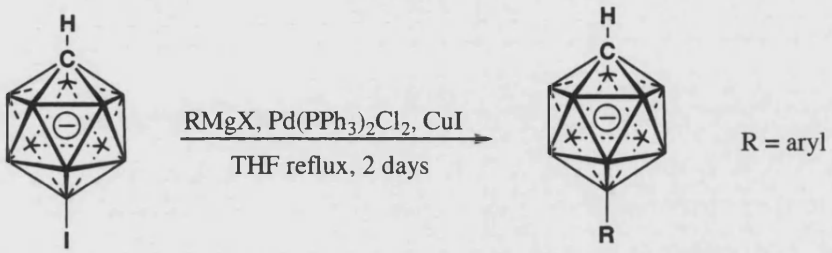

[*closo*-12-I-$CB_{11}H_{11}$] [*closo*-12-R-$CB_{11}H_{11}$]

Figure 1.23

Treatment of the [*closo*-$CB_{11}HMe_{11}]^-$ anion with F_2/N_2 in $CFCl_3$ followed with K_2NiF_6/HF, leads to the perfluorinated [*closo*-$CB_{11}H(CF_3)_{11}]^-$ anion (Figure 1.24). This anion has all the characteristics of an excellent weakly coordinated and nucleophilic anion, however, its explosive nature has prevented further development.[84]

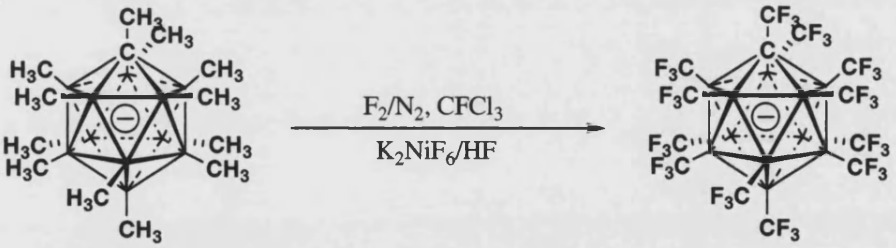

Figure 1.24 Synthesis of the explosive anion [*closo*-$CB_{11}(CF_3)_{12}]^-$.

Deuteration. The antipodal and lower pentagonal belt vertices are deuterated selectively by employment of D_2O/DCl mixture at room temperature.[85] This is an electrophilic substitution, similar to halogenation.

Mercuration. Addition of (HgX) groups is possible when [1-NMe_3-1-*closo*-$CB_{11}H_{11}]^-$ is used along with HgX_2 (X = $OCOCF_3$).[86]

Hydroxylation. Hydroxylation occurs by treatment of Cs[*closo*-$CB_{11}H_{12}$] in refluxing hydrogen peroxide (30% in volume), but it degrades to boric acid if kept under these conditions.[87] In contrast to other boranes, no explosions have been reported for the hydroxylation of [*closo*-$CB_{11}H_{12}]^-$. Mixed halo-hydroxylated derivative has been reported by Stasko et al.[88]

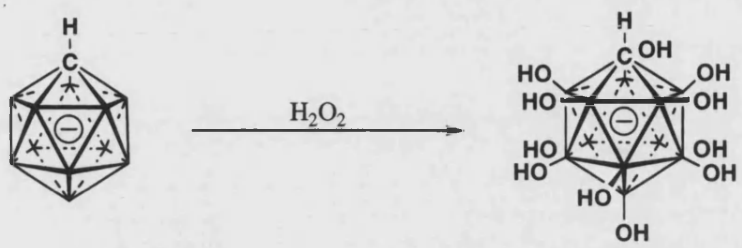

Figure 1.25 Complete hydroxylation of the cluster.[87]

Recently, an extensive review has been published describing many of the compounds derived from [*closo*-$CB_{11}H_{12}]^-$.[81]

1.2 Transition Metal Chemistry of [*closo*-$CB_{11}H_{12}]^-$ and its derivatives

1.2.1 Available starting materials

There are three main routes of forming transition metal complexes where {*closo*-$CB_{11}\}^-$ is on the coordination sphere of the metal centre. Simple metathesis of halide with the silver salt of the appropriate cage has been used in numerous cases. It is worth mentioning that sometimes the silver atom gets intimately attached to the molecule due to the weak nucleophilic character of the anion, as is detailed later. These silver salts are easily accessible by reaction of the corresponding caesium carborane salt with silver nitrate. Silver carborane complexes give access also to the trityl $[CPh_3]^+$ salts of carboranes, which are useful methyl or metal hydride abstraction agents for transition metal complex synthesis. However, it should be pointed out that it is not possible to

isolate the trityl salt of the parent carborane due to the electrophilic character of the trityl group that attacks antipodal {BH} protons and decomposes the cage.

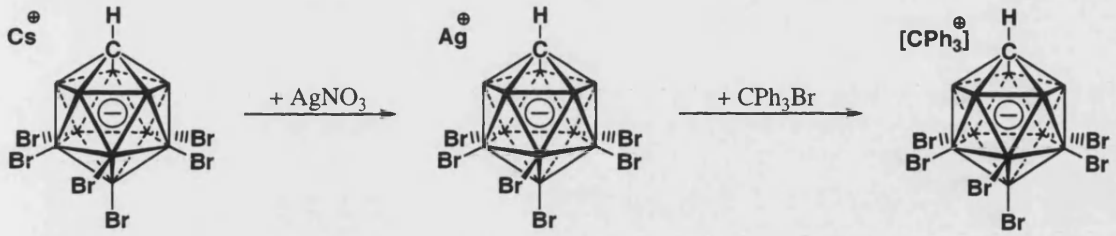

Figure 1.26 The reaction scheme for the formation of the silver and trityl salts of [*closo*-$CB_{11}H_6Br_6]^-$.

An ethereal solution of the carborane acid, $[H(OEt_2)_2][$*closo*-$CB_{11}H_{12}]$, has been employed to partner carboranes with platinum phosphine fragments too. Although the use of thallium salts has not been tried in halide abstraction in [*closo*-$CB_{11}H_{12}]^-$ chemistry, they are utilised with other weakly coordinating anions[89, 90] and carboranes.[91]

Diolefin metal complexes are excellent precursors of transition metal carborane complexes, and constitute another route to coordinate carboranes to transition metals as was initially demonstrated by Hawthorne with the synthesis of [*exo-nido*-$(H)_2(PPh_3)_2Ir(C_2B_9H_{12})$][92] or later on by Rifat *et al* more specifically for a series of rhodium complexes with [*closo*-$CB_{11}H_{12}]^-$.[9] Reduction of diolefin ligands such as norbornadiene or cyclooctadiene *via* hydrogenation allows the carborane to interact with the metal centre through two 3c2e bonds (Figure 1.27).

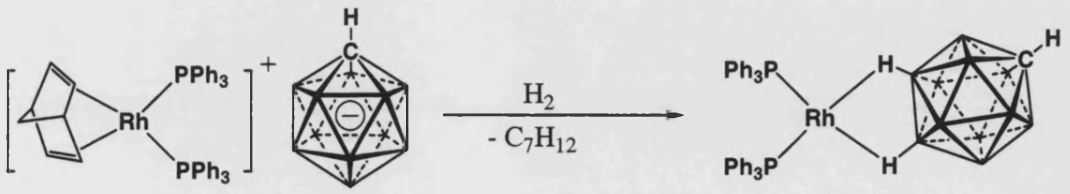

Figure 1.27 Formation of a rhodium-carborane complex *via* diolefin hydrogenation.[9]

1.2.2 [*closo*-$CB_{11}H_{12}$]$^-$ and derivative anions complexes

A few examples of transition metal complexes with the [*closo*-$CB_{11}H_{12}$]$^-$ anion and its derivatives have been mentioned in section 1.1.3, however, there are more than this. Ag, Rh, Zr, Fe and Mo metal complexes have been used, though there are also compounds of Pt, Pd, Ni and Ti, but are much less abundant. While some of them have interesting properties in catalysis, others do not show any catalytic activity but constitute examples of complexes showing 3c2e M-H-B bonding. Nevertheless, they are sometimes useful for the preparation of catalyst precursors, like [Rh(cod)(*closo*-$CB_{11}H_{12}$)][71], which is a starting material for the synthesis of [Rh(L_2)(*closo*-$CB_{11}H_{12}$)] (L = PCy_3, PPh_3, dppe, $P(OMe)_3$).[72]

Different silver complexes partnered with the carboranes [*closo*-$CB_{11}H_{12}$]$^-$, [*closo*-$CB_{11}H_6Br_6$]$^-$ and [*closo*-$CB_{11}HMe_{11}$]$^-$ have been reported. In the solid state, [*closo*-$CB_{11}H_{12}$]$^-$ coordinates always to [Ag]$^+$ *via* the antipodal {BH} vertex and one vertex from the lower pentagonal belt. The coordination sphere of the silver atom can be completed with benzene[93] or one or two molecules of triphenylphosphine (Figure 1.28).[10] N-containing ligands have been attached to silver and their complexes have been isolated and characterised.[94, 95]

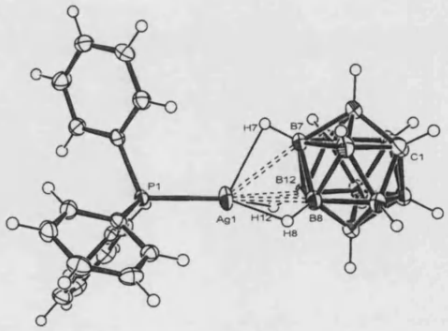

Figure 1.28 [(PPh_3)Ag(*closo*-$CB_{11}H_{12}$)].

A curious arrangement is observed in the carbene complex $[(IMes)_2Ag]_2[Ag_2(closo\text{-}CB_{11}H_{12})_4]$,[96] where each silver shows six different interactions (four shorter and two longer), as is depicted in Figure 1.29.

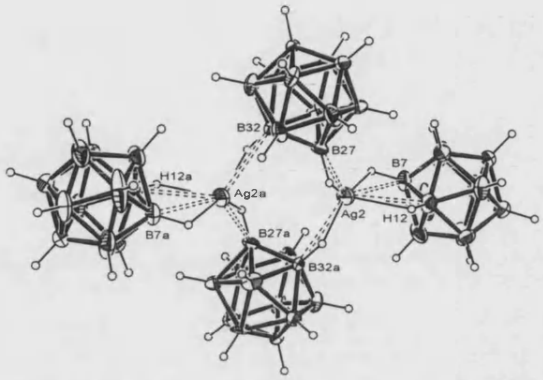

Figure 1.29 Solid state structure of the $[Ag_2(closo\text{-}CB_{11}H_{12})_4]^{2-}$ fragment.

The use of NMR spectroscopy, especially $^1H\{^{11}B\}$ and $^{11}B\{^1H\}$ frequently permits the identification of different species in solution, and provides reliable comparative data to solid-state structural determinations. The solid state structure of these Ag-carborane complexes is not kept in solution, and local C_{5v} symmetry for the anion is often observed with the corresponding cationic silver fragment being fluxional over the cage surface. Upfield values in ^{11}B chemical shifts indicate that interactions are taking place between the metal centre and $B_{7\text{-}12}$-H vertices.[96] The differences of chemical shifts in the $^1H\{^{11}B\}$ NMR spectrum of these silver complexes are minimum when compared to the values of the free carborane. As is described later, more upfield chemical shift values are found for those {BH} hydrogens involved in the coordination with other metal centres such as Rh, Mo or Zr, indicative of a stronger B-H-M interaction. In addition to the metal attached to the carborane in each specific case, the substituents attached to the metallic centre can also indicate how the cage coordinates (e.g. phosphine ligands magnitude of J(RhP)). Thus, in complexes with carboranes, NMR

spectroscopy is an excellent technique to evaluate the strength of the 3c2e interactions between metal and cage.

Similar complexes and results, both in solution and solid state, were observed after the synthesis of analogous silver complexes with mono, hexa and undeca-brominated cages. In some cases only the antipodal vertex was coordinated to silver,[38] while in others, the interaction with lower belt vertices was observed.[10, 97 41] Mixed halogenated complexes of silver show similar patterns in the solid state.[42] Ag[*closo*-$CB_{11}HMe_{11}$] and [$Ag(PPh_3)$(*closo*-$CB_{11}HMe_{11}$)] are well characterised compounds and exhibit interactions between silver and B-Me vertices in both solution and solid state.[98, 99] As described above, in solution these interactions are observed all over the lower belt surface. In contrast, no interactions between the carborane anion and silver were observed when [*closo*-$CB_{11}HF_{11}]^-$ was employed. Some of these silver complexes partnered with carborane anions have been tested in hetero Diels-Alder reactions. The complex [$Ag(PPh_3)$(*closo*-$CB_{11}H_6Br_6$)] provided the best results in the catalytic synthesis of N-benzylideneaniline compared with $[BF_4]^-$ or [*closo*-$CB_{11}H_{12}]^-$.[10]

Direct reaction of $[Rh(\mu\text{-}Cl)(COD)]_2$ with Ag[*closo*-$CB_{11}H_{12}$] in dichloromethane leads to the formation of [Rh(COD)(*closo*-$CB_{11}H_{12}$)],[71] which after addition of stoichiometric amounts of phosphines and hydrogenation gives access to other carborane complexes with two 3c2e bonds.[9, 72]

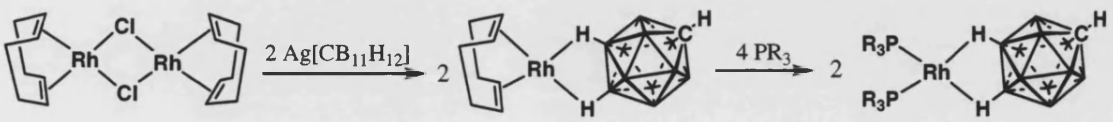

Figure 1.30

X-ray diffraction data have confirmed that, in the solid state, either one lower belt and the antipodal vertex (Figure 1.31) or two lower belt vertices are involved in the

coordination to rhodium.[72] Again in solution, $^{1}H\{^{11}B\}$ and ^{11}B NMR spectra show that the metal centre establishes contacts with all the lower belt and antipodal surface, indicating a local C_{5v} symmetry for the carborane cage, and thus a fluxional mechanism is occurring to render the B-H vertices equivalent.

Compound	δ (^{1}H) C-H (ppm)	*J*(RhP) (Hz)	δ (^{1}H) B_{12}-H (ppm)	*J*(BH) (Hz)
free $[CB_{11}H_{12}]^-$	2.20		1.55	135
$\{Rh(PPh_3)_2\}$	2.60	194	-1.97	119
$\{Rh(PCy_3)_2\}$	2.50	190	-2.32	130
$\{Rh(P(OMe)_3)_2\}$	2.55	294	-2.45	120
{Rh(dppe)}	2.55	189	-1.40	116

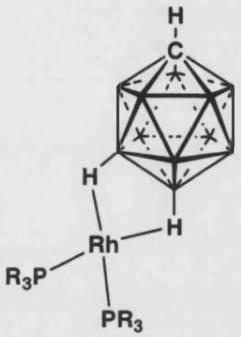

Table 1.5 Selected NMR data for four rhodium complexes.[72]

The rhodium complexes that appear in Table 1.5 represent a good example of how the electron density of the {BH} bond changes with metal coordination, and how this is reflected in NMR chemical shifts to higher field for the {BH} fragment and smaller *J*(BH) coupling constants. It is worth noting that the correlation between chemical shifts and coupling constants is not a linear one and thus, the most hydridic proton in the $^{1}H\{^{11}B\}$ spectrum does not imply the smallest *J*(BH) coupling constant in ^{11}B NMR spectrum.

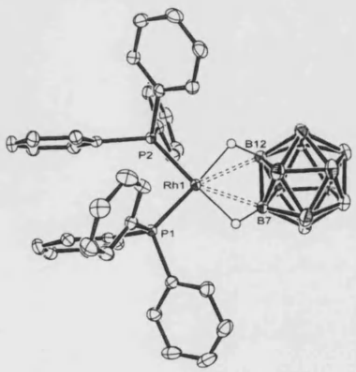

Figure 1.31 Solid state structure of $[Rh(PPh_3)_2(closo\text{-}CB_{11}H_{12})]$.[9]

Rhodium complexes with nitrogen containing ligands and [*closo*-$CB_{11}H_{12}$]$^-$ in its coordination sphere has been prepared and screened in catalysis.[100] There is not any example of the hexabromo carborane anion coordinated to rhodium, but it has been reported as a separate ion in the compounds [{Cp*Rh(μ_2-Cl)}$_3$(μ_3-Cl)][*closo*-$CB_{11}H_6Br_6$][101] and [(PPh_3)(PPh_2-η^6-C_6H_5)Rh]$_2$[*closo*-$CB_{11}H_6Br_6$]$_2$. This last compound, along with [Rh(PPh_3)$_2$(*closo*-$CB_{11}H_{12}$)] was examined in catalytic alkene hydrogenation.[9] In this study a large counteranion effect was observed, with the hexabromo-carborane complex shown to be more effective than [Rh(PPh_3)$_2$(*closo*-$CB_{11}H_{12}$)] due to the lower nucleophilicity of the anion. The {Rh(PPh_3)$_2$}$^+$ fragment has also been demonstrated to perform hydroboration on *exo-nido*-[Rh(PPh_3)$_2$(7,8-μ-$(CH_2)_3$-7,8-*closo*-$C_2B_9H_{10}$)]. The complex [Rh(PPh_3)$_2$(*closo*-$CB_{11}H_{12}$)] under ethene has also given evidence of dehydrogenative borylation.[102] More detailed information is discussed in Chapter 2.

The iridium complexes [(PPh_3)$_2$Ir(η^2-C_2H_4)$_3$][*closo*-$CB_{11}H_6Br_6$] and [(PPh_3)$_2$Ir(H)$_2$(*closo*-$CB_{11}H_6Br_6$)] have also shown catalytic activity in olefin hydrogenation.[103] More importantly, the anion has been demonstrated to play an important role in the catalytic cycle, stabilising the metal fragment after olefin consumption, in contrast to other weakly coordinating anions which force the metal to form inactive complexes (Figure 1.32).

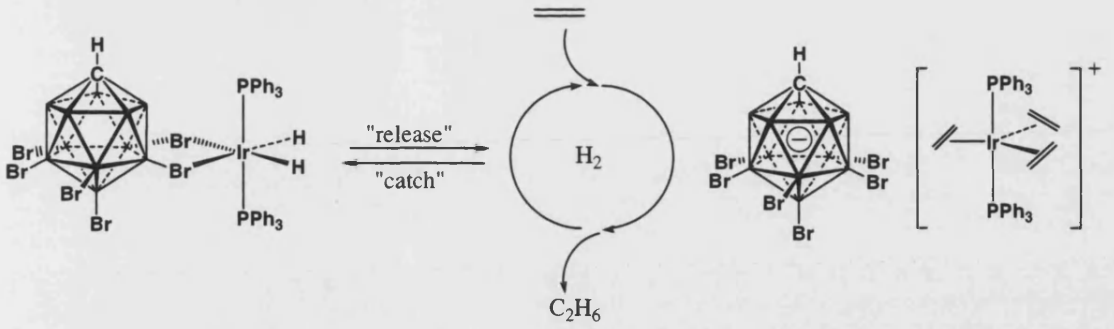

Figure 1.32 "Release and catch" mechanism of the [*closo*-$CB_{11}H_6Br_6$]$^-$ anion in the hydrogenation of olefins.[103]

Three zirconium complexes partnered with [*closo*-$CB_{11}H_{12}$]$^-$ have been synthesised by silver salt metathesis and tested in olefin polymerisation. Two of them, [$Cp_2Zr(\eta^2$-$CH_2Ph)$(*closo*-$CB_{11}H_{12}$)] and [$(C_5H_4Me)Zr(Me)$(*closo*-$CB_{11}H_{12}$)] show only interaction with the metal through the antipodal {BH} vertex and are catalytically active. However, the complex [Cp^*ZrMe_2(*closo*-$CB_{11}H_{12}$)] is stabilised *via* three {BH} interactions and is catalytically inactive.[69] An analogous complex, [Cp_2ZrMe(*closo*-$CB_{11}HMe_{11}$)], was prepared by methyl abstraction with the trityl salt in fluorobenzene.[104] Although it has not been tested, the complex is probably catalytically active due to the lower nucleophilicity of the [*closo*-$CB_{11}HMe_{11}$]$^-$ anion compared with [*closo*-$CB_{11}H_{12}$]$^-$.

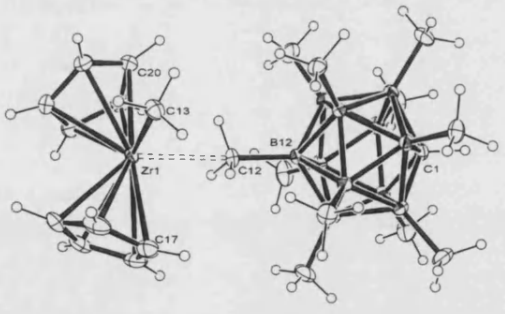

Figure 1.33 Molecular structure of [Cp_2ZrMe(*closo*-$CB_{11}HMe_{11}$)].[104]

NMR spectroscopic characterisation of these complexes (Table 1.6) demonstrates again the fluxional behaviour of the cage towards the metal, showing the local C_{5v} symmetry of the cage in solution. Similarly to the rhodium complexes, a downfield shift of the CH signal of *ca.* 0.3-0.4 ppm is observed as well as lower frequencies on the ^{11}B

NMR spectrum for those vertices involved in the interaction with the metal. The data provided for $[Cp_2Zr(PhCH_2)(closo\text{-}CB_{11}H_{12})]$ also proves the hydridic nature of the B_{12}-H proton because of its interaction with the metal, which is reflected in the smaller J(BH) value too.

Compound	δ (^{1}H) C-H	δ (^{1}H) B_{12}-H	δ (^{11}B) B_{12}-H	J(BH)
free $[CB_{11}H_{12}]^-$ [a]	2.20	1.55	-6.9	135
$[Cp_2Zr(PhCH_2)Cb]$ [b]	2.56	-3.15	-8.1	100
$[Cp_2ZrMeCb]$ [b]	2.60	n/a	-9.4	n/a
$[Cp'_2ZrMeCb]$ [b]	2.50	n/a	-8.4	n/a
$[Cp^*Zr(Me)_2Cb]$ [b]	2.49	n/a	-11.3	n/a

Table 1.6 NMR data for zirconium complexes of $[closo\text{-}CB_{11}H_{12}]^-$. Some values are missed since they were not reported. δ in ppm, J in Hz.

Another important set of transition metal complexes with carborane anions were obtained by iodide or hydride abstraction of the molybdenum complexes $[Cp(CO)_3MoX]$, X = I, H. Initially, the parent $[closo\text{-}CB_{11}H_{12}]^-$ anion was used for the synthesis of $[Cp(CO)_3Mo(closo\text{-}CB_{11}H_{12})]$ and $[Cp^*(CO)_3Mo(closo\text{-}CB_{11}H_{12})]$.[67, 68] An intermediate in the silver salt metathesis reaction of the iodide complex was isolated, $[CpMo(CO)_3I{\cdot}Ag\{closo\text{-}CB_{11}H_{12}\}]_2$ (Figure 1.14), and its X-ray crystal structure illustrates the Mo-I-Ag sequence of bonds with interactions between B_{12}-H of the carborane anion with the silver atom.

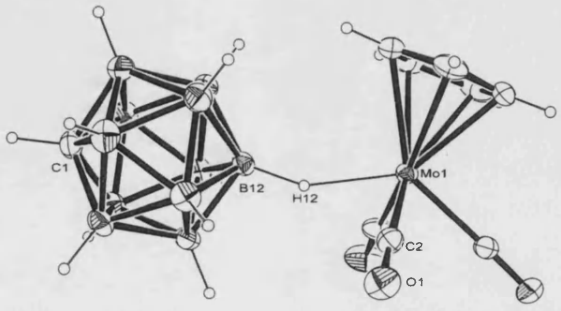

Figure 1.34 Solid state structure of $[Cp(CO)_3Mo(closo\text{-}CB_{11}H_{12})]$.[67]

According to ^{1}H NMR data, the hydridic character of the antipodal vertex has undergone a considerable increase from the values seen previously for Ag, Rh or Zr. This is also reflected on the higher ^{11}B chemical shift and smaller J(BH) coupling constant value shown in Table 1.7. The chemical shift for the {CH} proton follows the same trend observed for other metal-cage complexes of the [*closo*-$CB_{11}H_{12}]^-$ with variations between 0.3-0.4 ppm with respect the free anion.

Compound	δ (^{1}H) C-H	δ (^{1}H) B_{12}-H	δ (^{11}B) B_{12}-H	$J(B_{12}H)$
free $[CB_{11}H_{12}]^-$	2.20	1.55	-6.9	135
$[MoCp(CO)_3(CB_{11}H_{12})]$	2.53	-15.1	-10.4	90
$[MoCp^*(CO)_3(CB_{11}H_{12})]$	2.51	-13.5	-10.6	n/a
$[MoCp(CO)_3I{\cdot}Ag\ (CB_{11}H_{12})]$	2.56	2.12	-9.1	119

Table 1.7 NMR data for three different molybdenum complexes. δ in ppm, J in Hz.

Similar compounds were obtained with [12-Br-1-*closo*-$CB_{11}H_{11}]^-$, [*closo*-$CB_{11}H_6Br_6]^-$ and [*closo*-$CB_{11}HMe_{11}]^-$.[105] The monobrominated carborane anion has exposed monocoordination through the {BBr} vertex to the metallic centre. In solution once again, the solid state symmetry is lost and the carborane shows, by ^{11}B NMR, a local C_{5v} symmetry and an upfield chemical shift for the lower pentagonal belt signal, which indicates full interaction all lower belt {BH} vertices. The hexabromo carborane forms similar compounds, however, if the undecamethylated cage is utilized, the complex formed does not show any B-Me-Mo or B-Me-Ag-Mo interaction (Mo-I is more nucleophilic than {B-CH_3}) and this time each silver atom is surrounded by three $[Cp(CO)_3MoI]$ units.

Other transition metal complexes with carboranes have been synthesized with similar characteristics to those previously described, involving Pt,[73] Pd[106] or Ti[107] as metal centres.

Undecamethylated carborane salts have been reacted with different transition metal complexes in order to form B-Me-Metal interactions; however, in some cases the permethylated anion can suffer cage degradation with some metal fragments, which produce B-CH_3 cleavage (Figure 1.35).[108]

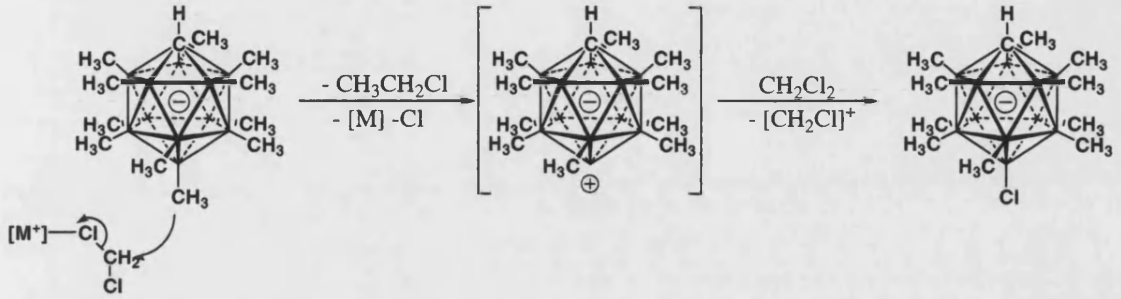

Figure 1.35 Possible mechanism for B-CH_3 cleavage and chloride abstraction from a CH_2Cl_2 molecule.

B-Cl vertices are formed when the reaction takes place in dichloromethane, while a B-aryl vertex is formed when fluorobenzene is used (Figure 1.36).[109]

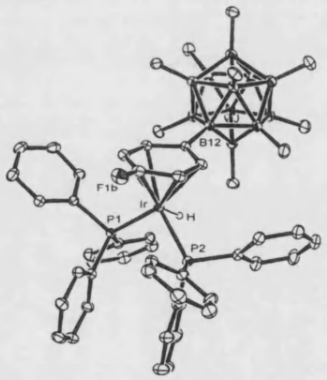

Figure 1.36 Cationic portion of $[(PPh_3)_2Ir(H)\{12\text{-}(\eta^6\text{-}C_6H_4F)\text{-}1\text{-}closo\text{-}CB_{11}H_{11}\}][12\text{-}(\eta^6\text{-}C_6H_4F)\text{-}1\text{-}closo\text{-}CB_{11}Me_{11}]^-$.

The formation of this boronium ylides had been described in earlier publications by Michl. Lithium induced methyl abstraction from the carborane produces multiple methyl substitutions by aryl groups, and this can be controlled when a dioxaborole ring is incorporated at the carbon to form the aryl substituted product at the antipodal position only, as demonstrated in Figure 1.37.[108]

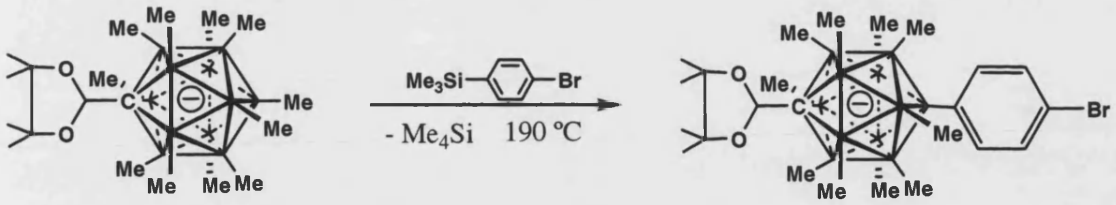

Figure 1.37 Lithium induced methyl abstraction at the antipodal position.[108]

More recently, the isolation of the intermediate boronium ylide [*closo*-$CB_{11}Me_{11}$] has been achieved at -60 °C,[110] albeit its difficult characterisation due to insolubility in alkane solvents. This species reacts easily with nucleophiles such as ethers, alcohols or $(SnMe_3)_2$.[81, 110]

1.2.3 Analogous *nido*-carborane complexes

Work by Hawthorne in the 1980s was focused on the catalytic study of *closo*-icosahedral bis(phosphine)hydridorhodacarboranes,[91, 111-115] which were found to be catalytically active in olefin hydrogenation and isomerisation. In solution some of these *closo* icosahedral complexes are in equilibrium with *exo-nido*-rhodium species showing 3c2e bonding (e.g. R = Me, R' = Me) (see Figure 1.38).[91]

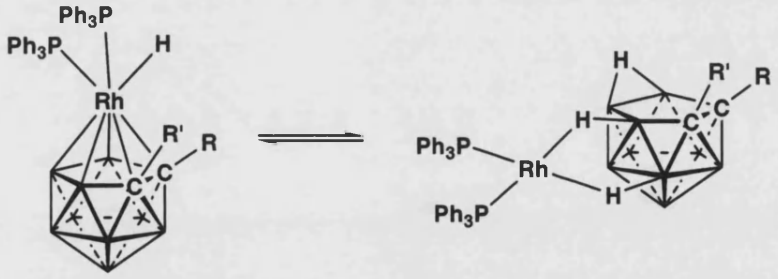

Figure 1.38 Equilibrium between *closo*-Rh^{3+} and *exo-nido*-Rh^{+} species.[111]

The tautomerism described in Figure 1.38 is a common phenomenon for many [1-*closo*-$Rh(PPh_3)_2(H)(2,3\text{-}C_2B_9H_{11})$] isomers and their carbon substituted derivatives; however due to steric bulk, there are derivatives (e.g. RR' = $-CH_2-CH_2-CH_2-$; R = Me, R' = Ph; R = R' = Ph) that only exist in the *exo-nido* form either in solution and solid

state.[91, 113, 116] The reaction of deuterium with derivatives of complexes depicted in Figure 1.38 produces deuterium exchange at the {BH} vertices and it is favoured at the most electron rich vertices, those furthest from the carbon atoms. Earlier deuteration studies had confirmed that transition metals generally catalyse this reaction that proceeds through an oxidative addition process.[117] This process would imply the formation of a metal-boryl bond. Examples of these species are numerous in the literature and have been reported with simple boryl groups (e.g. catecholborane)[118, 119] and also formed from carboranes.[120-122]

Teixidor and co-workers have focused on the functionalisation of one carbon atom of the *nido* cage with a phosphino or thiol group, which leads to the formation of monophosphino or monothio-carboranes respectively. These monoanionic species have been partnered with metallic centres such as rhodium or ruthenium to produce a series of *exo-nido* complexes with 3c2e interations as shown in Figure 1.39.[123-126]

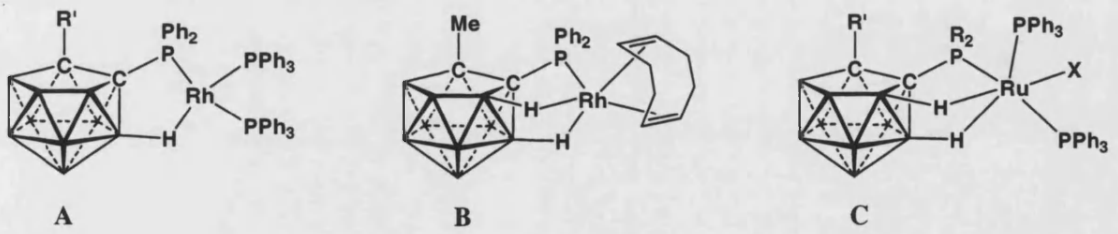

A B C

Figure 1.39

The ^{1}H NMR spectra for compounds **A** and **C** (Figure 1.39) show distinctive chemical shift values in the negative region for the B-H-M (M = Rh, Ru) protons, similar to those described for rhodium complexes of the [*closo*-$CB_{11}H_{12}]^{-}$. However, these resonances were absent for compound **B** and thus its characterisation by NMR was unclear. X-ray crystallographic studies confirmed these interactions, which show that, in contrast to compound **A**, the *nido*-carborane is tricoordinated to rhodium. This *extra* B-H interaction is explained due to the π–acceptor character of the dialkene ligand

in comparison to the more σ–donor capacity of two triphenylphosphine groups. These phosphino and thio-*exo-nido*carborane complexes were catalytically tested in cyclopropanation and also hydrogenation of alkenes. It was demonstrated that they are active catalysts in the hydrogenation of terminal alkenes but gave poor results with internal alkenes.[127]

1.3 Additional functionalisation methods of {BH} cluster vertices

1.3.1 Metal catalysed alkene hydroboration/borylation

Further methods have been reported for carborane and borane functionalisation which invoke the use of catalysts such as $PtBr_2$, $PdBr_2$, $H_2PtCl_6{\cdot}6H_2O$, $Cp_2Ti(CO)_2$. Sneddon *et al* have reported that these catalyst precursors react with *arachno*-6,8-$C_2B_7H_{12}$ to give olefin insertion *via* hydroboration and dehydrogenative borylation.[128, 129] The conditions of the reaction play an important role in obtaining alkyl or alkenyl substituents and are highly dependent on the temperature. The proposed mechanisms for the $PtBr_2$, $PdBr_2$, $H_2PtCl_6{\cdot}6H_2O$ catalytic reactions are shown in Figure 1.40.

These mechanisms are based in sequential oxidative additions and reductive eliminations, which are typical of late transition metals. Borane functionalisation with $Cp_2Ti(CO)_2$ is thought to proceed *via* formation of a metallocycle metal-olefin-borane, with the titanium bearing a formal oxidation state of IV. Subsequent reductive elimination would render the functionalised borane and a Ti(II) complex. This mechanism has also been proposed for early-transition-metal-catalysed hydroboration reactions of olefins with catecholborane.[130]

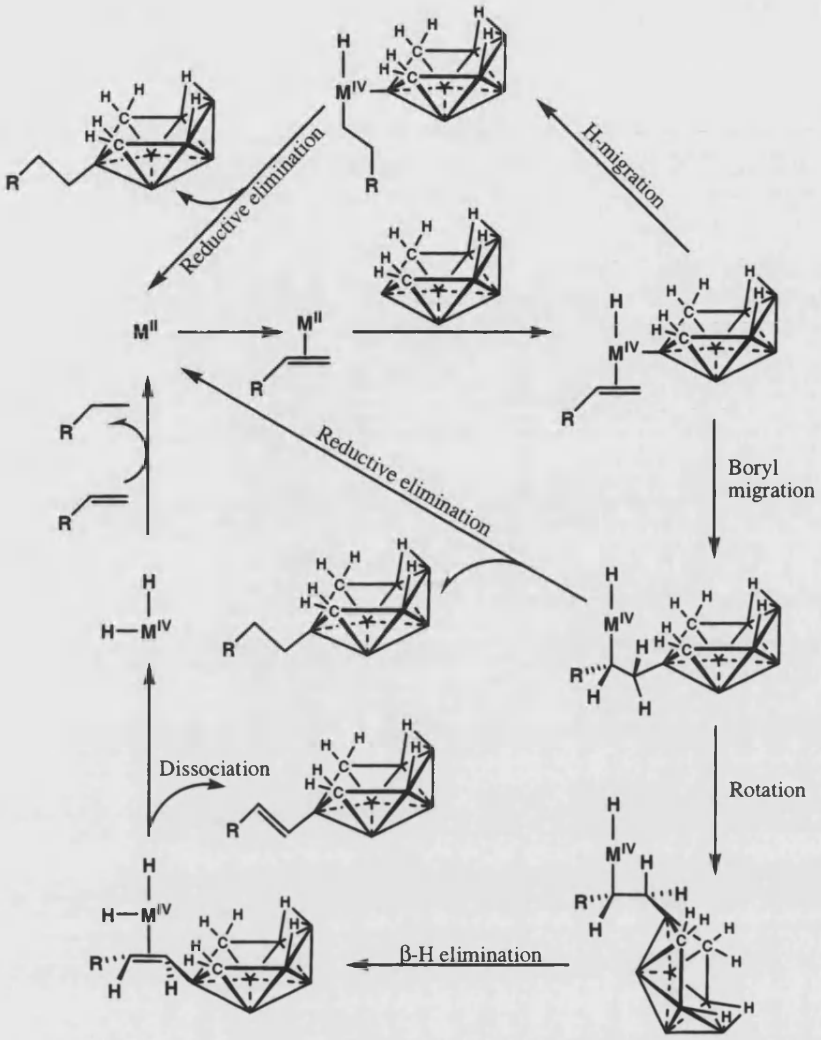

Figure 1.40 Catalytic cycle proposed for M (II) (M = Pt, Pd) for olefin hydroboration and borylation.[128]

Hawthorne has also reported the metal-promoted insertion of 1-butyl acrylate into a B-H bond of [7,8-μ-$(CH_2)_3$-7,8-*nido*-$C_2B_9H_{10}$] using *exo-nido*-[$Rh(PPh_3)_2$][7,8-μ-$(CH_2)_3$-7,8-$C_2B_9H_{10}$] (Figure 18).[116] In this reaction only the mono hydroboration product was obtained. The mechanism proposed for this hydroboration of 1-butyl acrylate consists of an oxidative addition of the B-H bond within the rhodium centre, followed by the formation of the alkyl-rhodium complex, a reductive elimination reaction and final formation of the B-alkyl bond. This system has been demonstrated to be active towards activated olefins such as acrylates; however, it does not show any reactivity with simple alkenes such as 1-hexene.[116]

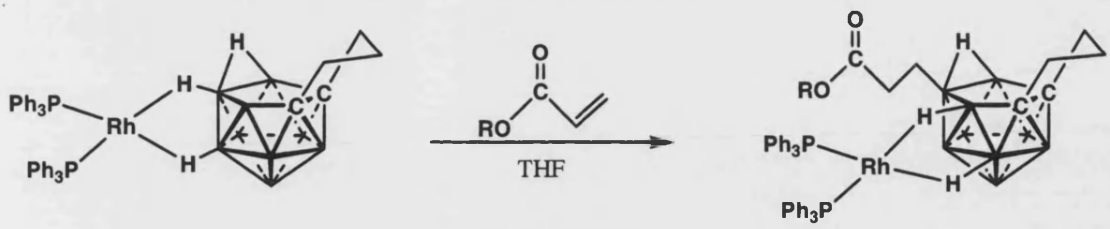

Figure 1.41

An analoguous rhodium complex has been described previously in section 1.2.2 with the [*closo*-$CB_{11}H_{12}$]$^-$ anion,[9] and similar compounds either with rhodium bearing different phosphines or variation on the groups tethered to the carbons on the *nido* cluster were investigated by Hawthorne et al in the 1980s[91, 111-115] and by Teixidor's group more recently (section 1.2.3).[123-126]

1.3.2 Metal induced alkyne hydroboration

Selective and stepwise substitutions at vertices B3 and B6 of an ortho-carborane cage were promoted by pentamethylcyclopentadienyl rhodium and iridium fragments, with sulphur and selenium atoms bridging the carborane with the metallic centre. The alkyne hydroboration reaction needed softer conditions for the rhodium complexes as can be seen in Figure 1.42[131] and higher temperatures when the iridium compounds were utilised. In the reaction, metal-boryl species are formed and have been detected and isolated for the iridium complex.[132] Similar compounds were found for analogous complexes of ruthenium and osmium.[133]

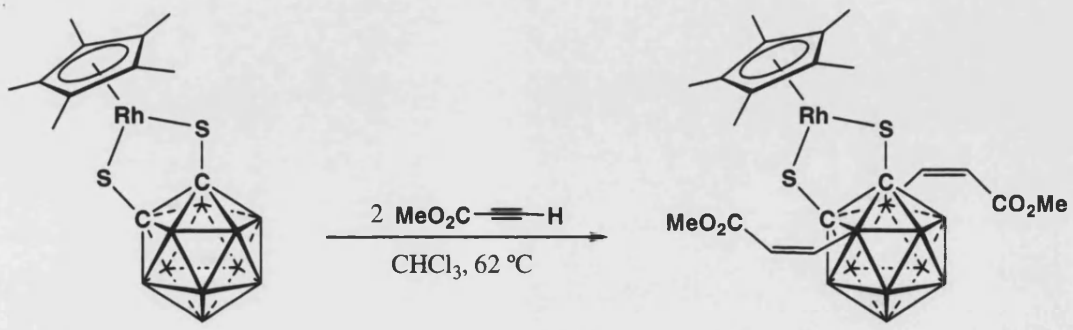

Figure 1.42

1.3.3 Friedel-Craft conditions

Hawthorne has reported another alternative for borane/carborane methylation. It consists of treatment of the borane or carborane under Friedel-Craft conditions using $MeI/AlMe_3$.[134-137] This technique yields good results in the complete methylation of $[closo\text{-}B_{12}H_{12}]^{2-}$ (Figure 1.43),[136] and high methyl substitution in 1,2-, 1,7- and 1,12-dicarbadodecaborane.[135] Similar results were obtain by Teixidor *et al* using $MeI/AlCl_3$ with *closo*-1,2-dicabadodecaborane.[138]

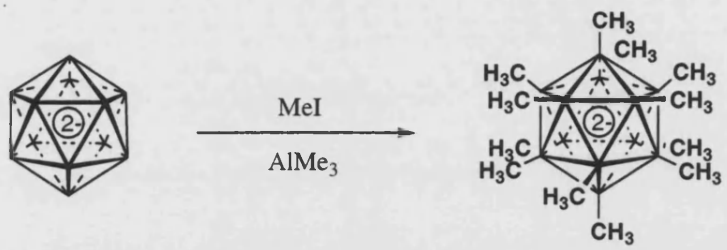

Figure 1.43 Complete methylation of $[closo\text{-}B_{12}H_{12}]^{2-}$.

1.3.4 Hydroxylation

Hydroxylation of the $[closo\text{-}B_{12}H_{12}]^{2-}$ cage, using similar conditions as described for the parent $[closo\text{-}CB_{11}H_{12}]^{-}$, leads to the dodecahydroxy-dodecaborate anion. However, the main limitation of these anions is that they cannot be used as weakly coordinating anions due to the presence of oxygen atoms with lone pairs of electrons. Further transformations of the hydroxyl groups are possible, for instance, by treatment the perhydroxyl carboranes with methyltriflate to render permethoxyl carboranes.[139] Use of typical organic reactions at elevated temperatures with activated carboxylic acids renders ester and ether-linked persubstituted *closo*-boranes (Figure 1.44).[140, 141]

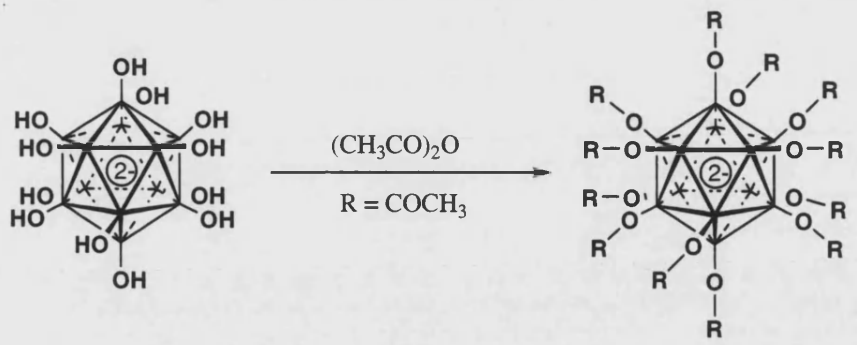

Figure 1.44 Example of one of the products reported by Li *et al.*[140]

1.3.5 Ionic liquids

The most recent method of B-H functionalisation has been published by Sneddon and it is based on the use of ionic liquids.[142] Olefins, in the presence of decaborane, undergo hydroboration in an ionic liquid media (1-butyl-3-methylimidazolium or 1-butyl-4-methylpyridium salts of $[BF_4]^-$) without a metal catalyst.(Figure 19)

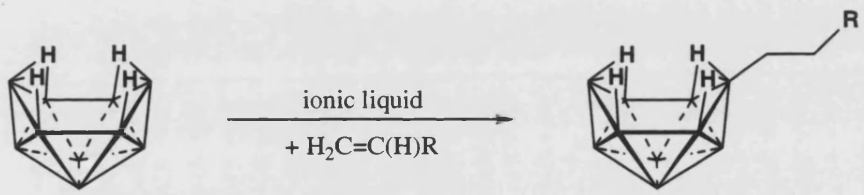

Figure 1.45 B-H functionalisation in ionic liquids of $B_{10}H_{14}$.[142]

Subsequent treatment of [6-(CH_2CH_2)R-*nido*-$B_{10}H_{13}$] in an ionic liquid (1-butyl-3-methylimidazolium chloride) with alkynes renders an icosahedral orthocarborane as Equation 1.3 shows.

$$6\text{-}(CH_2CH_2)R\text{-}B_{10}H_{13} + R'C{\equiv}CR'' \xrightarrow{\text{ionic liquid}} 1\text{-}R'\text{-}2R''\text{-}6(CH_2CH_2)R\text{-}C_2B_{10}H_9 + 2\,H_2 \quad (R'' = R', H)$$

Equation 1.3

Nowadays, the use of ionic liquids is opening new routes in organic and inorganic chemistry, and as can be seen in the results obtained by Sneddon, ionic liquids may be a new pathway for carborane polyfunctionalisation.

1.4 Bibliography

1 I. Krossing and I. Raabe, *Angew. Chem.-Int. Edit. Engl.*, 2004, **43**, 2066.

2 R. J. LeSuer and W. E. Geiger, *Angew. Chem.-Int. Edit. Engl.*, 2000, **39**, 248.

3 A. Bösmann, G. Franciò, E. Janssen, M. Solinas, W. Leitner, and P. Wasserscheid, *Angew. Chem.-Int. Edit. Engl.*, 2001, **40**, 2697.

4 T. J. Barbarich and P. F. Driscoll, *Electrochem. Solid-State Lett.* , 2003, **6**, A113.

5 T. J. Barbarich, P. F. Driscoll, S. Izquierdo, L. N. Zakharov, C. D. Incarvito, and A. L. Rheingold, *Inorg. Chem.*, 2004, **43**, 7764.

6 A. Macchioni, *Chem. Rev.*, 2005, **105**, 2039.

7 E. P. Kundig and C. M. Saudan, 'Lewis acids in Organic Synthesis', ed. H. Yamamoto, Weinheim, 2000.

8 M. C. Chen, J. A. S. Roberts, and T. J. Marks, *J. Am. Chem. Soc.*, 2004, **126**, 4605.

9 A. Rifat, N. J. Patmore, M. F. Mahon, and A. S. Weller, *Organometallics*, 2002, **21**, 2856.

10 N. J. Patmore, C. Hague, J. H. Cotgreave, M. F. Mahon, C. G. Frost, and A. S. Weller, *Chem.-Eur. J.*, 2002, **8**, 2088.

11 S. H. Strauss, *Chem. Rev.*, 1993, **93**, 927.

12 D. M. Branan, N. W. Hoffman, E. A. McElroy, N. Prokopuk, A. B. Salazar, M. J. Robbins, W. E. Hill, and T. R. Webb, *Inorg. Chem.*, 1991, **30**, 1200.

13 N. M. N. Gowda, S. B. Naikar, and G. K. N. Reddy, *Adv. Inorg. Chem.* , 1984, **28**, 255.

14 G. A. Lawrance, *Chem. Rev.*, 1986, **86**, 17.

15 W. Beck and K. Sunkel, *Chem. Rev.*, 1988, **88**, 1405.

16 H. Salem, Y. Ben-David, L. J. W. Shimon, and D. Milstein, *Organometallics*, 2006, **25**, 2292.

17 C. A. Reed, *Acc. Chem. Res.*, 1998, **31**, 133.

18 L. C. A. d. Carvalho, M. Dartiguenave, Y. Dartiguenave, and A. L. Beauchamp, *J. Am. Chem. Soc.*, 1984, **106**, 6848.

19 Z. L. Lutsenko, G. G. Aleksandrov, P. V. Petrovskii, E. S. Shubina, V. G. Andrianov, Y. T. Struchkov, and A. Z. Rubezhov, *J. Organomet. Chem.*, 1985, **281**, 349.

20 M. Bochmann, G. Karger, and A. J. Jaggar, *J. Chem. Soc.-Chem. Commun.*, 1990, 1038.

21 G. G. Hlatky, H. W. Turner, and R. R. Eckman, *J. Am. Chem. Soc.*, 1989, **111**, 2728.

22 A. D. Horton and J. H. G. Frijns, *Angew. Chem.-Int. Edit. Engl.*, 1991, **30**, 1152.

23 X. M. Yang, C. L. Stern, and T. J. Marks, *Organometallics*, 1991, **10**, 840.

24 M. Brookhart, B. Grant, and A. F. Volpe, *Organometallics*, 1992, **11**, 3920.

25 E. Y. X. Chen and T. J. Marks, *Chem. Rev.*, 2000, **100**, 1391.

26 M. Brookhart, F. C. Rix, J. M. Desimone, and J. C. Barborak, *J. Am. Chem. Soc.*, 1992, **114**, 5894.

27 X. G. Fang, J. Huhmann-Vincent, B. L. Scott, and G. J. Kubas, *J. Organomet. Chem.*, 2000, **609**, 95.

28 D. J. Huang, J. C. Bollinger, W. E. Streib, K. Folting, V. Young, O. Eisenstein, and K. G. Caulton, *Organometallics*, 2000, **19**, 2281.

[29] J. Huhmann-Vincent, B. L. Scott, and G. J. Kubas, *J. Am. Chem. Soc.*, 1998, **120**, 6808.

[30] J. B. Lambert, L. J. Lin, and V. Rassolov, *Angew. Chem.-Int. Edit. Engl.*, 2002, **41**, 1429.

[31] J. B. Lambert and S. H. Zhang, *J. Chem. Soc.-Chem. Commun.*, 1993, 383.

[32] W. V. Konze, B. L. Scott, and G. J. Kubas, *J. Am. Chem. Soc.*, 2002, **124**, 12550.

[33] W. V. Konze, B. L. Scott, and G. J. Kubas, *Chem. Commun.*, 1999, 1807.

[34] A. D. Horton and A. G. Orpen, *Organometallics*, 1991, **10**, 3910.

[35] R. D. Shannon, *Acta Crystallogr.*, 1976, **A32**, 751.

[36] W. H. Knoth, J. L. Little, J. R. Lawrance, F. R. Scholer, and L. J. Todd, *Inorg. Synth.*, 1968, **11**, 33.

[37] J. Plesek, T. Jelinek, S. Hermanek, and B. Stibr, *Collect. Czech. Chem. Commun.*, 1986, **51**, 81.

[38] T. Jelinek, P. Baldwin, W. R. Scheidt, and C. A. Reed, *Inorg. Chem.*, 1993, **32**, 1982.

[39] Z. Xie, J. Manning, R. W. Reed, R. Mathur, P. D. W. Boyd, A. Benesi, and C. A. Reed, *J. Am. Chem. Soc.*, 1996, **118**, 2922.

[40] S. V. Ivanov, J. J. Rockwell, O. G. Polyakov, C. M. Gaudinski, O. P. Anderson, K. A. Solntsev, and S. H. Strauss, *J. Am. Chem. Soc.*, 1998, **120**, 4224.

[41] Z. Xie, C. W. Tsang, E. T. P. Sze, Q. C. Yang, D. T. W. Chan, and T. C. W. Mak, *Inorg. Chem.*, 1998, **37**, 6444.

[42] C. W. Tsang, Q. C. Yang, E. T. P. Sze, T. C. W. Mak, D. T. W. Chan, and Z. Xie, *Inorg. Chem.*, 2000, **39**, 5851.

[43] B. T. King, Z. Janousek, B. Gruner, M. Trammell, B. C. Noll, and J. Michl, *J. Am. Chem. Soc.*, 1996, **118**, 3313.

[44] C. W. Tsang and Z. Xie, *Chem. Commun.*, 2000, 1839.

[45] K. Shelly, C. A. Reed, Y. J. Lee, and W. R. Scheidt, *J. Am. Chem. Soc.*, 1986, **108**, 3117.

[46] Z. Xie, R. Bau, and C. A. Reed, *Angew. Chem.-Int. Edit. Engl.*, 1994, **33**, 2433.

[47] Z. Xie, R. Bau, A. Benesi, and C. A. Reed, *Organometallics*, 1995, **14**, 3933.

[48] S. P. Hoffmann, T. Kato, F. S. Tham, and C. A. Reed, *Chem. Commun.*, 2006, 767.

[49] B. T. King, I. Zharov, and J. Michl, *Chemical Innovation*, 2001, **2001**, 23.

[50] M. Juhasz, S. Hoffmann, E. Stoyanov, K. C. Kim, and C. A. Reed, *Angew. Chem.-Int. Edit. Engl.*, 2004, **43**, 5352.

[51] E. S. Stoyanov, K. C. Kim, and C. A. Reed, *J. Am. Chem. Soc.*, 2006, **128**, 8500.

[52] C. A. Reed, *Chem. Commun.*, 2005, 1669.

[53] E. S. Stoyanov, K. C. Kim, and C. A. Reed, *J. Am. Chem. Soc.*, 2006, **128**, 1948.

[54] R. Hoffmann, *Angew. Chem.-Int. Edit. Engl.*, 1982, **21**, 711.

[55] K. Wade, *Adv. Inorg. Organometal. Chem.*, 1976, **18**, 1.

[56] M. J. S. Dewar and M. L. McKee, *Inorg. Chem.*, 1980, **19**, 2662.

[57] M. L. McKee, *J. Am. Chem. Soc.*, 1997, **119**, 4220.

[58] P. V. Schleyer and K. Najafian, *Inorg. Chem.*, 1998, **37**, 3454.

[59] W. H. Knoth, *Inorg. Chem.*, 1971, **10**, 598.

[60] J. Plesek, T. Jelinek, E. Drdakova, S. Hermanek, and B. Stibr, *Collect. Czech. Chem. Commun.*, 1984, **49**, 1559.

[61] A. S. Batsanov, M. A. Fox, A. E. Goeta, J. A. K. Howard, A. K. Hughes, and J. M. Malget, *J. Chem. Soc.-Dalton Trans.*, 2002, 2624.

[62] A. Franken, B. T. King, J. Rudolph, P. Rao, B. C. Noll, and J. Michl, *Collect. Czech. Chem. Commun.*, 2001, **66**, 1238.

[63] B. Brellochs, in 'Contemporaty boron chemistry', ed. M. G. Davidson, A. K. Hugues, T. B. Marder, and K. Wade, Royal Society of Chemistry, Cambridge, England, 2000.

[64] T. Jelinek, C. A. Kilner, M. Thornton-Pett, and J. D. Kennedy, *Chem. Commun.*, 2001, 1790.

[65] A. Franken, N. J. Bullen, T. Jelinek, M. Thornton-Pett, S. J. Teat, W. Clegg, J. D. Kennedy, and M. J. Hardie, *New J. Chem.* , 2004, **28**, 1499.

[66] D. J. Liston, Y. J. Lee, W. R. Scheidt, and C. A. Reed, *J. Am. Chem. Soc.*, 1989, **111**, 6643.

[67] N. J. Patmore, M. F. Mahon, J. W. Steed, and A. S. Weller, *J. Chem. Soc.-Dalton Trans.*, 2001, 277.

[68] N. J. Patmore, J. W. Steed, and A. S. Weller, *Chem. Commun.*, 2000, 1055.

[69] D. J. Crowther, S. L. Borkowsky, D. Swenson, T. Y. Meyer, and R. F. Jordan, *Organometallics*, 1993, **12**, 2897.

[70] S. V. Ivanov, J. J. Rockwell, S. M. Miller, O. P. Anderson, K. A. Solntsev, and S. H. Strauss, *Inorg. Chem.*, 1996, **35**, 7882.

[71] A. S. Weller, M. F. Mahon, and J. W. Steed, *J. Organomet. Chem.*, 2000, **614**, 113.

[72] A. Rifat, V. E. Laing, G. Kociok-Kohn, M. F. Mahon, G. D. Ruggiero, and A. S. Weller, *J. Organomet. Chem.*, 2003, **680**, 127.

[73] G. S. Mhinzi, S. A. Litster, A. D. Redhouse, and J. L. Spencer, *J. Chem. Soc.-Dalton Trans.*, 1991, 2769.

[74] T. Gadt, B. Grau, K. Eichele, I. Pantenburg, and L. Wesemann, *Chem.-Eur. J.*, 2006, **12**, 1036.

[75] W. H. Knoth, Jr., *Inorg. Chem.*, 1971, **10**, 598.

[76] K. Vyakaranam, S. Korbe, and J. Michl, *J. Am. Chem. Soc.*, 2006, **128**, 5680.

[77] T. Jelinek, J. Plesek, S. Hermanek, and B. Stibr, *Collect. Czech. Chem. Commun.*, 1986, **51**, 819.

[78] S. V. Ivanov, A. J. Lupinetti, S. M. Miller, O. P. Anderson, K. A. Solntsev, and S. H. Strauss, *Inorg. Chem.*, 1995, **34**, 6419.

[79] Z. Janousek, C. L. Hilton, P. J. Schreiber, and J. Michl, *Collect. Czech. Chem. Commun.*, 2002, **67**, 1025.

[80] A. Franken, C. A. Kilner, M. Thornton-Pett, and J. D. Kennedy, *Collect. Czech. Chem. Commun.*, 2002, **67**, 869.

[81] S. Körbe, P. J. Schreiber, and J. Michl, *Chem. Rev.*, 2006, **106**, 5208

[82] Z. Xie, in 'Personal Communication'.

[83] B. Gruner, Z. Janousek, B. T. King, J. N. Woodford, C. H. Wang, V. Vsetecka, and J. Michl, *J. Am. Chem. Soc.*, 1999, **121**, 3122.

[84] B. T. King and J. Michl, *J. Am. Chem. Soc.*, 2000, **122**, 10255.

[85] T. Jelinek, J. Plesek, F. Mares, S. Hermanek, and B. Stibr, *Polyhedron*, 1987, **6**, 1981.

[86] A. B. Yakushev, I. B. Sivaev, K. A. Solntsev, and N. T. Kuznetsov, *Koordinat. Khim.*, 1994, **20**, 429.

[87] T. Peymann, A. Herzog, C. B. Knobler, and M. F. Hawthorne, *Angew. Chem.-Int. Edit. Engl.*, 1999, **38**, 1061.

[88] D. J. Stasko, K. J. Perzynski, and M. A. Wasil, *Chem. Commun.*, 2004, 708.

[89] J. A. Casares, P. Espinet, J. M. Martin-Alvarez, G. Espino, M. Perez-Manrique, and F. Vattier, *Eur. J. Inorg. Chem.*, 2001, 289.

[90] C. Bartolome, R. de Blas, P. Espinet, J. M. Martin-Alvarez, and F. Villafane, *J. Organomet. Chem.*, 2006, **691**, 3862.

[91] J. A. Long, T. B. Marder, P. E. Behnken, and M. F. Hawthorne, *J. Am. Chem. Soc.*, 1984, **106**, 2979.

[92] J. A. Doi, R. G. Teller, and M. F. Hawthorne, *J. Chem. Soc.-Chem. Commun.*, 1980, 80.

[93] K. Shelly, D. C. Finster, Y. J. Lee, W. R. Scheidt, and C. A. Reed, *J. Am. Chem. Soc.*, 1985, **107**, 5955.

[94] A. Westcott, N. Whitford, and M. J. Hardie, *Inorg. Chem.*, 2004, **43**, 3663.

[95] L. Cunha-Silva, R. Ahmad, and M. J. Hardie, *Aust. J. Chem.* , 2006, **59**, 40.

[96] M. A. Fox, M. F. Mahon, N. J. Patmore, and A. S. Weller, *Inorg. Chem.*, 2002, **41**, 4567.

[97] C. Hague, N. J. Patmore, C. G. Frost, M. F. Mahon, and A. S. Weller, *Chem. Commun.*, 2001, 2286.

[98] A. J. Clarke, M. J. Ingleson, G. Kociok-Kohn, M. F. Mahon, N. J. Patmore, J. P. Rourke, G. D. Ruggiero, and A. S. Weller, *J. Am. Chem. Soc.*, 2004, **126**, 1503.

[99] M. J. Ingleson, M. F. Mahon, N. J. Patmore, G. D. Ruggiero, and A. S. Weller, *Angew. Chem.-Int. Edit. Engl.*, 2002, **41**, 3694.

[100] C. Moreau, C. Hague, A. S. Weller, and C. G. Frost, *Tetrahedron Lett.* , 2001, **42**, 6957.

[101] N. J. Patmore, M. F. Mahon, and A. S. Weller, *Appl. Organomet. Chem.*, 2003, **17**, 388.

[102] A. Rifat, 'PhD Thesis', University of Bath, Bath, 2003.

[103] A. Rifat, G. Kociok-Köhn, J. W. Steed, and A. S. Weller, *Organometallics*, 2004, **23**, 428.

[104] M. J. Ingleson, A. Clarke, M. F. Mahon, J. P. Rourke, and A. S. Weller, *Chem. Commun.*, 2003, 1930.

[105] N. J. Patmore, M. J. Ingleson, M. F. Mahon, and A. S. Weller, *Dalton Trans.*, 2003, 2894.

[106] P. G. Lassahn, V. Lozan, B. Wu, A. S. Weller, and C. Janiak, *Dalton Trans.*, 2003, 4437.

[107] S. L. Borkowsky, N. C. Baenziger, and R. F. Jordan, *Organometallics*, 1993, **12**, 486.

[108] Z. Janousek, U. Lehmann, J. Castulik, I. Cisarova, and J. Michl, *J. Am. Chem. Soc.*, 2004, **126**, 4060.

[109] M. J. Ingleson, G. Kociok-Kohn, and A. S. Weller, *Inorg. Chim. Acta*, 2005, **358**, 1571.

[110] I. Zharov, Z. Havlas, A. M. Orendt, D. H. Barich, D. M. Grant, M. G. Fete, and J. Michl, *J. Am. Chem. Soc.*, 2006, **128**, 6089.

[111] P. E. Behnken, J. A. Belmont, D. C. Busby, M. S. Delaney, R. E. King, C. W. Kreimendahl, T. B. Marder, J. J. Wilczynski, and M. F. Hawthorne, *J. Am. Chem. Soc.*, 1984, **106**, 3011.

[112] P. E. Behnken, D. C. Busby, M. S. Delaney, R. E. King, C. W. Kreimendahl, T. B. Marder, J. J. Wilczynski, and M. F. Hawthorne, *J. Am. Chem. Soc.*, 1984, **106**, 7444.

[113] C. B. Knobler, T. B. Marder, E. A. Mizusawa, R. G. Teller, J. A. Long, P. E. Behnken, and M. F. Hawthorne, *J. Am. Chem. Soc.*, 1984, **106**, 2990.

[114] J. A. Long, T. B. Marder, and M. F. Hawthorne, *J. Am. Chem. Soc.*, 1984, **106**, 3004.

[115] R. T. Baker, M. S. Delaney, R. E. King, C. B. Knobler, J. A. Long, T. B. Marder, T. E. Paxson, R. G. Teller, and M. F. Hawthorne, *J. Am. Chem. Soc.*, 1984, **106**, 2965.

[116] J. D. Hewes, C. W. Kreimendahl, T. B. Marder, and M. F. Hawthorne, *J. Am. Chem. Soc.*, 1984, **106**, 5757.

[117] E. L. Hoel, M. Talebinasabsavari, and M. F. Hawthorne, *J. Am. Chem. Soc.*, 1977, **99**, 4356.

[118] K. Burgess, W. A. Vanderdonk, S. A. Westcott, T. B. Marder, R. T. Baker, and J. C. Calabrese, *J. Am. Chem. Soc.*, 1992, **114**, 9350.

[119] G. J. Irvine, M. J. G. Lesley, T. B. Marder, N. C. Norman, C. R. Rice, E. G. Robins, W. R. Roper, G. R. Whittell, and L. J. Wright, *Chem. Rev.*, 1998, **98**, 2685.

[120] E. L. Hoel and M. F. Hawthorne, *J. Am. Chem. Soc.*, 1973, **95**, 2712.

[121] Y. J. Lee, J. D. Lee, S. J. Kim, J. J. Ko, I. H. Suh, M. S. Cheong, and S. O. Kang, *Organometallics*, 2004, **23**, 135.

[122] M. Herberhold, H. Yan, W. Milius, and B. Wrackmeyer, *Chem.-Eur. J.*, 2002, **8**, 388.

[123] R. Nunez, C. Vinas, F. Teixidor, and M. M. Abad, *Appl. Organomet. Chem.*, 2003, **17**, 509.

[124] C. Vinas, R. Nunez, F. Teixidor, R. Kivekas, and R. Sillanpaa, *Organometallics*, 1998, **17**, 2376.

[125] F. Teixidor, J. Rius, C. Miravitlles, C. Vinas, L. Escriche, E. Sanchez, and J. Casabo, *Inorg. Chim. Acta*, 1990, **176**, 61.

[126] F. Teixidor, R. Benakki, C. Vinas, R. Kivekas, and R. Sillanpaa, *Organometallics*, 1998, **17**, 4630.

[127] F. Teixidor, R. Nunez, M. A. Flores, A. Demonceau, and C. Vinas, *J. Organomet. Chem.*, 2000, **614**, 48.

[128] D. E. Kadlecek, P. J. Carroll, and L. G. Sneddon, *J. Am. Chem. Soc.*, 2000, **122**, 10868.

[129] M. J. Pender, P. J. Carroll, and L. G. Sneddon, *J. Am. Chem. Soc.*, 2001, **123**, 12222.

[130] C. N. Muhoro, X. He, and J. F. Hartwig, *J. Am. Chem. Soc.*, 1999, **121**, 5033.

[131] M. Herberhold, H. Yan, W. Milius, and B. Wrackmeyer, *Angew. Chem.-Int. Edit. Engl.*, 1999, **38**, 3689.

[132] M. Herberhold, H. Yan, W. Milius, and B. Wrackmeyer, *J. Chem. Soc.-Dalton Trans.*, 2001, 1782.

[133] M. Herberhold, H. Yan, W. Milius, and B. Wrackmeyer, *Chem.-Eur. J.*, 2000, **6**, 3026.

[134] T. Peymann, C. B. Knobler, and M. F. Hawthorne, *J. Am. Chem. Soc.*, 1999, **121**, 5601.

[135] A. Herzog, A. Maderna, G. N. Harakas, C. B. Knobler, and M. F. Hawthorne, *Chem.-Eur. J.*, 1999, **5**, 1212.

[136] T. Peymann, C. B. Knobler, S. I. Khan, and M. F. Hawthorne, *Inorg. Chem.*, 2001, **40**, 1291.

[137] W. Jiang, C. B. Knobler, and M. F. Hawthorne, *Angew. Chem.-Int. Edit. Engl.*, 1996, **35**, 2536.

[138] F. Teixidor, G. Barbera, A. Vaca, R. Kivekas, R. Sillanpaa, J. Oliva, and C. Vinas, *J. Am. Chem. Soc.*, 2005, **127**, 10158.

[139] A. Herzog, C. B. Knobler, and M. F. Hawthorne, *J. Am. Chem. Soc.*, 2001, **123**, 12791.

[140] T. J. Li, S. S. Jalisatgi, M. J. Bayer, A. Maderna, S. I. Khan, and M. F. Hawthorne, *J. Am. Chem. Soc.*, 2005, **127**, 17832.

[141] O. K. Farha, R. L. Julius, M. W. Lee, R. E. Huertas, C. B. Knobler, and M. F. Hawthorne, *J. Am. Chem. Soc.*, 2005, **127**, 18243.

[142] U. Kusari, Y. Li, M. G. Bradley, and L. G. Sneddon, *J. Am. Chem. Soc.*, 2004, **126**, 8662.

Chapter 2. Functionalisation of [*closo*-$CB_{11}H_{12}$]$^-$ with the {$Rh(PPh_3)_2$}$^+$ metal fragment

2.1 Introduction

The synthesis of new carboranes with longer alkyl substituents may avoid B-C activation as seen with B-Me substitution and, more importantly, the incorporation of long hydrocarbon chains into the [*closo*-$CB_{11}H_{12}$]$^-$ anion would permit the formation of less nucleophilic anions and, thus, possibly better catalysts. Another consequence would be an increment in alkane solubility, which would lead to the formation of alkane soluble salts that may provide a route to elusive metal-alkane complexes.

Utilisation of metal complexes as catalysts has been proved as a good route towards borane and carborane functionalisation. This chapter covers a brief introduction of active catalysts in carborane functionalisation, followed by the report of successful structural and spectroscopic characterisation of a series of new multi-substituted carborane anions derived from the parent [*closo*-$CB_{11}H_{12}$]$^-$ anion. The study of the metal-mediated reactions involved in their synthesis, the products derived thereof and their full characterisation are also discussed.

2.1.1 Metal complexes for catalytic carborane functionalisation

Mono and bis functionalisation of polyboranes with alkyl or alkenyl groups have been achieved using metal complexes in partnership with alkenes. Transition metal complexes such as $Cp_2Ti(CO)_2$, $PtBr_2$, $PdBr_2$, $Ir(Cl)(CO)(PPh_3)_2$ or cationic rhodium fragments such as {$Rh(PPh_3)_2$}$^+$ have been used to perform catalytic hydroboration or

dehydrogenative borylation on one {BH} vertex of pentaborane,[1, 2] decaborane,[3] *arachno*-6,8-$C_2B_7H_{13}$[4] and 7,8-μ-$(CH_2)_3$-7,8-$C_2B_9H_{10}$.[5] Two {BH} vertices on decaborane were functionalised with 1-alkenes by chloroplatinic acid or $PtBr_2$ as Figure 2.1 shows. A maximum of three {BH} alkenyl groups can be incorporated in ruthenacarborane complexes by reaction with alkynes that afford {BH} insertion products,[6] although this is not catalytic.

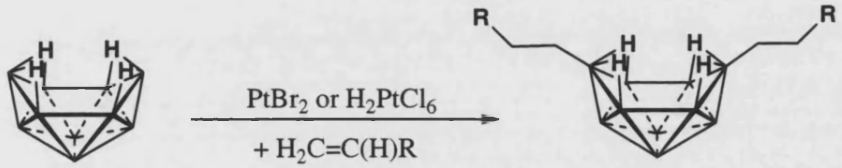

Figure 2.1

Palladium and platinum catalysts such as $PtBr_2$, $PdBr_2$, $H_2PtCl_6{\cdot}6H_2O$ have been successfully screened as alkene borylating agents for the functionalisation of pentaborane, decaborane and *arachno*-6,8-$C_2B_7H_{13}$. Two different but related types of processes can occur when using late transition metals: hydroboration and dehydrogenative borylation (Figure 2.2).

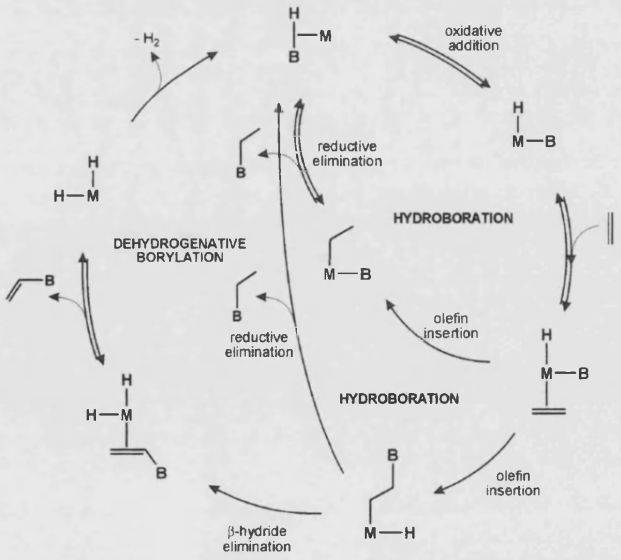

Figure 2.2 Basic steps in hydroboration-dehydrogenative borylation processes.

Both mechanisms imply initial oxidative addition of a B-H bond with coordination of an olefin to the metallic fragment, followed by insertion of the olefin. The next step may involve a reductive elimination with the formation of a B-alkyl product or a β-elimination reaction to form a B-alkenyl derivative and H_2. In the functionalisation of *arachno*-6,8-$C_2B_7H_{13}$, both species, alkyl and alkenyl derivatives are formed, and their formation depends upon the catalyst, temperature and olefin used. Competition between hydroboration and dehydrogenative borylation can exist and their respective products can be formed in one reaction, producing mixtures.[4]

As shown in Figure 2.3, only hydroboration takes place in the functionalisation of [7-R-8-R'-7,8-*nido*-$C_2B_9H_{10}$]$^-$ (R, R' = μ-($CH_2CH_2CH_2$); 1',2'-μ-$CH_2C_6H_4CH_2$; CH_3, CH_3; CH_3, C_6H_5 and C_6H_5, C_6H_5) with the {$Rh(PPh_3)_2$}$^+$ fragment. Since rhodium is a late transition metal, the same hydroboration mechanism (i.e. olefin coordination, oxidative addition, olefin insertion and reductive elimination), described above for platinum and palladium, has been postulated.[5]

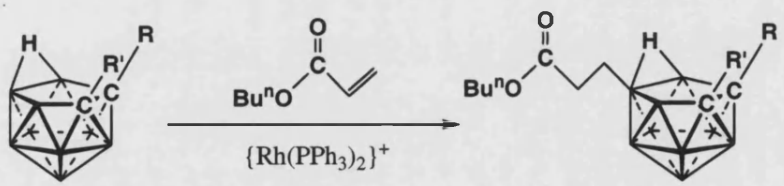

Figure 2.3 Rhodium catalysed hydroboration into a carborane {BH} vertex.

Detailed studies on the mechanistic aspects of transition metal mediated borylation have provided evidence of the intermediate on route to the formation of the final products. Since the first report of synthesis of metal-boryl compounds by Nöth and Schmid,[7] the chemistry of metal-boryl complexes has been extended enormously, and several reviews have been published.[8, 9, 11, 12] Because metal-boryl species are likely intermediates in hydroboration/borylation reactions, great effort has been made in their isolation, characterisation and study of their reactivity. Synthesis of metal boryl

complexes has been achieved in most cases utilising alkoxy-stabilised boranes such as catechol- and pinacol-boranes in preference of the less stable halo, alkyl or arylboranes. Compounds such as those represented in Figure 2.4 are examples of late transition metal-boryl species and can be considered intermediates in the borylation process.

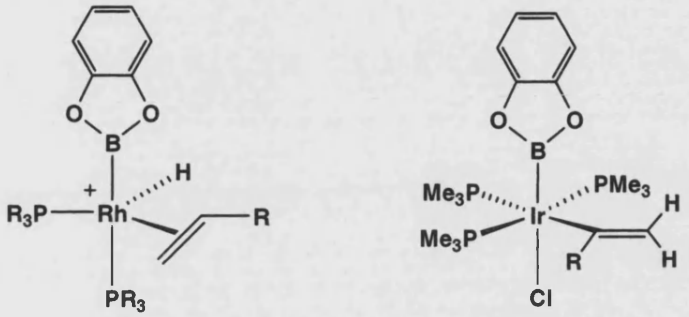

Figure 2.4 Catechol boryl compounds.

Metal-boryl carborane complexes have also been isolated and the first example of a B-H oxidative addition was reported in 1973 by Hoel and Hawthorne for the iridium complex shown in Figure 2.5 (left).[13] Intermediate species of metal-boryl compounds in metal-mediated hydroboration of alkynes have also been characterised and isolated (Figure 2.5, right).[14]

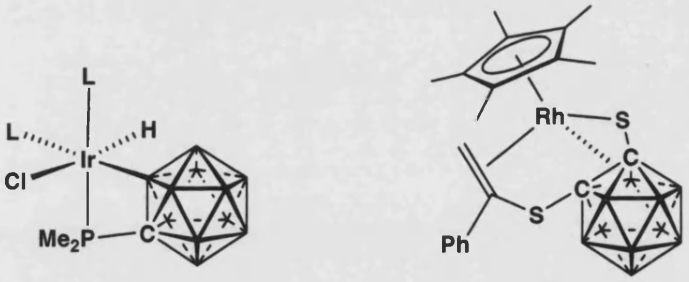

Figure 2.5

More evidence of the mechanistic aspects of metal-catalysed borylation has been found from metal-catalysed deuterium exchange experiments on boranes and carboranes. A qualitative study, based principally on ^{11}B NMR data, was performed on the three isomers of *closo*-$C_2B_{10}H_{12}$. Catalysts such as $(PPh_3)_3RuHCl$, $(PPh_3)_2(CO)IrCl$ and $(PPh_3)_2IrCl$ functionalise {BH} to {BD} vertices using deuterium gas.[15] Similar

experiments were carried out by Hawthorne et al. on the system described in Figure 2.3, where the H/D exchange reaction, catalysed by the $\{Rh(PPh_3)_2\}^+$, was found to be electrophilic in nature. Such a process favors substitution at the most electron-rich {BH} vertices, that is, those farthest from the cage carbon atoms.[16] In both studies, the postulated mechanisms involve oxidative addition of boron-hydrogen bonds to the catalytic species to form a metal-boryl intermediate.

The titanium catalysed hydroboration of decaborane with 1-alkenes produces the substitution of one {BH} vertex only. The hydroboration mechanism of this early transition metal complex is believed to follow a different pathway than the observed for late transition metals. Mechanistic studies, reported by Hartwig,[17] on titanium catalysed hydroboration of catecholborane with $Cp_2Ti(CO)_2$ and Cp_2TiMe_2 have been extended to decaborane by Sneddon.[3] The case of $Cp_2Ti(CO)_2$, as Figure 2.6 shows, involves the dissociation of a carbonyl ligand and the formation of a σ-complex (**D**). Further carbonyl decoordination with the consequent olefin coordination (**E**) would lead to the formation of a pentametallacycle (**F**), which after reductive elimination would produce the functionalised decaborane.

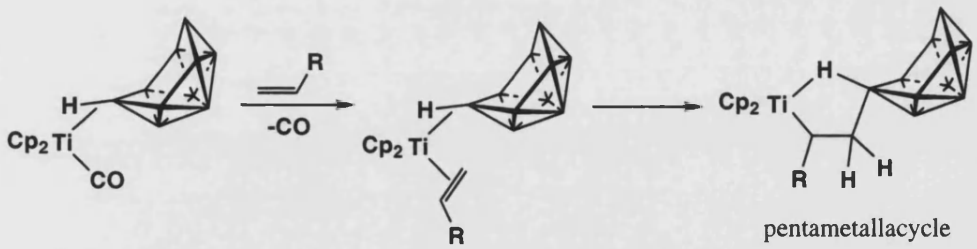

D **E** **F**

Figure 2.6 Proposed intermediates in titanium catalysed hydroboration.

This section has described that functionalisation of {BH} vertices with metal complexes has been demonstrated to be an effective route to functionalise boranes, although substitution of a maximum of three vertices on one cage has been achieved. It

is worth noting that metal-mediated alkyl functionalisation of one of the most utilised weakly coordinating anions, the [*closo*-$CB_{11}H_{12}$]$^-$, has never been reported; however, many routes exist for its functionalisation as commented in Chapter 1.

2.1.2 Scope of the chapter

This chapter will show that addition of alkene to a solution of {$Rh(PPh_3)_2$}$^+$ partnered with [1-X-1-*closo*-$CB_{11}H_{11}$]$^-$ (X = H, Me, $^iPr_3Si$) results in dehydrogenative borylation. This reaction permits the functionalisation of one of the cage {BH} vertices. Hydrogenation of the B-vinyl group affords a complex able to functionalise another vertex and thus, sequential addition of ethene and hydrogen permits multiple substitutions on the cage.

2.2 Results and discussion

2.2.1 Functionalisation of [*closo*-$CB_{11}H_{12}$]$^-$ with the {$Rh(PPh_3)_2$}$^+$ fragment

2.2.1.1 [$Rh(PPh_3)_2$(7/12-(H_2C=CH)-1-*closo*-$CB_{11}H_{11}$)]

The starting material [$Rh(PPh_3)_2$(*closo*-$CB_{11}H_{12}$)] was synthesized by the method reported in the literature.[18] This synthesis involved the hydrogenation of [$Rh(PPh_3)_2$(nbd)][*closo*-$CB_{11}H_{12}$] in dichloromethane to produce norbornane and the desired [$Rh(PPh_3)_2$(*closo*-$CB_{11}H_{12}$)] (**I**).

Addition of an excess of ethene to a solution of **I** in dichloromethane at room temperature for 15 hours affords the vinyl compound [$Rh(PPh_3)_2$(7/12-(H_2C=CH)-1-*closo*-$CB_{11}H_{11}$)] **1** (Figure 2.7), which is formed from dehydrogenative borylation of ethene. Quantitative conversion into the vinyl compound is observed when the reaction

is followed by NMR spectroscopy; however the isolated yield of the reaction was 61%, as an orange crystalline solid.

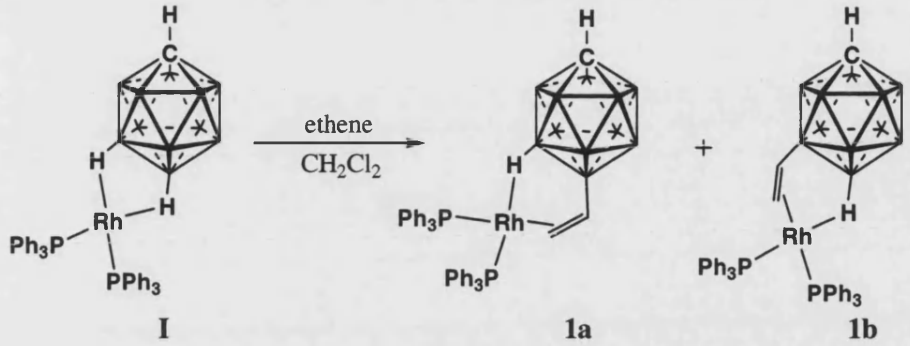

Figure 2.7 Synthesis of compounds **1a** and **1b**. Only hydrogen atoms on coordinated B-H vertices are shown.

NMR spectroscopy shows the formation of two different isomers in solution, $[Rh(PPh_3)_2(12\text{-}(H_2C{=}CH)\text{-}1\text{-}closo\text{-}CB_{11}H_{11})]$ **1a**, and $[Rh(PPh_3)_2(7\text{-}(H_2C{=}CH)\text{-}1\text{-}closo\text{-}CB_{11}H_{11})]$ **1b**, in a 7:3 ratio, according to the relative integrals in their ^1H and ^{11}B NMR spectra.

The $^1H\{^{11}B\}$ NMR signals for **1a** consists of two sets of doublets and a doublet of doublets between δ 4.83 and 2.56 ppm for the vinyl group; a broad singlet at δ 2.22 ppm for the cage C-H; and two broad singlets (in a 5:5 ratio) appear at δ 1.45 ppm for the $B_{2\text{-}6}$-H and -0.80 ppm for the $B_{7\text{-}11}$-H vertices. These chemical shifts reveal that these latter five B-H hydrogens are shifted upfield, compared to uncoordinated $[closo\text{-}CB_{11}H_{12}]^-$, and are characteristic of Rh-H-B 3c2e bonding.[19] This means that, in solution, all vertices of the lower belt are interacting with the metal on the NMR time-scale. Slightly downfield shifted, very similar vinyl signals are observed for **1b** between δ 4.95 and 2.59 ppm. The C-H signal appears at δ 2.36 ppm, however, the six B-*H* signals for **1b** from the expected 1:2:2:2:2:1 pattern cannot be observed clearly in the $^1H\{^{11}B\}$ NMR spectrum due to overlapping signals. Since NMR signals broaden when the cage is interacting with rhodium, assignment of the C-H and vinyl signals to the

correct isomer as determined by ^{11}B NMR spectroscopy was easier once the cage was no longer interacting with the metal fragment (compound **2,** section 2.2.1.2). The relative integrals between isomers in ^{11}B and ^{1}H NMR spectra along with the cages symmetries allow the assignment of signals for **2a/b** and therefore for compounds **1a/b**.

Evidence of cage coordination to the $\{Rh(PPh_3)_2\}^+$ fragment through the *B*-vinyl group is obtained from the upfield displacement of the vinyl chemical shifts when compared to a non-coordinated vinyl in a similar environment such as in [7-(CH_2=CH)-*arachno*-6,8-$C_2B_7H_{12}$]^4 (**II**) [δ 6.46-5.59 ppm], or in compounds **2a/b** [δ 6.35-5.18 ppm] (*vide infra*). A similar shift to higher field is observed in $[(PPh_3)_2Ir(C_2H_4)_3][closo$-$CB_{11}H_6Br_6]$ where ethene resonates at δ 3.09 ppm, while free ethene appears at δ 5.40 ppm.[20]

Compounds **1a/b** arise from the dehydrogenative borylation of ethene mediated by the *exo*-coordinated $\{Rh(PPh_3)_2\}^+$ metal fragment. In this process, the dehydrogenative borylation process is completed by a β-elimination reaction which promotes the formation of a vinyl group and dihydrogen. Prior to the β-elimination, insertion of ethene takes place into a putative Rh-boryl bond as Figure 2.8 shows. Hydroboration would invoke reductive elimination at intermediate **J**.

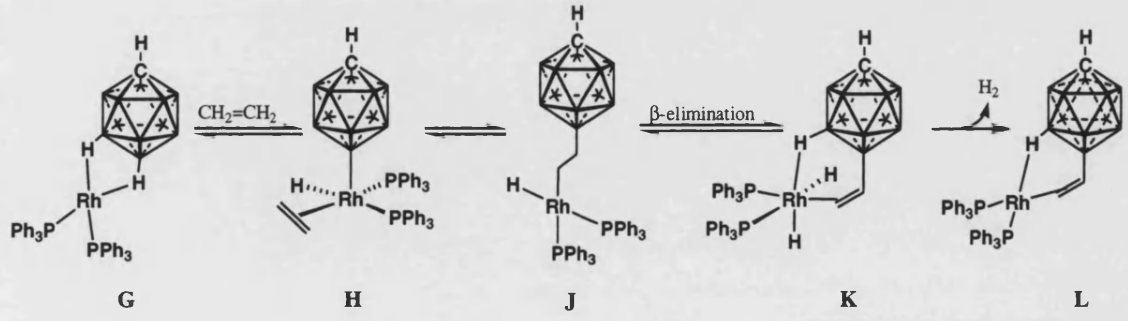

Figure 2.8 Suggested intermediate species in the synthesis of **1a** *via* dehydrogenative borylation.

Along with hydroboration, dehydrogenative borylation is a common reaction in catalytic synthesis of boron-alkenyl products derived from {BH} functionalisation of carborane, boranes and borazines with 1-alkenes. Extensive studies have been performed by Sneddon et al., who have used $PtBr_2$ and $PdBr_2$ as hydroboration-borylation catalysts.[2, 4, 21] Different factors have been found to induce the metal centre to perform β-elimination instead of reductive elimination, which would result in hydroboration to give boron-alkyl species. Steric bulk can force the metal-alkyl species to adopt a geometry that favors β-elimination. Coordinating molecules such us acetonitrile can block sites necessary for reductive elimination.[22] This could be the case for compounds **1a/b**, where the bulkiness and coordination ability of the carborane would favor β-elimination and therefore dehydrogenative borylation. The large excess of ethene in solution might disfavor reductive elimination too, by coordination to the metal, and also by consuming the hydrogen liberated after the dehydrogenative borylation reaction with formation of ethane.

If hydroboration were taking place, there would be a catalytic system since the ethyl group formed in the reaction would not coordinate to the rhodium fragment. Consequently, new {BH} vertices would be oxidatively added and functionalised *via* ethene insertion and reductive elimination. The dehydrogenative borylation to produce a B-vinyl group stops this, and the system does not turn over.

The use of higher temperatures or other solvents in this reaction such as THF, methanol or fluorobenzene, does not promote hydroboration, and always the vinyl-carborane derivative was obtained. Functionalisation occurs at the most electron rich vertices (twelfth or seventh) of the carborane, which demonstrates that the electrophilic $\{Rh(PPh_3)_2\}^+$ fragment follows the expected trend for carborane functionalisation *via*

insertion of the most electron rich B-H bond into the metal.[23, 24] B-vinyl substituted carboranes have previously been reported. They were prepared by metal mediated alkyne insertion[6] or by cross coupling reactions of a {B-halide} vertex and vinyl-Gringnards or zinc reagents.[25-27]

2.2.1.2 [Rh(PPh$_3$)$_2$(nbd)][7/12-(H$_2$C=CH)-1-*closo*-CB$_{11}$H$_{11}$]

Coordination of the cage to the rhodium fragment usually produces closely overlapping signals on the ^{11}B and ^{31}P{^{1}H} NMR spectra, therefore better characterisation of the cage is obtained when the cage is not bound with the metal. Addition of norbornadiene (nbd) to a solution of **1a/b** in CH_2Cl_2 generates compounds [Rh(PPh$_3$)$_2$(nbd)][7/12-(H$_2$C=CH)-1-*closo*-CB$_{11}$H$_{11}$] **2a/b** (Figure 2.9). Single crystals of the isomer **2a** were obtained from a CH_2Cl_2 solution of **2a/b** layered with pentane. Norbornadiene is added as is easily removed by hydrogenation, allowing for the isolation of intermediate species.

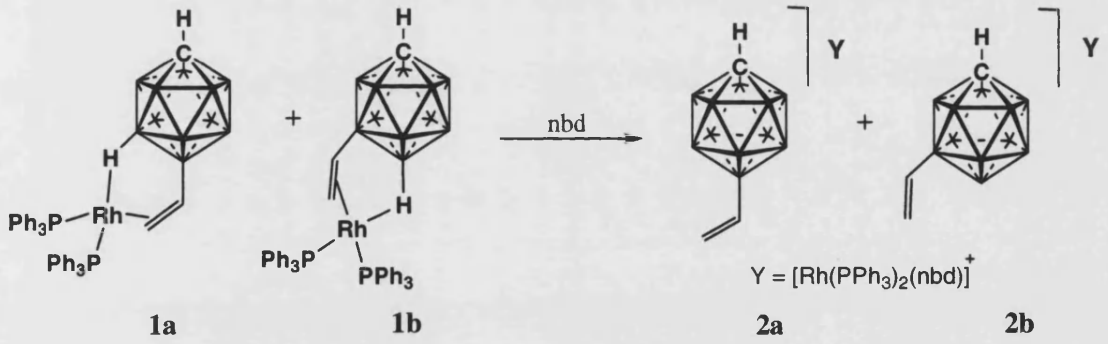

Figure 2.9 Synthesis of compounds **2a** and **2b**. Only hydrogen atoms on coordinated B-H vertices are shown.

In the ^{1}H NMR spectrum, **2a/b** displays downfield shifted signals for the vinyl protons compared to **1a/b**, which indicates that the cage is no longer interacting with the metal fragment. This is also supported by the disappearance of the Rh-*H*-B signals at the high field region in the ^{1}H{^{11}B} spectrum. As Table 2.1 shows vinyl protons for

2a/b are observed between δ 6.35 and 5.18 ppm, in the same ratio of 7:3 as commented for **1a/b**. These chemical shift values also agree with those presented for the vinyl protons in [7-(CH_2=CH)-*arachno*-6,8-$C_2B_7H_{12}$] (**II**) which appear between δ 6.56 and 5.59 ppm.[4] Multiple resonances are observed in the ^{11}B NMR spectrum, three of them belong to the B_{12}-vinyl isomer **2a** with a relative integral signal of 1:5:5 as anticipated for local C_{5v} symmetry; the isomer **2b**, with C_s symmetry, produces seven signals with relative intensities 1:1:2:2:2:2:1, with two of them overlapped with signals from **2a**. An ^{11}B-^{11}B COSY NMR experiment aided in the assignment of signals and identification of isomers with local C_{5v} (**2a**) and C_s (**2b**) symmetries (see Appendix A.1).

δ (ppm)	**1a***	**1b***	**2a***	**2b***	**II****
-C*H*=CH_2	4.83	4.95	6.23	6.35	6.46
-CH=C*H*$_2$	4.10-2.56	4.15-2.67	5.35-5.18	5.53-5.35	5.76-5.59

Table 2.1 Chemical shift change comparison of rhodium coordinated vinyl (**1a**, **1b**) and free vinyl (**2a**, **2b** and **II**). *CD_2Cl_2, **C_6D_6.

The solid state structure of **2a** is shown in Figure 2.10 with selected bond lengths and angles given in Table 2.2. The C(2)-C(3) bond length of 1.323(4) Å is consistent with a vinyl group, and is similar to the distance obtained from the solid-state structure of [Ru(CN^{t}Bu)(CO)(PPh_3){η^5-9-(CH_2=CH)-7,8-$C_2B_9H_{10}$}], 1.347(13) Å, or from DFT studies on [7-(CH_2=CH)-*arachno*-6,8-$C_2B_7H_{12}$] which suggest a C-C bond length of 1.336 Å. The B(12)-C(2) distance, 1.583(4) Å, and C(3)-C(2)-B(12) angle, 127.0(3)°, are in accordance with the values found on the ruthenium metallacarborane compound above of 1.571(13) Å and 124.2(8)° respectively. However, the B(12)-C(2) distance is slightly longer in compound **2a**, probably due to the different environment of the vinylic boron vertex, surrounded by five boron atoms in compound **2a**, and by a carbon, a ruthenium and three boron atoms in the metallacarborane cluster. However, the B-C

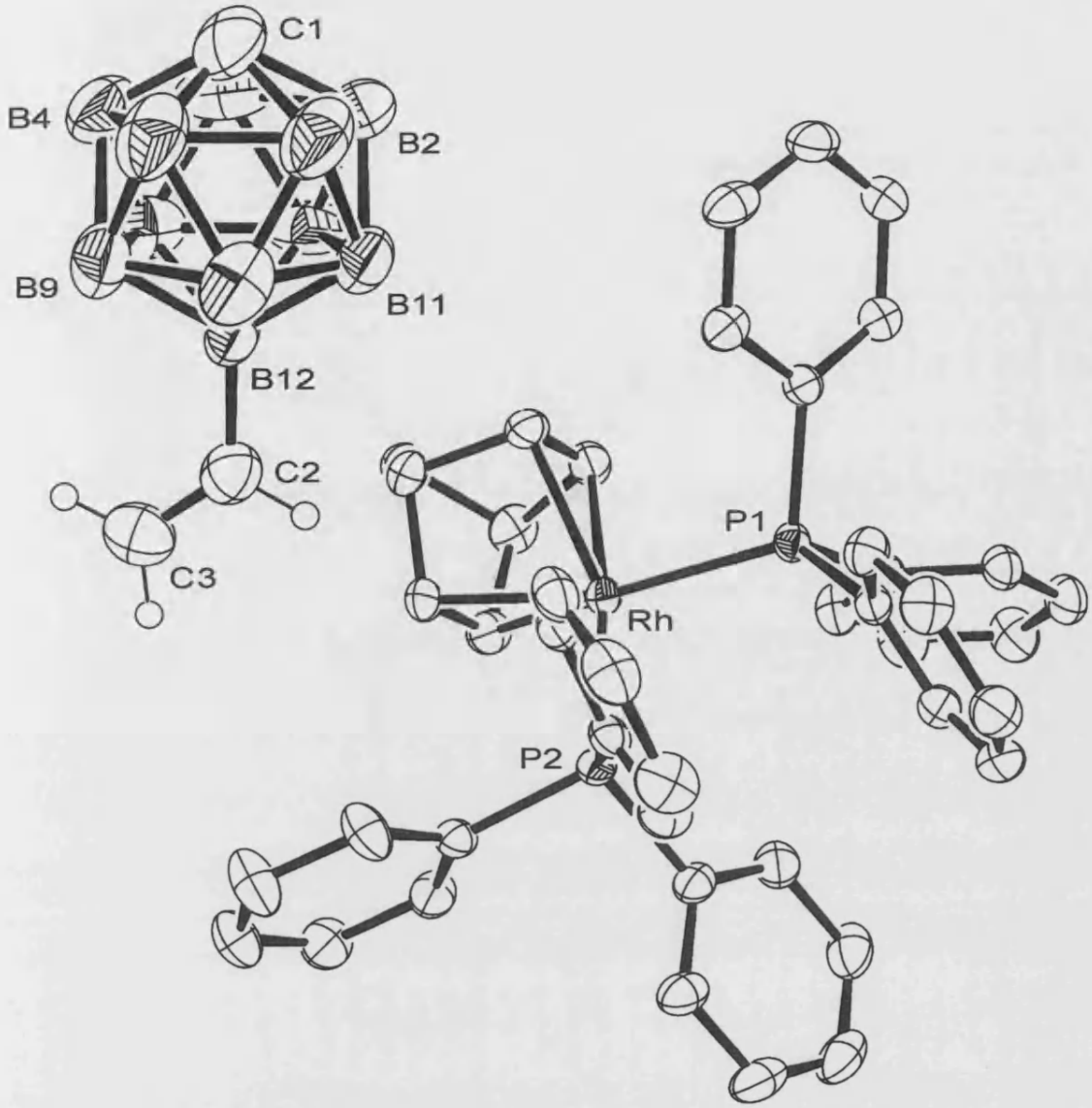

Figure 2.10 Molecular structure of the asymmetric unit of complex **2a**. Hydrogens have been omitted for clarity (except for the vinyl group). Thermal ellipsoids are drawn at the 50 % probability level.

Rh-P(1)	2.3409(4)	C(1)-B(2)	1.711(4)
Rh-P(2)	2.3056(4)	C(1)-B(3)	1.706(5)
B(12)-C(2)	1.583(4)	C(1)-B(4)	1.656(5)
C(2)-C(3)	1.323(4)	C(1)-B(5)	1.690(6)
C(3)-C(2)-B(12)	127.0(3)	C(1)-B(6)	1.719(6)

Table 2.2 Selected bond lengths (Å) and angles (°) for **2a**.

distance is similar to those B-CH_3 distances reported for the permethylated [*closo*-$CB_{11}Me_{12}]^-$.[28, 29] The location of the carbon atom in the cage is often difficult, since differentiation between carbon and boron is not easy by X-ray crystallography given the single-electron difference. However, the combination of short B-C distance and thermal parameters allows us to confidently identify the C-vertex bearing in mind the above caveat.

The presence of two isomers in solution before crystallisation also indicates that this assignment needs to be treated with caution, however, the C-B lengths [1.656(5) Å – 1.719(6) Å] are shorter than the rest of B-B distances [1.727(5) Å – 1.829(6) Å]. This indicates that the C atom has been located with a fair degree of reliability, although caution should be exercised in stating its position unequivocally.

Electrospray ionisation mass spectrometry (ESI-MS) shows the formation of a major product from the dehydrogenative borylation of ethene (m/z 169.3), e.g. **2a**, and a small amount of cage doubly substituted with an ethyl and a vinyl group (m/z 196.2) (Figure 2.11). The formation of the latter can be rationalised either by hydrogenation of a mono-vinyl cage with the hydrogen liberated after the β-elimination process, or after a reductive elimination. Both options would generate an ethyl group which unblocks the rhodium centre and allows dehydrogenative borylation of ethene onto the same cage to give [(CH_3-CH_2)(CH_2=CH)-1-*closo*-$CB_{11}H_{10}]^-$. The coordination of the second vinyl group to the cage prevents a further {BH} substitution and stops a possible catalytic cycle.

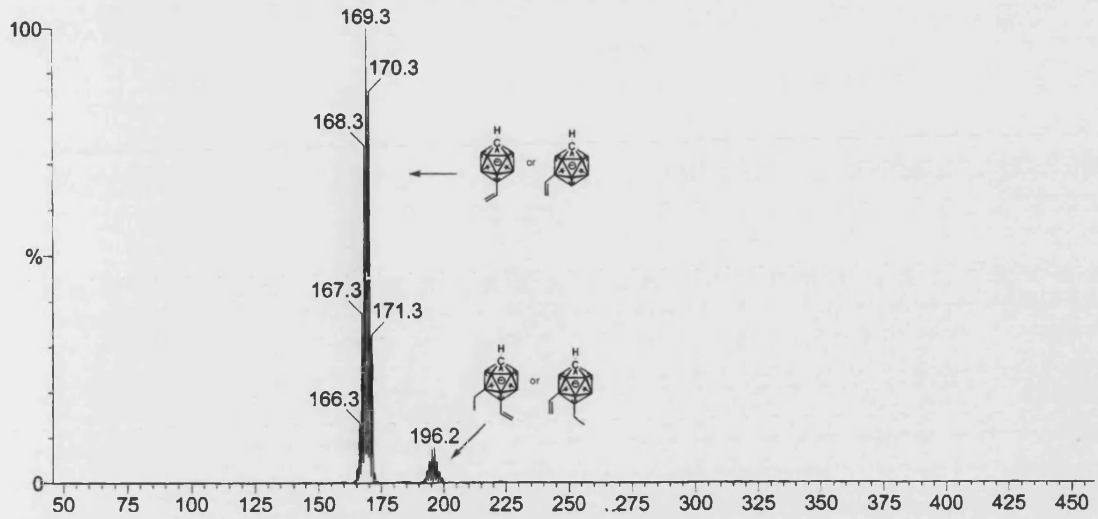

Figure 2.11 ESI-MS of **2a/b**.

2.2.1.3 [Rh(PPh$_3$)$_2$(7/12-(H$_3$C-H$_2$C)-1-*closo*-CB$_{11}$H$_{11}$)]

Addition of hydrogen to a CH_2Cl_2 solution of **1a/b** results in the hydrogenation of the *B*-vinyl group, mediated by the $\{Rh(PPh_3)_2\}^+$ fragment, to afford [Rh(PPh$_3$)$_2$(12-(Et)-1-*closo*-CB$_{11}$H$_{11}$)] **3a** (Figure 2.12) and [Rh(PPh$_3$)$_2$(7-(Et)-1-*closo*-CB$_{11}$H$_{11}$)] **3b**. A change in colour is produced after the hydrogenation from orange to dark red.

In the ^{1}H NMR spectrum, the resonances assigned to the vinyl group have disappeared and have been replaced for multiplets between δ 0.95 and 0.30 ppm which are assigned to ethyl groups. Characteristic signals of Rh-H-B interactions appear as a very broad 1:1:1:1 quartet, that is displayed at δ -0.84 [B$_{7\text{-}11}$-H-Rh], along with another small one at δ -2.11 ppm (remaining B$_{12}$-H-Rh). Both become significantly sharper in the ^{1}H{^{11}B} NMR spectrum. The ^{11}B{^{1}H} NMR spectrum shows five different environments, two for the substituted vertices at δ 8.51 (B$_{12}$) and 5.04 B$_7$, and overlapping signals signals for B-H borons between δ 2.69, -16.89. The ^{31}P{^{1}H} NMR spectrum displays two doublets at δ 46.0 [*J*(Rh-P) = 194 Hz] and 45.8 ppm [*J*(Rh-P) = 189 Hz] in an approximate 7:3 ratio, which agrees with that observed before

hydrogenation. These data suggest that the vinyl group has been hydrogenated and the cage is coordinated again via B-H vertices to the metal fragment through 3c2e bonding.

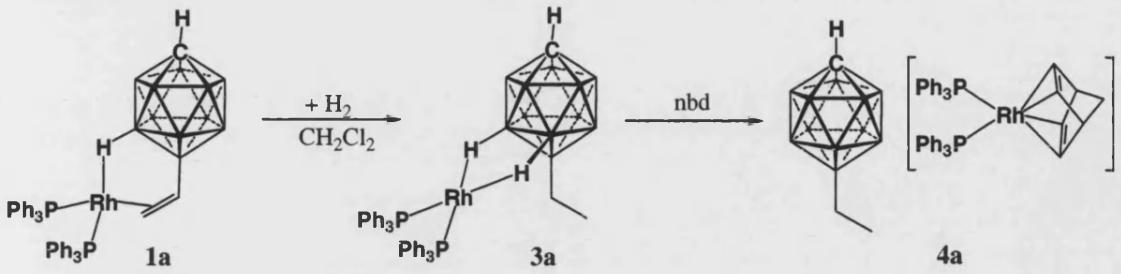

Figure 2.12

2.2.1.4 [Rh(PPh$_3$)$_2$(nbd)][7/12-(H$_3$C-H$_2$C)-1-*closo*-CB$_{11}$H$_{11}$]

Addition of norbornadiene (nbd) to an orange solution of **3a/b** in CH_2Cl_2 generates compounds [Rh(PPh$_3$)$_2$(nbd)][12-(Et)-1-*closo*-CB$_{11}$H$_{11}$] **4a** (Figure 2.9) and [Rh(PPh$_3$)$_2$(nbd)][7-(Et)-1-*closo*-CB$_{11}$H$_{11}$] **4b.** These were isolated as a dark red product in 85 % yield. ^{1}H NMR spectroscopy no longer shows high field resonances due to Rh-*H*-B interactions, while the ethyl resonances still appear between 1.06-0.70 as multiplets. The ^{11}B{^{1}H} spectrum is similar to that obtained for **2a/b,** three resonances belonging to the B12-ethyl isomer **4a** were obtained with a relative integral signal of 1:5:5. The isomer **4b** produces seven signals with relative intensities 1:1:2:2:2:2:1, two of them were overlapped with signals from compound **4a**. An ^{11}B-^{11}B COSY NMR experiment helped in the assignment of signals and identification of isomers with local C_{5v} (**4a** or *) and C_s (**4b** or ▪) symmetry (see Figure 2.13).

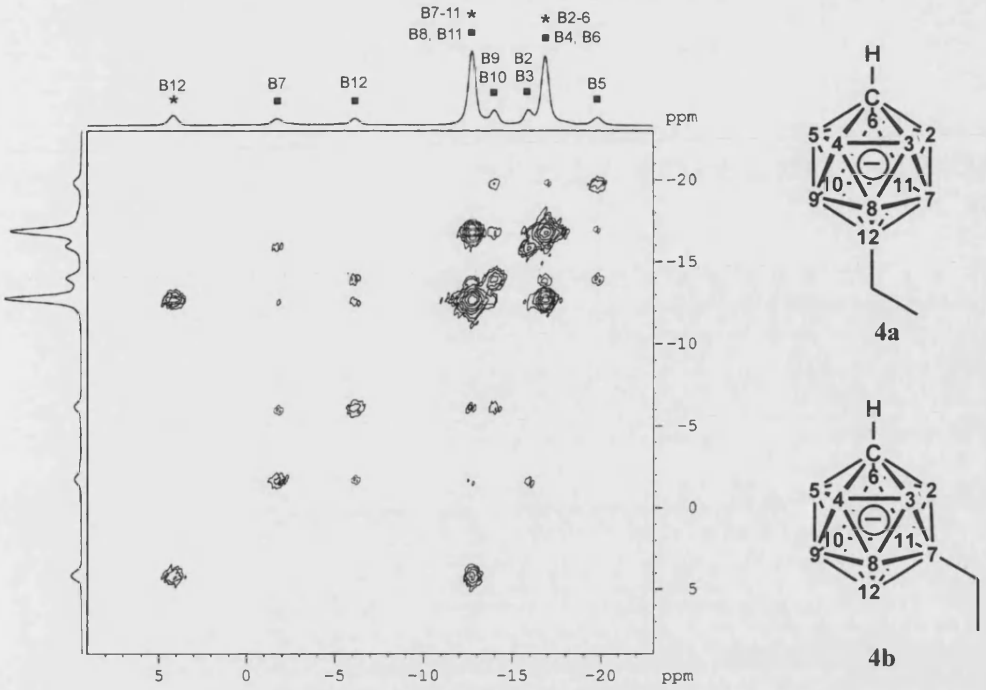

Figure 2.13 ^{11}B-^{11}B COSY NMR of compounds **4a** (*) and **4b** (▪).

ESI-MS spectrometry for **4a/b** displays one major signal at m/z 171.3 that belongs to the monosubstituted carborane (Appendix A.2) [7/12-Et-1-*closo*-$CB_{11}H_{11}$]. However there is also a small amount of cage with a mass of m/z 199.1 that indicates the existence of [7,12-Et_2-1-*closo*-$CB_{11}H_{10}$], with two substituted vertices. These arise from a probable hydrogenation or reductive elimination produced after the first ethene insertion into the cage as commented in section 2.2.1.2.

2.2.1.5 [$Rh(PPh_3)_2${7-(CH_2=CH)-12-Br-1-*closo*-$CB_{11}H_{10}$}]

Blocking the antipodal position of the carborane cage with a bromine atom permits the synthesis of a single compound since the 12-isomer is no longer possible.

Synthesis of [$(PPh_3)_2$Rh(12-Br-1-closo-$CB_{11}H_{11}$)]

Although this compound has already been prepared and studied,[30] a different synthetic pathway has been used: Triphenylphosphine was reacted with [Rh(μ-Cl)(nbd)]$_2$ in methanol at room temperature. To this clear suspension, Cs[12-Br-

1-*closo*-$CB_{11}H_{11}$] was added to afford an orange precipitate which was identified as [$(PPh_3)_2$Rh(nbd)][12-Br-1-*closo*-$CB_{11}H_{11}$] (**III**). After isolation of **III**, it was dissolved in CH_2Cl_2 and hydrogenated to produce [$(PPh_3)_2$Rh(12-Br-1-*closo*-$CB_{11}H_{11}$)] (**IV**) (Figure 2.14).

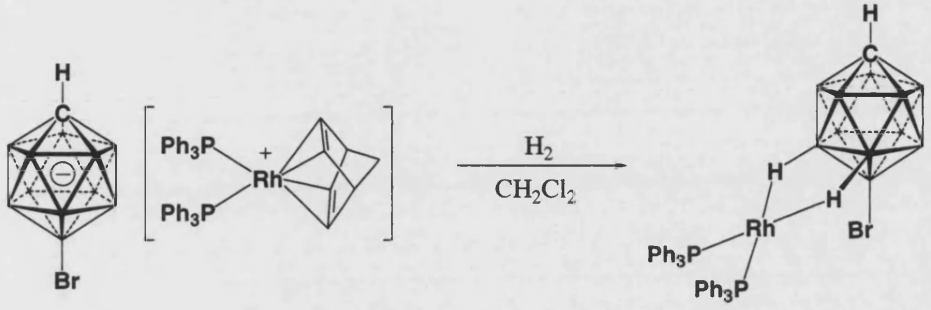

III **IV**

Figure 2.14

NMR spectra of compound **IV** display similar resonances as those found for [$Rh(PPh_3)_2$(nbd)][*closo*-$CB_{11}H_{12}$] since the cationic part of the molecule is the same in both cases. Small differences are found for the cage signals as Table 2.3 illustrates, with variation on the C-H and B-H chemical shifts due to the substitution of the 12-position of the carborane.

Compound	C-*H*	B-*H*	δ $^{31}P\{^1H\}$	*J*(RhP)
free $[CB_{11}H_{12}]^-$	2.35	1.95, 1.85, 1.79	30.5	155
I	2.60	1.70, -0.02, -1.77	49.0	194
III	2.29	1.85, 1.66	30.5	155
IV	2.61	1.77, -0.42	45.0	195

Table 2.3 δ in ppm, *J* in Hz.

$^1H\{^{11}B\}$ NMR spectrum for **IV** shows the interaction of the lower pentagonal belt {BH} vertices with the metallic fragment due to the upfield shift of their signals from δ 1.66 in **III** to δ -0.42 ppm. Therefore, in solution on the NMR time-scale, a dynamic

process takes place where all {BH} vertices on the lower belt are interacting with the $\{Rh(PPh_3)_2\}^+$ metallic centre on the NMR time-scale, affording local C_{5v} symmetry to the cage. All other resonances are similar to those found for complex **I** where the carborane is coordinated to rhodium after reduction of the chelating diolefin.[18, 30]

Synthesis of [Rh(PPh$_3$)$_2${7-(CH$_2$=CH-)-12-Br-1-closo-CB$_{11}$H$_{10}$}]

$[Rh(PPh_3)_2\{7\text{-}(CH_2{=}CH\text{-})\text{-}12\text{-}Br\text{-}1\text{-}closo\text{-}CB_{11}H_{10}\}]$ arises as a single product after the addition of ethene to a solution of **IV** in 47% isolated yield. The ^1H NMR spectrum displays three groups of vinylic signals between δ 5.03 and 3.81 ppm, suggestive of coordination to the metallic fragment. However, no low frequency resonances representative of B-*H*-Rh interactions are displayed, so it can be suggested that the metal is probably coordinated to the vinyl group and Br atom on vertex B_{12} as depicted in Figure 2.15. Coordination of the carborane through the {BBr} vertex has been previously observed in molybdenum complexes such as $[MoCp(CO)_3(12\text{-}Br\text{-}1\text{-}closo\text{-}CB_{11}H_{11})]$.[31]

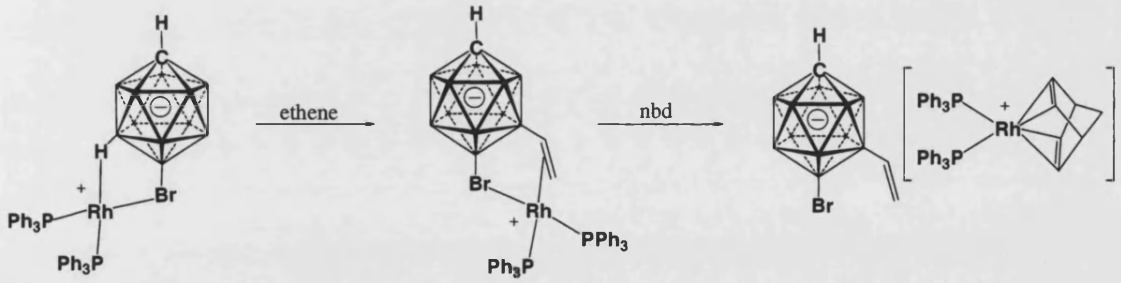

IV **5** **6**

Figure 2.15

The $^{11}B\{^1H\}$ NMR spectrum shows five different environments, two 1:1 broad singlets for the functionalized vertices at δ -2.35 and -3.64 ppm, and three broad 1:3:5 signals at -12.80, -14.33 and -17.07 ppm which become to broad doublets in the ^{11}B spectrum. The $^{31}P\{^1H\}$ NMR spectrum displays two broad signals at δ 57.9 and 20.0 ppm at room temperature. The non-equivalency of both PPh_3 groups is displayed clearly

upon cooling down to 258 K. The initial broad signals split into two well-defined doublets of doublets at δ 57.4 [*J*(RhP) 194, *J*(PP) 32] and 21.4 ppm [*J*(RhP) 155, *J*(PP) 32]. Given that vinyl is expected to be a stronger *trans*-effect ligand than bromine, the phosphine group *trans* to the bromine atom will suffer a smaller *trans*-influence and it will have the biggest coupling constant (194 Hz). On the other hand, the phosphine *trans* to the vinyl group will be more weakly coordinated to rhodium with a correspondingly smaller rhodium-phosphorus coupling constant.

Compound	C-*H*	B-*H*	$^{31}P\{^{1}H\}$	*J*(RhP)
III	2.29	1.85, 1.66	d, 30.5	155
IV	2.61	1.77, -0.42	d, 45.0	195
5	2.26	1.74, 1.60	dd, 57.4, 21.4	194, 155
6	2.40	2.14, 1.74	d, 29.8	156

Table 2.4 δ in ppm, *J* in Hz.

2.2.1.6 [Rh(PPh$_3$)$_2$(nbd)][12-Br-7-(CH=CH$_2$)-1-*closo*-CB$_{11}$H$_{10}$]

Addition of norbornadiene to a CH_2Cl_2 solution of compound **5** results in the formation of [Rh(PPh$_3$)$_2$(nbd)][12-Br-7-(CH=CH$_2$)-1-*closo*-CB$_{11}$H$_{10}$] (**6**), and the concomitant liberation of the cage from the coordination sphere of the metal. This eases the characterisation of the cage either by NMR spectroscopy and mass spectrometry.

In the ^{1}H NMR spectrum, the vinyl resonances have been shifted to higher frequencies by over 1 ppm compared to compound **5**, which indicates the cage is no longer bound to the $\{Rh(PPh_3)_2\}^+$ fragment. The signals displayed on the ^{11}B NMR spectrum are less broad and better resolved than for compound **5**, and show a 1:1:2:2:2:2:1 pattern between -2.2 and -18.9 ppm in agreement with the C_s symmetry of the carborane cage. Each of these signals has been assigned to the relevant vertex by

^{11}B-^{11}B COSY NMR experiment (Appendix A.3). ESI-MS mass spectrometry shows only one main peak at m/z 248.1 as expected (Appendix A.3).

It has been demonstrated with the previous reactions that dehydrogenative borylation of ethene does not proceed catalytically and stops after the first carborane substitution. Treatment with H_2 is necessary in order to hydrogenate the vinyl group and allow the next vertex substitution in the presence of ethene. Hence, sequential treatment with ethene and dihydrogen provides multiple substitutions as described in section 2.2.1.7.

2.2.1.7 [Rh(PPh$_3$)$_2$(nbd)][2,4,8,10,12-(Et)$_5$-1-*closo*-CB$_{11}$H$_7$]

As it has been commented previously, the reduction of the vinyl to an ethyl group unblocks the metal fragment, which only interacts with the carborane anion through 3c2e bonds. Then the metal is able to insert another molecule of ethene into the cage by dehydrogenative borylation. Consequently, sequential treatment of compounds **1a/b** with ethene and hydrogen for five repetitions (a total of six times if compound **I** is considered) results in a five-fold functionalised carborane cage with Rh-H-B interactions that can be formulated as [Rh(PPh$_3$)$_2$(2,4,8,10,12-(Et)$_5$-*closo*-CB$_{11}$H$_7$)] (**7**).

Compound **7** has been characterised by NMR spectroscopy. The ^1H NMR spectrum displays characteristic phenyl resonances between δ 7.45 and 7.00 ppm, the carborane CH cage resonance appears at δ 2.31 ppm, and ethyl multiplets are shown as broad signals between δ 0.86 and 0.14 ppm. BH signals are also observed at δ -4.95 ppm, characteristic of Rh-H-B bonding, as two overlapped quartets. Therefore, the coupling constant values for these interactions need to be calculated from the ^{11}B NMR spectrum, where they are represented by two sharp doublets at δ -17.85 ppm [*J*(BH) 92.7] and

δ -19.89 ppm [*J*(BH) 95.2 Hz]. The $^{31}P\{^{1}H\}$ NMR spectrum shows a broad peak at δ 45.1 ppm, that can not be resolved with low temperature NMR experiments.

Addition of excess of norbornadiene affords the compound $[Rh(PPh_3)_2(nbd)][2,4,8,10,12\text{-}(Et)_5\text{-}1\text{-}closo\text{-}CB_{11}H_7]$ (**8**) shown in Figure 2.16. Crystals suitable for X-ray diffraction studies were obtained by slow diffusion of pentane into a dichloromethane solution of **8**.

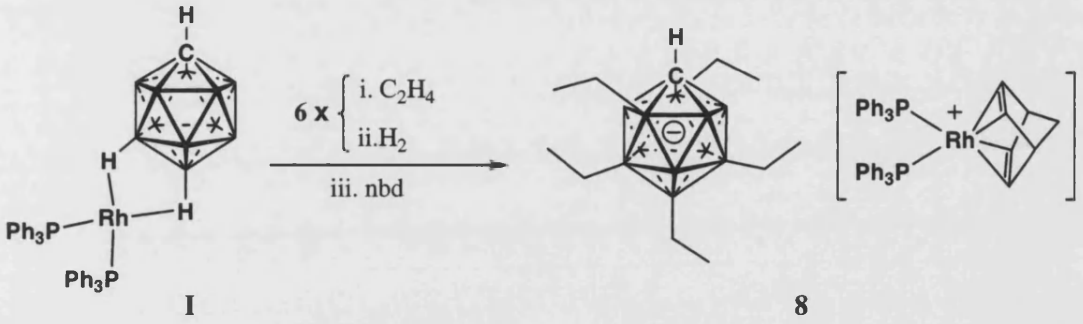

Figure 2.16 Schematic synthesis of compound **8**.

The solid state structure of the anionic part of compound **8** is shown in Figure 2.17, and this displays the carborane cage with five of its vertices functionalised. The substitution pattern is formed by the antipodal vertex, two vertices at the lower pentagonal belt and another two on the upper pentagonal belt. There are no two consecutive functionalised vertices at the same pentagonal belt. According to this substitution pattern none of the vertices are equivalent, and thus the cage has C_1 symmetry. The cage-carbon atom was located on the basis of shorter C-B distances compared to other vertices. The B-C bond distances in the cage [1.572(7) Å - 1.630(7) Å] are similar to those found in the permethylated carborane [*closo*-$CB_{11}Me_{12}]^-$ [1.58(2) Å -1.73(2) Å][28] and the ethyl substituted carborane [7-(Et)-*arachno*-6,8-$C_2B_7H_{12}$] (**II**)

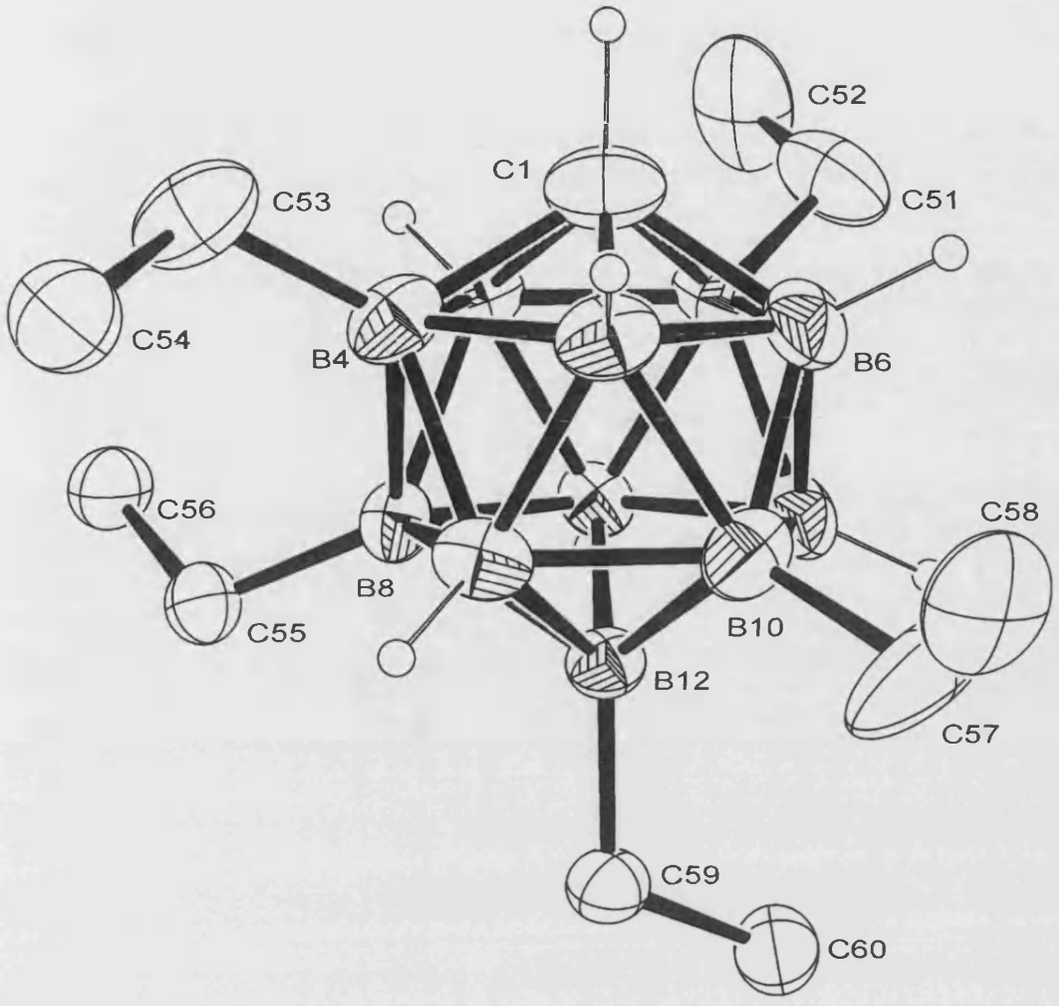

Figure 2.17 Solid-state structure of the anionic portion of **8**. The $[Rh(PPh_3)(nbd)]^+$ fragment is not shown. Thermal ellipsoids are shown at the 30% probability level. The minor disordered component of the ethyl groups has been omitted for clarity. Hydrogen atoms on the ethyl groups have been omitted for clarity.

C(1)-B(2)	1.743(7)	B(8)-C(55)	1.589(6)	C(59)-C(60)	1.522(6)
C(1)-B(3)	1.722(6)	B(10)-C(57)	1.588(16)	C(52)-C(51)-B(2)	118.3(8)
C(1)-B(4)	1.744(8)	B(12)-C(59)	1.605(5)	C(54)-C(53)-B(4)	117.7(5)
C(1)-B(5)	1.732(7)	C(51)-C(52)	1.333(14)	C(56)-C(55)-B(8)	115.7(3)
C(1)-B(6)	1.681(7)	C(53)-C(54)	1.558(11)	C(58)-C(57)-B(10)	119.2(14)
B(2)-C(51)	1.630(7)	C(55)-C(56)	1.533(5)	C(60)-C(59)-B(12)	115.2(4)
B(4)-C(53)	1.572(7)	C(57)-C(58)	1.33(2)	B(6)-C(1)-B(4)	109.2(4)

Table 2.5 Selected bond lengths (Å) and angles (°) for **8**.

[1.562(3) Å].[4] The B-C-C angles found in compound **8** [115.2(4)° - 118.3(8)°] are also similar to the one reported for **II** [115.4(2)°].[4]

The NMR spectra of compound **8** are fully consistent with the solid state structure. The B-Et signals are the most notable in the ^{1}H NMR spectrum and have a relative integral of 25 protons, being displayed as a set of multiplets between δ 0.96 and 0.36 ppm. The cage CH signal is observed at δ 2.02 ppm, which agrees with a partially-substituted cage if it is compared to that found for the unfunctionalised [*closo*-$CB_{11}H_{12}]^-$ δ 2.26 ppm,[18] and δ 1.15 ppm characteristic of free undecamethylated [*closo*-$CB_{11}HMe_{11}]^-$.[32]

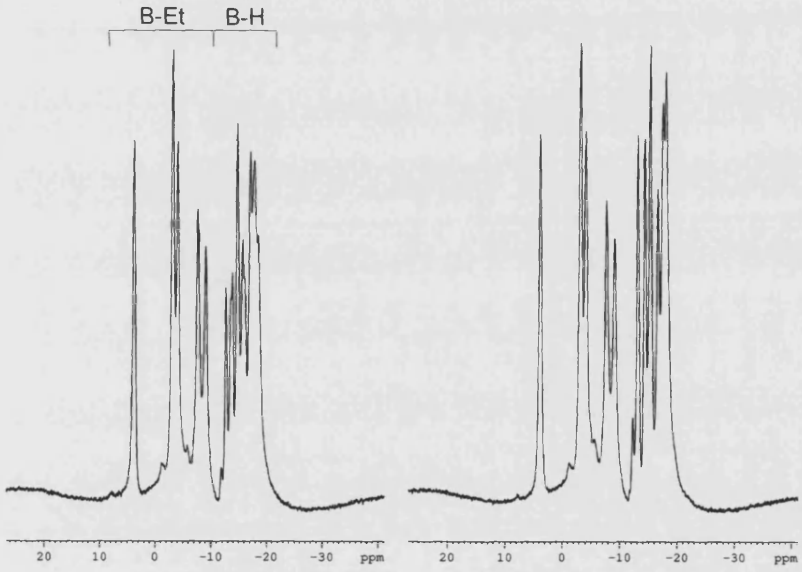

Figure 2.18 ^{11}B (left) and $^{11}B\{^{1}H\}$ NMR spectra of **8**.

The $^{11}B\{^{1}H\}$ NMR spectrum displays eleven resonances with a 1:1:1:1:1:1:1:1:1:1:1 pattern, fully consistent with the cage's C_1 symmetry. The first five of these signals do not split into doublets in the ^{11}B NMR spectrum and thus represent *B*-alkyl substituted vertices. ^{11}B-^{11}B COSY NMR experiment helped in the identification of B_{12} as the signal at δ 3.8 ppm- the lowest field resonance. Signals at δ -3.2 and -4.0 ppm can be assigned to lower pentagonal functionalised vertices, as well

as signals at δ -8.0 and -9.0 ppm to upper pentagonal belt substituted vertices. However accurate signal identification of each pairs of resonances and those from {BH} vertices to each specific vertex was problematic due to the close proximity of the signals, meaning the accurate determination of the origin of the cross-peaks in the COSY spectrum was problematic.

ESI-MS spectrometry of compound **8** shows the formation of a five-fold functionalised carborane anion, m/z 283.3 (see Appendix A.4). A very small amount of a six-fold substituted cage is also observed in the spectrum. Repeated recrystallisation affords compound **8** as pure material. It has been briefly mentioned in the introduction that late transition metal complexes are able to exchange hydrogen by deuterium at {BH} vertices. Exposure of a dichloromethane solution of **8** to deuterium provokes the substitution of the all remaining {BH} vertices of the cage by deuterium atoms. Therefore, it can be concluded that the $\{Rh(PPh_3)_2\}^+$ fragment is able to oxidatively add all {BH} vertices of the cage but steric factors may prevent further borylation with ethene.

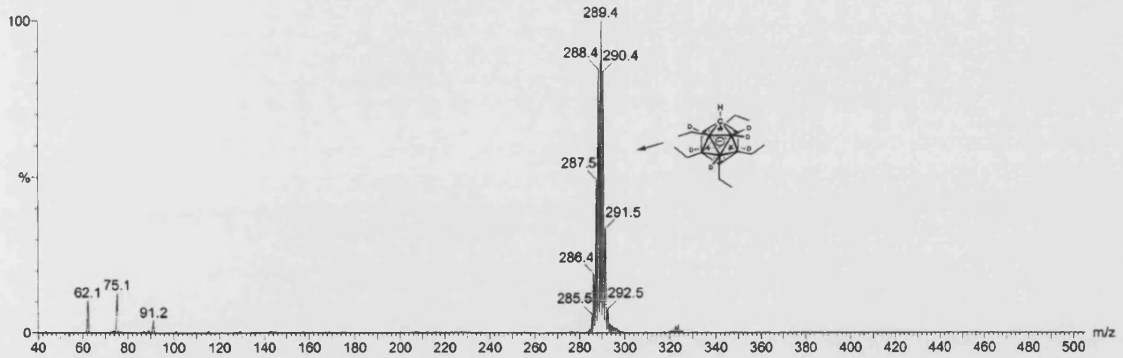

Figure 2.19 Negative ESI-MS spectrum of $[1\text{-H-}closo\text{-}CB_{11}Et_5D_6]^-$.

Figure 2.19 shows the ESI-MS spectrum obtained from the nbd salt of these deuterated cage, where a unique anion of m/z 289.4 is present and can be formulated as

[1-H-*closo*-$CB_{11}Et_5D_6$]$^-$. Deuteration of the [*closo*-$CB_{11}H_{12}$]$^-$ and other related anions with the $\{Rh(PPh_3)_2\}^+$ fragment will be discussed in more detail later on.

2.2.2 Functionalisation of [1-X-*closo*-$CB_{11}H_{11}$]$^-$ (X = Me, $^iPr_3Si$) with the $\{Rh(PPh_3)_2\}^+$ fragment

Michl has commented that for methyl substitution on [*closo*-$CB_{11}H_{12}$]$^-$, the introduction of a bulkier substituent on the carbon atom hampers the substitution at the upper pentagonal belt vertices.[33] Hence, in order to control the functionalisation of the cage by tailoring the substituents on the carbon atom, its hydrogen was replaced by a methyl and the larger triisopropylsilyl group.

2.2.2.1 $[Rh(PPh_3)_2$(1-X-*closo*-$CB_{11}H_{11}$)], (X = Me, $^iPr_3Si$)

Synthesis of the Cs salts of [closo-1-X-$CB_{11}H_{11}$]$^-$ anions

Reaction of Cs[*closo*-$CB_{11}H_{12}$] with 1.1 equivalents of BuLi results in the deprotonation of the acidic {CH} vertex and the production of the C-lithiated product CsLi[*closo*-$CB_{11}H_{11}$] as reported by Reed *et al.*[34] Reaction with alkyl halides such as MeI produces the isolation of 1-substituted carboranes such as [1-Me-*closo*-$CB_{11}H_{11}$]$^-$,[34] which is isolated as its caesium salt after addition of excess CsCl in aqueous solution.

Cs[1-$^iPr_3$Si-*closo*-$CB_{11}H_{11}$] (**9**) was prepared in a similar manner (Figure 2.20). Cs[*closo*-$CB_{11}H_{12}$] was treated with 1.1 equivalents of BuLi in THF. After stirring overnight, a solution of 1.1 equivalents of $^iPr_3SiCl$ in THF was added to the white suspension. The resulting mixture was stirred for 20 hours. The solvent was removed *in vacuo* to leave a pale yellow oil, which was dissolved in water. Addition of 5

equivalents of CsCl allows the precipitation of **9** which was recrystallised from slow evaporation of a THF/hexanes solution to render colourless suitable crystals for X-ray diffraction in 66 % yield.

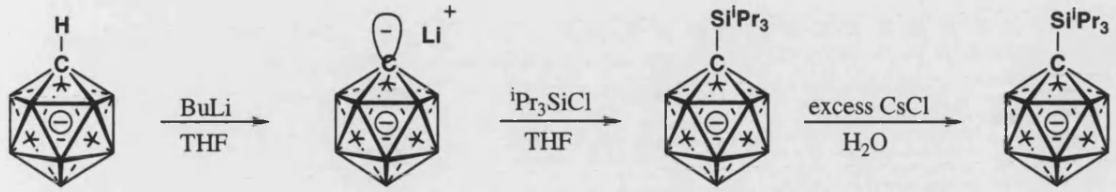

9

Figure 2.20 Functionalisation of the {CH} vertex with the $^{i}Pr_3Si$ group.

Compound **9** was characterized by NMR spectroscopy, mass spectrometry and X-ray diffraction studies. Its solid-state structure is displayed in Figure 2.22 along with selected bond lengths and angles in Table 2.6. This figure shows the position of the closest Cs^+ ion. Each Cs^+ ion establishes interactions with {BH} vertices of four $[1\text{-}^{i}Pr_3Si\text{-}closo\text{-}CB_{11}H_{11}]^-$ carborane clusters and one oxygen atom from a molecule of tetrahydrofuran, this environment is shown in Figure 2.21. It is worth noting that two {BH} interactions, of one of the cages, towards the caesium ion are with upper belt vertices rather to the more electronically favored lower belt or antipodal vertices.

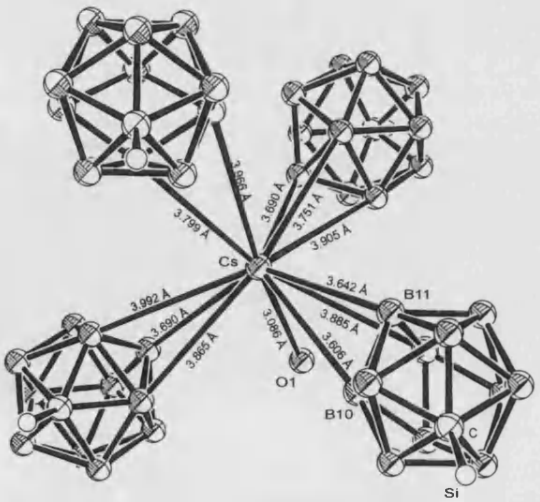

Figure 2.21 Stereoscopic diagram illustrating the environment of the caesium ion in $Cs[1\text{-}^{i}Pr_3Si\text{-}closo\text{-}CB_{11}H_{11}]$. Hydrogens, isopropyl groups and 1,4-dioxane atoms (except oxygen interacting with the Cs^+ ion) have been omitted for clarity.

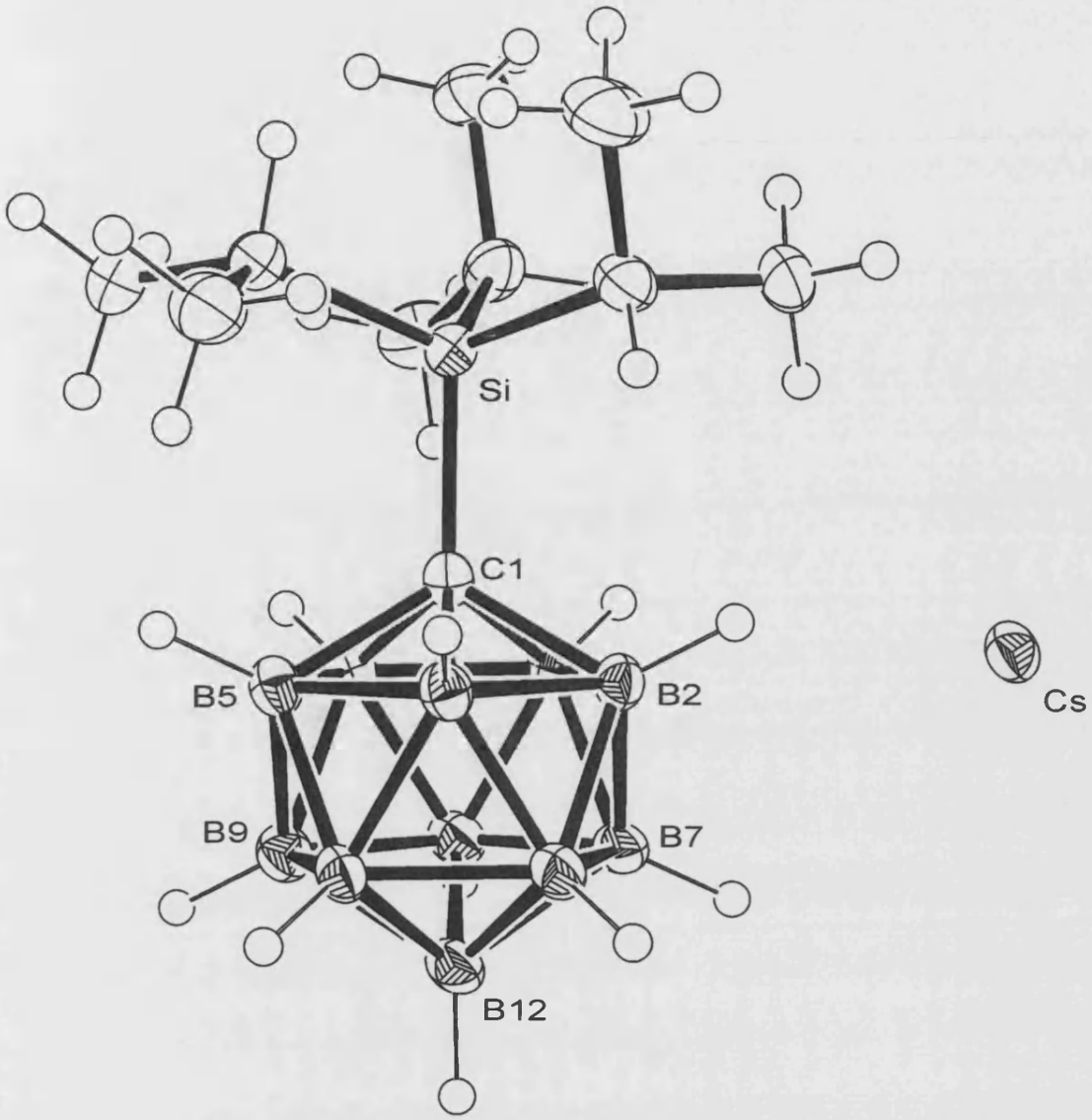

Figure 2.22 Molecular structure of the asymmetric unit of Cs[1-^{i}Pr$_3$Si-*closo*-CB$_{11}$H$_{11}$] (**9**). Ellipsoids are shown at the 50 % probability level. The position of the closest Cs^+ ion is shown.

Si-C(1)	1.934(3)	B(7)-B(12)	1.782(4)
C(1)-B(2)	1.734(4)	B(8)-B(12)	1.799(5)
C(1)-B(3)	1.714(4)	B(9)-B(12)	1.792(5)
C(1)-B(4)	1.723(4)	B(10)-B(12)	1.776(5)
C(1)-B(5)	1.734(4)	B(11)-B(12)	1.773(5)
C(1)-B(6)	1.739(4)	Cs···B(2)	3.865(3)

Table 2.6 Selected bond lengths (Å) for **9**.

This compound is best described as an ionic salt, since Cs···H distances range from 2.984 Å upward and Cs···B distances from 3.606 Å upward. The closest Cs···Cs distance in the crystal lattice equals to 5.636 Å. These values are similar to those reported for Cs[12-Br-1-*closo*-$CB_{11}H_{11}$],[34] where each caesium atom is surrounded by six carborane clusters and establishes interactions towards {BH} and {BBr} vertices.

In a d_6-acetone solution, the ^1H NMR spectrum of **9** consists of a highly second order septet at 1.24 ppm for the methide protons and a doublet at 1.17 ppm for the (C-CH_3) methyls. The $^1H\{^{11}B\}$ NMR shows, in addition to these, three broad singlets for the B-H bonds of the carborane at δ 1.94 (B_{12}-H), 1.88 ($B_{2\text{-}6}$-H) and 1.67 ($B_{7\text{-}11}$-H) which are shifted downfield compared with Cs[*closo*-$CB_{11}H_{12}$] [δ 1.71 (B_{12}-H), 1.65 ($B_{2\text{-}6}$-H), 1.56 ($B_{7\text{-}11}$-H)]. The $^{11}B\{^1H\}$ NMR spectrum displays three singlets at -1.93, -10.89 and -12.71 ppm for the B_{12}, $B_{7\text{-}11}$ and $B_{2\text{-}6}$ respectively in a 1:5:5 ratio. The mass spectrometry FAB- spectrum displays a peak m/z 299.2 with correct isotope pattern, as predicted theoretically.

*Synthesis of [$Rh(PPh_3)_2$(nbd)][(1-X-closo-$CB_{11}H_{11}$)], [X = Me (**10**), $^iPr_3Si$ (**11**)]*

A solution of 4 equivalents of triphenylphosphine in THF was added to a solution of [Rh(μ-Cl)(nbd)]$_2$ with 2 equivalents of Cs[1-X-*closo*-$CB_{11}H_{11}$] along with excess nbd. After stirring the reaction mixture overnight, the solvent was removed *in-vacuo* and dissolved with CH_2Cl_2 to allow complete precipitation of CsCl. The orange solution was filtered and concentrated *in vacuo*. Orange crystals of [$Rh(PPh_3)_2$(nbd)][(1-$^iPr_3$Si-*closo*-$CB_{11}H_{11}$)] (**11**) were obtained after diffusion of hexanes into the CH_2Cl_2 solution at room temperature.

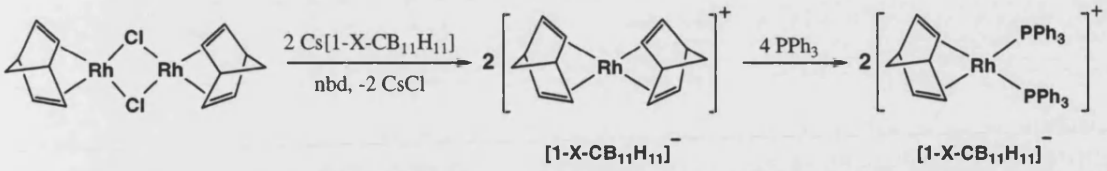

Figure 2.23 Schematic synthesis of **10** (X = Me) and **11** (X = $^{i}Pr_3Si$).

In $CDCl_3$, the ^{1}H NMR spectra of **10** and **11** are almost identical to that reported in the literature for $[Rh(PPh_3)_2(nbd)][closo\text{-}CB_{11}H_{12}]$,[18] the difference is the substitution of the C-H signal for a singlet at δ 1.67 ppm from the methyl when X = Me (compound **10**) and for highly second order septet and doublet from the isopropyl group when X = $^{i}Pr_3Si$ (compound **11**) at δ 1.27 and 1.16 ppm respectively. The signals from the PPh_3 groups and norbonadiene remain unchanged. The $^{1}H\{^{11}B\}$ spectrum for $[Rh(PPh_3)_2(nbd)][1\text{-}^{i}Pr_3Si\text{-}CB_{11}H_{11}]$ (**11**) shows a distinctive antipodal effect,[35] with a downfield shift of the B_{12}-H signal from δ = 1.90 ppm in the $[closo\text{-}CB_{11}H_{12}]^-$ anion to δ = 2.30 ppm in the $[1\text{-}^{i}Pr_3Si\text{-}closo\text{-}CB_{11}H_{11}]^-$ anion. Two more B-H resonances at δ 2.08 and 1.96 ppm are observed, from the upper and lower belt {BH} vertices respectively. The $^{31}P\{^{1}H\}$ NMR consists in a doublet at 30.59 ppm with a coupling constant of *J*(RhP) 155.5 Hz, as expected for a Rh(I) complex. ^{11}B and $^{11}B\{^{1}H\}$ NMR spectra present the same signals of the caesium salts of the respective carborane anions, consistent with non-coordination of the anions.

For $[Rh(PPh_3)_2(nbd)][(1\text{-}^{i}Pr_3Si\text{-}CB_{11}H_{11})]$ (**11**) the solution structure from NMR data was confirmed by X-ray diffraction studies of a single crystal. The molecular structure is shown in Figure 2.25 with selected bond lengths and angles displayed in Table 2.7. The bond lengths and angles are unremarkable and are consistent with other structurally characterised $[(PPh_3)_2Rh(nbd)]^+$ fragments.[30, 36]

Synthesis of [Rh(PPh$_3$)$_2$(1-X-closo-CB$_{11}$H$_{11}$)], (X = Me, ^{i}Pr$_3$Si)

The procedure for the [Rh(PPh$_3$)$_2$(*closo*-CB$_{11}$H$_{12}$)] (**I**) preparation[18] has been followed for the synthesis of [Rh(PPh$_3$)$_2$(1-X-*closo*-CB$_{11}$H$_{11}$)], [X = Me (**12**), ^{i}Pr$_3$Si (**13**)]. Treatment of a solution of **10** and **11** in CH_2Cl_2 with H_2 results in the formation of norbornane from the reduction of the diene, and the subsequent coordination of [1-X-*closo*-CB$_{11}$H$_{11}$], (X = Me, ^{i}Pr$_3$Si) anion to the metal fragment {(PPh$_3$)$_2$Rh}$^+$ (Figure 2.24). As previously described in the literature,[18] the formation of the new *exo*-rhodacarborane complex results in a colour change of the solution from orange to dark red for [Rh(PPh$_3$)$_2$(1-Me-*closo*-CB$_{11}$H$_{11}$)] (**12**) and from orange to dark pink-red for [Rh(PPh$_3$)$_2$(1-^{i}Pr$_3$Si-*closo*-CB$_{11}$H$_{11}$)] (**13**).

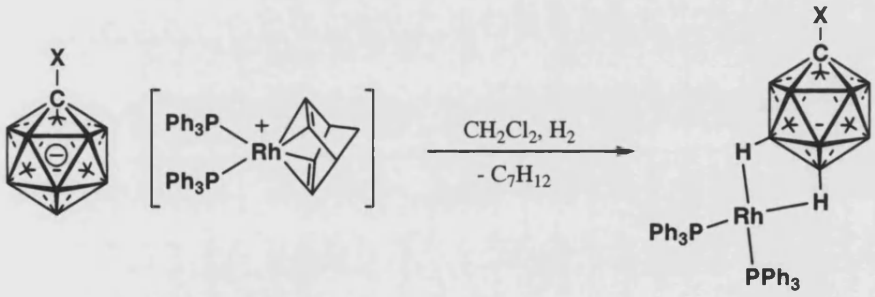

Figure 2.24 Synthesis of compounds **12** (X = Me) and **13** (X = Si^{i}Pr$_3$)

Complex **12** was characterised by multinuclear NMR spectroscopy. The ^{1}H NMR spectrum in CD_2Cl_2 at room temperature shows multiplets from 7.50 to 7.09 ppm for the triphenylphosphine protons, a singlet at δ 1.59 ppm for the methyl cage, with a relative integral of three protons, and two signals for cage {BH} vertices at 0.18 and -2.05 ppm. The ^{1}H{^{11}B} NMR spectrum shows three signals for cage {BH} vertices at 1.93, 0.18 and -2.05 ppm. The latter two are shifted to a higher field compared with the norbonadiene precursor [Δδ = -4.04 (B$_{12}$-H) and -1.68 ppm (B$_{7\text{-}11}$-H)] since they are involved in 3c2e bonding with the metal (Figure 2.26).

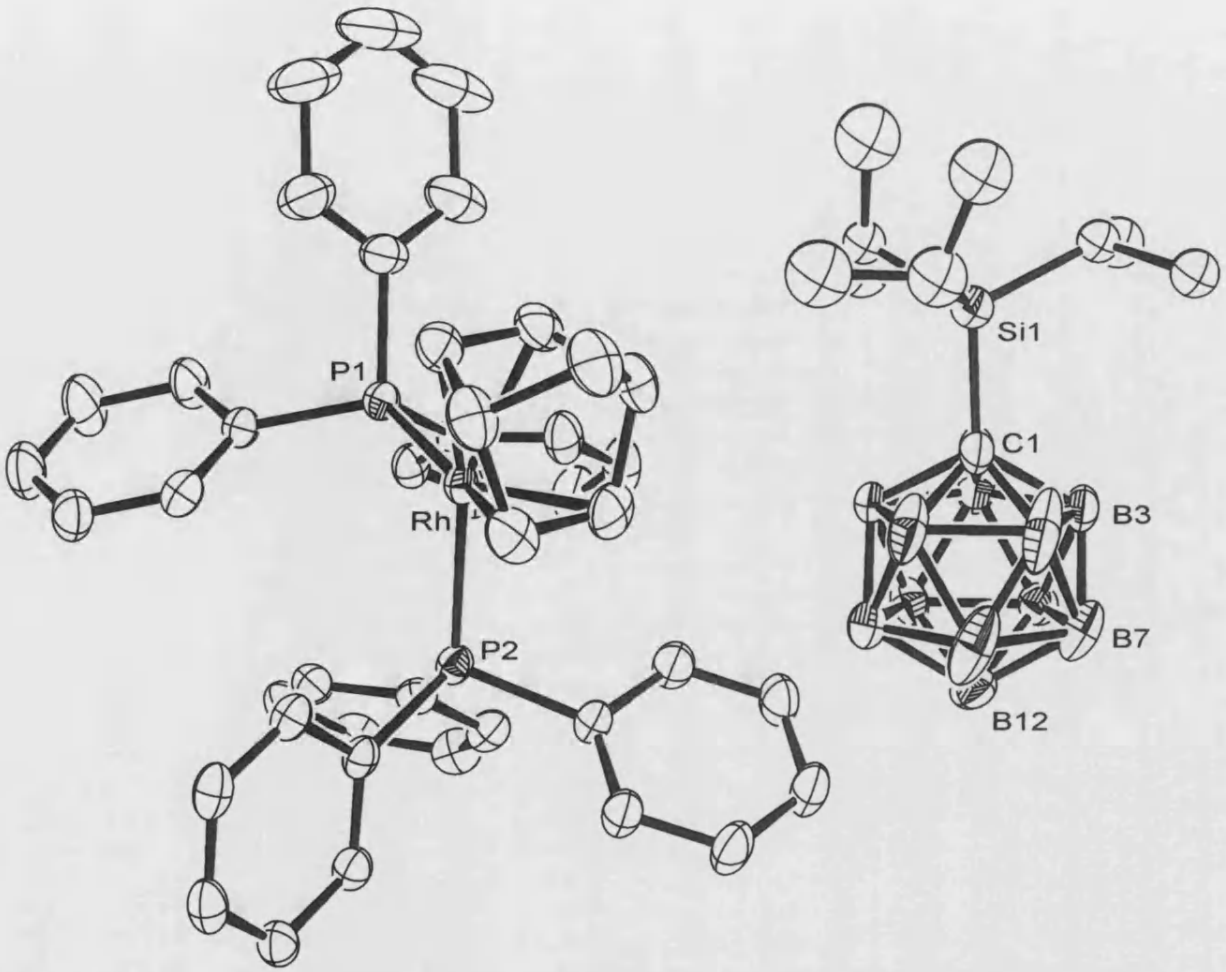

Figure 2.25 Molecular structure of the asymmetric unit of complex **2a**. Hydrogens have been omitted for clarity. Thermal ellipsoids are drawn at the 50 % probability level.

Rh-P(1)	2.3106(7)
Rh-P(2)	2.3493(7)
Si(1)-C(1)	1.942(4)
C(1)-B(2)	1.697(8)
C(1)-B(3)	1.737(5)
C(1)-B(4)	1.734(7)
C(1)-B(5)	1.724(5)
C(1)-B(6)	1.709(7)
P(1)-Rh-P(2)	96.89(2)

Table 2.7 Selected bond lengths (Å) and angles (°) for .

The integral 5H at δ 0.18 ppm can be assigned to the $B_{7\text{-}11}$-H protons and the integral 1H at δ -2.05 ppm is assigned to the antipodal vertex. The broad $B_{2\text{-}6}$-H singlet remains without any significant change at δ 1.93 ppm from the norbonadiene precursor, consistent with non-involvement of the upper pentagonal belt in Rh-H-B bonding. The methyl singlet has been slightly shifted upfield from δ 1.67 to 1.59 ppm.

In the $^{11}B\{^{1}H\}$ NMR spectrum, the signal from the upper pentagonal belt remains unchanged at δ -11.91 ppm, however the signals for the lower belt and antipodal vertices are upfield shifted compared to compound **10**, from δ -10.06 ppm (B_{12}) and -11.72 ppm ($B_{7\text{-}11}$) to δ -14.36 ppm (overlapped signals). $B_{7\text{-}11}$-H doublet shows, in ^{11}B NMR spectrum, a coupling constant *J*(BH) reduction from 143.2 Hz (in complex **10**) to 122.6 Hz (in **12**) due to a decrease of the B-H bond order upon coordination of the antipodal and lower pentagonal belt vertices to the metal via 3c2e bonding. The $^{1}H\text{-}^{11}B$ coupling constant for B_{12}-H can be calculated from the ^{1}H NMR spectrum, and has an approximate value of 156 Hz.

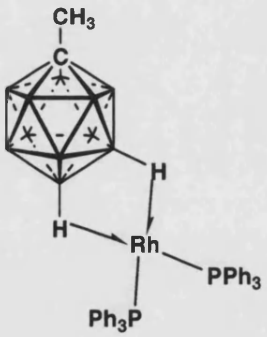

Figure 2.26 Schematic representation of complex **12**

The equivalent complex [$Rh(PPh_3)_2(1\text{-}^{i}Pr_3Si\text{-}closo\text{-}CB_{11}H_{11})$] (**13**) was characterized by X-ray crystallography and multinuclear NMR spectroscopy. The solid state structure of complex **13** is shown in Figure 2.27 with relevant bonds and angles given in Table 2.8.

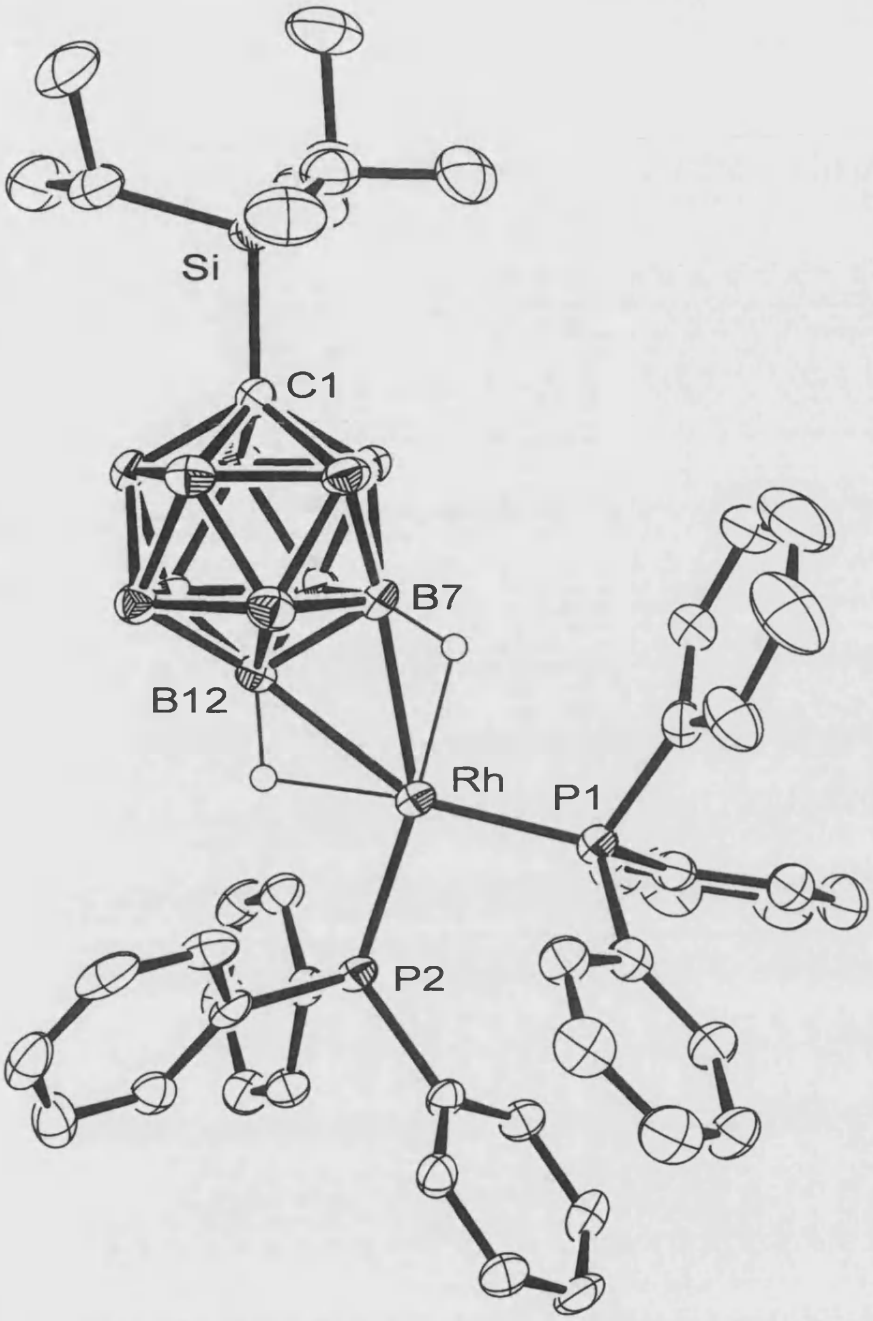

Figure 2.27 Solid-state structure of complex **13**. Thermal ellipsoids are shown at the 50% probability level. Hydrogen atoms, apart from those associated with cage vertices, have been omitted for clarity.

Rh-P(1)	2.2241(12)	P(1)-Rh-P(2)	95.47(4)
Rh-P(2)	2.2295(11)	P(1)-Rh-B(7)	112.95(12)
Rh-B(7)	2.387(5)	P(2)-Rh-B(12)	109.31(11)
Rh-B(12)	2.384(5)	B(7)-Rh-B(12)	42.28(16)

Table 2.8 Selected bond lengths (Å) and angles (°) for **13**.

The $\{B_{12}H\}$ and $\{B_7H\}$ vertices are coordinated to the rhodium via 3c2e Rh-H-B bonds. The metal centre is square planar coordinated to two PPh_3 ligands and two {BH} vertices with a dihedral angle [P(1)-P(2)-B(7)-B(8)] of 2.5°. The Rh-P lengths [2.2241(12) and 2.2295(11)] are comparable to those reported for $[Rh(PPh_3)_2(closo\text{-}CB_{11}H_{12})]$ [2.2192(6), 2.2391(6)].[18] The Rh-B distances [Rh-B(12) = 2.384(5), Rh-B(7) = 2.387(5)] are almost identical to those observed in other rhodium complexes like $[Rh(COD)(closo\text{-}CB_{11}H_{12})]$, [Rh-B(12) = 2.385(3), Rh-B(7) = 2.391(3)].[37]

In CD_2Cl_2 solution, the ^1H NMR spectrum at room temperature for **13** shows multiplets from 7.51 to 7.07 ppm for the triphenylphosphine protons, a second order septet and a doublet between δ 1.30-1.03 ppm (SiR_3) and two broad B-H vertex signals at δ 0.07 and -0.08 ppm in the ratio 5:1. The $^1H\{^{11}B\}$ NMR spectrum shows three B-H resonances at 2.05, 0.07 and -0.08 ppm. The latter two are shifted to a higher field compared with the norbonadiene precursor since they are involved in 3c2e bonds with the metal. Nevertheless, the B_{12}-H proton shows a smaller high field shift than in $[Rh(PPh_3)_2(closo\text{-}CB_{11}H_{12})]$ (δ = -1.97 ppm) due to the antipodal effect induced by the silyl group on the carbon atom. The 5H integral resonance at δ 0.07 ppm can be assigned as the $B_{7\text{-}11}$-H protons and the integral at δ -0.08 ppm being assigned to the antipodal B_{12}-H vertex. No variation from the norbonadiene precursor is observed at the $B_{2\text{-}6}$-H singlet, which appears at δ 2.05 ppm.

Two different environments are displayed in the ^{11}B NMR spectrum at -6.85 (B_{12}) and -13.17 ppm ($B_{2\text{-}11}$) with coupling constants of 110.1 and 112.4 Hz respectively, in a 1:10 pattern since the lower and upper belt signals are coincidently overlapped. The upfield shift and the reduction of the coupling constant values reflect the coordination of the metal to the carborane with the subsequent reduction of the B-H bond order. Finally,

the $^{31}P\{^{1}H\}$ NMR spectrum shows a doublet at δ 47.74 ppm [*J*(Rh-P) = 193.6 Hz]. Considering all these spectroscopic data, it can be suggested that on the NMR time-scale the metal interacts with all the protons of the lower pentagonal belt and the antipodal vertex as observed for other $\{L_2M\}^+$ fragments coordinated to [*closo*-$CB_{11}H_{12}]^-$ anion.[19, 37] If the solid state structure were retained a 1:1:2:2:2:2:1 pattern would be observed in the $^{11}B\{^{1}H\}$ NMR spectra. Figure 2.28 and Table 7 (*vide infra*) include selected spectroscopic data of complexes **I, 12, 13** and their precursors.

	Compound	δ(^{1}H)*BH* (ppm)[a]	*J(BH)* Hz	δ(^{11}B) ppm		
				B_{12}	$B_{7\text{-}11}$	$B_{2\text{-}6}$
	[Rh(PPh$_3$)$_2$(nbd)][1-H-*closo*-$CB_{11}H_{11}$]	*1.95*, 1.85, 1.79	135	-4.0	-10.3	-13.1
10	[Rh(PPh$_3$)$_2$(nbd)][1-Me-*closo*-$CB_{11}H_{11}$]	*1.99*, 1.86	132.2	-10.0	-11.7	-11.7
11	[Rh(PPh$_3$)$_2$(nbd)][1-^{i}Pr$_3$Si-*closo*-$CB_{11}H_{11}$]	*2.30*, 2.08, 1.96	133.9	-2.0	-10.8	-12.3
I	[Rh(PPh$_3$)$_2$(1-H-*closo*-$CB_{11}H_{11}$)]	1.70, -0.02, -*1.97*	119	-9.9	-13.5	-14.1
12	[Rh(PPh$_3$)$_2$(1-Me-*closo*-$CB_{11}H_{11}$)]	1.93, 0.18, -*2.05*	122.6	-11.9	-14.4	-14.4
13	[Rh(PPh$_3$)$_2$(1-^{i}Pr$_3$Si-*closo*-$CB_{11}H_{11}$)]	2.05, 0.07, -*0.08*	110.1	-6.8	-13.2	-13.2

Table 2.9 [Rh(nbd)(PPh$_3$)$_2$][*closo*-$CB_{11}H_{12}$] and [Rh(PPh$_3$)$_2$(*closo*-$CB_{11}H_{12}$)].[18] All measured in $CDCl_3$ or CD_2Cl_2 solutions. [a]Antipodal vertices in *italics*.

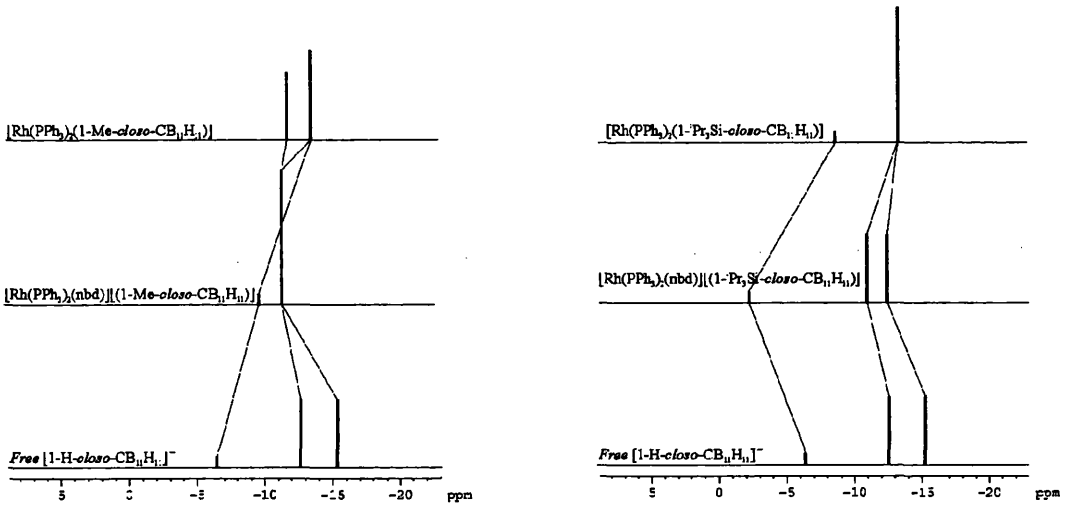

Figure 2.28 Correlation diagrams of chemical shifts and relative peak intensities in the $^{11}B\{^1H\}$ NMR spectra of compounds **10, 11, 12, 13** compared to free [*closo*-$CB_{11}H_{12}]^-$.

2.2.2.2 [Rh(PPh$_3$)$_2$(1-Me-9,11,12-(Et)$_3$-1-*closo*-CB$_{11}$H$_8$)]

Similar to that described in section 2.2.1 for **I**, treatment of **12** with ethene provokes the formation of B-vinyl by dehydrogenative borylation, and consequently the initial red solution becomes orange. Addition of hydrogen changes the solution to dark red again, indicative of the reduction of the vinyl group and the subsequent formation of a complex with Rh-H-B interactions via 3c2e bonding. Sequential treatment of compound **12** with ethene and hydrogen three times results in a three-fold functionalised carborane cage with Rh-H-B interactions that could be formulated as [Rh(PPh$_3$)$_2$(1-Me-9,11,12-(Et)$_3$-1-*closo*-CB$_{11}$H$_8$)]. The final complex has been characterized by X-ray diffraction studies, multinuclear NMR spectroscopy and ESI-MS.

Suitable crystals for X-ray crystallography were grown from a concentrated dichloromethane/hexane solution of **14** at -18°C. The solid state structure is shown in Figure 2.29 with relevant bond lengths and angles in Table 2.10. The three-fold functionalized cage displays the same substitution pattern as that found for the lower part of the anionic portion of compound **8**; though it is coordinated to rhodium through

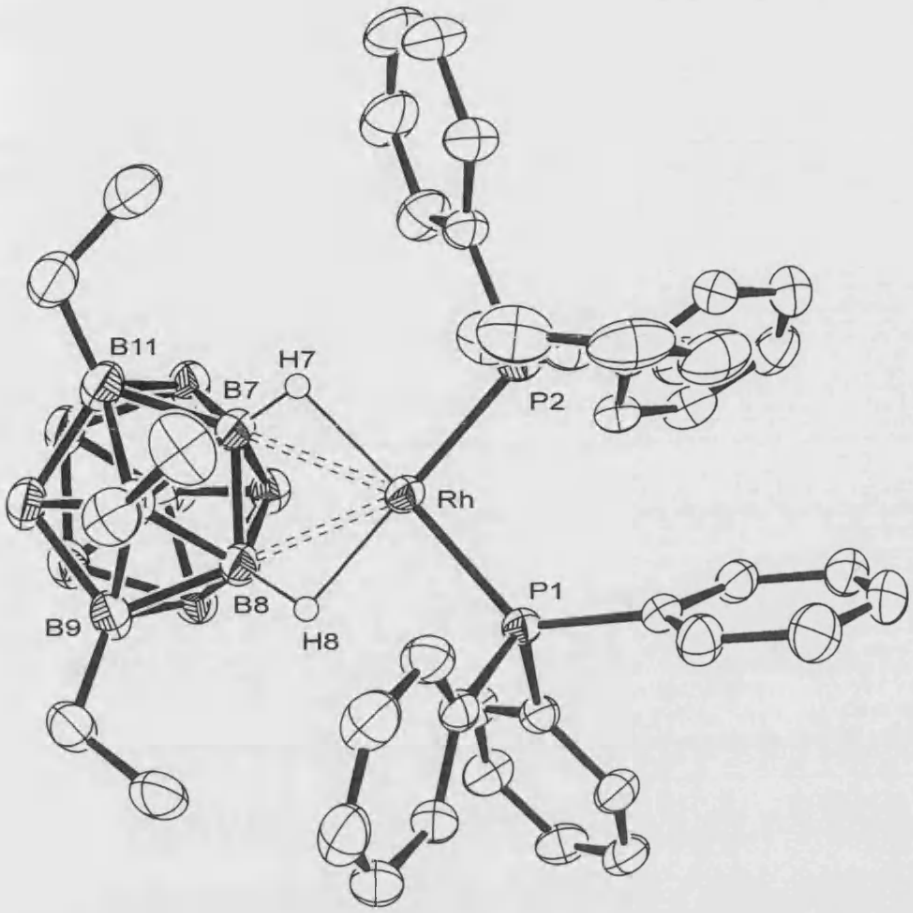

Figure 2.29 Molecular structure of the asymmetric unit of complex **14**. Hydrogen atoms have been omitted for clarity (except H7 and H8). Thermal ellipsoids are drawn at the 50 % probability level.

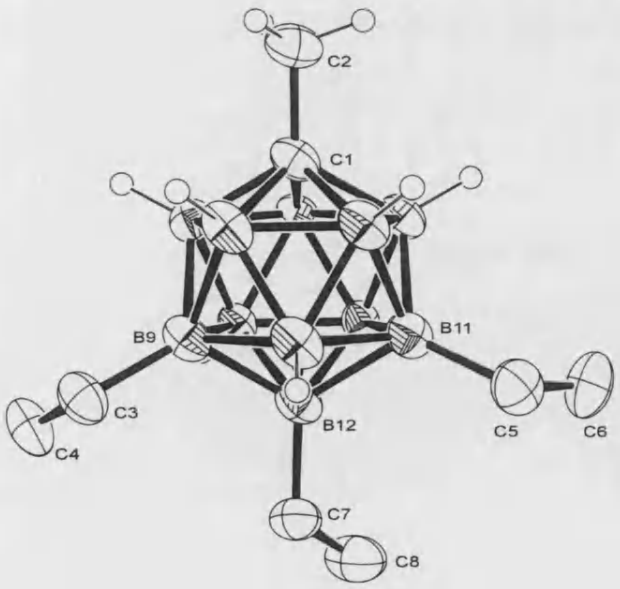

Figure 2.30 Solid state structure of the functionalised anion of complex **14**.

Rh-P1	2.2457(8)
Rh-P2	2.2129(9)
Rh-B7	2.401(4)
Rh-B8	2.405(4)
C(1)-C(2)	1.518(5)
C(1)-B(2)	1.723(6)
C(1)-B(3)	1.702(5)
B(12)-C(7)	1.597(5)
P1-Rh-P2	95.77(3)

Table 2.10 Selected bond lengths (Å) and angles (°) for **14**.

two 3c2e Rh-H-B bonds. The cage carbon atom has been reliably located due to the attached methyl group, and hence all boron vertices have been identified unambiguously. The B-C_{ethyl} distances [1.590(6) Å - 1.597(5) Å] fall into the same range as observed for **8** [1.572(7) Å - 1.630(7) Å]. The metal centre is square planar coordinated to two PPh_3 ligands and two separated lower pentagonal belt {BH} vertices with a dihedral angle [P(1)-P(2)-B(7)-B(8)] of -4.3°. The Rh-P lengths [2.2457(8) and 2.2129(8) Å] are comparable to those reported for [$Rh(PPh_3)_2$(*closo*-$CB_{11}H_{12}$)] [2.2192(6), 2.2391(6)].[18] The Rh-B distances [Rh-B(7) = 2.401(4), Rh- B(8) = 2.405(4)] are very similar to those observed in analogous rhodium complexes such as [Rh(COD)(*closo*-$CB_{11}H_{12}$)],[37] [Rh-B(12) = 2.385(3), Rh-B(7) = 2.391(3)]; [$Rh(PPh_3)_2$(1-$^{i}Pr_3$Si-*closo*-$CB_{11}H_{11}$)], [Rh-B(12) = 2.384(5), Rh-B(7) = 2.387(5)].

The ^{1}H NMR spectrum in CD_2Cl_2 shows a singlet for the carborane methyl group at δ 1.64 ppm and the ethyl groups are represented by multiplets between δ 1.02 and 0.11 ppm with a relative integral value of 15H. Rh-H-B interactions are observed at δ -4.64 ppm as a broad quartet with a coupling constant value [*J*(BH) 94.0 Hz], and it has been shifted upfield from δ 0.18 [$B_{7\text{-}11}$-H-Rh] in [$Rh(PPh_3)_2$(1-Me-*closo*-$CB_{11}H_{11}$)]. The ^{11}B{^{1}H} NMR spectrum consists of 3:3:3:2 pattern with three very broad signals at δ -2.11, -12.82 and -16.27 ppm, and a sharp singlet at δ -18.78 ppm. The last signal splits into a sharp doublet in the ^{11}B NMR spectrum with a coupling constant value [*J*(BH) 94.0 Hz], which suggests it is the vertex coordinated to the rhodium fragment since the coupling constant value is the same in both ^{1}H and ^{11}B NMR spectra. The ^{31}P{^{1}H} NMR spectrum displays a doublet at δ 45.0 ppm, [*J*(RhP) 193 Hz], equal to that found for [$Rh(PPh_3)_2$(1-Me-*closo*-$CB_{11}H_{11}$)] (**12**).

2.2.2.3 [Rh(PPh$_3$)$_2$(nbd)][1-Me-9,11,12-(Et)$_3$-1-*closo*-CB$_{11}$H$_8$]

Addition of excess nbd to a solution of **14** in CH_2Cl_2 affords [Rh(PPh$_3$)$_2$(nbd)][1-Me-9,11,12-(Et)$_3$-1-*closo*-CB$_{11}$H$_8$] (**15**).

The release of the cage facilitates the characterization of the anion since there is not interference from the rhodium fragment to any {BH} vertex. The $^1H\{^{11}B\}$ NMR spectrum shows a singlet for the carborane methyl group at δ 1.53 ppm and multiplets for the ethyl groups between δ 0.97 and 0.34 ppm. The existence of a smaller methyl signal at δ 1.62 ppm indicates the presence of a different functionalised cage in solution but in low concentration. Five B-H signals (from a 1:2:2:2:1 B-H pattern) are displayed between 1.66 and 1.31 ppm as broad singlets. The $^{11}B\{^1H\}$ NMR spectrum consists of seven different environments between δ -0.1 and -15.9 ppm with a ratio 1:2:1:2:2:1:2. The first two, more downfield, signals do not show coupling to ^1H in the ^{11}B NMR spectrum, being identified as B-ethyl vertices.

ESI-MS spectroscopy shows the main peak at m/z 241.0, which represents the three-fold functionalised anion (see Appendix A.5). However, this technique detects two more species at m/z 213.0 and 269.0, albeit in low concentration, due to respective formation of two and four-fold substituted cages. This agrees with the extra methyl resonance displayed in ^1H NMR spectrum. Since a four-fold substituted cage was detected, an additional reaction with ethene and hydrogen was carried out. However, it resulted only in a small increment of the *tetra*-functionalised carborane.

2.2.2.4 [Rh(PPh$_3$)$_2$(nbd)][1-(^{i}Pr$_3$Si)-9,11,12-(Et)$_3$-1-*closo*-CB$_{11}$H$_8$]

The incorporation of a bulkier substituent (Si^{i}Pr$_3$) on the cage carbon atom, sequential treatment of ethene and hydrogen three times produces the formation of a

single cage with three ethyls. Consequently, compound **13** is transformed in a compound that can be postulated as [Rh(PPh$_3$)$_2$(1-(^{i}Pr$_3$Si)-9,11,12-(Et)$_3$-1-*closo*-CB$_{11}$H$_8$)]. This complex is represented in Figure 2.31. Based in the NMR data of the nbd adduct **16** and the solid state structures obtained from X-ray diffraction studies of complexes **8** and **14**. However, full characterisation was performed on the nbd salt that is discussed next.

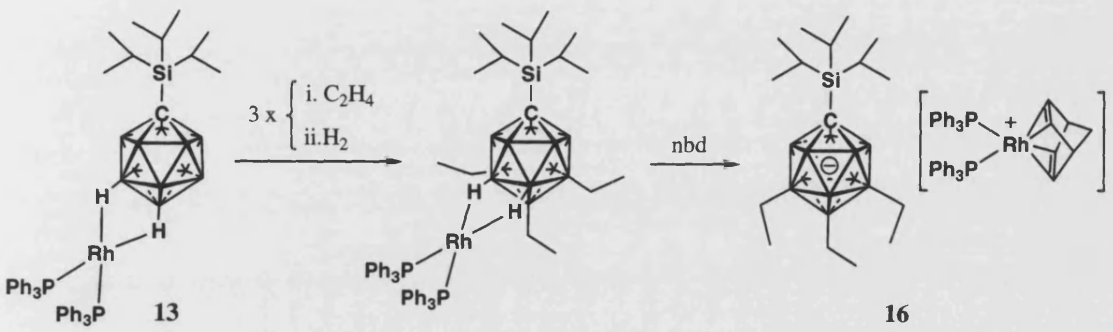

Figure 2.31 Proposed structure for [Rh(PPh$_3$)$_2$(1-(^{i}Pr$_3$Si)-9,11,12-(Et)$_3$-1-*closo*-CB$_{11}$H$_8$)].

Addition of nbd affords complex [Rh(PPh$_3$)$_2$(nbd)][1-(^{i}Pr$_3$Si)-9,11,12-(Et)$_3$-1-*closo*-CB$_{11}$H$_8$] (**16**) that has been isolated in 63% yield. In solution, ^{1}H NMR spectrum shows the characteristic resonances of the ^{i}Pr$_3$Si group at δ 1.17 and 1.10 ppm and ethyl signals as multiplets between δ 0.90-0.40 with a relative integral of 15H. The ^{11}B{^{1}H} displays a 1:2:1:2:2:3 pattern between δ 7.7 and -16.8 ppm, similar to that described for **15**. The signals at δ 7.7 and -1.4 ppm do not couple to ^{1}H in the ^{11}B NMR spectrum (Figure 2.32), thus they belong to {B-ethyl} vertices, most probably to the antipodal vertex and the substituted vertices at the lower pentagonal belt respectively. From this data it can be suggested that the substitution pattern of **16** is the same as **15**, although the exception of the most downfield signal is different in both. This difference may be caused by the antipodal effect as previously commented for other antipodal {BH} vertex resonances in **13**. The ESI-MS spectrum (Appendix A.6) shows a single peak at

m/z 383.5, whose isotopic distribution pattern is identical to the one calculated theoretically.

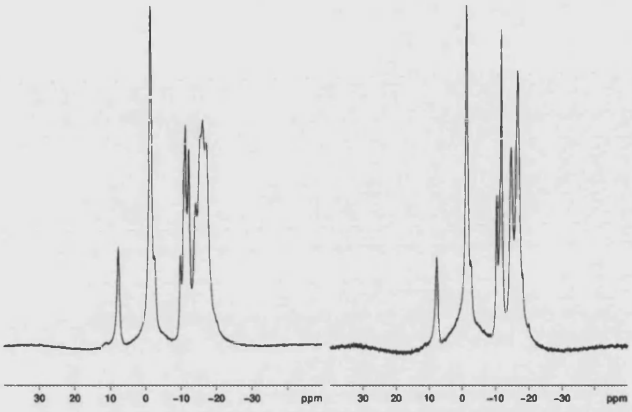

Figure 2.32 ^{11}B (left) and $^{11}B\{^{1}H\}$ NMR spectra of **16**.

The utilisation of the triisopropylsilyl group as a blocking group in order to avoid substitution on the upper pentagonal belt in [*closo*-$CB_{11}H_{12}$]$^-$ has been mentioned previously, when alkylation of the cage with MeOTf or EtOTf.[33, 38]

2.2.3 Studies on the mechanism of borylation

Rhodium-mediated dehydrogenative borylation in [*closo*-$CB_{11}H_{12}$]$^-$ occurs preferentially in the antipodal or a lower pentagonal belt vertex, as evidenced by the synthesis of **1a/b**. A simple charge distribution analysis in the [*closo*-$CB_{11}H_{12}$]$^-$ cage,[23, 24] has confirmed that the substitution sequence is favored on the most electron rich {BH} vertices, i.e. $B_{12} \approx B_{7\text{-}11} > B_{2\text{-}6}$, and this has been clearly demonstrated with cage halogenation[39] and DCl[40] reactions. This substitution pattern should be followed when multiple functionalisation of the carborane anion with the $\{Rh(PPh_3)_2\}^+$ fragment, if rhodium inserts into the most electron rich B-H bonds. The synthesis of compound **8** shows that once the lower part of the cage is sterically hindered due to two ethyl substitutions, the two upper pentagonal {BH} vertices undergo ethene insertion. Cage interactions to electrophilic metal fragments have also proved the trend in reactivity

with preferred coordination to {B_{7-12}-H} vertices.[33] The solid state structure of compound **14** confirms metal coordination to the two consecutive {BH} vertices at the lower pentagonal belt in preference to any less electron rich upper belt vertex. Hydroboration and exo-coordination to the metal fragment of the carborane [7,8-$(CH_2)_3$-*nido*-$C_2B_9H_{10}]^-$ also takes place at the most electron rich {BH} vertices, i.e. those furthest away from the cage carbon atoms.

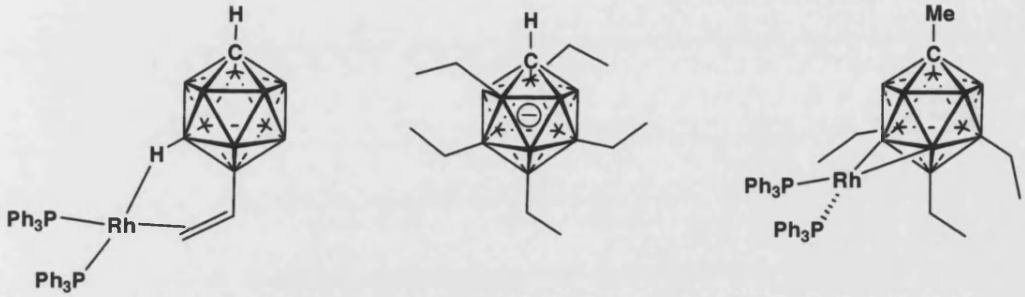

Figure 2.33 Compounds: **1a** (left), **8** (centre) and **14** (right).

Exposure of a dichloromethane solution of $Rh(PPh_3)_2$(1-X-*closo*-$CB_{11}H_{11}$) to a D_2 atmosphere (1 atm) results in gradual substitution of {BH} into {BD} vertices, as followed by $^1H\{^{11}B\}$ and ^{11}B NMR spectroscopy. B-H signals disappear from the $^1H\{^{11}B\}$ spectrum or become broad signals in the ^{11}B spectrum in the order expected from a sinple charge distribution analysis: B_{12} followed by B_{7-11} and eventually B_{2-6}, however the {CH} vertex remains undeuterated. HD (g) [1:1:1 triplet at δ 4.59, *J*(DH) 43 Hz] followed by H_2 (g) [singlet at δ 4.62 ppm] is also observed. This suggests an H/D exchange mechanism that implies the coordination of a molecule of deuterium to a putative rhodium-boryl species such as **M** (Figure 2.34), and closely related to [Rh(H)(B-cat)$(PR_3)_2(\eta^2$-CH_2=CHR')] (Figure 2.4, left). Similar mechanisms, involving metal-boryl intermediates, have been suggested in analogous deuterium experiments for *closo*-$C_2B_{10}H_{12}$ with ruthenium and iridium complexes,[15] or for the *exo*-[$Rh(PPh_3)_2$(7,8-R,R'-*nido*-$C_2B_9H_{10}$)].[16]

Compound **8**, as commented in section 2.2.1.7, undergoes deuterium exchange in all remaining {BH} vertices catalysed by the $\{Rh(PPh_3)_2\}^+$ fragment, although no further ethene insertion is possible. Probably, ethene coordination and/or migratory insertion of ethene into the putative rhodium-boryl species is blocked with increasing cage substitution.

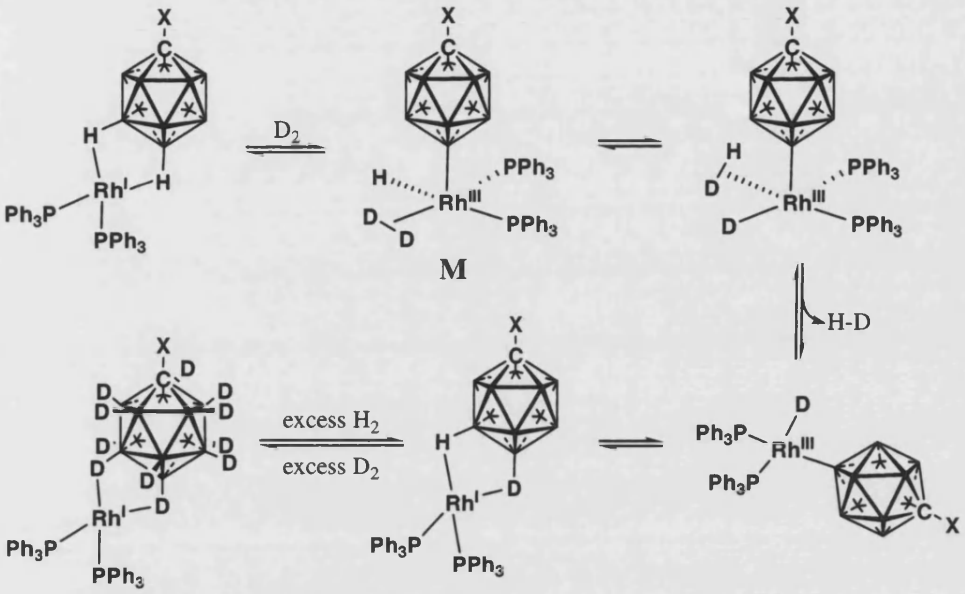

Figure 2.34 Proposed H/D exchange mechanism catalysed by the $[Rh(PPh_3)_2]^+$ fragment

2.2.3.1 $[Rh(PPh_3)_2(\eta^2\text{-}C_2H_4)_3][closo\text{-}CB_{11}H_{12}]$ and $[Rh(PPh_3)_2(\eta^2\text{-}C_2H_4)_3][closo\text{-}CB_{11}H_6Br_6]$

In an attempt to detect the postulated rhodium-boryl species, low temperature $^{31}P\{^1H\}$ and ^{11}B NMR experiments were performed for the reaction of **I** with ethene. In order to avoid immediate dehydrogenative borylation, ethene was added to a pre-cooled solution of **I** (red) at 200 K to produce a yellow solution, suggesting the presence of a new species. The experiment was monitored by NMR spectroscopy between 200 K and 298 K.

Only one species was observed in the $^{31}P\{^{1}H\}$ NMR spectrum between 200 K and 230 K, as a doublet at δ 35.5 [*J*(RhP) 93 Hz]. The ^{11}B NMR spectrum shows only three resonances as doublets with a 1:5:5 pattern characteristic of free [*closo*-$CB_{11}H_{12}]^-$; no downfield or upfield peaks that would be indicative of metal-boryl or Rh-H-B interactions respectively were observed.[41, 42] All this suggests that the cage is not interacting with the metal centre. Corroboration of this fact was obtained by changing to a more weakly coordinating anion such as $[BAr^F_4]^-$ and [*closo*-$CB_{11}H_6Br_6]^-$ which gives identical spectra for the metal fragment. Thus, addition of ethene to a solution of $[Rh(PPh_3)\{(\eta^6\text{-}C_6H_5)PPh_2\}]_2[BAr^F_4]_2$ or $[Rh(PPh_3)\{(\eta^6\text{-}C_6H_5)PPh_2\}]_2$[*closo*-$CB_{11}H_6Br_6]_2$ affords the formation of the same species detected previously by $^{31}P\{^{1}H\}$ NMR spectroscopy, with the same chemical shift and coupling constant value. These complexes have been characterised as the *tris*-ethene species *trans*-$[Rh(PPh_3)_2(\eta^2\text{-}C_2H_4)_3][Y]$, Y = [*closo*-$CB_{11}H_{12}]^-$, $[BAr^F_4]^-$ and [*closo*-$CB_{11}H_6Br_6]^-$. A related compound, $[Rh(PMe_3)_2(\eta^2\text{-}C_2H_4)_3][PF_6]$, has been characterised in solution by NMR spectroscopy.[43]

On warming the solution, the complex $[Rh(PPh_3)_2(\eta^2\text{-}C_2H_4)_3]$[*closo*-$CB_{11}H_{12}]$ (**17**) disappears gradually to give way to complex **I**, which is the major species at 273 K (Figure 2.35). The same low-temperature spectrum is obtained by cooling the solution again to 230 K, suggestive of a dynamic equilibrium. Once room temperature is reached, dehydrogenative borylation commences, and signals due to **1a/b** are observed.

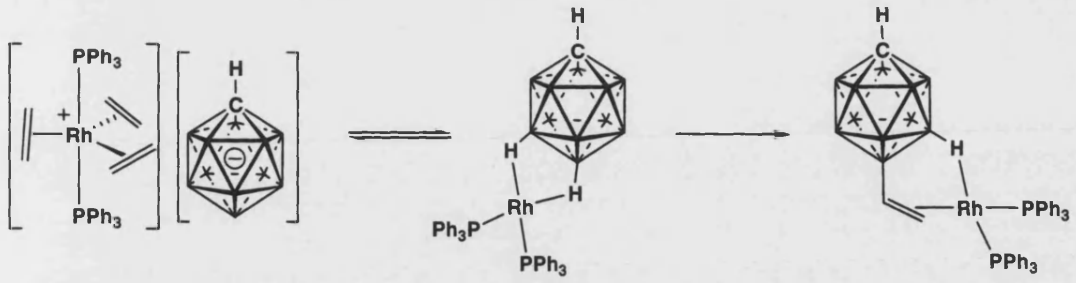

213 K 253 K 293 K

Figure 2.35 Complexes detected by reaction of **I** with ethene.

Crystals of the complex $[Rh(PPh_3)_2(\eta^2\text{-}C_2H_4)_3][closo\text{-}CB_{11}H_6Br_6]$ (**18**) suitable for X-ray crystallography were grown from a cooled solution at -78 °C under an atmosphere of ethene. Compound **18** starts losing ethene rapidly when removed from an ethene atmosphere above -20 °C in solution, therefore, crystals had to be mounted quickly on a pre-cooled diffractometer. The solid-state structure is shown in Figure 2.36. The cationic portion of complex **18** displays a trigonal bipyramidal structure in which the ethene ligands are arranged equatorially, adopting a geometry as expected from steric and electronic arguments.[44] The structure is analogous to the more thermally stable complex $[Ir(PPh_3)_2(\eta^2\text{-}C_2H_4)_3][closo\text{-}CB_{11}H_6Br_6]$,[20] and is similar to the acetonitrile complex $[Rh(NCMe)_2(\eta^2\text{-}C_2H_4)_3][BF_4]$.[45]

The C-C distances in the ethene ligand [1.362(7) - 1.375(7)] are slightly longer than for free ethene [*d*(CC) 1.337 Å] due to σ-donation from the ethene and little Rh→C back donation from the cationic rhodium fragment. The Rh-C_{ethene} distances [2.246(4) - 2.287(4) Å] are very similar to those found for the iridium analogue complex $[Ir(PPh_3)_2(\eta^2\text{-}C_2H_4)_3][closo\text{-}CB_{11}H_6Br_6]$ [2.220(8) - 2.273(9) Å]. Both complexes also show comparable bond distances for the *trans* phosphine ligands: Rh-P [2.3770(11), 2.3864(11)], Ir-P [2.370(2), 2.379(2)].[20, 30]

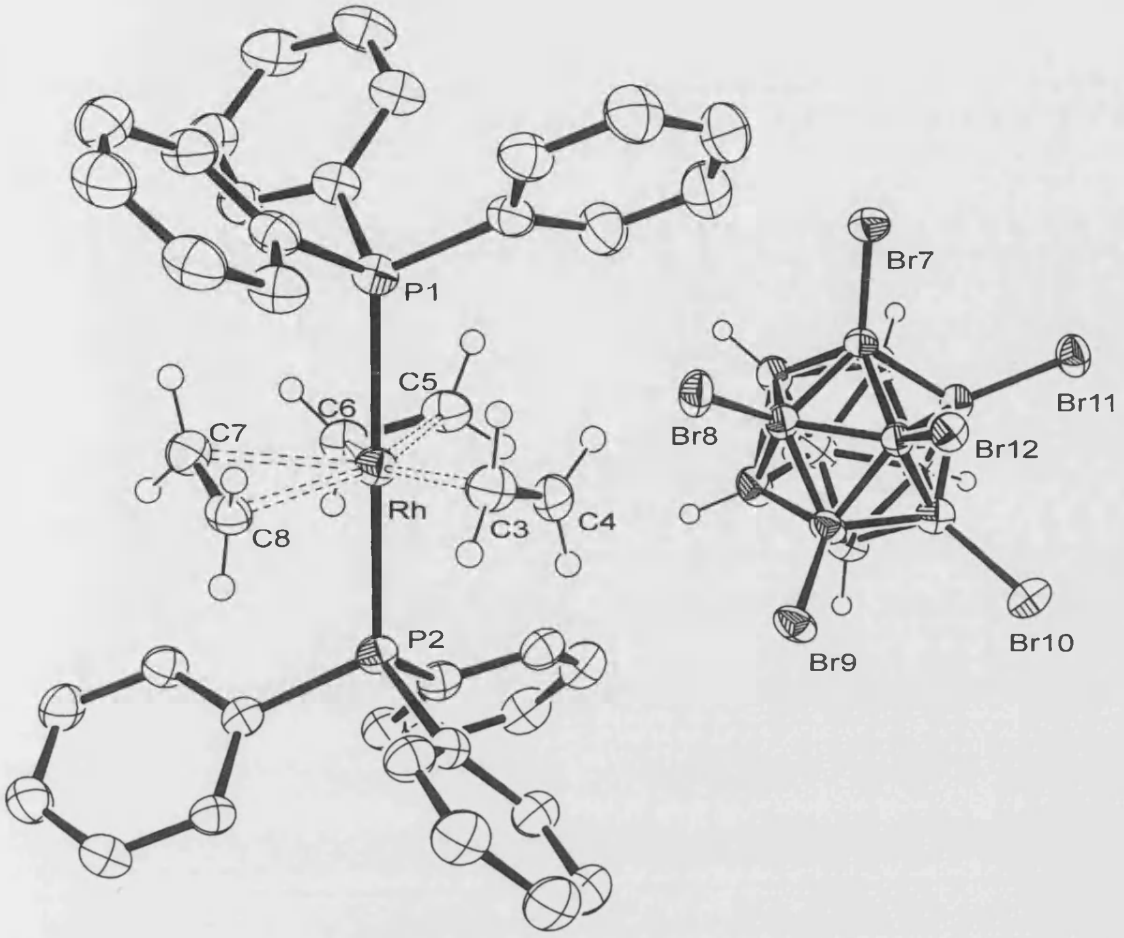

Figure 2.36 Solid-state structure of complex **18**. Thermal ellipsoids are shown at the 50% probability level. Hydrogen atoms on the phenyl groups have been omitted for clarity.

Rh-P(1)	2.3770(11)	Rh-C(7)	2.274(5)
Rh-P(2)	2.3864(11)	Rh-C(8)	2.252(4)
Rh-C(3)	2.246(4)	C(3)-C(4)	1.375(7)
Rh-C(4)	2.249(5)	C(5)-C(6)	1.362(7)
Rh-C(5)	2.273(4)	C(7)-C(8)	1.375(7)
Rh-C(6)	2.287(4)	P(1)-Rh-P(2)	178.13(4)

Table 2.11 Selected bond lengths and angle

A related complex to **17** and **18** has been prepared by replacement of a weakly coordinated carborane with carbonyls before: $Rh(PPh_3)_2(7,8\text{-}R_2\text{-}nido\text{-}C_2B_9H_{10})$ reacts with CO to afford $[Rh(PPh_3)_2(CO)_3][7,8\text{-}R_2\text{-}nido\text{-}C_2B_9H_{10}]$, (R = alkyl, Ph).[46]

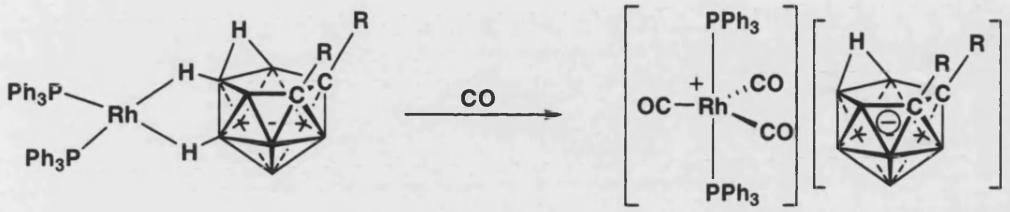

Figure 2.37 Formation of complex $[Rh(PPh_3)_2(CO)_3][7,8\text{-}R_2\text{-}nido\text{-}C_2B_9H_{10}]$.[46]

2.3 Conclusions

Ethylation of [1-X-*closo*-$CB_{11}H_{11}$]$^-$ (X = H, Me, $^iPr_3Si$) by a bisphosphine-rhodium fragment has been shown to be an effective route *via* dehydrogenative borylation / hydrogenation of ethene. A maximum of five ethyl groups on the [*closo*-$CB_{11}H_{12}$]$^-$ cage, and three on the [1-Me-*closo*-$CB_{11}H_{11}$]$^-$ and [1-$^iPr_3Si$-*closo*-$CB_{11}H_{11}$]$^-$ cages, has been achieved. The metallic fragment becomes reluctant to undergo further borylation due to the increasingly bulky ethyl substituted carboranes. In addition, the formation of a B-vinyl group in the first instance blocks the metal, upon coordination, not allowing the system to perform catalytically.

2.4 Bibliography

1 R. Wilczynski and L. G. Sneddon, *Inorg. Chem.*, 1981, **20**, 3955.
2 T. Davan, E. W. Corcoran, and L. G. Sneddon, *Organometallics*, 1983, **2**, 1693.
3 M. J. Pender, P. J. Carroll, and L. G. Sneddon, *J. Am. Chem. Soc.*, 2001, **123**, 12222.
4 D. E. Kadlecek, P. J. Carroll, and L. G. Sneddon, *J. Am. Chem. Soc.*, 2000, **122**, 10868.
5 J. D. Hewes, C. W. Kreimendahl, T. B. Marder, and M. F. Hawthorne, *J. Am. Chem. Soc.*, 1984, **106**, 5757.
6 S. W. Du, D. D. Ellis, P. A. Jelliss, J. A. Kautz, J. M. Malget, and F. G. A. Stone, *Organometallics*, 2000, **19**, 1983.
7 H. Nöth and G. Schmid, *Angew. Chem.-Int. Edit. Engl.*, 1963, **2**, 623.
8 G. Schmid, *Angew. Chem.-Int. Edit. Engl.*, 1970, **9**, 819.
9 G. J. Irvine, M. J. G. Lesley, T. B. Marder, N. C. Norman, C. R. Rice, E. G. Robins, W. R. Roper, G. R. Whittell, and L. J. Wright, *Chem. Rev.*, 1998, **98**, 2685.
10 J. M. Brown, *Modern Rhodium-Catalyzed Organic Reactions*, 2005, 33.
11 D. Mannig and H. Noth, *Angew. Chem.-Int. Edit. Engl.*, 1985, **24**, 878.
12 K. Burgess, W. A. Vanderdonk, S. A. Westcott, T. B. Marder, R. T. Baker, and J. C. Calabrese, *J. Am. Chem. Soc.*, 1992, **114**, 9350.
13 E. L. Hoel and M. F. Hawthorne, *J. Am. Chem. Soc.*, 1973, **95**, 2712.
14 M. Herberhold, H. Yan, W. Milius, and B. Wrackmeyer, *J. Organomet. Chem.*, 2000, **604**, 170.
15 E. L. Hoel, M. Talebinasabsavari, and M. F. Hawthorne, *J. Am. Chem. Soc.*, 1977, **99**, 4356.
16 P. E. Behnken, J. A. Belmont, D. C. Busby, M. S. Delaney, R. E. King, C. W. Kreimendahl, T. B. Marder, J. J. Wilczynski, and M. F. Hawthorne, *J. Am. Chem. Soc.*, 1984, **106**, 3011.
17 J. F. Hartwig and C. N. Muhoro, *Organometallics*, 2000, **19**, 30.
18 A. Rifat, N. J. Patmore, M. F. Mahon, and A. S. Weller, *Organometallics*, 2002, **21**, 2856.
19 A. Rifat, V. E. Laing, G. Kociok-Kohn, M. F. Mahon, G. D. Ruggiero, and A. S. Weller, *J. Organomet. Chem.*, 2003, **680**, 127.
20 A. Rifat, G. Kociok-Köhn, J. W. Steed, and A. S. Weller, *Organometallics*, 2004, **23**, 428.
21 A. T. Lynch and L. G. Sneddon, *J. Am. Chem. Soc.*, 1989, **111**, 6201.
22 R. B. Coapes, F. E. S. Souza, R. L. Thomas, J. J. Hall, and T. B. Marder, *Chem. Commun.*, 2003, 614.
23 I. Zharov, T. C. Weng, A. M. Orendt, D. H. Barich, J. Penner-Hahn, D. M. Grant, Z. Havlas, and J. Michi, *J. Am. Chem. Soc.*, 2004, **126**, 12033.
24 M. L. McKee, *J. Am. Chem. Soc.*, 1997, **119**, 4220.
25 L. I. Zakharkin, A. I. Kovredov, and V. A. Ol'shevskaya, *Izv. Akad. Nauk SSSR, Ser. Khim.*, 1985, 888.
26 J. M. Russell, M. Sabat, and R. N. Grimes, *Organometallics*, 2002, **21**, 4113.
27 V. N. Kalinin, N. I. Kobelkova, and L. I. Zakharkin, *Zh. Obshch. Khim.* , 1977, **47**, 963.
28 B. T. King, Z. Janousek, B. Gruner, M. Trammell, B. C. Noll, and J. Michl, *J. Am. Chem. Soc.*, 1996, **118**, 3313.
29 A. J. Clarke, M. J. Ingleson, G. Kociok-Kohn, M. F. Mahon, N. J. Patmore, J. P. Rourke, G. D. Ruggiero, and A. S. Weller, *J. Am. Chem. Soc.*, 2004, **126**, 1503.
30 A. Rifat, University of Bath, Bath, PhD Thesis 2003.
31 N. J. Patmore, M. J. Ingleson, M. F. Mahon, and A. S. Weller, *Dalton Trans.*, 2003, 2894.
32 M. J. Ingleson, M. F. Mahon, and A. S. Weller, *Chem. Commun.*, 2004, 2398.
33 S. Körbe, P. J. Schreiber, and J. Michl, *Chem. Rev.*, 2006, **106**, 5208
34 T. Jelinek, P. Baldwin, W. R. Scheidt, and C. A. Reed, *Inorg. Chem.*, 1993, **32**, 1982.
35 S. Hermanek, *Chem. Rev.*, 1992, **92**, 325.

[36] A. Miyashita, A. Yasuda, H. Takaya, K. Toriumi, T. Ito, T. Souchi, and R. Noyori, *J. Am. Chem. Soc.*, 1980, **102**, 7932.
[37] A. S. Weller, M. F. Mahon, and J. W. Steed, *J. Organomet. Chem.*, 2000, **614**, 113.
[38] B. T. King, I. Zharov, and J. Michl, *Chemical Innovation*, 2001, **2001**, 23.
[39] T. Jelinek, J. Plesek, S. Hermanek, and B. Stibr, *Collect. Czech. Chem. Commun.*, 1986, **51**, 819.
[40] T. Jelinek, J. Plesek, F. Mares, S. Hermanek, and B. Stibr, *Polyhedron*, 1987, **6**, 1981.
[41] N. P. Rath and T. P. Fehlner, *J. Am. Chem. Soc.*, 1987, **109**, 5273.
[42] S. Aldridge and D. L. Coombs, *Coord. Chem. Rev.*, 2004, **248**, 535.
[43] H. Werner and R. Feser, *Z. Naturforsch., B: Chem. Sci.* , 1980, **35**, 689.
[44] T. A. Albright, J. K. Burdett, and M. H. Whangbo, 'Orbital Interactions in Chemistry', Wiley, 1985.
[45] F. Maspero, Simonett.F, and E. Perrotti, *J. Organomet. Chem.*, 1972, **38**, C43.
[46] J. A. Long, T. B. Marder, P. E. Behnken, and M. F. Hawthorne, *J. Am. Chem. Soc.*, 1984, **106**, 2979.

Chapter 3. Monophosphine rhodium complexes partnered with [*closo*-$CB_{11}H_{12}]^-$

3.1 Introduction

As outlined in the Introduction Chapter, the mechanism proposed by Hawthorne for the butylacrylate functionalisation of the [*nido*-7,8-μ-$(CH_2)_3$-7,8-$C_2B_9H_{10}]^-$ with the $\{Rh(PPh_3)_2\}^+$ fragment suggests the dissociation of one triphenylphosphine ligand to generate monophophine-*exo*-*nido*-rhodacarborane intermediate species, as Figure 3.1 shows. Thus, a monophosphine complex is the catalytically active species in hydroboration.[1]

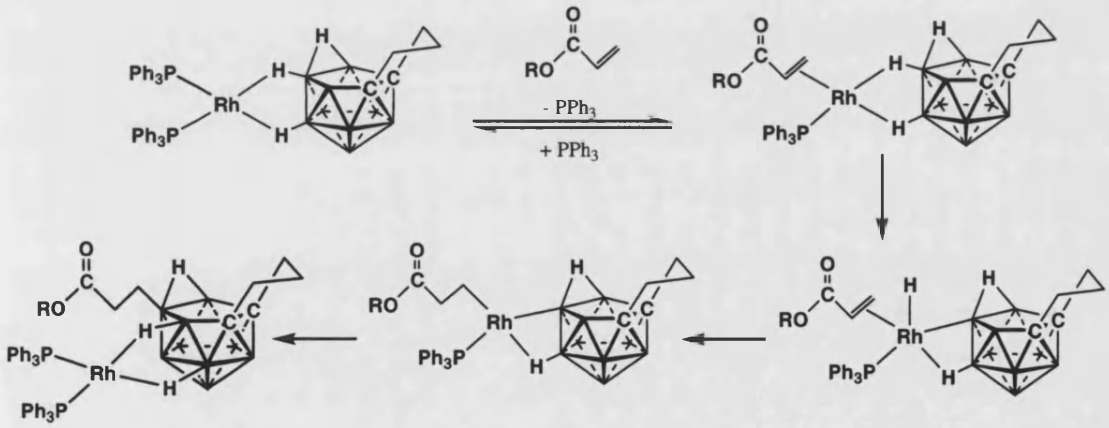

Figure 3.1 Intermediate species proposed in the hydroboration of [7,8-μ-$(CH_2)_3$-7,8-*nido*-$C_2B_9H_{10}]^-$.[1]

Hawthorne et al. also noted in alkene hydrogenation with rhodacarborane complexes that higher triphenylphosphine concentrations in solution decrease the rate of alkene hydrogenation.[2] This is consistent with a mechanism that involves phosphine dissociation. This observation led to the synthesis of the more active hydride-olefin-rhodacarborane complex [*closo*-1,3-μ-(η^2-3,4-CH_2=$CHCH_2CH_2$)-3-H-3-PPh_3-3,1,2-$RhC_2B_9H_{10}$] (Figure 3.2), which bears only one triphenylphosphine ligand. Exposure of

this monophosphine complex to hydrogen gas produces very reactive species (the terminal alkene is hydrogenated) with more vacant sites, and a resulting catalyst that show impressive turnover numbers.

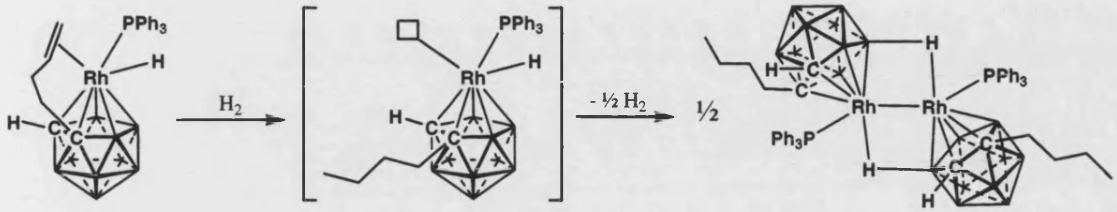

Figure 3.2[*closo*-1,3-μ-(η^2-3,4-CH_2=$CHCH_2CH_2$)-3-H-3-PPh_3-3,1,2-$RhC_2B_9H_{10}$] and suggested final product after hydrogenation of the vinyl group.[2]

In view of the fact that the more vacant sites exposed on a catalyst metal centre must result in an increase of reactivity, and considering the proposed mechanism for acrylate hydroboration with the $\{Rh(PPh_3)_2\}^+$ fragment described above, we decided to prepare monophosphine rhodium complexes stabilised by the parent [*closo*-$CB_{11}H_{12}]^-$ anion, and to screen these for olefin hydroboration. An added advantage of this approach is that sterically less bulky monophophines might allow greater substitution on the carborane anion.

3.1.1 Monophosphine rhodium complexes

Rhodium complexes bearing only one phosphine ligand are common;[3] however, our aim was the synthesis of monophosphine rhodium complexes with the weakly coordinating parent anion utilised in this thesis, i.e. [*closo*-$CB_{11}H_{12}]^-$. Rhodium monophosphine complexes stabilised by *nido*-carboranes have been reported. A phosphine disproportionation mechanism has been suggested for the synthesis of $[Rh(PR_3)(C_2B_9H_{11})]_2$ that is displayed in Figure 3.3. In this case a single bond between Rh(II)-Rh(II) is bridged by a B-H interation.[4, 5]

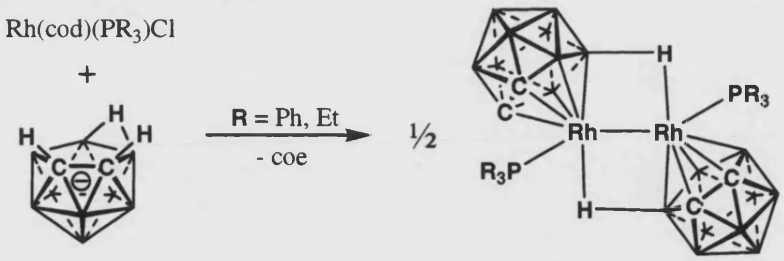

Figure 3.3 Synthesis of $[Rh(PR_3)(C_2B_9H_{11})]_2$

Hydrides and olefins are other ligands that can be easily eliminated to produce vacant sites. While olefins can also be reduced by H_2 in some rhodium complexes,[2, 6, 7] the opposite reaction has also been reported with conversion of a dihydride-metal compound into an olefin-stabilised complex shown in Figure 3.4.[8] Given this, hydride monophosphine complexes would be convenient starting materials in our case, as reaction with alkene affords an active complex that then catalyses hydroboration. The alkene would then act as both an activator and a reagent.

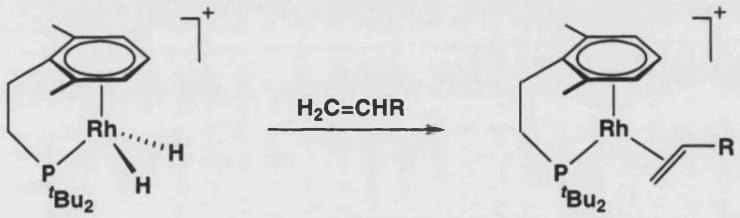

Figure 3.4

Two general strategies have been utilised previously in order to synthesise rhodium or iridium monophosphine complexes. The use of silver salts of weakly coordinating anions such as $[PF_6]^-$ or $[BF_4]^-$ in chloride-abstraction reactions (Figure 3.5),[9, 10] and the use of phosphonium salts of such anions with methoxy compounds (Figure 3.6),[7, 11, 12] leads to monophosphine metal complexes.

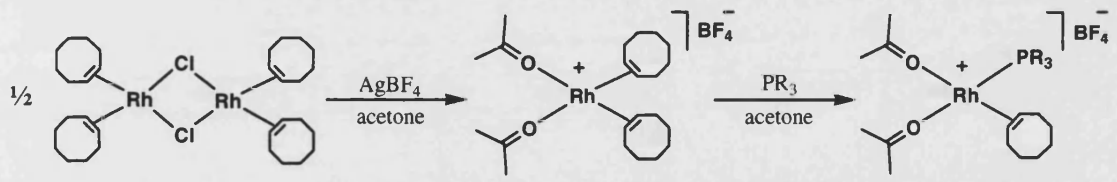

Figure 3.5 Silver-salt metathesis reaction

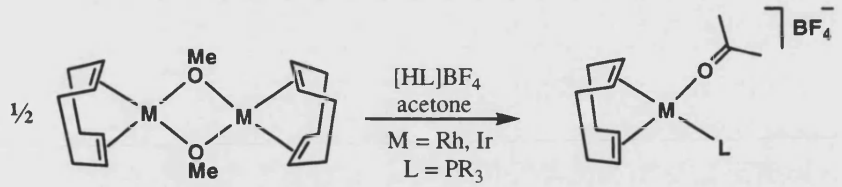

Figure 3.6 Use of phosphonium salts to obtain monophosphine compounds

3.1.2 Scope of the chapter

Monophosphine rhodium complexes are believed to be key intermediates in rhodium catalysed hydrogenation and hydroboration reactions. It is suggested that this is due to the presence of more vacant sites in these intermediates. The literature documents a range of group 9 monophosphine complexes with hydrides or olefin ligands that may favour the formation of vacant sites on their removal.

This chapter will describe the formation of rhodium species with only one phosphine ligand partnered with the [*closo*-$CB_{11}H_{12}$]$^-$ carborane anion, as well as their phosphonium salt precursors. These complexes lead to the formation of rhodium dimers that also confirm the existence of the putative Rh-boryl intermediate species in hydroboration reactions on [*closo*-$CB_{11}H_{12}$]$^-$ suggested in Chapter 2. These new complexes will be shown to be active in dehydrogenative borylation of alkenes.

3.2 Results and discussion

Both synthetic procedures outlined in Figure 3.5 and Figure 3.6 were tested in order to prepare monophosphine rhodium complexes partnered with the weakly coordinating [*closo*-$CB_{11}H_{12}$]$^-$ carborane anion. The silver metathesis reaction of [Rh(μ-Cl)(coe)$_2$]$_2$ with Ag[*closo*-$CB_{11}H_{12}$] was unsuccessful, probably due to the weak nucleophilic nature of the anion. However, the reaction of the phosphonium salt of the carborane [HPR_3][*closo*-$CB_{11}H_{12}$] (R = Cy, Cyp, ^{i}Pr) with the methoxy-bridged rhodium dimer

$[Rh(\mu\text{-}OMe)(nbd)]_2$ under H_2 proved to be a valid route to the formation of monophosphine rhodium complexes.

3.2.1 Synthesis of phosphonium salt precursors of [*closo*-$CB_{11}H_{12}]^-$

Treatment of a solution of phosphine in diethyl ether with acid carborane, $[(H(OEt)_x)(closo\text{-}CB_{11}H_{12})]$, leads to the formation of the desired carborane complexes of general formula $[HPR_3][closo\text{-}CB_{11}H_{12}]$.

3.2.1.1 $[HPCy_3][closo\text{-}CB_{11}H_{12}]$

$[(H(OEt)_x)(closo\text{-}CB_{11}H_{12})]$ can be prepared as described in the literature, as indicated in Equation 3.1.[13] The carborane acid is extracted with ether and consequently separated from the CsCl formed that remains in the aqueous phase.

$$Cs[closo\text{-}CB_{11}H_{12}] \xrightarrow[\text{ii. + HCl (pH = 1)}]{\text{i. water/ether 15:1}} [(H(OEt_2)_x)(closo\text{-}CB_{11}H_{12})] + CsCl$$

Equation 3.1

As Equation 3.2 indicates, addition of the carborane acid to the PCy_3 solution provokes the immediate precipitation of $[HPCy_3][closo\text{-}CB_{11}H_{12}]$ (**19**) as a white solid.

$$[(H(OEt_2)_x)(closo\text{-}CB_{11}H_{12})] + PCy_3 \xrightarrow{\text{ether}} [HPCy_3][closo\text{-}CB_{11}H_{12}]$$

Equation 3.2

The ^1H NMR spectrum of a solution of **19** in CD_2Cl_2 at room temperature displays a doublet of multiplets at δ 5.32 ppm with an H-P coupling constant of 448 Hz, which is characteristic of a P-H hydrogen. The cyclohexyl protons are observed as multiplets at δ 2.42 ppm and between 1.98-1.25 ppm. The C-H cage resonance appears at δ 2.31 ppm, characteristic of a free cage as demonstrated in Chapter 2 (Tables 2.3 &

2.9). The signals obtained in the ^{11}B and $^{1}H\{^{11}B\}$ NMR spectra for the {BH} vertices are also similar to those reported previously for a free cage without cation-anion interaction. The $^{31}P\{^{1}H\}$ NMR spectrum displays a singlet at δ 31.6 ppm, which is consistent with that reported for the similar $[HPCy_3][BF_4]$ salt.[11]

3.2.1.2 [HPCyp$_3$][*closo*-CB$_{11}$H$_{12}$]

The same synthetic procedure for $[HPCy_3][closo\text{-}CB_{11}H_{12}]$ (**19**) was employed for the synthesis of $[HPCyp_3][closo\text{-}CB_{11}H_{12}]$ (**20**).

The $^{1}H\{^{11}B\}$ NMR spectrum displays a doublet of multiplets at δ 5.90 ppm with a coupling constant value of *J*(PH) 455.0 Hz, three series of multiplets at δ 2.56, 2.22 and 1.81 ppm for the alkyl protons of the cyclopentyl groups, and two BH resonances at δ 1.64 and 1.46 ppm. According to integral values, the cage CH signal is under the multiplet displayed at δ 2.22 ppm and not observed. The $^{31}P\{^{1}H\}$ NMR spectrum shows a singlet at δ 34.0 ppm.

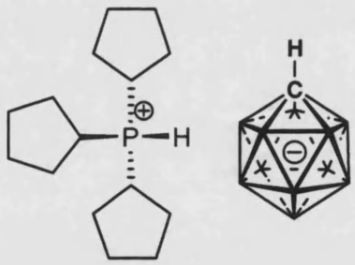

Figure 3.7 $[HPCyp_3][closo\text{-}CB_{11}H_{12}]$ (**20**)

3.2.1.3 [HP^{i}Pr$_3$][*closo*-CB$_{11}$H$_{12}$]

The $^{1}H\{^{11}B\}$ NMR spectrum of $[HP^{i}Pr_3][closo\text{-}CB_{11}H_{12}]$ (**21**) shows a doublet of multiplets at δ 5.65 ppm with a coupling constant value of 452.8 Hz. The cage C-H resonance is displayed at δ 2.33 ppm. Isopropyl signals appear at δ 2.75 for the C*H*

protons as a overlapped doublet of septets. A doublet of doublets at δ 1.48 is observed for CH_3 groups with coupling constants of *J*(PH) 17.8, *J*(HH) 7.6 Hz, which are almost equal to those reported for $[HP^iPr_3][BF_4]$.[12] Proton resonances for {BH} vertices are shown at δ 1.64, 1.58 and 1.48 ppm in a 5:1:5 ratio respectively. As expected, the ^{11}B NMR spectrum shows the same signals with similar chemical shifts when compared to the spectra obtained from compounds **19** and **20**. The $^{31}P\{^1H\}$ spectrum shows one singlet at δ 43.2 ppm.

The following table resumes the data obtained for compounds **19**, **20** and **21**.

Compound	^1H NMR P*H*	*J*(PH)	C*H* cage	^{11}B NMR	$^{31}P(^1H)$
19	5.32	448	2.31	-7.23, -13.45, -16.18	31.6
20	5.90	455	~ 2.22	-6.33, -12.58, -15.31	34.0
21	5.65	453	2.33	-7.16, -13.36, -16.07	43.2

Table 3.1 NMR data from CD_2Cl_2 solutions. δ in ppm, *J* in Hz.

3.2.2 Synthesis of $[Rh(PR_3)(H)_2(closo\text{-}CB_{11}H_{12})]$

Figure 3.8 shows that reaction of $[Rh(\mu\text{-}OMe)(nbd)]_2$ with phosphonium salts of general formula $[HPR_3][closo\text{-}CB_{11}H_{12}]$ (R = Cy, Cyp, ^{i}Pr) and hydrogen leads to the formation of a new series of monophosphine rhodium complexes. The reaction proceeds cleanly in C_6H_5F, but not in dichloromethane. However, the complexes are stable in CH_2Cl_2 once formed.

These complexes are also available from reaction of complexes **25**, **26** and **27** with H_2 in CH_2Cl_2 as reported later. For the purposes of characterisation of pure material, compounds **22**, **23** and **24** are best produced by this method.

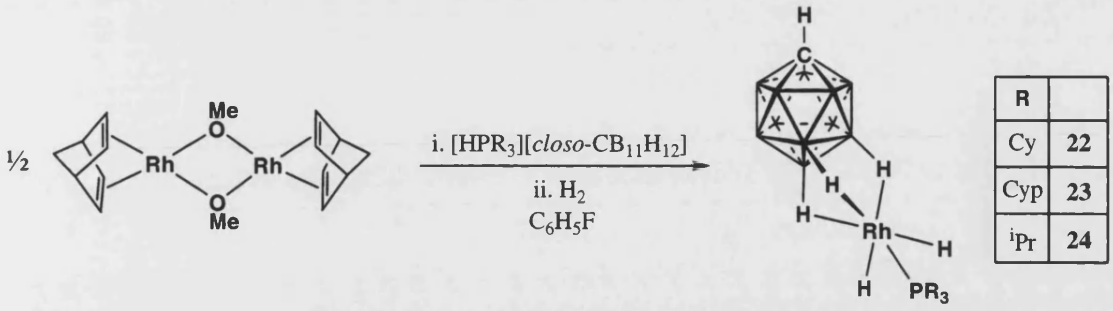

R	
Cy	**22**
Cyp	**23**
^{i}Pr	**24**

Figure 3.8 Schematic synthesis of $[Rh(PR_3)(H)_2(closo\text{-}CB_{11}H_{12})]$; R = Cy (**22**), Cyp (**23**), $^{i}Pr_3$ (**24**)

The initial yellow solution of the $[Rh(\mu\text{-}OMe)(nbd)]_2$ complex turns orange after the addition of the phosphonium salt to form an unidentified compound that decomposes slowly in solutions of dichloromethane or fluorobenzene. This compound is suggested to be a monophosphine-diene-rhodium complex with a molecule of methanol (formed in the reaction) coordinated to the metallic fragment (see Figure 3.9). Another possibility could be the formation of a formal 16 electron rhodium complex with one {BH} vertex coordinated. Addition of H_2 to this solution forms the final products **22**, **23** and **24**. We suggest the most likely formulation of the complex is one with methanol coordinated.

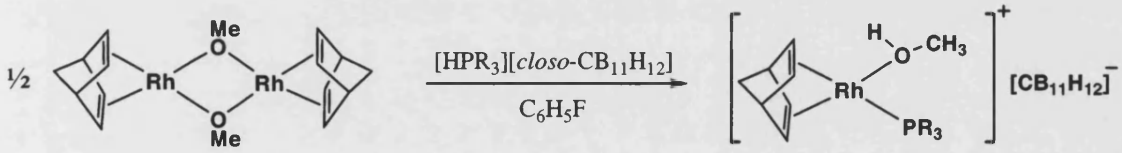

Figure 3.9

Rhodium complexes where a molecule of methanol is coordinated to the metal centre are common,[14-17] and similar diene rhodium complexes to that proposed in Figure 3.9 have been isolated and characterised, e.g. with an amino alcohol ligand[18] (Figure 3.10, left) or with a chelate phosphine (Figure 3.10, right).[7]

Figure 3.10

3.2.2.1 [Rh(PCy$_3$)(H)$_2$(*closo*-CB$_{11}$H$_{12}$)]

Slow addition of a fluorobenzene solution of [HPCy$_3$][*closo*-CB$_{11}$H$_{12}$] to a yellow solution of [Rh(μ-OMe)(nbd)]$_2$ affords an orange solution of the proposed intermediate [Rh(nbd)(PCy$_3$)(MeOH)]. The atmosphere of argon is changed to hydrogen to give, after filtration, a pale brown solution of [Rh(PCy$_3$)(H)$_2$(*closo*-CB$_{11}$H$_{12}$)] (**22**). Compound **22** was characterised exclusively by NMR spectroscopy, since in solution, it loses hydrogen on evaporating solvent. This compound is also accessible if a solution of complex **25** is placed under a H_2 atmosphere (*vide infra*).

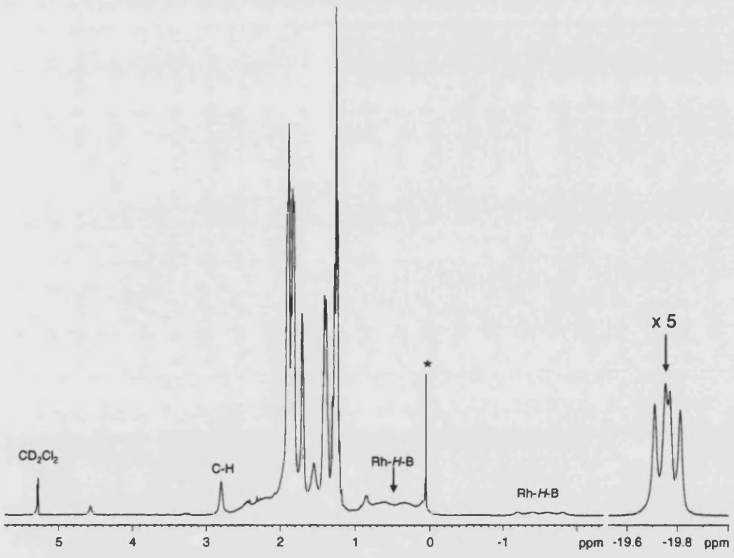

Figure 3.11 ^{1}H NMR spectrum in CD_2Cl_2 of **22** (*grease)

The solution of **22** under hydrogen atmosphere (1 atm) in CD_2Cl_2 at room temperature shows in the ^{1}H NMR spectrum (Figure 3.11) a doublet of doublets at δ -19.76 ppm with a Rh-H coupling constant of 30.5 Hz and a P-H coupling constant of 21.5 Hz, which indicates the presence of two hydrides *cis* to a phosphine ligand. The

coupling constant *J*(RhH) was measured using a selective decoupling $^{1}H\{^{31}P\}$ NMR experiment in which a single doublet [*J*(RhH) 30.5 Hz] was observed. The cage C-H resonance appears at δ 2.79 ppm and two broad {BH} quartets are observed at δ 0.47 and -1.51 ppm in a 5:1 relative integral ratio. These chemical shifts indicate that the [*closo*-$CB_{11}H_{12}]^-$ carborane cage is now bound to the rhodium fragment, by the observation that: the C-H resonance has been shifted downfield and {BH} vertices involved in Rh-H-B interaction are shifted to higher field compared with free anion. This is also demonstrated by the observation in the $^{1}H\{^{11}B\}$ NMR spectrum of three B-H resonances at δ 2.02 (5H), 0.47 (5H) and -1.51 ppm (1H), that correspond respectively to $B_{2\text{-}6}$, $B_{7\text{-}11}$ and B_{12} {BH} vertices. The observation of dissolved H_2 at δ 4.55 ppm as a slightly broad signal, plus sharp Rh-H resonances, suggests that exchange with H_2 is slow on the NMR time-scale. However, deuterium addition experiments shows that exchange occurs on the chemical timescale (*vide infra*). A solution of **22** in fluorobenzene under hydrogen shows effectively the same ^{1}H NMR spectrum, but slightly different chemical shifts of the {BH} resonances, as Table 3.2 displays. This fact also is consistent with the more downfield values obtained in C_6H_5F solution for the 'free' [*closo*-$CB_{11}H_{12}]^-$ anion.

Compound	CH cage	$B_{2\text{-}6}$-H	$B_{7\text{-}11}$-H	B_{12}-H	δ hydrides
'free' $[CB_{11}H_{12}]^-$ in CD_2Cl_2	2.31	1.64	1.46	1.58	n/a
22 in CD_2Cl_2	2.79	2.02	0.47	-1.51	-19.76
'free' $[CB_{11}H_{12}]^-$ in C_6H_5F	2.66	2.35	2.26	2.35	n/a
22 in C_6H_5F	2.82	2.51	~1.1	-1.08	-19.65

Table 3.2 $^{1}H\{^{11}B\}$ NMR chemical shifts of **22** and [NBu][*closo*-$CB_{11}H_{12}$].

The NMR data for **22** in CD_2Cl_2 are discussed below, but broadly similar patterns and chemical shifts are observed in C_6H_5F solution. The $^{11}B\{^{1}H\}$ NMR spectrum shows

three resonances at δ -14.32, -15.16 and -16.11 ppm. A ^{11}B-^{11}B COSY NMR experiment allowed the assignment of the signals to be $\{B_{2\text{-}6}H\}$, $\{B_{7\text{-}11}H\}$ and $\{B_{12}H\}$ respectively. Therefore, the signals for the lower pentagonal belt and antipodal vertices have been shifted upfield when compared to $[HPCy_3][CB_{11}H_{12}]$, from δ -7.23 and -13.45 ppm respectively (as Figure 3.12 shows), where the carborane anion was free in solution. This upfield chemical shift change is indicative of anion coordination.[19, 20] The presence of three signals in a 5:5:1 ratio suggests a fluxional mechanism where all lower pentagonal belt protons become equivalent. This mechanism grants local C_{5v} symmetry to the cage in solution, and is discussed in more detail in section 3.2.2.2.

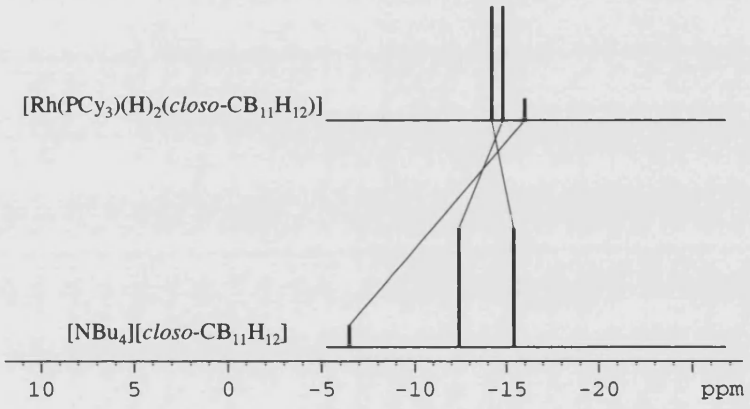

Figure 3.12 Schematic representation of the $^{11}B\{^1H\}$ NMR spectra

The $^{31}P\{^1H\}$ NMR spectrum of **22** displays a doublet at δ 86.1 ppm with a Rh-P coupling constant value of 150 Hz. These values are comparable to the chemical shifts and coupling constants reported for the similar compounds (see Figure 3.15 in section 3.2.2.3) $[Rh(^iPr_3P)(H)_2(\eta^6\text{-}C_6H_6)][PF_6]$, [δ 96.5 ppm and *J*(RhP) 142] and $[Rh(^iPr_3P)(H)_2(acetone)_3][PF_6]$, [δ 87.0 ppm and *J*(RhP) 158].[7]

3.2.2.2 $[Rh(PCyp_3)(H)_2(closo\text{-}CB_{11}H_{12})]$

In a similar way to **22**, a solution of $[Rh(PCyp_3)(H)_2(CB_{11}H_{12})]$ (**23**) can be prepared in a one-pot synthesis. Treatment of the complex $[Rh(\mu\text{-}OMe)(nbd)]_2$ with

$[HPCyp_3][CB_{11}H_{12}]$ in fluorobenzene and subsequent addition of H_2 results in the formation of complex **23** (Figure 3.13).

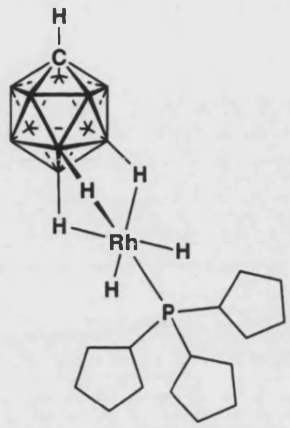

Figure 3.13 $[Rh(PCyp_3)(H)_2(CB_{11}H_{12})]$ (**23**)

Similar to compound **22**, the $^1H\{^{11}B\}$ NMR spectrum in CD_2Cl_2 of **23** under H_2 shows a downfield chemical shift change for the {CH} vertex from δ 2.22 ppm in the free cage to δ 2.80 ppm in **23**, which demonstrates that the cage is now coordinated to the rhodium fragment. This is also evident by the upfield shift of the antipodal and lower belt B-H resonances that are displayed at δ 0.43 ppm ($B_{7\text{-}11}$-H) and -1.59 ppm (B_{12}-H) as broad signals due to coupling with quadrupolar boron. Cyclopentyl resonances appear as multiplets at δ 1.74, 1.57 and 1.37 ppm. A doublet of doublets, characteristic of the hydride protons, is displayed at δ -19.19 ppm, with a Rh-H coupling constant of 29.5 Hz and a P-H coupling constant of 24.5 Hz. *J*(RhH) was determined from a $^1H\{^{31}P\}$ NMR experiment.

Three resonances are observed in the ^{11}B NMR spectrum with relative intensities 5:5:1 at δ -14.23, -15.22 and -16.44 ppm respectively, which demonstrate large upfield chemical shift changes from those shown for the free cage. This is especially the case for the antipodal {BH} vertex resonance that has been upfield shifted by Δδ 7.9 ppm. Assignment of the *B*-H resonances was made by a ^{11}B-^{11}B COSY NMR experiment,

which supports that upper, lower and antipodal resonances are displayed in that order, moving downfield to upfield, in the ^{11}B NMR spectrum. Both ^{11}B and $^{1}H\{^{11}B\}$ NMR spectra suggest local C_{5v} symmetry for the cage which means that all lower pentagonal {BH} vertices are equivalent on the NMR time-scale. Consequently a fluxional process must be occurring; a suggested process is depicted in Figure 3.14.

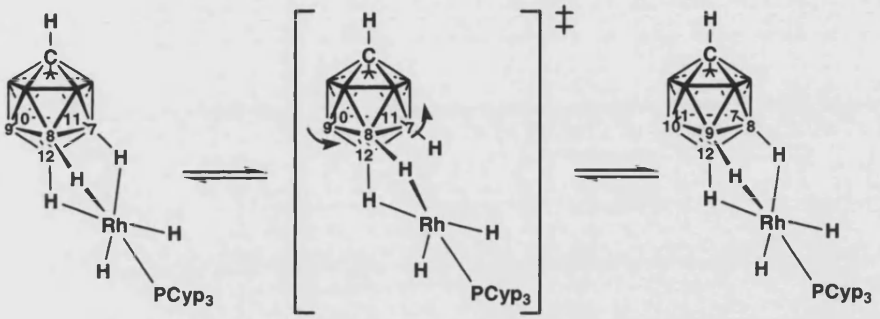

Figure 3.14 Proposed fluxional process for complex **23** in solution

The $^{31}P\{^{1}H\}$ NMR spectrum is almost the same as **22**, with a chemical shift for **23** at δ 91.1 ppm and a Rh-P coupling constant of 150 Hz.

3.2.2.3 [Rh(P^{i}Pr$_3$)(H)$_2$(*closo*-CB$_{11}$H$_{12}$)]

[Rh(P^{i}Pr$_3$)(H)$_2$(*closo*-CB$_{11}$H$_{12}$)] (**24**) can be prepared in a one-pot synthesis by treatment of the complex [Rh(μ-OMe)(nbd)]$_2$ with [HP^{i}Pr$_3$][*closo*-CB$_{11}$H$_{12}$] in fluorobenzene and subsequent addition of H_2.

A solution of **24** in CD_2Cl_2 under hydrogen (1 atm) shows broad peaks characteristic of Rh-H-B interactions at δ 0.47 ppm (for lower belt {BH} vertices) and -1.53 ppm (antipodal {BH} vertex) in the $^{1}H\{^{11}B\}$ NMR spectrum. Another broad peak is displayed at δ 2.03 ppm that is assigned to the upper belt {BH} vertices. The cage C-H proton is shown at δ 2.80 ppm and is consistent with the C-H chemical shift obtained in compounds **22** and **23**. Hydride resonances are shown as a doublet of

doublets at δ -19.54 ppm, with Rh-H coupling constant value of 29.0 Hz and a P-H coupling constant of 21.6 Hz. Isopropyl groups show as a multiplet at δ 2.03 ppm for the CH protons and a doublet of doublets at δ 1.21 ppm for CH_3 groups with a relative integral of 18 H.

The $^{11}B\{^1H\}$ NMR spectrum shows the pattern observed for complexes **22** and **23**, three resonances with a 5:5:1 ratio indicating local C_{5v} symmetry for the cage. Signals occur at δ -14.38 ppm ($B_{2\text{-}6}$), δ -15.30 ppm ($B_{7\text{-}11}$), and δ -16.52 ppm (B_{12}), which again indicates cage coordination since the resonances for the antipodal and lower belt {BH} vertices have been shifted to highfield. The largest shift is observed for the antipodal vertex with a Δδ of -9.4 ppm similar to those reported previously for **22** and **23**. The $^{31}P\{^1H\}$ NMR spectrum displays a doublet at δ 98.4 ppm with a Rh-P coupling constant value of 151.0 Hz. These values are comparable to the chemical shifts and couplings reported for complexes **22** and **23**.

The most relevant chemical shift and coupling constant values of complexes **22**, **23** and **24** are compared in Table 3.3 and also compared with **21**, $[Rh(^iPr_3P)(H)_2(\eta^6\text{-}C_6H_6)]^+$ and $[Rh(^iPr_3P)(H)_2(acetone)_3]^+$.

According to the data displayed in Table 3.3, and commented on previously in more detail, a tridentate coordination of the [*closo*-$CB_{11}H_{12}]^-$ anion can be suggested in complexes **22**, **23** and **24**. This would make the Rh(III) centre octahedrally coordinated. Also, evidence presented later for [*closo*-$CB_{11}H_6Br_6]^-$ makes tridentate ligation mode the most plausible. The presence of broad peaks at higher field values for lower pentagonal belt and antipodal {BH} vertices in complex **21**, is indicative of Rh-H-B interactions with 3-centre-2-electron bonding.

	Compound	$\delta^1H\{^{11}B\}$ NMR		^1H NMR Rh-hydrides			$^{31}P(^1H)$	
		CH cage	$B_{12}H$	δ	*J*(RhH)	*J*(PH)	δ	*J*(RhP)
21	$[HP^iPr_3][CB_{11}H_{12}]$	2.33	1.58	n/a	n/a	n/a	43.2	n/a
22	$[Rh(PCy_3)(H)_2(CB_{11}H_{12})]$	2.79	-1.51	-19.76	30.5	21.5	86.8	149.8
23	$[Rh(PCyp_3)(H)_2(CB_{11}H_{12})]$	2.80	-1.59	-19.19	29.5	24.5	91.1	149.8
24	$[Rh(P^iPr_3)(H)_2(CB_{11}H_{12})]$	2.80	-1.53	-19.54	29.0	21.6	98.4	151.0
	$[Rh(^iPr_3P)(H)_2(\eta^6\text{-}C_6H_6)]^+$ [7]	n/a	n/a	-14.54	28.1	24.1	96.5	142.5
	$[Rh(^iPr_3P)(H)_2(acetone)_3]^+$ [7]	n/a	n/a	-23.30	31.2	25.5	87.0	157.7

Table 3.3 CD_2Cl_2 solutions; δ in ppm, *J* in Hz

Tridentate coordination of borane clusters is well documented. The [*closo*-$CB_{11}H_{12}]^-$ anion shows this coordination with the $\{Ag(PPh_3)\}^+$ fragment.[21, 22] NMR studies on this system suggest a fluxional process where the metal ion moves over all triangular faces linking the antipodal vertex, as suggested for **22**, **23** and **24**. The low energy barrier from the tridentate coordination state to a bidentate mode, 12 $kJmol^{-1}$, supports a low energy fluxional process.[23] Another example of tridentate coordination was found with the $\{Cp^*Zr(Me)_2\}^+$ fragment, that also undergoes rapid migration over the triangular faces of [*closo*-$CB_{11}H_{12}]^-$ of the delimited by two lower pentagonal vertices and the antipodal vertex.[24] η^3-(B-H) coordination to metals has been reported with the stanna-*closo*-dodecaborate anion,[25, 26] and with the anionic rhenacarbaborane complex [3,3,3-$(CO)_3$-*closo*-3,1,2-$ReC_2B_9H_{11}]^-$.[27]

Similar monophosphine dihydride rhodium complexes to **22**, **23** and **24** have been prepared by Werner et al, where the carborane is substituted by 6-electron donor ligands, such as benzene, or by three 2-electron donor ligands such as acetone or acetonitrile shown in Figure 3.15.[7, 28] Oro has also reported the analogous iridium complexes.[11, 12]

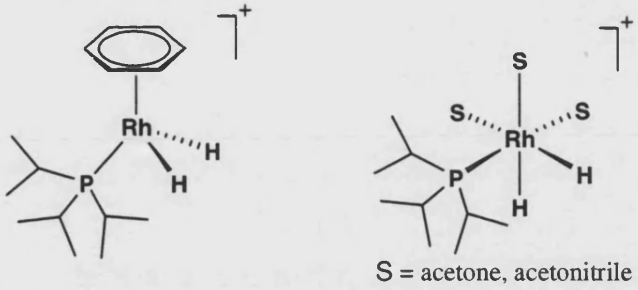

Figure 3.15

The similarities in chemical shifts and coupling constants between compounds **22**, **23** and **24**, and complexes $[Rh(^{i}Pr_3P)(H)_2(\eta^6\text{-}C_6H_6)][PF_6]$ and $[Rh(^{i}Pr_3P)(H)_2(acetone)_3][PF_6]$ (see Table 3.3) suggest that the carborane anion coordinates similarly to benzene or three acetones respectively, underscoring that three {BH} vertices are bound to the rhodium atom through 3c2e bonds.

Addition of D_2 to solutions of **22**, **23** and **24** shows the formation of HD (g) and deuteration of all {BH} vertices. Figure 3.16 shows a possible mechanism for this process, including intermediates suggested to be dihydrogen species.

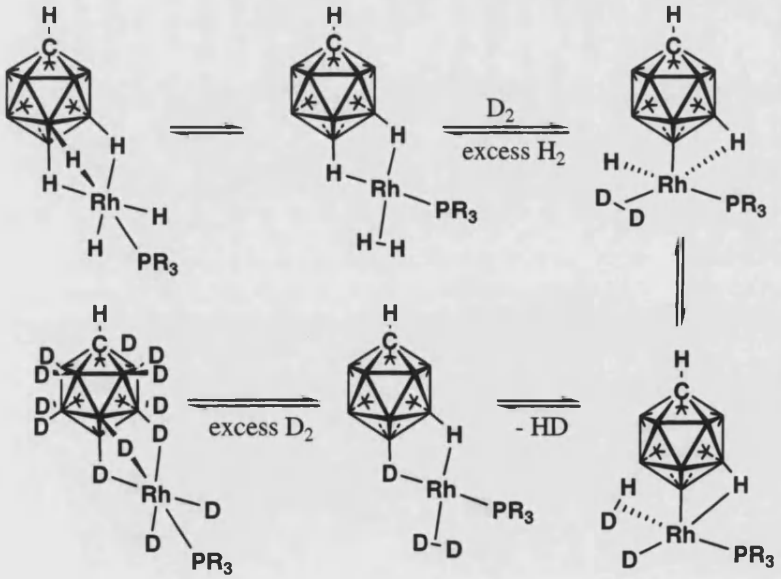

Figure 3.16

3.2.3 Monophosphine carborane rhodium dimers

While $[Rh(^{i}Pr_3P)(H)_2(\eta^6\text{-}C_6H_6)]$ can be isolated as a pale brown solid, $[Rh(^{i}Pr_3P)(H)_2(acetone)_3]$ decomposes even under an atmosphere of hydrogen.[7] Similarly, complexes **22**, **23** and **24** can be characterized only by NMR and if the solution is kept under a hydrogen atmosphere. When the solution is placed under vacuum, compounds **22**, **23** and **24** lose hydrogen and form a new and more stable set of complexes.

3.2.3.1 $[(PCy_3)(closo\text{-}CB_{11}H_{11})(H)Rh\text{-}Rh(PCy_3)(closo\text{-}CB_{11}H_{12})]$

A pale brown solution of **22** in fluorobenzene is degassed under vacuum to give a dark red solid that can be identified by NMR spectroscopy as a mixture of compound **22** and the new compound $[(PCy_3)(closo\text{-}CB_{11}H_{11})(H)Rh\text{-}Rh(PCy_3)(closo\text{-}CB_{11}H_{12})]$ (**25**). In order to obtain compound **25** as a single product, the residue needs to be dissolved in dichloromethane and evaporated to dryness twice. Complex **25** was obtained in 80 % yield.

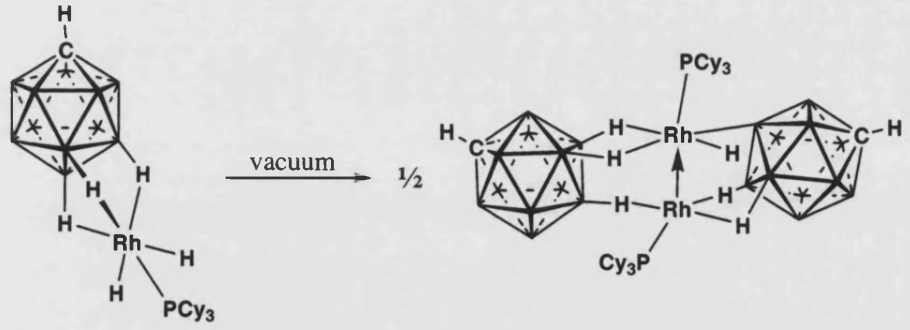

Figure 3.17 Synthesis of complex **25**

Single crystals suitable for X-ray crystallography were produced by passing a gentle flow of argon over a solution of $[(PCy_3)(closo\text{-}CB_{11}H_{11})(H)Rh\text{-}Rh(PCy_3)(closo\text{-}CB_{11}H_{12})]$ (**25**). The solid state structure is presented in Figure 3.18, with relevant bond lengths and angles in Table 3.4.

The solid-state crystal structure shows complex **25** as a dinuclear neutral complex with a single molecule of pentane in the crystal lattice. Complex **25** is formed by two rhodium atoms bridged through two [*closo*-$CB_{11}H_{12}]^-$ carborane cages with a single tricyclohexylphosphine ligand coordinated on each rhodium forming a $[Rh_2(PCy_3)_2]^{2+}$ fragment. One of the carborane anions has undergone B-H activation to form a hydride-boryl complex. Both metal centres exhibit different environments, with a potential intermetallic Rh-Rh bond separated by a distance of 2.7962(2) Å. This Rh-Rh separation is within the range of other Rh-Rh single bond complexes: e.g. 2.68 Å in $[(\eta^5\text{-}C_5H_5)_2Rh_2(CO)_3]$,[29] and 2.906 Å in $\{(\mu\text{-}Cl)(\mu\text{-}H)[(\eta^5\text{-}C_5Me_5)Rh(Cl)]_2\}$.[30, 31] The Rh-Rh distance in compound **25** is also similar to that observed in the related Rh(II)-Rh(II) rhodacarborane complex $[Rh(PPh_3)(C_2B_9H_{11})]_2$, 2.763 Å.[4] In complex **25**, considering a $\{Rh_2\}^{2+}$ fragment bridged by [*closo*-$CB_{11}H_{12}]^-$ the metal unit has 32 electrons.

Simple electron counting arguments are consistent with the formulation of a $Rh^I \rightarrow Rh^{III}$ dative bond, rather than a Rh(II)-Rh(II) complex, since this would invoke a symmetric geometry for the rhodium atoms.[32, 33] The possibility of a Rh(I)-Rh(I) dimer is unlikely because the dz^2 orbitals would be filled,[34] and consequently no covalent metal-metal bond would be possible. Complex **25** would have to be formulated as a bis boryl molecule to be considered a Rh(III)-Rh(III) dimer. This would also make the cluster have 32 electrons, but invoke a Rh=Rh double bond. The distance of 2.7962(2) Å is too long for this (e.g. less than 2.4 Å for a M=M).[32] Therefore, a $Rh^I \rightarrow Rh^{III}$ dative bond best describes the bonding in **25**. Analogous $Rh^I \rightarrow Rh^{II}$ and $Ir^I \rightarrow Ir^{III}$ dative bond have been reported in $[(COD)M(\mu\text{-form})_2M(OCOCF_3)_2(H_2O)]$, (M = Rh or Ir; form = N,N'-di-*p*-tolylformamidi-nato) [Figure 3.19 (left)].[33, 35]

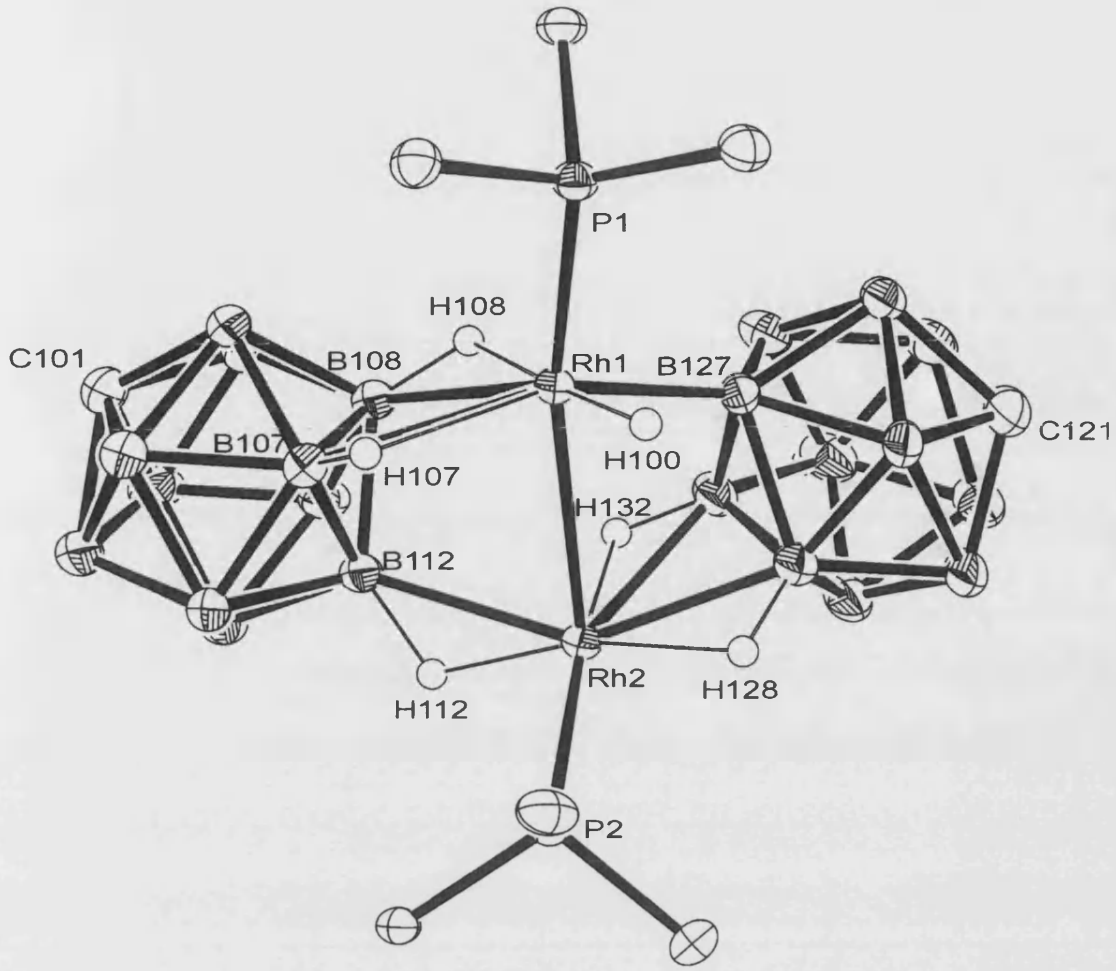

Figure 3.18 Solid-state structure of $[(PCy_3)(CB_{11}H_{11})(H)Rh\text{-}Rh(PCy_3)(CB_{11}H_{12})]$ (**25**). Thermal ellipsoids are shown at the 50% probability level. Only hydrogen atoms involved in rhodium coordination are shown. Cyclohexyl groups have been reduced to one carbon for clarity.

Rh(1)-Rh(2)	2.7962(2)	Rh(2)-P(2)	2.2572(6)
Rh(1)-P(1)	2.2324(6)	Rh(2)-B(112)	2.377(3)
Rh(1)-B(107)	2.587(3)	Rh(2)-B(128)	2.300(3)
Rh(1)-B(108)	2.479(3)	Rh(2)-B(132)	2.419(3)
Rh(1)-B(127)	2.061(3)	P(1)-Rh(1)-Rh(2)	167.506(18)
Rh(1)-H(100)	1.604(10)	H(112)-Rh(2)-B(112)	30.96(7)
Rh(1)-H(108)	1.95(3)	B(127)-Rh(1)-H(100)	81.76

Table 3.4 Selected bond lengths (Å) and angles (°) for $[(PCy_3)(CB_{11}H_{11})(H)Rh\text{-}Rh(PCy_3)(CB_{11}H_{12})]$ (**25**).

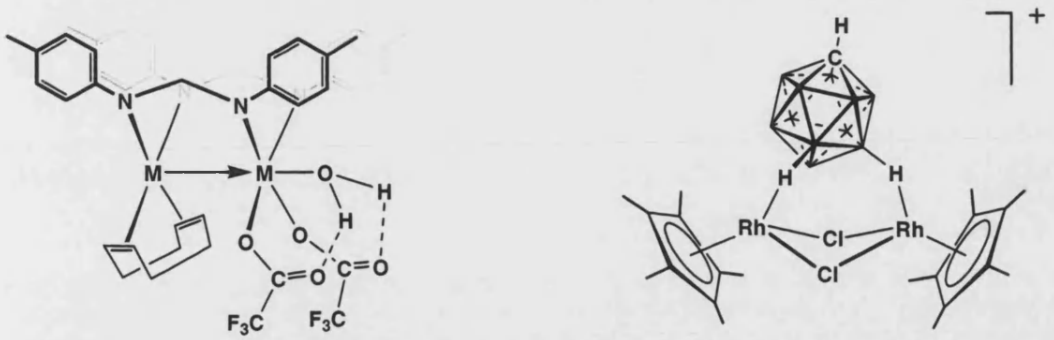

Figure 3.19 Ir(I)-Ir(III) dative bond in $[(COD)Ir(\mu\text{-form})Ir(OCOCF_3)_2(H_2O)]$ (left),[33] and $[(Cp^*)_2Rh_2(\mu\text{-}Cl)_2(closo\text{-}CB_{11}H_{12})]^+$ (right).[36]

The Rh-Rh bond in **25** is further supported by two Rh-H-B interactions in Rh(1) and three Rh-H-B interactions in Rh(2). Evidence for the $[closo\text{-}CB_{11}H_{12}]^-$ anion acting as a bridging ligand between two rhodium centres has been reported previously in the dinuclear complex $[(Cp^*)_2Rh_2(\mu\text{-}Cl)_2(closo\text{-}CB_{11}H_{12})][closo\text{-}CB_{11}H_{12}]$.[36] Rh(1) has a distorted octahedral coordination geometry with a boryl, a hydride and two {BH} vertex at the equatorial positions, and the phophine ligand situated *trans* to the Rh-Rh bond (Figure 3.20 right).

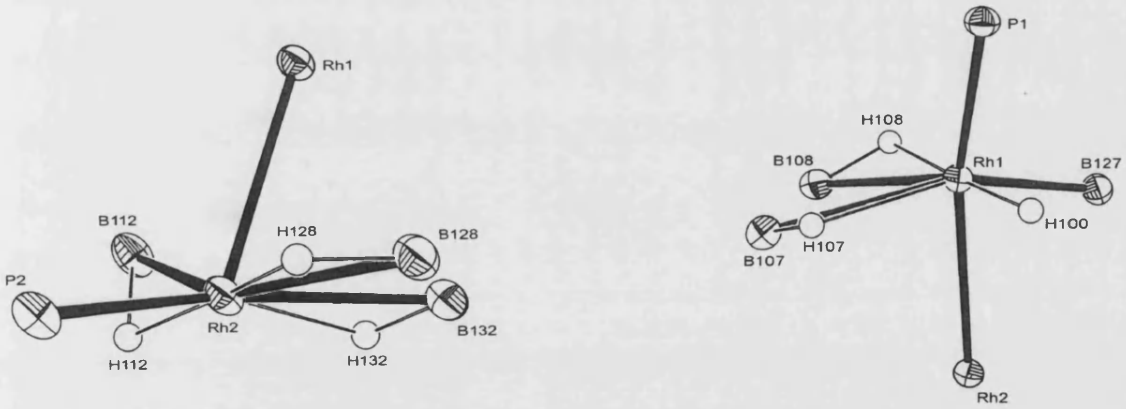

Figure 3.20 ORTEP representation of the metallic environment of complex **25** evidencing the square planar-like geometry of Rh2 (left) and the distorted octahedral geometry of Rh1(right).

The Rh(1)-B(127) distance of 2.061(3) Å unambiguously describes a Rh-boryl bond, comparable to that in the rhodium carborane complex $[(\eta^5\text{-}Cp^*)Rh(\eta^2\text{-}MeOCH_2CH{=}CH_2)(1,2\text{-}S_2\text{-}closo\text{-}C_2B_{10}H_{10})]$ shown in Figure 3.21 (left) where the Rh-B(3) distance is 2.125(3) Å,[37] or that reported for the boryl hydride complex

[Rh(Cp')(Bpin)(H)(PR_3)] (pin = pinacolate, 1,2-$O_2C_2Me_4$) (Figure 3.21, right), where the Rh-B distance is 2.0196(15) Å.[38] The Rh(1)-H(100) distance in compound **25** [1.604(10) Å] is slightly longer than that reported in [Rh(Cp')(Bpin)(H)(PR_3)], 1.508(17) Å. No covalent bond can be considered between B(127) and H(100) since they are separated by 2.423 Å, much greater than typical B-H bond (*ca* 1.2 Å).

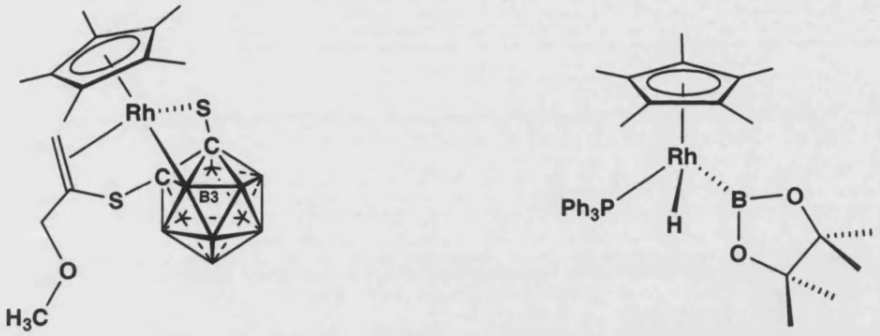

Figure 3.21

Another structural feature that supports the presence of a boryl ligand rather than a Rh-H-B 3c-2e interaction is the angle formed between B(127)-Rh(1)-H(100). For B-H···Rh interactions the B-Rh-H angles in **25** range from 25.16 up to 32.44°, indicating the presence of a covalent B-H bond. On the other hand, B(127)-Rh-H(100) forms an angle of 81.76°, which implies the existence of rhodium-hydride and rhodium-boryl bonds. A similar analysis has been used in hydrido-boryl complexes of niobium and tantalum.[39, 40] The Rh(1)-B distances are slightly longer than those reported for similar Rh-H-B interactions in carborane complexes. In complex **25**, Rh(1)-B(108) and Rh(1)-B(107) values are 2.479(3) and 2.587(3) Å respectively, however in [(PR_3)$_2$Rh(*closo*-$CB_{11}H_{12}$)], (R = Cy, Ph), the average Rh-B distance is 2.387 Å.[19, 20] This difference reflects the unusual bonding mode of the carborane anion.

The environment around Rh(2) can be described as distorted square pyramidal with the phosphine group and three {BH} vertexes forming the base of the pyramid in a

square planar-like arrangement and Rh(1) situated in the pyramid apex (Figure 3.20 left). Rh(2)-B distances fall into a range of 2.300(3) Å and 2.419(3) Å, being shorter than the Rh(1)-B distances.

Rh(II)-Rh(II) and mixed valence rhodium complexes are relatively common, with Rh(0)-Rh(II), and Rh(I)-Rh(III) complexes being the most abundant.[41-43] Similar Rh(I)-Rh(III) complexes with Rh-Rh dative metal bonds to that described for complex **25** have been reported.[35, 44, 45] However, these could also be a Rh(II)-Rh(II) with coordination of an axial ligand at one rhodium. This underscores the difficulty in assigning formal oxidation states and valence bonding descriptions to these dimeric species.[46] These complexes, shown in Figure 3.22, have the same structural environments around their rhodium atoms as complex **25**. The Rh(I) centres display a square planar geometry with a formal dative bond to the octahedral Rh(III) atom. The Rh-Rh distances in compounds **V** and **VI** are 2.532(2) and 2.558(1) Å respectively, which are shorter than the distance observed in complex **25** [2.7962(2) Å], probably due to the structural differences of the bridging ligands in each case.

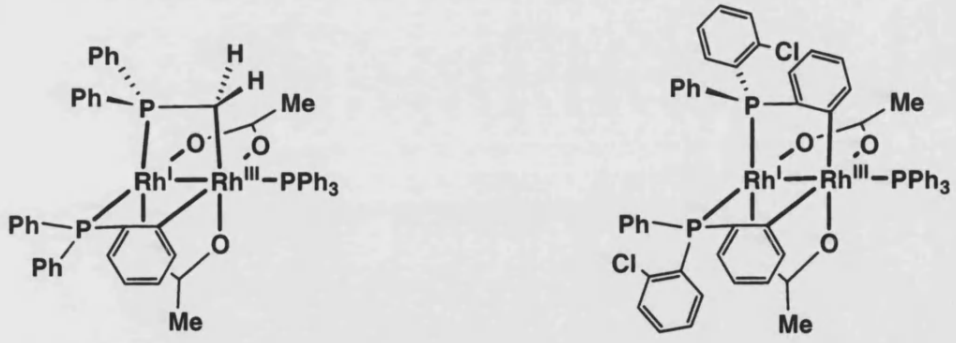

V **VI**

Figure 3.22 $\{Rh_2(\mu^2\text{-}O_2CMe)_2[\mu^2\text{-}(CH_2)PPh_2][\mu^2\text{-}(C_6H_4)PPh_2](PPh_3)\}$[45] (**V**) and $\{Rh_2(\mu^2\text{-}O_2CMe)_2[\mu^2\text{-}(C_6H_4)P(o\text{-}C_6H_4)Ph]_2(PPh_3)\}$[44] (**VI**)

In contrast to the solid-state structure, the NMR data for **25** indicate that at room temperature the cage anions are equivalent, as are the two phosphine ligands. The ^1H

NMR spectrum at 298 K of **25** shows the cyclohexyl proton signals of the phosphine ligand between δ 2.05 and 1.25 ppm. One cage C-H proton is observed at δ 2.65 ppm, upfield shifted when compared to its precursor **22** (δ 2.79 ppm). The Rh-H-B signals have shifted considerably to higher field from complex **22** [δ 0.47 ppm ($B_{7\text{-}11}$-*H*), δ -1.51 ppm (B_{12}-*H*)] and appear as two broad signals in a 5:1 ratio at δ -1.43 and -7.44 ppm respectively. This high value for a Rh-H-B interaction is indicative of a significant Rh-H interaction on the NMR time-scale. The $^{11}B\{^1H\}$ spectrum displays two broad resonaces at δ -13.43 and -16.05 ppm in a 6:5 ratio. The resonances observed in the ^1H and ^{11}B NMR spectra for the cage vertices suggest local C_{5v} symmetry, and thus rapid scrambling of the Rh-H-B interactions on the NMR time-scale. The $^{31}P\{^1H\}$ NMR spectrum shows a slighty broad doublet at δ 76.4 ppm with a *J*(RhP) coupling constant of 160 Hz. The NMR data of complex **25** suggests a dynamic process which makes equivalent the cage anions and the phosphine ligands (a possible mechanism is commented later).

3.2.3.2 [(PCyp$_3$)(*closo*-CB$_{11}$H$_{11}$)(H)Rh-Rh(PCyp$_3$)(*closo*-CB$_{11}$H$_{12}$)]

Complex [(PCyp$_3$)(*closo*-CB$_{11}$H$_{11}$)(H)Rh-Rh(PCyp$_3$)(*closo*-CB$_{11}$H$_{12}$)] (**26**) is obtained when a C_6H_5F solution of [Rh(PCyp$_3$)(H)$_2$(*closo*-CB$_{11}$H$_{12}$)] (**23**) is placed under vacuum. In order to isolate compound **26**, it is necessary to dissolve the residue in CH_2Cl_2 and evaporate at least twice more, until the $^{31}P\{^1H\}$ NMR spectrum shows the complete disappearance of the signal from compound **23**. Complex **26** is isolated as a dark orange solid in 77% yield.

The behaviour of complex **26** in solution is analogous to that observed for **25**. At room temperature the ^1H NMR spectrum displays signals a single C-*H* resonance at

δ 2.63 ppm, tricyclopentylphosphine protons between δ 2.30-1.30 ppm, and BH broad signals in the high field region at δ -1.14 and -7.74 ppm in a 5:1 relative ratio respectively, indicative of Rh-H-B interactions. The $^{11}B\{^1H\}$ NMR spectrum shows two resonances in a 6:5 ratio, at δ -13.44 ppm and δ -15.15 ppm. This pattern confirms a local C_{5v} symmetry for the cage, where all lower pentagonal belt are equivalent on the NMR time-scale as observed for compound **25**. The two resonances become broad doublets in the ^{11}B NMR spectrum. The $^{31}P\{^1H\}$ NMR spectrum exhibits one phosphorus environment at δ 64.2 ppm with *J*(RhP) of 154 Hz. Hence, the NMR data shows that on the NMR time-scale the metal centres interact with all the lower pentagonal belt and antipodal vertex protons, and indicate higher symmetry than expected for the solid-state structure of **25**.

3.2.3.3 [(P^{i}Pr$_3$)(*closo*-CB$_{11}$H$_{11}$)(H)Rh-Rh(P^{i}Pr$_3$)(*closo*-CB$_{11}$H$_{12}$)]

A pale brown solution of **24** in fluorobenzene is degassed under vacuum to give a dark red solid that can be identified by NMR spectroscopy as a mixture of compound **24** and [(P^{i}Pr$_3$)(*closo*-CB$_{11}$H$_{11}$)(H)Rh-Rh(P^{i}Pr$_3$)(*closo*-CB$_{11}$H$_{12}$)] (**27**). In order to obtain compound **27** as a single product, the residue needs to be dissolved in CH_2Cl_2 and evaporated until dryness in dichloromethane twice. Complex **27** was obtained in 59 % yield.

The ^1H NMR spectrum of complex **27** at 298 K is shown in Figure 3.23. This is comparable to those obtained for complexes **25** and **26**, although with characteristic triisopropyl resonances replacing the cyclic alkyls. The cage C-H signal appears at δ 2.65 ppm, the phosphine isopropyl groups are displayed at δ 2.31 and 1.33 ppm for the C*H* and CMe_2 respectively. {BH} vertices are observed at δ -1.51 ppm, assigned as

lower pentagonal belt protons, and δ -7.50 ppm assigned as the B_{12}-H. These resonances are complemented by upper pentagonal belt {BH} resonances at δ 1.88 ppm, clearly identified in the $^{1}H\{^{11}B\}$ NMR spectrum.

The $^{11}B\{^{1}H\}$ NMR spectrum displays two resonances in a 6:5 ratio, at δ -12.88 ppm and δ -14.98 ppm. The $^{31}P\{^{1}H\}$ NMR spectrum shows a single doublet at δ 66.4 ppm, with *J*(RhP) 156 Hz, indicating that both phosphorus atoms are equivalent on the NMR time-scale at room temperature.

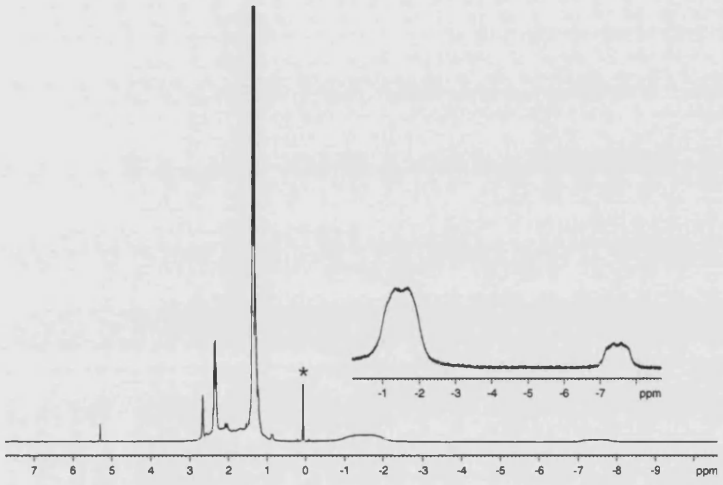

Figure 3.23 ^{1}H NMR spectrum of **27** at 298 K (*grease)

3.2.3.4 Low temperature studies

^{1}H, ^{11}B and $^{31}P\{^{1}H\}$ NMR experiments of **25**, **26** and **27** at 298 K show local C_{5v} symmetry for the carborane cage and one phosphorus environment respectively. This suggests there must be some fluxional process occurring at room temperature (Figure 3.24), and we suggest that this involves reversible breaking and making of the Rh-H-B bonds around two equal monophosphine-rhodium fragments. As we also show there is evidence to suggest the metal-metal bond also undergoes cleavage in solution. Nevertheless, we consider the rhodium dimer persists in solution since no exchange

between the different phosphine-rhodium fragments is observed on the NMR time-scale when compounds **25** and **27** are present in the same solution.

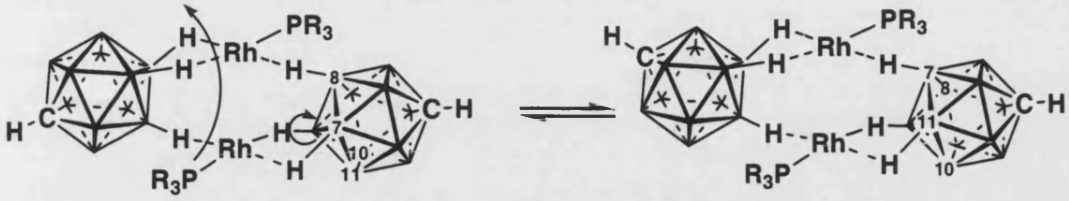

Figure 3.24 Possible fluxional process

If the solid state structure obtained for complex **25** were retained in solution, two different phosphorus resonances with different coupling constants [Rh(I)-P, Rh(III)-P] should be visible in the $^{31}P\{^{1}H\}$ NMR spectrum. Variable temperature NMR experiments of **25**, **26** and **27** show at 250K a flattening of the phosphorus signal that starts to resolve into two broad, independent, resonances at 190K for compounds **25** and **26**, and into a very broad resonance for complex **27**. The formation of these two multiplets is consistent with two different phosphorus environments as found in the solid state. Particularly for complex **25**, the $^{31}P\{^{1}H\}$ NMR spectrum shows a broad doublet of doublets at δ 69.1 ppm and coupling constants ^{1}J(RhP) 170 Hz and ^{2}J(RhP) 85 Hz that could be assigned to the phosphorus *cis* to the rhodium-rhodium bond. The second resonance is observed at δ 60.1 ppm as a virtual triplet [splitting 133 Hz] and would correspond to the phosphorus found *trans* to the metal-metal bond in the solid-state structure.

As can be observed in Figure 3.25, five broad Rh-*H*-B resonances are displayed in the high field region of the ^{1}H NMR spectrum at δ -0.36, -4.57 -8.56, -10.91 and -16.6 ppm in a 2:1:1:1:1 ratio. Similar chemical shifts are obtained for compounds **25** and **26**. Six hydride resonaces is in agreement with the solid state structure. The resonance that appears at the lowest frequency may correspond to the proton that

becomes a hydride in the solid-state structure as this is the sharpest high field signal. The broadness of this peak suggests the exchange process has not been completely frozen out at the lowest attainable temperature of 190 K. It would be necessary to lower the temperature even more in order to observe by NMR spectroscopy a static structure obtained by X-ray crystallography, that is Rh-H-B interactions along with a rhodium hydride in the ^{1}H NMR spectrum, rhodium boryl resonances in the ^{11}B and $^{11}B\{^{1}H\}$ NMR spectra, and two well-defined multiplets in the $^{31}P\{^{1}H\}$ NMR spectrum.

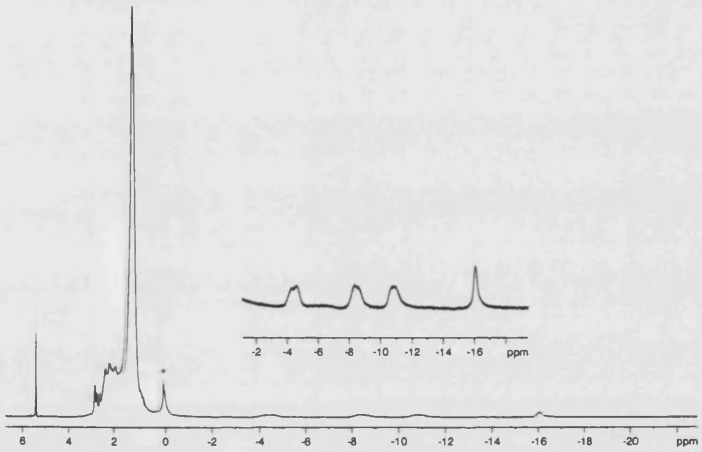

Figure 3.25 ^{1}H NMR spectrum of **27** in CD_2Cl_2 at 190 K (* grease)

3.2.3.5 Comments on the formation of 25, 26 and 27

We have seen that exposure of solutions of $[Rh(PR_3)(H)_2(CB_{11}H_{12})]$ [R = Cy (**22**), Cyp (**23**), ^{i}Pr (**24**)] to vacuum ($5x10^{-2}$ Torr) leads to the formation of compounds **25**, **26** and **27**. These complexes can be isolated and stored for months at 2 °C under argon without decomposing.

A possible intermediate species between the dihydride Rh(III) compound and the dinuclear Rh(I) complex could be formulated as a square planar complex with a dihydrogen molecule coordinated to a Rh(I) centre as shown in Figure 3.26. This could then lose H_2 on pumping. Such an intermediate is also consistent with the H/D exchange observed for **22**, **23** and **24**. The addition of H_2 to dichloromethane solutions of

complexes **25**, **26** and **27** results in the re-formation of compounds **22**, **23** and **24** in 1 hour.

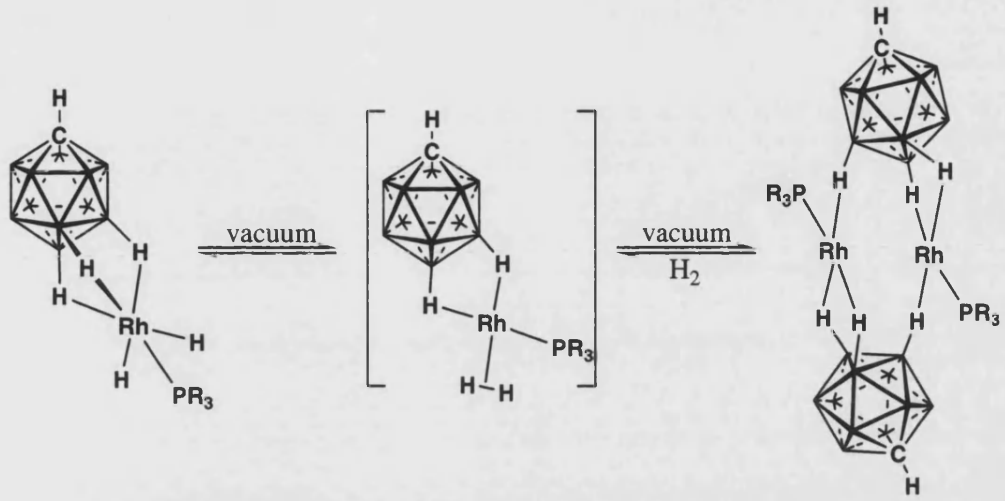

Figure 3.26 Proposed mechanism of hydrogen loss

Reversible addition of dihydrogen has been described in the literature for other metal complexes that are stable only under hydrogen atmosphere, but lose their hydrides when replaced by argon. This behaviour has been noted in an Ir-Ir dimer, where the hydrogen uptake occurred across the metal-metal bond.[47] A more similar complex to those described herein, the monophosphine-rhodium-arene shown in Figure 3.27, also exhibits reversible addition of dihydrogen. In the absence of H_2 or acetone both compounds decompose rapidly and cannot be isolated.[8]

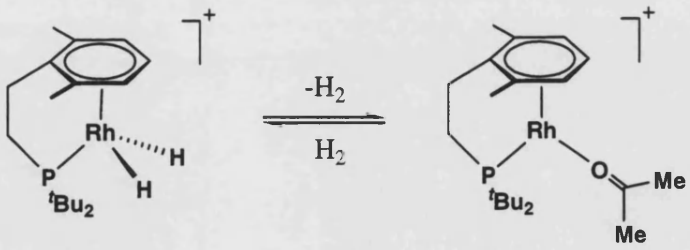

Figure 3.27 Reversible addition or release of H_2 by a rhodium complex[8]

Exposure of **25**, **26** and **27** to a D_2 atmosphere results in the gradual deuteration of the cage. ^2H NMR spectra show a resonance at about δ -20 ppm, which correlates with

the hydride resonance observed for **22**, **23** and **24.** Therefore, it can be suggested the formation of mononuclear deuterated complexes that could be formulated as $[Rh(PR_3)(D)_2(1\text{-H-}closo\text{-}CB_{11}D_{11})]$ (R = Cy, Cyp, ^{i}Pr) (Figure 3.28), similar to compounds **22**, **23** and **24**. Also evident is the formation of HD (g) (1:1:1 triplet at δ 4.55) suggesting a dihydrogen intermediate as suggested in Figure 3.16. ESI-MS has also given evidence of complete cage deutaration (except the {CH} vertex). A unique isotope-pattern corresponding of *per*-deuterium substitution is observed with a base peak at m/z 154.26.

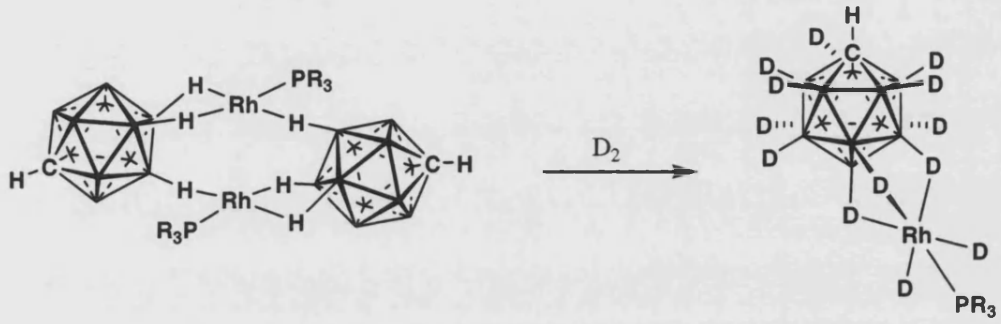

Figure 3.28 Deuteration of complexes **25**, **26** and **27**

3.2.4 Reactivity of $[(PR_3)(CB_{11}H_{11})(H)Rh\text{-}Rh(PR_3)(CB_{11}H_{12})]$ with olefins

Complexes **25**, **26** and **27** were screened for olefin hydroboration of ethene and 1-hexene. Dichloromethane solutions of the rhodium complexes were placed in a Young's ampoule with excess of olefin under an atmosphere of argon and stirred at room temperature. All three compounds were demonstrated to be active catalysts and react with the alkenes producing multiple substitutions after one day of reaction.

This data is in broad accordance with the ^{11}B and $^{11}B\{^{1}H\}$ NMR spectra, which show multiple signals due to a variety of different substituted products with no starting $[closo\text{-}CB_{11}H_{12}]^-$ present. It was observed that increasing the temperature (above 40 °C) still produced complex mixtures of hexyl-substituted cages when 1-hexene was used.

The utilisation of ethene instead of 1-hexene also rendered low selectivity, with mixtures of different products formed of variable substitution numbers.

Compound	n_{ethene}	$n_{1\text{-}hexene}$
25	2, 3	1, 2, 3, 4
26	1, 2, 3	1, 2, 3, 4
27	2, 3	1, 2, 3, 4

Table 3.5 Number of substitutions (**n**) observed by ESI-MS (negative mode) after 1 day of reaction

In the reactions of **25**, **26** and **27** with ethene, NMR spectroscopy shows vinyl resonances between δ 5.2 and 3.5 ppm, and the formation of ethane (δ 0.89 ppm). This is indicative of a dehydrogenative borylation process, as described for the $\{Rh(PPh_3)_2\}^+$ fragment in the previous chapter. The formation of ethane indicates that the hydrogen formed in the dehydrogenative borylation reaction is being consumed by the metal fragment in the hydrogenation of ethene. Resonances due to B-ethyl groups were not detected, as evidence for hydroboration of ethene. The ESI-MS spectra corroborate this data. The base peak appears at m/z 195.23, which corresponds with a carborane cage with two vinyl substituted vertices, i.e. the [1-H-*closo*-$(CH{=}CH_2)_2$-$CB_{11}H_9$]$^-$ anion. Exposure of this solution to a dihydrogen atmosphere resuts in the reduction of the vinyl into ethyl groups and the conversion of the base peak into m/z 199.27, that agrees with [7,12-Et_2-1-*closo*-$CB_{11}H_{10}$]$^-$. Consequently, sequential addition of ethene and hydrogen was performed at room temperature as Figure 3.29 shows. After four cycles, ESI-MS spectrometry shows a mixture of poly-substituted cages, where the number of substitutions (**n**) varies from two to nine. Therefore, this system results in greater substitution yet lower selectivity compared with the $\{Rh(PPh_3)_2\}^+$ system described in

Chapter 3. The formation of a compositionally pure product is not possible even with an increase in the number of cycles.

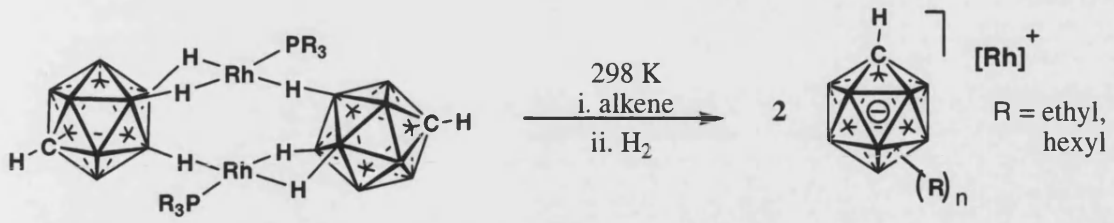

Figure 3.29 Sequential treatment with alkene and H_2

Similar to the reaction with ethene, reaction of 1-hexene with complexes **25**, **26** and **27** in dichloromethane at room temperature also renders dehydrogenative borylation after one day of reaction. After hydrogenation, the ESI-MS base peak shows (in the negative mode) a m/z 395.48, which agrees with a three-fold substituted cage. The selectivity of this system is again low as 1, 2, 3 and 4-fold substituted cages are observed. After cycling 1-hexene and hydrogen four times, higher substitution numbers are obtained without an increase of selectivity as Table 3.6 shows.

Compound	n_{ethene}	$n_{1\text{-}hexene}$
25	3-9	2-7
26	3-9	2-7
27	3-9	2-7

Table 3.6 Number of substitutions (**n**) observed by ESI-MS (negative mode) after 4 cycles

The dehydrogenative borylation mechanism involved in this monophosphine rhodium system will probably be very similar to that described for the $\{Rh(PPh_3)_2\}^+$ fragment in Chapter 2. However, the presence of only one phosphine ligand in the present system allows the metal centre to be more reactive and perform more than one substitution.

3.3 Conclusions

A range of rhodium complexes with only one phosphine ligand and the [*closo*-$CB_{11}H_{12}]^-$ carborane anion has been prepared. The solid-state structure of one of these compounds shows the B-H oxidative addition of one of the {BH} vertexes of this anion, confirming the existence of the putative Rh-boryl intermediate species in hydroboration reactions on [1-H-*closo*-$CB_{11}H_{11}]^-$. These new complexes react at room temperature with alkenes, such as ethene and 1-hexene, to produce dehydrogenative borylation. This monophosphine-rhodium system has been found to be more reactive than the $\{Rh(PPh_3)_2\}^+$ fragment, albeit less selective, for cage functionalisation.

3.4 Bibliography

1 J. D. Hewes, C. W. Kreimendahl, T. B. Marder, and M. F. Hawthorne, *J. Am. Chem. Soc.*, 1984, **106**, 5757.
2 M. S. Delaney, C. B. Knobler, and M. F. Hawthorne, *J. Chem. Soc.-Chem. Commun.*, 1980, 849.
3 R. Crabtree and D. M. P. Mingos, 'Comprehensive Organometallic Chemistry, 3rd Edition', Elsevier, 2007.
4 P. E. Behnken, T. B. Marder, R. T. Baker, C. B. Knobler, M. R. Thompson, and M. F. Hawthorne, *J. Am. Chem. Soc.*, 1985, **107**, 932.
5 R. T. Baker, R. E. King, C. Knobler, C. A. Ocon, and M. F. Hawthorne, *J. Am. Chem. Soc.*, 1978, **100**, 8266.
6 H. Werner, *Dalton Transactions*, 2003, 3829.
7 G. Canepa, C. D. Brandt, K. Ilg, J. Wolf, and H. Werner, *Chem.-Eur. J.*, 2003, **9**, 2502.
8 G. Canepa, C. D. Brandt, and H. Werner, *Organometallics*, 2004, **23**, 1140.
9 H. Werner, M. E. Schneider, M. Bosch, J. Wolf, J. H. Teuben, A. Meetsma, and S. I. Troyanov, *Chem.-Eur. J.*, 2000, **6**, 3052.
10 B. Windmuller, O. Nurnberg, J. Wolf, and H. Werner, *Eur. J. Inorg. Chem.*, 1999, 613.
11 F. Torres, E. Sola, M. Martin, C. Ochs, G. Picazo, J. A. Lopez, F. J. Lahoz, and L. A. Oro, *Organometallics*, 2001, **20**, 2716.
12 E. Sola, J. Navarro, J. A. Lopez, F. J. Lahoz, L. A. Oro, and H. Werner, *Organometallics*, 1999, **18**, 3534.
13 T. Jelinek, J. Plesek, S. Hermanek, and B. Stibr, *Collect. Czech. Chem. Commun.*, 1986, **51**, 819.
14 R. J. Cross, A. R. Kennedy, L. Manojlovicmuir, and K. W. Muir, *J. Organomet. Chem.*, 1995, **493**, 243.
15 D. P. Smith, M. T. Griffin, M. M. Olmstead, M. F. Maestre, and R. H. Fish, *Inorg. Chem.*, 1993, **32**, 4677.
16 F. E. Wood, J. Hvoslef, and A. L. Balch, *J. Am. Chem. Soc.*, 1983, **105**, 6986.
17 V. Noinville, B. Viossat, and N. H. Dung, *Acta Crystallogr., Sect. C: Cryst. Struct. Commun.* , 1993, **49**, 1297.
18 M. Enamullah, A. Sharmin, M. Hasegawa, T. Hoshi, A. C. Chamayou, and C. Janiak, *Eur. J. Inorg. Chem.*, 2006, 2146.
19 A. Rifat, V. E. Laing, G. Kociok-Kohn, M. F. Mahon, G. D. Ruggiero, and A. S. Weller, *J. Organomet. Chem.*, 2003, **680**, 127.
20 A. Rifat, N. J. Patmore, M. F. Mahon, and A. S. Weller, *Organometallics*, 2002, **21**, 2856.
21 N. J. Patmore, C. Hague, J. H. Cotgreave, M. F. Mahon, C. G. Frost, and A. S. Weller, *Chem.-Eur. J.*, 2002, **8**, 2088.
22 C. Hague, N. J. Patmore, C. G. Frost, M. F. Mahon, and A. S. Weller, *Chem. Commun.*, 2001, 2286.
23 M. A. Fox, M. F. Mahon, N. J. Patmore, and A. S. Weller, *Inorg. Chem.*, 2002, **41**, 4567.
24 D. J. Crowther, S. L. Borkowsky, D. Swenson, T. Y. Meyer, and R. F. Jordan, *Organometallics*, 1993, **12**, 2897.
25 T. Gadt, B. Grau, K. Eichele, I. Pantenburg, and L. Wesemann, *Chem.-Eur. J.*, 2006, **12**, 1036.
26 T. Gadt and L. Wesemann, *Organometallics*, 2007, **26**, 2474.
27 D. D. Ellis, A. Franken, P. A. Jelliss, J. A. Kautz, F. G. A. Stone, and P. Y. Yu, *J. Chem. Soc.-Dalton Trans.*, 2000, 2509.
28 H. Werner, G. Canepa, K. Ilg, and J. Wolf, *Organometallics*, 2000, **19**, 4756.
29 O. S. Mills and J. P. Nice, *J. Organomet. Chem.*, 1967, **10**, 337.
30 M. R. Churchill and S. W. Y. Ni, *J. Am. Chem. Soc.*, 1973, **95**, 2150.
31 F. A. Cotton and T. R. Felthouse, *Inorg. Chem.*, 1981, **20**, 584.

[32] F. A. Cotton and R. A. Walton, 'Multiple bonds between metal atoms', ed. Wiley, 1982.
[33] F. A. Cotton and R. Poli, *Inorg. Chem.*, 1987, **26**, 590.
[34] T. G. Gray and D. G. Nocera, *Chem. Commun.*, 2005, 1540.
[35] P. Piraino, G. Bruno, G. Tresoldi, S. Loschiavo, and P. Zanello, *Inorg. Chem.*, 1987, **26**, 91.
[36] N. J. Patmore, M. F. Mahon, and A. S. Weller, *Appl. Organomet. Chem.*, 2003, **17**, 388.
[37] M. Herberhold, H. Yan, W. Milius, and B. Wrackmeyer, *Chem.-Eur. J.*, 2002, **8**, 388.
[38] M. V. Campian, J. L. Harris, N. Jasim, R. N. Perutz, T. B. Marder, and A. C. Whitwood, *Organometallics*, 2006, **25**, 5093.
[39] J. F. Hartwig and S. R. Degala, *J. Am. Chem. Soc.*, 1994, **116**, 3661.
[40] D. R. Lantero, D. H. Motry, D. L. Ward, and M. R. Smith, *J. Am. Chem. Soc.*, 1994, **116**, 10811.
[41] J. A. Gaunt, V. C. Gibson, A. Haynes, S. K. Spitzmesser, A. J. P. White, and D. J. Williams, *Organometallics*, 2004, **23**, 1015.
[42] C. Tejel, M. A. Ciriano, L. A. Oro, A. Tiripicchio, and F. Ugozzoli, *Organometallics*, 2001, **20**, 1676.
[43] M. P. Garcia, M. V. Jimenez, T. Luengo, and L. A. Oro, *J. Organomet. Chem.*, 1996, **510**, 189.
[44] F. A. Cotton, F. Barcelo, P. Lahuerta, R. Llusar, J. Paya, and M. A. Ubeda, *Inorg. Chem.*, 1988, **27**, 1010.
[45] M. V. Borrachero, F. Estevan, S. Garciagranda, P. Lahuerta, J. Latorre, E. Peris, and M. Sanau, *J. Chem. Soc.-Chem. Commun.*, 1993, 1864.
[46] P. Piraino, G. Bruno, G. Tresoldi, S. L. Schiavo, and F. Nicolo, *Inorg. Chem.*, 1989, **28**, 139.
[47] A. F. Heyduk and D. G. Nocera, *J. Am. Chem. Soc.*, 2000, **122**, 9415.

Chapter 4. Monophosphine rhodium complexes partnered with [*closo*-$CB_{11}H_6Br_6$]$^-$

4.1 Introduction

As we have shown, the [*closo*-$CB_{11}H_{12}$]$^-$ anion is susceptible to B-H oxidative addition due to the hydridic character of the antipodal and lower pentagonal belt {BH} vertices. Consequently, the isolation of intermediate spices in hydroboration reactions of the [*closo*-$CB_{11}H_{12}$]$^-$ anion is likely to be complicated. The use of an anion with similar nucleophilic characteristics yet more stable toward oxidative addition may assist in isolating intermediate species and shedding more light on the mechanism. The hexa-halogenated derivatives of the parent [*closo*-$CB_{11}H_{12}$]$^-$ anion are potential candidates for its substitution since they avoid complication with B-H oxidative addition, as the lower surface of the cage is surrounded by B-X (X = halogen) groups. In terms of nucleophilicity, according to IR measurements of their respective trioctylammonium salts,[1, 2] the [*closo*-$CB_{11}H_6Br_6$]$^-$ anion becomes the most appropriate anion, in terms of ease of preparation, weakly coordinating ability and chemical robustness.

Both, the [*closo*-$CB_{11}H_{12}$]$^-$ and [*closo*-$CB_{11}H_6Br_6$]$^-$ anions, are known to coordinate to transition metal fragments although such complexes of the latter are still rare. There are examples where these anions coordinate in the same fashion, as Figure 4.1 shows. In these examples both anions coordinate through three vertices to an $\{Ag(PPh_3)\}^+$ fragment,[3, 4] and bidentate coordination has been observed when these carboranes are partnered to the $\{Ir(H)_2(PPh_3)_2\}^+$ fragment.[5, 6]

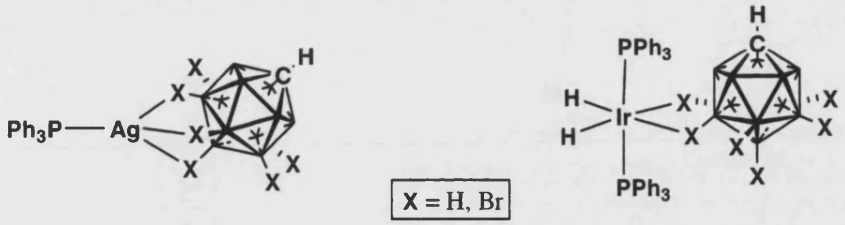

Figure 4.1 Same coordination of the [*closo*-$CB_{11}H_{12}$]$^-$ and [*closo*-$CB_{11}H_6Br_6$]$^-$ anions with equal metal fragments.

In contrast, with other metal fragments, the formation of different products has been observed depending on the carborane utilised. This is due to steric effects (Br is larger than H) as well as the difference in nucleophilicity between Br and H. The hydrogenation of $[(PPh_3)_2Rh(nbd)]^+$ shows this well. With [*closo*-$CB_{11}H_{12}$]$^-$ a complex with Rh-H-B interactions is observed, while with [*closo*-$CB_{11}H_6Br_6$]$^-$ an arene-bridged dimer is formed, as shown in Figure 4.2.[7] Similar behaviour has been observed with the $\{Cp^*RhCl\}^+$ metallic fragment.[8]

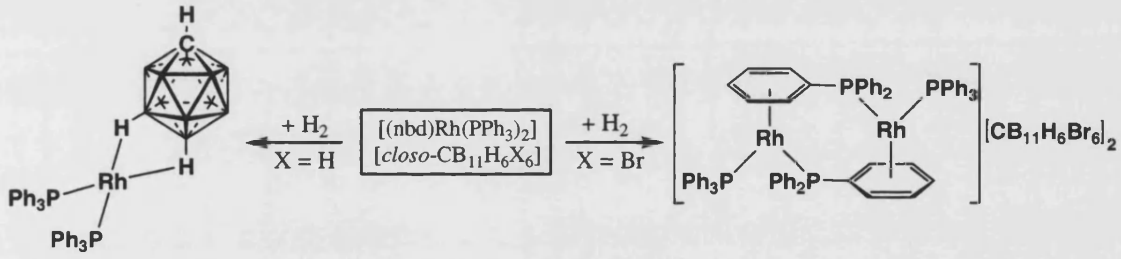

Figure 4.2 Example of complexes that share the same metal fragment but with different structural arrangement.

Similarly, partnering the $\{Mo(\eta^5\text{-}C_5H_5)(CO)_3\}^+$ fragment with the [*closo*-$CB_{11}H_{12}$]$^-$ and [*closo*-$CB_{11}H_6Br_6$]$^-$ anions showed the coordination of the [*closo*-$CB_{11}H_{12}$]$^-$ cage through one of its {BH} vertices, while in solution, the analogous [*closo*-$CB_{11}H_6Br_6$]$^-$ complex (with one Mo-Br-B interaction) was formed alongside with two more species where the carborane anion was believed to be out of the coordination sphere of the metal, one of which is suggested to be a dichloromethane complex.[9-11]

4.1.1 Scope of Chapter

In summary, although occasionally the more weakly coordinating nature of the [*closo*-$CB_{11}H_6Br_6$]$^-$ anion has led to different complexes from equivalent conditions of reaction and starting materials, analogous complexes have also been characterised of the weakly coordinating [*closo*-$CB_{11}H_{12}$]$^-$ and [*closo*-$CB_{11}H_6Br_6$]$^-$ carborane anions.

In order to better understand the processes described in the previous chapter and confirm the structure proposed for those complexes characterised only by NMR spectroscopy, i.e. **22**, **23** and **24**, we decided to substitute the [*closo*-$CB_{11}H_{12}$]$^-$ by the slightly more weakly coordinating [*closo*-$CB_{11}H_6Br_6$]$^-$ anion.

A range of new rhodium monophosphine complexes partnered with [*closo*-$CB_{11}H_6Br_6$]$^-$ have been synthesised and characterised in solution and the solid state. Such complexes give insight into the reactivity of a $\{Rh(PR_3)(H)_2\}^+$ fragment without involving reactivity of the cage.

4.2 Results and discussion

The preparation of monophosphine rhodium complexes with [*closo*-$CB_{11}H_6Br_6$]$^-$ has been achieved following the synthetic strategy used in the previous chapter namely, protonation of a methoxy group using [HPR_3][*closo*-$CB_{11}H_6Br_6$].

4.2.1 Synthesis of [HPR_3][*closo*-$CB_{11}H_6X_6$], R = Cy, Cyp, ^{i}Pr; X = Br, Cl

Phosphonium salts of carborane derivatives of the parent [*closo*-$CB_{11}H_6Br_6$]$^-$ anion are readily prepared by reacting the appropriate phosphine with a solution of the carborane acid in diethyl ether as shown in Figure 4.3.

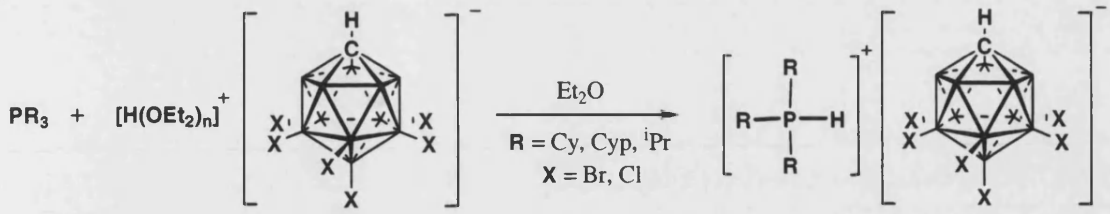

Figure 4.3 Schematic synthesis of phosphonium salts of [*closo*-$CB_{11}H_6X_6$]$^-$ derivatives.

4.2.1.1 [$HPCy_3$][*closo*-$CB_{11}H_6Br_6$]

Addition of a solution of tricyclohexylphosphine into an ethereal solution of the [$H(OEt_2)_x$][*closo*-$CB_{11}H_6Br_6$] carborane acid (prepared *in situ* as shown in Equation 1) leads to the formation of a white precipitate identified as [$HPCy_3$][*closo*-$CB_{11}H_6Br_6$] (**28**) in 84 % yield.

$$Cs[closo\text{-}CB_{11}H_6Br_6] \xrightarrow[\text{ii. + HCl (pH = 1)}]{\text{i. water/ether 15:1}} [H(OEt_2)_x][closo\text{-}CB_{11}H_6Br_6] + CsCl$$

Equation 1

In the $^1H\{^{11}B\}$ NMR spectrum, a CD_2Cl_2 solution of [$HPCy_3$][*closo*-$CB_{11}H_6Br_6$] (**28**) shows a resonance at δ 5.33 ppm with a large *J*(PH) coupling constant of 447 Hz. Cyclohexyl groups are displayed between δ 2.52-1.28 ppm, consistent with the chemical shift obtained for the same cation described in Chapter 3. The proton resonance from the cage C*H* is observed at δ 2.56 ppm. The ^{11}B NMR spectrum shows singlets for the antipodal and lower pentagonal {BBr} vertices at δ -1.05 and -9.09 ppm in 1:5 ratio. {BH} vertices appear as a doublet at δ -19.43 ppm with *J*(BH) 169 Hz. These chemical shifts identify the carborane as a free cage, and agree with data reported for other uncoordinated [*closo*-$CB_{11}H_6Br_6$]$^-$ salts, e.g. [$(Ph_3P)_2Ir(COD)$][*closo*-$CB_{11}H_6Br_6$].[5] The $^{31}P\{^1H\}$ NMR spectrum displays a unique singlet at 33.06 ppm.

4.2.1.2 [HPR_3][*closo*-$CB_{11}H_6X_6$], R = Cyp, ^{i}Pr; X = Br, Cl

The synthetic procedure described for compound **28** was utilised in the synthesis of [$HPCyp_3$][*closo*-$CB_{11}H_6Br_6$] (**29**), [HP^iPr_3][*closo*-$CB_{11}H_6Br_6$] (**30**) and [$HPCy_3$][*closo*-$CB_{11}H_6Cl_6$] (**31**). Isolated yields for these compounds are between 81 and 96 %. Their NMR spectra are similar to those described for the analogous phosphonium compounds of the parent [*closo*-$CB_{11}H_{12}$]$^-$ anion in Chapter 3, except for the carborane resonances, specific to [*closo*-$CB_{11}H_6Br_6$] and [*closo*-$CB_{11}H_6Cl_6$], respectively. The following table outlines the data obtained for compounds **28**, **29**, **30** and **31**.

Compound	^{1}H NMR δ PH	*J*(PH)	CH cage δ	^{11}B{^{1}H} NMR[a] δ	^{31}P(^{1}H) δ
28	5.33	447	2.56	-1.05, -9.09, -19.43	33.1
29	5.95	453	~2.50	-1.08, -9.08, -19.43	33.9
30	5.55	441	2.58	-0.94, -9.09, -19.43	45.1
31	5.28	447	2.15	1.71, -5.17, -22.53	33.20

Table 4.1 NMR data of CD_2Cl_2 solutions of **28**, **29**, **30** and **31**. δ in ppm, *J* in Hz. [a]The highest field peaks are a doublet in the ^{11}B NMR spectrum with *J*(BH) ≈ 168 Hz.

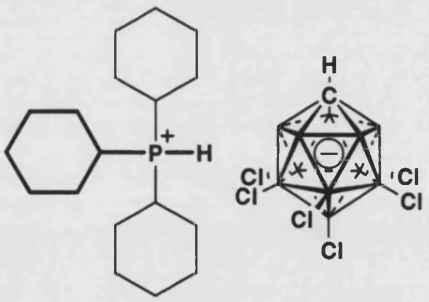

Figure 4.4 Schematic representation of compound **31**.

4.2.2 [$Rh(PR_3)(H)_2$(*closo*-$CB_{11}H_6Br_6$)]

The use of the [*closo*-$CB_{11}H_6Br_6$]$^-$ anion to synthesize the analogous dihydride-monophosphine rhodium compounds in a manner described in Chapter 3 allows the isolation of stable complexes of general formula $Rh(PR_3)(H)_2$(*closo*-$CB_{11}H_6Br_6$) (R =

Cy, Cyp and ^{i}Pr). The reaction proceeds cleanly in C_6H_5F but not in CH_2Cl_2, however these compounds are stable in the CH_2Cl_2 once formed. The NMR data of these compounds confirm the structures proposed in Chapter 3 for $[Rh(PR_3)(H)_2(closo\text{-}CB_{11}H_{12})]$ complexes, since the $\{Rh(PR_3)(H)_2\}^+$ fragment data is very similar. Attempts to synthesize analogous complexes with the more weakly coordinating $[closo\text{-}CB_{11}H_6Cl_6]^-$ anion and the $\{Rh(PR_3)(H)_2\}^+$ fragment failed.

4.2.2.1 $[Rh(PCy_3)(H)_2(closo\text{-}CB_{11}H_6Br_6)]$

Slow addition of two equivalents of $[HPCy_3][closo\text{-}CB_{11}H_6Br_6]$ (in fluorobenzene solution) to $[Rh(\mu\text{-}OMe)(nbd)]_2$ affords an orange solution that after treatment with hydrogen gas produces a pale brown solution of $[Rh(PCy_3)(H)_2(closo\text{-}CB_{11}H_6Br_6)]$ (**32**). Removal of the solvent *in vacuo* and recrystallisation of the compound in fluorobenzene and pentane yielded crystals suitable for X-ray crystallography.

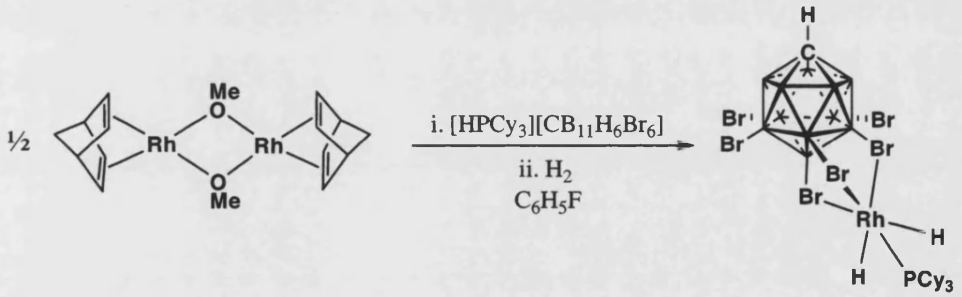

Figure 4.5 Schematic synthesis of $[Rh(PCy_3)(H)_2(closo\text{-}CB_{11}H_6Br_6)]$ (**32**).

The solid state structure of **32** is shown in Figure 4.6. One molecule of **32** is present in the asymmetric unit alongside with a molecule of uncoordinated fluorobenzene. Bond lengths and angles are shown in Table 4.2. As the structure shows, complex **32** is formed by the $[closo\text{-}CB_{11}H_6Br_6]^-$ carborane cage ligated to a $\{Rh(PCy_3)(H)_2\}^+$ cationic unit in a tridentate fashion. The rhodium atom displays an octahedral geometry as

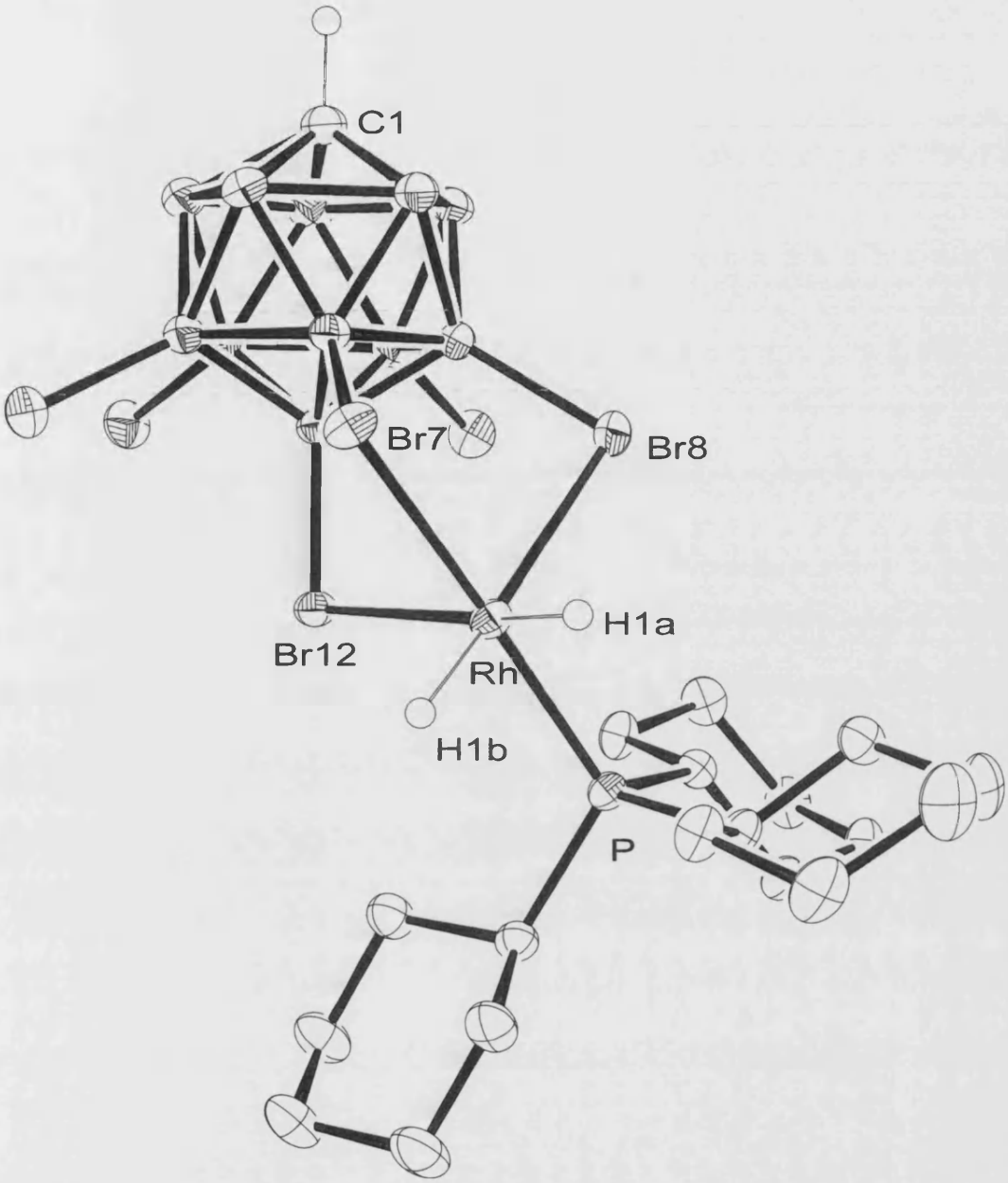

Figure 4.6 Solid-state structure of **32**. Thermal ellipsoids are shown at the 50% probability level and hydrogen atoms associated with the boron atoms and alkyl groups are omitted for clarity.

Rh-P	2.2165(7)	Rh-H(1b)	1.46(3)
Rh-Br(7)	2.6346(3)	P-Rh-Br(7)	167.786(18)
Rh-Br(8)	2.7187(3)	P-Rh-Br(8)	102.689(18)
Rh-Br(12)	2.7241(3)	P-Rh-Br(12)	104.818(18)
Rh-H(1a)	1.45(4)	Br(7)-Rh-Br(8)	85.627(10)

Table 4.2 Selected bond lengths (Å) and angles (°) for **32**.

expected for a formally Rh(III) centre. The cage binds through [B(7)-Br], [B(8)-Br] and [B(12)-Br] vertices, which are *trans* to tricyclohexylphosphine and hydride ligands respectively. The *trans* influence of the hydride ligands is clearly shown by the longer Rh-Br distances of the bromine atoms *trans* to hydrides, i.e. Br(8) and Br(12), with the Rh-Br(8) and Rh-Br(12) lengths [2.7187(3) and 2.7241(3) Å respectively] being about 0.09 Å longer than the Rh-Br(7) distance [2.6346(3) Å]. This *trans* influence is also observed in other dihydride rhodium complexes such as the $\{Rh(PMe)_4(H)_2\}^+$ fragment,[12] in which the phosphorus atoms situated *trans* to the hydride ligands are about 0.05 Å longer in the Rh-P bond length. The Rh-Br bond distances in complex **32** also reflect the weak coordination nature of the [*closo*-$CB_{11}H_6Br_6]^-$ cage. These distances are considerably longer than in $[Rh_2(\mu\text{-}Br)_2Br_4(dppm)_2]$, where the average Rh-(μ-Br)distance is 2.490 Å and for Rh-Br(terminal) 2.452 Å.[13] The B-Br bond lengths of the vertices coordinated to the rhodium atom are slightly longer [B(7)-Br 1.973(3) Å, B(8)-Br 1.970(3) Å, B(12)-Br 1.954(3) Å] than those not bound to the metal [1.941(3)-1.949(3) Å]. This is consistent with the values observed in a similar iridium-carborane complex, $[(PPh_3)_2Ir(H)_2$(*closo*-$CB_{11}H_6Br_6)]$,[5] in which the B-Br distances of the vertices bound to the metal, 1.974(9) and 1.984(11) Å, are longer than those uncoordinated, 1.943(12)-1.956(11) Å. The Rh-P distance in complex **32** [2.2165(7) Å] is similar to those found for $[(PCy_3)(CB_{11}H_{12})(H)Rh\text{-}Rh(PCy_3)(CB_{11}H_{12})]$ (**25**) [Rh(1)-P(1) 2.2324(6) Å and Rh(2)-P(2) 2.2572(6) Å]. Overall the molecule has C_1 symmetry in the solid-state.

According to the NMR spectra, the solid-state structure of **32** is not retained in solution since the carborane adopts local C_{5v} symmetry and there is only one hydride environment, meaning that there is rapid rotation of the cage on the NMR time-scale. A possible mechanism is displayed in Figure 4.7.

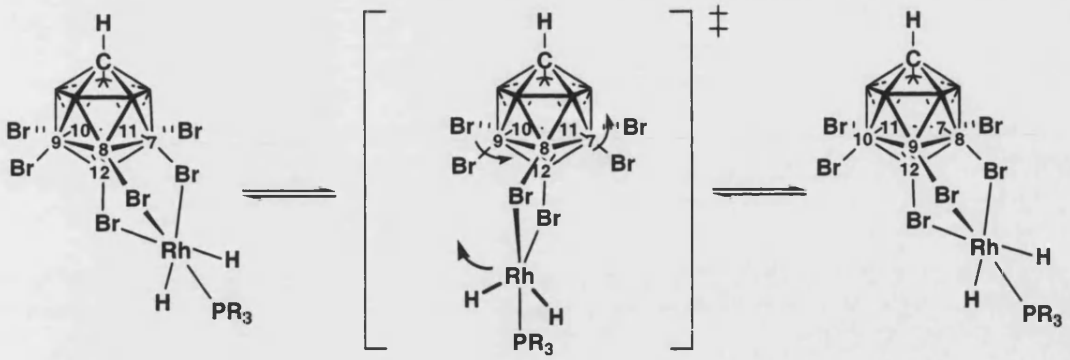

Figure 4.7 Proposed mechanism of fluxionality for **32**, **33** and **34**.

The $^{1}H\{^{11}B\}$ NMR spectrum in CD_2Cl_2 displays a set of multiplets for the phosphine cyclohexyl groups between δ 1.43-1.10 ppm. The cage C-H appears at δ 2.85 ppm, downfield shifted by 0.4 ppm compared to compound **28**. The single B-H resonance is displayed at δ 2.47 ppm. The two hydrides are shown at δ -21.25 ppm as a doublet of doublets with a Rh-H coupling constant of 28.8 Hz and a P-H coupling constant of 18.8 Hz. These values are similar to those observed for $[Rh(PCy_3)(H)_2(closo\text{-}CB_{11}H_{12})]$ [δ -19.65 ppm, *J*(RhH) 30.0 Hz, *J*(PH) 21.2 Hz], however the hydride resonance for **32** is observed at higher field probably due to the weaker nucleophilic nature of the anion. It is well established that the chemical shift of hydrides is sensitive to the nature of the *trans* group, the weaker the *trans* ligand interaction, the lower field the hydride resonance.[14] This has been demonstrated with a range of $[closo\text{-}CB_{11}H_{12}]^-$ derivatives when partnered with the $[Ir(PPh_3)_2(H)_2]^+$ fragment.[15] A large shift of the hydride resonance has been observed in dihydride-monophosphine rhodium complexes reported by Werner el al., with a chemical shift difference of about Δδ 8.8 ppm between $[Rh(P^iPr_3)(H)_2(Me_2CO)_3]^+$ and $[Rh(P^iPr_3)(H)_2(\eta^6\text{-}C_6H_6)]^+$ with the arene to lower field.[16] The ^{11}B NMR spectrum of **32** shows three resonances as expected for the hexabromo carborane anion under C_{5v} symmetry. {BBr} vertices resonate at δ 0.57, -8.77 ppm in a 1:5 ratio as broad singlets. A doublet is displayed for the {BH} vertices at δ -20.39 ppm with *J*(BH) 154 Hz. Thus,

there is a small upfield shift of Δδ 0.96 ppm and a reduction of the coupling constant [Δ*J*(BH) 15 Hz] from the values obtained for compound **28**, when the cage was unbound to any cationic fragment. A similar chemical shift change was observed in the {BH} resonance between the complexes $[(PPh_3)_2Ir(H)_2(closo\text{-}CB_{11}H_6Br_6)]$ and $[(PPh_3)_2Ir(C_2H_4)_3][closo\text{-}CB_{11}H_6Br_6]$.[5] The $^{31}P\{^1H\}$ NMR spectrum shows a doublet at δ 82.9 ppm with *J*(RhP) 161.0 Hz. Comparable chemical shift and coupling constant were reported for $[Rh(P^iPr_3)(H)_2(S)_3]$ (S = acetone), δ 87.0 ppm with *J*(RhP) 157.7 Hz.[16] Table 4.3 shows relevant chemical shifts and coupling constants values of **32** and related compounds.

	Compound	^{1}H NMR	^{1}H NMR Rh-hydrides			$^{31}P(^1H)$	
		CH cage	δ	*J*(RhH)	*J*(PH)	δ	*J*(RhP)
28	$[HPCy_3][closo\text{-}CB_{11}H_6Br_6]$	2.56	n/a	n/a	n/a	43.2	n/a
32	$[Rh(PCy_3)(H)_2(closo\text{-}CB_{11}H_6Br_6)]$	2.82	-21.25	28.8	18.8	82.9	161.0
22	$[Rh(PCy_3)(H)_2(closo\text{-}CB_{11}H_{12})]$	2.82	-19.65	30.0	21.2	86.1	149.8
	$[Rh(^iPr_3P)(H)_2(acetone)_3][PF_6]$[16]	n/a	-23.30	31.2	25.5	87.0	157.7

Table 4.3 Solution in CD_2Cl_2, δ in ppm, *J* in Hz.

4.2.2.2 $[Rh(PCyp_3)(H)_2(closo\text{-}CB_{11}H_6Br_6)]$

Slow addition of two equivalents of $[HPCyp_3][closo\text{-}CB_{11}H_6Br_6]$ (in fluorobenzene solution) to $[Rh(\mu\text{-}OMe)(nbd)]_2$ produces an orange solution that after treatment with hydrogen gas renders a pale brown solution of $[Rh(PCyp_3)(H)_2(closo\text{-}CB_{11}H_6Br_6)]$ (**33**). Removal of the solvent *in vacuo* and recrystallisation of the compound from dichloromethane and pentane yielded an off-white solid in 76 % yield.

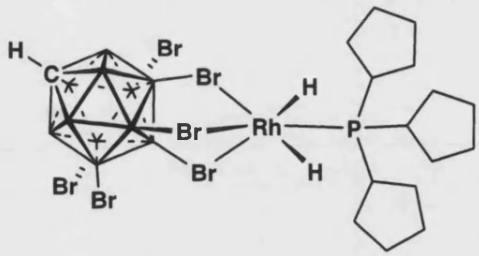

Figure 4.8 Schematic representation of the proposed structure for complex **33**.

A CD_2Cl_2 solution of **33** at room temperature shows in the high field region of the ^1H NMR spectrum a doublet of doublets at δ -20.95 ppm with a Rh-H coupling constant of 28.4 Hz and a P-H coupling constant of 19.6 Hz. This coupling pattern indicates the presence of two hydrides in *cis* position to a phosphine ligand as seen for complex **32**. The cage C-H resonance appears at δ 2.86 ppm and protons from the phosphine ligand lie between δ 2.27-1.49 ppm. The $^1H\{^{11}B\}$ NMR spectrum confirms the signals obtained in ^1H NMR spectrum, and additionally shows a broad singlet at δ 2.48 ppm for the cage {BH} vertices. The ^{11}B NMR spectrum shows the signals for the antipodal and lower pentagonal vertices as broad singlets at δ 0.73 and -8.71 ppm in the ratio 1:5 respectively. The {BH} resonances are displayed as a broad doublet at δ -20.33 ppm, with a B-H coupling constant of 155.3 Hz. These data agree with local C_{5v} symmetry for the [*closo*-$CB_{11}H_6Br_6$]$^-$ cage where all {BBr} vertices interact with the metallic fragment on the NMR time-scale. The B-H resonance has been shifted marginally upfield by Δδ 0.90 ppm when compared to [$HPCyp_3$][$CB_{11}H_6Br_6$] as observed in complex **32** and its phosphonium salt precursor. There is also a similar change in the coupling constant value of ΔJ(BH) -11.7 Hz. The $^{31}P\{^1H\}$ NMR spectrum displays a doublet at δ 86.38 ppm with a Rh-P coupling constant value of 163.6 Hz. These last values are comparable to the chemical shifts and coupling constants reported for the similar compounds [$Rh(PCy_3)(H)_2$(*closo*-$CB_{11}H_6Br_6$)] (**32**) and [$Rh(^iPr_3P)(H)_2(\eta^6$-$C_6H_6)$][16] as Table 4.3 shows.

4.2.2.3 $[Rh(P^iPr_3)(H)_2(closo\text{-}CB_{11}H_6Br_6)]$

$[Rh(P^iPr_3)(H)_2(closo\text{-}CB_{11}H_6Br_6)]$ (**34**) is prepared in a one-pot synthesis by treatment of the complex $[Rh(\mu\text{-}OMe)(nbd)]_2$ with a solution of $[HP^iPr_3][closo\text{-}CB_{11}H_6Br_6]$ in fluorobenzene. Subsequent addition of H_2, as Figure 4.9 shows, results in the formation of complex **34**.

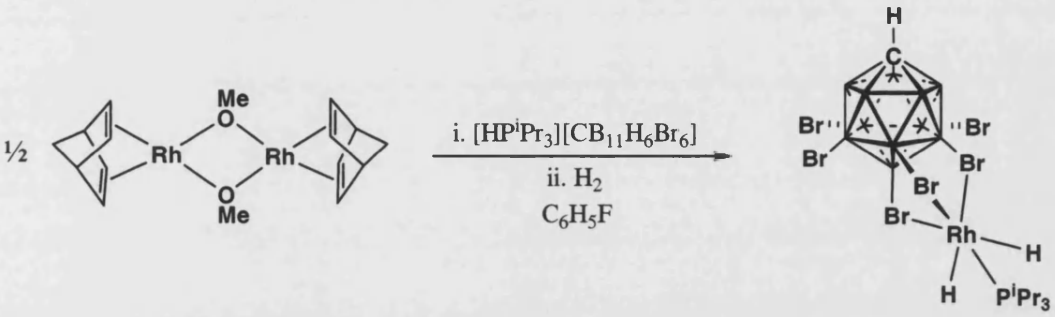

Figure 4.9 Schematic synthesis of complex **34**.

The $^1H\{^{11}B\}$ NMR spectrum of complex **34** (in $CDCl_3$) shows a doublet of doublets at δ -21.04 ppm for the hydrido ligands. The chemical shift is nearly identical to those of **32** and **33**, as well as the coupling constants. Compound **34** displays *J*(RhH) 28.0 Hz and *J*(PH) 18.8 Hz, this is comparable to **32** [*J*(RhH) 28.0 Hz and *J*(PH) 18.8 Hz] and **33** [*J*(RhH) 28.0 Hz and *J*(PH) 18.8 Hz], as Table 4.4 reports. The cage {CH} resonance is displayed at δ 2.79 ppm, and the {BH} resonances are shown as a broad signal at δ 2.54 ppm. Isopropyl groups are displayed at δ 2.19 ppm as a multiplet and at δ 2.79 ppm as a doublet of doublets for the CH and methyl protons respectively. The ^{11}B NMR spectrum shows a broad singlet for the $\{B_{12}\text{-}Br\}$ vertex at δ 1.05 ppm. The lower pentagonal {BBr} vertices resonate at δ -8.48 ppm and the {BH} vertices are observed at δ -20.21 ppm, slightly upfield shifted (Δδ 0.78 ppm) compared to the 'free' $[closo\text{-}CB_{11}H_6Br_6]^-$ carborane in $[HP^iPr_3][closo\text{-}CB_{11}H_6Br_6]$ (**30**). *J*(BH) in complex **34** is 166 Hz, and has been reduced by 5 Hz from compound **30** upon coordination of the

cage to the rhodium fragment. The $^{31}P\{^{1}H\}$ NMR spectrum displays a doublet at δ 94.4 ppm with a *J*(RhP) of 162 Hz. A similar coupling constant is found for the complex $[Rh(^{i}Pr_3P)(H)_2(acetone)_3][PF_6]$ [*J*(RhP) 158 Hz],[16] where three molecules of acetone replace the position that the carborane cage occupies in complex **34**, sitting facial on the metal centre. However, when benzene coordinates to the $\{Rh(^{i}Pr_3P)(H)_2\}^{+}$ fragment, a reduction of the coupling constant is observed [*J*(RhP) 142 Hz][16] due to the larger donation of electron density by the arene ligand. The chemical shifts and coupling constants tabulated in Table 4.4 support the proposed structure for **34** in Figure 4.9.

	Compound	^{1}H NMR	^{1}H NMR Rh-hydrides			$^{31}P(^{1}H)$	
		C*H* cage	δ	*J*(RhH)	*J*(PH)	δ	*J*(RhP)
30	$[HP^{i}Pr_3][closo\text{-}CB_{11}H_6Br_6]^{*}$	2.58	-21.04	n/a	n/a	45.1	n/a
34	$[Rh(P^{i}Pr_3)(H)_2(closo\text{-}CB_{11}H_6Br_6)]$	2.86	-20.95	28.0	18.8	94.4	162
32	$[Rh(PCy_3)(H)_2(closo\text{-}CB_{11}H_6Br_6)]$	2.82	-21.25	28.8	18.8	82.9	161
	$[Rh(^{i}Pr_3P)(H)_2(acetone)_3][PF_6]$[16]	n/a	-23.30	31.2	25.5	87.0	158

Table 4.4 Solution in CD_2Cl_2 ($^{*}CDCl_3$), δ in ppm, *J* in Hz.

4.2.2.3.1 Reactivity with benzene

Addition of benzene to a solution of **34** produces partial displacement of the $[closo\text{-}CB_{11}H_6Br_6]^{-}$ anion. Figure 4.10 shows the equilibrium formed between complex **34** and the new half-sandwich compound $[Rh(P^{i}Pr_3)(H)_2(\eta^6\text{-}C_6H_6)][closo\text{-}CB_{11}H_6Br_6]$ (**35**). Compound **35** has been characterised in solution by direct comparison with $[(P^{i}Pr_3)Rh(H)_2(\eta^6\text{-}C_6H_6)][PF_6]$.[16]

The $^{1}H\{^{11}B\}$ NMR spectrum shows a singlet at δ 6.94 ppm characteristic of coordinated benzene that has been upfield shifted by about 0.4 ppm compared to free benzene (δ benzene 7.36 ppm, in CD_2Cl_2).[17] The cage C-H and B-H resonances are

displayed at δ 2.60 and 2.39 ppm respectively, as observed in compound **30** where the cage was unbound. Isopropyl resonances are shown as a doublet of septets at δ 2.03 ppm for the C*H*, and as a doublet of doublets at δ 1.13 ppm for the C*Me*$_2$ protons. The hydride resonance has been downfield shifted by Δδ 6.4 ppm to lower field from that observed in complex **34** (δ -20.95 ppm) to δ -14.53 ppm, being effectively identical with the chemical shift reported for [(P^iPr_3)Rh(H)$_2$(η^6-C_6H_6)][PF_6] (δ -14.54 ppm).[16] The $^{31}P\{^1H\}$ NMR spectrum shows a doublet at δ 97.2 ppm with a coupling constant *J*(RhP) of 143 Hz as also reported for the [(P^iPr_3)Rh(H)$_2$(η^6-C_6H_6)]$^+$ fragment. The ^{11}B NMR spectrum displays three resonances as expected for an uncoordinated cage, two singlets in 1:5 ratio at δ -0.95 and -9.05 ppm, and a doublet at δ -19.41 ppm.

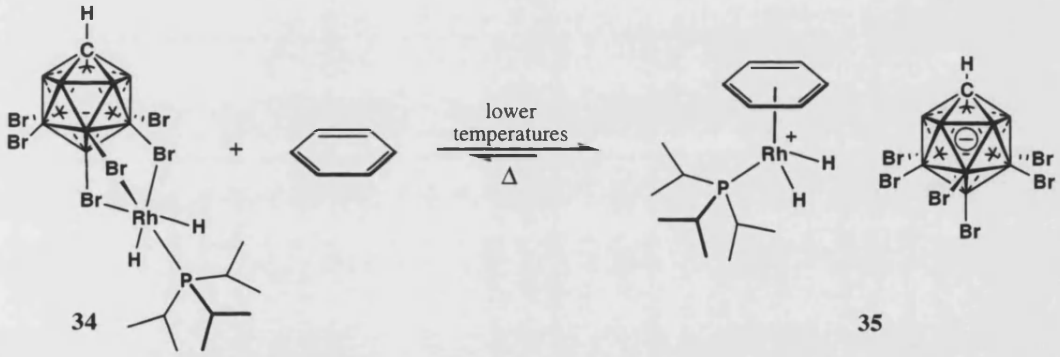

Figure 4.10 Equilibrium observed after addition of benzene to **34**.

The concentration of the species present in the equilibrium varies with the temperature. Complex **35** is favored at lower temperatures, therefore the displacement of the equilibrium towards **34** is an endothermic process. Unfortunately no equilibrium constant data was collected over a suitable temperature range, which means estimates of ΔH° and ΔS° are not available. However, the relative ratios of the species in solution have helped us to estimate ΔG° according to the equilibrium described in Figure 4.10. Therefore and using the equation $\Delta G^\circ = -RT \ln K_{eq}$, ΔG°(298K) = -8.4 kJmol^{-1}. Thus, benzene binds more strongly to the rhodium fragment than the carborane cage anion in

this system. The hexabromo carborane anion remains coordinated to the Rh(III) fragment when compound **34** is dissolved in neat fluorobenzene. This reflects the weaker coordinating nature of fluorobenzene against benzene and the preference of this Rh(III) centre for cage coordination through three Rh-Br interactions rather than the weak π-donor fluorobenzene.

Single crystals of $[Rh(P^iPr_3)(H)_2(\eta^6\text{-}C_6H_6)][CB_{11}H_6Br_6]$ (**35**) suitable for X-ray crystallography were obtained by addition of benzene to a highly concentrated solution of **34** in fluorobenzene. Elemental analysis from crystalline material suggests a formulation for the solid material that corresponds to five molecules of complex **35** and one molecule of **34**. Figure 4.11 displays the solid-state structure of **35** and relevant bond lengths and angles in Table 4.5. The rhodium atom exhibits a pseudo-octahedral geometry, with a typical three-legged piano-stool appearance. The metal centre is η^6-bonded to the benzene ligand and completes its coordination sphere with one triisopropylphosphine ligand and two hydrides. The carborane anion is well separated from the rhodium atom with the closest Rh-Br distance of 5.313 Å. The rhodium distances to the arene carbon atoms are moderately affected by the *trans* influence of the hydride ligands. C(2) and C(3) are the most affected [Rh(1)-C(2) 2.357(4) Å; Rh(1)-C(3) 2.362(4) Å] along with C(1). In contrast, the C(5) and C(6), *cis* to Rh-H bonds, show shorter Rh-C distances [Rh(1)-C(5) 2.286(4) Å; Rh(1)-C(6) 2.297(4) Å]. These distances are nearly identical to those reported for the arene-chelate complex $[(\eta^6\text{-}C_6H_5CH_2CH_2CH_2P^iPr_2\text{-}\kappa\text{-}P)Rh(C_8H_{14})][PF_6]$ [2.295(4)-2.355(4) Å],[18] or for the even more similar complex $[(\eta^6\text{-}C_6H_6)Rh(P^iPr_3)(C_8H_{14})]$ [2.296(5)-2.365(4) Å].[19] The Rh-P1 bond length of 2.2536(10) is also very similar to that found in $[(\eta^6\text{-}C_6H_6)Rh(P^iPr_3)(C_8H_{14})]$ [2.294(1) Å], complex **34** [2.2165(7) Å] or the solid-state structure of **25** [2.2324(6) and 2.2572(6) Å].

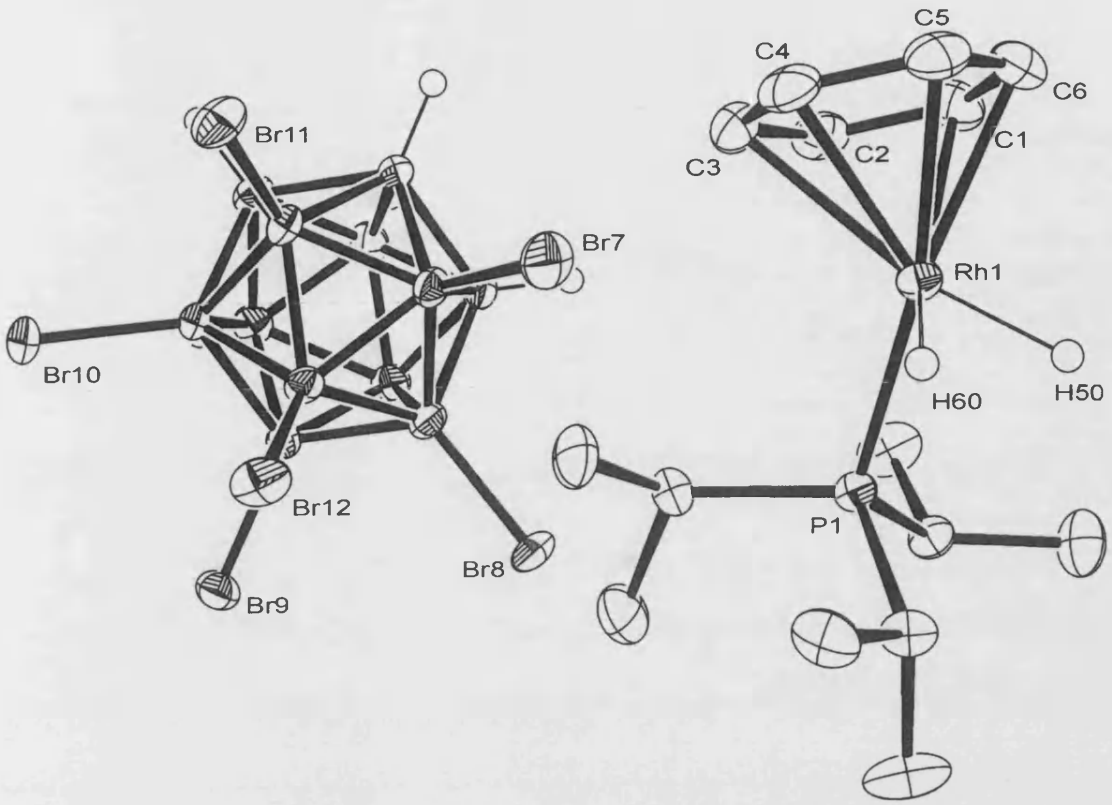

Figure 4.11 Solid-state structure of **35**. Thermal ellipsoids are shown at the 50% probability level and hydrogen atoms associated with carbon atoms are omitted for clarity.

Rh(1)-P(1)	2.2536(10)	Rh(1)-H(60)	1.52(5)
Rh(1)-C(1)	2.343(4)	C(1)-C(2)	1.389(6)
Rh(1)-C(2)	2.357(4)	C(2)-C(3)	1.409(6)
Rh(1)-C(3)	2.362(4)	C(3)-C(4)	1.390(6)
Rh(1)-C(4)	2.320(4)	C(4)-C(5)	1.409(7)
Rh(1)-C(5)	2.286(4)	C(5)-C(6)	1.395(7)
Rh(1)-C(6)	2.297(4)	C(1)-C(6)	1.423(6)
Rh(1)-H(50)	1.59(6)	H(50)-Rh(1)-P(1)	80(2)

Table 4.5 Selected bond lengths (Å) and angles (°) for **35**.

4.2.2.4 Reactivity of $[Rh(PR_3)(H)_2(closo\text{-}CB_{11}H_6Br_6)]$ with D_2

As determined by $^1H\{^{11}B\}$ and ^{11}B NMR spectroscopy, exposure of **32**, **33** and **34** to a D_2 atmosphere results in the deuteration of the all upper belt {BH} vertices and formation of Rh-D bonds. The latter is observed in the ^2H NMR spectra as a broad signal at about δ -21 ppm, which correlates with the hydride resonance observed for **32**, **33** and **34.** Therefore, it can be suggested the formation of mononuclear deuterated complexes that could be formulated as $[Rh(PR_3)(D)_2(1\text{-}H\text{-}closo\text{-}CB_{11}D_6Br_6)]$ (R = Cy, Cyp, ^{i}Pr) (Figure 4.12). It is also evident the formation of H/D(g) (1:1:1 triplet at δ 4.55) suggesting a mechanism as that displayed in Figure 3.16 (Chapter 3) for the $[closo\text{-}CB_{11}H_{12}]^-$ cage.

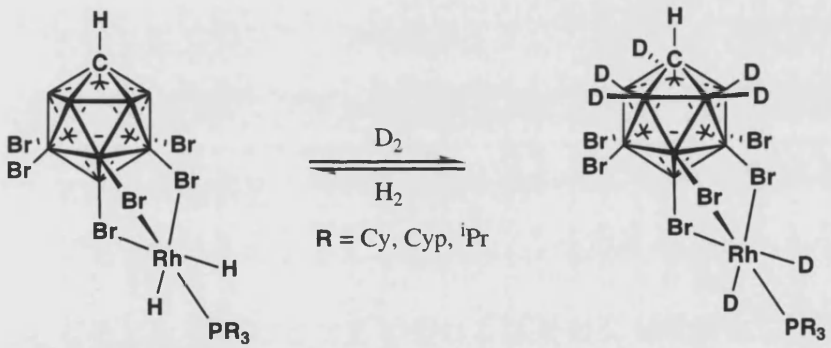

Figure 4.12 Deutaration of the upper {BH} vertices on the $[closo\text{-}CB_{11}H_6Br_6]^-$ anion.

4.2.3 Reactivity of $[Rh(PR_3)(H)_2(closo\text{-}CB_{11}H_6Br_6)]$ towards olefins

In Chapter 3 it was reported that exposure to vacuum of the compounds of formula $[Rh(PR_3)(H)_2(closo\text{-}CB_{11}H_{12})]$ (R = Cy, Cyp, ^{i}Pr) resulted in the formation of rhodium dimer species in which the cage anion had undergone B-H oxidative addition. Addition of olefins, such as ethene or 1-hexene, resulted in dehydrogenative borylation of {BH} vertices of the parent $[closo\text{-}CB_{11}H_{12}]^-$ anion. Complete deuteration of {BH} vertices was also observed when solutions of the dimer species were exposed to D_2, which suggests oxidative addition of B-H bonds.

Likewise, we have seen that exposing complexes **32**, **33** and **34** to a deuterium atmosphere while in solution results in the complete replacement of the upper pentagonal {BH} vertices for {BD}. This shows that in the chemical time-scale the {RhP} fragment inserts into the upper belt {BH} bonds. However, the metal does not promote olefin insertion (ethene, 1-hexene) despite being able to oxidatively add the upper pentagonal {B-H} vertices to substitute them by deuterium. Instead, addition of the hydrogen acceptor *tert*-butylethene produces C-H activation of one of the cyclohexyl and cyclopentyl rings in **32** and **33**, while in compound **34** a molecule of *tert*-butylethene coordinates to the metal after consuming one equivalent of the rhodium-hydrides.

4.2.3.1 [Rh{(η^2-C_6H_9)P(Cy_2)}(*closo*-$CB_{11}H_6Br_6$)]

Addition of excess of *tert*-butylethene to a pale yellow solution of **32** results in the formation of a dark red solution after 30 minutes that turns slowly orange. After one day of reaction the new orange solution contains one organometallic species identified by NMR spectroscopy as [Rh{(η^2-C_6H_9)P(Cy_2)}(*closo*-$CB_{11}H_6Br_6$)] (**36**) in which one of the cyclohexyl groups has undergone dehydrogenation. Addition of pentane affords a pale orange solid in 75 % yield.

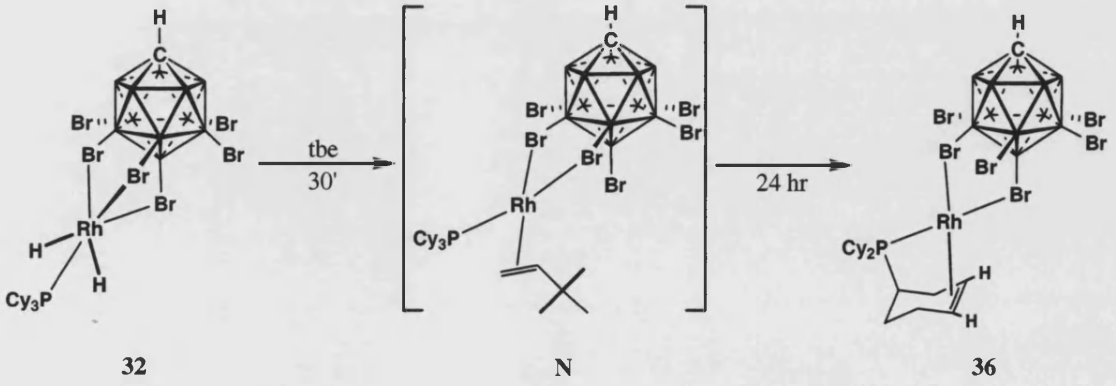

Figure 4.13 Schematic synthesis of compound **36**.

The ^{1}H NMR spectrum of complex **36** in CD_2Cl_2 shows a signal at δ 4.43 ppm for the coordinated alkene, although we should expect two resonances due to the C_1 symmetry of the complex. However, the $^{13}C\{^{1}H\}$ NMR spectrum displays two separate resonances for the CH=CH olefinic carbons at δ 68.88 ppm [d, *J*(RhC) 16.0] and δ 62.26 ppm [d, *J*(RhC) 16.7]. Thus, the two signals expected in the ^{1}H NMR spectrum are coincident. Identification of the double bond within the cyclohexyl ring was possible using $^{13}C\{^{1}H\}$ PENDANT, HMQC and ^{1}H-^{1}H COSY NMR experiments, and places it at the 3,4-positions of the ring. The cage C-H signal is displayed at δ 2.72 ppm, a downfield shifted when compared with compound **28** where the cage is uncoordinated (δ 2.56 ppm). Cyclohexyl protons appear between δ 2.28 and 1.24 ppm. The ^{11}B NMR spectrum shows three resonances, two broad singlets at δ -0.22 and -9.42 ppm for antipodal and lower pentagonal {BBr} vertices, and a doublet at δ -20.27 ppm [*J*(BH) 164 Hz] for the top {BH} vertices. This is consistent with a local C_{5v} symmetry for cage anion in solution, and thus invokes a fluxional process where all lower pentagonal vertices are equivalent on the NMR time-scale. The $^{31}P\{^{1}H\}$ NMR spectrum displays a doublet at δ 84.63 ppm with a coupling constant *J*(RhP) of 180 Hz. The chemical shift has been barely shifted downfield by Δδ 1.7 ppm when compared to the precursor compound **32**. However, the coupling constant value has been increased by about 20 Hz, consistent with a change in the oxidation state of the metal from Rh(III) to Rh(I).

When the reaction is followed *in situ* by $^{31}P\{^{1}H\}$ NMR spectroscopy, the initial signal at δ 82.9 ppm [*J*(RhP) 161] due to **32** decreases progressively accompanied by the growth of a doublet at δ 58.3 ppm [*J*(RhP) 180]. This new intermediate product (**N**) evolves eventually into complex **36** (δ 84.63 ppm) over 24 hours. The intermediate structure proposed in Figure 4.13, [Rh(PCy_3)(tbe)(*closo*-$CB_{11}H_6Br_6$)], is related to

compound **41** (*vide infra*) that is a *tert*-butylethene rhodium complex, i.e. [Rh(P^{i}Pr$_3$)(tbe)(*closo*-$CB_{11}H_6Br_6$)]. Similarly to **41**, whose $^{31}P\{^1H\}$ NMR resonance is shifted by $\Delta\delta$ 20 ppm upfield compared to its precursor [Rh(P^{i}Pr$_3$)(H)$_2$(*closo*-$CB_{11}H_6Br_6$)], the $^{31}P\{^1H\}$ NMR resonance for **N** appears upfield shifted by $\Delta\delta$ 24 ppm compared to **32**. In both cases the coupling constants also follow the same trend, as Table 4.6 shows. The increment of about 20 Hz is consistent with a new oxidation state for the metal centre that involves the reduction of the dihydride-Rh(III) fragments to Rh(I) species.

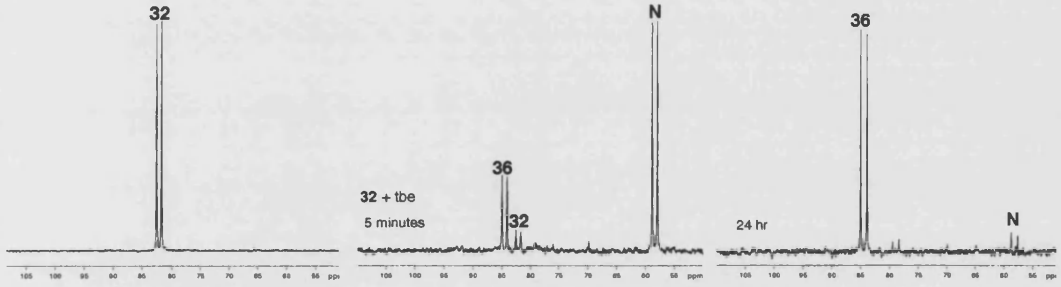

Figure 4.14 $^{31}P\{^1H\}$ NMR spectra of the reaction of complex **32** with tbe to form **36** through the proposed intermediate **N**.

Compound	δ(ppm)	*J*(RhP)	Compound	δ(ppm)	*J*(RhP)
32	82.9	161	**34**	94.4	162
N	58.3	180	**41**	74.0	183

Table 4.6 $^{31}P\{^1H\}$ NMR data of complexes **32**, **34, 41** and the proposed intermediate **N**.

C-H activation of a cyclohexyl moiety has been observed previously in ruthenium complexes bearing tricyclohexylphosphine ligand,[20-23] as well as in iridium-carbene complexes.[24, 25] The dehydrogenation of the cyclohexyl ring on the C3, C4 position to the phosphorus atom as observed in **36** has also been reported for the ruthenium complex {Cp*Ru[(η^2-C_6H_9)P(C_6H_{11})$_2$]}BF_4, shown in Figure 4.15 on the left.[21] Figure 4.15 provides examples of the possible metal-mediated C-H activations a cyclohexyl ring can undergo. The cyclohexyl ring also offers the possibility of dehydrogenation on

three carbon atoms to generate an allylic group. This has been widely studied by Sabo-Ethiene et al. upon dehydrogenation of the ruthenium complex $RuH_2(H_2)_2(PCy_3)_2$.[20] We see no evidence of such a process here.

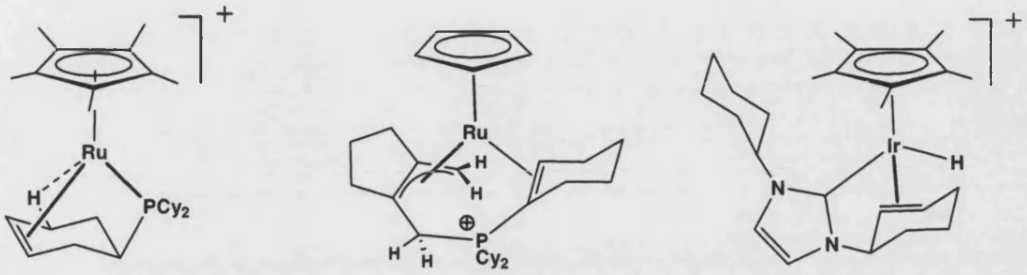

Figure 4.15 Dehydrogenation of a cyclohexyl ring at three different positions.

Figure 4.16 presents a suggested mechanism based on that established for alkane dehydrogenation.[26-28]

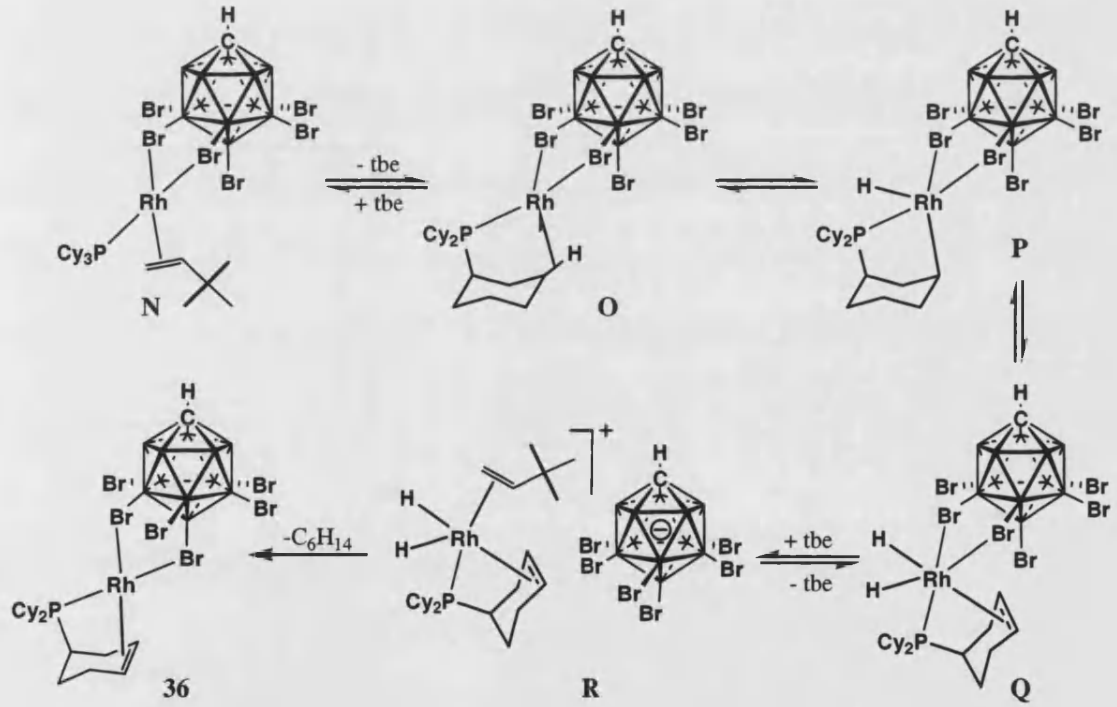

Figure 4.16 Suggested mechanism for alkane dehydrogenation in PCy_3.

After hydrogenation of one equivalent of *tert*-butylethene by complex **32**, we suggest the formation of an intermediate **N** (Figure 4.13), observed by $^{31}P\{^1H\}$ NMR spectroscopy as commented previously. The intermediate **O** arises by the dissociation of

the *tbe* ligand, and through a C-H activation step (**P**), β-elimination (**Q**) and reduction of another *tbe* molecule, compound **36** is formed. C-H activation is generally a higher energy process than the β-transfer and thus the transformation of **N** to **O** is suggested to be a likely rate-determining step.

4.2.3.1.1 Reactivity with toluene

Use of toluene as a co-solvent in the reaction mixture results in the formation of $\{(\eta^6\text{-}C_6H_5Me)Rh[(\eta^2\text{-}C_6H_9)P(Cy_2)]\}[closo\text{-}CB_{11}H_6Br_6]$ (**37**). Attempts to obtain single crystals in order to determine the X-ray crystal structure of **37** were unfruitful, and characterisation of this complex was based on NMR spectroscopy techniques and elemental analysis. Compound **37** can also be generated by addition of toluene to **36**.

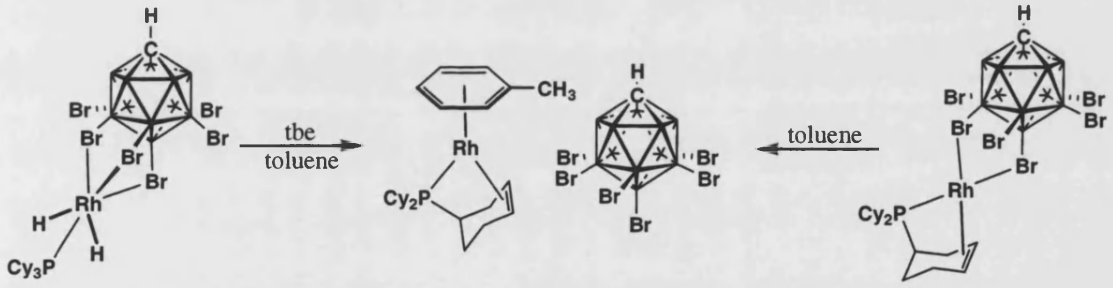

Figure 4.17 Schematic synthesis of compound **37**.

The ^1H NMR spectrum of **37** shows four signals for the coordinated toluene at δ 6.68, 6.63, 6.46 and 6.30 ppm, in a 1:2:1:1 ratio. These resonances have been shifted to higher field by about Δδ 0.6 ppm since free toluene resonances in CD_2Cl_2 appear between δ 7.28 and 7.10 ppm.[17] The toluene methyl singlet appears at δ 2.27 ppm. The C_1 symmetry of the molecule is further demonstrated by two different signals from the olefinic protons of the C-H activated cyclohexyl ring. These resonances are shown at δ 4.50 and 3.96 ppm, and their relative integrals correspond to one proton each. Coordination of the toluene has resulted in these signals now being no longer

isochronous. The cage C-H has been shifted upfield to δ 2.57 ppm when compared to the chemical shift in complex **36** (δ 2.72 ppm), consistent with its decoordination of the metal fragment. Alkyl protons of the cyclohexyl groups are displayed between δ 2.40 and 1.15 ppm. The $^{1}H\{^{11}B\}$ NMR spectrum confirms the resonances commented upon previously and also include the upper pentagonal B-*H* resonances at δ 2.33 ppm. The ^{11}B NMR spectrum shows three signals, two singlets are displayed at δ -1.64 and -9.81 ppm and a doublet at δ -20.15 ppm [*J*(BH) 167 Hz] as expected for a local C_{5v} symmetric anion.

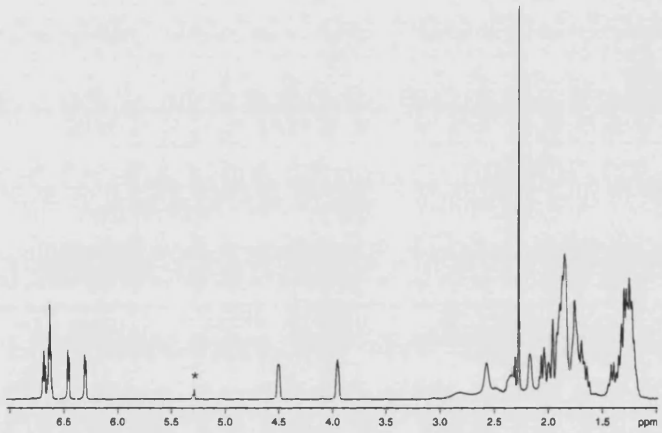

Figure 4.18 ^{1}H NMR spectrum of compound **37** (*residual solvent).

The $^{13}C\{^{1}H\}$ PENDANT NMR spectrum of **37** clearly shows six carbon environments for the toluene ligand between δ 120.16 and 99.58 ppm. The alkene carbons coordinated to rhodium appear at δ 68.04 ppm [*J*(RhC) 14.1, *J*(PC) 2.9] and δ 62.26 ppm [*J*(RhC) 14.1, *J*(PC) 1.9], and are nearly coincident to the chemical shifts of complex **36**, δ 68.88 ppm [*J*(RhC) 16.0] and δ 62.26 ppm [*J*(RhC) 16.7]. The cage carbon atom resonates at δ 41.49 ppm and alkyl signals of the cyclohexyl rings are shown between δ 38.66-22.45 ppm. The methyl carbon of the toluene ligand is diplayed at δ 19.79 ppm.

4.2.3.2 [Rh{P(Cyp$_2$)(η^2-C$_5$H$_7$)}(*closo*-CB$_{11}$H$_6$Br$_6$)]

Treatment of a solution of Rh(PCyp$_3$)(H)$_2$(*closo*-CB$_{11}$H$_6$Br$_6$) (**33**) with *tert*-butylethene, which acts as hydrogen acceptor, results in the dehydrogenation of the rhodium fragment. The dehydrogenation process occurs on one of the cyclopentyl rings with the consequent formation of the complex [Rh{P(Cyp$_2$)(η^2-C$_5$H$_7$)}(*closo*-CB$_{11}$H$_6$Br$_6$)] (**38**) in 69% isolated yield. Addition of H_2 results in the formation of complex **33** as Figure 4.19 shows.

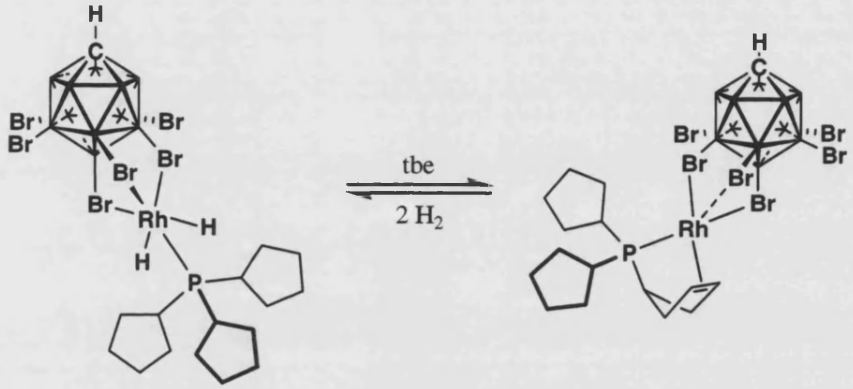

Figure 4.19

Single crystals suitable for X-ray crystallography were obtained from a concentrated solution of **38**, and its solid-state structure is shown in Figure 4.20. Table 4.7 shows relevant bond lengths and angles. The geometry of complex **38** can be described as pseudo trigonal bipyramidal with the alkene ligand and two bromine atoms in the equatorial position. The phosphorus and another bromine atom occupy the apices. The chelating phosphine-olefin ligand coordinates with the rhodium through two carbons and a phosphorus atom, the latter with a Rh-P distance of 2.1973(11) Å. This distance is slightly shorter than that found for the similar monophosphine rhodium complex [Rh{P(Cyp$_2$)(η^2-C$_5$H$_7$)}(η^6-C$_6$H$_5$F)][BAr$^F{}_4$] [Rh-P 2.2412(6) Å],[29] or in [Rh(PCy$_3$)(H)$_2$(CB$_{11}$H$_6$Br$_6$)] (**32**) [Rh-P 2.2165(7) Å].

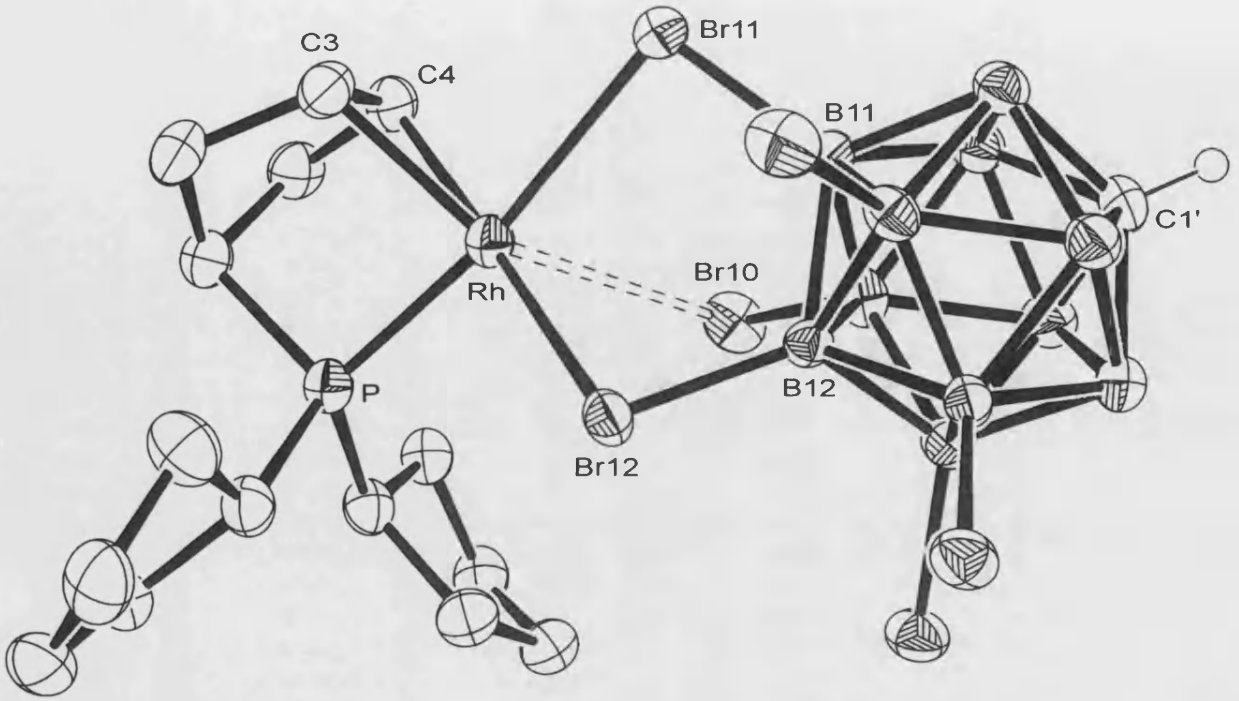

Figure 4.20 Solid-state structure of **38**. Thermal ellipsoids are shown at the 50% probability level and hydrogen atoms associated with the boron and phosphine carbon atoms are omitted for clarity.

Rh-P	2.1973(11)	Rh-Br(10)	2.9514(6)	C(3)-C(4)	1.415(7)	C(4)-Rh-Br(12)	173.66(13)
Rh-Br(11)	2.6504(5)	Rh-C(3)	2.109(5)	C(3)-Rh-P	84.24(13)	Br(11)-Rh-Br(12)	87.243(16)
Rh-Br(12)	2.6702(5)	Rh-C(4)	2.077(5)	C(4)-Rh-P	84.40(13)	C(4)-Rh-C(3)	39.51(18)

Table 4.7 Selected bond lengths (Å) and angles (°) for **38**.

The alkene carbon atoms are situated at 2.109(5) and 2.077(5) Å to the rhodium atom. Similar distances were observed for $[Rh\{P(Cyp_2)(\eta^2\text{-}C_5H_7)\}(\eta^6\text{-}C_6H_5F)][BAr^F{}_4]$ [2.125(2) and 2.128(2) Å] or in the non-chelated monophosphine-alkene complex $[\{\eta^6\text{-}C_6H_5(CH_2)_3P^iPr_2\text{-}\kappa\text{-}P\}Rh(\eta^2\text{-}C_8H_{14})][PF_6]$ (Figure 4.21 right) [2.151(4) and 2.127(4) Å].[18] The alkene C-C distance in complex **38**, 1.415(7) Å, is the same observed $[Rh\{P(Cyp_2)(\eta^2\text{-}C_5H_7)\}(\eta^6\text{-}C_6H_5F)][BAr^F{}_4]$ (Figure 4.21 left), 1.414(5) Å,[29] as expected for a Rh(I) alkene interaction.

The carborane anion coordinates to the rhodium fragment through three Rh-Br interactions. One of these is significantly longer than the other two [2.9514(6) Å versus 2.6504(5), 2.6702(5) Å], with one weaker equatorial Rh···Br interaction. Similar Rh-Br distances to the shortest two Rh-Br contacts are observed in complex **32**, situated with the range of 2.6346(3) and 2.7241(3) Å. However, the structure is still best described as trigonal bipyramidal than square planar or tetrahedral.

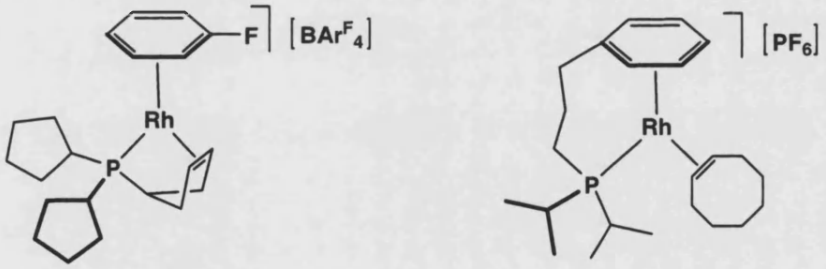

Figure 4.21 $[Rh\{P(Cyp_2)(\eta^2\text{-}C_5H_7)\}(\eta^6\text{-}C_6H_5F)][BAr^F{}_4]$[29] and $[\{\eta^6\text{-}C_6H_5(CH_2)_3P^iPr_2\text{-}\kappa\text{-}P\}Rh(\eta^2\text{-}C_8H_{14})][PF_6]$[18] complexes.

The C_1 symmetry observed for **38** in the solid state is not retained in solution (CD_2Cl_2), where the anion is fluxional and shows local C_{5v} symmetry. The ^{11}B NMR spectrum confirms this fluxionality in solution with three resonances observed at δ 0.01, -9.31 and -20.30 ppm in a 1:5:5 ratio. The $^1H\{^{11}B\}$ NMR spectrum shows only one resonance for the upper pentagonal {BH} vertices that indicates C_{5v} symmetry for the cage anion and one broad signal at δ 2.74 ppm for the cage C-H proton. This spectrum

also displays a single resonance for the alkene protons at δ 4.17 ppm, which are related to a doublet at δ 63.54 pmm [*J*(RhC) 19.7 Hz] in the $^{13}C\{^{1}H\}$ NMR spectrum by a HMQC experiment. This chemical shift is as expected for a metal alkene, and lies between the δ 3.89 and δ 4.30 ppm observed for the $[Rh\{P(Cyp_2)(\eta^2\text{-}C_5H_7)\}(\eta^6\text{-}C_6H_5F)][BAr^F{}_4]$ complex and its benzene analogue $[Rh\{P(Cyp_2)(\eta^2\text{-}C_5H_7)\}(\eta^6\text{-}C_6H_6)][BAr^F{}_4]$.[29] Comparable chemical shifts have been accounted for ruthenium complexes bearing the same chelating phosphine-alkene ligand, e.g. $[RuH\{PCy_2(\eta^3\text{-}C_6H_8)\}\{PCy_2(\eta^2\text{-}C_6H_9)\}]$.[30] Alkyl resonances are shown between δ 2.25 and 0.90 ppm, as expected. The $^{31}P\{^{1}H\}$ NMR spectrum shows a doublet at δ 116.60 ppm, which has been downfield shifted by Δδ 30.2 ppm when compared with its precursor compound **33**. This is as expected for incorporation of the phosphine in a chelate ring.[31] The *J*(RhP) coupling constant of 180 Hz is consistent with a Rh(I) monophosphine fragment, and is similar to those found in the literature.[29]

4.2.3.2.1 Reactivity with arenes

Addition of an excess of fluorobenzene or one equivalent of toluene to **38** results in the quantitative formation of the complexes $[(\eta^6\text{-}C_6H_5F)Rh\{(\eta^2\text{-}C_5H_7)P(Cyp_2)\}][\textit{closo}\text{-}CB_{11}H_6Br_6]$ (**39**) and $[(\eta^6\text{-}C_6H_5Me)Rh\{(\eta^2\text{-}C_5H_7)P(Cyp_2)\}][1\text{-}\textit{closo}\text{-}CB_{11}H_6Br_6]$ (**40**), respectively. Characterisation of **39** and **40** was performed by X-ray diffraction and NMR spectroscopy. The solid state-structures are shown in Figure 4.22 (**39**) and Figure 4.23 (**40**), and relevant bond lengths and angles in Table 4.8 (**39**) and Table 4.9 (**40**).

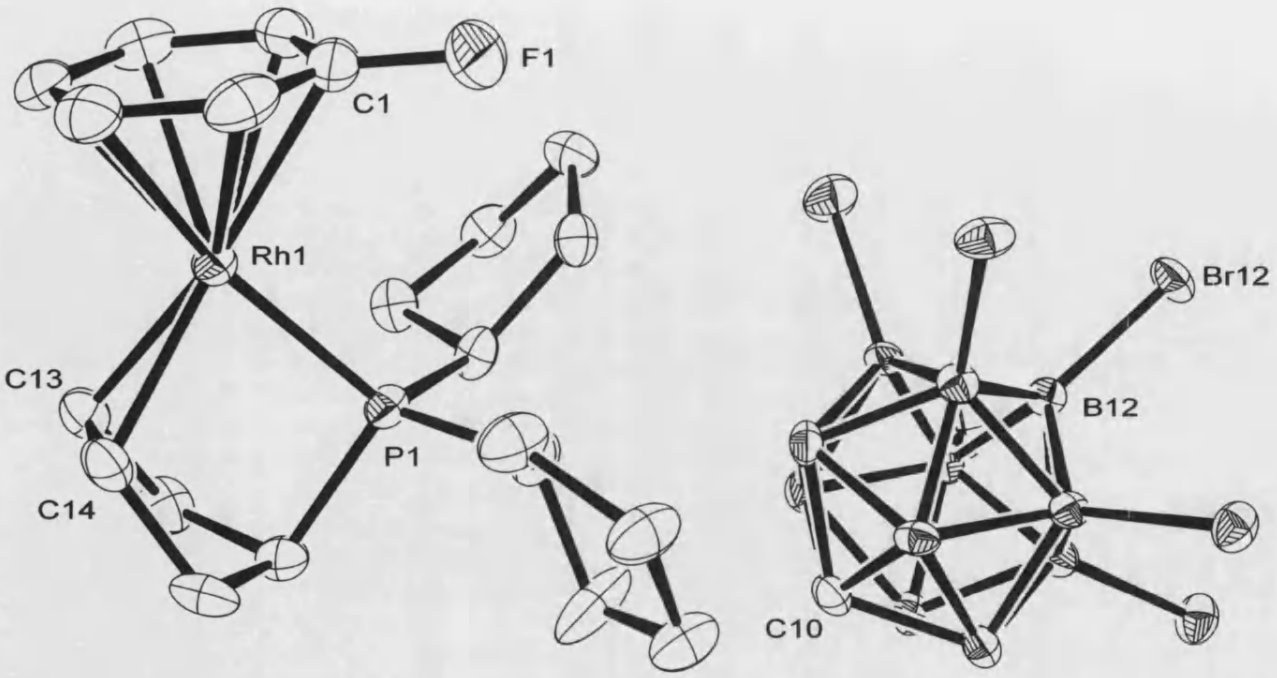

Figure 4.22 Solid-state structure of **39**. Thermal ellipsoids are shown at the 50% probability level and hydrogen atoms associated with the boron and carbon atoms are omitted for clarity.

Rh(1)-P(1)	2.2492(15)	Rh(1)-C(1)	2.277(7)	Rh(1)-C(4)	2.282(6)	C(13)-C(14)	1.431(10)
Rh(1)-C(13)	2.139(6)	Rh(1)-C(2)	2.314(7)	Rh(1)-C(5)	2.313(7)	C(13)-Rh(1)-P(1)	83.33(18)
Rh(1)-C(14)	2.146(6)	Rh(1)-C(3)	2.307(7)	Rh(1)-C(6)	2.369(7)	C(13)-Rh(1)-C(14)	39.0(3)

Table 4.8 Selected bond lengths (Å) and angles (°) for **39**.

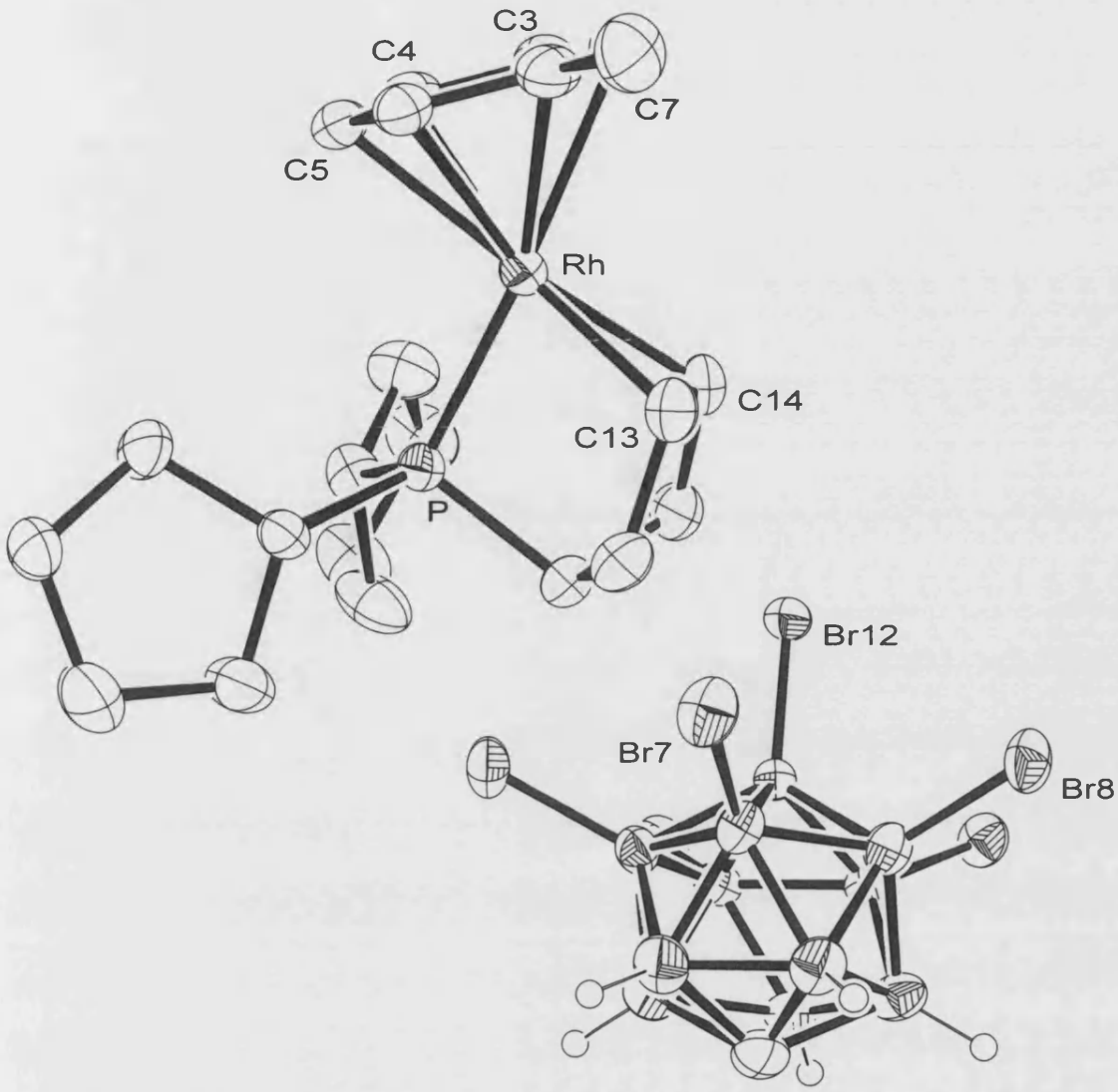

Figure 4.23 Solid-state structure of **40**. Thermal ellipsoids are shown at the 50% probability level and hydrogen atoms associated with the carbon atoms are omitted for clarity.

Rh-P	2.2305(10)	Rh-C(3)	2.327(4)	C(3)-C(4)	1.381(6)
Rh-C(13)	2.128(5)	Rh-C(4)	2.307(4)	C(4)-C(5)	1.395(6)
Rh-C(14)	2.127(4)	Rh-C(5)	2.249(4)	C(5)-C(6)	1.385(6)
C(13)-C(14)	1.409(8)	Rh-C(6)	2.300(4)	C(1)-C(7)	1.507(6)
Rh-C(1)	2.328(4)	C(1)-C(2)	1.431(6)	C(13)-Rh-P	82.77(13)
Rh-C(2)	2.291(4)	C(2)-C(3)	1.407(6)	C(14)-Rh-P	83.06(13)

Table 4.9 Selected bond lengths (Å) and angles (°) for **40**.

Complexes **39** and **40** show a configuration typical of half-sandwich arene complexes in which the other ligands on rhodium lies orthogonal to the arene ring. The Rh-P distances are found at 2.2492(15) Å and 2.2305(10) Å, respectively, and are similar to that observed for the same fluorobenzene fragment with the $[BAr^F_4]^-$ anion, 2.2412(6) Å, pictured in Figure 4.21.[29] Rh-C_{alkene} distances in **39** and **40** are found in the range [2.127(4)-2-146(6) Å], typical of Rh-olefin distances, such as those observed in [{η^6-$C_6H_5(CH_2)_3P^iPr_2$-κ-P}Rh(η^2-C_8H_{14})][PF_6] (Figure 4.21, right) and related complexes described therein.[18] Alkene C-C bond distances [1.431(10) Å in **39**, 1.409(8) Å in **40**] are also consistent with those metal-alkene complexes described by Werner,[18] or in similar monophosphine-iridium-arene complexes such as [Ir(η^6-C_6H_6)(P^iPr_3)(η^2-CH_2=CH_2)] [C=$C_{distance}$ 1.430(7) Å].[32] Rh-C_{arene} distances in complexes **39** and **40** are found between the range 2.249(4)-2.369(7) Å and show no significant differences with the complexes referenced above. The most significant distances of these complexes are recorded in Table 4.10.

Compound	Rh-P	Rh-C_{alkene}	Rh-C_{arene}	C=C_{alkene}
39	2.2492(15)	2.139(6)-2.146(6)	2.277(7)-2.369(7)	1.431(10)
40	2.2305(10)	2.127(4)-2.128(5)	2.249(4)-2.328(4)	1.381(6)
[Rh{$P(Cyp_2)(\eta^2$-$C_5H_7)$}(η^6-C_6H_5F)][BAr^F_4][29]	2.2412(6)	2.125(2)-2.128(2)	2.244(2)-2.330(2)	1.401(4)
[{η^6-$C_6H_5(CH_2)_3P^iPr_2$-κ-P}Rh(η^2-C_8H_{14})][PF_6][18]	2.265(1)	2.127(4)-2.151(4)	2.295(4)-2.355(4)	1.403(6)

Table 4.10 Bond lengths in Å.

When compound **39** is dissolved in CD_2Cl_2, without excess fluorobenzene present, the carborane cage competes with the fluorobenzene ligand in order to coordinate to rhodium. This results in an equilibrium between compounds **38** and **39** as shown in

Figure 4.24. On the other hand, only one compound (the fluorobenzene adduct) is observed when compound **39** is dissolved in neat fluorobenzene. The [*closo*-$CB_{11}H_6Br_6]^-$ does not displace the toluene ligand in compound **40**, and consequently a single compound is observed in a CD_2Cl_2 solution.

The $^1H\{^{11}B\}$ NMR spectrum of complex **39** in CD_2Cl_2 shows three resonances due to the coordinated arene at δ 6.82, 6.71 and 6.11 ppm. These signals have been shifted upfield by about Δδ *ca* 0.4 to 0.9 ppm compared to free fluorobenzene [δ 7.42, 7.12 and 7.04 ppm]. The alkene resonance is displayed at δ 4.38 ppm and is shifted downfield by Δδ 0.2 ppm when compared to complex **38**, but coincides with the chemical shift reported for the $[BAr^F{}_4]^-$ analogous formula (Figure 4.21).[29] The carborane cage C-H proton is shown at δ 2.58 ppm, consistent with a non-coordinated $[CB_{11}H_6Br_6]^-$ cage. Alkyl signals from the phosphine ligand arise between δ 2.20 and 1.45 ppm. The ^{11}B NMR spectrum confirms the C_{5v} symmetry of the carborane cage observed in the solid-state structure. The antipodal and lower pentagonal {BBr} vertices appear at δ -1.08 ppm and δ -9.33 ppm respectively as two broad singlets in a 1:5 ratio. The upper pentagonal vertices are represented by a doublet at δ -19.94 ppm with a *J*(BH) coupling constant of 150 Hz. The $^{31}P\{^1H\}$ NMR spectrum shows a doublet of doublets at δ 111.24 ppm, with a *J*(RhP) coupling constant of 178 Hz and an additional *J*(FP) of 3.8 Hz due to phosphorus coupling to fluorine. The ^{19}F NMR spectrum shows a singlet at δ -120.6 ppm, which has been upfield shifted by Δδ 7 ppm compared to free fluorobenzene resonance (δ -113.6 ppm). Similar chemical shifts and coupling constants are observed in complex **40**, except for the arene resonances that vary slightly due to the substitution of the fluorine by the methyl group.

A solution of **39** in CD_2Cl_2 establishes an equilibrium between **38** and **39**, with their relative concentration at room temperature in a 1:2.7 ratio, respectively.

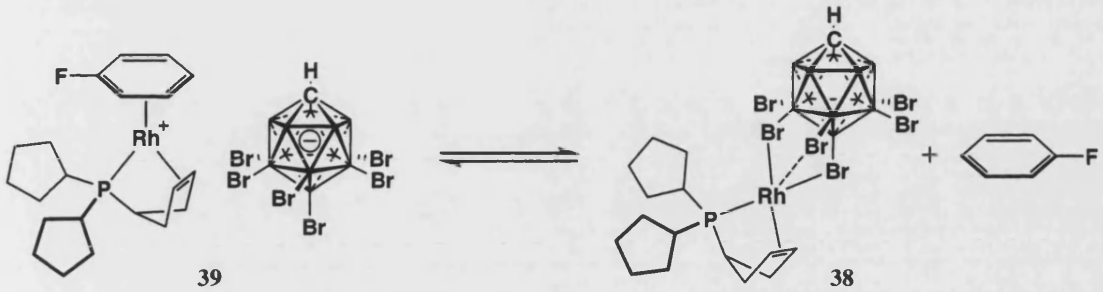

Figure 4.24 Equilibrium between complexes **39** and **38**.

$$K_{eq} = \frac{\left[Rh\{(\eta^2\text{-}C_5H_7)P(C_5H_9)_2\}(\textit{closo}\text{-}CB_{11}H_6Br_6)\right]\left[C_6H_5F\right]}{\left[(\eta^6\text{-}C_6H_5F)Rh\{(\eta^2\text{-}C_5H_7)P(C_5H_9)_2\}(\textit{closo}\text{-}CB_{11}H_6Br_6)\right]}$$

Equation 2

Equation 2 represents the equilibrium constant between **38** and **39** as described in Figure 4.24, assuming tight ion-pair formation. Recent studies reported on ion-pairing with halogenated carborane anions suggest similar diffusion coefficients between compounds where the carborane is coordinated and those where it is unbound, thus suggesting an ion-pair formulation is sensible at the first approximation.[15] By measuring the relative ratios of these two complexes over the temperature range 260-310 K, a van't Hoff plot has been obtained (Figure 4.25).

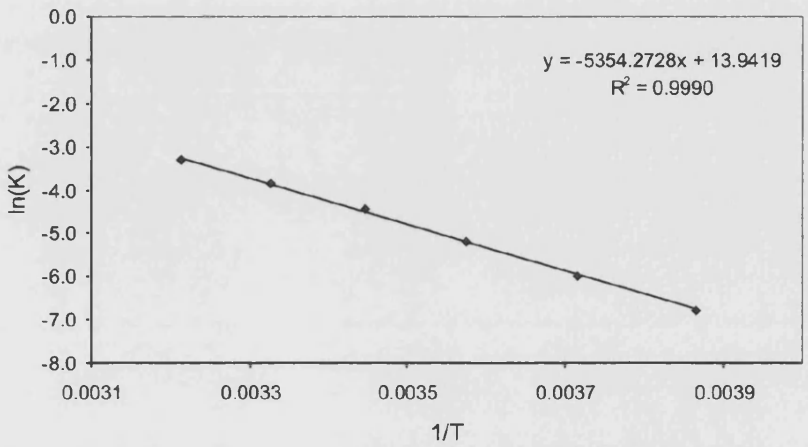

Figure 4.25 van't Hoff plot obtain for the equilibrium described in Figure 4.24.

From this plot, it has been possible to determine that, enthalpically, fluorobenzene binds more strongly than the carborane cage in this system, since ΔH° is positive, +44.5 ± 2.1 kJ·mol^{-1}. As expected, the entropy of the system increases when the equilibrium is displaced towards the formation of **38** and free fluorobenzene, ΔS° = +115.9 ± 7.5 J K^{-1} mol^{-1}. Therefore, ΔG is positive with a value of ΔG°(298 K) = +9.97 ± 4.5 kJ·mol^{-1}. Thus overall, fluorobenzene binds more strongly to the rhodium fragment than [*closo*-$CB_{11}H_6Br_6$]$^-$ anion in this system.

Any suggested ion-pair effect on the equilibrium can be suppressed by substituting the neutral arene ligand for a similar anionic one and assuming that ion pairing is the same for both. It was observed that addition of one equivalent of the weakly coordinating [NBu_4][$BAr^F{}_4$] salt results in a similar equilibrium between **38** and [Rh{P(Cyp)$_2$(η^2-C_5H_7)}{η^6-$C_6H_3(CF_3)$}$BAr^F{}_3$] (**VII**). This complex was prepared by T.M. Douglas of the Weller group, and full characterisation is given in reference [33].

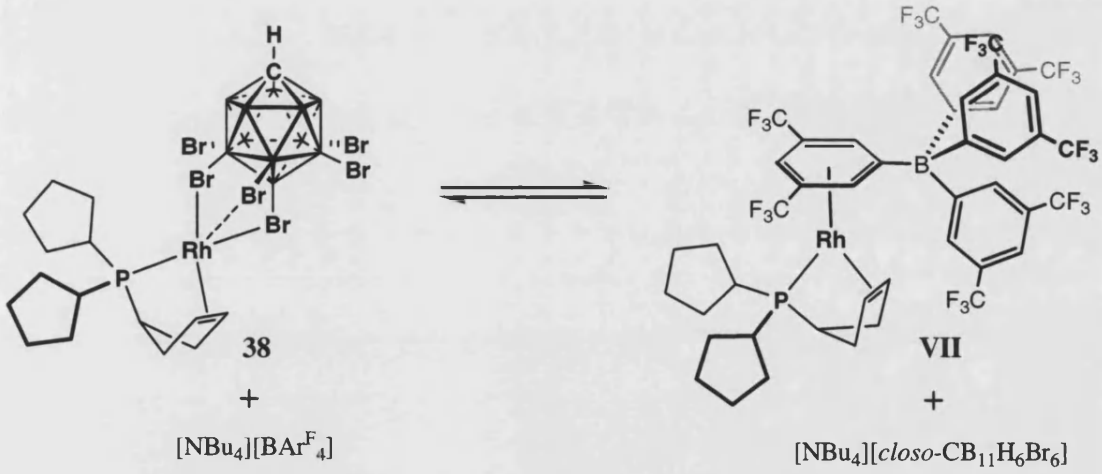

Figure 4.26 Equilibrium between **38** and **VII**.

$$K_{eq} = \frac{[Rh\{(\eta^2\text{-}C_5H_7)P(C_5H_9)_2\}(BAr^F{}_4)][(NBu_4)(closo\text{-}CB_{11}H_6Br_6)]}{[Rh\{(\eta^2\text{-}C_5H_7)P(C_5H_9)_2\}(closo\text{-}CB_{11}H_6Br_6)][(NBu_4)(BAr^F{}_4)]}$$

Equation 3

Measuring the relative ratios of these two complexes over the temperature range 275-313 K affords a van't Hoff plot from which ΔH° = -19.0 ± 0.3 kJ mol^{-1}, ΔS° -87.6 ± 0.8 J K^{-1} mol^{-1}, and $\Delta G^\circ(298)$ = +7.0 ± 0.5 kJ mol^{-1} were determined. Interestingly, this shows that although enthalpically the $[BAr^F{}_4]^-$ anion binds more strongly than the carborane anion (ΔH° is negative), it is the large negative entropic contribution involved in the coordination of the $[BAr^F{}_4]^-$ anion/dissociation and solvation of the carborane anion that overall results in the [*closo*-$CB_{11}H_6Br_6]^-$ anion being marginally favored (ΔG° is small but positive).

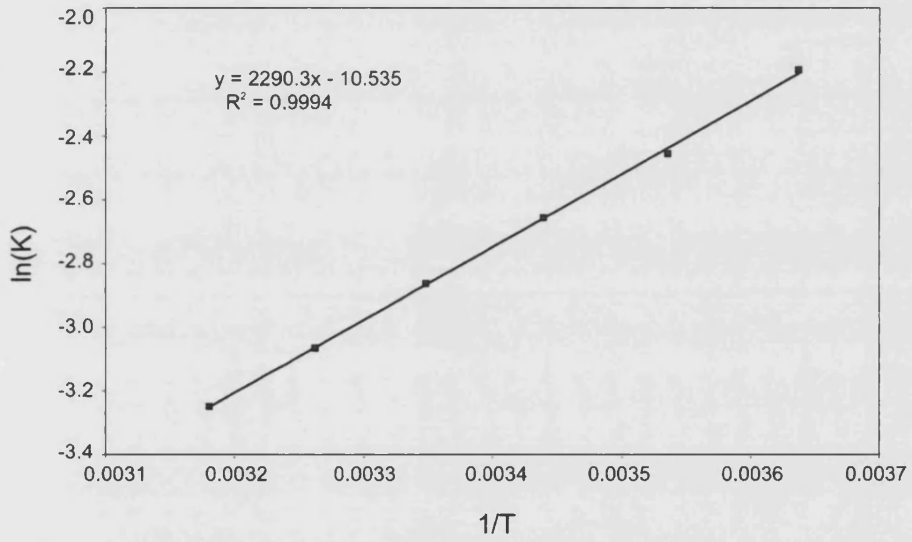

Figure 4.27 van't Hoff plot obtain for the equilibrium described in Figure 4.26.

Addition of 1 equiv of [NBu_4][*closo*-$CB_{11}H_6Cl_6$], an anion which is ranked as being less basic that its bromo congener, to **VII** did *not* result in an equilibrium being established to the detection limits of ^{1}H and ^{31}P NMR spectroscopy after 24 h at room temperature, with **VII** remaining unchanged and no decomposition observed. This demonstrates that, in this system at least, [*closo*-$CB_{11}H_6Cl_6]^-$ must be more weakly coordinating even than $[BAr^F{}_4]^-$.

4.2.3.3 [Rh(P^{i}Pr$_3$)(η^2-CH$_2$=CH^{t}Bu)(*closo*-CB$_{11}$H$_6$Br$_6$)]

In contrast to the dehydrogenation of the cyclohexyl or cyclopentyl rings of the phosphine ligand observed in complexes [Rh(PR$_3$)(H)$_2$(*closo*-CB$_{11}$H$_6$Br$_6$)] (R = Cy, Cyp), treatment of a solution of [Rh(P^{i}PR$_3$)(H)$_2$(*closo*-CB$_{11}$H$_6$Br$_6$)] (**33**) with an excess of *tert*-butylethene results in the coordination of the olefin and no dehydrogenation of the alkene. Consequently, after the reduction of one equivalent of *tert*-butylethene with the metal hydrides, complex [Rh(P^{i}Pr$_3$)(tbe)(*closo*-CB$_{11}$H$_6$Br$_6$)] (**41**) is formed in 55 % isolated yield (Figure 4.28). A similar complex must be formed prior the insertion of the olefin into a [*closo*-CB$_{11}$H$_{12}$]$^-$ vertex in the dehydrogenative borylation process described in section 3.2.4. Thus, the more stable [*closo*-CB$_{11}$H$_6$Br$_6$]$^-$ anion has been proved to be helpful in isolating reactive species containing the [*closo*-CB$_{11}$H$_{12}$]$^-$ carborane anion.

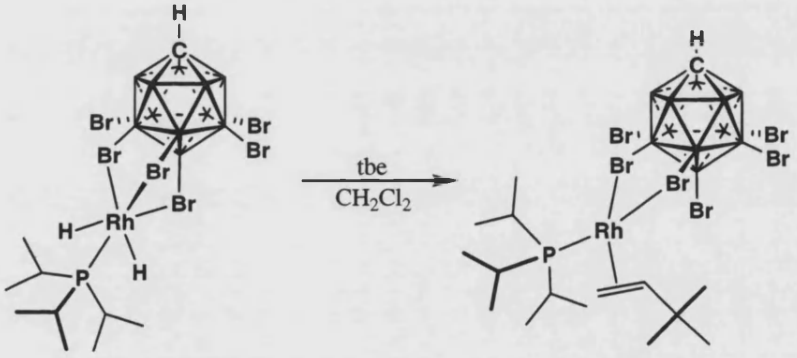

Figure 4.28 Schematic synthesis of complex **41**.

In this particular example, coordination of the olefin is more favored than the dehydrogenation of one isopropyl group that would lead to a less stable metallocycle. Nevertheless, dehydrogenation of triisopropylphosphine is known and has been reported in octahedral osmium complexes by Esteruelas et al[34-36] and Tilley.[37]

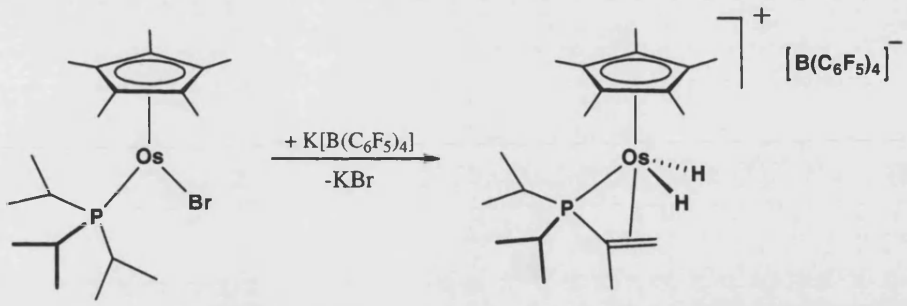

Figure 4.29 Example of dehydrogenation of triisoprophylphosphine.[37]

Crystals suitable for X-ray diffraction analysis were grown by slow diffusion of pentane into a solution of **41** in dichloromethane. The solid-state structure is shown in Figure 4.30 and relevant bond lengths and angles in Table 4.11.

In contrast to the square-planar geometry expected for a Rh(I) complex, the metal adopts a flattened-tetrahedral conformation. The *trans* P-Rh-Br(8) angle is 152.39(2)°, and the *trans* C(11)-Rh-Br(7) and C(12)-Rh-Br(7) angles are found to be 167.52(9)° and 133.78(10)°, respectively. Similar flattened-tetrahedral geometries have been found common in some complexes with two or three bulky phosphines,[38-40] such as in *trans*-[(^{t}Bu$_3$P)$_2$Rh(CO)(Cl)].[40] All bond lengths are comparable to those found in similar complexes: The Rh-P distance of 2.2319(7) Å is within the range of distances reported for the monophosphine complexes that appears in Table 4.10 [2.2305(10)-2.265(1) Å]. In the same way, the Rh-C_{alkene} distances in complex **41** [2.107(3) Å and 2.124(3) Å] are comparable in those compounds, which show an Rh-C average distance of 2.134 Å. The C=C length in *tbe* ligand is found to be 1.426(5) Å, slightly longer to the distances observed in similar platinum(II) [1.40(2) Å][41] and copper[1.384 Å][42] complexes pictured in Figure 4.31, perhaps suggesting increased back donation for the Rh(I) metal centre to the alkene.

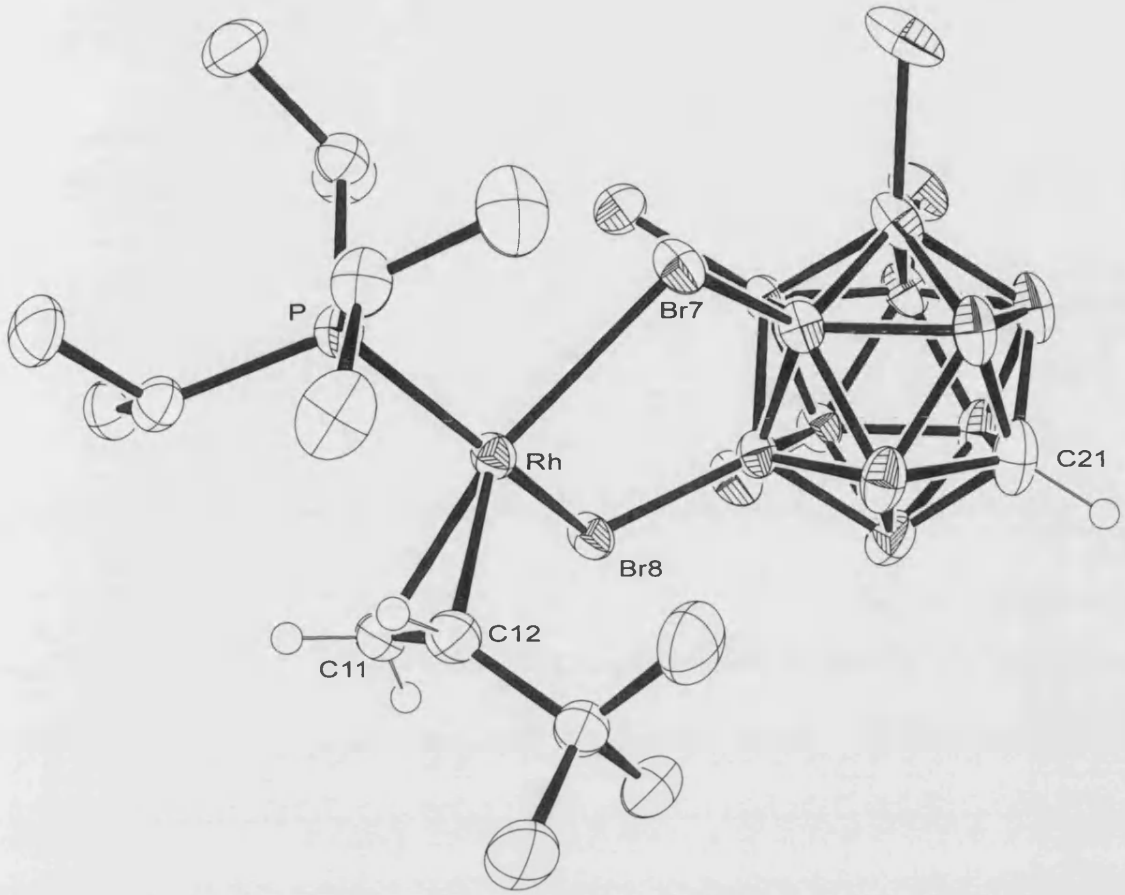

Figure 4.30 Solid-state structure of **41**. Thermal ellipsoids are shown at the 50% probability level and hydrogen atoms associated with the boron atoms and alkyl groups are omitted for clarity.

Rh-P	2.2319(7)	C(11)-C(12)	1.426(5)	C(11)-Rh-Br(7)	167.52(9)
Rh-Br(7)	2.6140(3)	P-Rh-Br(8)	152.39(2)	C(12)-Rh-Br(7)	133.78(10)
Rh-Br(8)	2.6264(3)	P-Rh-Br(7)	94.12(2)	C(11)-Rh-Br(8)	85.28(9)
Rh-C(11)	2.107(3)	C(11)-Rh-P	96.32(9)	C(12)-Rh-Br(8)	106.84(9)
Rh-C(12)	2.124(3)	C(12)-Rh-P	90.94(9)	Br(7)-Rh-Br(8)	88.642(10)

Table 4.11 Selected bond lengths (Å) and angles (°) for **41**.

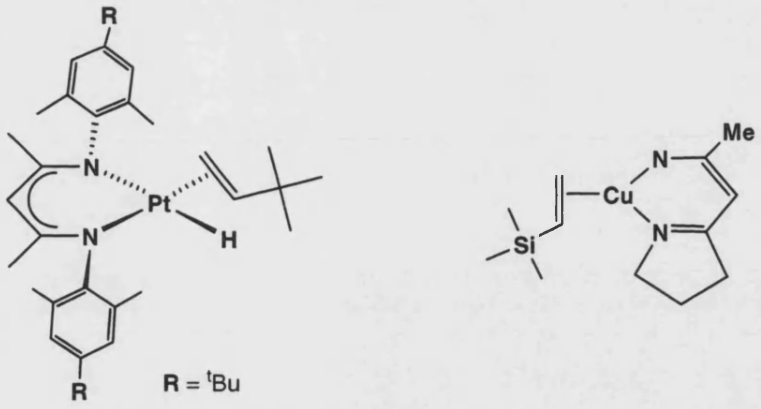

Figure 4.31

The Rh-Br distances in complex **41** [Rh-Br7 2.6140(3) Å and Rh-Br8 2.6264(3) Å] are similar to those observed in complexes **32** and **38,** or in $[(PPh_3)_2(Ir(H)_2(closo\text{-}CB_{11}H_6Br_6)]$ [2.6554(9)-2.6799(10) Å].[5] These distances reflect the weak interaction of the cage anion to the metal centre when compared to the Rh-Br range of distances reported in $[Rh_2(\mu\text{-}Br)_2Br_4(dppm)_2]$ [2.447(5)-2.491(4) Å].[13]

NMR spectroscopy studies in a CD_2Cl_2 solution show complex **41** as a diamagnetic compound, as expected for a square planar Rh(I) complexes. This suggests that the flattened tetrahedral ligand distribution observed in the solid state is not retained in solution. The $^1H\{^{11}B\}$ NMR spectrum shows three resonances for the alkene protons at δ 4.07, 2.91 and 2.26 ppm. Correlation of these signals was found with resonances at δ 74.39 [*J*(RhC) = 19.1 Hz] and at δ 38.11 [*J*(RhC) = 16.1 Hz] in the $^{13}C\{^1H\}$ NMR spectrum. Comparable chemical shifts are observed in similar rhodium complexes with coordinated *tbe* or vinyl-containing ligands, such as in $[(\eta^6\text{-}2,6\text{-}Me_2C_6H_3CH_2CH_2PtBu_2\text{-}\kappa\text{-}P)Rh(CH_2{=}CHtBu)][PF_6]$.[43] The cage C-*H* signal appears at δ 2.69 ppm, and the upper belt B-H resonance at δ 2.41 ppm. Isopropyl C*H* is observed as a multiplet at δ 1.96 ppm. Due to the C_1 symmetry of the molecule, isopropyl CMe_2 groups are inequivalent and show as two doublets of doublets at δ 1.36 and 1.38 ppm. The *tert*-butyl group of the *tbe* ligand is observed as a singlet at δ 1.17 ppm. The $^{31}P\{^1H\}$

NMR spectrum shows one phosphine resonance at δ 74.0 ppm as a doublet with a *J*(RhP) coupling constant of 183.4 Hz.

Despite of the coordination of the cage to rhodium *via* two {BBr} vertices, only three resonances are observed in the ^{11}B spectrum. Two broad singlets are shown at δ -0.31 and -8.51 ppm due to {BBr} vertices, and a doublet at δ -19.50 ppm from the upper belt {BH} vertices. Consequently, the cage is involved in a fluxional process that to affords the C_{5v} symmetry observed in the ^{11}B NMR spectrum for the anion. Figure 4.32 postulates a mechanism where one of the B-Br-Rh bonds breaks. Rotation of the cage around the C_5 axis allows the metal to coordinate to a different B-Br-Rh bond.

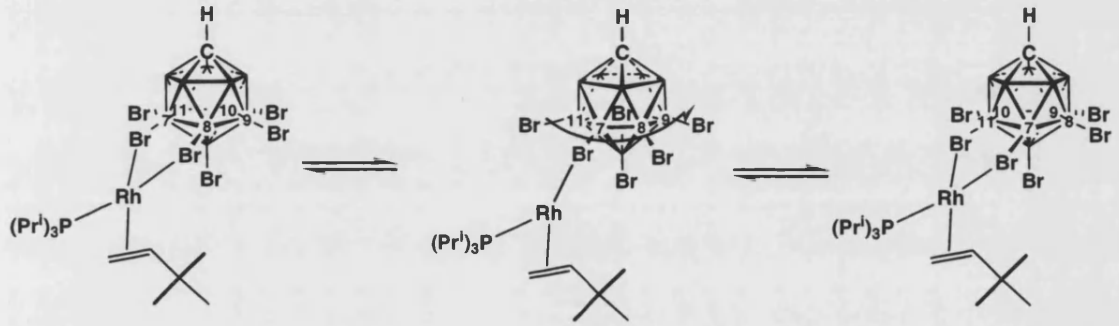

Figure 4.32 Proposed fluxional process in complex **41**.

4.3 Conclusions

A range of new rhodium monophosphine complexes partnered with [*closo*-$CB_{11}H_6Br_6]^-$ have been synthesised and characterised in solution and the solid state. The solid state and solution studies of the complexes [$Rh(PR_3)(H)_2$(*closo*-$CB_{11}H_6Br_6$)] (R = Cy, Cyp, ^iPr) have confirmed the structure proposed in Chapter 3 for the analogous complexes partnered with the [*closo*-$CB_{11}H_{12}]^-$ anion. Although deuteration at the {BH} vertices mediated by the metal fragment is observed, reaction of these complexes with olefins does not lead to hydroboration. In contrast on reaction with *tert*-butylethene, after the hydridic protons have been utilised to reduce one equivalent of the olefin, the metal promotes C-H activation in one of the rings of the phosphine (R = Cy, Cyp), forming a bidentate phosphine-alkene ligand. Dehydrogenation of an isopropyl group is not observed for the reaction of [$Rh(P^iPr_3)(H)_2$(*closo*-$CB_{11}H_6Br_6$)] with excess of *tert*-butylethene, which produces [$Rh(P^iPr_3)(\eta^2$-CH_2=$CH^tBu)$(*closo*-$CB_{11}H_6Br_6$)] instead, which is a model for alkene coordination to a $\{Rh(PR_3)\}^+$ fragment prior to insertion into a B-H bond.

Reactivity of these complexes with arenes has shown that Rh(III) complexes prefer to coordinate to the [*closo*-$CB_{11}H_6Br_6]^-$ anion rather than to a weakly coordinating arene ligand such as fluorobenzene. This tendency changes when a stronger donor arene is used (benzene). In contrast, coordination of fluorobenzene to Rh(I) complexes is favored when compared to the [*closo*-$CB_{11}H_6Br_6]^-$ anion.

Not only have these complexes provided insight into how [*closo*-$CB_{11}H_{12}]^-$ binds to a metal centre and olefins initially react with {$Rh(PR_3)$(*closo*-$CB_{11}H_{12}$)}, but they also extend considerably the number of transition-metal fragments partnered with the weakly

coordinating [*closo*-$CB_{11}H_6Br_6$]$^-$ anion. Given that cationic rhodium phosphine complexes are extensively used in catalysis, such complexes as reported here might prove useful in the future.

4.4 Bibliography

1 M. Juhasz, S. Hoffmann, E. Stoyanov, K. C. Kim, and C. A. Reed, *Angew. Chem.-Int. Edit. Engl.*, 2004, **43**, 5352.

2 C. A. Reed, *Chem. Commun.*, 2005, 1669.

3 C. Hague, N. J. Patmore, C. G. Frost, M. F. Mahon, and A. S. Weller, *Chem. Commun.*, 2001, 2286.

4 N. J. Patmore, C. Hague, J. H. Cotgreave, M. F. Mahon, C. G. Frost, and A. S. Weller, *Chem.-Eur. J.*, 2002, **8**, 2088.

5 A. Rifat, G. Kociok-Köhn, J. W. Steed, and A. S. Weller, *Organometallics*, 2004, **23**, 428.

6 A. Rifat, University of Bath, Bath, PhD Thesis 2003.

7 A. Rifat, N. J. Patmore, M. F. Mahon, and A. S. Weller, *Organometallics*, 2002, **21**, 2856.

8 N. J. Patmore, M. F. Mahon, and A. S. Weller, *Appl. Organomet. Chem.*, 2003, **17**, 388.

9 N. J. Patmore, J. W. Steed, and A. S. Weller, *Chem. Commun.*, 2000, 1055.

10 N. J. Patmore, M. F. Mahon, J. W. Steed, and A. S. Weller, *J. Chem. Soc.-Dalton Trans.*, 2001, 277.

11 N. J. Patmore, M. J. Ingleson, M. F. Mahon, and A. S. Weller, *Dalton Trans.*, 2003, 2894.

12 W. Clegg, M. R. J. Elsegood, A. J. Scott, T. B. Marder, C. Y. Dai, N. C. Norman, N. L. Pickett, and E. G. Robins, *Acta Crystallogr., Sect. C: Cryst. Struct. Commun.* , 1999, **55**, 733.

13 F. A. Cotton, K. R. Dunbar, C. T. Eagle, L. R. Falvello, and A. C. Price, *Inorg. Chem.*, 1989, **28**, 1754.

14 B. E. Hauger, D. Gusev, and K. G. Caulton, *J. Am. Chem. Soc.*, 1994, **116**, 208.

15 G. L. Moxham, T. M. Douglas, S. K. Brayshaw, G. Kociok-Kohn, J. P. Lowe, and A. S. Weller, *Dalton Trans.*, 2006, 5492.

16 G. Canepa, C. D. Brandt, K. Ilg, J. Wolf, and H. Werner, *Chem.-Eur. J.*, 2003, **9**, 2502.

17 H. E. Gottlieb, V. Kotlyar, and A. Nudelman, *J. Org. Chem.* , 1997, **62**, 7512.

18 H. Werner, G. Canepa, K. Ilg, and J. Wolf, *Organometallics*, 2000, **19**, 4756.

19 H. Werner, M. Bosch, M. E. Schneider, C. Hahn, F. Kukla, M. Manger, B. Windmuller, B. Weberndorfer, and M. Laubender, *J. Chem. Soc.-Dalton Trans.*, 1998, 3549.

20 S. Sabo-Etienne and B. Chaudret, *Coord. Chem. Rev.*, 1998, **180**, 381.

21 T. Arliguie, B. Chaudret, F. A. Jalon, A. Otero, J. A. Lopez, and F. J. Lahoz, *Organometallics*, 1991, **10**, 1888.

22 T. Arliguie, B. Chaudret, G. Chung, and F. Dahan, *Organometallics*, 1991, **10**, 2973.

23 K. Mauthner, K. M. Soldouzi, K. Mereiter, R. Schmid, and K. Kirchner, *Organometallics*, 1999, **18**, 4681.

24 M. Prinz, M. Grosche, E. Herdtweck, and W. A. Herrmann, *Organometallics*, 2000, **19**, 1692.

25 S. Hietkamp, D. J. Stufkens, and K. Vrieze, *J. Organomet. Chem.*, 1978, **152**, 347.

26 K. I. Goldberg and A. S. Goldman, 'Activation and Functionalisation of C-H Bonds', American Chemical Society, Washington, 2004.

27 M. J. Burk and R. H. Crabtree, *J. Am. Chem. Soc.*, 1987, **109**, 8025.

28 C. M. Jensen, *Chem. Commun.*, 1999, 2443.

29 T. M. Douglas, H. Le Notre, S. K. Brayshaw, C. G. Frost, and A. S. Weller, *Chem. Commun.*, 2006, 3408.

30 M. Grellier, L. Vendier, and S. Sabo-Etienne, *Angew. Chem.-Int. Edit. Engl.*, 2007, **46**, 2613.

31 P. S. Pregosin and R. W. Kunz, '^{31}P and ^{13}C NMR of Transition Metal Phosphine Complexes', Springer, Berlin, 1979.

32 F. Torres, E. Sola, M. Martin, C. Ochs, G. Picazo, J. A. Lopez, F. J. Lahoz, and L. A. Oro, *Organometallics*, 2001, **20**, 2716.

[33] T. M. Douglas, E. Molinos, S. K. Brayshaw, and A. S. Weller, *Organometallics*, 2007, **26**, 463.
[34] M. Baya, M. L. Buil, M. A. Esteruelas, and E. Onate, *Organometallics*, 2004, **23**, 1416.
[35] A. J. Edwards, M. A. Esteruelas, F. J. Lahoz, A. M. Lopez, E. Onate, L. A. Oro, and J. I. Tolosa, *Organometallics*, 1997, **16**, 1316.
[36] M. A. Esteruelas and A. M. Lopez, *Organometallics*, 2005, **24**, 3584.
[37] P. B. Glaser and T. D. Tilley, *Organometallics*, 2004, **23**, 5799.
[38] M. A. Fernandes, V. Circu, R. Weber, T. Varnali, and L. Carlton, *J. Chem. Crystallogr.*, 2002, **32**, 273.
[39] D. L. Thorn and R. L. Harlow, *Inorg. Chem.*, 1990, **29**, 2017.
[40] R. L. Harlow, S. A. Westcott, D. L. Thorn, and R. T. Baker, *Inorg. Chem.*, 1992, **31**, 323.
[41] U. Fekl, W. Kaminsky, and K. I. Goldberg, *J. Am. Chem. Soc.*, 2003, **125**, 15286.
[42] K. H. Park, A. Z. Bradley, J. S. Thompson, and W. J. Marshall, *Inorg. Chem.*, 2006, **45**, 8480.
[43] G. Canepa, C. D. Brandt, and H. Werner, *Organometallics*, 2004, **23**, 1140.

Chapter 5. [1-Me-1-*closo*-$SnB_{11}H_{11}$]$^-$ as a potential weakly coordinating anion

5.1 Introduction

The cage species [1-Me-*closo*-$SnB_{11}H_{11}$]$^-$, isolectronic with [1-*closo*-$CB_{11}H_{12}$]$^-$, was first reported by Todd in 1992 by methylation of the dianion [1-*closo*-$SnB_{11}H_{11}$]$^{2-}$.[1] This dianion, in turn, is available in two steps from $Na[BH_4]$ in good yield and reasonable preparative scale (62%, ~5 g) as Figure 5.1 shows.

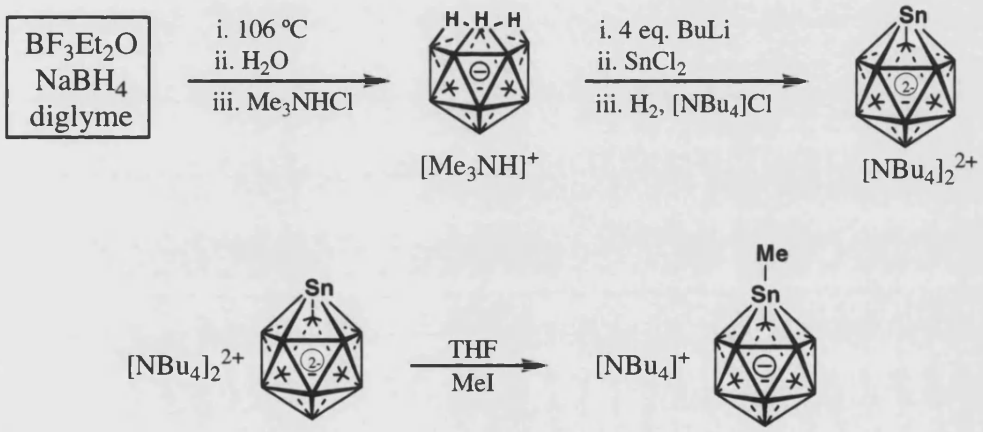

Figure 5.1 Schematic synthesis of [NBu_4][*closo*-$SnB_{11}H_{11}$]$^-$.[1]

The coordination chemistry of $[SnB_{11}H_{11}]^{2-}$ has been investigated by Wesemann[2-6] and this has centred around the interaction of the *exo*-lone pair on the cluster tin atom with metal centres. However, there are no reports of the use of mono-anionic [1-R-*closo*-$SnB_{11}H_{11}$]$^-$ (R = alkyl) anions as potential weakly coordinating anion with transition metal fragments. The potential to use such anions has been recognised[5] and as such they have been recently used to prepare ionic-liquids when partnered with imidazolium cations,[7] and there are examples where the $[SnB_{11}H_{11}]^{2-}$ cage has stablished M-H-B interactions with transition metal complexes[8] as Figure 5.2 shows.[9]

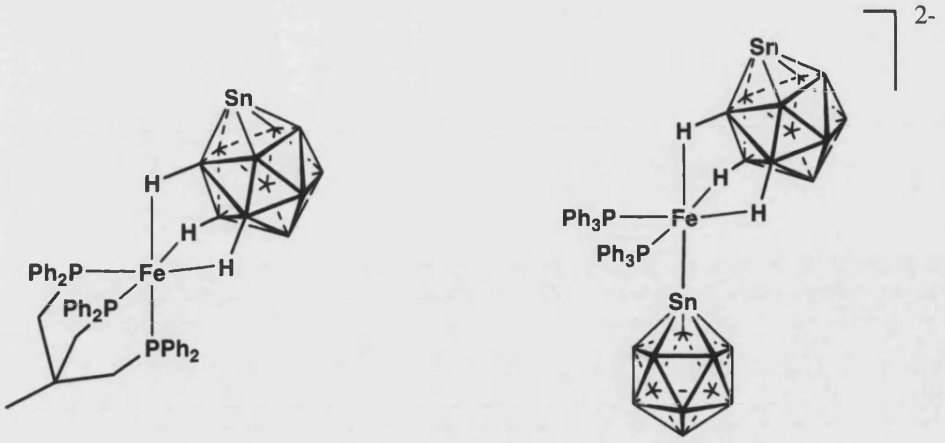

Figure 5.2 Examples of M-H-B interactions of the $[SnB_{11}H_{11}]^{2-}$ cage.[9]

5.1.1 Scope of Chapter

The use of the stannaborane [1-Me-*closo*-$SnB_{11}H_{11}$]$^-$ anion can be considered an alternative approach to the formation of precursors to weakly coordinating *closo*-icosahedral mono anionic borane species. The $\{Rh(PPh_3)_2\}^+$ metal fragment has been chosen to partner the [1-Me-*closo*-$SnB_{11}H_{11}$]$^-$cage as it has been previously reported on the synthesis and structures of this cation with anion derivatives of the parent [*closo*-$CB_{11}H_{12}$]$^-$ anion, and thus this provides a useful spectroscopic and structural comparison.[10]

This short chapter reports the synthesis of $[Rh(PPh_3)_2(nbd)][1\text{-Me-}closo\text{-}SnB_{11}H_{11}]$ and its subsequent treatment with dihydrogen to afford $Rh(PPh_3)_2$(1-Me-*closo*-$SnB_{11}H_{11}$). Attempts to functionalise the stannaborane cage with alkenes are also described.

5.2 Results and Discussion

5.2.1 [Rh(PPh$_3$)$_2$(nbd)][1-Me-*closo*-SnB$_{11}$H$_{11}$]

[Rh(PPh$_3$)$_2$(nbd)][1-Me-*closo*-SnB$_{11}$H$_{11}$] (**42**) is prepared by reaction of [Rh(nbd)Cl]$_2$ (nbd = norbornadiene), [Bu$_4$N][1-CH$_3$-*closo*-SnB$_{11}$H$_{11}$] and PPh$_3$ in methanol, and has been characterised by multinuclear NMR spectroscopy and microanalysis.

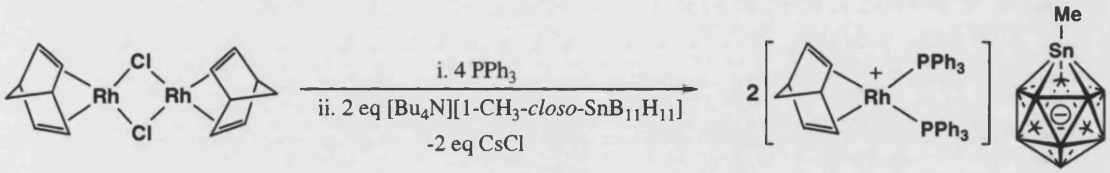

Figure 5.3 Synthesis of compound **42**.

The ^{1}H{^{11}B} spectrum shows three B-H signals that also show coupling to $^{117/119}$Sn (I = 1/2 for both isotopes ^{117}Sn and ^{119}Sn, natural abundance 7.7 and 8.6 % respectively) at: δ 2.97 ppm [1H, *J*(SnH) 87], δ 2.06 ppm [5H, *J*(SnH) 58] and δ 1.56 ppm [5H, *J*(SnH) 35]. The ^{11}B NMR spectrum ($CDCl_3$) shows two environments, at δ -10.4 and -15.7 ppm in a 1:10 ratio respectively, and ^{11}B-Sn coupling is not resolved, even in the ^{11}B{^{1}H} NMR spectrum. In d_6-acetone these signals resolve into three signals in the ratio 1:5:5. As is well established that chemical shifts and *J*(BH) coupling constants can provide useful spectroscopic guides to the coordination of a cationic metal fragment with [*closo*-CB$_{11}$H$_{12}$]$^-$,[11] ^{11}B-^{11}B and ^{11}B-^{1}H correlation experiments have been performed on **42** to establish the identity of the signals. Todd has previously reported the ^{11}B-^{11}B COSY NMR data for the anion [1-Me-*closo*-SnB$_{11}$H$_{11}$][PPh$_3$CH$_3$][1] and our results concur with these. In addition, a ^{1}H-^{11}B HMQC experiment allow the assignment of the ^{1}H signals to specific cluster vertices. These follow the pattern (low field to high field): B$_{12}$H, B$_{7\text{-}11}$H and B$_{2\text{-}6}$H. The magnitude of ^{1}H-Sn coupling follows the reverse

order, with $B_{12}H$ displaying the largest couple [J(SnH) 87] and $B_{2\text{-}6}H$ the smallest [J(SnH) 35]: a demonstration of the antipodal effect in the NMR spectra of boranes.[12] The $^{31}P\{^{1}H\}$ NMR spectrum shows a single environment, δ 30.6 [J(RhP) 153].

5.2.2 [Rh(PPh$_3$)$_2$(1-Me-*closo*-SnB$_{11}$H$_{11}$)]

Treatment of **42** with H_2 in CH_2Cl_2 solution results in a colour change from orange to red/orange. $^{1}H\{^{11}B\}$ and $^{11}B\{^{1}H\}$ NMR spectroscopy indicate the formation of Rh(PPh$_3$)$_2$(1-Me-*closo*-SnB$_{11}$H$_{11}$) **43** (Figure 5.4), the structure of which was confirmed in the solid-state by a X-ray diffraction study (Figure 5.5).

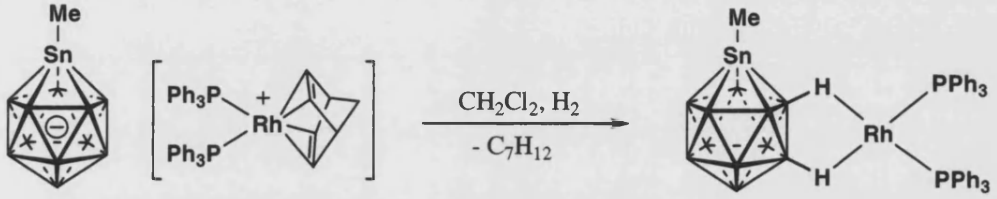

Figure 5.4 Schematic synthesis of [Rh(PPh$_3$)$_2$(1-Me-*closo*-SnB$_{11}$H$_{11}$)] (**43**).

Compound **43** crystallises with no close intermolecular contacts in the solid-state. The refinement shows that the molecule crystallises with a minor disordered component (10%). For the major (90%) component the $\{Rh(PPh_3)_2\}^+$ fragment is coordinated through one upper pentagonal belt {BH} vertex (B_2) and one lower pentagonal belt {BH} vertex (B_{11}) through 3-centre-2electron Rh-H-B interactions. The Rh-P bond lengths in **43** [2.2155(8) and 2.2417(8) Å] are very similar to those observed in [Rh(PPh$_3$)$_2$(*closo*-CB$_{11}$H$_{12}$)] [2.2192(6) and 2.2391(6) Å],[10] and [(Rh(PPh$_3$)$_2${7-Me-8-Ph-*nido*-C$_2$B$_9$H$_{10}$)] [2.231(4) and 2.232(5) Å].[13] Similar Rh-B distances were observed between **43** [2.369(4), 2.372(4) Å], [Rh(PPh$_3$)$_2$(*closo*-CB$_{11}$H$_{12}$)] [2.359(3), 2.407(3) Å] and [Rh(cod)(*closo*-CB$_{11}$H$_{12}$)] [2.385(3), 2.391(3) Å].[14] The Rh(I) fragment in **43** is square planar (sum of angles 360.0°).

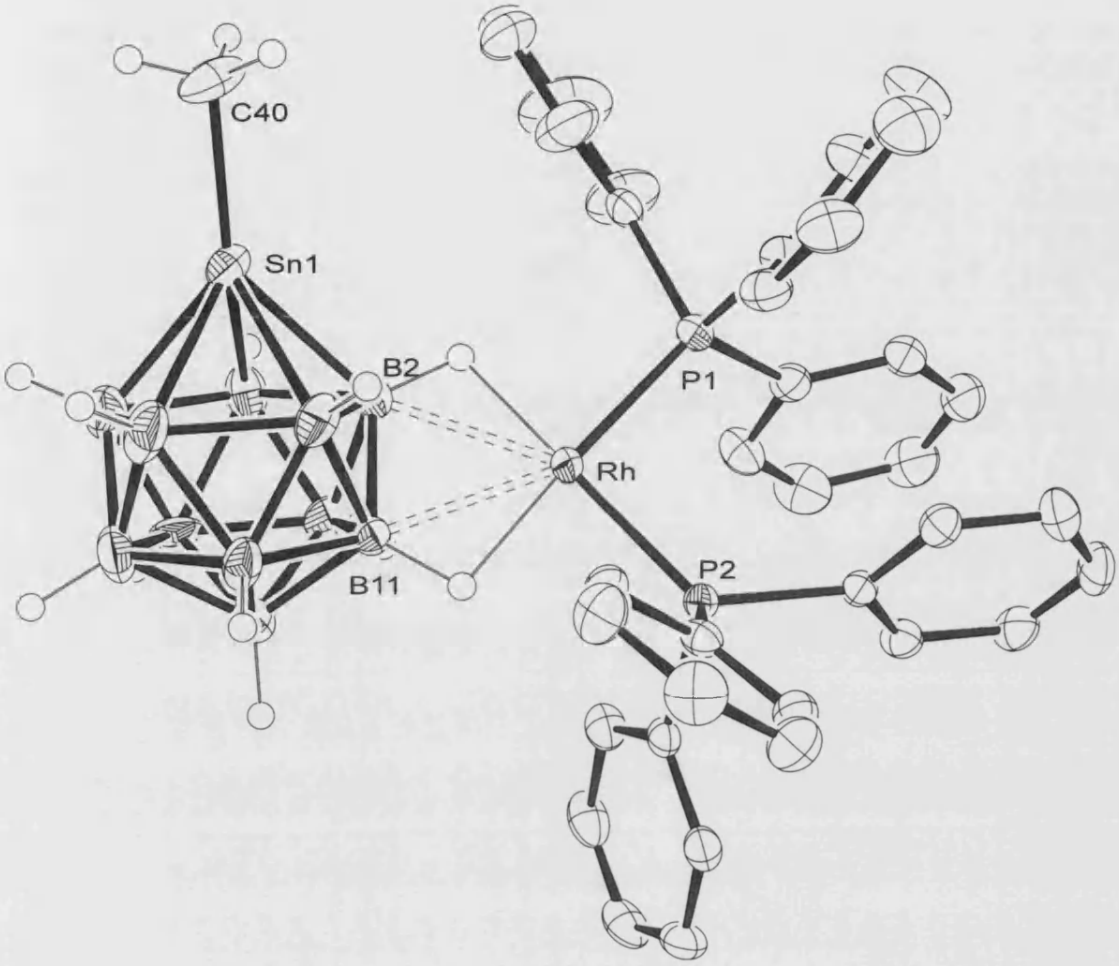

Figure 5.5 Solid-state structure of $[Rh(PPh_3)_2(1\text{-Me-}closo\text{-}SnB_{11}H_{11})]$ **43**. Thermal ellipsoids are shown at the 50% probability level and hydrogen atoms associated with the phenyl groups are omitted for clarity. The major (90%) disordered component is shown.

Rh-P1	2.2155(8)	Rh-H11	1.89(3)	Sn-B6	2.323(4)
Rh-P2	2.2417(8)	Sn-B2	2.273(4)	P1-Rh-P2	95.64(3)
Rh-B2	2.369(4)	Sn-B3	2.292(4)	P1-Rh-B2	111.53(10)
Rh-B11	2.372(4)	Sn-B4	2.263(5)	B2-Rh-B11	42.71(13)
Rh-H2	1.85(4)	Sn-B5	2.322(5)	B11-Rh-P2	110.15(9)

Table 5.1 Selected bond lengths (Å) and angles (°) for **43**.

In the cluster, the Sn-B distances span the range 2.263(5) to 2.323(4) Å which are similar to those observed in the parent [1-Me-*closo*-$SnB_{11}H_{11}$]$^-$ anion [2.288(3) to 2.306(3) Å],[1] while there are no close contacts between the phenyl groups and the cage methyl group. The minor component in the crystal resolves best as the 7,8-isomer, in which the {$Rh(PPh_3)_2$}$^+$ fragment coordinates to two {BH} vertices on the lower pentagonal belt. A B-H-M interaction between a upper belt {BH} vertex and an Au(I) centre has been noted previously,[5, 8, 9] e.g. [Bu_3MeN][Au(1-Ph_2PCH_2-*closo*-$SnB_{11}H_{11})_2$].[5] This coordination mode of a metal fragment is unusual for the directly analogous [*closo*-$CB_{11}H_{12}$]$^-$ anion, as charge distributions in this cage means that metal fragments preferentially interact with the lower hemisphere of the cage. However, as we show later, the replacement of {CH} for {SnMe} results in a change in charge distribution, and thus a 2,7-coordination mode is perfectly reasonable.

In solution NMR spectroscopic data show that the {$Rh(PPh_3)_2$}$^+$ fragment is fluxional over the surface of the cage, affording C_{5v} symmetry for the anion, in contrast to the C_1 symmetry observed in the solid-state. This fluxional process is not frozen out at -70°C in CD_2Cl_2 solution. The ^{1}H NMR spectrum shows signals due to PPh_3 and Sn-*CH*$_3$ in the ratio 30:3. The ^{1}H{^{11}B} NMR spectrum reveals three signals assigned to B*H* that also show coupling to Sn: δ 2.00 [1H, *J*(SnH) 80], δ 0.53 [5H, *J*(SnH) 50] and δ 0.05 [5H, *J*(SnH) ~40]. As ^{11}B-^{1}H HMQC NMR experiments are not suitable for the assignments of these signals due to overlapping peaks in the ^{11}B NMR spectrum (*vide infra*), the magnitude of the *J*(SnH) coupling constant has been used to assign the B*H* signals, using the peak assignments made for **42** as a guide. These follow the order (high field to low field): $B_{12}H$, $B_{7\text{-}11}H$ and $B_{2\text{-}6}H$. Although this order follows that found in **42**, all the signals are shifted by approximately 1-2 ppm to higher field in **43**. Specifically, $B_{12}H$ is shifted by Δδ 0.97, $B_{7\text{-}11}H$ Δδ 1.53 and $B_{2\text{-}6}H$ Δδ 1.51 ppm. It is

well established that the coordination of a metal fragment *exo* to the cage results in upfield chemical shift changes for those {BH} vertices interacting with the metal.[10, 15, 16] That $B_{2\text{-}6}H$ and $B_{7\text{-}11}H$ are shifted more than $B_{12}H$ suggests that, in solution, the $\{Rh(PPh_3)_2\}^+$ fragment interacts on the NMR time-scale more with the $B_{2\text{-}11}H$ vertices and less with $B_{12}H$, consistent with the observed solid-state structure that shows 2,11-coordination. The ^{11}B NMR spectrum shows two signals at δ -14.0 and -17.8 ppm, in the ratio 1:10 - the latter being a 5+5 coincidence. These signals have also been shifted upfield from **42**, by ca. Δδ 4 ppm, again suggesting that the $\{Rh(PPh_3)_2\}^+$ fragment interacts with the entire BH surface of the cage anion.

5.2.3 Reactivity of [Rh(PPh$_3$)$_2$(1-Me-*closo*-SnB$_{11}$H$_{11}$)] with ethene

The conditions utilized in Chapter 2 for the functionalisation of {BH} vertices *via* dehydrogenative borylation were tested with the [1-Me-*closo*-$SnB_{11}H_{11}]^-$ anion. Addition of ethene to a solution of [$Rh(PPh_3)_2$(1-Me-*closo*-$SnB_{11}H_{11}$)] (**43**) in dichloromethane produces, after one week, a mixture of unreacted cage and a vinyl-substituted cage in an approximate 3:1 ratio respectively. After addition of nbd to the solution, ^1H NMR spectroscopy shows the presence of a vinyl group with three pairs of resonances as doublet of doublets at δ 6.50, 5.45 and 5.18 ppm. Similar resonances were observed for [$Rh(PPh_3)_2$(nbd)][7-($CH{=}CH_2$)-*closo*-$CB_{11}H_{11}$] (**2b**) at δ 6.35, 5.37 and 5.32 ppm.

As is shown in section 5.2.4, the strong Rh-H-B interaction of the cage with the metal fragment must be the responsible for the slow rate of reactivity of the metal with ethene to produce hydroboration.

5.2.4 DFT calculations[17]

Reduction of the norbornadiene ligand in **42** with H_2 results in a coordinatively unsaturated $\{Rh(PPh_3)_2\}^+$ fragment that coordinates with the stannaborane [1-Me-*closo*-$SnB_{11}H_{11}]^-$ anion through two B-H-Rh 3-centre-2-electron bonds. Both the solid-state and solution data for **43** can be contrasted with those for the carborane anion complexes $Rh(PR_3)_2$(*closo*-$CB_{11}H_{12}$) (R = Ph **I**,[10] Cy **VIII**[11]) (Figure 5.6). Both **I** and **VIII** show interactions with the lower hemisphere of the carborane cage. In solution the $^1H\{^{11}B\}$ NMR spectra show this by large ($\Delta\delta$ *ca.* 5 ppm) upfield shifts of $B_{12}H$, smaller upfield shifts for $B_{7\text{-}11}$ of $\Delta\delta$ *ca.* 1 to 2 ppm and virtually no chemical shift change for $B_{2\text{-}6}$. Similar chemical shift changes are also observed in the $^{11}B\{^1H\}$ NMR spectrum. In the solid-state **I** coordinates through $B_{12}H$ and B_7H while **VIII** coordinates through B_7H and B_8H, both being consistent with NMR data; and with the model complex [$Rh(PMe_3)_2$(*closo*-$CB_{11}H_{12}$)] in which there is essentially no difference energetically between these two isomers.[11] In contrast, stannaborane **43** coordinates in the solid-state through one upper pentagonal belt {BH} vertex and one lower pentagonal belt vertex. However, in solution the metal fragment must be fluxional over the *whole* {BH} surface as all the B-H signals show upfield shifts on coordination of the $\{Rh(PPh_3)_2\}^+$ fragment. That $B_{2\text{-}6}H$ and $B_{7\text{-}11}H$ show larger chemical shifts ($\Delta\delta$ *ca.* –1.5) than $B_{12}H$ ($\Delta\delta$ *ca.* –1) suggests that the metal fragment spends relatively less time coordinated with $B_{12}H$ on the NMR timescale.

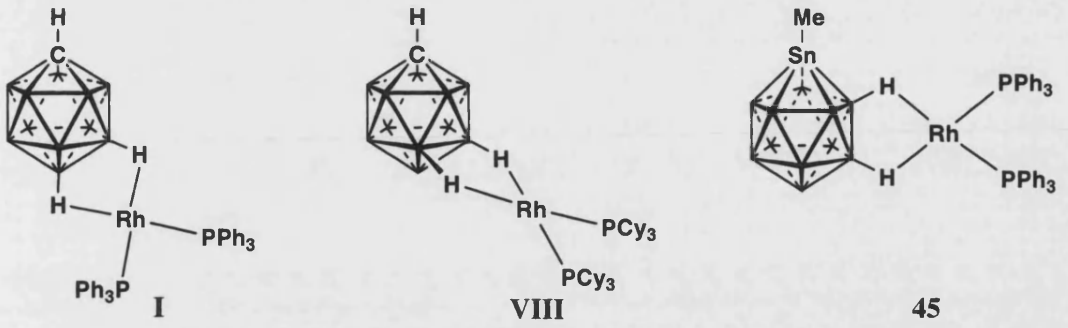

Figure 5.6 Examples of coordination of the $\{Rh(PPh_3)_2\}^+$ fragment.

The different coordination modes of the $\{Rh(PPh_3)_2\}^+$ fragment between the stannaborane and carborane cages can explained at a basic level - ignoring the orbital contributions to the bonding - by using a simple analysis of the charge distribution in the two cages. For [*closo*-$CB_{11}H_{12}]^-$ the relative electronegativity of carbon and boron means that upper belt vertices, $B_{2\text{-}6}H$, would be expected to be relatively positively charged while the lower hemisphere of the cage would be relatively negatively charged. Previous calculations at the DFT level have confirmed this.[18, 19] For comparison with [1-Me-*closo*-$SnB_{11}H_{11}]^-$ we have performed calculations at the B3LYP/DZVP level on [1-Me-*closo*-$CB_{11}H_{11}]^-$ and this shows a very similar charge distribution (based on NBO analysis) as reported previously for [*closo*-$CB_{11}H_{12}]^-$ (Figure 5.7).[18, 19] For the stannaborane [1-Me-*closo*-$SnB_{11}H_{11}]^-$ this polarisation would be expected to be reversed, as the tin is electropositive compared with boron, and DFT calculations show all the {BH} vertices as having a negative charge, with $B_{2\text{-}6}H$ being more negative, followed by $B_{7\text{-}11}H$ and $B_{12}H$ (Figure 5.7). On purely electrostatic grounds coordination of a metal fragment with [*closo*-$CB_{11}H_{12}]^-$ would be expected to occur with the lower hemisphere of the cage – as is observed both in the solid-state (e.g. **I** and **VIII**) and in solution. With [1-Me-*closo*-$SnB_{11}H_{11}]^-$, having all BH vertices negatively charged, a metal fragment would be expected to coordinate with the entire {BH} surface of the cage. That, for **43**, all the B-H signals shift to high-field in the $^1H\{^1B\}$ and ^{11}B NMR

spectra, with $B_{2\text{-}11}$ shifting the most, and the X-ray structure shows coordination of the metal fragment to B_2H and $B_{11}H$, is consistent with this analysis.

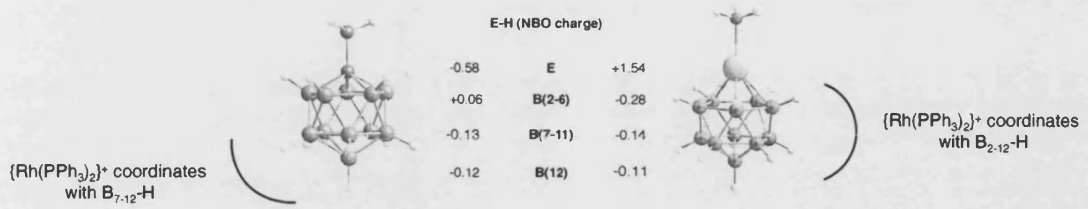

Figure 5.7 Charges on each unique {BH} and {E} vertex as calculated by NBO analysis at the B3LYP/DZVP level.

The greater negative charge on the {BH} vertices compared with [*closo*-$CB_{11}H_{12}]^-$ suggests the stronger binding of a cation metal fragment such as $\{Rh(PPh_3)_2\}^+$. Experimentally this is the case, as **43** only undergoes dehydrogenative borylation very slowly, presumably due to the tighter bond between the metal and cage.

5.3 Conclusions

The synthesis of $[NBu_4][1\text{-Me-1-}closo\text{-}SnB_{11}H_{11}]$ in multigram quantities from $Na[BH_4]$ suggests that it might be a more accessible alternative to $[closo\text{-}CB_{11}H_{12}]^-$, the derivatives of which have been shown to be some of the most robust weakly coordinating anions currently known.

The synthesis of $[Rh(PPh_3)_2(1\text{-Me-}closo\text{-}SnB_{11}H_{11})]$ has been achieved. Its solid-state structure shows unusual Rh-H-B interactions between the upper and lower pentagonal {BH} vertices. These interactions are retained in solution, as well as contacts between the antipodal vertex and the metal fragment. The preferred binding mode to the upper portion of the cage has been confirmed by DFT studies, which has also suggested that the slow dehydrogenative borylation of ethene may be due to the stronger Rh-H-B interactions in $[Rh(PPh_3)_2(1\text{-Me-}closo\text{-}SnB_{11}H_{11})]$ than in $[Rh(PPh_3)_2(closo\text{-}CB_{11}H_{12})]$.

5.4 Bibliography

1 R. W. Chapman, J. G. Kester, K. Folting, W. E. Streib, and L. J. Todd, *Inorg. Chem.*, 1992, **31**, 979.

2 L. Wesemann, *Z. Anorg. Allg. Chem.* , 2004, **630**, 1349.

3 T. Marx, B. Mosel, I. Pantenburg, S. Hagen, H. Schulze, and L. Wesemann, *Chem.-Eur. J.*, 2003, **9**, 4472.

4 S. Hagen, I. Pantenburg, F. Weigend, C. Wickleder, and L. Wesemann, *Angew. Chem.-Int. Edit.*, 2003, **42**, 1501.

5 B. Ronig, H. Schulze, I. Pantenburg, and L. Wesemann, *Eur. J. Inorg. Chem.*, 2005, 314.

6 S. Hagen, L. Wesemann, and I. Pantenburg, *Chem. Commun.*, 2005, 1013.

7 B. Ronig, I. Pantenburg, and L. Wesemann, *Eur. J. Inorg. Chem.*, 2002, 319.

8 T. Gadt, B. Grau, K. Eichele, I. Pantenburg, and L. Wesemann, *Chem.-Eur. J.*, 2006, **12**, 1036.

9 T. Gadt and L. Wesemann, *Organometallics*, 2007, **26**, 2474.

10 A. Rifat, N. J. Patmore, M. F. Mahon, and A. S. Weller, *Organometallics*, 2002, **21**, 2856.

11 A. Rifat, V. E. Laing, G. Kociok-Kohn, M. F. Mahon, G. D. Ruggiero, and A. S. Weller, *J. Organomet. Chem.*, 2003, **680**, 127.

12 S. Hermanek, *Chem. Rev.*, 1992, **92**, 325.

13 C. B. Knobler, T. B. Marder, E. A. Mizusawa, R. G. Teller, J. A. Long, P. E. Behnken, and M. F. Hawthorne, *J. Am. Chem. Soc.*, 1984, **106**, 2990.

14 A. S. Weller, M. F. Mahon, and J. W. Steed, *J. Organomet. Chem.*, 2000, **614**, 113.

15 N. J. Patmore, M. F. Mahon, J. W. Steed, and A. S. Weller, *J. Chem. Soc.-Dalton Trans.*, 2001, 277.

16 D. J. Crowther, S. L. Borkowsky, D. Swenson, T. Y. Meyer, and R. F. Jordan, *Organometallics*, 1993, **12**, 2897.

17 performed by Dr Gus Ruggeiro, Department of Chemistry, University of Bath.

18 I. Zharov, T. C. Weng, A. M. Orendt, D. H. Barich, J. Penner-Hahn, D. M. Grant, Z. Havlas, and J. Michi, *J. Am. Chem. Soc.*, 2004, **126**, 12033.

19 M. L. McKee, *J. Am. Chem. Soc.*, 1997, **119**, 4220.

Chapter 6. Experimental

6.1 General

All manipulations were carried out under an atmosphere of argon, using standard Schlenk-line and glove box techniques, unless otherwise stated. Glassware was pre-dried in an oven at 130°C and flamed with a blowtorch under vacuum prior to use. Solvents were dried over activated alumina, copper and molecular sieve columns using a MBraun solvent purification system. $CDCl_3$ and CD_2Cl_2 were distilled under vacuum from CaH_2. All other chemicals were used as received. Mass spectrometry was performed by the EPSRC Service at the University of Swansea or at the University of Bath using a Bruker MicroToF mass spectrometer equipped with an electrospray ionisation source.

6.1.1 NMR spectroscopy

^{1}H, $^{1}H\{^{11}B\}$, $^{11}B\{^{1}H\}$, ^{11}B and $^{31}P\{^{1}H\}$ NMR spectra were recorded on Brüker Avance 300 MHz, 400 MHz or 500 MHz spectrometers. Residual protio solvent was used as reference for ^{1}H and $^{1}H\{^{11}B\}$ NMR spectra ($CDCl_3$: $\delta = 7.24$; CD_2Cl_2: $\delta = 5.32$; C_3D_6O: $\delta = 2.09$) and $^{13}C\{^{1}H\}$ NMR spectra (CD_2Cl_2: $\delta = 53.8$). ^{11}B, $^{11}B\{^{1}H\}$ and $^{31}P\{^{1}H\}$ spectra were referenced against $BF_3.OEt_2$ (external) and 85% H_3PO_4 (external) respectively. Values are quoted in ppm. Coupling constants are quoted in Hz.

6.1.2 X-ray crystallography

Intensity data for all structures were collected at 150 K on a Nonius KappaCCD diffractometer equipped with a low temperature device, using graphite monochromated

MoKα radiation (λ= 0.71070 Å). Structure solution followed by full-matrix least squares refinement was performed by using the SHELX suite of programs throughout.

6.2 Synthesis and characterization

6.2.1 Starting materials

The starting materials Cs[*closo*-$CB_{11}H_{12}$],[1] Ag[*closo*-$CB_{11}H_{12}$],[1] Cs[1-Me-*closo*-$CB_{11}H_{11}$],[2] [Rh(μ-Cl)(C_7H_8)]$_2$,[3] [Rh(μ-Cl)(C_7H_{12})]$_2$, [Rh(PPh_3)$_2$(*closo*-$CB_{11}H_{12}$)],[4] [Rh(PPh_3)$_2$(12-Br-*closo*-$CB_{11}H_{11}$)][5]. All other chemicals were used as received from Aldrich, Acros, Alfa Aesar, Fisher, Fluka or Strem Chemicals.

6.2.2 Synthesis

Rh(PPh_3)$_2$(7 or 12-(CH=CH_2)-*closo*-$CB_{11}H_{11}$), 12-isomer (1a), 7-isomer (1b)

[Rh(PPh_3)$_2$(*closo*-$CB_{11}H_{12}$)] (45 mg, 0.058 mmol) was placed in a 15 ml Young's ampoule and CH_2Cl_2 (5 ml) was added *via* cannula. The solution was freeze-pump-thawed three times. On the third cycle the solution was charged with ethene (0.500 g) the ampoule closed and then allowed to warm to room temperature with stirring. After 15 hours, the solvent was evaporated under vacuum, residue washed with pentane and dried to afford a dark orange product (28 mg, 61 %). $C_{39}H_{44}B_{11}P_2Rh$ requires %C 58.81 %H 5.57. Found %C 57.57 %H 5.57.

^{1}H NMR (δ/ppm CD_2Cl_2): 7.81-7.06 (m, 30H, PPh_3), 4.95 [d, 1H, B-CH=CH_2, *J*(HH) 16, 7 isomer], 4.83 [d, 1H, B-CH=CH_2, *J*(HH) 16, 12 isomer], 4.15 [d, 1H, B-CH=CH_2, *J*(HH) 9, 7 isomer], 4.10 [d, 1H, B-CH=CH_2, *J*(HH) 9, 12 isomer], 2.67 [dd, 1H, B-C*H*=CH_2, *J*(HH) 16, ^{3}*J*(H-H) 9 Hz, 7 isomer], 2.56 [dd, 1H, B-C*H*=CH_2, *J*(HH) 16,

J(H-H) 9, 12 isomer], 2.37 (s, 1H, Ccage-*H*, 7 isomer), 2.22 (s, 1H, Ccage-*H*, 12 isomer).

selected - $^{1}H\{^{11}B\}$ NMR (δ/ppm CD_2Cl_2): 1.86 (br s, B-*H*, 7 isomer), 1.80 (br s, B-*H*, 7 isomer), 1.64 (br s, B-*H*, 7 isomer),1.52 (br, B-*H*, 12 isomer), 1.24 (br s, B-*H*, 7 isomer), 0.18 (br s, B-*H*, 7 isomer), 0.56 (br , B-*H*, 12 isomer), -0.80 (br s, B-*H*-Rh, 7 isomer), -1.72 (br, B-*H*-Rh, 12 isomer), -2.15 (br s, B-*H*-Rh, 7 isomer).

^{11}B NMR (δ/ppm CD_2Cl_2): 2.71 (s, *B*-C), -2.18 (s, *B*-C), -14.93 (br, overlapping signals).

$^{31}P\{^{1}H\}$ NMR (δ/ppm CD_2Cl_2, 298 K): 40.7 (br).

[$Rh(PPh_3)_2$(nbd)][7 or 12-($CH=CH_2$)-*closo*-$CB_{11}H_{11}$] 12-isomer (2a), 7-isomer (2b)

Norbornadiene (100 equivalents) was added to a CH_2Cl_2 solution of **1a/1b** as described above and stirred for 3 hours. The solvent was evaporated under vacuum and the residue redissolved in CH_2Cl_2 (2 ml) and precipitated with pentane (15 ml) to afford an orange precipitate. The solvent was decanted *via* cannula and the product dried under vacuum. (44 mg, 85 %). FAB- (NOBA matrix), m/z: 169.2 showing the correct isotope pattern for $B_{11}C_3H_{14}$. $C_{46}H_{52}B_{11}P_2Rh$ requires %C 62.17 %H 5.90. Found %C 61.75 %H 6.08.

^{1}H NMR (δ/ppm CD_2Cl_2): 7.50-7.26 (m, 30H, PPh_3), 6.35 [dd, B-C*H*=CH_2, *J*(HH) 19, *J*(HH) 13, 7 isomer], 6.23 [dd, B-C*H*=CH_2, *J*(HH) 19, *J*(HH) 13, 12 isomer], 5.53 (br s, B-CH=CH_2, 12 isomer), 5.37 (br s, B-CH=CH_2, 7 and 12 isomers), 5.32 (br s, B-CH=CH_2, 7 and 12 isomers), 5.18 (br s, B-CH=CH_2, 12 isomer), 4.50 (br s, 4H, C_7H_8), 4.08 (br s, 2H, C_7H_8), 2.44 (br s, C_{cage}- *H*, 7 isomer), 2.31 (br s, 1H, C_{cage}-*H*, 12 isomer), 1.56 (s, 2H, C_7H_8).

$^{11}B\{^1H\}$ NMR (δ/ppm CD_2Cl_2), assignments from ^{11}B-^{11}B COSY and ^{11}B NMR, primed numbers indicate 7 isomer: 1.2 (*B12*-$CH{=}CH_2$), -4.6 (*B7'*-$CH{=}CH_2$), -5.8 (*B12'*-H), -12.4 (*B7-11,8',11'*-H, coincident signal), -13.4 (*B9',10'*-H), -15.6 (*B2',3'*-H), -16.4 (*B2-6,4',6'*-H, coincident signal), -18.5 (*B5'*-H).

$^{31}P\{^1H\}$ NMR (δ/ppm CD_2Cl_2, 298 K): 29.6 [d, *J*(RhP) 156].

[$Rh(PPh_3)_2$(7 or 12-(Et)-*closo*-$CB_{11}H_{11}$)], 12-isomer (3a), 7-isomer (3b)

[$Rh(PPh_3)_2$(1-H-*closo*-$CB_{11}H_{11}$)] (45 mg, 0.058 mmol) was placed in a 15 ml Young's ampoule and CH_2Cl_2 (5 ml) was added *via* cannula. The solution was freeze-pump-thawed three times. On the third cycle the solution was charged with ethene (1.012 g) and allowed to warm to room temperature with stirring. After 15 hours, excess of ethene was removed under vacuum and replaced with hydrogen (1 atm). After one hour, the solvent was evaporated under vacuum to afford a red product (25 mg 54 %). $C_{39}H_{46}B_{11}P_2Rh$ requires %C 58.66 %H 5.81. Found %C 58.04 %H 5.85.

^1H NMR (δ/ppm CD_2Cl_2): 7.80-7.06 (m, 30H, PPh_3), 2.51 (br s, 1H, C_{cage}-*H*, 12 isomer), 2.46 (s, 1H, C_{cage}-*H*, 7 isomer), 0.95-0.30 (m, B-*Et*), -0.84 (br q, B-*H*-Rh) , -2.11 (br q, B-*H*-Rh).

Selected-$^1H\{^{11}B\}$ NMR (δ /ppm CD_2Cl_2): 2.51 (br s, 1H, C_{cage}-*H*,. 12 isomer), 2.46 (s, 1H, C_{cage}- *H*, 7 isomer), 1.98 (br s, B-*H*), 1.64 (br s, B-*H*), 1.55 (br s, B-*H*), 1.44 (br s, B-*H*), 0.95-0.30 (m, B-*Et*), -0.84 (br s, B-*H*-Rh) , -2.11 (br s, B12-*H*-Rh).

$^{11}B\{^1H\}$ NMR (δ/ppm CD_2Cl_2): 8.51 (s, *B*-Et), 5.04 (s, *B*-Et), 2.67 (s, *B*-H), 0.89 (s, *B*-H), -12.00 (s, *B*-H), -14.18 (s, *B*-H), -16.12 (s, *B*-H), -16.89 (s, *B*-H).

$^{31}P\{^1H\}$ NMR (δ/ppm CD_2Cl_2, 298 K): 12 isomer: 46.0 [d, *J*(RhP) 194]; 7 isomer: 45.8 [d, *J*(RhP) 189].

[Rh(PPh$_3$)$_2$(nbd)][7 or 12-(Et)-*closo*-CB$_{11}$H$_{11}$] 12-isomer (4a) 7-isomer (4b)

[Rh(PPh$_3$)$_2$(CB$_{11}$H$_{12}$)] (45 mg, 0.058 mmol) was placed in a 15 ml Young's ampoule and CH_2Cl_2 (5 ml) was added *via* cannula. The solution was freeze-pump-thawed three times. On the third cycle the solution was charged with ethene (1.012 g) and allowed to warm to room temperature with stirring. After 15 hours, excess of ethene was removed under vacuum and replaced with hydrogen (1 atm). After one hour, the solvent was evaporated under vacuum. The residue was redissolved in CH_2Cl_2 and norbornadiene (0.5 ml, 4.63 mmol) was added. After stirring for 3 hours, the solvent was evaporated under vacuum and the orange residue redissolved in CH_2Cl_2 (2 ml) and precipitated with pentane (15 ml). The solvent was decanted *via* cannula and the product dried under vacuum (44 mg, 85 %). FAB- (NOBA matrix), m/z: 171.1 showing the correct isotope pattern for $B_{11}C_3H_{16}$. $C_{46}H_{54}B_{11}P_2Rh$ requires %C 62.03 %H 6.11. Found %C 61.70 %H 6.22.

^{1}H NMR (δ/ppm CD_2Cl_2): 7.37-7.27 (m, 30H, PPh_3), 4.47 (br s, 4H, C_7H_8), 3.99 (br s, 2H, C_7H_8), 2.26 (br s, C_{cage}-*H*), 2.16 (br s, C_{cage}-*H*), 1.59 (br s, 2H, C_7H_8), 1.06-0.70 (m, B-*Et*).

^{1}H{^{11}B} NMR (δ/ppm CD_2Cl_2): 7.37-7.27 (m, 30H, PPh_3), 4.47 (br s, 4H, C_7H_8), 3.99 (br s, 2H, C_7H_8), 2.26 (br s, C_{cage}-*H*), 2.16 (br s, C_{cage}-*H*), 1.63 (br s, B-*H*), 1.61 (br s, B-*H*), 1.59 (br s, 2H, C_7H_8), 1.55 (br s, B-*H*), 1.06-0.70 (m, B-*Et*).

^{11}B NMR (δ/ppm CD_2Cl_2) assignments from ^{11}B-^{11}B COSY, primed numbers indicate 7 isomer: 4.13 (s, *B12*-Et), -1.78 (s, *B7'*-Et), -6.20 [d, *B12'*-H, *J*(BH) 133], -12.77 [d, *B7-11,8',11'*-H, *J*(BH) 136], -14.03 (d br, *B9',10'*-H), -16.00 (d br, *B2',3'*-H), -16.90 [d, *B2-6,4',6'*-H, *J*(BH) 147], -19.81 [d, *B5'*-H, *J*(BH) 149].

^{31}P{^{1}H} NMR (δ/ppm CD_2Cl_2, 298 K): 29.4 [d, *J*(RhP) 155].

[$Rh(PPh_3)_2${12-Br-7-($CH=CH_2$)-*closo*-$CB_{11}H_{10}$}] (5)

[$Rh(PPh_3)_2$(nbd)][12-Br-*closo*-$CB_{11}H_{11}$] (50 mg, 0.053 mmol) was placed in a 15 ml Young's ampoule equipped with a magnetic stir bar and CH_2Cl_2 (5 ml) was added *via* cannula. The solution was freeze-pump-thawed three times. On the third cycle the solution was allowed to warm to room temperature with stirring under an atmosphere of hydrogen to obtain [$Rh(PPh_3)_2$(12-Br-$CB_{11}H_{11}$)]. After 30 minutes excess of hydrogen was removed with vacuum and ethene condensed (1.407 g). After 24 hours excess of ethene was released, the solvent evaporated under vacuum and the residue redissolved with CH_2Cl_2. The solution was concentrated under reduced pressure to a volume of 3 ml, and hexanes (20 ml) was added to afford an orange precipitate. Solvents were removed by decantation, product washed with hexane (2 x 5 ml) and dried in vacuo to afford the title compound (22 mg, 47%) as an orange solid. $C_{39}H_{43}B_{11}BrP_2Rh(CH_2Cl_2)_2$ requires %C 47.11 %H 4.53. Found %C 47.97 %H 4.83.

^{1}H NMR (δ/ppm CD_2Cl_2 298K): 7.44-7.14 (m, 30H, PPh_3), 5.03 [d, 1H, B-CH=C*H*$_2$, *J*(HH) 16], 4.45 [d, 1H, B-CH=C*H*$_2$, *J*(HH) 9.6], 3.18 [dd, 1H, B-C*H*=CH_2, *J*(HH) 16, ^{3}*J*(HH) 9.6, 2.26 (s, 1H, Ccage-*H*).

selected - ^{1}H{^{11}B} NMR (δ/ppm CD_2Cl_2 298K): 1.74 (br s, B-*H*), 1.60 (br s, B-*H*).

^{11}B{1H} NMR (δ/ppm CD_2Cl_2 298K): -2.35 (s, *B*-C), -3.64 (s, *B*-Br), -12.80 (br s, *B*-H), -14.33 (br s, *B*-H), -17.07 (br s, *B*-H).

^{31}P{^{1}H} NMR (δ/ppm CD_2Cl_2 298K): 57.4(br s), 21.4 (br s).

^{31}P{^{1}H} NMR (δ/ppm CD_2Cl_2 258K): 57.4 (dd, *J*(RhP) 194, *J*(PP) 32), 21.4 (dd, *J*(RhP) 194, *J*(PP) 32).

[Rh(PPh$_3$)$_2$(nbd)][12-Br-7-(CH=CH$_2$)-*closo*-CB$_{11}$H$_{10}$] (6)

[Rh(PPh$_3$)$_2$(nbd)][12-Br-*closo*-CB$_{11}$H$_{11}$] (100 mg, 0.106 mmol) was placed in a 15 ml Young's ampoule equipped with a magnetic stir bar and CH_2Cl_2 (5 ml) was added *via* cannula. The solution was freeze-pump-thawed three times. On the third cycle the solution was allowed to warm to room temperature with stirring under an atmosphere of hydrogen to obtain [Rh(PPh$_3$)$_2$(12-Br-CB$_{11}$H$_{11}$)]. After 30 minutes excess of hydrogen was removed with vacuum and ethene condensed (1.542 g). After 2 hours, ethene was released, the solvent evaporated under vacuum and the residue redissolved with CH_2Cl_2. Norbornadiene (0.5 ml, 4.63 mmol) was added to the CH_2Cl_2 solution and stirred for 3 hours. The solvent was evaporated under vacuum and the residue redissolved in CH_2Cl_2 (2 ml) and precipitated with pentane (15 ml) to afford an orange precipitate. Solvents were removed by decantation, product washed with pentane (2 x 5 ml) and dried in vacuo to afford the title compound (85 mg, 83%) as an orange solid. FAB-(NOBA matrix), m/z: 248.2 showing the correct isotope pattern for $C_3H_{13}B_{11}Br$. $C_{46}H_{51}B_{11}BrP_2Rh$ requires %C 57.10 %H 5.31. Found %C 57.16 %H 5.33.

^{1}H NMR (δ/ppm $CDCl_3$): 7.40-7.27 (m, 30H, PPh$_3$), 6.32 (dd, B-C*H*=CH$_2$, *J*(HH) 19, *J*(HH) 13), 5.61 (br s, 1H, B-CH=C*H*$_2$), 5.45 (br s, 1H, B-CH=C*H*$_2$), 4.50 (br s, 4H, C_7H_8), 4.08 (br s, 2H, C_7H_8), 2.40 (br s, C$_{cage}$- *H*), 1.57 (s, 2H, C_7H_8).

^{1}H{^{11}B} NMR (δ/ppm $CDCl_3$): 7.40-7.27 (m, 30H, PPh$_3$), 6.32 (dd, B-C*H*=CH$_2$, *J*(HH) 19, *J*(HH) 13), 5.61 (dd, 1H, B-CH=C*H*$_2$, *J*(HH) 19, *J*(HH) 4.6), 5.45 (dd, 1H, B-CH=C*H*$_2$, *J*(HH) 13, *J*(HH) 4.6), 4.50 (br s, 4H, C_7H_8), 4.08 (br s, 2H, C_7H_8), 2.40 (br s, C$_{cage}$- *H*), 2.14 (br s, 2H, B-*H*), 2.07 (br s, 2H, B-*H*), 1.93 (br s, 2H, B-*H*), 1.81 (br s, 2H, B-*H*), 1.74 (br s, 1H, B-*H*), 1.57 (s, 2H, C_7H_8).

$^{11}B\{^1H\}$ NMR (δ/ppm $CDCl_3$), assignments from ^{11}B-^{11}B COSY and ^{11}B NMR, -2.16 (s, 1B, *B*-Br), -5.38 (s, 1B, *B*-C), -11.73 (s, 2B, *B*-H), -12.63 (s, 2B, *B*-H), -16.48 (s, 2B, *B*-H), -17.43 (s, 2B, *B*-H), -18.87 (s, 1B, *B*-H).

$^{31}P\{^1H\}$ NMR (δ/ppm $CDCl_3$): 29.8 [d, *J*(RhP) 156].

[$Rh(PPh_3)_2$(*closo*-$CB_{11}H_7Et_5$)] (7)

A solution of compound [$Rh(PPh_3)_2$(*closo*-$CB_{11}H_{12}$)] (**I**) (60 mg, 0.078 mmol) in CH_2Cl_2 (10 ml) was freeze-pump-thawed three times. After the third cycle the solution was placed under an ethene atmosphere. After stirring for 24 hours, the solution was degassed again and hydrogen was placed in the Young's ampoule and the solution stirred for 2 hours. Sequential treatment with ethene and hydrogen as explained was repeated a total of six times. The dark pink-red solution was reduced *in vacuo* to dryness.

^1H NMR (δ/ppm CD_2Cl_2): 7.45-7.00 (m, 30 H, PPh_3), 2.31 (br s, C_{cage}-*H*), 2.21 (br s, C_{cage}-*H*), 0.86-0.14 (m, 26H, B-*Et*), -4.95 (br q, B-*H*-Rh).

^{11}B NMR (δ/ppm CD_2Cl_2): 7.83 (br s, *B*-Et), -4.26 (br s, *B*-Et), -9.18 (br d), -12.81 (br d, *B*-H), -17.85 (d, *B*-H, *J*(H-B) = 92.7 Hz), -19.89 (d, *B*-H, *J*(H-B) = 95.2 Hz).

$^{11}B\{^1H\}$ NMR (δ/ppm CD_2Cl_2): 7.83 (br s, *B*-Et), -4.26 (br s, *B*-Et), -9.18 (br s), -12.81 (br s, *B*-H), -17.85 (s, *B*-H, *J*(H-B) = 92.7 Hz), -19.89 (s, *B*-H, *J*(H-B) = 95.2 Hz).

$^{31}P\{^1H\}$ NMR (δ/ppm CD_2Cl_2, 298 K): 45.1 (br m).

[$Rh(PPh_3)_2$(nbd)][$(Et)_5$-*closo*-$CB_{11}H_7$] (8)

A solution of [$Rh(PPh_3)_2$(*closo*-$CB_{11}H_{12}$)] (179 mg, 0.232 mmol) in CH_2Cl_2 (10 ml) was freeze-pumpthawed three times. On the third cycle ethene (~ 0.600 g) was added to

the solution, the ampoule closed and warmed up to room temperature. After stirring for 24 hours, the solution was degassed again and hydrogen was placed in the Young's ampoule and the solution stirred for 2 hours. This sequential treatment with ethene / hydrogen was repeated a total of 6 times. Following the last hydrogenation the solvent was degassed and norbornadiene (1 ml, 9.27 mmol) added. After stirring overnight, the solvent was evaporated under vacuum, the orange residue redissolved in CH_2Cl_2 (2 ml) and precipitated with hexane (20 ml). The solvent was decanted via cannula and the product dried under vacuum (175 mg, 75 %). Crystals suitable for an X-ray diffraction study were grown from CH_2Cl_2/pentane solutions. $RhP_2B_{11}C_{54}H_{70}$ requires %C 64.67 % H 7.04, found %C 63.63 %H 6.92. FAB- (NOBA matrix), m/z: 283.3. This preparation has been successfully scaled up to 1.5 g of material with only a small overall loss in yield (~70%).

^{1}H NMR (δ/ppm CD_2Cl_2): 7.49-7.20 (m, 30H, PPh_3), 4.44 (br s, 4H, C_7H_8), 3.96 (br s, 2H, C_7H_8), 2.02 (br s, C_{cage}-*H*), 1.55 (br s, 2H, C_7H_8), 0.96-0.36 (m, 25H, B-*Et*).

^{1}H{^{11}B} NMR (δ /ppm CD_2Cl_2): 7.49-7.20 (m, 30H, PPh_3), 4.44 (br s, 4H, C_7H_8), 3.96 (br s, 2H, C_7H_8), 2.02 (br s, C_{cage}-*H*), 1.55 (br s, 2H, C_7H_8), 1.48 (br s, B-*H*), 1.40 (br s, B-*H*), 1.36 (br s, B*H*), 1.29 (br s, B-*H*), 1.21 (br s, B-*H*), 1.08 (br s, B-*H*), 0.96-0.36 (m, 25H, B-*Et*).

^{11}B NMR (δ /ppm CD_2Cl_2): 4.6 (br s, 1B, *B*-Et), -2.5 (br s, 2B, *B*-Et), -3.3 (br s, 1B, *B*-Et), -7.0 (br s, 1B, *B*-Et), -8.4 (br d, 1B, *B*-H) -12.5 (br d, 1B *B*-H), -13.7 (br d,1B *B*-H), -14.6 (br d, *B*-H, 1B), -17.3 (br d, *B*-H, 2B overlapping coincidence).

^{31}P{^{1}H} NMR (δ /ppm CD_2Cl_2, 298 K): 30.5 [d, *J*(RhP) 155].

Cs[1-^{i}Pr$_3$Si-*closo*-CB$_{11}$H$_{11}$] (9)

Butyllithium (1.45 ml, 3.63 mmol of a 2.5 M solution in hexane) was added to a solution of Cs[CB$_{11}$H$_{12}$] (1.002 g, 3.63 mmol) in THF (15 ml) at -70 °C. The new solution was allowed to warm up to room temperature and the resulting white suspension stirred overnight. ^{i}Pr$_3$SiCl (0.86 ml, 3.63 mmol) in THF (10 ml) was added and the mixture stirred for 20 hours. The new solution was filtered and the solvent removed to give a residue which was dissolved in water. A white precipitate was obtained after addition of excess of CsCl (3.056 g, 66 %). The solid was filtered, washed with water, dried and dissolved in ethanol. This was removed by rotary evaporation and the solid vacuum dried.

^{1}H NMR (δ/ppm d$_6$-acetone): 1.24 (sept., 3H, Si(C*H*(CH$_3$)$_2$)$_3$); 1.17 (d, 18H, Si(CH(C*H*$_3$)$_2$)$_3$).

^{1}H{^{11}B} NMR (δ/ppm d$_6$-acetone): 1.94 (br s, 1H, B-*H*); 1.88 (br s, 5H, B-*H*); 1.67 (br s, 5H, B-*H*); 1.24 (2 sept., 3H, Si(C*H*(CH$_3$)$_2$)$_3$); 1.17 (d, 18H, Si(CH(C*H*$_3$)$_2$)$_3$).

^{11}B NMR (δ/ppm d$_6$-acetone): -1.93 (d, 1B, *B(12)*-H, *J*(B-H) = 134.0 Hz); -10.89 (d, 5B, *B(2-11)*-H, *J*(B-H) = 151.0 Hz); -12.71 (d, 5B, *B(2-11)*-H, *J*(B-H) = 166.1 Hz).

^{11}B{^{1}H} NMR (δ/ppm d$_6$-acetone): -1.94(s, 1B, *B(12)*-H); -10.89 (s, 5B, *B(12)*-H); -12.71 (s, 5B, *B(2-11)*-H).

[Rh(PPh$_3$)$_2$(nbd)][1-Me-*closo*-CB$_{11}$H$_{11}$] (10):

[Rh(μ-Cl)(nbd)]$_2$ (50 mg, 0.108 mmol), nbd (26 μl, 28 mmol) and Cs[1-Me-CB$_{11}$H$_{11}$] (62.5 mg, 0.216 mmol) were stirred in THF (15 ml) for 3 hours. PPh$_3$ (115 mg, 0.435 mmol) was added to the reaction which was stirred overnight. THF was pumped off and the residue dissolved in CH_2Cl_2 and cannula filtered. The compound

was crystallised by addition of hexanes to yield 169 mg (0.193 mmol, 88 %) of $[Rh(PPh_3)_2(nbd)][1\text{-}Me\text{-}CB_{11}H_{11}]$. The orange crystals were washed with hexane twice and dried *in vacuo*.

^{1}H NMR (δ/ppm $CDCl_3$): 7.36 (m, 30H, PPh_3), 4.48 (s, 4H, C_7H_8), 4.08 (s, 2H, C_7H_8), 1.67 (s, 3H, C-Me_{cage}), 1.54 (s, 2H, C_7H_8).

^{1}H{^{11}B} NMR (δ/ppm $CDCl_3$): 7.36 (m, 30H, PPh_3), 4.49 (s, 4H, C_7H_8), 4.08 (s, 2H, C_7H_8), 1.99 (br s, 6H, B(2-6, 12)-*H*), 1.86 (br s, 5H, B(7-11)-*H*), 1.67 (s, 3H, C_{cage}-*Me*), 1.54 (s, 2H, C_7H_8).

^{11}B NMR (δ/ppm $CDCl_3$): -10.08 (d, 1B, *B(12)*-H, *J*(B-H) = 132.2 Hz), -11.72 (d, 10B, *B(2-11)*-H, *J*(B-H) = 143.2 Hz)).

^{11}B{^{1}H} NMR (δ/ppm $CDCl_3$): -10.08 (s, 1B, *B(12)*-H), -11.72 (s, 10B, *B(7-12)*-H).

^{31}P{^{1}H} NMR (δ/ppm $CDCl_3$): 30.6 (d, *J*(Rh-P) = 156 Hz, PPh_3).

$[Rh(PPh_3)_2(nbd)][1\text{-}^iPr_3Si\text{-}closo\text{-}CB_{11}H_{11}]$ (11)

$[Rh(\mu\text{-}Cl)(nbd)]_2$ (50 mg, 0.108 mmol), nbd (26 µl, 28 mmol) and $Cs[1\text{-}^iPr_3Si\text{-}closo\text{-}CB_{11}H_{11}]$ (94 mg, 0.216 mmol) were stirred in THF (15 ml) for 3 hours. PPh_3 (115 mg, 0.435 mmol) was added to the reaction which was stirred overnight. THF was pumped off and the residue dissolved in CH_2Cl_2 and cannula filtered. The compound was crystallised by addition of hexanes to yield 189 mg (0.185 mmol, 85 %) of $[Rh(PPh_3)_2(nbd)][1\text{-}^iPr_3Si\text{-}CB_{11}H_{11}]$. The orange crystals were washed with hexane twice and dried *in vacuo*.

^{1}H NMR (δ/ppm $CDCl_3$): 7.34 (m, 30H, PPh_3), 4.48 (s, 4H, C_7H_8), 4.08 (s, 2H, C_7H_8), 1.52 (s, 2H, C_7H_8), 1.27 (sept, 3H, $Si(CH(CH_3)_2)_3$), 1.16 (d, 18H, $Si(CH(CH_3)_2)_3$).

$^{1}H\{^{11}B\}$ NMR (δ/ppm $CDCl_3$): 7.34 (m, 30H, PPh_3), 4.48 (s, 4H, C_7H_8), 4.09 (s, 2H, C_7H_8), 2.30 (br s, 1H, B(12)-*H*), 2.08 (br s, 5H, B(2-6)-*H*), 1.96 (br s, 5H, B(7-11)-*H*), 1.52 (s, 2H, C_7H_8), 1.27 (sept, 3H, $Si(CH(CH_3)_2)_3$), 1.16 (d, 18H, $Si(CH(CH_3)_2)_3$).

^{11}B NMR (δ/ppm $CDCl_3$): -2.04 (d, 1B, *B(12)*-H, *J*(B-H) = 133.9 Hz)), -10.75 (d, 5B, *B(7-11)*-H, *J*(B-H) = 147.7 Hz)), -12.29 (d, 5B, *B(2-6)*-H, *J*(B-H) = 138.0 Hz)).

$^{11}B\{^{1}H\}$ NMR (δ/ppm $CDCl_3$): -2.04 (s, 1B, *B(12)*-H), -10.75 (s, 5B, *B(7-12)*-H), -12.29 (s, 5B, *B(2-6)*-H).

$^{31}P\{^{1}H\}$ NMR (δ/ppm $CDCl_3$): 30.6 (d, *J*(RhP) = 155 Hz)

[$Rh(PPh_3)_2$ (1-Me-*closo*-$CB_{11}H_{11}$)] (12):

[$Rh(PPh_3)_2$(nbd)][1-Me-$CB_{11}H_{11}$] (30 mg, 0.034 mmol) was placed in a 15 ml Young's ampoule and CH_2Cl_2 (5 ml) was added *via* cannula. The solution was freeze-pump-thawed three times. On the third cycle the solution was allowed to warm to room temperature with stirring, under an atmosphere of H_2. Conversion was quantitative by NMR spectroscopy. Addition of hexanes along with solvent evaporation under vacuum afforded a dark red product.

^{1}H NMR (δ/ppm $CDCl_3$): 7.50-7.09 (m, 30H, PPh_3), 1.59 (s, 3H, C-Me_{cage}), 0.18 (br q, 5H, B(7-11)-*H*), -2.05 (br q, 1H, B(12)-*H*).

$^{1}H\{^{11}B\}$ NMR (δ/ppm $CDCl_3$): 7.50-7.09 (m, 30H, PPh_3), 1.93 (s, 5H, B(2-6)-*H*), 1.59 (s, 3H, C-Me_{cage}), 0.18 (br s, 5H, B(7-11)-*H*), -2.05 (br s, 1H, B(12)-*H*).

^{11}B NMR (δ/ppm $CDCl_3$): -11.91 (br d overlapping, *B*-H), -13.17 (d, *B*-H, $J(^{11}B\text{-}^{1}H)$ = 122.6 Hz).

$^{11}B\{^{1}H\}$ NMR (δ/ppm $CDCl_3$): -11.91 (s, *B*-H), -13.17 (s, *B*-H).

$^{31}P\{^{1}H\}$ NMR (δ/ppm $CDCl_3$): 47.7 (d, $J(^{103}Rh\text{-}^{31}P)$ = 193 Hz, PPh_3).

[Rh(PPh$_3$)$_2$(1-^{i}Pr$_3$Si-*closo*-CB$_{11}$H$_{11}$)] (13)

[Rh(PPh$_3$)$_2$(nbd)][1-^{i}Pr$_3$Si-*closo*-CB$_{11}$H$_{11}$] (30 mg, 0.029 mmol) was placed in a 15 ml Young's ampoule and CH_2Cl_2 (5 ml) was added *via* cannula. The solution was freeze-pump-thawed three times. On the third cycle the solution was allowed to warm to room temperature with stirring, under an atmosphere of H_2. Conversion was quantitative by NMR spectroscopy. Addition of hexanes along with solvent evaporation under vacuum afforded a dark red product. Suitable crystals for X-ray diffraction studies were obtained from a concentrated CH_2Cl_2 solution at -18°C. Anal. Calcd for $C_{46}H_{62}P_2RhSiB_{11}$: C, 59.61 %; H, 6.74 %. Found: C, 60.3 %; H, 6.54 %.

^{1}H NMR (δ/ppm $CDCl_3$): 7.51-7.07 (m, 30H, PPh$_3$), 1.18 (sept, 3H, Si(C*H*(CH$_3$)$_2$)$_3$), 1.11 (d, 18H, Si(CH(C*H*$_3$)$_2$)$_3$), 0.07 (br q, 5H, B(7-11)-*H*), -0.08 (br q, 1H, B(12)-*H*).

^{1}H{^{11}B} NMR (δ/ppm $CDCl_3$): 7.51-7.07 (m, 30H, PPh$_3$), 2.05 (s, 5H, B(2-6)-*H*), 1.18 (sept, 3H, Si(C*H*(CH$_3$)$_2$)$_3$), 1.11 (d, 18H, Si(CH(C*H*$_3$)$_2$)$_3$), 0.07 (br s, 5H, B(7-11)-*H*), -0.08 (br s, 1H, B(12)-*H*).

^{11}B NMR (δ /ppm $CDCl_3$): -6.85 (d, 1B, *B(12)*-H, *J*(B-H) = 110.1 Hz)), -13.17 (d, 10B, *B(2-11)*-H, *J*(B-H) = 112.4 Hz)).

^{11}B{^{1}H} NMR (δ /ppm $CDCl_3$): -6.85 (s, 1B, *B(12)*-H), -13.17 (s, 10B, *B(2-12)*-H).

^{31}P{^{1}H} NMR (δ /ppm $CDCl_3$): 47.7 (d, *J*(RhP) = 194 Hz).

[Rh(PPh$_3$)$_2$(1-Me-(Et)$_3$-*closo*-CB$_{11}$H$_8$)] (14)

[Rh(PPh$_3$)$_2$(nbd)][1-Me-*closo*-CB$_{11}$H$_{11}$] (50 mg, 0.057 mmol) was placed in a 15 ml Young's ampoule and CH_2Cl_2 (5 ml) was added *via* cannula. The solution was freeze-pump-thawed three times. On the third cycle the solution was allowed to warm to room temperature with stirring under an atmosphere of hydrogen to obtain

$[Rh(PPh_3)_2(1\text{-Me-}CB_{11}H_{11})]$. After 30 minutes excess of hydrogen was removed with vacuum and replaced with ethene. After 24 hours, the solution was degassed again and hydrogen was placed in the Young's ampoule and the solution stirred for 2 hours. This procedure was repeated a total of six times. The solution was then reduced *in vacuo* to dryness to afford a dark red residue. Crystals suitable for an X-ray diffraction experiment were grown from CH_2Cl_2/pentane solutions. Mass 12 mg, Yield 25%. FAB-(NOBA matrix), m/z: 241.2 that shows the correct isotope pattern for $B_{11}C_8H_{26}$. Compound **14** was always formed with a small (~ 10%) of another carborane anion that could not be removed by bulk purification methods. Mass spectroscopy suggests that the identity of this may be $[1\text{-H-}closo\text{-}(C_2H_5)_4\text{-}CB_{11}H_7]^-$.

^{1}H NMR (δ/ppm CD_2Cl_2): 7.52-7.10 (m, 30H, PPh_3), 1.64 (s, 3H, C_{cage}-*CH*$_3$), 1.02-0.11 (m, 15H, B-*CH*$_2$*CH*$_3$), -4.64 (br q, 2H, B-*H*-Rh).

^{11}B NMR (δ/ppm CD_2Cl_2): -2.1 (vbr, 3B), -12.7 (vbr , 3B), -16.3 (vbr, 3B), -18.8 [d, 2B *B*-H, *J*(HB) 94].

^{31}P{^{1}H} NMR (δ/ppm CD_2Cl_2, 298 K): 45.0 [d, *J*(RhP) 193].

$[Rh(PPh_3)_2(nbd)][1\text{-Me-}(Et)_3\text{-}closo\text{-}CB_{11}H_8]$ (15)

A solution of $[Rh(PPh_3)_2(nbd)][1\text{-Me-}closo\text{-}CB_{11}H_{11}]$ (60 mg, 0.068 mmol) in CH_2Cl_2 (10 ml) was placed in a 20 ml Young's ampoule equipped with a magnetic stir bar. The solution was degassed with vacuum and then stirred under an atmosphere of hydrogen to obtain $[Rh(PPh_3)_2(1\text{-Me-}closo\text{-}CB_{11}H_{11})]$. After 30 minutes excess of hydrogen was removed with vacuum and ethene condensed (0.259 g). After 4 hours, ethene was released, the solution degassed under vacuum again and charged with hydrogen. Sequential treatment with ethene and hydrogen as previously described were

performed twice more (with reaction times of 16 hours and 40 minutes respectively). The solvent was evaporated under vacuum and the residue redissolved with CH_2Cl_2. Norbornadiene (0.5 ml, 4.63 mmol) was added to the CH_2Cl_2 solution and stirred for 4 hours. The solvent was evaporated under vacuum and the residue redissolved in CH_2Cl_2 (2 ml) and precipitated with pentane (15 ml) to afford a dark orange precipitate. Solvents were removed by decantation, product washed with pentane (2 x 4 ml) and dried in vacuo to afford the title compound (46 mg, 70.0 %) as a dark orange solid. FAB (negative mode): *m/z* 241.31, showing the correct isotope pattern for $C_8H_{26}B_{11}$.

^{1}H NMR (δ/ppm CD_2Cl_2): 7.45-7.28 (m, 30H, PPh_3), 4.46 (br s, 4H, C_7H_8), 3.97 (br s, 2H, C_7H_8), 1.56 (s, C_{cage}-*CH*$_3$), 1.53 (br s, 2H, C_7H_8), 1.50 (s, C_{cage}-*CH*$_3$), 0.91-0.42 (m, 15H, B-*Et*).

^{1}H{^{11}B} NMR (δ/ppm CD_2Cl_2): 7.45-7.28 (m, 30H, PPh_3), 4.46 (br s, 4H, C_7H_8), 3.97 (br s, 2H, C_7H_8), 1.70 (br s, B-*H*), 1.64 (br s, B-*H*), 1.56 (s, C_{cage}-*CH*$_3$), 1.53 (br s, 2H, C_7H_8), 1.50 (s, C_{cage}-*CH*$_3$), 1.44 (br s, B-*H*), 1.38 (br s, B-*H*), 1.33 (br s, B-*H*), 0.91-0.42 (m, 15H, B-*Et*).

^{11}B NMR (δ/ppm CD_2Cl_2): -0.1 (br s, 1B, *B*-Et), -2.3 (br s, 2B, *B*-Et), -8.8 (br s, 1B, *B*-H), -11.2 (br s, 1B, *B*-H), -12.7 (br d, 2B, *B*-H) -13.9 (br d, 2B *B*-H), -15.9 (br d, 2B, *B*-H).

^{31}P{^{1}H} NMR (δ/ppm CD_2Cl_2, 298 K): 29.4 (d, *J*(RhP) 155).

[Rh(PPh_3)$_2$(nbd)][1-(^{i}Pr$_3$Si)-(Et)$_3$-*closo*-$CB_{11}H_8$] (16)

A solution of [Rh(PPh_3)$_2$(1-^{i}Pr$_3$Si-*closo*-$CB_{11}H_{11}$)] (179 mg, 0.232 mmol) in CH_2Cl_2 (10 ml) was freeze-pump-thawed three times. On the third cycle ethene (~ 0.600 g) was added to the solution, the ampoule closed and warmed up to room

temperature. After stirring for 24 hours, the solution was degassed again and hydrogen was placed in the Young's ampoule and the solution stirred for 2 hours. This sequential treatment with ethene / hydrogen was repeated a total of 3 times. Following the last hydrogenation the solvent was degassed and norbornadiene (1 ml, 9.27 mmol) added. After stirring overnight, the solvent was evaporated under vacuum, the orange residue redissolved in CH_2Cl_2 (2 ml) and precipitated with hexane (20 ml). The solvent was decanted via cannula and the product dried under vacuum (161 mg, 63%) . Anal. Calcd for $C_{59}H_{82}P_2RhSiB_{11}$: C, 64.2; H, 7.49. Found: C, 64.4; H, 7.56. ESI-MS (negative mode): *m/z* 383.5 (obsd), showing the correct isotope pattern for $SiB_{11}C_{16}H_{44}$.

^{1}H NMR (δ/ppm CD_2Cl_2, 298 K): 7.50-7.25 (m, 30H, PPh_3), 4.46 (br s, 4H, C_7H_8), 3.97 (br s, 2H, C_7H_8), 1.56 (br s, 2H, C_7H_8), 1.17 (sept, 3H, (Si-(C*H*$(CH_3)_2)_3$), 1.10 (d, 18H, (Si-(CH(C*H*$_3)_2)_3$), 0.90-0.40 (m, 15H, B-*Et*).

^{1}H{^{11}B} NMR (δ/ppm CD_2Cl_2, 298 K): 7.50-7.25 (m, 30H, PPh_3), 4.46 (br s, 4H, C_7H_8), 3.97 (br s, 2H, C_7H_8), 1.74 (s, 2H, B-*H*), 1.66 (s, 2H, B-*H*), 1.47 (s, 1H, B-*H*), 1.43 (s, 1H, B-*H*), 1.39 (s, 2H, B-*H*) 1.56 (br s, 2H, C_7H_8), 1.17 (sept, 3H, (Si-(C*H*$(CH_3)_2)_3$), 1.10 (d, 18H, (Si-(CH(C*H*$_3)_2)_3$), 0.90-0.40 (m, 15H, B-*Et*).

^{11}B{^{1}H} NMR (δ/ppm CD_2Cl_2, 298 K): 7.7 (br s, 1B, *B*-Et), -1.4 (br s, 2B, *B*-Et), -10.4 (br s, 1B, *B*-H), -11.9 (br s, 2B, *B*-H), -14.8 (br s, 2B, *B*-H) -16.8 (br s, 3B, *B*-H).

^{31}P{^{1}H} NMR (δ/ppm CD_2Cl_2, 298 K): 30.5 (d, *J*(RhP) 155).

$[Rh(PPh_3)_2(\eta^2\text{-}CH_2{=}CH_2)_3][closo\text{-}CB_{11}H_{12}]$ (17)

A solution of $[Rh(PPh_3)_2(nbd)][CB_{11}H_{12}]$ (20 mg, 0.023 mmol) in CH_2Cl_2 was freeze-pump-thawed three times. On the third cycle hydrogen (1 atm) was added to the solution to give $[Rh(PPh_3)_2(CB_{11}H_{12})]$. After 30 minutes the solution was freeze-pumped and ethene added. NMR experiments were performed at 230, 260 and 298 K.

^{1}H NMR (δ/ppm CD_2Cl_2, 298 K): 7.60-7.10 (m, 30H, PPh_3), (5.2, excess ethene), 2.35 (br s, 1H, C_{cage}-*H*).

^{1}H{^{11}B} NMR (δ/ppm CD_2Cl_2, 298 K): 7.60-7.10 (m, 30H, PPh_3), (5.2, excess ethene), 2.35 (br s, 1H, C_{cage}-*H*), 1.62 (br s, 6H, BH), 1.47 (br s, 5H, BH).

^{11}B NMR (δ/ppm CD_2Cl_2, 298 K): -7.18 (d, 1B, *B*-Br, *J*(BH) 130), -12.40 (d, 5B, *B*-Br, *J*(BH) 137), -16.17 (d, 5B, *B*-H, *J*(BH) 150).

^{31}P{^{1}H} NMR (δ/ppm CD_2Cl_2, 230 K): 35.8 (d, *J*(RhP) 95).

^{31}P{^{1}H} NMR (δ/ppm CD_2Cl_2, 260 K): $[Rh(PPh_3)_2(CB_{11}H_{12})]$ and **17** were observed.

^{31}P{^{1}H} NMR (δ/ppm CD_2Cl_2, 298 K): **1a/b** was formed.

$[Rh(PPh_3)_2(\eta^2\text{-}CH_2{=}CH_2)_3][closo\text{-}CB_{11}H_6Br_6]$ (18)

A solution of $[Rh(PPh_3)_2(nbd)][CB_{11}H_6Br_6]$ (20 mg, 0.015 mmol) in CH_2Cl_2 was freeze-pump-thawed three times. On the third cycle hydrogen (1 atm) was added to the solution to give $[(PPh_3)Rh(PPh_2\text{-}\eta^6\text{-}C_6H_5)]_2[CB_{11}H_6Br_6]_2$. After 30 minutes the solution was evaporated and the residue dissolved in CH_2Cl_2 under an atmosphere of ethene. Suitable crystals for X-ray diffraction studies were grown at -80°C by layering ethene-saturated pentane over the CH_2Cl_2 solution. *Insitu* low temperature ^{31}P{^{1}H} NMR spectra for the $[closo\text{-}CB_{11}H_{12}]^-$(**17**) and $[BAr^F{}_4]^-$ analogues are identical to (**18**).

^{1}H NMR (δ/ppm CD_2Cl_2, 298 K): 7.60-7.11 (m, 30H, PPh_3), (5.2, excess ethene), 2.59 (br s, 1H, C_{cage}-*H*).

^{1}H{^{11}B} NMR (δ/ppm CD_2Cl_2, 298 K): 7.60-7.11 (m, 30H, PPh_3), (5.2, excess ethene), 2.59 (br s, 1H, C_{cage}-*H*), 2.35 (br s, 5H, B-*H*).

^{11}B NMR (δ/ppm CD_2Cl_2, 298 K): -1.55 (s, 1B, *B*-Br), -9.80 (s, 5B, *B*-Br), -20.25 (d, 5B, *B*-H, *J*(BH) 156.6).

^{31}P{^{1}H} NMR (δ/ppm CD_2Cl_2, 298 K): 33.3 (d, *J*(RhP) 105.3).

^{31}P{^{1}H} NMR (δ/ppm CD_2Cl_2, 238 K): 34.5 (d, *J*(RhP) 102).

[$HPCy_3$][*closo*-$CB_{11}H_{12}$] (19)

HCl was added to a suspension of Cs[*closo*-$CB_{11}H_{12}$] (200 mg, 0.725 mmol) in water (50 ml) with ether (2 ml) to give a pH 1 solution. Ether (30 ml) was added to extract the acid carborane and the mixture transferred into a separating funnel, which was shaken and ether phase collected in a Schlenk tube. Ether was added twice more (2 x 30 ml) to the aqueous phase in order to extract all acid carborane. The ether solution was degassed, reduced up to ~5 ml under vacuum and placed under Argon. A PCy_3 (203 mg, 0.725 mmol) solution in ether (5 ml) was prepared in another Schlenk tube under inert atmosphere and cannula transferred to the acid carborane solution. [$HPCy_3$][*closo*-$CB_{11}H_{12}$] appeared as a white precipitate, which was washed three times with ether and dried under vacuum overnight (293 mg, 95.0 %). Anal. Calc. for $C_{19}H_{46}B_{11}P$: C, 53.76; H, 10.92. Found: C, 53.09; H, 11.15.

^{1}H NMR (δ/ppm, 400.1 MHz, CD_2Cl_2): 5.32 (d m, 1H, *H*PCy_3, *J*(PH) 448), 2.42 (m, PCy_3), 2.31 (br s, 1H, CcageH), 1.98-1.25 (m, PCy_3).

^{1}H{^{11}B} NMR (δ/ppm, 400.1 MHz, CD_2Cl_2): 5.32 (d m, 1H, *H*PCy_3, *J*(PH) 448), 2.42 (m, PCy_3), 2.31 (br s, 1H, CcageH), 1.63 (br s, 5H, BH), 1.46 (br s, 5H, BH), 1.98-1.25 (m, PCy_3), .

^{11}B NMR (δ/ppm, 128.4 MHz, CD_2Cl_2): -7.23 (d, 1B, B_{12}-H, *J*(BH) 137), -13.45 (d, 5B, $B_{7\text{-}11}$-H, *J*(BH) 136), -16.18 (d, 5B, $B_{2\text{-}6}$-H, *J*(BH) 149).

$^{11}B\{^1H\}$ NMR (δ/ppm, 128.4 MHz, CD_2Cl_2): -7.23 (s, 1B, B_{12}-H), -13.45 (s, 5B, $B_{7\text{-}11}$ H), -16.18 (s, 5B, $B_{2\text{-}6}$-H).

$^{31}P\{^1H\}$ NMR (δ/ppm, 162.0 MHz, CD_2Cl_2): 31.6 (s, H*P*Cy_3).

[$HPCyp_3$][*closo*-$CB_{11}H_{12}$] (20)

HCl was added to a suspension of Cs[*closo*-$CB_{11}H_{12}$] (310 mg, 1.123 mmol) in water (50 ml) with ether (2 ml) to give a pH 1 solution. Ether (30 ml) was added to extract the acid carborane and the mixture transferred into a separating funnel, which was shaken and ether phase collected in a Schlenk tube. Ether was added twice more (2 x 30 ml) to the aqueous phase in order to extract all acid carborane. The ether solution was degassed and reduced up to ~5 ml under Argon. A $PCyp_3$ (3 ml, 0.37 M in pentane, 1.123 mmol) solution in ether (10 ml) was prepared in another Schlenk tube under inert atmosphere and cannula transferred to the acid carborane solution. [$HPCyp_3$][*closo*-$CB_{11}H_{12}$] appeared as a white precipitate, which was washed three times with ether and dried under vacuum overnight (385 mg, 89.7 %). Anal. Calc. for $C_{16}H_{40}B_{11}P$: C, 50.26; H, 10.54. Found: C, 49.93; H, 10.74.

^1H NMR (δ/ppm CD_2Cl_2): 5.90 (d m, 1H, *H*PCyp_3, *J*(PH) 455), 2.56 (m, PCyp_3), 2.22 (m, PCyp_3), 1.81 (m, PCyp_3).

$^1H\{^{11}B\}$ NMR (δ/ppm CD_2Cl_2): 5.90 (d m, 1H, *H*PCyp_3, *J*(PH) 455.0), 2.56 (m, PCyp_3), 2.22 (m, PCyp_3 and CcageH), 1.81 (m, PCyp_3), 1.64 (br s, 5H, B-*H*), 1.46 (br s, 5H, B-*H*).

^{11}B NMR (δ/ppm CD_2Cl_2): -6.33 (d, 1B, B_{12}-H, *J*(BH) 132), -12.58 (d, 5B, $B_{7\text{-}11}$-H, *J*(BH) 134), -15.31 (d, 5B, $B_{2\text{-}6}$-H, *J*(BH) 153).

$^{31}P\{^1H\}$ NMR (δ/ppm CD_2Cl_2, 298 K): 34.0 (s, H*P*Cyp_3).

[HP^{i}Pr$_3$][*closo*-CB$_{11}$H$_{12}$] (21)

HCl was added to a suspension of Cs[*closo*-CB$_{11}$H$_{12}$] (200 mg, 0.725 mmol) in water (50 ml) with ether (2 ml) to give a pH 1 solution. Ether (30 ml) was added to extract the acid carborane and the mixture transferred into a separating funnel, which was shaken and ether phase collected in a Schlenk tube. Ether was added twice more (2 x 30 ml) to the aqueous phase in order to extract all acid carborane. The ether solution was degassed and reduced up to ~5 ml. A P^{i}Pr$_3$ (1.73 ml, 0.42 M in pentane, 0.725 mmol) solution in ether was prepared in another Schlenk tube under inert atmosphere and cannula transferred to the acid carborane solution. [HP^{i}Pr$_3$][*closo*-CB$_{11}$H$_{12}$] appeared as a white precipitate, which was washed three times with ether and dried under vacuum overnight (180 mg, 81.6 %). Anal. Calc. for C$_{10}$H$_{34}$B$_{11}$P: C, 39.47; H, 11.26. Found: C, 39.54; H, 11.45.

^{1}H NMR (δ/ppm CD_2Cl_2): 5.65 (d m, 1H, *H*P^{i}Pr$_3$, *J*(PH) 452.8), 2.75 (m, 3H, C*H* ^{i}Pr), 2.33 (br s, C$_{cage}$-*H*), 1.48 (dd, 18H, C*H*$_3$ ^{i}Pr, *J*(PH) 17.8, *J*(HH) 7.4).

^{1}H{^{11}B} NMR (δ/ppm CD_2Cl_2): 5.65 (d m, 1H, *H*P^{i}Pr$_3$, *J*(PH) 452.8), 2.75 (m, 3H, C*H* ^{i}Pr), 2.33 (br s, C$_{cage}$-*H*), 1.64 (br s, 5H, B-*H*), 1.58 (br s, 1H, B-*H*), 1.48 (dd, 18H + 5H, C*H*$_3$ ^{i}Pr + B-*H*, *J*(PH) 17.8, *J*(HH) 7.6, overlapping signals).

^{11}B NMR (δ/ppm CD_2Cl_2): -7.16 (d, 1B, *B*$_{12}$-H, *J*(BH) 141.2), -13.36 (d, 5B, *B*$_{7\text{-}11}$-H, *J*(BH) 136.1), -16.07 (d, 5B, *B*$_{2\text{-}6}$-H, *J*(BH) 150.2).

^{31}P{^{1}H} NMR (δ/ppm CD_2Cl_2, 298 K): 43.2 (s, H*P*^{i}Pr$_3$).

[Rh(PCy$_3$)(H)$_2$(*closo*-CB$_{11}$H$_{12}$)] (22)

A suspension of [HPCy$_3$][*closo*-CB$_{11}$H$_{12}$] (19 mg, 0.044 mmol) in C_6H_5F was slowly cannula transferred to a C_6H_5F solution of [Rh(μ-OMe)(nbd)]$_2$ (10 mg,

0.022 mmol) to give an orange solution. The solution was degassed under vacuum and H_2 introduced to give a pale yellow solution of [Rh(PCy_3)$(H)_2$(*closo*-$CB_{11}H_{12}$)].

^{1}H NMR (δ/ppm, 400.1 MHz, C_6H_5F): 2.82 (br s, 1H, C_{cage}-*H*), 1.84-0.98 (m, PCy_3), -1.08 (br q, 1H, B-*H*), -19.65 [dd, 2H, *J*(RhH) 30.0, *J*(PH) 21.2, Rh$(H)_2$].

^{1}H{^{11}B} NMR (δ/ppm, 400.1 MHz, C_6H_5F): 2.82 (br s, 1H, C_{cage}-*H*), 2.51 (br s, 5H, B-*H*), 1.84-0.98 (m, 33H PCy_3 + 5H B-*H*), -1.08 (br s, 1H, B-*H*), -19.65 [dd, 2H, *J*(RhH) 30.0, *J*(PH) 21.2, Rh$(H)_2$].

^{11}B NMR (δ/ppm, 128.4 MHz, C_6H_5F): -15.16 (d, 11B, *B*-H, *J*(BH) 114).

^{11}B{^{1}H} NMR (δ/ppm, 128.4 MHz, C_6H_5F): -15.16 (s, 11B, *B*-H).

^{31}P{^{1}H} NMR (δ/ppm, 128.4 MHz, C_6H_5F): 86.1 (d, *P*Cy_3, *J*(RhP) 150).

^{1}H NMR (δ/ppm, 500.13 MHz, CD_2Cl_2): 2.79 (br s, 1H, C_{cage}-*H*), 1.91-1.20 (m, PCy_3), 0.47 [br q, 5H, B-*H*, *J*(BH) 124.5], -1.51 (br q, 1H, B-*H*, *J*(BH) 102.7), -19.76 [dd, 2H, *J*(RhH) 30.5, *J*(PH) 21.5, Rh$(H)_2$].

^{1}H{^{11}B} NMR (δ/ppm, 500.13 MHz, CD_2Cl_2): 2.79 (br s, 1H, C_{cage}-*H*), 2.02 (br s, 5H, B-*H*), 1.91-1.20 (m, PCy_3), 0.47 (br s, 5H, B-*H*), -1.51 (br s, 1H, B-*H*), -19.76 [dd, 2H, *J*(RhH) 30.5, *J*(PH) 21.5, Rh$(H)_2$].

^{1}H{^{31}P} NMR (δ/ppm, 500.13 MHz, CD_2Cl_2): 2.79 (br s, 1H, C_{cage}-*H*), 1.91-1.20 (m, PCy_3), 0.47 [br q, 5H, B-*H*, *J*(BH) 124.5], -1.51 (br q, 1H, B-*H*, *J*(BH) 102.7), -19.76 [d, 2H, *J*(RhH) 30.5, Rh$(H)_2$].

^{11}B NMR (δ/ppm, 160.46 MHz, CD_2Cl_2): -14.32 (d, 5B, *B*-H, *J*(BH) ~ 152), -15.16 (d, 5B, *B*-H, *J*(BH) ~ 138), -16.11 [d, 1B, *B*-H, *J*(BH) ~ 132].

^{11}B{^{1}H} NMR (δ/ppm, 160.46 MHz, CD_2Cl_2): -14.32 (s, 5B, *B*-H), -15.16 (s, 5B, *B*-H), -16.11 (s, 1B, *B*-H).

^{31}P{^{1}H} NMR (δ/ppm, 202.47 MHz, CD_2Cl_2, 298 K): 86.8 (d, *P*Cy_3, *J*(RhP) 150).

[Rh(PCyp$_3$)(H)$_2$(*closo*-CB$_{11}$H$_{12}$)] (23)

A suspension of [HPCyp$_3$][*closo*-CB$_{11}$H$_{12}$] (25 mg, 0.066 mmol) in C_6H_5F was slowly cannula transferred to a C_6H_5F solution of [Rh(μ-OMe)(nbd)]$_2$ (15 mg, 0.033 mmol) to give an orange solution. The solution was degassed under vacuum and H_2 introduced to give a pale brown solution of [Rh(PCyp$_3$)(H)$_2$(*closo*-CB$_{11}$H$_{12}$)].

NMR data:

^{1}H NMR (δ/ppm C_6H_5F): 2.81 (br s, 1H, C_{cage}-*H*), 1.74 (m, PCyp$_3$), 1.57 (m, PCyp$_3$), 1.37 (m, PCyp$_3$), -1.24 (br q, 1H, B-*H*), -19.14 [dd, 2H, *J*(RhH) 28.0, *J*(PH) 22.0, Rh(H)$_2$].

^{1}H{^{11}B} NMR (δ/ppm C_6H_5F): 2.81 (br s, 1H, C_{cage}-*H*), 2.51 (br s, 5H, B-*H*), 1.74 (m, PCyp$_3$), 1.57 (m, PCyp$_3$), 1.37 (m, PCyp$_3$), 0.96 (br s, 5H, B-*H*), -1.24 (br s, 1H, B-*H*), -19.14 [dd, 2H, *J*(RhH) 28.0, *J*(PH) 22.0, Rh(H)$_2$].

^{11}B NMR (δ/ppm C_6H_5F): -16.32 (d, 5B, *B*-H, *J*(BH) ~ 132), -17.20 (d, 5B, *B*-H, *J*(BH) ~ 134), -18.67 (d, 1B, *B*-H, *J*(BH) ~ 157).

^{11}B{^{1}H} NMR (δ/ppm C_6H_5F): -16.32 (s, 5B, *B*-H), -17.20 (s, 5B, *B*-H), -18.67 (s, 1B, *B*-H).

^{31}P{^{1}H} NMR (δ/ppm C_6H_5F, 298 K): 87.9 (d, *P*Cyp$_3$, *J*(RhP) 152).

^{1}H NMR (δ/ppm, 500.13 MHz, CD_2Cl_2): 2.80 (br s, 1H, C_{cage}-*H*), 2.13 (m, PCyp$_3$), 1.89 (m, PCyp$_3$), 1.60 (m, PCyp$_3$), -1.59 (br q, 1H, B-*H*, *J*(BH) 101.7), -19.19 [vt, 2H, *J*(RhH) 29.5, *J*(PH) 24.5, Rh(H)$_2$].

^{1}H{^{11}B} NMR (δ/ppm, 500.13 MHz, CD_2Cl_2): 2.80 (br s, 1H, C_{cage}-*H*), 2.02 (br s, 5H, B-*H*), 2.13 (m, PCyp$_3$), 1.89 (m, PCyp$_3$), 1.60 (m, PCyp$_3$), 0.43 (br s, 5H, B-*H*), -1.59 (br s, 1H, B-*H*), -19.19 [vt, 2H, *J*(RhH) 29.5, *J*(PH) 24.5, Rh(H)$_2$].

$^{1}H\{^{31}P\}$ NMR (δ/ppm, 500.13 MHz, CD_2Cl_2): 2.80 (br s, 1H, C_{cage}-*H*), 2.13 (m, $PCyp_3$), 1.89 (m, $PCyp_3$), 1.60 (m, $PCyp_3$), -1.59 (br q, 1H, B-*H*), -19.19 [d, 2H, *J*(RhH) 29.5].

^{11}B NMR (δ/ppm, 160.46 MHz, CD_2Cl_2): -14.23 (d, 5B, *B*-H, *J*(BH) ~ 175), -15.22 (d, 5B, *B*-H, *J*(BH) ~ 140), -16.44 [d, 1B, *B*-H, *J*(BH) ~ 116].

$^{11}B\{^{1}H\}$ NMR (δ/ppm, 160.46 MHz, CD_2Cl_2): -14.23 (s, 5B, *B*-H), -15.22 (s, 5B, *B*-H), -16.44 (s, 1B, *B*-H).

$^{31}P\{^{1}H\}$ NMR (δ/ppm, 202.47 MHz, CD_2Cl_2, 298 K): 91.1 (d, *P*Cyp_3, *J*(RhP) 150).

$[Rh(P^{i}Pr_3)(H)_2(closo\text{-}CB_{11}H_{12})]$ (24)

A suspension of $[HP^{i}Pr_3][closo\text{-}CB_{11}H_{12}]$ (33.8 mg, 0.111 mmol) in C_6H_5F was slowly cannula transferred to a C_6H_5F solution of $[Rh(\mu\text{-}OMe)(nbd)]_2$ (25 mg, 0.055 mmol) to give an orange solution. The solution was degassed under vacuum and H_2 introduced to give a pale brown solution of $[Rh(P^{i}Pr_3)(H)_2(closo\text{-}CB_{11}H_{12})]$.

^{1}H NMR (δ/ppm CD_2Cl_2): 2.80 (br s, 1H, C_{cage}-*H*), 2.15 (m, 3H, C*H* ^{i}Pr), 1.21 (dd, 18H, C*H*$_3$ ^{i}Pr, *J*(PH) 15.4, *J*(HH) 7.0), -1.53 (br q, 1H, B_{12}-*H*), -19.54 [dd, 2H, *J*(RhH) 29.0, *J*(PH) 21.6, $Rh(H)_2$].

$^{1}H\{^{11}B\}$ NMR (δ/ppm CD_2Cl_2): 2.80 (br s, 1H, C_{cage}-*H*), 2.15 (m, 3H, C*H* ^{i}Pr), 2.03 (br s, 5H, $B_{2\text{-}6}$-*H*), 1.21 (dd, 18H, C*H*$_3$ ^{i}Pr, *J*(PH) 15.4, *J*(HH) 7.0), 0.47 (br s, 5H, $B_{7\text{-}11}$-*H*), -1.53 (br s, 1H, B_{12}-*H*), -19.54 [dd, 2H, *J*(RhH) 29.0, *J*(PH) 21.6, $Rh(H)_2$].

^{11}B NMR (δ/ppm CD_2Cl_2): -14.38 (d, 5B, *B*-H, *J*(BH) ~ 140), -15.30 (d, 5B, *B*-H, *J*(BH) ~ 128), -16.52 (d, 1H, *B*-H, *J*(BH) ~ 130).

$^{11}B\{^{1}H\}$ NMR (δ/ppm CD_2Cl_2): -14.38 (s, 5B, *B*-H), -15.30 (s, 5B, *B*-H), -16.52 (s, 1B, *B*-H).

$^{31}P\{^{1}H\}$ NMR (δ/ppm CD_2Cl_2): 98.4 (d, *P*$^{i}Pr_3$, *J*(RhP) 151).

[(PCy$_3$)(*closo*-CB$_{11}$H$_{11}$)(H)Rh-Rh(PCy$_3$)(*closo*-CB$_{11}$H$_{12}$)] (25)

A suspension of [HPCy$_3$][*closo*-CB$_{11}$H$_{12}$] (75.1 mg, 0.177 mmol) in C_6H_5F was slowly cannula transferred to a C_6H_5F solution of [Rh(μ-OMe)(nbd)]$_2$ (40 mg, 0.089 mmol) to give an orange solution. The solution was degassed under vacuum and H_2 introduced to give a pale brown solution of [Rh(PCy$_3$)(H)$_2$(*closo*-CB$_{11}$H$_{12}$)]. After 40 minutes, the solution was degassed under vacuum to dryness. The residue was dissolved with CH_2Cl_2 (~10 ml) and the new solution again evaporated to dryness. One more time, the residue was dissolved in dichloromethane (~ 10 ml) and the solution cannula filtered and reduced this time to a volume of ~ 2 ml. Addition of pentane (~ 10 ml) afforded a dark red product (74 mg, 80 %) that was dried under vacuum overnight. Anal. Calc. for $C_{43}H_{102}B_{22}P_2Rh_2$: C, 45.91; H, 9.14. Found: C, 45.58; H, 8.78.

^{1}H NMR (δ/ppm, 400.1 MHz, CD_2Cl_2): 2.65 (br s, 1H, C_{cage}-*H*), 2.05-1.25 (m, 33H, PCy$_3$), -1.43 (vbr s, 5H, $B_{7\text{-}11}$-*H*), -7.44 (vbr s, 1H, B_{12}-*H*).

^{1}H{^{11}B} NMR (δ/ppm, 400.1 MHz, CD_2Cl_2): 2.65 (br s, 1H, C_{cage}-*H*), 2.05-1.25 (m, 33H, PCy$_3$ + 5H, $B_{2\text{-}6}$-*H*), -1.43 (vbr s, 5H, $B_{7\text{-}11}$-*H*), -7.44 (vbr s, 1H, B_{12}-*H*).

^{11}B NMR (δ/ppm, 128.4 MHz, CD_2Cl_2): -13.54 (d, 6B, *B*-H, *J*(BH) ~ 115), -16.05 (d, 5B, *B*-H, *J*(BH) ~ 145).

^{31}P{^{1}H} NMR (δ/ppm, 162.0 MHz, CD_2Cl_2): 66.4 (d, *P*Cy$_3$, *J*(RhP) 160).

[(PCyp$_3$)(*closo*-CB$_{11}$H$_{11}$)(H)Rh-Rh(PCyp$_3$)(*closo*-CB$_{11}$H$_{12}$)] (26)

A suspension of [HPCyp$_3$][*closo*-CB$_{11}$H$_{12}$] (100 mg, 0.262 mmol) in C_6H_5F was slowly cannula transferred to a C_6H_5F solution of [Rh(μ-OMe)(nbd)]$_2$ (59 mg, 0.131 mmol) to give an orange solution. The solution was degassed under vacuum and

H_2 introduced to give a pale brown solution of [Rh(PCyp$_3$)(H)$_2$(*closo*-$CB_{11}H_{12}$)]. After 40 minutes, the solution was degassed under vacuum to dryness. The residue was dissolved with CH_2Cl_2 (~10 ml) and the new solution again evaporated to dryness. One more time, the residue was dissolved in dichloromethane (~ 10 ml) and the solution cannula filtered and reduced this time to a volume of ~ 2 ml. Addition of pentane (~ 10 ml) afforded a dark red product (98 mg, 77 %) that was dried under vacuum overnight. Anal. Calc. for $C_{32}H_{78}B_{22}P_2Rh_2$: C, 39.68; H, 8.12. Found: C, 40.50; H, 8.01.

^{1}H NMR (δ/ppm, 400.1 MHz, C_6H_5F): 2.63 (br s, 1H, C_{cage}-*H*), 2.30 (m, 3H, PC*H*, PCyp$_3$), 2.01-1.30 (m, 30H, C*H*$_2$, PCyp$_3$), -1.14 (vbr q, 5H, $B_{7\text{-}11}$-*H*), -7.74 (vbr q, 1H, B_{12}-*H*).

^{1}H{^{11}B} NMR (δ/ppm, 400.1 MHz, C_6H_5F): 2.63 (br s, 1H, C_{cage}-*H*), 2.34 (br s, 5H, $B_{2\text{-}6}$H), 2.30 (m, 3H, PC*H*, PCyp$_3$), 2.01-1.30 (m, 30H, C*H*$_2$, PCyp$_3$), -1.14 (vbr s, 5H, $B_{7\text{-}11}$-*H*), -7.74 (vbr s, 1H, B_{12}-*H*).

^{11}B NMR (δ/ppm, 128.4 MHz, C_6H_5F): -13.44 (br d, overlapping signals), -15.15 (br d, overlapping signals).

^{11}B{^{1}H} NMR (δ/ppm, 128.4 MHz, C_6H_5F): -13.44 (br s), -15.15 (br s).

^{31}P{^{1}H} NMR (δ/ppm, 162.0 MHz, C_6H_5F): 64.2 (d, *P*Cyp$_3$, *J*(RhP) 154).

[(P^{i}Pr$_3$)(*closo*-$CB_{11}H_{11}$)(H)Rh-Rh(P^{i}Pr$_3$)(*closo*-$CB_{11}H_{12}$)] (27)

A suspension of [HP^{i}Pr$_3$][*closo*-$CB_{11}H_{12}$] (80.8 mg, 0.265 mmol) in C_6H_5F was slowly cannula transferred to a C_6H_5F solution of [Rh(μ-OMe)(nbd)]$_2$ (60 mg, 0.133 mmol) to give an orange solution. The solution was degassed under vacuum and H_2 introduced to give a pale brown solution of [Rh(P^{i}Pr$_3$)(H)$_2$(*closo*-$CB_{11}H_{12}$)]. After 40 minutes, the solution was degassed under vacuum to dryness. The residue was

dissolved with CH_2Cl_2 (~10 ml) and the new solution again evaporated to dryness. One more time, the residue was dissolved in dichloromethane (~ 10 ml) and the solution cannula filtered and reduced this time to a volume of ~ 2 ml. Addition of pentane (~ 10 ml) afforded a dark red product (64 mg, 59 %) that was dried under vacuum overnight. Anal. Calc. for $C_{20}H_{66}B_{22}P_2Rh_2$: C, 29.57; H, 8.19. Found: C, 29.06; H, 7.79.

^{1}H NMR (δ/ppm CD_2Cl_2): 2.65 (br s, 1H, C_{cage}-*H*), 2.31 (m, 3H, C*H* ^{i}Pr), 1.33 (dd, 18H, C*H*$_3$ ^{i}Pr, *J*(PH) 15, *J*(HH) 7.1), -1.51 (vb s, 5H, $B_{7\text{-}11}$-*H*), -7.50 (vb s, 1H, B_{12}-*H*).

^{1}H{^{11}B} NMR (δ/ppm CD_2Cl_2): 2.65 (br s, 1H, C_{cage}-*H*), 2.31 (m, 3H, C*H* ^{i}Pr), 1.88 (b s, 5H, $B_{2\text{-}6}$-*H*), 1.33 (dd, 18H, C*H*$_3$ ^{i}Pr, *J*(PH) 15, *J*(HH) 7.1), -1.51 (vb s, 5H, $B_{7\text{-}11}$-*H*), -7.50 (vb s, 1H, B_{12}-*H*).

^{11}B NMR (δ/ppm CD_2Cl_2): -12.88 (d, 6B, *B*-H, *J*(BH) 129), -14.98 (d, 5B, *B*-H, *J*(BH) ~ 196).

^{11}B{^{1}H} NMR (δ/ppm CD_2Cl_2): -12.88 (s, 6B, *B*-H), -14.98 (s, 5B, *B*-H).

^{31}P{^{1}H} NMR (δ/ppm CD_2Cl_2): 76.4 (d, *P*^{i}Pr$_3$, *J*(RhP) 156).

[HPCy$_3$][*closo*-CB$_{11}$H$_6$Br$_6$] (28)

HCl was added to a suspension of Cs[*closo*-$CB_{11}H_6Br_6$] (267 mg, 0.357 mmol) in water (50 ml) with ether (3 ml) to give a pH 1 solution. Ether (30 ml) was added to extract the acid carborane and the mixture transferred into a separating funnel, which was shaken and the ether phase collected. Ether was added twice more (2 x 30 ml) to the aqueous phase in order to extract all acid carborane. The ether solution was degassed and reduced up to ~5 ml. A PCy_3 (100 mg, 0.357 mmol) solution in ether was prepared in another Schlenk tube under inert atmosphere and cannula transferred to the acid carborane solution. [$HPCy_3$][*closo*-$CB_{11}H_6Br_6$] appeared as a white precipitate, which

was washed three times with ether and dried under vacuum overnight (269 mg, 84%). Anal. Calc. for $C_{19}H_{40}B_{11}Br_6P$: C, 25.42; H, 4.49. Found: C, 25.84; H, 4.55.

^{1}H NMR (300.2 MHz, CD_2Cl_2): 5.33 [d, 1H, *J*(PH) 447, PH], 2.56 (br s, 1H, CcageH), 2.52-1.28 (m, 33H and PCy_3).

^{11}B NMR (96.3 MHz, CD_2Cl_2): -1.05 (s, 1B, BBr), -9.09 (s, 5B, BBr), -19.43 [d, *J*(BH) 169, 5B, BH].

^{11}B{^{1}H} NMR (96.3 MHz, CD_2Cl_2): -1.05 (s, 1B, BBr), -9.09 (s, 5B, BBr), -19.43 (s, 5B, BH).

^{31}P{^{1}H} NMR (121.5 MHz, CD_2Cl_2): 33.1 (s).

[$HPCyp_3$][*closo*-$CB_{11}H_6Br_6$] (29)

In air, HCl was added to a mixture of Cs[*closo*-$CB_{11}H_6Br_6$] (200 mg, 0.267 mmol) in water (40 ml) and ether (4 ml) to give a pH 1 solution. Ether (30 ml) was added and the mixture was transferred into a separating funnel, which was shaken and ether phase was collected. The aqueous layer was extracted with additional ether (2 x 30 ml) and the combined ethereal solution was degassed and reduced to ~10 ml *in vacuo*. Under argon, $PCyp_3$ (0.53 ml, 0.52M in pentane, 0.267 mmol) was added to the acid carborane solution. [$HPCyp_3$][*closo*-$CB_{11}H_6Br_6$] appeared as a white precipitate, which was washed three times with ether and dried *in vacuo* overnight (219 mg, 96 %). $C_{16}H_{34}B_{11}Br_6P$ requires %C 22.46, %H 4.00. Found %C 22.73, %H 4.24.

^{1}H NMR (300.1 MHz, CD_2Cl_2): 5.95 [d, 1H, *J*(PH) 453, PH], 2.73-1.70 (m, 28H, CcageH and $PCyp_3$).

^{1}H{^{11}B} NMR (300.1 MHz, CD_2Cl_2): 5.95 [d, 1H, *J*(PH) 453, PH], 2.73-1.70 (m, 28H, CcageH and $PCyp_3$), 2.35 (br s, 5H, BH).

^{11}B NMR (96.3 MHz, CD_2Cl_2): -1.08 (s, 1B, BBr), -9.08 (s, 5B, BBr), -19.42 [d, *J*(BH) 167, 5B, BH].

^{11}B{^{1}H} NMR (96.3 MHz, CD_2Cl_2): -1.08 (s, 1B, BBr), -9.08 (s, 5B, BBr), -19.42 (s, 5B, BH).

^{31}P{^{1}H} NMR (121.5 MHz, CD_2Cl_2): 33.9 (s).

[HP^{i}Pr$_3$][*closo*-$CB_{11}H_6Br_6$] (30)

HCl was added to a suspension of Cs[*closo*-$CB_{11}H_6Br_6$] (204 mg, 0.272 mmol) in water (50 ml) with ether (3 ml) to give a pH 1 solution. Ether (30 ml) was added to extract the acid carborane and the mixture transferred into a separating funnel, which was shaken and ether phase collected. Ether was added twice more (2 x 30 ml) to the aqueous phase in order to extract all acid carborane. The ether solution was degassed and reduced up to ~5 ml. A P^{i}Pr$_3$ (0.65 ml, 0.42 M, 0.272 mmol) solution in ether was prepared in another Schlenk tube under inert atmosphere and cannula transferred to the acid carborane solution. [HP^{i}Pr$_3$][*closo*-$CB_{11}H_6Br_6$] appeared as a white precipitate, which was washed three times with ether and dried under vacuum overnight (185 mg, 87%). Anal. Calc. for $C_{10}H_{28}B_{11}Br_6P$: C, 15.44; H, 3.63. Found: C, 16.21; H, 3.72.

^{1}H NMR (300.2 MHz, CD_2Cl_2): 5.55 [d, 1H, *J*(PH) 441, PH], 2.74 (m, 3H, C*H* ^{i}Pr$_3$), 2.58 (br s, 1H, CcageH), 1.48 (dd, 18H, C*H*$_3$ ^{i}Pr, *J*(PH) 17.9, *J*(HH) 7.1).

^{1}H{^{11}B} NMR (300.2 MHz, CD_2Cl_2): 5.55 [d, 1H, *J*(PH) 441, PH], 2.74 (m, 3H, C*H* ^{i}Pr$_3$), 2.58 (br s, 1H, CcageH), 2.35 (br s, 5H, BH), 1.48 (dd, 18H, C*H*$_3$ ^{i}Pr, *J*(PH) 17.9, *J*(HH) 7.1).

^{11}B NMR (96.3 MHz, CD_2Cl_2): -0.94 (s, 1B, BBr), -9.09 (s, 5B, BBr), -19.43 [d, *J*(BH) 171, 5B, BH].

$^{11}B\{^1H\}$ NMR (96.3 MHz, CD_2Cl_2): -0.94 (s, 1B, BBr), -9.09 (s, 5B, BBr), -19.43 (s, 5B, BH).

$^{31}P\{^1H\}$ NMR (121.5 MHz, CD_2Cl_2): 45.1 (s).

[$HPCy_3$][*closo*-$CB_{11}H_6Cl_6$] (31)

HCl was added to a suspension of $Cs[CB_{11}H_6Cl_6]$ (150 mg, 0.311 mmol) in water (50 ml) with ether (3 ml) to give a pH 1 solution. Ether (30 ml) was added to extract the acid carborane and the mixture transferred into a separating funnel, which was shaken and ether phase collected. Ether was added twice more (2 x 30 ml) to the aqueous phase in order to extract all acid carborane. The ether solution was degassed and reduced up to ~5 ml. A PCy_3 (87 mg, 0.311 mmol) solution in ether was prepared in another Schlenk tube under inert atmosphere and cannula transferred to the acid carborane solution. $[HPCy_3][CB_{11}H_6Cl_6]$ appeared as a white precipitate, which was washed three times with ether and dried under vacuum overnight (159 mg, 81%). Anal. Calc. for $C_{19}H_{40}B_{11}Cl_6P{\cdot}½CH_2Cl_2$: %C, 34.77; %H, 6.14. Found: %C, 34.16; %H, 6.51.

^1H NMR (300.2 MHz, CD_2Cl_2): 5.28 [d, 1H, *J*(PH) 447, PH], 2.43 (m, 3H, PCy_3), 2.15 (br s, 1H, CcageH), 2.04-1.25 (m, 30H and PCy_3).

$^1H\{^{11}B\}$ NMR (300.2 MHz, CD_2Cl_2): 5.28 [d, 1H, *J*(PH) 447, PH], 2.43 (m, 3H, PCy_3), 2.15 (br s, 1H, CcageH), 2.04-1.25 (m, 30H and PCy_3), 1.95 (br s, 5H, B*H*).

^{11}B NMR (96.3 MHz, CD_2Cl_2): 1.71 (s, 1B, BBr), -5.17 (s, 5B, BBr), -22.53 [d, 5B, *B*H, *J*(BH) 162].

$^{11}B\{^1H\}$ NMR (96.3 MHz, CD_2Cl_2): 1.71 (s, 1B, BBr), -5.17 (s, 5B, BBr), -22.53 (s, 5B, *B*H).

$^{31}P\{^1H\}$ NMR (121.5 MHz, CD_2Cl_2): 33.2 (s).

[Rh(PCy$_3$)(H)$_2$(*closo*-CB$_{11}$H$_6$Br$_6$)]·C$_6$H$_5$F (32)

A suspension of [HPCy$_3$][*closo*-CB$_{11}$H$_6$Br$_6$] (127 mg, 0.141 mmol) in C$_6$H$_5$F (10 ml) was slowly cannula transferred to [Rh(μ-OMe)(nbd)]$_2$ (32 mg, 0.070 mmol) in C$_6$H$_5$F (10 ml) to give an orange solution. The solution was degassed and placed under a H_2 atmosphere to produce after 30 minutes a pale brown solution of [Rh(PCy$_3$)(H)$_2$(*closo*-CB$_{11}$H$_6$Br$_6$)]. After addition of pentane (15 ml), the solution was filtered through celite and the filtrate was evaporated to dryness. The off-white product was dried under vacuum overnight (109 mg, 77 %). Crystals were obtained from a saturated solution of the compound in C$_6$H$_5$F and pentane. $C_{25}H_{46}B_{11}Br_6FPRh$ requires %C 27.35, %H 4.22. Found %C 27.20, %H 4.08.

^{1}H NMR (400.1 MHz, C$_6$H$_5$F): 2.38 (br s, 1H, CcageH), 1.88-1.05 (m, 33H, PCy$_3$), -21.12 [dd, *J*(RhH) 28.8, *J*(PH) 18.8, 2H, Rh(H)$_2$].

^{1}H{^{11}B} NMR (400.1 MHz, C$_6$H$_5$F): 2.65 (br s, 5H, BH), 2.38 (br s, 1H, CcageH), 1.88-1.05 (m, 33H, PCy$_3$), -21.12 [dd, *J*(RhH) 28.8, *J*(PH) 18.8, 2H, Rh(H)$_2$].

^{11}B NMR (128.4 MHz, C$_6$H$_5$F): 0.29 (s, 1B, BBr), -9.22 (s, 5B, BBr), -21.08 [br d, 5B, BH].

^{11}B{^{1}H} NMR (128.4 MHz, C$_6$H$_5$F): 0.29 (s, 1B, BBr), -9.22 (s, 5B, BBr), -21.08 (s, 5B, BH).

^{31}P{^{1}H} NMR (162.0 MHz, C$_6$H$_5$F): 82.7 [d, *J*(RhP) 161].

^{1}H NMR (400.1 MHz, CD$_2$Cl$_2$): 2.85 (br s, 1H, CcageH), 1.96-1.68 (m, 18H, PCy$_3$), 1.43-1.10 (m, 15H, PCy$_3$), -21.25 [dd, *J*(RhH) 28.8, *J*(PH) 18.8, 2H, Rh(H)$_2$].

^{1}H{^{11}B} NMR (400.1 MHz, CD$_2$Cl$_2$): 2.85 (br s, 1H, CcageH), 2.47 (br s, 5H, BH), 1.96-1.68 (m, 18H, PCy$_3$), 1.43-1.10 (m, 15H, PCy$_3$), -21.25 [dd, *J*(RhH) 28.8, *J*(PH) 18.8, 2H, Rh(H)$_2$].

^{11}B NMR (128.4 MHz, CD_2Cl_2): 0.57 (s, 1B, BBr), -8.77 (s, 5B, BBr), -20.39 [br d, 5B, BH, *J*(BH) 154].

^{11}B{^{1}H} NMR (128.4 MHz, CD_2Cl_2): 0.57 (s, 1B, BBr), -8.77 (s, 5B, BBr), -20.39 (s, 5B, BH).

^{31}P{^{1}H} NMR (162.0 MHz, CD_2Cl_2): 82.9 [d, *J*(RhP) 161].

[Rh(PCyp$_3$)(H)$_2$(*closo*-$CB_{11}H_6Br_6$)] (33)

A suspension of [HPCyp$_3$][*closo*-$CB_{11}H_6Br_6$] (200 mg, 0.233 mmol) in C_6H_5F (10 ml) was slowly cannula transferred to [Rh(μ-OMe)(nbd)]$_2$ (53 mg, 0.117 mmol) in C_6H_5F (10 ml) to give an orange solution. The solution was degassed and placed under a H_2 atmosphere to produce after 30 minutes a pale brown solution of [Rh(PCyp$_3$)(H)$_2$(*closo*-$CB_{11}H_6Br_6$)]. After addition of pentane (15 ml), the solution was filtered through celite and the filtrate was evaporated to dryness. The product was dried under vacuum overnight (170 mg, 76 %). $C_{16}H_{35}B_{11}Br_6PRh$ requires %C 20.02, %H 3.68. Found %C 20.24, %H 3.82.

^{1}H NMR (400.1 MHz, CD_2Cl_2): 2.86 (br s, 1H, CcageH), 2.27-1.49 (m, 27H, Cyp), -20.95 [dd, *J*(RhH) 28.4, *J*(PH) 18.6, 2H, Rh(H)$_2$].

^{1}H{^{11}B} NMR (400.1 MHz, CD_2Cl_2): 2.86 (br s, 1H, CcageH), 2.48 (br s, 5H, BH), 2.27-1.49 (m, 27H, Cyp), -20.95 [dd, 2H, *J*(RhH) 28.4, *J*(PH) 18.6, Rh(H)$_2$].

^{11}B NMR (128.4 MHz, CD_2Cl_2): 0.73 (s, 1B, BBr), -8.71 (s, 5B, BBr), -20.33 [d, *J*(BH) 155.3, 5B, BH].

^{11}B{^{1}H} NMR (128.4 MHz, CD_2Cl_2): 0.73 (s, 1B, BBr), -8.71 (s, 5B, BBr), -20.33 (s, 5B, BH).

^{31}P{^{1}H} NMR (162.0 MHz, CD_2Cl_2): 86.4 [d, *J*(RhP) 164].

[Rh(P^{i}Pr$_3$)(H)$_2$(*closo*-CB$_{11}$H$_6$Br$_6$)] (34)

A suspension of [HP^{i}Pr$_3$][*closo*-CB$_{11}$H$_6$Br$_6$] (138 mg, 0.177 mmol) in C_6H_5F (10 ml) was slowly cannula transferred to [Rh(μ-OMe)(nbd)]$_2$ (40 mg, 0.089 mmol) in C_6H_5F (10 ml) to give an orange solution. The solution was degassed and placed under a H_2 atmosphere to produce after 30 minutes a pale brown solution of [Rh(P^{i}Pr$_3$)(H)$_2$(*closo*-CB$_{11}$H$_6$Br$_6$)]. After addition of pentane (15 ml), the solution was filtered through celite and the filtrate was evaporated to dryness. The pale yellow product was dried under vacuum overnight (92 mg, 59 %). $C_{10}H_{29}B_{11}Br_6PRh$ requires %C 13.62, %H 3.32. Found %C 14.70, %H 3.48.

^{1}H NMR (400.1 MHz, CDCl$_3$): 2.79 (br s, 1H, CcageH), 2.19 (m, 3H, C*H* ^{i}Pr$_3$), 1.25 (dd, 18H, C*H*$_3$ ^{i}Pr, *J*(PH) 15.2, *J*(HH) 6.8), -21.04 [dd, *J*(RhH) 28.0, *J*(PH) 18.8, 2H, Rh(H)$_2$].

^{1}H{^{11}B} NMR (400.1 MHz, CDCl$_3$): 2.79 (br s, 1H, CcageH), 2.19 (m, 3H, C*H* ^{i}Pr$_3$), 2.54 (br s, 5H, BH), 1.25 (dd, 18H, C*H*$_3$ ^{i}Pr, *J*(PH) 15.2, *J*(HH) 6.8), -21.04 [dd, *J*(RhH) 28.0, *J*(PH) 18.8, 2H, Rh(H)$_2$].

^{11}B NMR (128.4 MHz, CDCl$_3$): 1.05 (s, 1B, BBr), -8.48 (s, 5B, BBr), -20.21 [d, *J*(BH) 166, 5B, BH].

^{11}B{^{1}H} NMR (128.4 MHz, CDCl$_3$): 1.05 (s, 1B, BBr), -8.48 (s, 5B, BBr), -20.21 (s, 5B, BH).

^{31}P{^{1}H} NMR (162.0 MHz, CDCl$_3$): 94.4 [d, *J*(RhP) 162].

[Rh(P^{i}Pr$_3$)(H)$_2$(η^6-C$_6$H$_6$)][*closo*-CB$_{11}$H$_6$Br$_6$] (35)

A suspension of [HP^{i}Pr$_3$][*closo*-CB$_{11}$H$_6$Br$_6$] (106 mg, 0.136 mmol) in CH_2Cl_2 (10 ml) was slowly cannula transferred to [Rh(μ-OMe)(nbd)]$_2$ (30.8 mg, 0.068 mmol) in CH_2Cl_2 (10 ml) to give an orange solution. Benzene (2 ml) was added to the solution

and this was degassed and placed under a H_2 atmosphere to produce after 30 minutes a pale brown solution of [Rh(P^iPr_3)$(H)_2$(*closo*-$CB_{11}H_6Br_6$)]. After addition of pentane (15 ml), the solution was filtered through celite and the filtrate was evaporated to dryness. The off-white solid was recrystallised from a solution of CH_2Cl_2 and benzene which was layered with pentane at -18°C. The crystalline solid was under vacuum for 4 hours (52 mg, 54 %). [5x($C_{16}H_{33}B_{11}Br_6PRh$) + ($C_{10}H_{29}B_{11}Br_6PRh$)] requires %C 19.03, %H 3.62. Found %C 19.08, %H 3.51.

^{1}H NMR (300.2 MHz, CD_2Cl_2): 6.94 (s, 6H, C_6H_6), 2.60 (br s, 1H, CcageH), 2.03 (m, 3H, C*H* ^{i}Pr$_3$), 1.13 (dd, 18H, C*H*$_3$ ^{i}Pr, *J*(PH) 15.9, *J*(HH) 7.1), -14.53 [dd, *J*(RhH) 27.8, *J*(PH) 23.7, 2H, Rh$(H)_2$].

^{1}H{^{11}B} NMR (300.2 MHz, CD_2Cl_2): 6.94 (s, 6H, C_6H_6), 2.60 (br s, 1H, CcageH), 2.39 (br s, 5H, BH), 2.03 (m, 3H, C*H* ^{i}Pr$_3$), 1.13 (dd, 18H, C*H*$_3$ ^{i}Pr, *J*(PH) 15.9, *J*(HH) 7.1), -14.53 [dd, *J*(RhH) 27.8, *J*(PH) 23.7, 2H, Rh$(H)_2$].

^{11}B NMR (96.3 MHz, CD_2Cl_2): -0.95 (s, 1B, BBr), -9.05 (s, 5B, BBr), -19.41 [d, *J*(BH) 167, 5B, BH].

^{11}B{^{1}H} NMR (96.3 MHz, CD_2Cl_2): -0.95 (s, 1B, BBr), -9.05 (s, 5B, BBr), -19.41 (s, 5B, BH).

^{31}P{^{1}H} NMR (121.5 MHz, CD_2Cl_2): 97.2 [d, *J*(RhP) 143].

[Rh{P(Cy_2)(η^2-C_6H_9)}(*closo*-$CB_{11}H_6Br_6$)] (36)

tert-Butylethene (0.2 ml, 1.552 mmol, excess) was added to a solution of [Rh(PCy_3)$(H)_2$(*closo*-$CB_{11}H_6Br_6$)] (40 mg, 0.040 mmol) in CD_2Cl_2 (0.5 ml). After 24 hr the reaction was complete and addition of pentane produced an orange suspension. The solvent was pumped off and the residue washed twice with pentane to afford an orange

product (30 mg, 75 %) which was dried under vacuum. $C_{19}H_{37}B_{11}Br_6PRh$ requires %C 22.87, %H 3.74. Found %C 22.30, %H 3.52.

^{1}H NMR (400.1 MHz, CD_2Cl_2): 4.43 (br s, 2H, CH=CH), 2.72 (br s, 1H, CcageH), 2.28-1.24 (m, 29H, $Cy_2P(C_6H_9)$).

^{1}H{^{11}B} NMR (400.1 MHz, CD_2Cl_2): 4.43 (br s, 2H, CH=CH), 2.72 (br s, 1H, CcageH), 2.43 (br s, 5H, BH), 2.28-1.24 (m, 29H, $Cy_2P(C_6H_9)$).

^{11}B NMR (128.4 MHz, CD_2Cl_2): -0.22 (s, 1B, BBr), -9.42 (s, 5B, BBr), -20.27 [d, *J*(BH) 164, 5B, BH].

^{11}B{^{1}H} NMR (128.4 MHz, CD_2Cl_2): -0.22 (s, 1B, BBr), -9.42 (s, 5B, BBr), -20.27 (s, 5B, BH).

^{31}P{^{1}H} NMR (162.0 MHz, CD_2Cl_2): 84.6 [d, *J*(RhP) 180].

^{13}C{^{1}H} NMR (125.8 MHz, CD_2Cl_2): 66.88 [d, *J*(RhC) 16.0, HC=CH], 62.26 [d, *J*(RhC) 16.7, HC=CH], 42.96 (br s, Ccage), 36.91 [d, *J*(PC) 21.3, PCH], 36.73 [d, *J*(PC) 24.0, PCH], 34.24 [d, *J*(PC) 6.1, CH_2], 32.89 (s, CH_2), 30.55 [d, *J*(PC) 2.4, CH_2], 30.40 [d, *J*(PC) 2.8, CH_2], 29.31 (s, CH_2), 28.25 [d, *J*(PC) 11.7, CH_2], 30.55 [d, *J*(PC) 2.4, CH_2], 27.95 [d, *J*(PC) 10.7, CH_2], 27.73 [d, *J*(PC) 9.91, CH_2], 27.65 [d, *J*(PC) 10.3, CH_2], 26.38 (s, CH_2), 25.26 [d, *J*(PC) 27.4, PCH], 23.96 (s, CH_2), 23.10 [d, *J*(PC) 5.0, CH_2].

[Rh{P(Cy_2)(η^2-C_6H_9)}(η^6-C_6H_5Me)][*closo*-$CB_{11}H_6Br_6$] (37)

Toluene (0.5 ml, 4.694 mmol, excess) was added to a solution of [Rh{P(Cy_2)(η^2-C_6H_9)}(*closo*-$CB_{11}H_6Br_6$)] (25 mg, 0.025 mmol) in CH_2Cl_2 (5 ml). After 1 hr the reaction was complete and addition of pentane produced a pale orange suspension. The solvent was pumped off and the residue washed twice with pentane to afford a pale

orange product (17 mg, 62 %) which was dried under vacuum. $C_{26}H_{45}B_{11}Br_6PRh$ requires %C 28.65, %H 4.16. Found %C 29.03, %H 3.92.

^{1}H NMR (500.1 MHz, CD_2Cl_2): 6.68 (m, 1H, η^6-C_6H_5Me), 6.63 (m, 2H, η^6-C_6H_5Me), 6.46 (d, 1H, η^6-C_6H_5Me), 6.30 (d, 1H, η^6-C_6H_5Me), 4.50 (m, 1H, CH=CH, P(C_6H_9)), 3.96 (m, 1H, CH=CH, P(C_6H_9)), 2.57 (br s, 1H, CcageH), 2.27 (s, 3H, CH_3, C_7H_8), 2.40-1.15 (m, 29H, $Cy_2P(C_6H_9)$).

^{1}H{^{11}B} NMR (500.1 MHz, CD_2Cl_2): 6.68 (m, 1H, CH_2=CH_2, C_7H_8), 6.63 (m, 2H, CH_2=CH_2, C_7H_8), 6.46 (d, 1H, CH_2=CH_2, C_7H_8), 6.30 (d, 1H, CH_2=CH_2, C_7H_8), 4.50 (m, 1H, CH=CH, P(C_6H_9)), 3.96 (m, 1H, CH=CH, P(C_6H_9)), 2.57 (br s, 1H, CcageH),2.33 (br s, 5H, BH), 2.27 (s, 3H, CH_3, C_7H_8), 2.40-1.15 [m, 29H, $Cy_2P(C_6H_9)$].

^{11}B NMR (160.5 MHz, CD_2Cl_2): -1.64 (s, 1B, BBr), -9.81 (s, 5B, BBr), -20.15 [d, *J*(BH) 167, 5B, BH].

^{11}B{^{1}H} NMR (160.5 MHz, CD_2Cl_2): -1.64 (s, 1B, BBr), -9.81 (s, 5B, BBr), -20.15 (s, 5B, BH).

^{31}P{^{1}H} NMR (202.5 MHz, CD_2Cl_2): 78.9 [d, *J*(RhP) 179].

^{13}C{^{1}H} NMR (125.8 MHz, CD_2Cl_2): 120.16 (m, 1C, ipso-C_6H_5Me), 104.36 (m, 1C, C_6H_5Me), 104.03 (m, 1C, C_6H_5Me), 102.78 [d, 1C, *J*(RhC) 2.5, C_6H_5Me], 107.88 [d, 1C, *J*(RhC) 2.5, C_6H_5Me], 99.58 [d, 1C, *J*(RhC) 2.5, C_6H_5Me], 68.04 [dd, *J*(RhC) 14.1, *J*(PC) 2.9, HC=CH, P(C_6H_9)], 62.26 [dd, *J*(RhC) 14.1, *J*(PC) 1.9, HC=CH, P(C_6H_9)], 41.49 (br s, Ccage), 38.66 [d, *J*(PC) 22.9, PCH], 36.69 [d, *J*(PC) 22.2, PCH], 34.49 [d, *J*(PC) 7.2, CH_2], 31.44 (d, *J*(PC) 1.5, CH_2), 30.09 [s, CH_2], 29.79 [d, *J*(PC) 1.5, CH_2], 29.74 (s, CH_2), 27.85 [d, *J*(PC) 12.6, CH_2], 27.64 [d, *J*(PC) 10.3 CH_2], 27.55 [d, *J*(PC) 11.3, CH_2], 27.42 [d, *J*(PC) 11.3, CH_2], 26.15 [d, *J*(PC) 1.0, CH_2], 26.13 (s, CH_2), 25.84 [d, *J*(PC) 27.7, PCH], 23.99 (s, CH_2), 22.45 [d, *J*(PC) 6.4, CH_2], 19.79 (s, CH_3, C_7H_8)

[Rh{P(Cyp$_2$)(η^2-C$_5$H$_7$)}(*closo*-CB$_{11}$H$_6$Br$_6$)] (38)

tert-Butylethene (0.2 ml, 1.552 mmol, excess) was added to a solution of [Rh(PCyp$_3$)(H)$_2$(*closo*-CB$_{11}$H$_6$Br$_6$)] (82 mg, 0.085 mmol) in CH_2Cl_2 (0.5 ml). After 24 hr, orange crystals suitable for X-ray diffraction studies were obtained (56 mg, 69 %). The crystals were collected and dried *in vacuo* overnight. $C_{16}H_{31}B_{11}Br_6PRh$ requires %C 20.11, %H 3.27. Found %C 20.29, %H 3.32.

^{1}H NMR (400.1 MHz, CD_2Cl_2): 4.17 (br s, 2H, CH=CH), 2.74 (br s, 1H, CcageH), 2.25-1.49 (m, 21H, Cyp), 1.15-0.90 (m, 2H, Cyp).

^{1}H{^{11}B} NMR (400.1 MHz, CD_2Cl_2): 4.17 (br s, 2H, CH=CH), 2.74 (br s, 1H, CcageH), 2.43 (br s, 5H, BH), 2.25-1.49 (m, 21H, Cyp), 1.15-0.90 (m, 2H, Cyp).

^{11}B NMR (128.4 MHz, CD_2Cl_2): 0.01 (s, 1B, BBr), -9.31 (s, 5B, BBr), -20.30 [d, *J*(BH) 167, 5B, BH].

^{11}B{^{1}H} NMR (128.4 MHz, CD_2Cl_2): 0.01 (s, 1B, BBr), -9.31 (s, 5B, BBr), -20.30 (s, 5B, BH).

^{31}P{^{1}H} NMR (162.0 MHz, CD_2Cl_2): 116.6 [d, *J*(RhP) 180].

^{13}C{^{1}H} NMR (100.6 MHz, CD_2Cl_2): 63.54 [d, *J*(RhC) 19.7, HC=CH], 43.11 (br s, Ccage), 36.75 [d, *J*(PC) 2.8, CH_2], 34.52 [d, *J*(PC) 25.4, PCH], 31.69 (s, CH_2), 30.31 [dd, *J*(PC) 27.8, *J*(RhC) 3.3, PCH], 30.14 (s, CH_2), 27.16 [d, *J*(PC) 8.5, CH_2], 26.25 [d, *J*(PC) 9.0, CH_2].

[Rh{P(Cyp$_2$)(η^2-C$_5$H$_7$)}(η^6-C$_6$H$_5$F)][*closo*-CB$_{11}$H$_6$Br$_6$] (39)

tert-Butylethene (0.2 ml, 1.552 mmol, excess) was added to a solution of [Rh(PCyp$_3$)(H)$_2$(*closo*-CB$_{11}$H$_6$Br$_6$)] (70 mg, 0.073 mmol) in C_6H_5F (0.5 ml). A pale yellow suspension was obtained after stirring for 24 hr. The precipitate was washed

twice with pentane and dried *in vacuo* overnight to yield a pale yellow solid (60 mg, 78 %). $C_{16}H_{31}B_{11}Br_6PRh$ requires %C 25.12, %H 3.45. Found %C 25.72, %H 3.63.

^{1}H NMR (500.1 MHz, CD_2Cl_2): 6.82 (m, 2H, η^6-C_6H_5F), 6.71 (m, 2H, η^6-C_6H_5F), 6.11 (m, 1H, η^6-C_6H_5F), 4.38 (d, 2H, CH=CH), 2.58 (br s, 1H, CcageH), 2.20-1.45 (m, 23H, Cyp).

^{1}H NMR (400.1 MHz, C_6H_5F/CD_2Cl_2): 6.49 (m, 2H, η^6-C_6H_5F), 6.27 (m, 2H, η^6-C_6H_5F), 5.82 (m, 1H, η^6-C_6H_5F), 4.06 (d, *J*(RhH) 2.8, 2H, CH=CH), 2.35 (br s, 1H, CcageH), 1.86-1.06 (m, 23H, Cyp).

^{1}H{^{11}B} NMR (400.1 MHz, C_6H_5F/CD_2Cl_2): 6.49 (m, 2H, η^6-C_6H_5F), 6.27 (m, 2H, η^6-C_6H_5F), 5.82 (m, 1H, η^6-C_6H_5F), 4.06 (d, *J*(RhH) 2.8, 2H, CH=CH), 2.61 (br s, 5H, BH), 2.35 (br s, 1H, CcageH), 1.86-1.06 (m, 23H, Cyp).

^{11}B NMR (128.4 MHz, C_6H_5F/CD_2Cl_2): -1.08 [s, 1B, B(12)-Br], -9.33 [s, 5B, B(7-11)-Br], -19.94 [d, *J*(BH) 150, 5B, BH].

^{11}B{^{1}H} NMR (128.4 MHz, C_6H_5F/CD_2Cl_2): -1.08 (s, 1B, BBr), -9.33 (s, 5B, BBr), -19.94 (s, 5B, BH).

^{31}P{^{1}H} NMR (128.4 MHz, C_6H_5F/CD_2Cl_2): 111.2 [dd, *J*(RhP) 178, *J*(PF) 3.8].

^{19}F NMR (162.0 MHz, C_6H_5F/CD_2Cl_2): -120.6 (s).

[Rh{P(Cyp$_2$)(η^2-C_5H_7)}(η^6-C_6H_5Me)][*closo*-$CB_{11}H_6Br_6$] (40)

Toluene (2 μL, 0.018 mmol) was added to a solution of Rh{(η^2-C_5H_7)P(Cyp)$_2$}(*closo*-$CB_{11}H_6Br_6$) (11.4 mg, 0.12 mmol) in CH_2Cl_2 (1 ml). After 15 minutes the solvent was removed under vacuum and the yellow residue dried overnight. CD_2Cl_2 was added to collect the NMR data.

^{1}H NMR (400.1 MHz, CD_2Cl_2): 6.60 (m, 2H, η^6-C_6H_5Me), 6.51 (m, 1H, η^6-C_6H_5Me), 6.38 (m, 2H, η^6-C_6H_5Me), 4.09 (d, 2H, *J* 2.8, CH=CH), 2.56 (br s, 1H, $C_{cage}H$), 2.32 (s, 3H, C_6H_5*Me*), 2.15-1.41 (m, 23H, Cyp).

^{1}H{^{11}B} NMR (400.1 MHz, C_6H_5F/CD_2Cl_2): 6.60 (m, 2H, η^6-C_6H_5Me), 6.51 (m, 1H, η^6-C_6H_5Me), 6.38 (m, 2H, η^6-C_6H_5Me), 4.09 (d, 2H, *J* 2.8, CH=CH), 2.56 (br s, 1H, $C_{cage}H$), 2.35 (s, 5H, BH), 2.32 (s, 3H, C_6H_5*Me*), 2.15-1.41 (m, 23H, Cyp).

^{11}B NMR (128.4 MHz, C_6H_5F/CD_2Cl_2): -1.75 [s, 1B, B(12)-Br], -9.86 [s, 5B, B(7-11)-Br], -20.20 [d, *J*(BH) 169.5, 5B, BH].

^{31}P{^{1}H} NMR (162.0 MHz, C_6H_5F/CD_2Cl_2): 110.6 [d, *J*(RhP) 180].

[Rh(P^iPr_3)(η^2-tbe)(*closo*-$CB_{11}H_6Br_6$)] (41)

tert-Butylethene (0.1 ml, 0.776 mmol, excess) was added to a solution of [Rh(P^iPr_3)$(H)_2$(*closo*-$CB_{11}H_6Br_6$)] (30 mg, 0.034 mmol) in CH_2Cl_2 (0.5 ml). After 20 hr, the solvent was evaporated under reduced pressure to afford an orange solid which was washed with pentane and dried under vacuum overnight (18 mg, 55%). Crystals suitable for X-ray diffraction studies were obtained at 4°C by layering a CH_2Cl_2 solution of the title compound with pentane. $C_{16}H_{37}B_{11}Br_6PRh$ requires %C 19.94, %H 4.08. Found %C 20.39, %H 4.15.

^{1}H NMR (δ/ppm CD_2Cl_2): 4.07 (m, 1H, CH_2=C*H*-$C(CH_3)_3$), 2.91 (d, 1H, CH_2=CH-$C(CH_3)_3$, *J*(HH) = 12.84), 2.69 (br s, 1H, CH_{cage}), 2.26 (d, 1H, CH_2=CH-$C(CH_3)_3$, *J*(HH) = 8.05), 1.96 (m, 3H, C*H* ^{i}Pr, *J*(HH) = 7.30), 1.38, 1.36 (both dd, 9H, CH_3 ^{i}Pr, *J*(H-H) = 7.30, *J*(PH) = 7.30), 1.17 (s, 9H, CH_2=CH-C(*CH_3)$_3$).

^{1}H{^{11}B} NMR (δ/ppm CD_2Cl_2): 4.07 (m, 1H, CH_2=C*H*-$C(CH_3)_3$), 2.91 (d, 1H, CH_2=CH-$C(CH_3)_3$, *J*(HH) = 12.84), 2.69 (br s, 1H, CH_{cage}), 2.41(s, 5H, B*H*), 2.26 (d,

1H, CH_2=CH-C(CH_3)$_3$, *J*(HH) = 8.05), 1.96 (m, 3H, C*H* ^{i}Pr, *J*(HH) = 7.30), 1.38, 1.36 (both dd, 9H, CH_3 ^{i}Pr, *J*(H-H) = 7.30, *J*(PH) = 7.30), 1.17 (s, 9H, CH_2=CH-C(*CH_3*)$_3$).

^{11}B NMR (δ/ppm CD_2Cl_2): -0.31 (s, 1B, *B(12)*-Br), -8.51 (s, 5B, *B(7-11)*-Br), -19.50 (d, 5B, *B(2-7)*-H, *J*(BH) = 158.0).

^{11}B{^{1}H} NMR (δ/ppm CD_2Cl_2): -0.31 (s, 1B, *B(12)*-Br), -8.51 (s, 5B, *B(7-11)*-Br), -19.50 (s, 5B, *B(2-7)*-H).

^{31}P{^{1}H} NMR (δ/ppm CD_2Cl_2): 74.0 (d, *J*(RhP) = 183, ^{i}Pr$_3$P).

^{13}C{^{1}H} NMR (δ/ppm CD_2Cl_2): 74.39 (d, CH_2=*C*H-C(CH_3)$_3$, *J*(RhC) = 19.1), 41.74 (s, *C*H$_{cage}$), 38.11 (d, *C*H_2=CH-C(CH_3)$_3$, *J*(RhC) = 16.1), 34.45 (s, CH_2=CH-*C*(CH_3)$_3$), 29.50 (s, CH_2=CH-C(*C*H_3)$_3$), 24.83 (d, P(*C*H(CH_3)$_2$)$_3$, *J*(PC) = 25.2), 19.98 (s, P(CH(*C*H_3)$_2$)$_3$), 19.77 (s, P(CH(*C*H_3)$_2$)$_3$).

Other NMR exp: Hcosy, HMQC, ^{1}H{^{31}P} helped to signal assignment.

[Rh(PPh$_3$)$_2$(nbd)][1-Me-*closo*-SnB$_{11}$H$_{11}$] (42)

[Rh(nbd)Cl]$_2$ (39.2 mg, 0.085 mmol) was placed in a Schlenk tube and MeOH (5 ml) added *via* cannula to give a yellow suspension. After addition of triphenylphosphine (89.1mg, 0.34 mmol), the reaction mixture was stirred until complete dissolution. Addition of [Bu$_4$N][1-CH_3-*closo*-SnB$_{11}$H$_{11}$] (86.0 mg, 0.17 mmol) led to the formation of an orange precipitate which was washed with cold MeOH (2 x 1 ml) and dried under vacuum. The product was recrystalised from CH_2Cl_2/pentane to afford 107 mg (0.108 mmol, yield = 64%). $C_{46}H_{58}B_{11}P_2RhSn$ requires % C, 54.52; % H, 5.77; Found % C 54.1, % H 6.68.

(assignments from ^{11}B-^{11}B COSY and ^{11}B-^{1}H HMQC)

$^{1}H\{^{11}B\}$ ($CDCl_3$, 298 K): 7.34 (m, 30H, Ph), 4.50 (s, 4H, nbd), 4.11 (s, 2H, nbd), 2.97 [s, 1H, BH(12), *J*(SnH) 87], 2.06 [s, 5H, BH(7-11), *J*(SnH) 58], 1.69 [s, 3H, Sn-CH_3, *J*(SnH) 88], 1.56 [s, 5H, BH(2-6), *J*(SnH) 35].

^{11}B ($CDCl_3$, 298 K): -10.4 [d, 1B, B(12), *J*(HB) 133], -15.7 [d, 10B, B(2-11), *J*(HB) 153].

^{11}B [$(CD_3)_2CO$, 298 K]: -11.5 [d, 1B, B(12), *J*(HB) 134], -16.6 [d, 5B, B(7-11), *J*(HB) 116], -17.4 [d, 5B, B(2-6), *J*(HB) 122].

$^{31}P\{^{1}H\}$ ($CDCl_3$, 298 K): 30.6 [d, 2P, *J*(RhP) 153].

[$Rh(PPh_3)_2$(1-Me-*closo*-$SnB_{11}H_{11}$)] (43)

[$Rh(PPh_3)_2$(nbd)][1-CH_3-*closo*-$SnB_{11}H_{11}$] (10 mg, 0.010 mmol) was placed in a 15 ml Young's ampoule and CH_2Cl_2 (4 ml) was added via cannula. The solution was freeze-pump-thawed three times. After the third cycle the solution was opened to a H_2 atmosphere (1 atm). The ampoule was closed and the solution stirred for 30 minutes. Then the solvent was evaporated and the red residue dried in vacuo. Yield was quantitative by NMR spectroscopy. Crystals suitable for an X-ray diffraction study were grown from a CD_2Cl_2/pentane solution at room temperature. $C_{37}H_{44}B_{11}P_2RhSn$ requires % C, % 49.86; H, 4.98. Found % C 50.5, % H 4.94.

$^{1}H\{^{11}B\}$ (CD_2Cl_2, 298 K): 7.40 [m, 12H, Ph], 7.28 [m, 6H, Ph], 7.14 [m, 12H, Ph], 2.00 [s, 1H, BH(12), *J*(SnH) 80], 1.53 [s, 3H, Sn-CH_3, *J*(SnH) 92], 0.53 [s, 5H, B(7-11), *J*(SnH) 50], 0.05 [s, 5H, BH(2-6), *J*(SnH) ~40].

^{11}B (CD_2Cl_2, 298 K): -14.0 [d, 1B, B(12), *J*(HB) 129], -17.8 [d, 5 + 5 coincidence, *J*(HB) 120].

$^{31}P\{^{1}H\}$ (CD_2Cl_2, 298 K): 45.7 [d, 2P, *J*(RhP) 188].

6.3 Bibliography

1 K. Shelly, D. C. Finster, Y. J. Lee, W. R. Scheidt, and C. A. Reed, *J. Am. Chem. Soc.*, 1985, **107**, 5955.

2 T. Jelinek, P. Baldwin, W. R. Scheidt, and C. A. Reed, *Inorg. Chem.*, 1993, **32**, 1982.

3 J. A. Osborn and R. R. Schrock, *J. Am. Chem. Soc.*, 1971, **93**, 2397.

4 A. Rifat, N. J. Patmore, M. F. Mahon, and A. S. Weller, *Organometallics*, 2002, **21**, 2856.

5 A. Rifat, 'PhD Thesis', University of Bath, Bath, 2003.

Appendix A

A.1 ^{11}B-^{11}B COSY NMR and ESI-MS spectra of **2a/b**

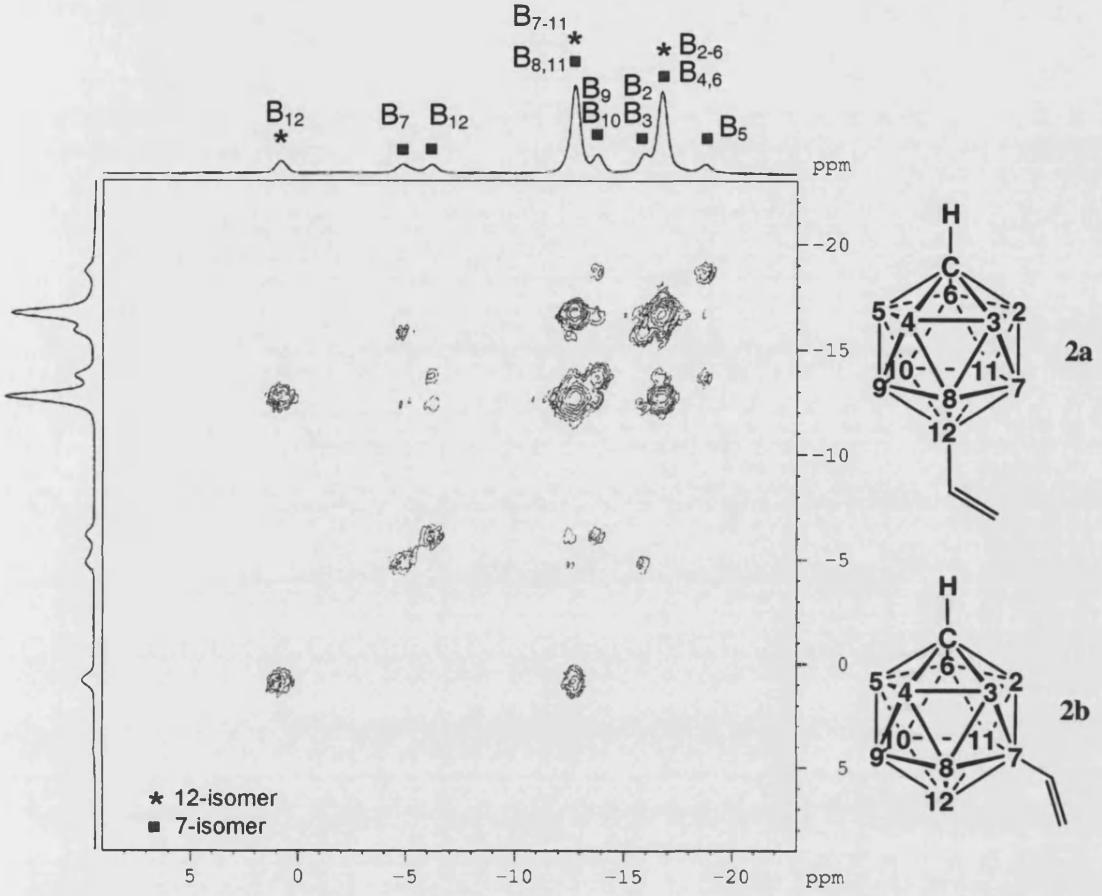

A.2 ^{11}B-^{11}B COSY NMR spectrum of **4a/b**

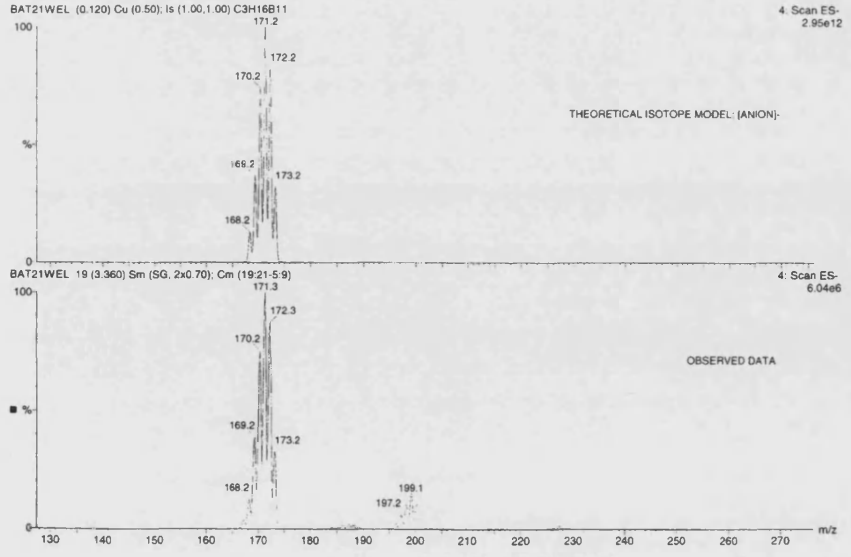

ESI-MS spectrum of **4a/b**

A.3 ^{11}B-^{11}B COSY NMR and ESI-MS spectra of **6**

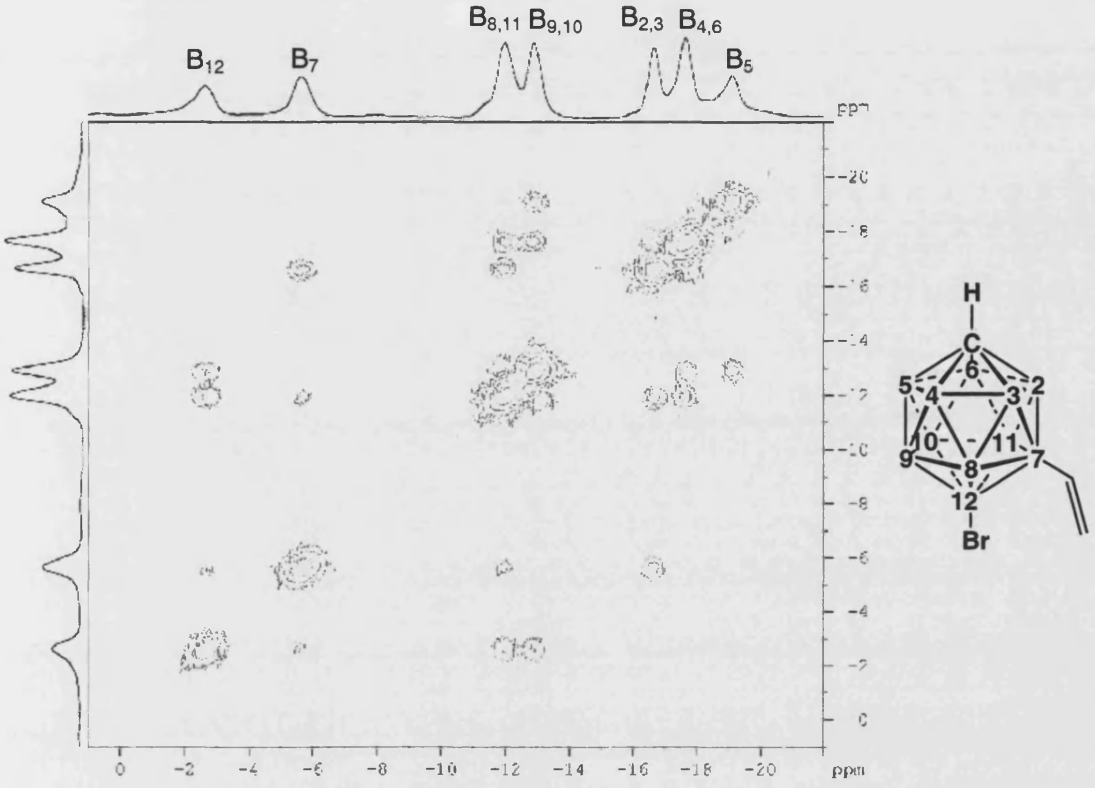

^{11}B-^{11}B COSY NMR spectrum of **6**

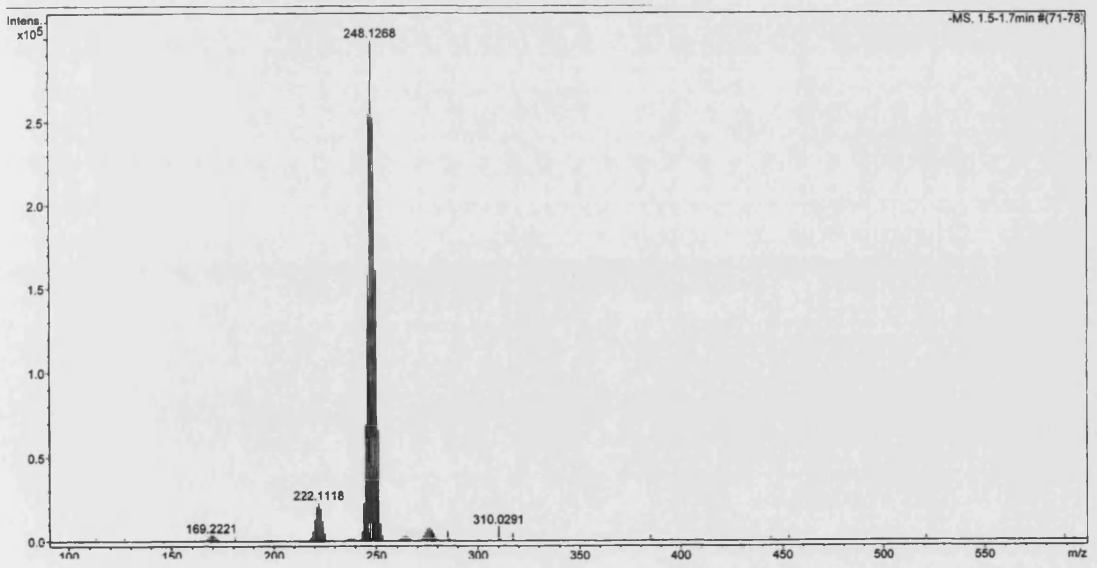

ESI-MS spectrum of **6**

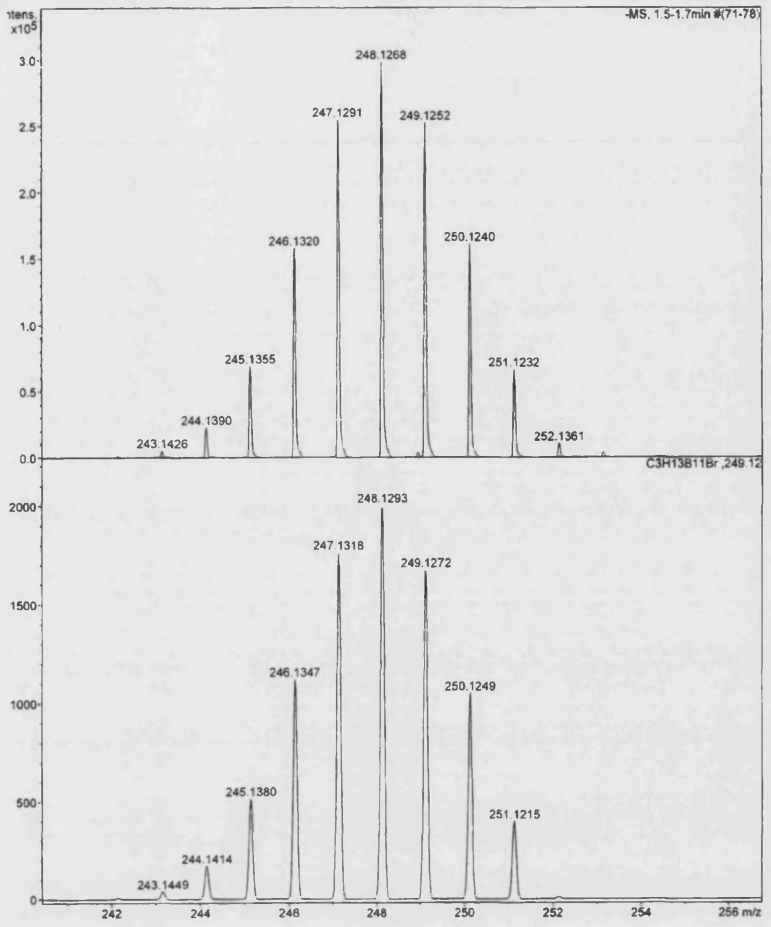

Observed and calculated ESI-MS spectra of **6**.

A.4 ESI-MS spectrum of **8**

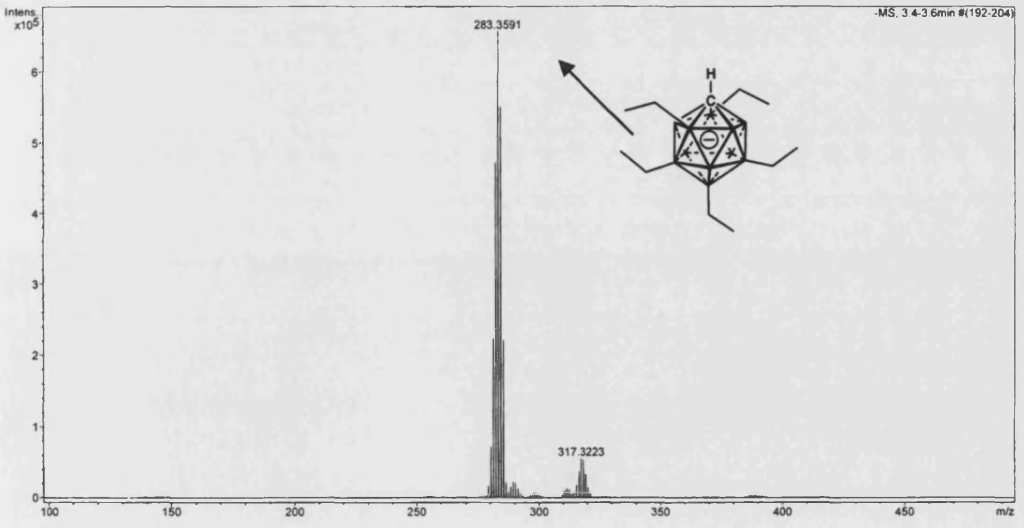

ESI-MS spectrum of **8**.

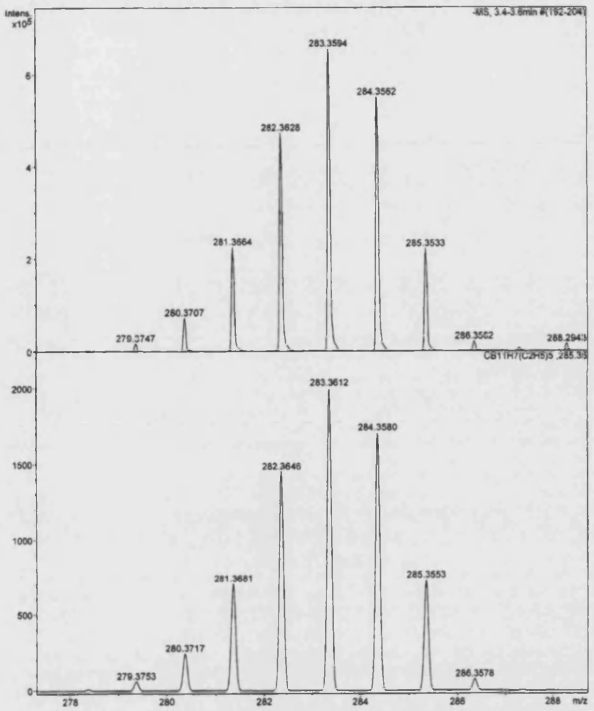

Observed and calculated ESI-MS spectra of **8**.

A.5 ESI-MS spectrum of **15**

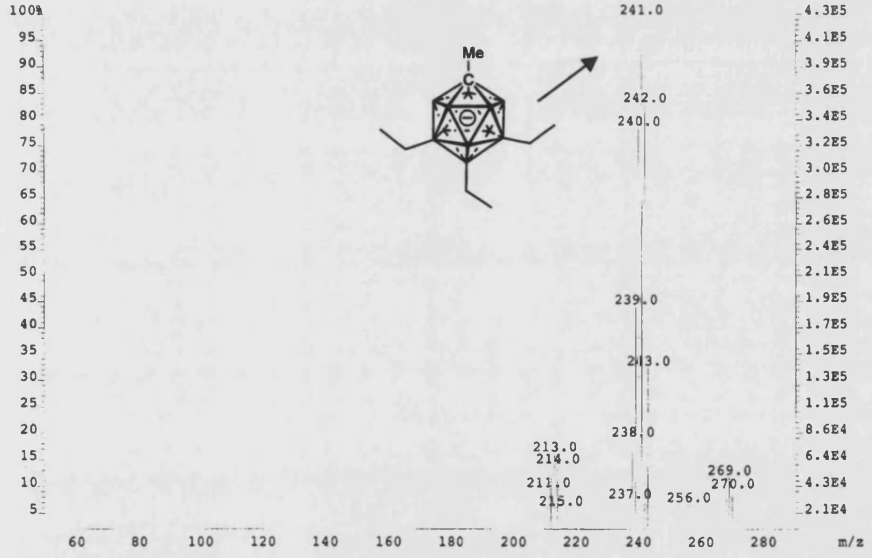

ESI-MS spectrum of **15**.

A.6 ESI-MS spectrum of **16**

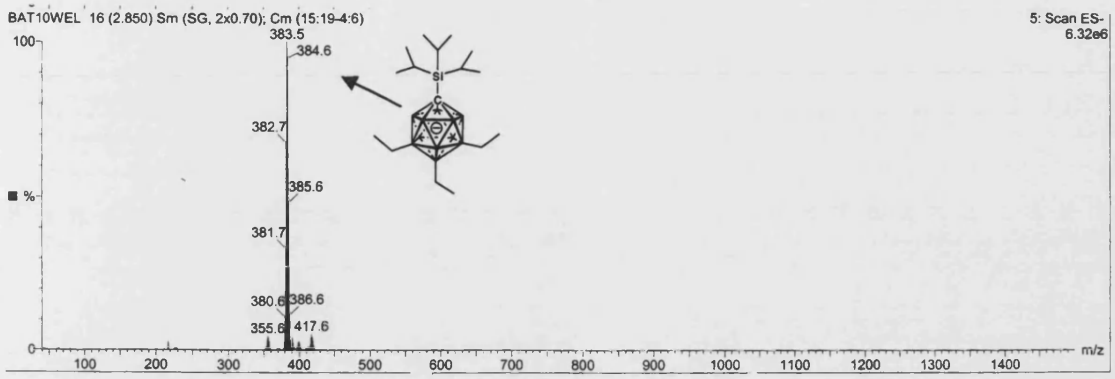

ESI-MS spectrum of **16**.

Appendix B.1 Selected Crystallographic Data

	2a	**8**	**9**	**11**	**13**	**14**	**18**
formula	$C_{46}H_{52}B_{11}P_2Rh$	$C_{54}H_{70}B_{11}P_2Rh$	$C_{12}H_{36}B_{11}CsO_{0.50}Si$	$C_{53}H_{70}B_{11}P_2RhSi$	$C_{46}H_{59}B_{11}P_2RhSi$	$C_{44}H_{56}B_{11}P_2Rh$	$C_{47}H_{56}B_{11}Br_6Cl_8P_2Rh$
fw	888.64	1002.86	468.32	1018.94	923.78	868.65	1667.74
cryst size, mm	0.55 × 0.55 × 0.30	0.20 × 0.10 × 0.05	0.63 × 0.63 × 0.13	0.62 × 0.40 × 0.20	0.25 × 0.13 × 0.08	0.20 × 0.13 × 0.03	0.50 × 0.25 × 0.20
T (K)	150(2)	150(2)	150(2)	150(2)	150(2)	150(2)	150(2)
cryst syst	monoclinic	monoclinic	monoclinic	triclinic	monoclinic	triclinic	triclinic
space group	P 2_1/c	P 2_1/c	C 2/c	P $\bar{1}$	P 2_1/a	*P* $\bar{1}$	P $\bar{1}$
a, Å	17.0670(2)	16.7380(2)	30.2090(10)	10.15100(10)	18.8890(3)	9.8660(2)	11.3130(2)
b, Å	15.6010(2)	18.0910(2)	7.9490(2)	13.58700(10)	14.4860(3)	13.3420(4)	14.2250(2)
c, Å	17.4360(2)	18.5710(2)	14.8200(4)	20.7780(2)	20.2760(3)	17.7310(6)	22.6530(5)
α, deg	90	90	90	88.3950(10)	90	83.5920(10)	96.5970(10)
β, deg	101.8950(10)	111.6180(10)	93.5750(10)	80.080(10)	116.2720(10)	75.7420(10)	92.3760(10)
γ, deg	90	90	90	76.97	90	78.438(2)	112.9980(10)
V, Å^3	4542.86(9)	5227.88(10)	4492.4(2)	2751.91(4)	4974.94(15)	2211.41(11)	3318.63(10)
Z	4	4	8	2	4	2	2
μ, mm^{-1}	0.479	0.424	1.699	0.425	0.463	0.491	4.272
F_{000}	1832	2096	1888	1064	1916	900	1628
θ range (deg)	3.58 to 28.70	3.45 to 27.49	4.02 to 30.06	3.34 to 29.14	5.54 to 25.00	5.57 to 27.44	3.64 to 27.51
D_{calcd}, g cm^{-3}	1.299	1.274	1.385	1.230	1.233	1.305	1.669
Index ranges (*h*, *k*, *l*)	-22/23, -20/21, ±23	±21, ±23, ±24	±53, ±11, ±20	±13, -18/17, -26/28	±22, ±17, ±24	±12, ±17, ±22	±14, ±18, ±29
Reflexions collected/ unique	78738/11612	76466/11940	21081/6484	44942/14634	55055/8611	26014/9894	36589/15044
No. of data/restraints/params	11612/0/541	11940/0/677	6484/0/241	14634/18/653	8611/0/558	9894/0/532	15044/9/808
R1/wR2 [$I > 2\sigma(I)$]	0.0325/0.0798	0.0498/0.1095	0.0409/0.0785	0.0531/0.1390	0.0545/0.1017	0.0491/0.0905	0.0484/0.1226
R1/wR2 (all data)	0.0381/0.0854	0.0664/0.1173	0.0815/0.0891	0.0652/0.1488	0.0863/0.1209	0.0813/0.1028	0.0688/0.1352
GOF on F^2	1.050	1.052	1.004	1.037	1.108	1.034	1.048
max./min.Δρ, e Å^{-3}	0.680, -1.006	0.645, -0.476	0.805, -1.363	2.487, -0.907	0.951, -0.683	0.452, -0.678	1.470, -1.108

Appendix B.2 Selected Crystallographic Data

	25	**32**	**35**	**38**	**39**	**40**	**41**
formula	$C_{43}H_{102}B_{22}P_2Rh_2$	$C_{25}H_{46}B_{11}Br_6FPRh$	$C_{16}H_{35}B_{11}Br_6PRh$	$C_{16}H_{31}B_{11}Br_6PRh$	$C_{22}H_{36}B_{11}Br_6FPRh$	$C_{23}H_{39}B_{11}Br_6PRh$	$C_{16}H_{39}B_{11}Br_6PRh$
Fw	1124.86	1097.87	959.69	955.66	1051.76	1047.79	963.72
cryst size, mm	0.25 × 0.23 × 0.08	0.50 × 0.40 × 0.30	0.20 × 0.15 × 0.05	0.25 × 0.18 × 0.15	0.20 × 0.20 × 0.06	0.50 × 0.40 × 0.30	0.40 × 0.35 × 0.20
T (K)	150(2)	150(2)	150(2)	150(2)	150(2)	150(2)	150(2)
cryst syst	monoclinic	monoclinic	monoclinic	orthorhombic	monoclinic	Orthorhombic	monoclinic
space group	P 2_1/n	C 2/c	P 2_1/c	P 2_1 2_1 2_1	P c	P bca	*C* c
a, Å	12.34400(10)	25.7860(3)	12.96500(10)	12.9014(1)	10.90900(10)	12.6807(1)	16.62600(10)
b, Å	20.10800(10)	13.1630(2)	12.14600(10)	13.8202(1)	12.7830(2)	20.6068(2)	19.10400(10)
c, Å	23.4140(2)	23.1100(2)	20.5620(3)	16.3616(2)	17.3700(2)	27.3058(2)	13.73500(10)
α, deg	90	90	90	90	90	90	90
β, deg	93.3490(3)	100.8460(10)	102.3162(4)	90	90.4200(10)	90	121.2435(3)
γ, deg	90	90	90	90	90	90	90
V, Å^3	5801.74(7)	7703.90(16)	3163.44(6)	2917.23(5)	1724.95(4)	7135.24(10)	3729.87(4)
Z	4	8	4	4	2	8	4
μ, mm^{-1}	0.655	6.733	8.178	8.868	7.513	7.261	6.937
F_{000}	2360	4240	1824	1808	1004	4016	1840
θ range (deg)	3.46 to 30.51	4.25 to 27.53	3.55 to 29.59	5.32 to 29.13	3.66 to 32.02	3.45 to 27.47	4.75 to 33.18
D_{calcd}, g cm^{-3}	1.288	1.893	2.015	2.176	2.025	1.951	1.716
Index ranges (*h, k , l*)	±17, ±28, ±33	±33, ±17, -29/30	-18/17, ±16, ±28	±17, ±18, -21/22	-16/15, -18/19, -18/16	±16, ±26, -34/35	±25, -29/28, ±21
Reflexions collected/ unique	127863/17673	42541/8692	52075/8855	61703/7799	30694/10764	127873/8156	48929/13829
no. of data/restraints/params	17673/1/643	8692/0/423	8855/0/324	7799/11/330	10764/2/379	8156/1/398	13829/5/328
R1/wR2 [$I > 2\sigma(I)$]	0.0453/0.0950	0.0264/0.0645	0.0432/0.0969	0.0311/0.0649	0.0465/0.1172	0.0364/0.0815	0.0330/0.0823
R1/wR2 (all data)	0.0633/0.1015	0.0310/0.0666	0.0622/0.1042	0.0390/0.0680	0.0528/0.1209	0.0541/0.0890	0.0380/0.0845
GOF on F^2	1.057	1.060	1.035	1.034	1.056	1.082	1.046
max./min.Δρ, e Å^{-3}	3.079, -0.998	0.723, -0.719	1.061, -1.224	1.021, -0.798	5.613, -1.316	0.577, 0.323	0.792, -1.189

Appendix B.3 Selected Crystallographic Data

	43
formula	$C_{37}H_{44}B_{11}P_2RhSn$
fw	891.17
cryst size, mm	0.40 × 0.33 × 0.33
T (K)	150(2)
cryst syst	Monoclinic
space group	C 2/c
a, Å	32.1840(3)
b, Å	14.7560(2)
c, Å	18.9180(2)
α, deg	90
β, deg	117.4640(10)
γ, deg	90
V, Å^3	7971.77(16)
Z	8
μ, mm^{-1}	1.149
F_{000}	3568
θ range (deg)	3.02 to 27.53
D_{calcd}, g cm^{-3}	1.485
Index ranges (*h, k , l*)	±41, ±19, ±24
Reflexions collected/ unique	68622/9139
no. of data/restraints/params	9139/0/495
R1/wR2 [$I > 2\sigma(I)$]	0.0481/0.0803
R1/wR2 (all data)	0.0650/0.0803
GOF on F^2	1.143
max./min.Δρ, e Å^{-3}	0.7030-0.6565

Appendix C Publications

- **Molinos, E.**; Kociok-Kohn, G.; Weller, A. S., Polyethyl substituted weakly coordinating carborane anions: a sequential dehydrogenative borylation-hydrogenation route. *Chemical Communications* **2005**, (28), 3609-3611.

- **Molinos, E.**; Player, T. P. H.; Kociok-Kohn, G.; Ruggerio, G. D.; Weller, A. S., 1-Me-1-*closo*-SnB11 H-11 (-) as a potential weakly coordinating anion: Synthesis of $Rh(PPh_3)_2$(1-Me-*closo*-$SnB_{11}H_{11}$) and comparisons with $Rh(PR_3)_2$(1-H-*closo*-$CB_{11}H_{11}$). *Heteroatom Chemistry* **2006,** 17, (3), 174-180.

- Douglas, T. M.; **Molinos, E.**; Brayshaw, S. K.; Weller, A. S., Rhodium Phosphine Olefin Complexes of the Weakly Coordinating Anions $[BAr^F_4]^-$ and [1-*closo*-$CB_{11}H_6Br_6]^-$. Kinetic versus Thermodynamic Factors in Anion Coordination and Complex Reactivity. *Organometallics* **2006,** 26, (3), 463 - 465.

- Brayshaw, S. K.; **Molinos, E.**; Weller, A. S., catena-Poly[[(tetrafluoroborato-F)silver(I)]--triphenylphosphine-2P:C3]. *Acta Crystallographica* **2007,** E63, m302-m303.

- **Molinos, E.**; Brayshaw, S. K.; Kociok-Köhn, G.; Weller, A. S., Sequential Dehydrogenative Borylation/Hydrogenation Route to Polyethyl-Substituted, Weakly Coordinating Carborane Anions. *Organometallics* **2007,** 26, (9), 2370 -2382.

Polyethyl substituted weakly coordinating carborane anions: a sequential dehydrogenative borylation–hydrogenation route†

Eduardo Molinos, Gabriele Kociok-Köhn and Andrew S. Weller*

Received (in Cambridge, UK) 5th April 2005, Accepted 16th May 2005
First published as an Advance Article on the web 9th June 2005
DOI: 10.1039/b504630k

Polyethylated carborane monoanions based on [*closo*-$CB_{11}H_{12}]^-$ with up to five *B*-ethyl groups can be prepared by a sequential Rh-catalysed dehydrogenative borylation then hydrogenation.

Functionalised carborane monoanions based upon [*closo*-$CB_{11}H_{12}]^-$ (Fig. 1) are an important subset of the "least coordinating anions",[1] and find application in catalysis,[2] the stabilisation of reactive species such as naked protons or unsaturated main-group cations,[3] and complexes that show intermolecular [M]···H_3C interactions.[4] Given this interest, reliable synthetic routes to poly-functionalise the B–H periphery of the anion are few: methylation using MeOTf,[5] halogenation (*e.g.* using Br_2)[6] and sequential iodination/Pd-catalysed cross-coupling with aryl Grignards.[7] We report here an extension of a route that has been previously shown to be useful in effecting the clean mono and bis-functionalisation of boranes—transition metal catalysed hydroboration[8–11]—to sequentially, and regioselectively, functionalise [*closo*-$CB_{11}H_{12}]^-$ with up to 5 alkyl groups under mild conditions. Perethylation of [*closo*-$CB_{11}H_{12}]^-$ has previously been reported[12] using relatively harsh conditions (sealed tube, 220 °C).

Treatment of $(PPh_3)_2Rh$(*closo*-$CB_{11}H_{12}$)[13] in CH_2Cl_2 solution with ethene (excess) in a sealed J. Young's tube at room temperature affords mono-substituted $(PPh_3)_2Rh$(*x*-(C_2H_3)-*closo*-$CB_{11}H_{11}$) (*x* = 12, 7) **1** in quantitative yield (Scheme 1). Compound **1** is characterised as having a *B*-vinyl substituted cage anion in the 12- or 7-positions, with the metal fragment bound to the vinyl and one B–H group. In particular two sets of vinylic protons are observed in the ^1H NMR spectrum in the ratio 7 : 3, while a ^{11}B–^{11}B COSY NMR experiment (on the $[Rh(PPh_3)_2(nbd)]^+$salt) indicates the formation of both 12- and 7-isomers. Compound **1** results from dehydrogenative borylation of ethene by [*closo*-$CB_{11}H_{12}]^-$ mediated by *exo*-coordinated $\{Rh(PPh_3)_2\}^+$ (no reaction is observed between ethene and [*closo*-$CB_{11}H_{12}]^-$). Transition metal mediated catalytic dehydrogenative borylation of alkenes using simple boron sources {*e.g.* $B_2(OR)_4$} is well established,[14] and Sneddon has previously commented on such a process occurring during mono-functionalisation of boranes, carboranes and borazines with 1-alkenes using $PtBr_2$ as the hydroboration catalyst.[8,11,15]

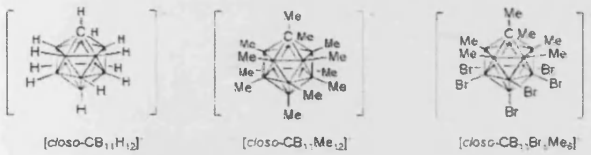

Fig. 1 Representative carborane monoanions based upon [*closo*-$CB_{11}H_{12}]^-$.

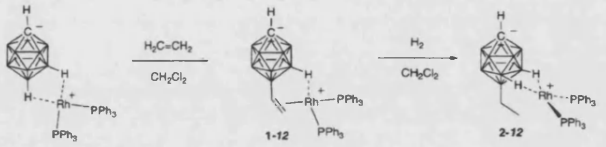

Scheme 1 (Only 12-isomer shown.)

Compound **1** does not react further with ethene, presumably due to the firmly bound cage vinyl group. Treatment with H_2 results in the $\{Rh(PPh_3)_2\}^+$ mediated hydrogenation of the vinyl group to form $(PPh_3)_2Rh$(*x*-C_2H_5-*closo*-$CB_{11}H_{11}$) (*x* = 12, 7) **2** in which the ratio of the two isomers remains the same as in **1**. NMR data are fully consistent with the metal fragment remaining coordinated *exo* to the cage anion, in particular two quadrupolar broadened peaks at δ −0.84 and δ −2.11 ppm are observed—indicative of Rh–H–B interactions in each isomer.[16] With the vinyl group removed, **2** now reacts with ethene, resulting in further dehydrogenative borylation. However a number of products are formed, which by FAB-mass spectrometry are identified as having polysubstituted cages (*n* = 2–5). Cycling the dehydrogenative borylation–hydrogenation process a further 4 times (6 in total) results in a single compositionally pure product that has been identified by NMR spectroscopy as the penta-ethyl substituted cage anion complex, $(PPh_3)_2Rh((C_2H_5)_5$-*closo*-$CB_{11}H_7)$ **3** (Scheme 2). Addition of nbd (nbd = norbornadiene) to **3** affords the separated ion-pair $[(PPh_3)_2Rh(nbd)][(C_2H_5)_5$-*closo*-$CB_{11}H_7)]$ **4**, which has been characterised by NMR spectroscopy and an X-ray diffraction

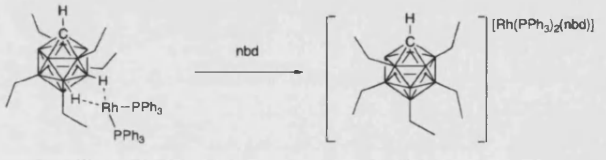

Scheme 2

† Electronic supplementary information (ESI) available: full experimental data and details of X-ray diffraction experiments. See http://www.rsc.org/suppdata/cc/b5/b504630k/

Department of Chemistry, University of Bath, Bath, UK BA2 7AY.
E-mail: a.s.weller@bath.ac.uk; Fax: +44(0)1225386231;
Tel: +44(0)1225383394
*a.s.weller@bath.ac.uk

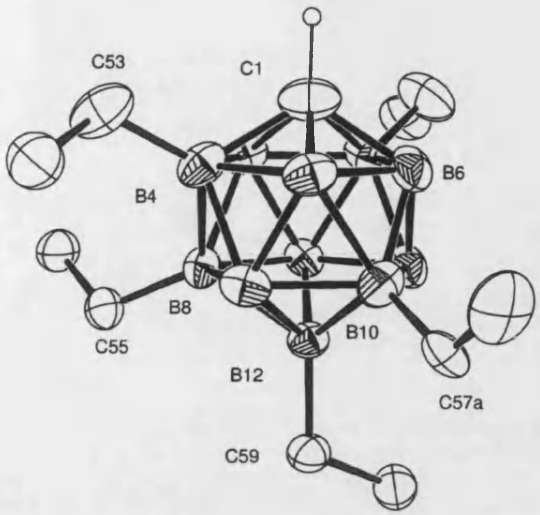

Fig. 2 Crystal structure of the anionic portion of $[Rh(PPh_3)_2(nbd)][(C_2H_5)_5$-*closo*-$CB_{11}H_7)]$ **4**. Thermal ellipsoids are shown at the 30% probability level. Hydrogen atoms, apart from the cage C–H, are omitted for clarity.

study. In our hands gram ($\sim$1.5 g) quantities of **4** can be prepared using this method in good yield (75% isolated yield).

The solid-state structure of the substituted anion in salt **4** is shown in Fig. 2.‡ This demonstrates five-fold B–H substitution has occurred: at the antipodal (B12) vertex, two vertices on the lower pentagonal belt and two on the upper belt. On the basis of charge distribution in the $[$*closo*-$CB_{11}H_{12}]^-$ cage substitution of all the lower-hemisphere B–H vertices would be expected to occur first.[17] However, the combination of steric bulk of the $\{(PPh_3)_2Rh\}^+$ fragment and the cage-bound ethyl groups results in vertices that are distal from one another to be substituted preferentially. This steric bulk (Fig. 3) presumably also disfavours further substitution of B–H vertices beyond 5-substitution under the mild conditions used. The substitution pattern observed in the solid state is supported by ^{11}B–^{11}B COSY NMR experiments in solution.

The degree of ethyl substitution can be modulated by introducing a methyl group onto the cage carbon atom. This has the effect of retarding substitution on the upper pentagonal belt so that after six successive dehydrogenative borylation–hydrogenation cycles the tri-substituted cage anion complex

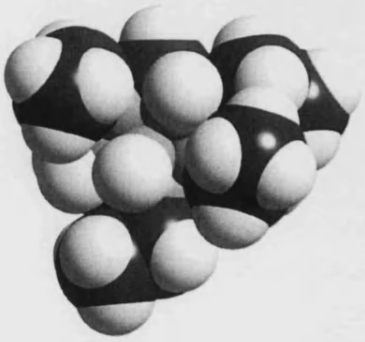

Fig. 3 Space filling representation (van der Waals radii) of the anionic portion of $[Rh(PPh_3)_2(nbd)][(C_2H_5)_5$-*closo*-$CB_{11}H_7)]$ **4**.

$(PPh_3)_2Rh(1\text{-Me-}(C_2H_5)_3$-*closo*-$CB_{11}H_8)$ **5** results as the major ($\sim$90%) product. **5** has been characterised by NMR spectroscopy, X-ray crystallography and mass spectrometry.‡ Addition of MeCN to **5** affords the separated ion-pair $[(PPh_3)_2Rh(MeCN)_x][1\text{-Me-}(C_2H_5)_3$-*closo*-$CB_{11}H_8]$ **6**, as characterised by NMR spectroscopy. Compounds **5** and **6** were not formed as compositionally pure materials, a small amount (*ca.* 10%) of another cage anion was always present, which FAB-mass spectroscopy suggests to be $[1\text{-Me-}(C_2H_5)_4$-*closo*-$CB_{11}H_7]^-$.

Fig. 4 shows the solid-state structure of **5** and demonstrates both the three fold-substitution and coordination of the $\{(PPh_3)_2Rh\}^+$ fragment through two Rh–H–B 3-centre 2-electron interactions, similar to that observed for $(PPh_3)_2Rh($*closo*-$CB_{11}H_{12})$.[13] These Rh–H–B interactions are retained in solution as shown in the ^1H NMR spectrum by the observation of a characteristic, integral 2-H, quadrupolar broadened, signal at δ – 4.64 ppm.[16] This signal disappears on addition of excess MeCN, consistent with the formation of the separated ion-pair **6**. ^1H, and ^{11}B NMR spectra are consistent with the C_s symmetry observed in the solid-state being retained in solution for **5** and **6**.

The mechanism of alkene (dehydrogenative) borylation has been discussed for both mono borane sources[9,14] and cluster species,[8] with the first step of such transformations being insertion of a low valent metal fragment into a B–H bond to give a metal–boryl intermediate such as **A** (Scheme 3). For the systems under discussion here H/D exchange experiments are fully consistent with a similar mechanism operating. Thus treatment of $(PPh_3)_2Rh($*closo*-$CB_{11}H_{12})$ with D_2 (1 atm) in CD_2Cl_2 solution slowly (days) results in perdeuteration of all the B–H vertices (by ^1H and ^{11}B NMR spectroscopy). Moreover HD *and* H2 are also observed in the ^1H NMR spectrum, fully consistent with a putative Rh(III)–boryl intermediate **B** for this H/D exchange process. Replacement of D_2 for an alkene in structure **B** would afford an intermediate closely related to **A**. Similar Rh(III)–boryl intermediates have been proposed for the mono-functionalisation of a $\{$*nido*-$C_2B_9\}$ cage using a $\{Rh(PPh_3)_2\}^+$ catalyst, although in this case activated alkenes (acrylates) needed to be used.[10] Noteworthy is that by ^{11}B and $^1H\{^{11}B\}$ NMR spectroscopy H/D exchange occurs in the order B(12)/B(7–11) and finally B(2–6), consistent with the charge distribution in the $[$*closo*-$CB_{11}H_{12}]^-$ cage,[17] with the $\{Rh(PPh_3)_2\}^+$ fragment preferentially inserting into the B–H vertices carrying the most negative charge. As indicated by the sequence of compounds **1** $\rightarrow$ **5** $\rightarrow$ **4** a similar order of substitution occurs in the hydroboration of ethene.

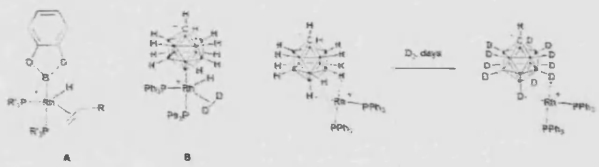

Scheme 3

With the bulkier alkene 1-hexene, dehydrogenative borylation is suppressed to the extent that the hydroboration product represents $\sim$90% of the isolated product (by ^1H NMR) and polyalkyl-functionalised cages result directly from addition of excess 1-hexene to $(PPh_3)_2Rh(1\text{-Me-}$*closo*-$CB_{11}H_{11})$ at 40 °C followed

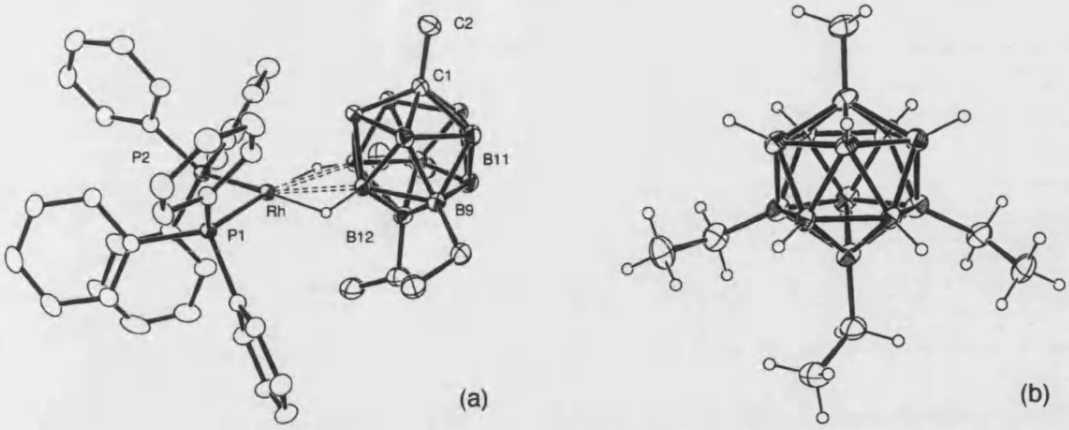

Fig. 4 (a) Crystal structure of complex **5**. Hydrogen atoms, apart from those associated with the Rh–H–B interaction are omitted for clarity. (b) The anion without the $\{Rh(PPh_3)_2\}^+$ fragment. Thermal ellipsoids are shown at the 30% probability level.

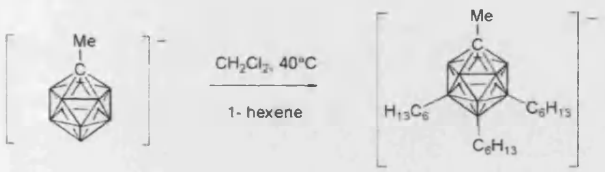

Scheme 4

by workup with MeCN (Scheme 4). NMR spectroscopy and FAB-mass spectrometry demonstrate that, as for ethene, 3-fold substitution takes place to afford [1-Me-$(C_6H_{13})_3$-*closo*-$CB_{11}H_8$][$(PPh_3)_2$Rh(MeCN)$_x$] **7**. Interestingly, the reaction with $(PPh_3)_2$Rh(1-H-*closo*-$CB_{11}H_{11}$) under the same conditions is much slower, suggesting that the cage-bound methyl group plays a role in activating the cage towards hydroboration of unactivated 1-hexene. In our hands **7** has been difficult to isolate in analytically pure form as it readily forms oily material on recrystallisation—a consequence of the increased length of the alkyl groups surrounding the cage. Nevertheless $^{11}B\{^1H\}$ NMR spectroscopy shows a very similar pattern compared with the ethyl counterparts (*e.g.* **6**) and we thus suggest a similar substitution pattern.

In summary, we have demonstrated that polyalkyl-functionalised monocarborane anions can be synthesised by multiple hydroboration of alkenes by a single [*closo*-$CB_{11}H_{12}]^-$ cage anion. Efforts are currently directed to using this, and related routes, to produce compositionally pure *per*-alkyl substituted carborane monoanions in synthetically useful quantities.

We acknowledge the EPSRC (GR/S42750/01) and the Royal Society for funding. Professor Larry Sneddon (University of Pennsylvania, USA) for useful discussions at the beginning of this project which were enabled by a Royal Society of Chemistry/J. W. T. Jones travelling fellowship awarded to A.S.W. Dr Adem Rifat is thanked for preliminary experiments.

Notes and references

‡ *Crystallographic data.* Intensity data were collected at 150 K on a Nonius Kappa CCD diffractometer, using graphite monochromated MoKα radiation (λ = 0.71073 Å). **4** $C_{54}H_{70}B_{11}P_2Rh$, M = 1002.86, $P2_1/c$, a = 16.7380(2) Å, b = 18.0910(2) Å, c = 18.5710(2) Å, β = 111.6180(10)° V = 5227.88(10) Å^3, Z = 4, μ = 0.424 mm^{-1}, unique reflections = 11940 [R(int) = 0.0545], R_1 = 0.0498, wR_2 = 0.1095 [$I > 2\sigma(I)$]. CCDC 268853. **5** $C_{44}H_{56}B_{11}P_2Rh$, M = 868.65, $P\bar{1}$, a = 9.8660(2) Å, b = 13.3420(4) Å, c = 17.7310(6) Å, α = 83.5920(10)°, β = 75.7420(10)°, γ = 78.438(2)° V = 2211.41(11) Å^3, Z = 2, μ = 0.491 mm^{-1}, unique reflections = 9894 [R(int) = 0.0741], R_1 = 0.0491, wR_2 = 0.0905 [$I > 2\sigma(I)$]. CCDC 268854. See http://www.rsc.org/suppdata/cc/b5/b504630k/ for crystallographic data in CIF or other electronic format.

1 I. Krossing and I. Raabe, *Angew. Chem., Int. Ed.*, 2004, **43**, 2066; C. A. Reed, *Acc. Chem. Res.*, 1998, **31**, 133; S. H. Strauss, *Chem. Rev.*, 1993, **93**, 927.
2 N. J. Patmore, C. Hague, J. H. Cotgreave, M. F. Mahon, C. G. Frost and A. S. Weller, *Chem. Eur. J.*, 2002, **8**, 2088; A. Rifat, G. Kociok-Köhn, J. W. Steed and A. S. Weller, *Organometallics*, 2004, **23**, 428.
3 C. A. Reed, *Chem. Commun.*, 2005, 1669.
4 L. Zharov, T.-C. Weng, A. M. Orendt, D. H. Barich, J. Penner-Hahn, D. M. Grant, Z. Havlas and J. Michl, *J. Am. Chem. Soc.*, 2004, **126**, 12033; M. J. Ingleson, N. J. Patmore, G. Kociok-Köhn, M. F. Mahon, G. D. Ruggiero, A. S. Weller, A. J. Clarke and J. P. Rourke, *J. Am. Chem. Soc.*, 2004, **126**, 1503.
5 B. T. King, Z. Janousek, B. Gruner, M. Trammell, B. C. Noll and J. Michl, *J. Am. Chem. Soc.*, 1996, **118**, 3313; D. Stasko and C. A. Reed, *J. Am. Chem. Soc.*, 2002, **124**, 1148.
6 J. Plesek, T. Jelinek, E. Drdakova, S. Hermanek and B. Stibr, *Collect. Czech. Chem. Commun.*, 1984, **49**, 1559.
7 A. Franken, C. A. Kilner, M. Thornton-Pett and J. D. Kennedy, *Chem. Commun.*, 2002, 2048.
8 D. E. Kadlecek, P. J. Carroll and L. G. Sneddon, *J. Am. Chem. Soc.*, 2000, **122**, 10868.
9 K. Mazighi, P. J. Caroll and L. G. Sneddon, *Inorg. Chem.*, 1993, **32**, 1963.
10 J. D. Hewes, C. W. Kreimendahl, T. B. Marder and M. F. Hawthorne, *J. Am. Chem. Soc.*, 1984, **106**, 5757.
11 T. Davan, E. W. Corcoran and L. J. Sneddon, *Organometallics*, 1983, **2**, 1693.
12 C. W. Tsang and Z. W. Xie, *Chem. Commun.*, 2000, 1839.
13 A. Rifat, N. J. Patmore, M. F. Mahon and A. S. Weller, *Organometallics*, 2002, **21**, 2856.
14 R. B. Coapes, F. E. S. Souza, R. L. Thomas, J. J. Hall and T. B. Marder, *Chem. Commun.*, 2003, 614 and references cited therein.
15 A. T. Lynch and L. G. Sneddon, *J. Am. Chem. Soc.*, 1989, **111**, 6201.
16 A. Rifat, V. E. Laing, G. Kociok-Köhn, M. F. Mahon, G. D. Ruggiero and A. S. Weller, *J. Organometallic Chem.*, 2003, **680**, 127.
17 M. L. McKee, *J. Am. Chem. Soc.*, 1997, **119**, 4220.

Heteroatom Chemistry
Volume 17, Number 3, 2006

[1-Me-1-*closo*-$SnB_{11}H_{11}$]$^-$ as a Potential Weakly Coordinating Anion: Synthesis of $Rh(PPh_3)_2$(1-Me-*closo*-$SnB_{11}H_{11}$) and Comparisons with $Rh(PR_3)_2$(1-H-*closo*-$CB_{11}H_{11}$)

Eduardo Molinos, Thomas P. H. Player, Gabriele Kociok-Köhn, Giuseppe D. Ruggerio, and Andrew S. Weller

Department of Chemistry, University of Bath, Bath BA2 7AY, UK

Received 18 April 2005; revised 10 August 2005

ABSTRACT: *The closo-stannaborane salt [Rh(PPh$_3$)$_2$(nbd)][1-Me-1-closo-SnB$_{11}$H$_{11}$] reacts with H$_2$ in CH$_2$Cl$_2$ solution to afford the contact ion-pair Rh(PPh$_3$)$_2$(1-Me-closo-SnB$_{11}$H$_{11}$), which has been characterized in solution and the solid state by X-ray diffraction.* © 2006 Wiley Periodicals, Inc. Heteroatom Chem 17:174–180, 2006; Published online in Wiley InterScience (www.interscience.wiley.com). DOI 10.1002/hc.20218

INTRODUCTION

"Weakly coordinating" carborane monoanions based upon derivatives of [*closo*-$CB_{11}H_{12}$]$^-$ **I** find application in catalysis mediated by transition metal cations [1], the isolation of superacids [2], and the generation of coordinatively unsaturated complexes [3] that can have interesting structural features such as [M]$\cdots$$H_3C$ intermolecular interactions [4,5]. Given this, these anions are not as widely used as the fluorinated aryl borates, such as [$B(C_6H_3(CF_3)_2)_4$]$^-$ [6], even though they exhibit attractive properties such as being more chemically robust [2]. This, in part, may be due to the perception that the precursor to these carborane anions, [*closo*-$CB_{11}H_{12}$]$^-$, is not straightforward to prepare, needing multistep routes from non-routine starting materials that are relatively expensive and toxic, i.e., decaborane $B_{10}H_{14}$. Attractive routes to alleviate this problem by reducing the number of synthetic steps from *nido*-$B_{10}H_{14}$ [7,8], synthetic routes that start with Na[BH_4] to form *nido*-[$B_{11}H_{14}$]$^-$ and subsequent insertion of a {CR} vertex [9,10], or derivatization of [*closo*-$B_{12}H_{12}$]$^{2-}$ [11] have recently been reported. We report here an alternative approach to form precursors to weakly coordinating *closo*-icosahedral monoanionic borane species by use of the stanna borane [1-Me-*closo*-$SnB_{11}H_{11}$]$^-$, **II**. This cage species was first reported by Todd in 1992 by methylation of the dianion [*closo*-$SnB_{11}H_{11}$]$^{2-}$ [12]. This dianion, in turn, is available in two steps from Na[BH_4] in good yield and reasonable preparative scale (62%, ~5 g). The coordination chemistry of [$SnB_{11}H_{11}$]$^{2-}$ has recently been elegantly explored by Wesemann [13–16] and this has centered around the interaction of the *exo*-lone pair on the cluster tin atom with metal centers. However, there are no reports of the use of monoanionic

Correspondence to: Andrew S. Weller; e-mail: a.s.weller@bath.ac.uk.
Contract grant sponsor: The Royal Society and the EPSRC.
Contract grant number: GR/S4270/01.

[1-R-*closo*-$SnB_{11}H_{11}$]$^-$ as potential weakly coordinating anion with transition metal fragments, although the potential to use such anions has been recognized [16] and as such they have been recently used to prepare ionic-liquids when partnered with imidazolium cations [17]. This short article reports a preliminary exploration of the transition metal chemistry of [1-R-*closo*-$SnB_{11}H_{11}$]$^-$ in the synthesis of the well-separated ion pair [$Rh(PPh_3)_2$(nbd)][1-Me-*closo*-$SnB_{11}H_{11}$] and its subsequent treatment with dihydrogen to afford $Rh(PPh_3)_2$(1-Me-*closo*-$SnB_{11}H_{11}$). The {$Rh(PPh_3)_2$}$^+$ metal fragment has been chosen to partner the cage as we have previously reported on the synthesis and structures of this cation with anion **I**, and thus serves as a useful comparison to compare with stannaborane **II** [18].

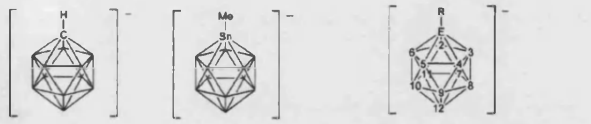

I **II** Numbering scheme for the [1-R-*closo*-$EB_{11}H_{11}$] anions

RESULTS

[$Rh(PPh_3)_2$(nbd)][1-Me-*closo*-$SnB_{11}H_{11}$] **1** is prepared by reaction of [Rh(nbd)Cl]$_2$ (nbd = norbornadiene), [Bu_4N][1-CH_3-*closo*-$SnB_{11}H_{11}$], and PPh_3 in methanol, and has been characterized by multinuclear NMR spectroscopy and microanalysis. In particular, the $^1H\{^{11}B\}$ spectrum shows three BH signals that also show coupling to $^{117/119}Sn$ at δ 2.97 (1H, J(SnH) 87), δ 2.06 (5H, J(SnH) 58), and δ 1.56 (5H, J(SnH) 35). The ^{11}B NMR spectrum ($CDCl_3$) shows two environments, at δ −10.4 (1 B) and δ −15.7 (10 B), and ^{11}B–Sn coupling is not resolved, even in the $^{11}B\{^1H\}$ NMR spectrum. In d_6-acetone, these signals resolve into three signals in the ratio 1:5:5. As it is well established that chemical shifts and J(BH) coupling constants can provide useful spectroscopic guides to the coordination of a cationic metal fragment with [*closo*-$CB_{11}H_{12}$]$^-$ [19], we have performed ^{11}B–^{11}B and ^{11}B–^1H correlation experiments on **1** to establish the identity of the signals. Todd has previously reported the ^{11}B–^{11}B COSY NMR data for the anion [1-Me-*closo*-$SnB_{11}H_{11}$][PPh_3CH_3] [12] and our results concur with these (see Experimental). In addition, a ^1H–^{11}B HMQC experiment allows the assignment of the ^1H signals to specific cluster vertices. These follow the pattern (low field to high field): BH(12), BH(7–11), and BH(2–6). The magnitude of ^1H–Sn coupling follows the reverse order, with BH(12) displaying the largest couple (J(SnH) 87) and BH(2–6) the smallest (J(SnH) 35): a demonstration of the antipodal effect in the NMR spectra of boranes [20]. The $^{31}P\{^1H\}$ NMR spectrum shows a single environment, δ 30.6 (J(RhP) 153).

Treatment of **1** with H_2 in CH_2Cl_2 solution results in a color change from orange to red/orange. $^1H\{^{11}B\}$ and $^{11}B\{^1H\}$ NMR spectroscopy indicate the formation of $Rh(PPh_3)_2$(1-Me-*closo*-$SnB_{11}H_{11}$) **2** (Scheme 1), the structure of which was confirmed in the solid state by an X-ray diffraction study (Fig. 1).

Compound **2** crystallizes with no close intermolecular contacts in the solid state. The refinement shows that the molecule crystallizes with a minor disordered component (10%). For the major (90%) component, the {$Rh(PPh_3)_2$}$^+$ fragment is coordinated through one upper pentagonal belt BH vertex (B2) and one lower pentagonal belt BH vertex (B11) through three center-two electron Rh–H–B interactions. The bond lengths around rhodium (see Table 1) are very similar to those observed in $Rh(PPh_3)_2$(1-H-*closo*-$CB_{11}H_{11}$) [18], Rh(cod)(1-H-*closo*-$CB_{11}H_{11}$) [21], and [($Rh(PPh_3)_2$\{7-Me-8-Ph-*nido*-$C_2B_9H_{10}$)] [22]. The Rh(I) fragment in **2** is square planar (sum of angles 360.0°). In the cluster, the Sn—B distances span the range 2.263(5)–2.323(4) Å which are similar to those observed in the parent [1-Me-*closo*-$SnB_{11}H_{11}$]$^-$ [12] anion, while there are no close contacts between the phenyl groups and the cage methyl group. The minor component in the

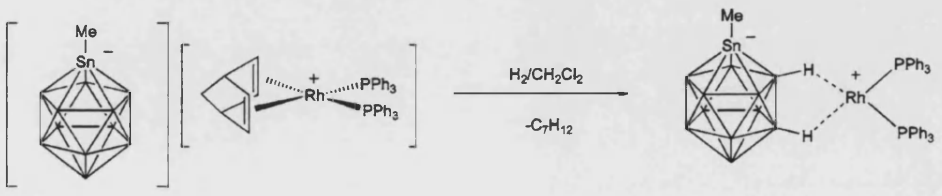

(1) **(2)**

SCHEME 1

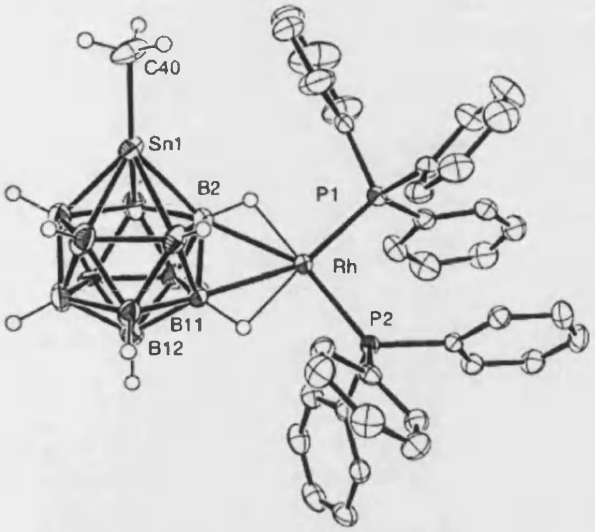

FIGURE 1 Solid-state structure of $Rh(PPh_3)_2$(1-Me-*closo*-$SnB_{11}H_{11}$) **2**. Thermal ellipsoids are shown at the 50% probability level, and hydrogen atoms associated with the phenyl groups are omitted for clarity. The major (90%) disordered component is shown.

crystal resolves best as the 7,8-isomer in which the $\{Rh(PPh_3)_2\}^+$ fragment coordinates to two BH vertices on the lower pentagonal belt. A B–H–[M] interaction between an upper belt BH vertex and an Au(I) center has been noted previously in $[Bu_3MeN][Au(1\text{-}Ph_2PCH_2\text{-}closo\text{-}SnB_{11}H_{11})_2]$ [16].

In solution, NMR spectroscopic data show that the $\{Rh(PPh_3)_2\}^+$ fragment is fluxional over the surface of the cage, affording C_5 symmetry for the anion, in contrast to the C_1 symmetry observed in the solid state. This fluxional process is not frozen out at −70°C in CD_2Cl_2 solution. The ^1H NMR spectrum shows signals due to PPh_3 and Sn–CH_3 in the ratio 30:3. The $^1H\{^{11}B\}$ NMR spectrum reveals three signals assigned to BH that also show coupling to Sn: δ 2.00 (1H, J(SnH) 80), δ 0.53 (5H, J(SnH) 50), and δ 0.05 (5H, J(SnH) ~40). As ^{11}B–^1H HMQC NMR experiments are not suitable for the assignments of these signals due to overlapping peaks in the ^{11}B NMR spectrum (vide infra), the magnitude of the J(SnH) coupling constant has been used to assign the BH signals, using the peak assignments made for **1** as a guide. These follow the order (high field to low field): BH(12), BH(7–11), and BH(2–6). Although this order follows that found in **1**, all the signals are shifted by approximately 1–2 ppm to higher field in **2**. Specifically, BH(12) is shifted by $\Delta\delta$ −0.97, BH(7–11) $\Delta\delta$ −1.53, and BH(2–6) $\Delta\delta$ −1.51. It is well established that the coordination of a metal fragment *exo* to the cage results in upfield chemical shift changes for those BH vertices interacting with the metal [18,23,24]. That BH(2–6) and BH(7–11) are shifted more than BH(12) suggests that, in solution, the $\{Rh(PPh_3)_2\}^+$ fragment interacts on the NMR timescale more with the BH(2–11) vertices and less with BH(12), consistent with the observed solid state structure that shows 2,11-coordination. The ^{11}B NMR spectrum shows two signals at δ −14.0 and δ −17.8, in the ratio 1:10—the latter being a 5 + 5 coincidence. These signals have also been shifted upfield from **1**, by ca. $\Delta\delta$ −4 ppm, again suggesting that the $\{Rh(PPh_3)_2\}^+$ fragment interacts with the entire BH surface of the cage anion.

DISCUSSION

Reduction of the norbornadiene ligand in **1** with H_2 results in a coordinatively unsaturated $\{Rh(PPh_3)_2\}^+$ fragment that coordinates with the stannaborane [1-Me-*closo*-$SnB_{11}H_{11}]^-$ anion through two B—H—Rh three center-two electron bonds. Both the solid state and solution data for **2** can be contrasted with those for the carborane anion complexes $Rh(PR_3)_2$(1-H-*closo*-$CB_{11}H_{11}$) (R = Ph **III** [18], Cy **IV** [19]) (Scheme 2). Both **III** and **IV** show interactions with the lower hemisphere of the carborane cage. In solution, the $^1H\{^{11}B\}$ NMR spectra show this by large ($\Delta\delta$ca. −5 ppm) upfield shifts of BH(12), smaller shifts for B(7–11) of $\Delta\delta$a. −1 to −2 ppm and virtually no chemical shift change for B(2–6). Similar chemical shift changes are also observed

TABLE 1 Selected Bond Lengths (Å) and Angles (°) for **2**

Bond length (Å)					
Rh—P1	2.2155(8)	Rh—P2	2.2417(8)	Rh—B2	2.369(4)
Rh—B11	2.372(4)	Sn—B2	2.273(4)	Sn—B3	2.292(4)
Sn—B4	2.263(5)	Sn—B5	2.322(5)	Sn—B6	2.323(4)
Rh—H2	1.85(4)	Rh—H11	1.89(3)		
Bond angle (°)					
P1—Rh—P2	95.64(3)	P1—Rh—B2	111.53(10)	B2—Rh—B11	42.71(13)
B11—Rh—P2	110.15(9)	C40—Sn1—B12	173.1(1)		

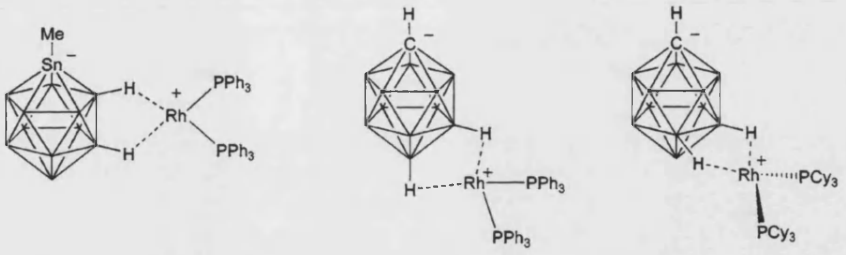

(2) III IV

SCHEME 2

in the $^{11}B\{^1H\}$ NMR spectrum. In the solid state, **III** coordinates through BH(12)/BH(7) while **IV** coordinates through BH(7)/BH(8), both being consistent with NMR data and with the model complex $Rh(PMe_3)_2$(1-H-*closo*-$CB_{11}H_{11}$) in which there is essentially no difference energetically between these two isomers [19]. In contrast, stannaborane **2** coordinates in the solid state through one upper pentagonal belt BH vertex and one lower pentagonal belt vertex. However, in solution, the metal fragment must be fluxional over the *whole* BH surface as all the BH signals show upfield shifts on coordination of the $\{Rh(PPh_3)_2\}^+$ fragment. That BH(2–6) and BH(7–11) show larger chemical shifts ($\Delta\delta$ca. −1.5) than BH(12) ($\Delta\delta$ca. −1) suggests that the metal fragment spends relatively less time coordinated with BH(12) on the NMR timescale.

The different coordination modes of the $\{Rh(PPh_3)_2\}^+$ fragment between the stannaborane and carborane cages can be explained at a basic level—ignoring the orbital contributions to the bonding—by using a simple analysis of the charge distribution in the two cages. For [1-H-*closo*-$CB_{11}H_{11}]^-$, the relative electronegativity of carbon and boron means that upper belt vertices, BH(2–6), would be expected to be relatively positively charged, while the lower hemisphere of the cage would be relatively negatively charged. Previous calculations at the DFT level have confirmed this [4,25]. For comparison with [1-Me-*closo*-$SnB_{11}H_{11}]^-$, we have performed calculations at the B3LYP/DZVP level on [1-Me-*closo*-$CB_{11}H_{11}]^-$ and this shows a very similar charge distribution (based on NBO analysis) as reported previously for [1-H-*closo*-$CB_{11}H_{11}]^-$ [4,25] (Fig. 2). For the stannaborane [1-Me-*closo*-$SnB_{11}H_{11}]^-$, this polarization would be expected to be reversed, as the tin is electropositive compared with boron, and DFT calculations show all the BH vertices as having a negative charge, with BH(2–6) being more negative, followed by BH(7–11) and BH(12) (Fig. 2). On purely electrostatic grounds, coordination of a metal fragment with [*closo*-$CB_{11}H_{12}]^-$ would be expected to occur with the lower hemisphere of the cage—as is observed both in the solid state (e.g., **III** and **IV**) and in solution. With [1-Me-*closo*-$SnB_{11}H_{11}]^-$, having all BH vertices negatively charged, a metal fragment would be expected to coordinate with the entire BH surface of the cage. That, for **2**, all the BH signals shift to high-field in the $^1H\{^1B\}$ and ^{11}B NMR spectra, with B(2–11) shifting the most, and the X-ray structure shows coordination of the metal fragment to BH(2) and BH(11), is consistent with this analysis.

CONCLUSIONS

The synthesis of [1-Me-1-*closo*-$SnB_{11}H_{11}$][NBu_4] in multigram quantities from Na[BH_4] suggests that it might be a more accessible alternative to [*closo*-$CB_{11}H_{12}]^-$, the derivatives of which have been shown to be some of the most robust weakly coordinating anions currently known. Although this cage is relatively tightly bound to metal fragment in **2**, it is well documented that introducing between 6 and 11 halogen or methyl groups to the periphery of [*closo*-$CB_{11}H_{12}]^-$ make the resulting anion significantly more weakly coordinating. It will be interesting to see if analogous derivatives of [1-Me-1-*closo*-$SnB_{11}H_{11}]^-$ can be prepared and if these show the same attractive properties as their carborane analogous.

EXPERIMENTAL

General

All manipulations were carried out under an atmosphere of argon, using standard Schlenk-line and glove-box techniques. Glassware were pre-dried in an oven at 130°C and flamed with a blowtorch under vacuum prior to use. Solvents were purified using an MBaun SPS column system. CD_2Cl_2 was dried over

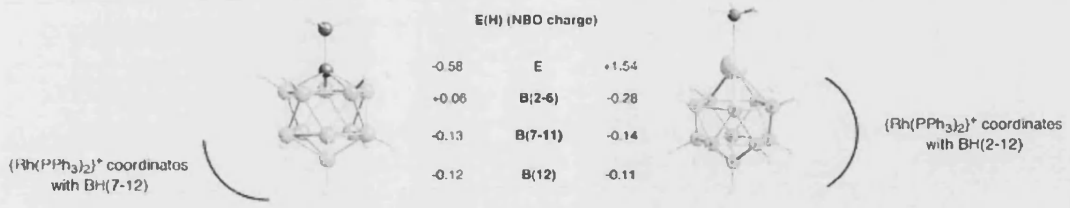

FIGURE 2 Charges on each unique {BH} and {E} vertex as calculated by the NBO analysis at the B3LYP/DZVP level.

CaH_2 and distilled under vacuum. $[Rh(nbd)Cl]_2$ [26] was prepared as described previously. $[Bu_4N][1\text{-}CH_3\text{-}closo\text{-}SnB_{11}H_{11}]$ was prepared by addition of MeI to $[NBu_4]_2[closo\text{-}SnB_{11}H_{11}]$ as described by Todd for the $[MePPh_3]$ salt [12]. The $[NBu_4]_2[closo\text{-}SnB_{11}H_{11}]$ is prepared exactly as outlined by Todd [12] for $[MePPh_3]_2[closo\text{-}SnB_{11}H_{11}]$ from $[Me_3NH][B_{11}H_{14}]$ substituting $[NBu_4]Cl$ for $[MePPh_3]Cl$ in the final step. Microanalyses were performed by Mr. Alan Carver (University of Bath microanalytical service).

NMR Spectroscopy

^1H, $^1H\{^{11}B\}$, ^{11}B, $^{11}B\{^1H\}$, and $^{31}P\{^1H\}$ NMR spectra were recorded on Bruker Avance 300 or 400 MHz spectrometers. Residual protio solvent was used as reference for ^1H. ^{11}B and ^{31}P were referenced to external $BF_3{\cdot}OEt_2$ and 85% H_3PO_4, respectively. Values are quoted in ppm. Coupling constants are given in Hz.

X-ray Crystallography

The crystal structure data for **2** were collected on a Nonius KappaCCD diffractometer with details provided in Table 2. Structure solution, followed by full-matrix least squares refinement was performed using the SHELXL suite of programs throughout [27]. Hydrogen atoms were included in calculated positions apart from those associated with the Rh—H—B bonds, which were located in the final difference map and refined without constraints. Crystallographic data files have been deposited with the Cambridge Crystallographic Data Centre (CCDC xxxxxx), 12 Union Road, Cambridge CB2 1EZ, UK; Tel.: (+44) 1223-336-408; Fax: (+44) 1223-336-033; e-mail: deposit@ccdc.cam.ac.uk.

$[Rh(PPh_3)_2(nbd)][1\text{-}Me\text{-}closo\text{-}SnB_{11}H_{12}]$ **1**. $[Rh(nbd)Cl]_2$ (39.2 mg, 0.085 mmol) was placed in a Schlenk tube and MeOH (5 cm^3) added via cannula to give a yellow suspension. After addition of triphenylphosphine (89.1 mg, 0.34 mmol), the reaction mixture was stirred until complete dissolution. Addition of $[Bu_4N][1\text{-}CH_3\text{-}closo\text{-}SnB_{11}H_{11}]$ (86.0 mg, 0.17 mmol) led to the formation of an orange precipitate, which was washed with cold MeOH (2 × 1 mL) and dried under vacuum. The product was recrystallized from CH_2Cl_2/pentane to afford 107 mg (0.108 mmol, yield = 64%).

NMR data (assignments from ^{11}B–^{11}B COSY and ^{11}B–^1H HMQC). δ $^1H\{^{11}B\}$ ($CDCl_3$, 298 K): 7.34 (m, 30H, Ph), 4.50 (s, 4H, nbd), 4.11 (s, 2H, nbd), 2.97 (s, 1H, BH(12), J(SnH) 87), 2.06 (s, 5H, BH(7–11), J(SnH) 58), 1.69 (s, 3H, Sn—CH_3, J(SnH) 88), 1.56 (s, 5H, BH(2–6), J(SnH) 35). $\delta^{11}B$ ($CDCl_3$, 298 K): −10.4 (d, 1B, B(12), J(HB) 133), −15.7 (d, 10B, B(2–11), J(HB) 153). $\delta^{11}B$ ($(CD_3)_2CO$, 298 K): −11.5 (d, 1B, B(12), J(HB) 134), −16.6 (d, 5B, B(7–11), J(HB) 116), −17.4 (d, 5B, B(2–6), J(HB) 122). $\delta^{31}P$ ($CDCl_3$, 298 K): 30.6 (d, 2P, J(RhP) 153). $C_{46}H_{58}B_{11}P_2RhSn$ requires: C, 54.52; H, 5.77%; Found: C 54.1, H 6.68%.

$Rh(PPh_3)_2(1\text{-}Me\text{-}closo\text{-}SnB_{11}H_{11})$ **2**. $[Rh(PPh_3)_2(nbd)][1\text{-}CH_3\text{-}closo\text{-}SnB_{11}H_{11}]$ (10 mg, 0.010 mmol) was placed in a 15 cm^3 Young's ampoule and CH_2Cl_2 (4 cm^3) was added via cannula. The solution was freeze–pump–thawed three times. After the third cycle, the solution was opened to a H_2 atmosphere (1 atm). The ampoule was closed and the solution stirred for 30 min. Then, the solvent was evaporated and the red residue dried in vacuo. Yield was quantitative by NMR spectroscopy. Crystals suitable for an X-ray diffraction study were grown from a CD_2Cl_2/pentane solution at room temperature.

NMR data. δ $^1H\{^{11}B\}$ (CD_2Cl_2, 298 K): 7.40 (m, 12H, Ph), 7.28 (m, 6H, Ph), 7.14 (m, 12H, Ph), 2.00 (s, 1H, BH(12), J(SnH) 80), 1.53 (s, 3H, Sn—CH_3, J(SnH) 92), 0.53 (s, 5H, B(7–11), J(SnH) 50), 0.05 (s, 5H, BH(2–6), J(SnH) ~40). $\delta^{11}B$ (CD_2Cl_2, 298 K): −14.0 (d, 1B, B(12), J(HB) 129), −17.8 (d, 5 + 5 coincidence, J(HB) 120). $\delta^{31}P$ (CD_2Cl_2, 298 K): 45.7 (d, 2P, J(RhP) 188). $C_{37}H_{44}B_{11}P_2RhSn$ requires: C, 49.86; H, 4.98%; Found: C 50.5, H 4.94%.

DFT Calculations

The Gaussian 98 program was employed with the DZVP basis set for B3LYP gas-phase geometry

TABLE 2 Crystal Data and Structure Refinement for Compound **1**

Empirical formula	$C_{37}H_{44}B_{11}P_2RhSn$
Formula weight	891.17
Temperature (K)	150(2)
Wavelength (Å)	0.71073
Crystal system	Monoclinic
Space group	*C2/c*
a (Å)	32.1840(3)
b (Å)	32.1840(3)
c(Å)	18.9180(2)
α (°)	90
β(°p)	117.4640(10)
(γ°)	90
Volume (Å^3)	7971.77(16)
Z	8
Density (calculated) (mg/m^3)	1.485
Absorption coefficient (mm^{-1})	1.149
F(0 0 0)	3568
Crystal size (mm)	0.40 × 0.33 × 0.33
Theta range for data collection (°)	3.02–27.53
Reflections collected	68622
Independent reflections	9139 (R_{int} = 0.0697)
Absorption correction	Semi-empirical from equivalents
Data Completeness	99.4
Refinement method	Full-matrix least-squares on F^2
Data/restraints/parameters	9139/0/495
Goodness-of-fit on F^2	1.143
Final *R* indices ($I > 2\sigma(I)$)	R_1 = 0.0481, wR_2 = 0.0803
R indices (all data)	R_1 = 0.0650, wR_2 = 0.0847
Largest diff. peak and hole (e Å^{-3})	0.999 and −0.879

optimizations, using the Berny routine algorithm [28]. No symmetry constraints were imposed, and the nature of each stationary point was verified through frequency calculations.

REFERENCES

[1] (a) Macchioni, A. Chem Rev 2005, 105, 2039; (b) Krossing, I.; Raabe, I. Angew Chem, Int Ed 2004, 43, 2066.

[2] Reed, C. A. Chem Commun 2005, 1669.

[3] Reed, C. A. Acc Chem Res 1998, 31, 133.

[4] Zharov, I.; Weng, T.-C.; Orendt, A. M.; Barich, D. H.; Penner-Hahn, J.; Grant, D. M.; Havlas, Z.; Michl, J. J Am Chem Soc 2004, 126, 12033.

[5] Ingleson, M. J.; Patmore, N. J.; Kociok-Köhn, G.; Mahon, M. F.; Ruggiero, G. D.; Weller, A. S.; Clarke, A. J.; Rourke, J. P. J Am Chem Soc 2004, 126, 1503.

[6] Chen, E. Y. X.; Marks, T. J Chem Rev 2000, 100, 1391.

[7] Batsanov, A. S.; Fox, M. A.; Goeta, A. E.; Howard, J. A. K.; Hughes, A. K.; Malget, J. M. J Chem Soc, Dalton Trans 2002, 2624.

[8] Brellochs, B.; Backovsky, J.; Stibr, B.; Jelinek, T.; Holub, J.; Bakardjiev, M.; Hnyk, D.; Hofmann, M.; Cisarova, I.; Wrackmeyer, B. Eur J Inorg Chem 2004, 3605.

[9] Franken, A.; King, B. T.; Rudolph, J.; Rao, P.; Noll, B. C.; Michl, J. Coll Czech Chem Commun 2001, 66, 1238.

[10] Korbe, S.; Sowers, D. B.; Franken, A.; Michl, J. Inorg Chem 2004, 43, 8158.

[11] Ivanov, S. V.; Davis, J. A.; Miller, S. M.; Anderson, O. P.; Strauss, S. H. Inorg Chem 2003, 42, 4489.

[12] Chapman, R. W.; Kester, J. G.; Folting, K.; Streib, W. E.; Todd, L. J. Inorg Chem 1992, 31, 979.

[13] Wesemann, L. Z. Anorg All Chem 2004, 630, 1349.

[14] Marx, T.; Mosel, B.; Pantenburg, I.; Hagen, S.; Schulze, H.; Wesemann, L. Chem Eur J 2003, 9, 4472.

[15] Hagen, S.; Pantenburg, I.; Weigend, F.; Wickleder, C.; Wesemann, L. Angew Chem 2003, 42, 1501.

[16] Ronig, B.; Schulze, H.; Pantenburg, I.; Wesemann, L. Eur J Inorg Chem 2005, 314.

[17] Ronig, B.; Pantenburg, I.; Wesemann, L. Eur J Inorg Chem 2002, 319.

[18] Rifat, A.; Patmore, N. J.; Mahon, M. F.; Weller, A. S. Organometallics 2002, 21, 2856–2865.

[19] Rifat, A.; Laing, G.; Kociok-Köhn, G.; Mahon, M. F.; Ruggiero, G. D.; Weller, A. S. J Organometal Chem 2003, 680, 127.

[20] Hermánek, S. Chem Rev 1992, 92, 325.

[21] Weller, A. S.; Mahon, M. F.; Steed, J. W. J Organomet Chem 2000, 614–615, 113–119.

[22] Knobler, C. B.; Marder, T. B.; Mizusawa, E. A.; Teller, R. G.; Long, J. A.; Behnken, P. E.; Hawthorne, M. F. J Am Chem Soc 1984, 106, 2990.

[23] Patmore, N. J.; Mahon, M. F.; Steed, J. W.; Weller, A. S. J Chem Soc, Dalton Trans 2001, 277.

[24] Crowther, D. J.; Borkowsky, S. L.; Swenson, D.; Meyer, T. Y.; Jordan, R. F. Organometallics 1993, 12, 2897–2903.
[25] McKee, M. L. J Am Chem Soc 1997, 119, 4220.
[26] Haines, L. M. Inorg Chem 1970, 9, 1517.
[27] Sheldrick, G. M. SHELX-97. University of Göttingen; A computer program for refinement of crystal structures; 1997.
[28] Frisch, M. J.; Trucks, G. W.; Schlegel, H. B.; Scuseria, G. E.; Robb, M. A.; Cheeseman, J. R.; Zakrzewski, V. G.; Montgomery, J. A.; Stratmann, R. E.; Burant, J. C.; Dapprich, S.; Millam, J. M.; Daniels, A. D.; Kudin, K. N.; Strain, M. C.; Farkas, O.; Tomasi, J.; Barone, V.; Cossi, M.; Cammi, R.; Mennucci, B.; Pomelli, C.; Adamo, C.; Cliord, S.; Ochterski, J.; Petersson, G. A.; Ayala, P. Y.; Cui, Q.; Morokuma, K.; Malick, D. K.; Rabuck, A. D.; Raghavachari, K.; Foresman, J. B.; Cioslowski, J.; Ortiz, J. V.; Stefanov, B. B.; Liu, G.; Liashenko, A.; Piskorz, P.; Komaromi, I.; Gomperts, R.; Martin, R. L.; Fox, D. J.; Keith, T.; Al-Laham, M. A.; Peng, C. Y.; Nanayakkara, A.; Gonzalez, C.; Challacombe, M.; Gill, P. M. W.; Johnson, B.; Chen, W.; Wong, M. W.; Andres, J. L.; Gonzalez, C.; Head-Gordon, M.; Replogle, E. S.; Pople, J. A.; Gaussian, Inc.: Pittsburgh, PA, 1998.

Rhodium Phosphine Olefin Complexes of the Weakly Coordinating Anions $[BAr^F_4]^-$ and $[1\text{-}closo\text{-}CB_{11}H_6Br_6]^-$. Kinetic versus Thermodynamic Factors in Anion Coordination and Complex Reactivity

Thomas M. Douglas, Eduardo Molinos, Simon K. Brayshaw, and Andrew S. Weller*

Department of Chemistry, University of Bath, Bath BA2 7AY, U.K.

Received October 23, 2006

Summary: Solution and solid-state structures for the pair of complexes $Rh\{P(Cyp_2)(\eta^2\text{-}C_5H_7)\}\{\eta^6\text{-}(C_6H_3(CF_3)_2)BAr^F_3\}$ *and* $Rh\{P(Cyp_2)(\eta^2\text{-}C_5H_7)\}(1\text{-}closo\text{-}CB_{11}H_6Br_6)$*, which contain bound weakly coordinating anions, are reported. While thermochemical data show that enthalpically* $[1\text{-}closo\text{-}CB_{11}H_6Br_6]^-$ *binds less strongly with the metal fragment and it is the large entropy loss for the overall process of coordination of the* $[BAr^F_4]^-$ *anion that results in the latter anion being thermodynamically more weakly coordinating. Qualitative kinetic data arising from reaction with* H_2 *indicates that the carborane anion is displaced more readily, attributable to the ability of the carborane to lift a Rh−Br interaction.*

The $[1\text{-}closo\text{-}CB_{11}H_6Br_6]^-$- and $[BAr^F_4]^-$-type anions (Chart 1; $Ar^F = C_6H_3(CF_3)_2$) are commonly referred to as being among the least nucleophilic and most stable anions known.[1] Comparisons between these classes of anions have been reported in terms of the synthesis of free silylium cations[2] and protonated arenes,[3] in relative anion basicities,[4] and in catalysis when partnered with cationic transition-metal fragments.[5] The solid-state structures of Ag^+ salts of these two anions are also known.[6,7] However, systems where a direct structural and thermochemical comparison can be made between the coordination properties of these counterions when they are partnered with transition-metal fragments, as far as we are aware, have not been reported. This is because, in order to do this, each anion must cleanly form a complex in both the solution and the solid state with the transition-metal fragment, and this is understandably difficult to achieve, given their weakly coordinating properties. Thermochemical data are well established for early-transition-metal (metallocene) cations partnered with $[MeB(Ar^F_3)]^-$ anions where complexes between cation and anion can be systematically made.[8] We communicate here the synthesis and solid-state and solution structures of a cationic rhodium phosphine fragment partnered with either a coordinated $[BAr^F_4]^-$ or $[1\text{-}closo\text{-}CB_{11}H_6Br_6]^-$ anion. This affords, for the first time we believe, a comparison of simple structural, thermodynamic, and kinetic factors that influence anion coordination between these two anions.

Chart 1

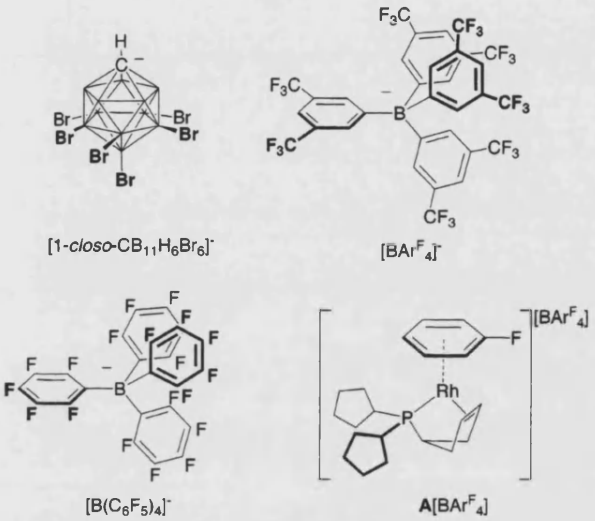

Scheme 1

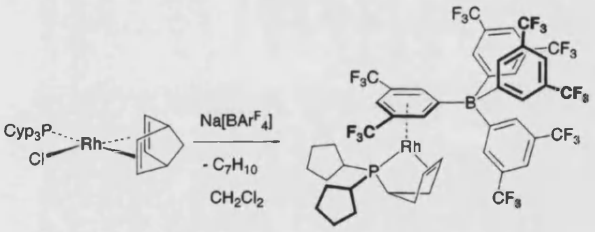

We have recently reported that addition of $Na[BAr^F_4]$ to $Rh(nbd)(PCyp_3)Cl$ ($PCyp_3$ = tricyclopentylphosphine) in fluorobenzene solvent results in the elimination of NaCl and the facile dehydrogenation of one of the cyclopentyl groups to afford $[Rh(\eta^6\text{-}C_6H_5F)\{P(Cyp_2)(\eta^2\text{-}C_5H_7)\}][BAr^F_4]$ ($A[BAr^F_4]$; Chart 1), which has a chelating phosphine−olefin ligand and coordinated fluorobenzene ligand.[9] We reasoned that repeating this reaction in CH_2Cl_2, a solvent much less likely to coordinate to

* To whom correspondence should be addressed. E-mail: a.s.weller@bath.ac.uk. Fax: +44 (0)1225 383394.

(1) Krossing, I.; Raabe, I. *Angew. Chem., Int. Ed.* **2004**, *43*, 2066−2090. Reed, C. A. *Acc. Chem. Res.* **1998**, *31*, 133−139. Reed, C. A. *Chem. Commun.* **2005**, 1669−1677.

(2) Kim, K. C.; Reed, C. A.; Elliott, D. W.; Mueller, L. J.; Tham, F.; Lin, L. J.; Lambert, J. B. *Science* **2002**, *297*, 825−827. Lambert, J. B.; Zhao, Y. *Angew. Chem., Int. Ed.* **1997**, *36*, 400−401.

(3) Reed, C. A.; Kim, K. C.; Stoyanov, E. S.; Stasko, D.; Tham, F. S.; Mueller, L. J.; Boyd, P. D. W. *J. Am. Chem. Soc.* **2003**, *125*, 1796−1804. Reed, C. A.; Fackler, N. L. P.; Kim, K. C.; Stasko, D.; Evans, D. R.; Boyd, P. D. W.; Rickard, C. E. F. *J. Am. Chem. Soc.* **1999**, *121*, 6314−6315.

(4) Stoyanov, E. S.; Kim, K. C.; Reed, C. A. *J. Am. Chem. Soc.* **2006**, *128*, 8500−8508.

(5) Macchioni, A. *Chem. Rev.* **2005**, *105*, 2039−2073.

(6) Powell, J.; Lough, A.; Saeed, T. *J. Chem. Soc., Dalton Trans.* **1997**, 4137−4138.

(7) Xie, Z. W.; Jelinek, T.; Bau, R.; Reed, C. A. *J. Am. Chem. Soc.* **1994**, *116*, 1907−1913.

(8) Deck, P. A.; Beswick, C. L.; Marks, T. J. *J. Am. Chem. Soc.* **1998**, *120*, 1772−1784.

(9) Douglas, T. M.; Le Notre, H.; Brayshaw, S. K.; Frost, C. G.; Weller, A. S. *Chem. Commun.* **2006**, 3408−3410.

10.1021/om060975d CCC: $37.00
Publication on Web 12/20/2006

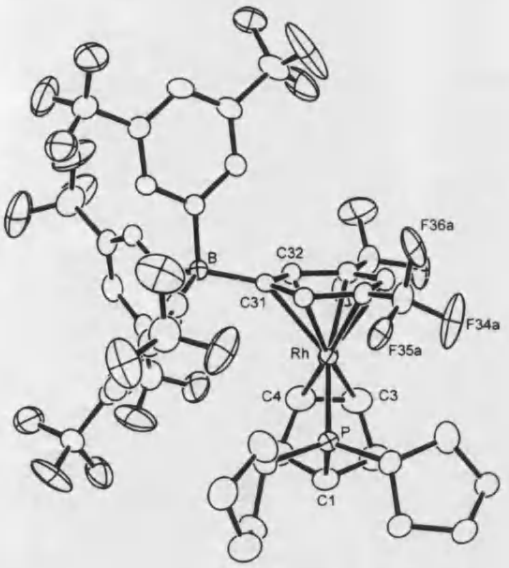

Figure 1. Solid-state structure of **1**. Thermal ellipsoids are shown at the 50% probability level. Hydrogen atoms are omitted for clarity. Selected bond lengths (Å) and angles (deg): Rh−C(31) = 2.426(3), Rh−C(32) = 2.308(3), Rh−P = 2.2608(8), Rh−C(4) = 2.131(3), Rh−C(3) = 2.158(3); B−C(31)−C(34) = 167.3(2).

the metal center, would afford the new complex Rh{P(Cyp$_2$)-(η^2-C$_5$H$_7$)}{η^6-(C$_6$H$_3$(CF$_3$)$_2$)BAr$^F_3$} (**1**), in which the [BAr$^F_4$]$^-$ anion is now a ligand coordinated through one of its aryl rings. This is indeed the case, and complex **1** can be isolated in 54% yield (Scheme 1). Solutions of **1** slowly decompose to unidentified products, some of which appear to have undergone B−C cleavage of the anion.[10] The solid-state structure of **1** is shown in Figure 1 and clearly demonstrates the η^6 coordination of the weakly coordinating [BAr$^F_4$]$^-$ anion through one of its aryl rings (d(Rh−C$_{aryl}$) = 2.263(3)−2.426(3) Å), with the longest Rh−C$_{aryl}$ interaction being not surprisingly with the ipso carbon, C(31). Solution NMR data demonstrate that the anion also remains coordinated in CD_2Cl_2 solution. In particular the coordinated aryl protons are shifted upfield in the ^{1}H NMR spectrum and the ^{19}F NMR spectrum displays two environments in the ratio 1:3. As far as we are aware, there are only two other examples of [BAr$^F_4$]$^-$ coordinated to a metal center, with {Rh(cod)}$^+$ and Ag$^+$ fragments,[6] while there are only a handful of crystallographically characterized examples of the analogous [B(C$_6$F$_5$)$_4$]$^-$ anion coordinated through M···F interactions, all with early transition metals or lanthanides.[11] Although it is η^6-coordinated, the [BAr$^F_4$]$^-$ anion in **1** can be displaced by weak ligands. Addition of 1 equiv of fluorobenzene establishes an equilibrium between **1** and **A**[BAr$^F_4$], so that a ratio of 1:1, respectively, is observed at 298 K. Addition of excess fluorobenzene affords **A**[BAr$^F_4$] quantitatively.

In order to compare the two anions, we have developed a synthesis of the complex directly analogous to **1** with the [1-*closo*-CB$_{11}$H$_6$Br$_6$]$^-$ anion (Scheme 2). Reaction of the hydrogen acceptor *tert*-butylethene with Rh(PCyp$_3$)H$_2$(1-*closo*-CB$_{11}$H$_6$Br$_6$) (**3**; see the Supporting Information for the synthesis

Scheme 2

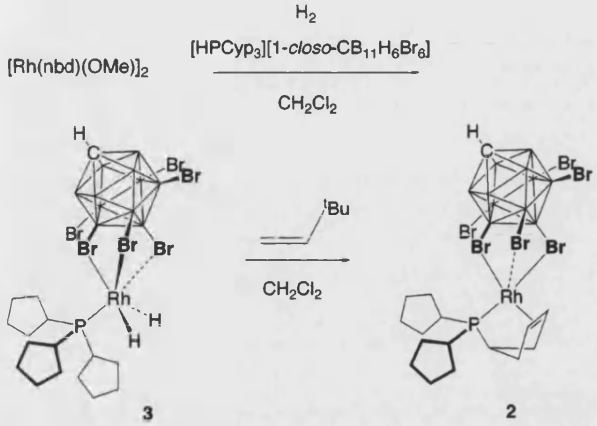

of **3**) results in the dehydrogenation of one cyclopentyl ring and formation of Rh{P(Cyp$_2$)(η^2-C$_5$H$_7$)}(1-*closo*-CB$_{11}$H$_6$Br$_6$) (**2**) in 69% isolated yield. By comparison, the analogous complex using the [1-*closo*-CB$_{11}$H$_6$Cl$_6$]$^-$ anion could not be prepared cleanly by this route. The solid-state structure of **2** is shown in Figure 2. The carborane anion coordinates with the rhodium fragment through three Rh−Br interactions. One of these is significantly longer than the other two (2.9514(6) Å versus 2.6504(5), 2.6702(5) Å), and we describe the geometry of **2** as pseudo trigonal bipyramidal with one weaker equatorial Rh···Br interaction. In solution (CD_2Cl_2) the anion is fluxional, as C_{5v} symmetry is observed for the boron cage, in contrast to the approximate C_s symmetry observed in the solid state. As with **1**, addition of 1 equiv of fluorobenzene to **2** results in an equilibrium between **2** and **A**[1-*closo*-CB$_{11}$H$_6$Br$_6$], being observed in a 1:2.7 ratio, respectively. Addition of an excess of fluorobenzene results in the quantitative formation of **A**[1-*closo*-CB$_{11}$H$_6$Br$_6$], which has been spectroscopically characterized by independent synthesis (see the Supporting Information).

With complexes **1** and **2** in hand, we have a unique opportunity to determine the relative strengths of binding of these two anions with a late-transition-metal fragment. Addition of 1 equiv of [NBu$_4$][BAr$^F_4$] to **2** slowly (hours at 298 K) establishes an equilibrium between **1** and **2** (Scheme 3). Measuring the relative ratios of these two complexes over the

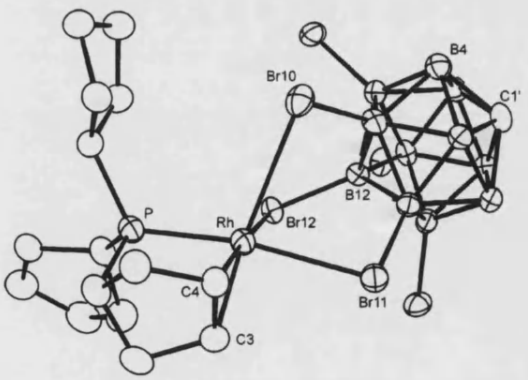

Figure 2. Solid-state structure of **2**. Thermal ellipsoids are shown at the 50% probability level. Hydrogen atoms are omitted for clarity. Selected bond lengths (Å) and angles (deg): Rh−Br(11) = 2.6504(5), Rh−Br(12) = 2.6702(5), Rh−Br(10) = 2.9514(6), Rh−P = 2.197(1), Rh−C(4) = 2.077(5), Rh−C(3) = 2.109(5); P−Rh−centC(3)/C(4) = 84.0(2), Br(12)−Rh−centC(3)/C(4) = 153.8(2), P−Rh−Br(11) = 171.32(4).

(10) Konze, W. V.; Scott, B. L.; Kubas, G. J. *J. Chem. Soc., Chem. Commun.* **1999**, 1807−1808.

(11) Bouwkamp, M. W.; Budzelaar, P. H. M.; Gercama, J.; Del, Hierro, Morales, I.; de Wolf, J.; Meetsma, A.; Troyanov, S. I.; Teuben, J. H.; Hessen, B. *J. Am. Chem. Soc.* **2005**, *127*, 14310−14319. Yang, X. M.; Stern, C. L.; Marks, T. J. *J. Am. Chem. Soc.* **1994**, *116*, 10015−10031. Yang, X. M.; Stern, C. L.; Marks, T. *J. Organometallics* **1991**, *10*, 840−842.

Scheme 3[a]

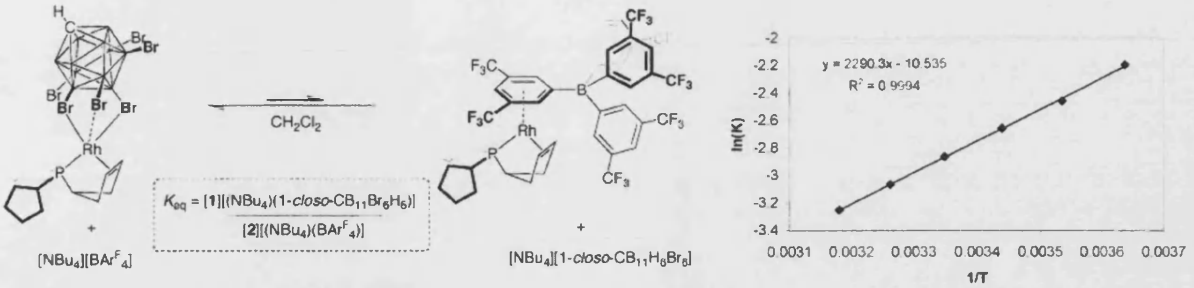

[a] The insert gives a van't Hoff plot for the equilibrium established between **1** and **2**.

temperature range 275−313 K[13] affords a van't Hoff plot from which $\Delta H° = -19.0 \pm 0.3$ kJ mol^{-1}, $\Delta S° = -87.6 \pm 0.8$ J K^{-1} mol^{-1}, and $\Delta G°(298) = +7.0 \pm 0.5$ kJ mol^{-1} were determined. Interestingly, this shows that although enthalpically the $[BAr^F_4]^-$ anion binds more strongly than the carborane anion ($\Delta H°$ is negative), it is the large negative entropic contribution involved in the coordination of the $[BAr^F_4]^-$ anion/dissociation and solvation of the carborane anion that overall results in the [1-*closo*-$CB_{11}H_6Br_6]^-$ anion being marginally favored ($\Delta G°$ is small but positive). Addition of 1 equiv of [NBu_4][1-*closo*-$CB_{11}H_6Cl_6$], an anion which is ranked as being less basic that its bromo congener,[4] to **2** did *not* result in an equilibrium being established to the detection limits of ^{1}H and ^{31}P NMR spectroscopy after 24 h at room temperature, with **2** remaining unchanged and no decomposition observed. This demonstrates that, in this system at least, [1-*closo*-$CB_{11}H_6Cl_6]^-$ must be more weakly coordinating even than $[BAr^F_4]^-$.

Reaction of H_2 (1 atm, 298 K) with **2** affords **3** in 3 h, whereas no reaction is observed with **1**, even after 12 h. We explain this by the $[BAr^F_4]^-$ anion being unable to create a vacant site on the 18-electron metal center in **1** required for addition of H_2, whereas the [1-*closo*-$CB_{11}H_6Br_6]^-$ can presumably lift the already weak Rh−Br interaction to reveal a reactive 16-electron rhodium center. With stronger ligands such as THF or MeCN reaction is effectively instantaneous for both to form the previously reported metal fragment [Rh{P(Cyp_2)(η^2-C_5H_7)}-$(L)_2]^+$ (L = MeCN, THF).[9]

In conclusion we report a rare example of $[BAr^F_4]^-$ coordinated to a transition-metal center and present the first comparative structural, thermodynamic, and reactivity data with the weakly coordinating carborane anion [1-*closo*-$CB_{11}H_6Br_6]^-$ in a transition-metal system. These show that although the $[BAr^F_4]^-$ anion forms a slightly weaker complex than [1-*closo*-$CB_{11}H_6Br_6]^-$, kinetically it is substitutionally less labile with the weak ligand H_2 in the weakly coordinating solvent CH_2Cl_2. This is a consequence of the η^6 binding of the $[BAr^F_4]^-$ compared with the carborane anion that can act in a hemilabile manner. Given that there are a growing number of organic transformations mediated by cationic late-transition-metal fragments in weakly coordinating solvents such as CH_2Cl_2 (e.g. hydrogenation, hydroacylation, cyclizations, and cycloadditions[12]) such subtle differences between anions as we disclose here may prove to be important.

Acknowledgment. We thank the Royal Society and the EPSRC for support.

Supporting Information Available: Text, tables, figures, and CIF files giving full experimental data for the synthesis of complexes **1**, **2**, and **3**, details of the anion exchange experiments, NMR spectra for complex **1**, and crystallographic data for complexes **1** and **2**. This material is available free of charge via the Internet at http://pubs.acs.org.

OM060975D

(12) *Modern Rhodium-Catalysed Organic Reactions*; Evans, P. A., Ed.; Wiley-VCH: Weinheim, Germany, 2005.

(13) The collection of equilibrium data over a wider temperature range was frustrated by the very slow time taken to reach equilibrium at each temperature: e.g., 16 h at 275 K.

Acta Crystallographica Section E
Structure Reports Online
ISSN 1600-5368

catena-Poly[[(tetrafluoroborato-κF)silver(I)]-μ-triphenylphosphine-$\kappa^2 P$:C^3]

Simon K. Brayshaw,* Eduardo Molinos and Andrew S. Weller

Department of Chemistry, University of Bath, Bath BA2 7AY, England

Correspondence e-mail: sb285@bath.ac.uk

Received 29 November 2006
Accepted 15 December 2006

The title compound, $[Ag(BF_4)(C_{18}H_{15}P)]_n$, crystallizes from dichloromethane–pentane as a one-dimensional coordination polymer in which the Ag atom is bound to a phosphine P atom, one F atom of tetrafluoroborate and one C atom of a neighbouring triphenylphosphine ligand.

Key indicators

Single-crystal X-ray study
T = 150 K
Mean σ(C–C) = 0.003 Å
R factor = 0.028
wR factor = 0.072
Data-to-parameter ratio = 22.6

For details of how these key indicators were automatically derived from the article, see http://journals.iucr.org/e.

Comment

Complexes of silver in which close metal–arene interactions are present in the solid state are not uncommon, with the first example reported by Smith & Rundle (1958). Typically, in such complexes, the silver is partnered with weakly or non-coordinating anions such as trifluoromethanesulfonate or perchlorate. On the other hand, there have been few reports of solid state structures of silver complexes which contain bound tetrafluoroborate.

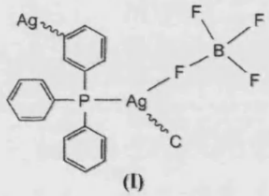

(I)

We have previously described (tertiary phosphine)silver complexes of functionalized 1-*closo*-carborane anions (Patmore *et al.*, 2002; Clarke *et al.*, 2004). Whilst attempting to prepare one such complex from silver tetrafluoroborate and $[(PPh_3)_2Rh(nbd)]\cdot CB_{11}H_7Et_5$ (Molinos *et al.*, 2005), colourless single crystals suitable for an X-ray diffraction experiment were obtained. The crystals were determined to be the title complex, (I), and the results of the diffraction study are described below.

In (I) (Fig. 1), the coordination of the silver is quasi-trigonal, the silver bonding to P, F1 and $C3^i$ [symmetry code: (i) $\frac{3}{2} - x$, $y - \frac{1}{2}$, $\frac{1}{2} - z$], with the silver having only slight deviation from the P—F—C ligand plane [0.0672 (7) Å]. The Ag—$C3^i$ and Ag—F1 distances are long (Table 1), but are consistent with bonding interactions, and the coordination of $C3^i$ results in a one-dimensional coordination polymer. As expected, the coordination of F1 results in a B—F1 distance greater than the other B—F distances.

There are two other Ag···F contacts within van der Waals radii. An Ag···F2 contact is accommodated by a small Ag—F1—B—F2 torsion angle and a reduced F1—B—F2 angle. The effect of this close contact is also seen in an increased P—Ag—F1 angle relative to P—Ag—$C3^i$ and F1—Ag—$C3^i$. Finally, an Ag···F contact occurs between Ag and $F3^{ii}$ [symmetry code:

(ii) $1-x, -y, -z$] in a pairwise manner, with a matching contact between the symmetry-related Ag^{ii} and F3 (Fig. 2).

Experimental

A solution containing equimolar quantities of silver tetrafluoroborate and $[(PPh_3)_2Rh(nbd)]\cdot CB_{11}H_7Et_5$ (Molinos *et al.*, 2005) in dichloromethane was layered with pentanes and held at 278 K for one week to crystallize. A crystal of (I) suitable for a single-crystal X-ray diffraction study was selected directly from the sample.

Crystal data

$[Ag(BF_4)(C_{18}H_{15}P)]$
$M_r = 456.95$
Monoclinic, $P2_1/n$
$a = 12.0606$ (1) Å
$b = 11.2379$ (1) Å
$c = 12.9254$ (1) Å
$\beta = 90.093$ (7)°
$V = 1751.85$ (3) Å^3
$Z = 4$
$D_x = 1.733$ Mg m^{-3}
Mo $K\alpha$ radiation
$\mu = 1.28$ mm^{-1}
$T = 150$ (2) K
Block, colourless
0.33 × 0.25 × 0.18 mm

Data collection

Nonius KappaCCD diffractometer
φ and ω scans
Absorption correction: multi-scan (*SORTAV*; Blessing, 1995)
$T_{min} = 0.678$, $T_{max} = 0.803$
31041 measured reflections
5109 independent reflections
4717 reflections with $I > 2\sigma(I)$
$R_{int} = 0.042$
$\theta_{max} = 30.0°$

Refinement

Refinement on F^2
$R[F^2 > 2\sigma(F^2)] = 0.028$
$wR(F^2) = 0.073$
$S = 1.04$
5109 reflections
226 parameters
H-atom parameters constrained
$w = 1/[\sigma^2(F_o^2) + (0.0322P)^2 + 1.6142P]$ where $P = (F_o^2 + 2F_c^2)/3$
$(\Delta/\sigma)_{max} < 0.001$
$\Delta\rho_{max} = 1.01$ e Å^{-3}
$\Delta\rho_{min} = -1.37$ e Å^{-3}

Table 1
Selected geometric parameters (Å, °).

Ag—P	2.3903 (4)	B—F2	1.372 (3)
Ag—F1	2.4242 (13)	B—F3	1.380 (2)
Ag—C3^i	2.5706 (18)	B—F1	1.411 (3)
B—F4	1.367 (3)		
Ag···F3^{ii}	2.6912 (14)	Ag···F2	2.913 (2)
P—Ag—F1	148.19 (4)	F4—B—F1	109.54 (19)
P—Ag—C3^i	129.96 (5)	F2—B—F1	107.37 (18)
F1—Ag—C3^i	81.56 (6)	F3—B—F1	108.32 (17)
F4—B—F3	109.72 (17)	B—F1—Ag	112.70 (12)
F2—B—F3	110.87 (19)		
Ag—F1—B—F2	−5.7 (2)		

Symmetry codes: (i) $-x+\frac{3}{2}, y-\frac{1}{2}, -z+\frac{1}{2}$; (ii) $-x+1, -y, -z$.

H atoms were located in difference Fourier maps and placed in idealized positions, with C—H = 0.95 Å and with $U_{iso}(H) = 1.2U_{eq}(C)$. The largest peak and deepest hole in the final difference map are located 0.75 and 0.60 Å from the Ag atom, respectively.

Data collection: *COLLECT* (Nonius, 1998); cell refinement: *SCALEPACK* (Otwinowski & Minor 1997); data reduction: *SCALEPACK* and *DENZO* (Otwinowski & Minor, 1997); program(s) used to solve structure: *SIR97* (Altomare *et al.*, 1999); program(s) used to refine structure: *SHELXL97* (Sheldrick, 1997); molecular graphics: *ORTEP-3 for Windows* (Farrugia, 1997); software used to prepare material for publication: *SHELXL97*.

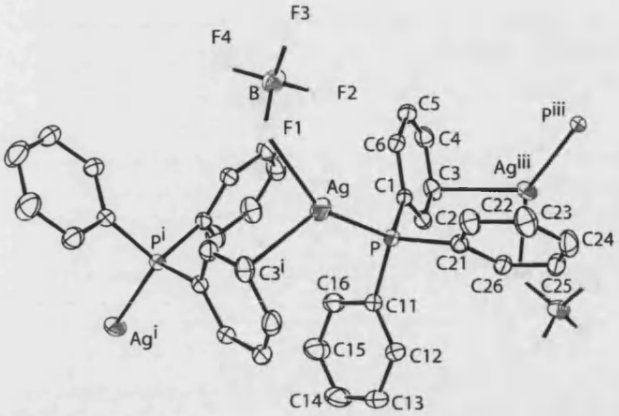

Figure 1
Part of the polymeric structure of (I), showing its polymeric nature. Displacement ellipsoids are shown at the 50% probability level. H atoms have been omitted for clarity. [Symmetry codes: (i) $\frac{3}{2}-x, y-\frac{1}{2}, \frac{1}{2}-z$; (iii) $\frac{3}{2}-x, \frac{1}{2}+y, \frac{1}{2}-z$.]

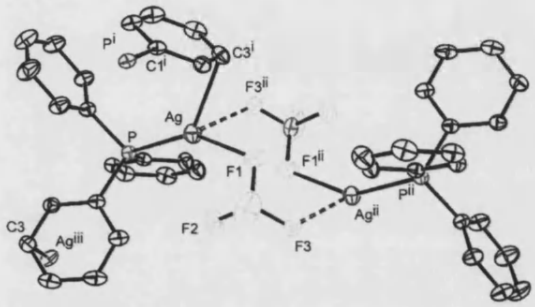

Figure 2
Two asymmetric units of (I), together with neighbouring Ag^{iii} and $C_6H_5P^{ii}$ groups, showing the pairwise packing. Displacement ellipsoids are shown at the 50% probability level. H atoms have been omitted for clarity. [Symmetry codes: (i) $\frac{3}{2}-x, y-\frac{1}{2}, \frac{1}{2}-z$; (ii) $1-x,-y,-z$; (iii) $\frac{3}{2}-x, \frac{1}{2}+y, \frac{1}{2}-z$.]

The EPSCR and Royal Society are thanked for financial support.

References

Altomare, A., Burla, M. C., Camalli, M., Cascarano, G. L., Giacovazzo, C., Guagliardi, A., Moliterni, A. G. G., Polidori, G. & Spagna, R. (1999). *J. Appl. Cryst.* **32**, 115–119.
Blessing, R. H. (1995). *Acta Cryst.* A**51**, 33–38.
Clarke, A. J., Ingleson, M. J., Kociok-Köhn, G., Mahon, M. F., Patmore, N. J., Rourke, J. P., Ruggiero, G. D. & Weller, A. S. (2004). *J. Am. Chem. Soc.* **126**, 1503–1517.
Farrugia, L. J. (1997). *J. Appl. Cryst.* **30**, 565.
Molinos, E., Kociok-Köhn, G. & Weller, A. S. (2005). *Chem. Commun.* pp. 3609–3611.
Nonius (1998). *COLLECT*. Nonius BV, Delft, The Netherlands.
Otwinowski, Z. & Minor, W. (1997). *Methods in Enzymology*, Vol. 276, *Macromolecular Crystallography*, Part A, edited by C. W. Carter Jr & R. M. Sweet, pp. 307–326. New York: Academic Press.
Patmore, N. J., Hague, C., Cotgreave, J. H., Mahon, M. F., Frost, C. G. & Weller, A. S. (2002). *Chem. Eur. J.* **8**, 2088–2098.
Sheldrick, G. M. (1997). *SHELXL97*. University of Göttingen, Germany.
Smith, H. G. & Rundle, R. E. (1958). *J. Am. Chem. Soc.* **80**, 5075–5080.

Organometallics **2007**, *26*, 2370−2382

Sequential Dehydrogenative Borylation/Hydrogenation Route to Polyethyl-Substituted, Weakly Coordinating Carborane Anions

Eduardo Molinos, Simon K. Brayshaw, Gabriele Kociok-Köhn, and Andrew S. Weller*

Department of Chemistry, University of Bath, Bath BA2 7AY, U.K.

Received January 16, 2007

Treatment of $Rh(PPh_3)_2$(1-H-*closo*-$CB_{11}H_{11}$) with ethene results in dehydrogenative borylation to form the vinyl−borate complex $Rh(PPh_3)_2$(1-H-7/12-(H_2C=CH)-*closo*-$CB_{11}H_{10}$) as a mixture of 7- and 12-isomers. Further dehydrogenative borylation does not occur; this is accounted for by the strong binding of the vinylcarborane to the $\{Rh(PPh_3)_2\}^+$ fragment through C=C and B−H interactions. Addition of H_2 results in hydrogenation of the vinyl group and the quantitative formation of the *B*-ethylcarborane complex $Rh(PPh_3)_2$(1-H-7/12-(Et)-*closo*-$CB_{11}H_{10}$). The crystal structure of the norbornadiene adduct of one the isomers, $[Rh(PPh_3)_2(nbd)]$[1-H-12-(H_2C=CH)-*closo*-$CB_{11}H_{10}$], has been determined. Addition of ethene to the complex $Rh(PPh_3)_2$(1-H-12-Br-*closo*-$CB_{11}H_{10}$), in which the 12-position on the cage is blocked, results in only one isomer: $Rh(PPh_3)_2$(1-H-7-(CH_2=CH)-12-Br-*closo*-$CB_{11}H_9$). Sequential addition of ethene/H_2 to $Rh(PPh_3)_2$(1-H-7/12-(Et)-*closo*-$CB_{11}H_{10}$) results, after six cycles, in the pentaethyl-substituted complex (characterized as the nbd salt) $[Rh(PPh_3)_2(nbd)]$[1-H-2,4,8,10,12-$(Et)_5$-*closo*-$CB_{11}H_6$]. The solid-state structure shows that the antipodal boron vertex, two lower pentagonal belt vertices, and two upper-belt vertices have been functionalized, with no two adjacent vertices on the same pentagonal belt substituted. The degree of ethylation can be controlled. Replacing the hydrogen on the cage carbon with a bulkier substituent (methyl or Si^iPr_3) affords products in which only three B−H vertices have been substituted, and the solid-state structure of $Rh(PPh_3)_2$(1-Me-7,11,12-$(Et)_3$-*closo*-$CB_{11}H_8$) shows that the antipodal boron vertex and two lower pentagonal belt vertices have undergone dehydrogenative borylation. Mechanistic insight into the dehydrogenative borylation comes from addition of D_2 to a CH_2Cl_2 solution of $Rh(PPh_3)_2$(*closo*-$CB_{11}H_{12}$), which results in H/D exchange of the B−H vertices, suggesting that the metal fragment reversibly inserts into a B−H bond of the cage anion to form a boryl species. Attempts to observe intermediates in the actual hydroboration process by addition of ethene to $Rh(PPh_3)_2$(1-H-*closo*-$CB_{11}H_{11}$) resulted in the observation of the tris(ethene) complex $[Rh(PPh_3)_2(\eta^2\text{-}C_2H_4)_3]$[1-H-*closo*-$CB_{11}H_{11}$], which has been characterized crystallographically as the [*closo*-$CB_{11}H_6Br_6$] salt.

Introduction

Within the landscape of metal catalysis, transformations mediated by cationic transition-metal centers occupy an important position. Such metal centers need to be partnered with anions, and the role of the anion in influencing the rate of the reaction, the stability of the catalyst, and even product distributions is now widely recognized, especially the influence that the so-called weakly coordinating anions have on catalytic systems.[1−4] Central to the development of weakly coordinating anions have been the carborane anions based upon [1-*closo*-$CB_{11}H_{11}]^-$ (Chart 1).[5,6] When surrounded by halogens, e.g., [1-H-*closo*-$CB_{11}Cl_{11}]^-$, these anions complement other weakly coordinating or noncoordinating anions such as $[BAr^F_4]^-$ (BAr^F_4 = $B\{C_6H_3(CF_3)_2\}_4$) and $[Al(OC(CF_3)_3)_4]^-$ [7] and in particular show impressive chemical resistance to decomposition or oxidation.[6,8] A particularly interesting subset of the carborane monoanions are those surrounded by alkyl groups, such as [*closo*-$CB_{11}Me_{12}]^-$ (Chart 1), accessed by electrophilic substitution of the {BH} vertices in the parent [*closo*-$CB_{11}H_{12}]^-$ anion

Chart 1

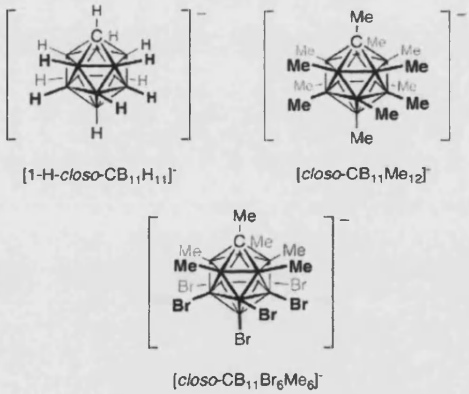

* To whom correspondence should be addressed. E-mail: a.s.weller@bath.ac.uk.

(1) Macchioni, A. *Chem. Rev.* **2005**, *105*, 2039−2073.
(2) Chen, E. Y. X.; Marks, T. J. *Chem. Rev.* **2000**, *100*, 1391−1434.
(3) Pregosin, P. S.; Kumar, P. G. A.; Fernández, I. *Chem. Rev.* **2005**, *105*, 2977−2998.
(4) Krossing, I.; Raabe, I. *Angew. Chem., Int. Ed.* **2004**, *43*, 2066.
(5) Reed, C. A. *Acc. Chem. Res.* **1998**, *31*, 133−139.
(6) Reed, C. A. *Chem. Commun.* **2005**, 1669−1677.
(7) Krossing, I.; Raabe, I. *Angew. Chem., Int. Ed.* **2004**, *43*, 2066−2090.
(8) Kato, T.; Stoyanov, E.; Geier, J.; Grutzmacher, H.; Reed, C. A. *J. Am. Chem. Soc.* **2004**, *126*, 12451−12457.

10.1021/om070043p CCC: $37.00
Publication on Web 03/28/2007

Scheme 1

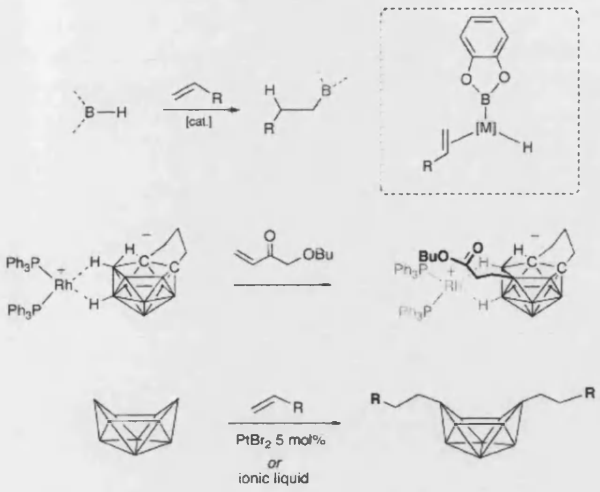

using methyl triflate.[9−11] Although these monoanions are less stable than their halogenated counterparts with respect to B−Me cleavage by strong acids or electrophiles,[12−14] they can possess the very attractive properties of showing appreciable solubility as their lithium salts in low-dielectric solvents such as hexane. When partnered with main-group or d-block metal cations, they can also show intermolecular M···H_3C interactions which have relevance to C−H activation processes and metal alkane complexes.[15,16] Extending the range of alkyl-substituted carborane monoanions by functionalization of the B−H vertices in [*closo*-$CB_{11}H_{12}]^-$ with alkyl groups other than methyl has proved to be problematic. There is a single report of perethylation using EtBr, but this uses conditions that are not necessarily suitable for large-scale synthesis (sealed tube, 220 °C).[17] Arylation of iodo-substituted monocarboranes using palladium cross-coupling with aryl Grignards has been reported,[11,18,19] but this leads to functionalized carboranes that are not ideally set up for use as weakly coordinating anions, due to the arene groups that are well-established to coordinate to metal centers. Cage-carbon functionalization is easier, given the ease of deprotonation of the C−H group and subsequent nucleophilic substitution strategies.[11,20] Although per-{BH} substitution is not well established outside methylation, peralkylation of [*closo*-$B_{12}(OH)_{12}]^{2-}$ with R−X at elevated temperatures leads to a variety of ether-linked closomers in good yield.[21]

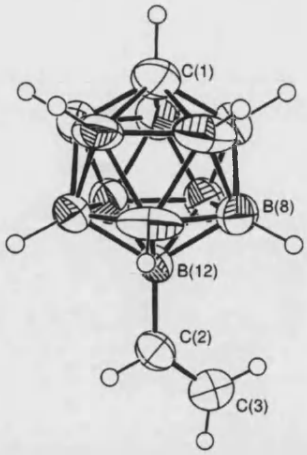

Figure 1. Solid-state structure of the anionic portion of **2a**. The $[Rh(PPh_3)_2(nbd)]^+$ cation is not shown. Thermal ellipsoids are shown at the 50% probability level.

Transition-metal-mediated catalytic borylation of alkenes using simple boron sources (e.g., $HB(OR)_2$) is well-known (Scheme 1, top).[22−24] With polyboranes, Sneddon[25−31] and Hawthorne[32] have shown that one or two {BH} vertices on, for example, *arachno*-$B_{10}H_{14}$, [*nido*-7,8-$C_2B_9H_{12}]^-$, or borazines can be alkylated using transition-metal catalysts such as the $\{Rh(PPh_3)_2\}^+$ fragment, $Cp_2Ti(CO)_2$, and $PtBr_2$ (Scheme 1, bottom), although recent work has shown that the use of ionic liquids removes the necessity of the metal catalyst in some systems.[33] Given this precedent, we speculated whether such routes could be extended to [1-H-*closo*-$CB_{11}H_{11}]^-$ to effect multiple substitutions of the anion with alkenes, thus leading to polyalkyl-substituted carborane monoanions with potentially interesting properties as weakly coordinating anions. We report here that the sequential, and regioselective, functionalization of [1-H-*closo*-$CB_{11}H_{11}]^-$ with up to five ethyl groups under mild conditions can be achieved using $\{Rh(PPh_3)_2\}^+$ fragments as catalysts but further substitution is disfavored by increasing steric hindrance. We also comment on the mechanistic aspects of this process and describe an unstable intermediate ethene complex

(9) King, B. T.; Janousek, Z.; Gruner, B.; Trammell, M.; Noll, B. C.; Michl, J. *J. Am. Chem. Soc.* **1996**, *118*, 3313−3314.
(10) Vyakaranam, K.; Janousek, Z.; Eriksson, L.; Michl, J. *Heteroat. Chem.* **2006**, *17*, 217−223.
(11) Korbe, S.; Schreiber, P. J.; Michl, J. *Chem. Rev.* **2006**, *106*, 5208−5249.
(12) King, B. T.; Zharov, I.; Michl, J. *Chem. Innovation* **2001**, 23−31.
(13) Zharov, I.; Havlas, Z.; Orendt, A. M.; Barich, D. H.; Grant, D. M.; Fete, M. G.; Michl, J. *J. Am. Chem. Soc.* **2006**, *128*, 6089−6100.
(14) Ingleson, M. J.; Kociok-Kohn, G.; Weller, A. S. *Inorg. Chim. Acta* **2005**, *358*, 1571−1580.
(15) Zharov, I.; Weng, T.-C.; Orendt, A. M.; Barich, D. H.; Penner-Hahn, J.; Grant, D. M.; Havlas, Z.; Michl, J. *J. Am. Chem. Soc.* **2004**, *126*, 12033−12046.
(16) Ingleson, M. J.; Patmore, N. J.; Kociok-Köhn, G.; Mahon, M. F.; Ruggiero, G. D.; Weller, A. S.; Clarke, A. J.; Rourke, J. P. *J. Am. Chem. Soc.* **2004**, *126*, 1503−1517.
(17) Tsang, C. W.; Xie, Z. W. *Chem. Commun.* **2000**, 1839−1840.
(18) Franken, A.; Kilner, C. A.; Thornton-Pett, M.; Kennedy, J. D. *Chem. Commun.* **2002**, 2048−2049.
(19) Franken, A.; Kilner, C. A.; Thornton-Pett, M.; Kennedy, J. D. *Collect. Czech. Chem. Commun.* **2002**, *67*, 869−912.
(20) Jelinek, T.; Baldwin, P.; Scheidt, W. R.; Reed, C. A. *Inorg. Chem.* **1993**, *32*, 1982−90.
(21) Farha, O. K.; Julius, R. L.; Lee, M. W.; Huertas, R. E.; Knobler, C. B.; Hawthorne, M. F. *J. Am. Chem. Soc.* **2005**, *127*, 18243−18251.
(22) Irvine, G. J.; Lesley, M. J. G.; Marder, T. B.; Norman, N. C.; Rice, C. R.; Robins, E. G.; Roper, W. R.; Whittell, G. R.; Wright, L. J. *Chem. Rev.* **1998**, *98*, 2685−2722.
(23) Burgess, K.; Vanderdonk, W. A.; Westcott, S. A.; Marder, T. B.; Baker, R. T.; Calabrese, J. C. *J. Am. Chem. Soc.* **1992**, *114*, 9350−9359.
(24) Mannig, D.; Noth, H. *Angew. Chem., Int. Ed.* **1985**, *24*, 878−879.
(25) Wilczynski, R.; Sneddon, L. G. *Inorg. Chem.* **1981**, *20*, 3955−3962.
(26) Davan, T.; Corcoran, E. W.; Sneddon, L. J. *Organometallics* **1983**, *2*, 1693−1694.
(27) Lynch, A. T.; Sneddon, L. G. *J. Am. Chem. Soc.* **1989**, *111*, 6201−6209.
(28) Mazighi, K.; Caroll, P. J.; Sneddon, L. G. *Inorg. Chem.* **1993**, *32*, 1963−1969.
(29) Kadlecek, D. E.; Carroll, P. J.; Sneddon, L. G. *J. Am. Chem. Soc.* **2000**, *122*, 10868−10877.
(30) Pender, M. J.; Carroll, P. J.; Sneddon, L. G. *J. Am. Chem. Soc.* **2001**, *123*, 12222−12231.
(31) Wei, X. L.; Carroll, P. J.; Sneddon, L. G. *Organometallics* **2004**, *23*, 163−165.
(32) Hewes, J. D.; Kreimendahl, C. W.; Marder, T. B.; Hawthorne, M. F. *J. Am. Chem. Soc.* **1984**, *106*, 5757−5759.
(33) Kusari, U.; Li, Y. Q.; Bradley, M. G.; Sneddon, L. *J. Am. Chem. Soc.* **2004**, *126*, 8662−8663.

Scheme 2 [a]

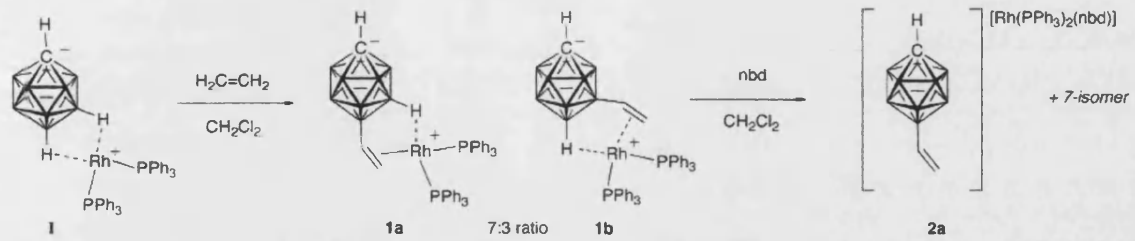

[a] Hydrogen atoms on B−H vertices are only shown when they are coordinated to the metal.

Scheme 3 [a]

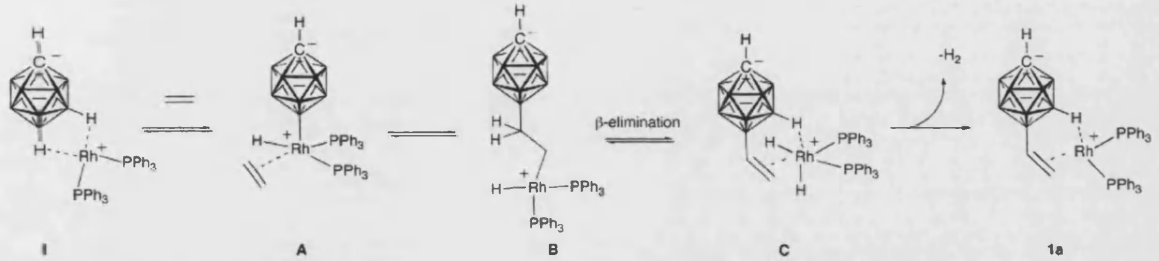

[a] Only the 12-isomer is shown.

Scheme 4 [a]

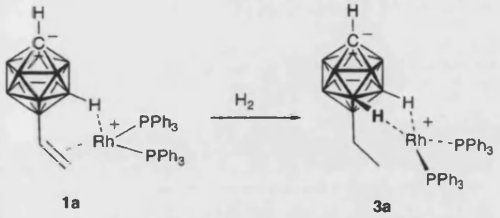

[a] Only the 12-isomer is shown.

characterized by spectroscopic and crystallographic techniques. Aspects of the work have been communicated previously.[34]

Results and Discussion

Sequential Dehydrogenative Borylation Reactions. We have previously reported the complex $Rh(PPh_3)_2$(1-H-*closo*-$CB_{11}H_{11}$) (**I**; Scheme 2), in which the metal fragment interacts with the carborane through two, lower hemisphere {BH} vertices.[35] Addition of D_2 (1 atm) to **I** in CD_2Cl_2 solution in a NMR tube resulted in the gradual (days) H/D exchange at the {BH} vertices, as evidenced by the disappearance of BH signals in the $^1H\{^{11}B\}$ NMR spectrum and the loss of B−H coupling in the ^{11}B NMR spectrum. Speculating that the H/D exchange process most probably occurs via reversible insertion of the metal fragment into a B−H bond of the carborane, leading to a putative hydrido−boryl intermediate (e.g., Scheme 1, top), and that such an intermediate is well set up for hydroboration of an alkene by the cage, we added a range of alkenes to **I**. Although a selection of alkenes (ethene, 1-hexene, *tert*-butylethene, butyl acrylate) did undergo hydroboration to afford the corresponding functionalized borane cages, only ethene resulted in the compositionally purest products. Other olefins gave mixtures of multiply substituted cage anions as determined by ESI-MS and were not studied in detail. Other catalysts that have proved useful in the past led to either a mixture of products ($PtBr_2$ or $PdBr_2$) or no reaction ($Cp_2Ti(CO)_2$).[25−31]

Addition of excess ethene to **I** in CH_2Cl_2 solution at room temperature for 15 h affords the vinyl complex $Rh(PPh_3)_2$(1-H-(H_2C=CH)-*closo*-$CB_{11}H_{10}$) (**1**) in reasonable isolated yield (61%), although as monitored by in situ NMR spectroscopy the conversion is essentially quantitative. Compound **1** arises from dehydrogenative borylation of ethene. No reaction is observed between ethene and [1-H-*closo*-$CB_{11}H_{11}$]$^-$. NMR spectroscopy shows that this compound is formed as a mixture of two isomers: $Rh(PPh_3)_2$(1-H-12-(H_2C=CH)-*closo*-$CB_{11}H_{10}$) (**1a**) and $Rh(PPh_3)_2$(1-H-7-(H_2C=CH)-*closo*-$CB_{11}H_{10}$) (**1b**). These two compounds are formed in a 7:3 ratio on the basis of relative integrals in the ^1H and ^{11}B NMR spectra. Both isomers show three separate vinylic resonances in the ^1H NMR spectrum, between δ 4.95 and 2.56, which were aided in their identification by $^1H-^1H$ COSY experiments. These vinylic signals are shifted to high field compared to [$Rh(PPh_3)_2$(nbd)][1-H-7/12-(H_2C=CH)-*closo*-$CB_{11}H_{10}$] (**2a**,**b**), complexes in which the metal fragment is not associated with the cage anion (vide infra), indicative of coordination of the C=C bond to the metal center in **1a**,**b**.[36,37] The high-field region of the $^1H\{^{11}B\}$ NMR spectrum shows broad peaks characteristic of Rh−*H*−B interactions between δ −0.80 and −2.15,[38] which broaden considerably in the ^1H NMR spectrum due to coupling to quadrupolar boron. Overall, these data suggest a solution structure in which the $\{Rh(PPh_3)_2\}^+$ fragment in each isomer binds to the *B*-vinyl group of the cage and one B−H vertex through a three-center−two-electron interaction.

The presence of a *B*-vinyl group was ultimately confirmed by an X-ray diffraction study of **2a**, [$Rh(PPh_3)_2$(nbd)][1-H-12-(H_2C=CH)-*closo*-$CB_{11}H_{10}$], which is formed on addition of norbornadiene (nbd) to a CH_2Cl_2 solution of **1a**,**b** to afford **2a**,**b**, from which crystals of **2a** could be isolated. The ^1H NMR data

(34) Molinos, E.; Kociok-Kohn, G.; Weller, A. S. *Chem. Commun.* **2005**, 3609−3611.

(35) Rifat, A.; Patmore, N. J.; Mahon, M. F.; Weller, A. S. *Organometallics* **2002**, *21*, 2856−2865.

(36) Crabtree, R. H. *The Organometallic Chemistry of the Transition Metals*; Wiley: Hoboken, NJ, 2005.

(37) Du, S.; Ellis, D. D.; Jelliss, P. A.; Kautz, J. A.; Malget, J. M.; Stone, F. G. A. *Organometallics* **2000**, *19*, 1983−1992.

(38) Rifat, A.; Laing, V. E.; Kociok-Kohn, G.; Mahon, M. F.; Ruggiero, G. D.; Weller, A. S. *J. Organomet. Chem.* **2003**, *680*, 127−135.

Scheme 5

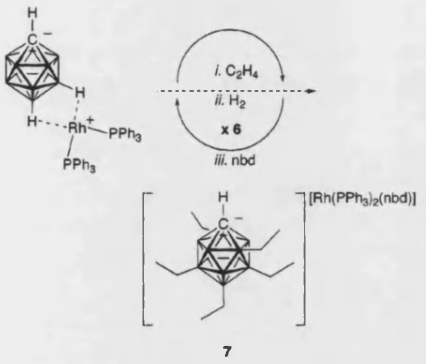

7

of the mixture **2** show the same ratio of vinyl protons, but these are now observed between δ 6.35 and 5.18, while the $^1H\{^{11}B\}$ NMR spectrum no longer shows distinctive Rh−*H*−B resonances at high field—all indicating that the metal fragment is not interacting with the cage anion. In the ^{11}B NMR spectrum, multiple environments are observed, and a $^{11}B-^{11}B$ COSY experiment allowed cage anions with approximate C_{5v} symmetry (**2a**) and C_s symmetry (**2b**) to be identified. The relative ratio of these two species in the ^{11}B NMR spectrum is ~7:3, which mirrors that found in the ^1H NMR spectrum and allows the vinylic protons to be identified with a particular isomer. The solid-state structure of the anion in **2a** is shown in Figure 1. Although differentiation between cage carbon and boron atoms by X-ray diffraction can be problematic, the B−C distances (1.656(5)−1.719(6) Å) in **2a** all being shorter than the other B−B distances (1.727(5)−1.829(6) Å) in the cage is a good indicator that the cage carbon atom was reliably located and indicates 12-substitution on the cage. However, without a labeled vertex (e.g, C_{cage}−Me) this assignment must be treated with a degree of caution, especially given the existence of both 7- and 12-isomers in solution. A short C(2)−C(3) distance (1.323(4) Å) is consistent with a vinyl group. The associated B(12)−C(2) bond length of 1.583(4) Å is longer than those in the alkenyl-substituted carborane 7-$(CH_2(CH_2)_2CH{=}CH)$-*arachno*-6,8-$C_2B_7H_{12}$ (1.546(2) Å),[29] in which there is suggested to be a π-bonding component to the interaction between the boron and vinyl atoms, reminiscent of conjugated olefins. In the case of **2a** we suggest no such bonding is present, on the basis of the long B−C bond length and the short C(2)−C(3) distance for the vinyl group. Indeed, the B−C distance is similar to that reported for *B*-methyl groups in methylated carborane monoanions[9,16] and those observed in the ethyl-substituted carborane **7** (vide infra).

Compounds **1a**,**b** (and derivatives **2a**,**b**) result from dehydrogenative borylation of ethene by [1-H-*closo*-$CB_{11}H_{11}]^-$ mediated by an exo-coordinated $\{Rh(PPh_3)_2\}^+$ fragment, which occurs by β-elimination from the insertion product of ethene into the Rh−boryl bond (Scheme 3). Transition-metal-mediated catalytic dehydrogenative borylation of alkenes using simple boron sources is well established,[25,39,40] and Sneddon has previously commented on such a process occurring during monofunctionalization of boranes, carboranes, and borazines with 1-alkenes using transition-metal catalysts such as $PdBr_2$ and $PtBr_2$ as the hydroboration mediator.[26,27,29] It has been suggested that dehydrogenative borylation occurs in preference

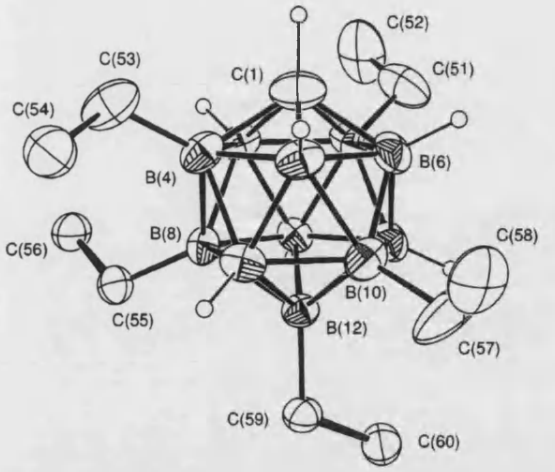

Figure 2. Solid-state structure of the anionic portion of **7**. The $[Rh(PPh_3)_2(nbd)]^+$ cation is not shown. Thermal ellipsoids are shown at the 30% probability level. The minor disordered components of the ethyl groups have been omitted for clarity.

to reductive elimination of alkyl borate (which would result in hydroboration) when steric bulk forces the metal alkyl to adopt a geometry that favors β-elimination. Coordinating solvents, such as acetonitrile, also disfavor reductive elimination and favor β-elimination.[40] The bulky carborane anion in **1** fulfils the first criterion, while the large excess of ethene present might also disfavor reductive elimination by filling a vacant site and also removing the H_2 liberated by β-elimination, by the formation of ethane. The 12-/7-substitution pattern is also consistent with initial insertion of the $\{Rh(PPh_3)_2\}^+$ fragment into the most electron-rich B−H vertices at the bottom of the cage.[15,41] *B*-Vinyl-substituted carboranes have been reported previously as arising from cross-coupling reactions between *B*-halide cages and vinyl Grignards or zinc reagents[42−44] or by metal-mediated B−H insertion of an alkyne into a metallacarborane.[37]

Electrospray ionization mass spectrometry (ESI-MS—see the Supporting Information) also shows that by far the major product is the one that arises from dehydrogenative borylation (*m/z* 169.3). However, there is also a small amount of cage anion that has a mass envelope (*m/z* 196.2) which indicates a further B−H substitution has occurred to afford the mixed ethylvinylcarborane anion [1-H-$(CH_3CH_2)(CH_2{=}CH)$-*closo*-$CB_{11}H_9]^-$. This small amount of product was always formed, irrespective of reaction conditions. B−H substitution in **1a**,**b** does not proceed further than this, even on heating, and we suggest that this is due to the coordination of the vinyl group to the rhodium metal center, which inhibits further substitution. The small amount of the bis-substituted cage presumably arises from reductive elimination of ethylcarborane from **B** (Scheme 3), which is in competition with β-elimination. This would lead to a small amount of ethyl-substituted cage that then undergoes a further dehydrogenative borylation. Consistent with this mechanism, there is a very small amount of the tris-substituted product also observed in the ESI-MS spectrum.

Intentional addition of H_2 to CH_2Cl_2 solutions of **1** results in rapid hydrogenation of the vinyl group, mediated by the rhodium

(39) Brown, J. M.; Lloyd-Jones, G. C. *J. Am. Chem. Soc.* **1994**, *116*, 866−878.
(40) Coapes, R. B.; Souza, F. E. S.; Thomas, R. L.; Hall, J. J.; Marder, T. B. *Chem. Commun.* **2003**, 614−615 and references cited therein.
(41) McKee, M. L. *J. Am. Chem. Soc.* **1997**, *119*, 4220−4223.
(42) Zakharkin, L. I.; Kovredov, A. I.; Ol'shevskaya, V. A. *Izv. Akad. Nauk SSSR, Ser. Khim.* **1985**, 888−92.
(43) Kalinin, V. N.; Kobel'kova, N. I.; Zakharkin, L. I. *Zh. Obshch. Khim.* **1977**, *47*, 963.
(44) Russell, J. M.; Sabat, M.; Grimes, R. N. *Organometallics* **2002**, *21*, 4113−4128.

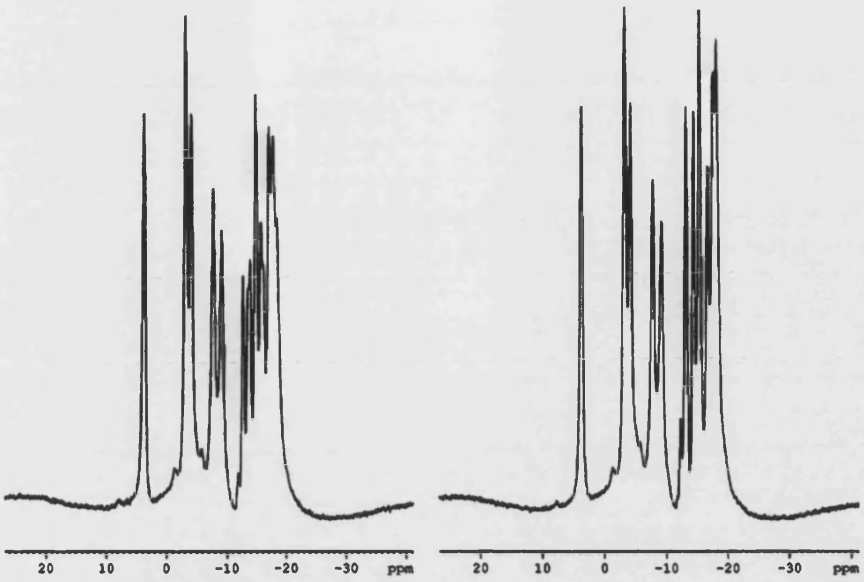

Figure 3. ^{11}B (left) and $^{11}B\{^1H\}$ (right) NMR spectra of **7** (160.46 MHz).

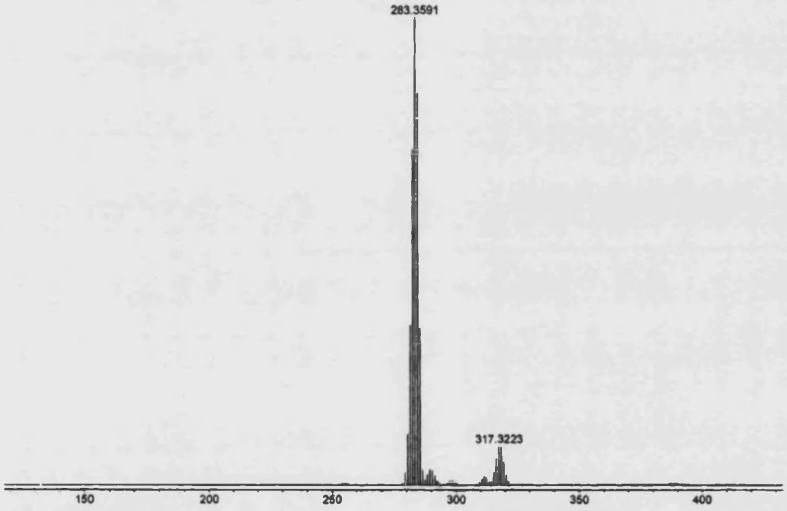

Figure 4. ESI-MS (negative mode) of **7**.

fragment,[35,45] to afford $Rh(PPh_3)_2$(1-H-12-(Et)-*closo*-$CB_{11}H_{10}$) (**3a**) and $Rh(PPh_3)_2$(1-H-7-(Et)-*closo*-$CB_{11}H_{10}$) (**3b**) (Scheme 4). A ^1H NMR spectrum of **3** shows the conversion of the vinyl group to ethyl, while the high-field region of the $^1H\{^{11}B\}$ NMR spectrum shows two broad signals attributed to the B−*H*−Rh bonds in either isomer, which broaden considerably in the ^1H NMR spectrum into poorly resolved quartets. Addition of nbd forms the salt $[Rh(PPh_3)_2(nbd)]$[1-H-7/12-(Et)-*closo*-$CB_{11}H_{10}$] (**4a**,**b**), which can be crystallized as an inseparable mixture of isomers. The ratio of 7- and 12-isomers remains the same throughout these transformations. On addition of nbd the high-field resonances due to Rh−*H*−B interactions in the ^1H NMR spectrum disappear.

Blocking the 12-position in the carborane cage with a bromine results in a single product. Addition of ethene to $Rh(PPh_3)_2$(1-H-12-Br-*closo*-$CB_{11}H_{10}$) gives the exclusive formation of $Rh(PPh_3)_2$(1-H-7-(CH_2=CH)-12-Br-*closo*-$CB_{11}H_9$) (**5**), which was

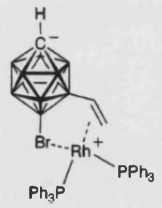

5

characterized by NMR spectroscopy. The ^1H NMR spectrum of **5** displays no low-frequency shifts that are indicative of Rh−*H*−B interactions, while the vinyl protons are observed between δ 5.03 and 3.81, suggestive of coordination to the $\{Rh(PPh_3)_2\}^+$ fragment, as when nbd is added to **5**, to produce $[Rh(PPh_3)_2$-(nbd)][1-H-7-(CH_2=CH)-12-Br-*closo*-$CB_{11}H_9$] (**6**), these vinyl signals now shift downfield by over 1 ppm. These observations

(45) Behnken, P. E.; Busby, D. C.; Delaney, M. S.; King, R. E.; Kreimendahl, C. W.; Marder, T. B.; Wilczynski, J. J.; Hawthorne, M. F. *J. Am. Chem. Soc.* **1984**, *106*, 7444−7450.

Table 1. X-ray Crystallographic Data Collection and Refinement Details

	2a	7	9	10	13
formula	$C_{46}H_{52}B_{11}P_2Rh$	$C_{54}H_{70}B_{11}P_2Rh$	$C_{46}H_{59}B_{11}P_2RhSi$	$C_{44}H_{56}B_{11}P_2Rh$	$C_{47}H_{56}B_{11}Br_6Cl_8P_2Rh$
fw	888.64	1002.86	923.78	868.65	1667.74
cryst size, mm	0.55 × 0.55 × 0.30	0.20 × 0.10 × 0.05	0.25 × 0.13 × 0.08	0.20 × 0.13 × 0.03	0.50 × 0.25 × 0.20
T, K	150(2)	150(2)	150(2)	150(2)	150(2)
cryst syst	monoclinic	monoclinic	monoclinic	triclinic	triclinic
space group	$P2_1/c$	$P2_1/c$	$P2_1/a$	$P\bar{1}$	$P\bar{1}$
a, Å	17.0670(2)	16.7380(2)	18.8890(3)	9.8660(2)	11.3130(2)
b, Å	15.6010(2)	18.0910(2)	14.4860(3)	13.3420(4)	14.2250(2)
c, Å	17.4360(2)	18.5710(2)	20.2760(3)	17.7310(6)	22.6530(5)
α, deg	90	90	90	83.592(1)	96.597(1)
β, deg	101.895(1)	111.618(1)	116.272(1)	75.742(1)	92.376(1)
γ, deg	90	90	90	78.438(2)	112.9980(10)
V, Å^3	4542.86(9)	5227.88(10)	4974.94(15)	2211.41(11)	3318.63(10)
Z	4	4	4	2	2
μ, mm^{-1}	0.479	0.424	0.463	0.491	4.272
F_{000}	1832	2096	1916	900	1628
θ range, deg	3.58−28.70	3.45−27.49	5.54−25.00	5.57−27.44	3.64−27.51
D_{calcd}, g cm^{-3}	1.299	1.274	1.233	1.305	1.669
no. of collected/unique rflns	78 738/11 612	76 466/11 940	55 055/8611	26 014/9894	36 589/15 037
R1/wR2 ($I > 2\sigma(I)$)	0.0325/0.0798	0.0498/0.1095	0.0545/0.1017	0.0491/0.0905	0.049/0.136
R1/wR2 (all data)	0.0381/0.0854	0.0664/0.1173	0.0863/0.1209	0.0813/0.1028	0.0688/0.1352
GOF on F^2	1.050	1.052	1.108	1.034	1.04
max, min diff Fourier peaks, e Å^{-3}	0.680, −1.006	0.645, −0.476	0.951, −0.683	0.452, −0.678	1.49, −1.10

suggest a structure for **5** that has the metal phosphine fragment coordinated to the cage through a Rh−Br and a Rh−vinyl interaction. Monobrominated cages interacting with a metal fragment through the antipodal {BBr} vertex have been reported before.[46] Consistent with this structure that has inequivalent phosphines, the $^{31}P\{^1H\}$ NMR spectrum shows two broad environments at room temperature that sharpen into two well-resolved doublets of doublets at 258 K. There must be some fluxional process occurring to broaden the peaks at room temperature, and this might involve reversible breaking and making of the Rh−Br bond. The $^{11}B\{^1H\}$ NMR spectrum of **5** shows five broad environments, which resolve better in the nbd salt **6** to give a 1:1:2:2:2:2:1 pattern between δ −2.2 and −18.9 ppm, consistent with C_s symmetry. The first two signals are assigned by a combination of $^{11}B-^{11}B$ COSY and ^{11}B NMR spectroscopy as being due to BBr and *B*-vinyl groups, respectively. The nbd salt also shows only one environment in the $^{31}P\{^1H\}$ NMR spectrum, as expected.

Once the vinyl group has been hydrogenated in **3a**, the metal center becomes available to perform further dehydrogenative borylations. Addition of excess ethene to **3a** results in a mixture of products that can be identified by ESI-MS as resulting from two or three vertices being dehydrogenatively borylated. Addition of H_2 hydrogenates the vinyl groups to *B*-ethyls. Further cycling of ethene/H_2 addition four times (a total of six times in all) and addition of nbd results a compound that is identified by NMR spectroscopy, ESI-MS, and X-ray crystallography as $[Rh(PPh_3)_2(nbd)][1\text{-H-}2,4,8,10,12\text{-}(Et)_5\text{-}closo\text{-}CB_{11}H_6]$ (**7**; Scheme 5). This reaction affords product in ~75% yield based on complex **I** and has been scaled to ~1.5 g. The reaction mixture before addition of nbd shows broad, poorly resolved peaks in the ^{11}B NMR spectrum and evidence of Rh−H−B interactions in the high-field portion of the ^1H NMR spectrum (δ −4.95, br, B−*H*−Rh). Addition of a large excess of nbd to the reaction mixture results in decoordination of the cage from the carborane anion and a sharpening of the ^{11}B NMR spectrum, and for this reason full characterization has been carried out on this salt.

The solid-state structure of the anionic part of salt **7** is shown in Figure 2, and this shows fivefold substitution of the cage anion. There is some minor disorder associated with some of the ethyl groups, but this can be satisfactorily modeled. The cage carbon atom was identified on the basis of shorter C−B distances compared to distance for the other vertices. The substitution pattern is one in which the antipodal boron vertex, two lower pentagonal belt vertices, and two upper-belt vertices have been functionalized. No two adjacent vertices on the same pentagonal belt have been functionalized. This pattern presumably reflects that the sterically bulky $\{Rh(PPh_3)_2\}^+$ metal fragment sequentially inserts ethene into the B−H bonds which are least hindered and after five substitutions the resulting anion is too bulky to undergo further reaction. Although this results in no further substitutions, the benefit is that the metal fragment controls the substitution pattern and, thus, excellent regioselectvity is obtained. The B−C bonds in the cage (1.58(2)−1.630(7) Å) are similar to those found in the methylated carborane $[closo\text{-}CB_{11}Me_{12}]^-$ (1.59(2)−1.73(2) Å)[9] and the alkyl-substituted borane 6-$(CH_2{=}CHCH_2SiMe_2(CH_2)_3)$-*nido*-$B_{10}H_{13}$ (1.577(3) Å).[30]

The NMR spectra of **7** are consistent with the solid-state structure. In the ^1H NMR spectrum a broad (relative integral 25 H) set of signals is observed between δ 0.96 and 0.36 that is assigned to the ethyl groups. In the $^{11}B\{^1H\}$ NMR spectrum (160 MHz) nine resonances are observed in the ratio 1:1:1:1:1:1:1:1:1 (Figure 3) between δ 3.8 and −18.0. The first five of these signals (those most downfield) remain singlets in the ^{11}B NMR spectrum, identifying them as the B−Et vertices. ESI-MS of the reaction mixtures (Figure 4, *m*/*z* 283) demonstrates that fivefold substitution accounts for ~95% of the products, with a very small amount of sixfold-substituted product also being observed (~5%; see Figure 4). Analytically pure material can be obtained by repeated recrystallization. Multiple substitutions on polyborane cages using hydroboration methodology have been reported previously. $B_{10}H_{14}$ can be cleanly bisfunctionalized with alkenes by either $PtBr_2$ or stepwise incorporation using a $Cp_2Ti(CO)_2/PtBr_2$ combination.[28,30] Higher substitution products in the borylation of *arachno*-6,8-$C_2B_7H_{13}$ have been briefly mentioned but not characterized.[29] Up to three alkenyl groups can be incorporated in ruthenacarborane complexes by reactions with alkynes, affording B−H insertion products.[37] As far as we are aware, however, fivefold substitu-

(46) Patmore, N. J.; Ingleson, M. J.; Mahon, M. F.; Weller, A. S. *Dalton Trans.* **2003**, 2894−2904.

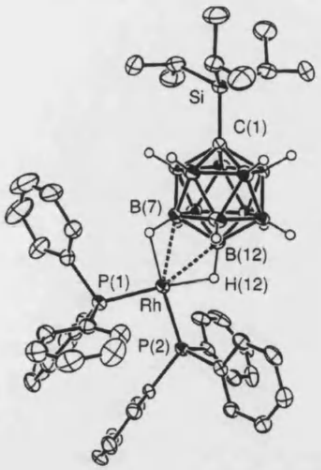

Figure 5. Solid-state structure of complex **9**. Thermal ellipsoids are shown at the 50% probability level. Hydrogen atoms, apart from those associated with cage vertices, have been omitted for clarity.

tion by hydroboration of a polyborane, as seen in **7**, has not been reported.

The degree of ethylation can be controlled by replacing the hydrogen on the cage carbon with a bulkier substituent. The rhodacarborane complexes $(PPh_3)_2Rh(1\text{-}R\text{-}closo\text{-}CB_{11}H_{11})$ have been prepared (R = Me (**8**), Si^iPr_3 (**9**)) by hydrogenation of the precursor complexes $[(PPh_3)_2Rh(nbd)][1\text{-}R\text{-}closo\text{-}CB_{11}H_{11}]$. Both complexes have been fully characterized by NMR spectroscopy and show the expected resonances due to Rh−H−B interactions in both the $^1H\{^{11}B\}$ and $^{11}B\{^1H\}$ NMR spectra.[35,38] The solid-state structure of **9** has also been determined (Figure 5), and this shows the $\{Rh(PPh_3)_2\}^+$ fragment to bind with the carborane cage with the antipodal (B12) and one lower pentagonal belt (B7) {BH} vertex, just as observed for the closely related complex **I**.[35]

Sequential addition of ethene/H_2 for three cycles to the methyl-substituted cage complex **8** afforded the new complex $Rh(PPh_3)_2(1\text{-}Me\text{-}9,11,12\text{-}(Et)_3\text{-}closo\text{-}CB_{11}H_8)$ (**10**), in which substitution has occurred in three places on the lower hemisphere of the cage, but the cage substituent has retarded further substitution on the upper-pentagonal belt of the anion (Scheme 6). Complex **10** has been characterized by NMR spectroscopy and ESI-MS. This latter technique shows the predominant product to be the triply substituted product, with a small amount (ca. 10%) of the doubly and quadruply substituted products also evident. Changing the reaction times, number of cycles, or temperature did not improve the ratio, and we could not isolate the material in bulk as a compositionally pure solid even after repeated crystallizations. Although the conversion was complete as measured by ^{11}B NMR spectroscopy, the isolated yields of impure solid **10** are low (25% based on Rh).

In the solid-state structure of **10** (Figure 6) the $\{Rh(PPh_3)_2\}^+$ fragment is coordinated through two Rh−H−B bonds on the lower pentagonal belt of the cage anion. B−H substitution has occurred in the antipodal and two separated lower belt {BH} vertices, a pattern that mirrors that observed in **7** for the same part of the cage. The labeled cage carbon vertex made the assignment of the substitution pattern unambiguous and also strengthens assignments made for the complexes which only had a {CH} vertex on the cage (e.g., **7**). The C−B distances in the substituted vertices fall into the same range as observed for **7** (1.590(6)−1.597(5) Å).

In solution, the Rh−H−B interactions are evidenced by a quadrupolar broadened integral 2H quartet at δ −4.64 ppm, while a broad (integral ~15 H) signal between δ 1.02 and 0.11 ppm is observed for the B−Et groups. The ^{11}B NMR spectrum shows four resonances in the ratio 3:3:3:2, although some of these are overlapping resonances. The expected (for C_s symmetry) 1:2:1:2:2:1:2 pattern between δ −0.1 and −15.9 ppm is observed when excess nbd is added to afford $[Rh(PPh_3)_2(nbd)][1\text{-}Me\text{-}7,11,12\text{-}(Et)_3\text{-}closo\text{-}CB_{11}H_8]$ (**11**), in which the cage is no longer bound with the metal center (the Rh−*H*−B signals disappear). The two low-field resonances do not display coupling to ^1H in the ^{11}B NMR spectrum, identifying them as being due to *B*-Et vertices.

That the tris-substituted methylcarborane is not formed in compositionally pure form can be remedied by using the bulkier carbon substitutent Si^iPr_3. Cycling ethene/H_2 addition three times and then adding nbd affords $[Rh(PPh_3)_2(nbd)][1\text{-}(Si^iPr_3)\text{-}9,11,12\text{-}(Et)_3\text{-}closo\text{-}CB_{11}H_8]$ (**12**) as pure material in a reasonable yield (63%). Complex **12** has been characterized by NMR spectroscopy and ESI-MS. The $^{11}B\{^1H\}$ NMR spectrum of **12** (Figure 7) shows a pattern very similar to that of **11**, 1:2:1:2:2:3 between δ 7.7 and −16.8, again with the two lowest frequency peaks observed as singlets, showing that they can be assigned to *B*-Et vertices. Although the chemical shifts are not identical with those of **11**, they are similar enough to suggest that the substitution pattern is the same. The ESI-MS spectrum (Figure 8) shows one cage anion species with a mass and isotopic distribution appropriate for the composition (*m/z* 383). The bulkier Si^iPr_3 groups thus inhibit further substitution past three times better than the methyl group. Similarly, it has been briefly reported that incorporation of the silyl group in $[1\text{-}Si^iPr_3\text{-}closo\text{-}CB_{11}H_{11}]^-$ directs electrophilic methylation with MeOTf to occur only at the lower hemisphere of the cage.[11,12,47]

Attempts to make any of these transformations catalytic, for example using 20 mol % of **I** and $[1\text{-}Si^iPr_3\text{-}closo\text{-}CB_{11}H_{11}][NBu_4]$, did not lead to appreciable turnover, even though a variety of anion/metal fragment/solvent combinations were tried. Catalytic turnover has been observed in monohydroborations of *nido* cages using the $\{Rh(PPh_3)_2\}^+$ fragment and butyl acrylate.[32] The lack of reactivity in the systems under discussion here suggests that the cage anion is strongly bound to the metal fragment and cannot undergo ready exchange with the unsubstituted $[1\text{-}H\text{-}closo\text{-}CB_{11}H_{11}]^-$ cage. This is consistent with the dehydrogenative borylation process operating that results in a tightly bound vinylcarborane (e.g., **1a**,**b**). Hydrogenation of vinyl groups should remove this bottleneck, and indeed addition of $[NBu_4][1\text{-}H\text{-}closo\text{-}CB_{11}H_{11}]$ to **7** (the sterically most hindered carborane) results in partial exchange after 1 h to afford **I** and **7** in an approximate 1:4 ratio. However, the system is not catalytic in the sense that it does not turn over, as further addition of ethene results in the formation of vinylcarborane **1a**,**b**, which requires addition of H_2 to promote further B−H substitution. Attempts to generate metal-free salts using simple cations such as $[PPN]^+$ and $[NBu_4]^+$ also met with limited success, and we have not pursued this further.

Comments on the Mechanism of Borylation. The substitution pattern for dehydrogenative borylation follows from a simple charge distribution analysis in the $[1\text{-}H\text{-}closo\text{-}CB_{11}H_{11}]^-$ cage,[15,41] as well as the order of electrophilic substitution by either halogens[48] or DCl.[49] The electronegative cage carbon atom induces a dipole in the {BH} vertices in the cage that leads to the most negative boron vertices being BH(12)/BH(7-11). If it

(47) King, B. T. University of Colorado, Boulder, CO, 2000.
(48) Jelinek, T.; Plesek, J.; Hermanek, S.; Stibr, B. *Collect. Czech. Chem. Commun.* **1986**, *51*, 819−829.
(49) Jelinek, T.; Plesek, J.; Mares, F.; Hermanek, S.; Stibr, B. *Polyhedron* **1987**, *6*, 1981−1986.

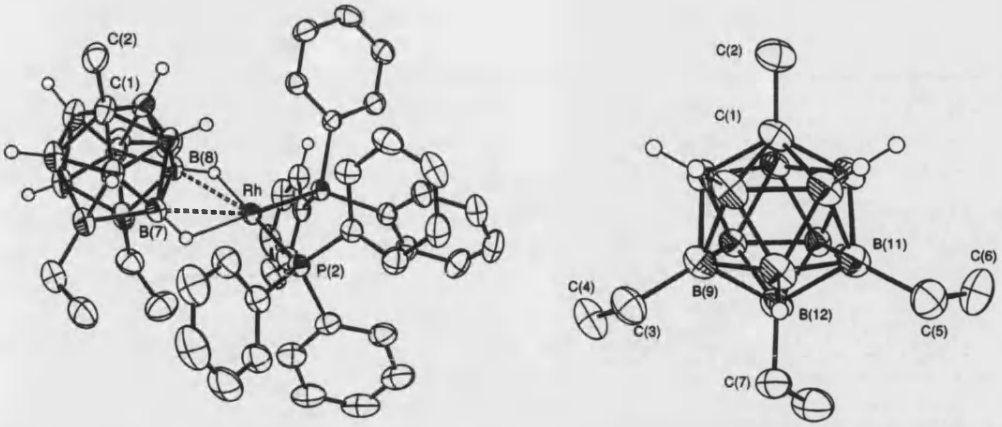

Figure 6. Solid-state structure of complex **10** (left) and of just the anion (right). Thermal ellipsoids are shown at the 50% probability level. Hydrogen atoms, apart from those associated with cage vertices, have been omitted for clarity.

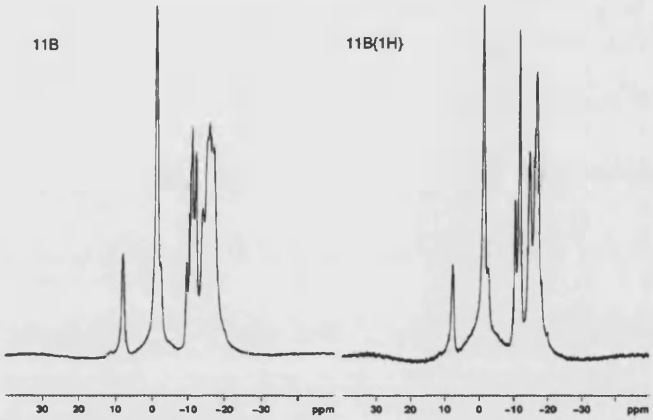

Figure 7. ^{11}B (left) and $^{11}B\{^1H\}$ (right) NMR spectra of **12**.

is assumed that the most electron rich {B−H} vertex undergoes preferential insertion with the $\{Rh(PPh_3)_2\}^+$ fragment in the absence of overriding steric effects, then the observed substitution pattern of B(12) → B(7-11) → B(2-5) is as expected when both electronic and steric factors are considered. Hydroboration using the carborane [7,8-$(CH_2)_3$-*nido*-$C_2B_9H_{10}]^-$ also occurs at the {BH} vertex farthest away from the cage carbon atoms.[32]

Exposure of $Rh(PPh_3)_2$(1-R-*closo*-$CB_{11}H_{11}$) (R = H, Me, Si^{i}Pr$_3$) to a D_2 atmosphere (1 atm) results in gradual (2 days) H/D exchange of all the {BH} vertices, as followed by ^{11}B and $^1H\{^{11}B\}$ NMR spectroscopy. The order of substitution, as determined from the $^1H\{^{11}B\}$ NMR spectrum, is as expected: B(12) followed by B(7-11) and finally B(2-5). The cage {CH} vertex is not deuterated. During this H/D exchange significant amounts of dissolved HD(g) were also observed (1:1:1 triplet at δ 4.55, J(DH) = 43 Hz), suggesting a mechanism for H/D exchange that involves an accessible dihydrogen/boryl intermediate such as **D** (Scheme 7). This is closely related to intermediate **A** in

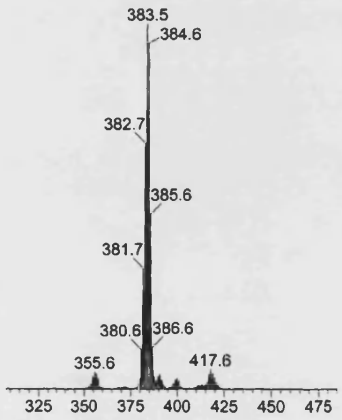

Figure 8. ESI-MS (negative mode) of **12**.

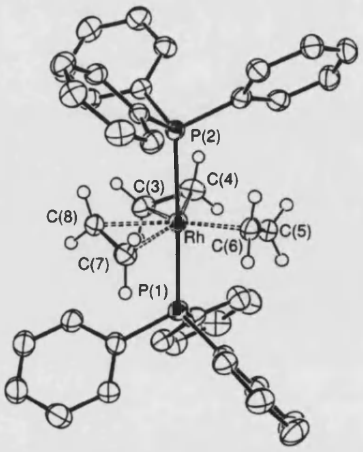

Figure 9. Solid-state structure of the cationic portion of complex **13**. Thermal ellipsoids are shown at the 50% probability level. Hydrogen atoms, apart from the olefin hydrogens, have been omitted for clarity.

Scheme 6

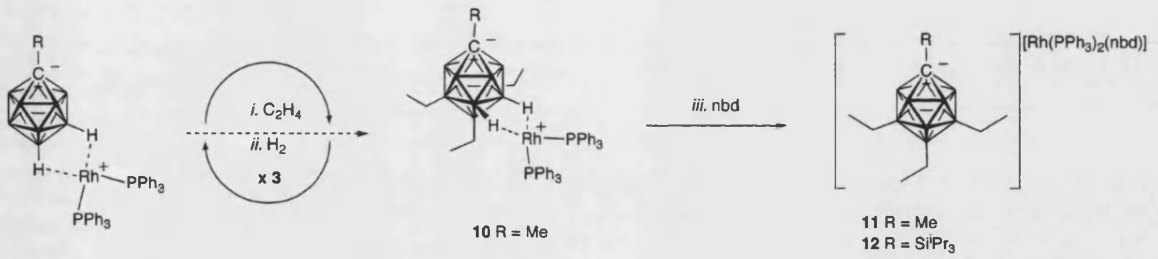

Scheme 7

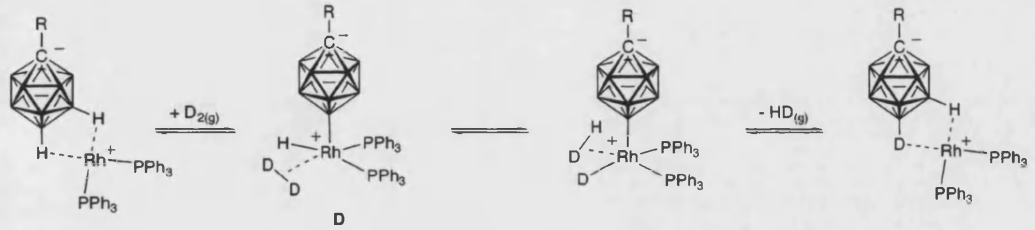

Scheme 8

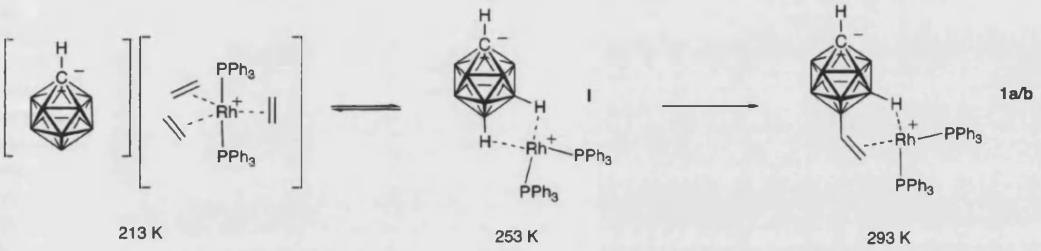

Scheme 3. Similar mechanisms, involving metal−boryl intermediates, have been proposed for the *exo-nido* complexes Rh(PPh$_3$)$_2$(7,8-R$_2$-*nido*-C$_2$B$_9$H$_{10}$).[45,50]

H/D exchange of every {BH} vertex also occurs in the ethyl-substituted complexes, even though no further dehydrogenative borylation occurs. For example, exposing **7** to a D_2 atmosphere for 2 days results in the complete replacement of the remaining {BH} vertices for {BD}, as measured by ^{1}H{^{11}B} and ^{11}B NMR spectroscopy and ESI-MS. This complete substitution suggests that the metal fragment is still able to insert into sterically protected {BH} vertices to generate intermediate boryl species but is not capable of further reaction with ethene. We suggest that it is the coordination of ethene and/or migratory insertion into the Rh−boryl bond which is disfavored with increasing cage substitution.

In an attempt to observe these putative Rh−boryl intermediates, reaction between **I** and excess ethene was monitored between 200 K and room temperature by ^{31}P{^{1}H} and ^{11}B{^{1}H} NMR spectroscopy. Between 200 and 230 K one species is observed in the ^{31}P{^{1}H} NMR spectrum, as a doublet at δ 35.5 (J(RhP) = 93 Hz). The ^{11}B{^{1}H} NMR spectrum shows no high-frequency peaks that would be indicative of direct metal boryl interactions,[51,52] while the distinctive 1:5:5 pattern for free [1-H-*closo*-CB$_{11}$H$_{11}$]$^-$ anion is observed at chemical shifts very close to those reported for the [NBu$_4$]$^+$ salt.[53] This suggests that the carborane cage is not interacting with the metal center. Confirming this, when the anion is changed to the weakly coordinating anions [BAr$^F_4$]$^-$ and [*closo*-CB$_{11}$H$_6$Br$_6$]$^-$ (by adding ethene to the aryl-bridged species [Rh(PPh$_3$){(η^6-C$_6$H$_5$)PPh$_2$}]$_2$[BAr$^F_4$]$_2$ or [Rh(PPh$_3$){(η^6-C$_6$H$_5$)PPh$_2$}]$_2$[1-*closo*-CB$_{11}$H$_6$Br$_6$]$_2$[35]), the ^{31}P{^{1}H} NMR spectrum remains the same. This complex has been characterized as the tris(ethene) species [Rh(PPh$_3$)$_2$(η^2-C$_2$H$_4$)$_3$][1-H-*closo*-CB$_{11}$H$_{11}$]. When the temperature is raised, signals due to **I** become increasingly intense at the expense of [Rh(PPh$_3$)$_2$(η^2-C$_2$H$_4$)$_3$][1-H-*closo*-CB$_{11}$H$_{11}$], and at 273 K **I** is the major species (Scheme 8). Cooling again establishes the same low-temperature spectrum, suggesting a dynamic equilibrium. When the temperature is raised to room temperature, dehydrogenative borylation commences, and signals due to **1a,b** are observed.

A crystal structure of the [*closo*-CB$_{11}$H$_6$Br$_6$]$^-$ salt unambiguously characterizes the low-temperature complex as the tris(ethene) species [Rh(PPh$_3$)$_2$(η^2-C$_2$H$_4$)$_3$][*closo*-CB$_{11}$H$_6$Br$_6$] (**13**). As **13** rapidly loses olefin when removed from an ethene atmosphere and also starts to lose ethene above −20 °C in solution, the crystals were grown from a cooled solution at −78 °C under an ethene atmosphere and mounted quickly on a precooled diffractometer. The solid-state structure is shown in Figure 9. Complex **13** shows a trigonal-bipyramidal structure in which the ethene ligands are arranged equatorially, adopting a geometry as expected from steric and electronic arguments.[54]

(50) Behnken, P. E.; Belmont, J. A.; Busby, D. C.; Delnay, M. S.; King, R. E.; Kreimendahl, C. W.; Marder, T. B.; Wilczynski, J. J.; Hawthorne, M. F. *J. Am. Chem. Soc.* **1984**, *106*, 3011−3025.
(51) Rath, N. P.; Fehlner, T. P. *J. Am. Chem. Soc.* **1987**, *109*, 5273−5274.
(52) Aldridge, S.; Coombs, D. L. *Coord. Chem. Rev.* **2004**, *248*, 535−559.
(53) Fox, M. A.; Mahon, M. F.; Patmore, N. J.; Weller, A. S. *Inorg. Chem.* **2002**, *41*, 4567−4573.
(54) Albright, T. A.; Burdett, J. K.; Whangbo, M.-H. *Orbital Interactions in Chemistry*; Wiley: New York, 1985.

The structure is very similar to the structure we have reported for $[Ir(PPh_3)_2(\eta^2\text{-}C_2H_4)_3][closo\text{-}CB_{11}H_6Br_6]$[55] and is also similar to that of the acetonitrile complex $[Rh(NCMe)_2(\eta^2\text{-}C_2H_4)_3][BF_4]$.[56] The analogous complex $[Rh(PMe_3)_2(\eta^2\text{-}C_2H_4)_3][PF_6]$ has been spectroscopically characterized in solution.[57] The Rh–C_{ethene} distances and C–C distances for **13** are as expected (2.246(4)–2.287(4) and 1.362(7)–1.375(7) Å, respectively) for a cationic metal center with three π-accepting ligands with little Rh→C back-donation (free ethene d(CC) = 1.337 Å). The analogous complex $[Ir(PPh_3)_2(\eta^2\text{-}C_2H_4)_3][closo\text{-}CB_{11}H_6Br_6]$ is significantly more stable than **13** toward ethene loss,[55] a consequence of the stronger Ir–C bonds. Replacement of weakly bound carboranes via other ligands has been reported before. For example, $Rh(PPh_3)_2(7,8\text{-}R_2\text{-}nido\text{-}C_2B_9H_{10})$ reacts with CO to afford $[Rh(PPh_3)_2(CO)_3][7,8\text{-}R_2\text{-}nido\text{-}C_2B_9H_{10}]$, in which the cation is directly related to **13** (R = alkyl, Ph).[58]

Conclusions

Ethylation of $[1\text{-}H\text{-}closo\text{-}CB_{11}H_{11}]^-$ by a rhodium phosphine mediated route has been shown to be effective for the introduction of up to five ethyl groups on the cage through sequential dehydrogenative borylation/hydrogenation of ethene. Although this accesses new substitution patterns, per-boron-vertex substitution using this route was not achieved, due to the increasingly bulky ethyl-substituted carborane becoming reluctant to undergo further borylation with ethene. Unfortunately, the fact that the functionalized cage is difficult to produce in pure form without an associated metal fragment and that the overall process does not turnover in a catalytic sense means that this methodology is somewhat limited for producing functionalized carborane cage anions. Studies to improve both the scope and possibility of catalytic turnover in this process are underway.

Experimental Section

General Considerations. All manipulations were carried out under an atmosphere of argon, using standard Schlenk-line and glovebox techniques, unless otherwise stated. Glassware was predried in an oven at 130 °C and flamed with a blowtorch under vacuum prior to use. Solvents were dried over activated alumina, copper, and molecular sieve columns using an MBraun solvent purification system. CD_2Cl_2 was distilled under vacuum from CaH_2. $(PPh_3)_2Rh(1\text{-}H\text{-}closo\text{-}CB_{11}H_{11})$ and $(PPh_3)_2Rh(1\text{-}Me\text{-}closo\text{-}CB_{11}H_{11})$ (**8**) were prepared by the published literature routes or slight variations thereof.[35,38] $[(PPh_3)_2Rh(nbd)][1\text{-}^iPr_3Si\text{-}closo\text{-}CB_{11}H_{11}]$ and $(PPh_3)_2Rh(1\text{-}H\text{-}12\text{-}Br\text{-}closo\text{-}CB_{11}H_{10})$ were prepared as outlined in the Supporting Information. All other chemicals were used as received from Aldrich. Microanalyses were performed by Elemental Microanalysis Limited. Mass spectrometry was performed by the EPSRC Service at the University of Swansea or at the University of Bath using a Bruker MicroToF mass spectrometer equipped with an electrospray ionization source.

NMR Spectroscopy. ^1H, $^1H\{^{11}B\}$, $^{11}B\{^1H\}$, ^{11}B, and $^{31}P\{^1H\}$ NMR spectra were recorded on Brüker Avance 300, 400, and 500 MHz spectrometers. Residual protio solvent was used as reference for ^1H and $^1H\{^{11}B\}$ NMR spectra (CD_2Cl_2, δ = 5.33). ^{11}B and $^{11}B\{^1H\}$ and $^{31}P\{^1H\}$ spectra were referenced against $BF_3{\cdot}OEt_2$ (external) and 85% H_3PO_4 (external), respectively. Values are quoted in ppm. Coupling constants are quoted in Hz.

X-ray Crystallography. Intensity data for all structures were collected at 150 K on a Nonius KappaCCD diffractometer equipped with a low-temperature device, using graphite-monochromated Mo Kα radiation (λ = 0.710 73 Å). Data were processed using the Nonius software.[59] For **13** a symmetry-related (multiscan) absorption correction was applied. Crystal parameters and details on the data collection, solution, and refinement for the complexes are provided in Table 1. Structure solution, followed by full-matrix least-squares refinement, was performed using the WINGX-1.70 suite of programs throughout.[60] The crystal data are available from the Cambridge Crystallographic Database: CCDC reference numbers 268853 (**10**), 268854 (**7**), 632281 (**2a**), 632282 (**9**), and 632283 (**13**). For **9** and **10** the bridging Rh–*H*–B hydrogen atoms were located in the difference Fourier map and freely refined. For **7** one phenyl ring of the PPh_3 ligand showed rotational disorder in the ratio of 85:15. Three out of the five ethyl group substituents of the anion borane cage were refined with site occupation of 60:40, and due to partial overlap of the ellipsoids the disordered atom pair C54/C54A was refined isotropically. Complex **13** crystallizes with four molecules of CH_2Cl_2 spread over six sites. The CH_2Cl_2 pair of C81/C81A was refined in a ratio of 90:10 with the minor C atom refined isotropically, and the pair C84/C85 showed a site occupancy of 1:1. Cl9 in the CH_2Cl_2 molecule associated with C85 was disordered in the ratio 1:1. The CH_2Cl_2 atoms C82 and C83 were fully occupied, but one of the Cl atoms in each molecule showed disorder in the ratios of 1:1 (Cl4/Cl4A) and 3:2 (Cl5/Cl5A). Most C–Cl bond lengths were idealized. Vinyl hydrogen atoms were located in the difference Fourier map and freely refined. Full bond lengths and angles are provided in the Supporting Information.

$Rh(PPh_3)_2(1\text{-}H\text{-}7/12\text{-}(CH{=}CH_2)\text{-}closo\text{-}CB_{11}H_{10})$ (12-Isomer (1a), 7-Isomer (1b)). $(PPh_3)_2Rh(1\text{-}H\text{-}closo\text{-}CB_{11}H_{11})$ (45 mg, 0.058 mmol) was placed in a 15 cm^3 Young ampule, and CH_2Cl_2 (5 cm^3) was added via cannula. The solution was freeze–pump–thawed three times. On the third cycle the solution was charged with ethene (0.500 g) the ampule was closed, and the mixture was warmed to room temperature with stirring. After 15 h, the solvent was evaporated under vacuum and the residue washed with pentane and dried to afford a dark orange product (28 mg, 61%). Anal. Calcd for $C_{39}H_{44}B_{11}P_2Rh$: C, 58.81; H, 5.57. Found: C, 58.57; H, 5.57.

^1H NMR (δ, CD_2Cl_2): 7.81–7.06 (m, 30H, PPh_3), 4.95 (d, 1H, B–CH=C*H*$_2$, J(HH) = 9, 7-isomer), 4.83 (d, 1H, B–CH=C*H*$_2$, J(HH) = 16, 12-isomer), 4.15 (d, 1H, B–CH=C*H*$_2$, J(HH) = 9, 7 isomer), 4.10 (d, 1H, B–CH=C*H*$_2$, J(HH) = 9, 12-isomer), 2.67 (dd, 1H, B–C*H*=CH$_2$, J(HH) = 16, ^3J(HH) = 9, 7-isomer), 2.56 (dd, 1H, B–C*H*=CH$_2$, J(HH) = 16, J(HH) = 9, 12-isomer), 2.37 (s, 1H, C_{cage}–*H*, 7-isomer), 2.22 (s, 1H, C_{cage}–*H*, 12-isomer). Selected $^1H\{^{11}B\}$ NMR (δ, CD_2Cl_2): 1.86 (br s, B–*H*, 7-isomer), 1.80 (br s, B–*H*, 7-isomer), 1.64 (br s, B–*H*, 7-isomer), 1.52 (br, B–*H*, 12-isomer), 1.24 (br s, B–*H*, 7-isomer), 0.18 (br s, B–*H*, 7-isomer), −0.56 (br, B–*H*, 12-isomer), −0.80 (br s, B–*H*–Rh, 7-isomer), −1.72 (br, B–*H*–Rh, 12-isomer), −2.15 (br s, B–*H*–Rh, 7-isomer). ^{11}B NMR (δ CD_2Cl_2): 2.71 (s, *B*–C), −2.18 (s, *B*–C), −14.93 (br, overlapping signals). $^{31}P\{^1H\}$ NMR (δ, CD_2Cl_2, 298 K): 40.7 (br).

$[Rh(PPh_3)_2(nbd)][1\text{-}H\text{-}7/12\text{-}(CH{=}CH_2)\text{-}closo\text{-}CB_{11}H_{10}]$ (12-Isomer (2a), 7-Isomer (2b)). Norbornadiene (100 equiv) was added to a CH_2Cl_2 solution of **1a,b** as described above, and the mixture was stirred for 3 h. The solvent was evaporated under vacuum and the residue redissolved in CH_2Cl_2 (2 cm^3) and precipitated with pentane (15 cm^3) to afford an orange precipitate. The solvent was decanted via cannula and the product (44 mg, 85%) dried under vacuum. ESI-MS (negative mode): *m/z* 169.2, showing the correct

(55) Rifat, A.; Kociok-Kohn, G.; Steed, J. W.; Weller, A. S. *Organometallics* **2004**, *23*, 428–432.
(56) Maspero, F.; Perrotti, E.; Simonetti, F. *J. Organomet. Chem.* **1972**, *38*, C43–C45.
(57) Werner, H.; Feser, R. Z *Naturforsch., B: Anorg. Chem. Org. Chem.* **1980**, *35B*, 689–693.
(58) Long, J. A.; Marder, T. B.; Behnken, P. E.; Hawthorne, M. F. *J. Am. Chem. Soc.* **1984**, *106*, 2979–2989.
(59) Otwinowski, Z.; Minor, W. In *Methods Enzymol.* **1997**, *276*.
(60) Farrugia, L. J. *J. Appl. Crystallogr.* **1999**, *32*, 837–838.

isotope pattern for $B_{11}C_3H_{14}$. Anal. Calcd for $C_{46}H_{52}B_{11}P_2Rh$: C, 62.17; H, 5.90. Found: C, 61.75; H, 6.08.

^1H NMR (δ, CD_2Cl_2): 7.50−7.26 (m, 30H, PPh_3), 6.35 (dd, BC*H*=CH_2, *J*(HH) = 19, *J*(HH) = 13, 7-isomer), 6.23 (dd, B−C*H*=CH_2, *J*(HH) = 19, *J*(HH) = 13, 12-isomer), 5.53 (br s, B−CH=C*H*$_2$, 7-isomer), 5.35 (br s, B−CH=C*H*$_2$, 7- and 12-isomers), 5.18 (br s, B−CH=C*H*$_2$, 12-isomer), 4.50 (br s, 4H, C_7H_8), 4.08 (br s, 2H, C_7H_8), 2.44 (br s, C_{cage}−*H*, 7-isomer), 2.31 (br s, 1H, C_{cage}−*H*, 12-isomer), 1.56 (s, 2H, C_7H_8). $^{11}B\{^1H\}$ NMR (δ, CD_2Cl_2; assignments from $^{11}B-^{11}B$ COSY and ^{11}B NMR, primed numbers indicate 7-isomer): 1.2 (*B12*−CH=CH_2), −4.6 (*B7′*−CH=CH_2), −5.8 (*B12′*−H), −12.4 (*B7′−11,8′,11′*−H, coincident signal), −13.4 (*B9′,10′*−H), −15.6 (*B2′,3′*−H), −16.4 (*B2−6,4′,6′*-H, coincident signal), −18.5 (*B5′*−H). $^{31}P\{^1H\}$ NMR (δ, CD_2Cl_2, 298 K): 29.6 (d, *J*(RhP) = 156).

Rh(PPh$_3$)$_2$(1-H-7/12-(Et)-*closo*-CB$_{11}$H$_{10}$) (12-Isomer (3a), 7-Isomer (3b)). (PPh_3)$_2$Rh(1-H-*closo*-$CB_{11}H_{11}$) (45 mg, 0.058 mmol) was placed in a 15 cm^3 Young ampule, and CH_2Cl_2 (5 cm^3) was added via cannula. The solution was freeze−pump−thawed three times. On the third cycle the solution was charged with ethene (1.012 g) and warmed to room temperature with stirring. After 15 h, excess ethene was removed under vacuum and replaced with hydrogen (1 atm). After 1 h, the solvent was evaporated under vacuum to afford a red product (25 mg, 54%). Anal. Calcd for $C_{39}H_{46}B_{11}P_2Rh$: C, 58.66; H, 5.81. Found: C, 58.04; H, 5.85.

^1H NMR (δ CD_2Cl_2): 7.80−7.06 (m, 30H, PPh_3), 2.51 (br s, 1H, C_{cage}−*H*, 12-isomer), 2.46 (s, 1H, C_{cage}−*H*, 7-isomer), 0.95−0.30 (m, B−*Et*), -0.84 (br q, B−*H*−Rh), −2.11 (br q, B−*H*−Rh). Selected $^1H\{^{11}B\}$ NMR (δ, CD_2Cl_2): 2.51 (br s, 1H, C_{cage}−*H*, 12-isomer), 2.46 (s, 1H, C_{cage}−*H*, 7-isomer), 1.98 (br s, B−*H*), 1.64 (br s, B−*H*), 1.55 (br s, B−*H*), 1.44 (br s, B−*H*), 0.95−0.30 (m, B−*Et*), −0.84 (br s, B−*H*−Rh), −2.11 (br s, B12−*H*−Rh). $^{11}B-\{^1H\}$ NMR (δ, CD_2Cl_2): 8.51 (s, *B*−H), 5.04 (s, *B*−H), 2.67 (s, *B*−H), 0.89 (s, *B*−H), −12.00 (s, *B*−H), −14.18 (s, *B*−H), −16.12 (s, *B*−H), −16.89 (s, *B*−H). $^{31}P\{^1H\}$ NMR (δ, CD_2Cl_2, 298 K): 12-isomer, 46.0 (d, *J*(RhP) = 194); 7-isomer, 45.8 (d, *J*(RhP) = 189).

[Rh(PPh$_3$)$_2$(nbd)][1-H-7/12-(Et)-*closo*-CB$_{11}$H$_{10}$] (12-Isomer (4a), 7-Isomer (4b)). (PPh_3)$_2$Rh(1-H-*closo*-$CB_{11}H_{11}$) (45 mg, 0.058 mmol) was placed in a 15 cm^3 Young ampule, and CH_2Cl_2 (5 cm^3) was added via cannula. The solution was freeze−pump−thawed three times. On the third cycle the solution was charged with ethene (1.012 g) and warmed to room temperature with stirring. After 15 h, excess ethene was removed under vacuum and replaced with hydrogen (1 atm). After 1 h, the solvent was evaporated under vacuum. The residue was redissolved in CH_2Cl_2, and norbornadiene (0.5 cm^3, 4.63 mmol) was added. After the mixture was stirred for 3 h, the solvent was evaporated under vacuum and the orange residue redissolved in CH_2Cl_2 (2 cm^3) and precipitated with pentane (15 cm^3). The solvent was decanted via cannula and the product (44 mg, 85%) dried under vacuum. ESI-MS (negative mode): *m/z* 171.1, showing the correct isotope pattern for $B_{11}C_3H_{16}$. Anal. Calcd for $C_{46}H_{54}B_{11}P_2Rh$: C, 62.03; H, 6.11. Found: C, 61.70; H, 6.22. ^1H NMR (δ, CD_2Cl_2): 7.37−7.27 (m, 30H, PPh_3), 4.47 (br s, 4H, C_7H_8), 3.99 (br s, 2H, C_7H_8), 2.26 (br s, C_{cage}−*H*), 2.16 (br s, C_{cage}−*H*), 1.59 (br s, 2H, C_7H_8), 1.06-0.70 (m, B−*Et*). $^1H\{^{11}B\}$ NMR (δ, CD_2Cl_2): 7.37−7.27 (m, 30H, PPh_3), 4.47 (br s, 4H, C_7H_8), 3.99 (br s, 2H, C_7H_8), 2.26 (br s, C_{cage}−*H*), 2.16 (br s, C_{cage}−*H*), 1.63 (br s, B−*H*), 1.61 (br s, B−*H*), 1.59 (br s, 2H, C_7H_8), 1.55 (br s, B−*H*), 1.06−0.70 (m, B−*Et*). ^{11}B NMR (δ, CD_2Cl_2; assignments from $^{11}B-^{11}B$ COSY, primed numbers indicate 7-isomer): 4.13 (s, *B12*−Et), -1.78 (s, *B7′*−Et), −6.20 (d, *B12′*−H, *J*(BH) = 133), −12.77 (d, *B7−11,8′,11′*−H, *J*(BH) = 136), −14.03 (d br, *B9′,10′*−H), −16.00 (d br, *B2′*,3′−H), −16.90 (d, *B2−6,4′*,6′−H, *J*(BH) = 147), −19.81 (d, *B5′*−H, *J*(BH) = 149). $^{31}P\{^1H\}$ NMR (δ, CD_2Cl_2, 298 K): 29.4 (d, *J*(RhP) = 155).

Rh(PPh$_3$)$_2${1-H-7-(CH=CH$_2$)-12-Br-*closo*-CB$_{11}$H$_9$} (5). [Rh(PPh$_3$)$_2$(nbd)][1-H-12-Br-*closo*-$CB_{11}H_{10}$] (50 mg, 0.053 mmol) was placed in a 15 cm^3 Young ampule equipped with a magnetic stirrer, and CH_2Cl_2 (5 cm^3) was added via cannula. The solution was freeze−pump−thawed three times. On the third cycle the solution was warmed to room temperature with stirring under an atmosphere of hydrogen to give [(PPh$_3$)$_2$Rh(1-H-12-Br-*closo*-$CB_{11}H_{11}$)] (see the Supporting Information for NMR data). After 30 min excess hydrogen was removed with vacuum and ethene was condensed in (1.407 g). After 24 h excess ethene was released, the solvent evaporated under vacuum, and the residue redissolved with CH_2Cl_2. The solution was concentrated under reduced pressure to a volume of 3 cm^3, and hexanes (20 cm^3) was added to afford an orange precipitate. Solvents were removed by decantation and the product was washed with hexane (2 × 5 cm^3) and dried in vacuo to afford the title compound (22 mg, 47%) as an orange solid. Anal. Calcd for $C_{39}H_{43}B_{11}BrP_2Rh(CH_2Cl_2)_2$: C, 47.11; H, 4.53. Found: C, 47.97; H, 4.83.

^1H NMR (δ, CD_2Cl_2, 298 K): 7.44−7.14 (m, 30H, PPh_3), 5.03 (d, 1H, B−CH=C*H*$_2$, *J*(HH) = 16), 4.45 (d, 1H, B−CH=C*H*$_2$, *J*(HH) = 9.6), 3.18 (dd, 1H, B−C*H*=CH_2, *J*(HH) = 16, *J*(HH) = 9.6), 2.26 (s, 1H, C_{cage}−*H*). Selected $^1H\{^{11}B\}$ NMR (δ, CD_2Cl_2 298 K): 1.74 (br s, B−*H*), 1.60 (br s, B−*H*). $^{11}B\{^1H\}$ NMR (δ, CD_2Cl_2, 298 K): −2.35 (s, *B*−C), -3.64 (s, *B*−Br), -12.80 (br s, *B*−H), −14.33 (br s, *B*−H), −17.07 (br s, *B*−H). $^{31}P\{^1H\}$ NMR (δ, CD_2Cl_2, 298 K): 57.4 (br s), 21.4 (br s). $^{31}P\{^1H\}$ NMR (δ, CD_2Cl_2, 258 K): 57.4 (dd, *J*(RhP) = 194, *J*(PP) = 32), 21.4 (dd, *J*(RhP) = 194, *J*(PP) = 32).

[Rh(PPh$_3$)$_2$(nbd)][1-H-7-(CH=CH$_2$)-12-Br-*closo*-CB$_{11}$H$_9$] (6). [Rh(PPh$_3$)$_2$(nbd)][1-H-12-Br-*closo*-$CB_{11}H_{10}$] (100 mg, 0.106 mmol) was placed in a 15 cm^3 Young ampule equipped with a magnetic stirrer, and CH_2Cl_2 (5 cm^3) was added via cannula. The solution was freeze−pump−thawed three times. On the third cycle the solution was warmed to room temperature with stirring under an atmosphere of hydrogen to give [(PPh$_3$)$_2$Rh(12-Br-$CB_{11}H_{11}$)]. After 30 min excess hydrogen was removed with vacuum and ethene condensed (1.542 g). After 2 h, ethene was released, the solvent evaporated under vacuum, and the residue redissolved with CH_2Cl_2. Norbornadiene (0.5 cm^3, 4.63 mmol) was added to the CH_2Cl_2 solution and stirred for 3 h. The solvent was evaporated under vacuum and the residue redissolved in CH_2Cl_2 (2 cm^3) and precipitated with pentane (15 cm^3) to afford an orange precipitate. Solvents were removed by decantation, and the product was washed with pentane (2 × 5 cm^3) and dried in vacuo to afford the title compound (85 mg, 83%) as an orange solid. ESI-MS (negative mode), *m/z* 248.2, showing the correct isotope pattern for $C_3H_{13}B_{11}$-Br. Anal. Calcd for $C_{46}H_{51}B_{11}BrP_2Rh$: C, 57.10; H, 5.31. Found: C, 57.16; H, 5.33.

^1H NMR (δ, $CDCl_3$): 7.40−7.27 (m, 30H, PPh_3), 6.32 (dd, B−C*H*=CH_2, *J*(HH) = 19, *J*(HH) = 13), 5.61 (br s, 1H, B−CH=C*H*$_2$), 5.45 (br s, 1H, B−CH=C*H*$_2$), 4.50 (br s, 4H, C_7H_8), 4.08 (br s, 2H, C_7H_8), 2.40 (br s, C_{cage}−*H*), 1.57 (s, 2H, C_7H_8). $^1H\{^{11}B\}$ NMR (δ, $CDCl_3$): 7.40−7.27 (m, 30H, PPh_3), 6.32 (dd, B−C*H*=CH_2, *J*(HH) = 19, *J*(HH) = 13), 5.61 (dd, 1H, B−CH=C*H*$_2$, *J*(HH) = 19, *J*(HH) = 4.6), 5.45 (dd, 1H, B−CH=C*H*$_2$, *J*(HH) = 13, *J*(HH) = 4.6), 4.50 (br s, 4H, C_7H_8), 4.08 (br s, 2H, C_7H_8), 2.40 (br s, C_{cage}−*H*), 2.14 (br s, 2H, B−*H*), 2.07 (br s, 2H, B−*H*), 1.93 (br s, 2H, B−*H*), 1.81 (br s, 2H, B−*H*), 1.74 (br s, 1H, B−*H*), 1.57 (s, 2H, C_7H_8). $^{11}B\{^1H\}$ NMR (δ, $CDCl_3$; assignments from $^{11}B-^{11}B$ COSY and ^{11}B NMR): −2.16 (s, 1B, *B*−Br), −5.38 (s, 1B, *B*−C), −11.73 (s, 2B, *B*−H), −12.63 (s, 2B, *B*−H), −16.48 (s, 2B, *B*−H), −17.43 (s, 2B, *B*−H), −18.87 (s, 1B, *B*−H). $^{31}P-\{^1H\}$ NMR (δ, $CDCl_3$): 29.8 (d, *J*(RhP) = 156).

[Rh(PPh$_3$)$_2$(nbd)][1-H-2,4,8,10,12-(Et)$_5$-*closo*-CB$_{11}$H$_6$] (7). A solution of (PPh_3)$_2$Rh(1-H-*closo*-$CB_{11}H_{11}$) (179 mg, 0.232 mmol) in CH_2Cl_2 (10 cm^3) was freeze−pump−thawed three times. On the third cycle ethene (~0.600 g) was added to the solution and

the ampule closed and warmed to room temperature. After it was stirred for 24 h, the solution was degassed again, hydrogen was placed in the Young ampule, and the solution was stirred for 2 h. This sequential treatment with ethene/hydrogen was repeated a total of six times. Following the last hydrogenation the solvent was degassed and norbornadiene (1 cm^3, 9.27 mmol) added. After the mixture was stirred overnight, the solvent was evaporated under vacuum and the orange residue redissolved in CH_2Cl_2 (2 cm^3) and precipitated with hexane (20 cm^3). The solvent was decanted via cannula and the product (175 mg, 75%) dried under vacuum. Crystals suitable for an X-ray diffraction study were grown from CH_2Cl_2/pentane solutions. Anal. Calcd for $RhP_2B_{11}C_{54}H_{70}$: C, 64.67; H, 7.04. Found: C, 64.50; H, 7.23. ESI-MS (negative mode): *m/z* 283.3. This preparation has been successfully scaled up to 1.5 g of material with only a small overall loss in yield (~70%).

^1H NMR (δ, CD_2Cl_2): 7.49−7.20 (m, 30H, PPh_3), 4.44 (br s, 4H, C_7H_8), 3.96 (br s, 2H, C_7H_8), 2.02 (br s, C_{cage}−*H*), 1.55 (br s, 2H, C_7H_8), 0.96−0.36 (m, 25H, B−*Et*). $^1H\{^{11}B\}$ NMR (δ, CD_2Cl_2): 7.49−7.20 (m, 30H, PPh_3), 4.44 (br s, 4H, C_7H_8), 3.96 (br s, 2H, C_7H_8), 2.02 (br s, C_{cage}−*H*), 1.55 (br s, 2H, C_7H_8), 1.48 (br s, B−*H*), 1.40 (br s, B−*H*), 1.36 (br s, B−*H*), 1.29 (br s, B−*H*), 1.21 (br s, B−*H*), 1.08 (br s, B−*H*), 0.96-0.36 (m, 25H, B−*Et*). $^{11}B\{^1H\}$ NMR (δ, CD_2Cl_2): 3.8 (br s, 1B, *B*−Et), −3.2 (br s, 1B, *B*−Et), −4.0 (br s, 1B, *B*−Et), −8.0 (br s, 1B, *B*−Et), −9.0 (br s, 1B, *B*−Et), -13.0 (br s, 1B, *B*−Et) −14.3 (br s, 1B, *B*−H), −15.2 (br s, 1B, *B*−H), −16.6 (br s, 1B, *B*−H), −17.4 (br s, 1B, *B*−H), −18.0 (br s, 1B, *B*−H). $^{31}P\{^1H\}$ NMR (δ, CD_2Cl_2, 298 K): 30.5 (d, *J*(RhP) = 155).

(PPh_3)$_2$Rh(1-^{i}Pr$_3$Si-*closo*-$CB_{11}H_{11}$) (9). [(PPh_3)$_2$Rh(nbd)][1-^{i}Pr$_3$Si-*closo*-$CB_{11}H_{11}$] (30 mg, 0.029 mmol) was placed in a 15 cm^3 Young ampule, and CH_2Cl_2 (5 cm^3) was added via cannula. The solution was freeze−pump−thawed three times. On the third cycle the solution was warmed to room temperature with stirring, under an atmosphere of H_2. Conversion was quantitative by NMR spectroscopy. Addition of hexanes along with solvent evaporation under vacuum afforded a dark red product. Suitable crystals for X-ray diffraction studies were obtained from a concentrated CH_2Cl_2 solution at −18 °C. Anal. Calcd for $C_{46}H_{62}P_2RhSiB_{11}$: C, 59.61; H, 6.74. Found: C, 60.3; H, 6.54.

^1H NMR (δ, $CDCl_3$): 7.51−7.07 (m, 30H, PPh_3), 1.18 (sept, 3H, Si(C*H*(CH$_3$)$_2$)$_3$), 1.11 (d, 18H, Si(CH(C*H*$_3$)$_2$)$_3$), 0.07 (br q, 5H, B(7−11)−*H*), −0.08 (br q, 1H, B(12)−*H*). $^1H\{^{11}B\}$ NMR (δ, $CDCl_3$): 7.51−7.07 (m, 30H, PPh_3), 2.05 (s, 5H, B(2−6)−*H*), 1.18 (sept, 3H, Si(C*H*(CH$_3$)$_2$)$_3$), 1.11 (d, 18H, Si(CH(C*H*$_3$)$_2$)$_3$), 0.07 (br s, 5H, B(7−11)−*H*), −0.08 (br s, 1H, B(12)−*H*). ^{11}B NMR (δ, $CDCl_3$): −6.85 (d, 1B, *B(12)*−H, *J*(BH) = 110), −13.17 (d, 10B, *B(2−11)*−H, *J*(BH) = 112). $^{11}B\{^1H\}$ NMR (δ, $CDCl_3$): −6.85 (s, 1B, *B(12)*−H), −13.17 (s, 10B, *B(2−12)*−H). $^{31}P\{^1H\}$ NMR (δ, $CDCl_3$): 47.74 (d, *J*(RhP) = 194).

Rh(PPh_3)$_2$(1-Me-9,11,12-(Et)$_3$-*closo*-$CB_{11}H_8$) (10). [(PPh_3)$_2$Rh(nbd)][1-Me-*closo*-$CB_{11}H_{11}$] (50 mg, 0.057 mmol) was placed in a 15 cm^3 Young ampule, and CH_2Cl_2 (5 cm^3) was added via cannula. The solution was freeze−pump−thawed three times. On the third cycle the solution was warmed to room temperature with stirring under an atmosphere of hydrogen to give [(PPh_3)$_2$Rh(1-Me−$CB_{11}H_{11}$)]. After 30 min excess hydrogen was removed with vacuum and replaced with ethene. After 24 h, the solution was degassed again, hydrogen was placed in the Young ampule, and the solution was stirred for 2 h. This procedure was repeated a total of four times. The solution was then reduced in vacuo to dryness to afford a dark red residue (12 mg, 25%). Crystals suitable for an X-ray diffraction experiment were grown from CH_2Cl_2/pentane solutions. ESI-MS (negative mode): *m/z* 241.2, showing the correct isotope pattern for $B_{11}C_8H_{26}$. Compound **10** was always formed with a small (~10%) of another carborane anion that could not be removed by bulk purification methods. Mass spectroscopy suggests that the identity of this may be [1-H-*closo*-$(C_2H_5)_4$-$CB_{11}H_7]^-$.

^1H NMR (δ, CD_2Cl_2): 7.52−7.10 (m, 30H, PPh_3), 1.64 (s, 3H, C_{cage}−C*H*$_3$), 1.02−0.11 (m, 15H, B−C*H*$_2$C*H*$_3$), −4.64 (br q, 2H, B−*H*−Rh). ^{11}B NMR (δ, CD_2Cl_2): −2.1 (vbr, 3B), −12.7 (vbr, 3B), −16.3 (vbr, 3B), −18.8 (d, 2B, *B*−H, *J*(HB) = 94). $^{31}P\{^1H\}$ NMR (δ, CD_2Cl_2, 298 K): 45.0 (d, *J*(RhP) = 193).

[Rh(PPh_3)$_2$(nbd)][1-Me-9,11,12-(Et)$_3$-*closo*-$CB_{11}H_8$] (11). A solution of [(PPh_3)$_2$Rh(nbd)][1-Me-*closo*-$CB_{11}H_{11}$] (60 mg, 0.068 mmol) in CH_2Cl_2 (10 cm^3) was placed in a 20 cm^3 Young ampule equipped with a magnetic stir bar. The solution was degassed with vacuum and then stirred under an atmosphere of hydrogen to give [(PPh_3)$_2$Rh(1-Me-*closo*-$CB_{11}H_{11}$)]. After 30 min excess hydrogen was removed with vacuum and ethene condensed in (0.259 g). After 4 h, ethene was released, the solution degassed under vacuum again, and the ampule charged with hydrogen. Sequential treatment with ethene and hydrogen as previously described was performed twice more (with reaction times of 16 h and 40 min, respectively). The solvent was evaporated under vacuum and the residue redissolved with CH_2Cl_2. Norbornadiene (0.5 cm^3, 4.63 mmol) was added to the CH_2Cl_2 solution and the mixture stirred for 4 h. The solvent was evaporated under vacuum and the residue redissolved in CH_2Cl_2 (2 cm^3) and precipitated with pentane (15 cm^3) to afford a dark orange precipitate. Solvents were removed by decantation and the product washed with pentane (2 × 4 cm^3) and dried in vacuo to afford the title compound (46 mg, 70.0%) as a dark orange solid. ESI-MS (negative mode): *m/z* 241.31, showing the correct isotope pattern for $C_8H_{26}B_{11}$.

^1H NMR (δ, CD_2Cl_2): 7.45−7.28 (m, 30H, PPh_3), 4.46 (br s, 4H, C_7H_8), 3.97 (br s, 2H, C_7H_8), 1.56 (s, C_{cage}−*CH*$_3$), 1.53 (br s, 2H, C_7H_8), 1.50 (s, C_{cage}−*CH*$_3$), 0.91−0.42 (m, 15H, B−*Et*). $^1H\{^{11}B\}$ NMR (δ, CD_2Cl_2): 7.45−7.28 (m, 30H, PPh_3), 4.46 (br s, 4H, C_7H_8), 3.97 (br s, 2H, C_7H_8), 1.70 (br s, B−*H*), 1.64 (br s, B−*H*), 1.56 (s, C_{cage}−*CH*$_3$), 1.53 (br s, 2H, C_7H_8), 1.50 (s, C_{cage}−*CH*$_3$), 1.44 (br s, B−*H*), 1.38 (br s, B−*H*), 1.33 (br s, B−*H*), 0.91-0.42 (m, 15H, B−*Et*). ^{11}B NMR (δ, CD_2Cl_2): −0.1 (br s, 1B, *B*−Et), −2.3 (br s, 2B, *B*−Et), −8.8 (br s, 1B, *B*−H), −11.2 (br s, 1B, *B*−H), −12.7 (br d, 2B, *B*−H), −13.9 (br d, 2B, *B*−H), −15.9 (br d, 2B, *B*−H). $^{31}P\{^1H\}$ NMR (δ, CD_2Cl_2, 298 K): 29.4 (d, *J*(RhP) = 155).

[Rh(PPh_3)$_2$(nbd)][1-(^{i}Pr$_3$Si)-9,11,12-(Et)$_3$-*closo*-$CB_{11}H_8$] (12). A solution of (PPh_3)$_2$Rh(1-^{i}Pr$_3$Si-*closo*-$CB_{11}H_{11}$) (179 mg, 0.232 mmol) in CH_2Cl_2 (10 cm^3) was freeze−pump−thawed three times. On the third cycle ethene (~0.600 g) was added to the solution and the ampule closed and warmed to room temperature. After the solution was stirred for 24 h, it was degassed again, hydrogen was placed in the Young ampule, and the solution stirred for 2 h. This sequential treatment with ethene/hydrogen was repeated a total of three times. Following the last hydrogenation the solvent was degassed and norbornadiene (1 cm^3, 9.27 mmol) added. After the mixture was stirred overnight, the solvent was evaporated under vacuum and the orange residue redissolved in CH_2Cl_2 (2 cm^3) and precipitated with hexane (20 cm^3). The solvent was decanted via cannula and the product dried under vacuum (161 mg, 63%). Anal. Calcd for $C_{59}H_{82}P_2RhSiB_{11}$: C, 64.2; H, 7.49. Found: C, 64.4; H, 7.56. ESI-MS (negative mode): *m/z* 383.5 (obsd), showing the correct isotope pattern for $SiB_{11}C_{16}H_{44}$.

^1H NMR (δ, CD_2Cl_2, 298 K): 7.50−7.25 (m, 30H, PPh_3), 4.46 (br s, 4H, C_7H_8), 3.97 (br s, 2H, C_7H_8), 1.56 (br s, 2H, C_7H_8), 1.17 (sept, 3H, (Si−(C*H*(CH$_3$)$_2$)$_3$), 1.10 (d, 18H, (Si−(CH(C*H*$_3$)$_2$)$_3$), 0.90-0.40 (m, 15H, B−*Et*). $^1H\{^{11}B\}$ NMR (δ, CD_2Cl_2, 298 K): 7.50−7.25 (m, 30H, PPh_3), 4.46 (br s, 4H, C_7H_8), 3.97 (br s, 2H, C_7H_8), 1.74 (s, 2H, B−*H*), 1.66 (s, 2H, B−*H*), 1.47 (s, 1H, B−*H*), 1.43 (s, 1H, B−*H*), 1.39 (s, 2H, B−*H*), 1.56 (br s, 2H, C_7H_8), 1.17 (sept, 3H, (Si−(C*H*(CH$_3$)$_2$)$_3$), 1.10 (d, 18H, (Si−(CH(C*H*$_3$)$_2$)$_3$), 0.90−0.40 (m, 15H, B−*Et*). $^{11}B\{^1H\}$ NMR (δ, CD_2Cl_2, 298 K): 7.7 (br

s, 1B, *B*−Et), −1.4 (br s, 2B, *B*−Et), −10.4 (br s, 1B, *B*−H), −11.9 (br s, 2B, *B*−H), −14.8 (br s, 2B, *B*−H), −16.8 (br s, 3B, *B*−H). $^{31}P\{^1H\}$ NMR (δ, CD_2Cl_2, 298 K): 30.5 (d, J(RhP) = 155).

[Rh(PPh$_3$)$_2$(η^2-CH$_2$=CH$_2$)$_3$][*closo*-CB$_{11}$H$_6$Br$_6$] (13). A solution of [(PPh$_3$)$_2$Rh(nbd)][*closo*-CB$_{11}$H$_6$Br$_6$] (20 mg, mmol) in CH_2Cl_2 was freeze−pump−thawed three times. On the third cycle hydrogen (1 atm) was added to the solution to give [(PPh$_3$)(PPh$_2$-η^6-C$_6$H$_5$)Rh]$_2$[*closo*-CB$_{11}$H$_6$Br$_6$]$_2$.[35] After 30 min the solution was evaporated and the residue dissolved in CH_2Cl_2 under an atmosphere of ethene. Suitable crystals for X-ray diffraction studies were grown at −80 °C by layering ethene-saturated pentane over the CH_2Cl_2 solution. In situ low-temperature $^{31}P\{^1H\}$ NMR spectra for the [1-H-*closo*-CB$_{11}$H$_{11}$]$^-$ and [BAr$^F_4$]$^-$ analogues are identical with those of **13**.

^1H NMR (δ, CD_2Cl_2, 298 K): 7.60−7.11 (m, 30H, PPh_3), 5.2 (excess ethene), 2.59 (br s, 1H, C_{cage}−*H*). $^1H\{^{11}B\}$ NMR (δ, CD_2Cl_2, 298 K): 7.69−7.11 (m, 30H, PPh_3), 5.2 (excess ethene), 2.59 (br s, 1H, C_{cage}−*H*), 2.35 (br s, 5H, B−*H*). ^{11}B NMR (δ, CD_2Cl_2, 298 K): −1.55 (s, 1B, *B*−Br), −9.80 (s, 5B, *B*−Br), −20.25 (d, 5B, *B*−H, J(BH) = 156.6). $^{31}P\{^1H\}$ NMR (δ, CD_2Cl_2, 298 K): 33.3 (d, J(RhP) = 105). $^{31}P\{^1H\}$ NMR (δ, CD_2Cl_2, 238 K): 34.5 (d, J(RhP) = 102).

Acknowledgment. We thank the EPSRC (No. GR/S42750/01) and the Royal Society for funding, Professor Larry Sneddon (University of Pennsylvania) for useful discussions at the beginning of this project, which were enabled by a Royal Society of Chemistry/J. W. T. Jones travelling fellowship awarded to A.S.W., the EPSRC national mass spectrometry service at Swansea University, and Drs. John Lowe and Anneke Lubben at the University of Bath for NMR and mass spectrometric support, respectively. We also thank the reviewers for useful comments.

Supporting Information Available: Text, tables, and figures giving additional experimental and characterization data, full crystallographic data, including bond lengths and angles, for **2a**, **7**, **9**, **10**, and **13**, and ESI-MS spectra for the new complexes. This material is available free of charge via the Internet at http://pubs.acs.org.

OM070043P